

ANTIMICROBIAL BACTERIAL CELLULOSE AND ITS
DERIVED SOFT GELS DEVELOPED FROM SMECTITE
CLAY AND NATURAL BIOCIDES

ELENA HUNTER

A thesis submitted in partial fulfilment of the requirements of Nottingham Trent
University for the degree of Doctor of Philosophy

July 2019

Copyright statement

This work is the intellectual property of the author and supervisors: Fengge Gao and Michael Loughlin. You may copy up to 5% of this work for private study, or personal, non-commercial research. Any re-use of the information contained within this document should be fully referenced, quoting the author, title, university, degree level and pagination. Queries or requests for any other use, or if a more substantial copy is required, should be directed in the owner of the Intellectual Property Right.

Abstract

Bacterial cellulose (BC) is a homopolysaccharide synthesised mainly by species of the genera *Acetobacter*. Due to the porous matrix, BC possesses high water-absorption and -holding capacities. This non-toxic, biodegradable and biocompatible material is widely used in medical, cosmological, textile and food industries. In the medical field, BC has found potential in wound, burn and reconstructive surgeries. However, the major drawback of BC is that it does not provide a barrier against infections. Infections are one of the most challenging aspects of burn recovery and wound healing systems that can delay a healing process due to contamination by foreign bodies, such as bacteria. There is, thus, a need to generate BC with additional antibacterial activity. While most antibacterial agents are harmful to mammalian cells, they can also leach, which causes the uncontrolled release of the agents into the environment.

Therefore, the overall aim of this project was to use nanofillers such as smectite clay and natural biocides such as chitosan to give BC permanent, non-toxic, antimicrobial properties without biocide leaching. This research has made three major findings that are based on natural and non-toxic minerals or biomaterials. One of the major results obtained was that natural Cloisite Na⁺ and synthetic SWN clays showed antibacterial activity against both Gram-positive MRSA and Gram-negative *E. coli* bacteria in its exfoliated state. Exfoliated clays were then incorporated into BC to provide such antibacterial properties to the final composite. Another major finding was the synthesis of new BC-based material, named bacterial chitosan. Bacterial chitosan was developed using chitosan as the main carbon source. This material showed antibacterial activity against MRSA and *E. coli*. Bacterial chitosan cannot be dissolved in acid. This can solve problems associated with using chitosan in antibacterial applications. The third major finding was the enhancement of antibacterial activity of BC/chitosan hybrid hydro and hydrated gels by using exfoliated Cloisite Na⁺ clay. In addition to these major findings, other results were obtained using clay with organo-modifiers and

chitosan as biocides. Some of these synthesised materials had strong antibacterial activity. However, the leaching behaviour of biocides may have potential health and safety concerns.

Acknowledgements

Undertaking this Ph.D. has been a truly life-changing experience for me. It would not be possible to accomplish without the support that I received from many people.

I would like to express my deepest gratitude to my supervisor Dr. Fengge Gao for his continuous support, guidance and help throughout my Ph.D. His constant feedback during our discussions and immersed knowledge made this research achievable. I would like to convey my sincere gratitude to my second supervisor Dr. Michael Loughlin for his support, help, motivation and encouragement.

I would like to thank Dr. Luigi De Girolamo for his help in the cytotoxicity part of the research. Many thanks also go out to the support I received from the University staff and colleagues.

I would like to give my deepest gratitude to my parents, Galina and Alexander, for encouraging me to follow my dreams and continuously supporting me in my life. I would like to thank my husband Nick, who has been by my side, for his continuous love. I thank my best friend Maria for her encouragement and moral support. I am also very grateful for my Mother-in-law Elena for her continues care and help.

Abbreviations

ATP:	Adenosine triphosphate
BC-CH:	Bacterial chitosan
BC:	Bacterial cellulose
CFs:	Cotton fibers
CFU:	Colony-forming unit
CH:	Chitosan
DDA:	Degree of deacetylation
DLS	Dynamic laser scattering
DMEM:	Dulbecco's modified Eagle's medium
DMSO:	Dimethyl sulfoxide
DSA:	Drop shape analyser
FBS:	Fetal bovine serum
FT-IR	Fourier Transform Infrared spectroscopy
<i>G. xylinus:</i>	<i>Gluconacetobacter xylinus</i>
HS:	Hestrin Schramm
IM:	Isolated microorganisms
KB:	Kombucha beverage
KC:	Kombucha cellulose
kDa:	Kilodalton
LPS:	Lipopolysaccharides
MRSA:	Methicillin resistant <i>Staphylococcus aureus</i>
MTT:	MTT (3-(4,5-Dimethylthiazol-2-yl)-2,5-Diphenyltetrazolium Bromide)
MW:	Molecular weight
N/A	Not available
NaMMT:	Na ⁺ Montmorillonite
NIR:	Near-infrared

Non-ox:	Non-oxidised
OD:	Optical density
Ox:	Oxidised
<i>P. aeruginosa:</i>	<i>Pseudomonas aeruginosa</i>
PBS:	Phosphate buffered saline
QAC:	Quaternary ammonium compounds
RCF:	Relative centrifugal force
RIU:	Reflective index unit
RPM:	Revolutions per minute
SCOBY	Symbiotic culture of bacteria and yeasts
SEM:	Scanning electron microscopy
SWN:	Lithium magnesium sodium silicate
TSA:	Tryptic soy agar
TSB:	Tryptic soy broth
UV:	Ultraviolet
VIS:	Visible
WA:	Widely-available

Table of Contents

Copyright statement	i
Abstract	ii
Acknowledgements	iv
Abbreviations	v
List of Figures	xvii
List of Tables	xxvii
Chapter 1. Introduction	1
1.1. Bacterial cellulose	1
1.1.1. Structure of bacterial cellulose	1
1.1.2. Synthesis of bacterial cellulose	3
1.1.2.1. Acetic acid bacteria: genus <i>Gluconacetobacter</i>	3
1.1.3. The process of BC biosynthesis	4
1.1.4. Transport of cellulose through the membrane.....	6
1.1.5. The comparison of BC and cotton fibres	8
1.1.6. Applications of bacterial cellulose.....	10
1.2. Bacterial cellulose-based composites	13
1.2.1. Modification of BC	13
1.2.2. Overview of <i>in situ</i> modification of BC	15
1.2.3. <i>Ex situ</i> modification of BC with antibacterial metal particles.....	17
1.2.3.1. Gram-positive and Gram-negative bacteria.....	18
1.2.3.2. Antibacterial activity against Gram-positive and Gram-negative bacteria	21
1.2.4. Limitations of the current BC modification techniques	26
1.3. Bacterial cellulose composites with clay particles and their applications	28
1.3.1. Smectite clay	28

1.3.1.1. Montmorillonite (MMT) clay	29
1.3.2. Properties of MMT	32
1.3.2.1. Physical properties of MMT	32
1.3.2.2. Antimicrobial properties of MMT	33
1.3.3. Mammalian toxicity of MMT clay	34
1.3.4. Current progress on BC/MMT composites	36
1.3.5. BC/MMT composites for wound healing applications.....	37
1.4. BC/chitosan composites	41
1.4.1. Chitosan overview	41
1.4.1.1. Chitosan as chitin derivative.....	41
1.4.2. Structure and properties of chitosan.....	43
1.4.2.1. Solubility of chitosan.....	44
1.4.3. Antimicrobial properties of chitosan.....	45
1.4.3.1. Mechanism of antibacterial action of chitosan.....	46
1.4.3.2. Effect of DDA of chitosan on antibacterial activity	49
1.4.3.3. Effect of molecular weight on antibacterial activity	50
1.4.4. BC/chitosan composites for wound dressing applications	54
1.4.4.1. Mammalian toxicity of BC/chitosan composites	55
1.5. Kombucha as an alternative to conventional BC.....	57
1.5.1. The structure of Kombucha cellulose	58
1.5.2. Microbial composition of Kombucha.....	59
1.5.3. Fermentation of Kombucha cellulose	60
1.5.4. Benefits of Kombucha beverage	60
1.5.5. Antimicrobial properties of Kombucha beverage.....	61
1.6. Need for the research	63
1.7. Aim and objectives of the study	64
Chapter 2. Experimental Methodology.....	66
2.1. Materials used in the current study.....	66
2.2. Synthesis of BC.....	68
2.2.1. Maintenance of bacterial species	68

2.2.2.	Incubation of bacteria in liquid medium	69
2.2.3.	Treatment of BC after incubation.....	69
2.3.	Optimisation of BC growing conditions	70
2.3.1	The effect of optical density	70
2.3.2	The effect of temperature	70
2.3.3	The duration of incubation	70
2.3.4	The effect of carbon source.....	71
2.4.	The growth of BC in a clay environment	71
2.4.1.	Preparation of clay suspensions.....	71
2.4.1.1.	Exfoliation of clay suspensions.....	72
2.4.1.2.	Characterisation of exfoliation state of the clay suspensions using dynamic laser scattering	73
2.4.2.	The rheological characterisation of gel formation.....	73
2.4.3.	Inoculation of <i>G. xylinus</i> with clay suspensions on a small scale	73
2.4.4.	Inoculation of <i>G. xylinus</i> with clay suspensions on a large scale	74
2.4.5.	Investigation of leaching behaviour	74
2.5.	Growth of BC in chitosan environment	75
2.5.1.	Preparation of chitosan solutions	75
2.5.2.	Replacing glucose with a chitosan solution in HS medium	75
2.5.2.1.	Inoculation of <i>G. xylinus</i> with modified HS medium.....	75
2.5.2.2.	Investigation of leaching behaviour of BC/chitosan composites .	76
2.5.3.	Investigation of solubility of BC-CH	76
2.6.	<i>Ex situ</i> modification of BC	77
2.6.1.	Oxidation of BC	77
2.6.2.	Preparation of additive materials	77
2.6.2.1.	Preparation of clay suspensions.....	77
2.6.2.2.	Preparation of chitosan solutions	78
2.6.2.3.	Preparation of chitosan hydrogels	78
2.6.2.4.	Introducing exfoliated Cloisite Na ⁺ clay to chitosan hydrogels	78
2.6.3.	Incorporation of additive materials into pure BC.....	78
2.6.3.1.	Vacuum self-assembly method	79

2.6.3.2. The immersion method.....	79
2.7. Antibacterial activity of modified bacterial cellulose	80
2.7.1. Bacterial strains used in antibacterial assays.....	80
2.7.2. Production of bacterial lawns.....	80
2.7.3. Antibacterial assay of the components incorporated into BC.....	80
2.7.3.1. Antibacterial assay using clay suspensions	81
2.7.3.2. The disc diffusion method using compressed powder handmade discs.....	81
2.7.3.3. Antibacterial activity of chitosan	82
2.7.4. Antibacterial activity of synthesised BC-based materials	82
2.8. Synthesis of Kombucha cellulose.....	83
2.8.1. Optimisation of KC growing conditions.....	83
2.8.2. Preparation of tea	84
2.8.3. Effect of OD on the growth of KC	84
2.8.4. The effect of temperature on the growth of KC	84
2.8.5. Effect of tea concentration on the growth of KC.....	85
2.8.6. Effect of pH on the growth of KC.....	85
2.8.7. Effect of carbon source.....	85
2.8.8. Treatment of KC after incubation.....	86
2.9. Growth of Kombucha in clay environment.....	86
2.9.1. Inoculation of Kombucha with clay suspensions on a small scale	86
2.9.2. Inoculation of Kombucha with clay suspensions on a large scale	86
2.9.3. Antibacterial activity of synthesised KC-based materials	87
2.10. Characterisation of developed materials.....	87
2.10.1. Surface energy measurement.....	87
2.10.2. Characterisation of chemical structure using Fourier Transform- Infrared spectroscopy (FT-IR).....	87
2.10.3. Powder X-Ray diffraction analysis.....	88
2.10.4. Solid state UV-VIS-NIR spectroscopy	88
2.10.5. Scanning electron microscopy.....	88

2.11. Investigation of mammalian cell cytotoxicity of developed materials.....	89
2.11.1. Maintenance of NIH 3t3 cells.....	90
2.11.2. Reviving 3t3 cells from frozen	90
2.11.3. Passaging of 3t3 cells.....	90
2.12. Mammalian cell cytotoxicity.....	91
2.12.1. MTT reduction assay	91
2.12.2. Effect of non-exfoliated clay suspensions on NIH 3t3 cells	91
2.12.3. Effect of exfoliated clay suspensions on MTT reduction in 3T3 cells.....	92
2.12.4. Effect of nanoparticles on 3T3 cell using coated slides.....	92
2.12.5. Effect of chitosan on 3t3 cells.....	92
2.12.5.1. Addition of chitosan to culture medium.....	92
2.12.5.2. Effect of chitosan on 3T3 cell using coated slides.....	93
2.12.6. Effect of pure and modified BC on 3T3 cells	93
2.13. Statistical analysis	93
Chapter 3. The growth of BC in clay environment.....	94
3.1. Results	94
3.1.1. Optimisation of BC growing conditions on a small scale	94
3.1.2. Synthesis of BC on a large scale.....	102
3.1.3. Investigation of clay suspensions for in situ modification of BC	104
3.1.3.1. The morphology of the clay	104
3.1.3.2. Exfoliation of Cloisite Na ⁺ clay suspensions	105
3.1.3.2.1. Analysis of Cloisite Na ⁺ clay suspensions without exfoliation treatment.....	105
3.1.3.2.2. Exfoliation of Cloisite Na ⁺ suspension through magnetic stirring	106
3.1.3.2.3. Exfoliation of Cloisite Na ⁺ suspension through high power sonication.....	107
3.1.3.2.4. Exfoliation of Cloisite Na ⁺ suspension through blender.....	108
3.1.3.3. Exfoliation of SWN clay suspensions	111
3.1.3.3.1. Analysis of SWN suspension without exfoliation treatment.....	111

3.1.3.3.2. Exfoliation of SWN suspension through magnetic stirring.....	113
3.1.3.3.3. Exfoliation of SWN suspension through high power sonication.....	115
3.1.3.3.4. Exfoliation of SWN suspension through blending.....	116
3.1.4. Effect of exfoliation of clay on BC growth on a small scale	118
3.1.5. Synthesis of BC in clay environment on a large scale	123
3.1.6. Leaching behaviour of clay.....	125
3.1.7. Characterisation of <i>in situ</i> synthesised BC/clay composites	128
3.1.7.1. UV-VIS-NIR analysis of BC/Cloisite Na ⁺ composites	128
3.1.7.2. UV-VIS-NIR analysis of BC/SWN composites.....	130
3.1.8. Antibacterial activity of non-exfoliated clay suspensions.....	132
3.1.9. Antibacterial activity of exfoliated clay suspensions	134
3.1.10. Antibacterial activity of <i>in situ</i> synthesised BC/clay composites	135
3.1.11. Cytotoxicity of Cloisite Na ⁺ and SWN clay.....	137
3.1.12. Cytotoxicity of non-exfoliated clay	138
3.1.12.1. Effect of non-exfoliated Cloisite Na ⁺ clay on 3t3 cells	138
3.1.12.2. Effect of non-exfoliated SWN clay on 3t3 cells.....	139
3.1.13. Cytotoxicity of exfoliated suspensions.....	141
3.1.13.1. Effect of time on MTT reduction in 3t3 cells	141
3.1.13.2. The effect of the reduction of the medium on MTT reduction in 3t3 cells.....	142
3.1.13.3. Cytotoxicity of exfoliated Cloisite Na ⁺ clay suspensions.....	144
3.1.13.4. Cytotoxicity of exfoliated SWN clay suspensions	146
3.2. Discussion	148
3.2.1. Growth of pure BC in HS medium	148
3.2.2. Swelling and exfoliation of clays.....	149
3.2.3. Growth of BC in clay environment.....	152
3.2.4. Antibacterial activity of natural clay	154
3.2.5. Effect of clay on MTT reduction in 3t3 cells.....	157
Chapter 4. <i>Ex situ</i> synthesis of BC/clay composites.....	160
4.1. Results	160
4.1.1. <i>Ex situ</i> synthesised BC/Cloisite Na ⁺ and BC/SWN composites	160

4.1.2. Antibacterial activity of <i>ex situ</i> modified BC/SWN and BC/Cloisite Na ⁺ composites.....	160
4.1.3. Cytotoxicity of BC/clay composites.....	163
4.1.4. <i>Ex situ</i> synthesised BC/organoclay composites.....	165
4.1.4.1. Antibacterial activity of organoclay.....	165
4.1.4.2. Investigation of leaching behaviour of organoclay.....	166
4.1.5. Antibacterial activity of <i>ex situ</i> synthesised BC/clay composites.....	171
4.1.6. Antibacterial activity of <i>ex situ</i> synthesised BC/organoclay composites.....	171
4.1.7. Mammalian cytotoxicity of organoclay.....	175
4.1.8. Cytotoxicity assays on 3t3 cells using clay coated cover glass.....	181
4.1.9. The mammalian toxicity of BC/organoclay composites.....	183
4.2. Discussion.....	186
4.2.1. Attachment of clay to BC.....	186
4.2.2. Antibacterial activity of synthesised <i>ex situ</i> composites.....	187
4.2.2.1. Quaternary ammonium compounds.....	187
4.2.2.2. Effect of zeta potential on the antibacterial activity of organoclay.....	191
4.2.2.3. Leaching behaviour of organoclay.....	192
4.2.2.4. Comparison of antibacterial activity of BC/clay composites.....	195
4.2.3. Effect of organoclay on 3t3 cells.....	197
Chapter 5. Incorporation of chitosan into BC through synthesis <i>in situ</i>.....	199
5.1. Results.....	199
5.1.1. <i>In situ</i> synthesis of BC/chitosan composite involving glucose... ..	199
5.1.1.1. Characterisation of <i>in situ</i> produced BC/chitosan composite....	199
5.1.1.2. Leaching behaviour of BC/chitosan composite.....	200
5.1.1.3. UV-VIS-NIR analysis of synthesised <i>in situ</i> BC/chitosan composite.....	202
5.1.1.4. Antibacterial activity of chitosan.....	204
5.1.1.5. Antibacterial activity of BC/chitosan composite.....	205

5.1.1.6.	Mammalian cytotoxicity of chitosan	208
5.1.1.6.1.	Evaluation of toxicity of chitosan powder.....	209
5.1.1.6.2.	Cytotoxicity assay using cover glass coated with chitosan.....	210
5.1.2.	<i>In situ</i> synthesis of BC-CH using chitosan as the main carbon source.....	211
5.1.2.1.	Effect of pH on the synthesis of BC-CH	212
5.1.3.	Understanding the structure of BC-CH.....	213
5.1.4.	Solubility of BC-CH.....	214
5.1.5.	UV-VIS-NIR analysis of BC-CH.....	216
5.1.6.	Analysis of BC-CH using FT-IR.....	217
5.1.7.	X-ray diffraction analysis of BC-CH.....	219
5.1.8.	Antibacterial activity of BC-CH	221
5.2.	Discussion	222
5.2.1.	Attachment of chitosan to BC.....	223
5.2.2.	The dependence of microbial growth on medium	223
5.2.3.	Antibacterial activity of chitosan	228
5.2.4.	Mammalian cytotoxicity of chitosan	229
Chapter 6.	<i>Ex situ</i> integration of chitosan into BC matrix	231
6.1.	Results	231
6.1.1.	Comparison of oxidised and non-oxidised BC	231
6.1.2.	Comparison of different types of chitosan	234
6.1.3.	Modification <i>ex situ</i> of BC through immersion	238
6.1.4.	Non-oxidised BC/chitosan composites	238
6.1.5.	Ox BC/chitosan composites	241
6.1.6.	Incorporation of chitosan into BC using vacuum self-assembly method.....	244
6.1.7.	Analysis of synthesised <i>ex situ</i> non-ox BC/chitosan composites.....	244
6.1.8.	Analysis of synthesised <i>ex situ</i> ox BC/chitosan composites	248
6.1.9.	Antibacterial activity of synthesised <i>ex situ</i> BC/chitosan composites.....	250

6.1.9.1. Antibacterial activity of non-ox BC/chitosan composite produced through immersion	250
6.1.9.2. Antibacterial activity of non-ox BC/chitosan composites prepared through vacuum self-assembly technique.....	253
6.1.9.3. Antibacterial activity of ox BC/chitosan composites synthesised through vacuum self-assembly technique.....	256
6.2. Discussion	258
6.2.1. Oxidation of BC	259
6.2.2. Antibacterial activity of BC/chitosan composites	260
6.2.3. Cytotoxicity of BC/chitosan composites.....	263
Chapter 7. Synthesis of BC/chitosan hybrid gel through chemical attachment.....	266
7.1. Results	266
7.1.1. Synthesis of BC/chitosan hybrid gel through chemical attachment of chitosan.....	266
7.1.2. Analysis of BC/CH hybrid	267
7.1.3. UV-VIS-NIR spectroscopy of BC/CH hybrid gel	268
7.1.4. Introduction of exfoliated Cloisite Na ⁺ to BC/CH hybrid.....	270
7.1.5. Antibacterial activity of BC/CH hybrid and BC/CH/Cloisite Na ⁺ composite.....	272
7.2. Discussion.....	275
7.2.1. Cross-linking of chitosan by genipin.....	275
7.2.2. Antibacterial activity of BC/chitosan hybrid gels.....	277
7.2.3. Mammalian toxicity of genipin	278
Chapter 8. Kombucha cellulose as an alternative to the conventional BC.....	279
8.1. Results	279
8.1.1. Optimisation of growing conditions of KC on a small scale	279
8.1.2. Synthesis of KC on a large scale involving glucose	283
8.1.3. <i>In situ</i> incorporation of clay into KC on a small scale	286

8.1.4.	<i>In situ</i> incorporation of clay into KC on a large scale	287
8.1.4.1.	UV-VIS-NIR analysis of synthesised KC/Clay composites.....	289
8.1.4.2.	Antibacterial activity of synthesised KC/Clay composites	291
8.1.5.	<i>In situ</i> synthesis of KC/Chitosan using chitosan as the main carbon source on a large scale.....	294
8.1.5.1.	UV-VIS-NIR analysis of <i>in situ</i> synthesised KC/Chitosan.....	296
8.1.6.	Synthesis of KC/Chitosan/Clay composites	297
8.1.7.	Antibacterial activity of synthesised KC/Chitosan and KC/Chitosan/Clay composites	299
8.2.	Discussion	302
Chapter 9.	Final discussion	305
9.1.	Summary of mechanisms of antibacterial action.....	305
9.2.	<i>Ex situ</i> and <i>in situ</i> synthesised materials and their significance for antibacterial action.....	306
9.3.	Antibacterial correlation of materials synthesised to other antibacterial agents.....	310
9.4.	Mechanical properties of the materials synthesised	314
9.4.1.	O ₂ diffusion through BC/clay and BC/chitosan composites.....	315
Chapter 10.	Conclusion	318
Chapter 11.	Future work	320
References		324

List of Figures

Figure 1. Inter- and intra-hydrogen bonding of bacterial cellulose ^[1]	2
Figure 2. Schematic representation of bacterial cellulose organisation ^[4]	3
Figure 3. A schematic representation of the biosynthesis of cellulose by <i>Acetobacter xylinum</i> ^[7]	4
Figure 4. Organisation of cellulose synthase operon of the genus <i>Gluconacetobacter</i> ^[3]	5
Figure 5. BcsA-BcsB complex ^[9]	6
Figure 6. SEM image showing a coherent 3-D network of BC ^[16]	9
Figure 7. SEM image of cotton fibres ^[12]	9
Figure 8. BC produced in various shapes.....	11
Figure 9. Schematic representation of BC modification methods.	14
Figure 10. Summary of various biomedical and pharmaceutical applications of BC-based nanocomposites ^[29]	15
Figure 11. The structure of the cell walls of Gram-negative (top) and Gram-positive (bottom) bacteria ^[44]	19
Figure 12. The mechanism of antibacterial action of nanoparticles ^[47]	21
Figure 13. Schematic presentation of silica tetrahedron and alumina octahedron.....	30
Figure 14. Chemical structure of montmorillonite ^[85]	30
Figure 15. The structure of MMT.....	31
Figure 16. Representative wound photographs of BC/CuMMT, BC/NaMMTC and BC/CaMMT treated group, negative control (without BC), pure BC, unmodified MMT-BC group and positive control group (silver sulfadiazine) during the course of treatment ^[94]	40
Figure 17. Effect of conversion of chitin into chitosan on the molecular structure through four steps: deproteinisation, demineralisation, decolourisation, deacetylation ^[135]	42
Figure 18. Schematic molecular structure of chitosan ^[137]	43
Figure 19. Interactions between bacterial cell walls and chitosan ^[46]	46
Figure 20. TEM image showing the structure of the KC matrix and fibres ^[162] ..	58

Figure 21. SEM images showing the structure KC matrix.....	59
Figure 22. Schematic structure of synthetic SWN clay ^[205]	67
Figure 23. Reduction of MTT to formazan ^[207]	89
Figure 24. The relationship between OD ₆₀₀ and concentration of <i>Gluconacetobacter xylinus</i>	95
Figure 25. Images of wet (left) and dried (right) BC.....	96
Figure 26. The effect of bacterial density on BC growth.....	97
Figure 27. The mass of wet BC produced at 25°C, 30°C and 37°C temperature on a small scale.....	98
Figure 28. The effect of temperature on the mass of dried BC.....	99
Figure 29. The mass of wet BC produced after 24, 48 and 72 hours on a small scale.....	100
Figure 30. The mass of dried BC produced after 24, 48 and 72 hours on a small scale.....	101
Figure 31. Effect of glucose on BC growth.....	102
Figure 32. The effect of the time of incubation on the synthesis of BC on a large scale using 7.9×10^7 CFU/ml bacterial concentration at 30°C.....	103
Figure 33. The effect of incubation time on the mass of wet BC on a large scale.....	104
Figure 34. SEM images of a) Cloisite Na ⁺ and b) SWN clay.....	105
Figure 35. The particle size distribution of Cloisite Na ⁺ clay suspension at concentration of 6 mg/ml without exfoliation treatment.....	106
Figure 36. The particle size distribution of Cloisite Na ⁺ suspension exfoliated using magnetic stirring.....	107
Figure 37. The particle size distribution of Cloisite Na ⁺ suspension exfoliated using ultrasound.....	108
Figure 38. The structure of blades of the chopper grinder (red; left picture) and coffee grinder (brown; right picture).....	109
Figure 39. The particle size distribution of Cloisite Na ⁺ suspension exfoliated using Tefal blender.....	109
Figure 40a. The particle size distribution of Cloisite Na ⁺ suspension exfoliated by using the coffee grinder.....	110

Figure 40b. The particle size distribution of Cloisite Na ⁺ suspension exfoliated by using the coffee grinder.....	111
Figure 41a. The particle size distribution of non-exfoliated SWN suspension.	112
Figure 41b. The particle size distribution of non-exfoliated SWN suspension.	113
Figure 42a. The particle size distribution of SWN suspension exfoliated using magnetic stirring (Stuard).....	114
Figure 42b. The particle size distribution of SWN suspension exfoliated using magnetic stirring (Stuard).....	114
Figure 43a. The particle size distribution of SWN suspension exfoliated using ultrasound..	115
Figure 43b. The particle size distribution of SWN suspension exfoliated using ultrasound.	116
Figure 44a. The particle size distribution of SWN suspension exfoliated using the coffee grinder..	117
Figure 44b. The particle size distribution of SWN suspension exfoliated using the coffee grinder.	117
Figure 45. Effect of non-exfoliated Cloisite Na ⁺ and SWN clay suspensions on the growth of BC on a small scale.....	119
Figure 46. Effect of exfoliated Cloisite Na ⁺ and SWN clay suspensions on the growth of BC on a small scale.....	120
Figure 47. Images of BC synthesised under different treatments.....	121
Figure 48. Elastic modulus of non-exfoliated and exfoliated Cloisite Na ⁺ /medium and SWN/medium suspensions after 0 and 48 hours.....	122
Figure 49. Viscous modulus of non-exfoliated and exfoliated Cloisite Na ⁺ /medium and SWN/medium suspensions after 0 and 48 hours.....	123
Figure 50. The synthesised BC with 3 mg/ml of non-exfoliated Cloisite Na ⁺ clay suspension.....	124
Figure 51. The synthesised BC in the presence of 3 mg/ml of exfoliated Cloisite Na ⁺ (a) and SWN (b) clay suspensions.....	124
Figure 52. Mass of wet, centrifuged pure BC, BC/Cloisite Na ⁺ and BC/SWN produced with exfoliated clay, respectively.....	125

Figure 53. The relationship between absorbance and concentration of Cloisite Na ⁺ suspension.....	126
Figure 54. The relationship between absorbance and concentration of SWN suspension.....	127
Figure 55. The concentration of leached clay of BC/Cloisite Na ⁺ and BC/SWN, respectively, from 0 to 24 hours.....	128
Figure 56. UV-VIS spectra of BC/Cloisite Na ⁺ composite, pure BC and Cloisite Na ⁺	129
Figure 57. NIR spectra of BC/Cloisite Na ⁺ composite, pure BC and Cloisite Na ⁺	130
Figure 58. UV-VIS spectra of BC/SWN, pure BC and SWN clay powder.....	131
Figure 59. NIR spectra of BC/SWN composite, pure BC and SWN clay powder.....	131
Figure 60. Antibacterial activity of non-exfoliated Cloisite Na ⁺ and SWN suspensions against MRSA (NCTC 10418).....	132
Figure 61. Antibacterial activity of non-exfoliated Cloisite Na ⁺ and SWN suspensions against <i>E. coli</i> (NCTC 12493).....	133
Figure 62. Antibacterial activity of exfoliated Cloisite Na ⁺ and SWN suspensions against MRSA (NCTC 10418).....	134
Figure 63. Antibacterial activity of exfoliated Cloisite Na ⁺ and SWN suspensions against <i>E. coli</i> (NCTC 12493).....	135
Figure 64. Antibacterial activity of BC/Cloisite Na ⁺ and BC/SWN against MRSA.....	136
Figure 65. Antibacterial activity of BC/Cloisite Na ⁺ and BC/SWN against <i>E. coli</i> (NCTC 12493).....	137
Figure 66. The effect of non-exfoliated Cloisite Na ⁺ suspensions at 3t3 cells.....	139
Figure 67. The effect of SWN/medium suspension on 3t3 cells.....	140
Figure 68. The effect of time of incubation on the MTT reduction in 3t3 cells after 24, 48 and 72 hours at 37°C.....	142
Figure 69. The effect of reduction of the medium on the MTT reduction in 3t3 cells.....	143

Figure 70. The effect of exfoliated Cloisite Na ⁺ clay suspension on a level of MTT reduction in 3t3 cells.	145
Figure 71. The effect of exfoliated SWN clay suspension on a level of MTT reduction in 3t3 cells..	146
Figure 72. Schematic representation of exfoliation of clay particles ^[223]	150
Figure 73. A proposed antibacterial mechanism of NaMMT ^[234]	154
Figure 74. Antibacterial activity of pure BC, BC/Cloisite Na ⁺ and BC/SWN against MRSA after 24 hours.....	161
Figure 75. Antibacterial activity of BC/Cloisite Na ⁺ and BC/SWN against <i>E. coli</i> after 24 hours.....	162
Figure 76. Antibacterial activity of BC/Cloisite Na ⁺ and BC/SWN against <i>P. aeruginosa</i> after 24 hours.).....	163
Figure 77. The effect of pure BC, BC/Cloisite Na ⁺ and BC/SWN composites on MTT reduction in 3t3 cells.....	164
Figure 78. The zones of inhibition of Cloisite organoclay against MRSA, <i>E. coli</i> and <i>P. aeruginosa</i>	166
Figure 79. The time-dependent contact angle of Cloisite 10A.....	167
Figure 80. The time-dependent contact angle of Cloisite 15A.....	168
Figure 81. The time-dependent contact angle of Cloisite 20A.....	169
Figure 82. The time-dependent contact angle of Cloisite 30B.....	170
Figure 83. The time-dependent contact angle of Cloisite 93A.....	170
Figure 84. Antibacterial activity of BC/organoclay composites against MRSA. BC/organoclay composites were prepared by pumping 6 mg/ml of organoclay into BC matrix.....	172
Figure 85. Antibacterial activity of BC/organoclay composites against <i>E. coli</i>	173
Figure 86. Antibacterial activity of BC/organoclay composites against <i>P. aeruginosa</i>	174
Figure 87. The effect of Cloisite 10A/medium suspension on the level of MTT reduction in 3t3 cells.	176
Figure 88. The effect of Cloisite 15A/medium suspension on the level of MTT reduction in 3t3 cells.....	177

Figure 89. The effect of Cloisite 20A/medium suspension on the level of MTT reduction in 3t3 cells..	178
Figure 90. The effect of Cloisite 30B/medium suspension on the level of MTT reduction in 3t3 cells..	179
Figure 91. The effect of Cloisite 93A/medium suspension on the level of MTT reduction in 3t3 cells..	181
Figure 92. The effect of Cloisite 10A, 15A, 20A, 30B and 93A at a concentration of 6 mg/ml on 3t3 cells..	182
Figure 93. The effect of pure BC and BC/organoclay composites on 3t3 cells after 24 of incubation at 37°C.....	183
Figure 94. The effect of pure BC and BC/organoclay composites on 3t3 cells after 48 of incubation at 37°C.....	184
Figure 95. The effect of pure BC and BC/organoclay composites on 3t3 cells after 72 of incubation at 37°C.....	185
Figure 96. A photograph of the synthesised BC/chitosan composite..	200
Figure 97. The relationship between absorbance at wavelength of 325 nm and concentration of chitosan.	201
Figure 98. The concentration of chitosan leached from the composite during washing from 1 to 80 hours.....	202
Figure 99. UV-VIS spectra of medium MW chitosan, pure BC and BC/chitosan composite.....	203
Figure 100. NIR spectra of MW chitosan, pure BC and BC/chitosan composite.....	203
Figure 101. Antibacterial activity of chitosan against MRSA.....	204
Figure 102. Antibacterial activity of chitosan against <i>E. coli</i>	205
Figure 103. Antibacterial activity of BC/chitosan composite against MRSA....	206
Figure 104. Antibacterial activity of BC/chitosan composite against <i>E. coli</i>	207
Figure 105. Antibacterial activity of BC/chitosan composite against <i>P. aeruginosa</i>	208
Figure 106. The effect of chitosan powder on 3t3 cells after 24, 48 and 72 hours.....	209

Figure 107. The effect of chitosan coated coverslips on MTT reduction in 3t3 cells.....	211
Figure 108. Photographs of BC-CH growth at pH6, 5 and 4 on a large scale..	212
Figure 109. The mass of wet BC-CH produced <i>in situ</i>	213
Figure 110. SEM micrograph of BC-CH and pure BC.....	214
Figure 111. The centrifuge tube containing 3 grams of BC-CH inside the pure vinegar at pH2 after 48 hours.....	215
Figure 112. UV-VIS spectra of washing vinegar liquid, which contained BC-CH for 48 hours, chitosan and pure vinegar.	216
Figure 113. UV-VIS-NIR spectra of chitosan powder, pure BC and BC-CH..	217
Figure 114. IR spectra of chitosan, pure BC and BC-CH using FT-IR spectroscopy.	218
Figure 115. XRD patterns of chitosan, pure BC and BC-CH.	220
Figure 116. Antibacterial properties of BC-CH composite against MRSA.	221
Figure 117. Antibacterial properties of BC-CH composite against <i>E. coli</i>	222
Figure 118. UV-VIS-NIR spectra of non-oxidised and oxidised BC.	232
Figure 119. IR spectrum of non-oxidised BC.	233
Figure 120. IR spectrum of oxidised BC.	234
Figure 121. UV-VIS-NIR spectra of WA, low and medium MW chitosan.	235
Figure 122. IR spectra of WA, low and medium MW chitosan.....	237
Figure 123. UV-VIS-NIR spectra of non-ox BC/WA, non-ox BC/Low and non-ox BC/Medium MW chitosan composites.	239
Figure 124. IR spectrum of non-ox BC/WA chitosan composite using FT-IR equipment.	240
Figure 125. The FT-IR spectrum of non-ox BC/Low MW chitosan composite.	240
Figure 126. The FT-IR spectrum of non-ox BC/Medium MW chitosan composite.....	241
Figure 127. UV-VIS-NIR spectra of ox BC/WA, ox BC/Low and ox BC/Medium MW chitosan composites.	242
Figure 128. IR spectra of ox BC/WA, ox BC/Low and ox BC/Medium MW chitosan composites.....	243

Figure 129. SEM image of BC/WA chitosan synthesised using vacuum self-assembly method.....	245
Figure 130. UV-VIS-NIR spectra of non-ox BC/WA, non-ox BC/ Low MW and non-ox BC/Medium MW chitosan composites	246
Figure 131. IR spectra of non-ox BC/WA, non-ox BC/ Low MW and non-ox BC/Medium MW chitosan composites	247
Figure 132. UV-VIS-NIR spectra of ox BC/WA, ox BC/Low and ox BC/Medium MW chitosan composites prepared using the pump.	248
Figure 133. IR spectra of ox BC/WA, ox BC/Low and ox BC/Medium MW chitosan composites prepared using the pump.....	249
Figure 134. Antibacterial activity of non-ox BC/chitosan composites against MRSA.....	251
Figure 135. Antibacterial activity of non-ox BC/chitosan composites against <i>E. coli</i>	252
Figure 136. Antibacterial activity of non-ox BC/chitosan composites against <i>P. aeruginosa</i>	253
Figure 137. Antibacterial activity of non-ox BC/CH composites prepared through vacuum self-assembly technique against MRSA.....	254
Figure 138. Antibacterial activity of non-ox BC/chitosan composites prepared through vacuum self-assembly technique against <i>E. coli</i>	255
Figure 139. Antibacterial activity of non-ox BC/CH composites prepared through vacuum self-assembly technique against <i>P. aeruginosa</i>	255
Figure 140. Antibacterial activity of ox BC/chitosan composites prepared through vacuum self-assembly technique against MRSA.....	256
Figure 141. Antibacterial activity of ox BC/chitosan composites prepared through vacuum self-assembly technique against <i>E. coli</i>	257
Figure 142. Antibacterial activity of ox BC/CH composites prepared through vacuum self-assembly technique against <i>P. aeruginosa</i>	258
Figure 143. Periodate oxidation of cellulose ^[294]	259
Figure 144. Schematic image of genipin crosslinks with chitosan ^[301]	266
Figure 145. The appearance of chitosan hydrogel (a) BC/CH hybrid gel (b) after 24 hours.	267

Figure 146. SEM image of BC/CH hybrid gel.....	268
Figure 147. UV-VIS spectrum of BC/Genipin composite.	269
Figure 148. UV-VIS spectrum of BC/CH/Genipin hybrid.....	269
Figure 149. NIR spectrum of BC/CH/Genipin hybrid.....	270
Figure 150. UV-Vis spectrum of BC/CH/Genipin/Cloisite Na ⁺ composite.	271
Figure 151. NIR spectrum of BC/CH/Genipin/Cloisite Na ⁺ composite.	272
Figure 152. Antibacterial activity of synthesised BC/CH hybrid and BC/CH/Cloisite Na ⁺ composite against MRSA.....	273
Figure 153. Antibacterial activity of synthesised BC/CH hybrid and BC/CH/Cloisite Na ⁺ composite against <i>E. coli</i>	274
Figure 154. Antibacterial activity of synthesised BC/CH hybrid and BC/CH/Cloisite Na ⁺ composite against <i>P. aeruginosa</i>	275
Figure 155. The effect of IM density ranging on the mass of wet KC after 48 hours.....	280
Figure 156. The mass of wet KC produced at 25°C, 30°C and 37°C temperature.....	281
Figure 157. The effect of pH on KC growth.	282
Figure 158. The effect of the concentration of tea broth the mass of wet KC.	283
Figure 159. Image of KC produced.....	284
Figure 160. SEM image of KC (a) and pure BC (b) produced on a large scale, respectively.....	285
Figure 161. The mass of wet KC produced using either tea or distilled water..	286
Figure 162. The effect of non-exfoliated and exfoliated Cloisite Na ⁺ and SWN clay suspensions on a mass of KC.....	287
Figure 163. Images of KC/Exfoliated Cloisite Na ⁺ (a) and KC/Exfoliated SWN (b) composites.....	288
Figure 164. The effect of non-exfoliated and exfoliated Cloisite Na ⁺ and SWN clay suspensions on a mass of wet KC.....	289
Figure 165. UV-VIS-NIR spectra of pure KC, SWN powder and KC/SWN composite.....	290
Figure 166. UV-VIS-NIR spectra of pure KC, Cloisite Na ⁺ powder and KC/Cloisite Na ⁺ composite.....	290

Figure 167. Antibacterial activity of pure KC, KC/Cloisite Na ⁺ and KC/SWN composites against MRSA.....	291
Figure 168. Antibacterial activity of pure KC, KC/Cloisite Na ⁺ and KC/SWN composites against <i>E. coli</i>	292
Figure 169. Antibacterial activity of pure KC, KC/Cloisite Na ⁺ and KC/SWN composites against <i>P. aeruginosa</i>	293
Figure 170. Image of the produced KC/Chitosan using tea.....	294
Figure 171. Image of the produced KC/Chitosan using sterile distilled water..	295
Figure 172. The mass of wet KC/Chitosan produced with either tea broth or distilled water	296
Figure 173. UV-VIS-NIR spectra of pure KC, WA chitosan powder and KC/WA chitosan composite.....	297
Figure 174. The mass of wet KC/Chitosan, KC/Chitosan/Cloisite Na ⁺ and KC/Chitosan/SWN composites on a small scale.....	298
Figure 175. The mass of wet KC/Chitosan, KC/Chitosan/Cloisite Na ⁺ and KC/Chitosan/SWN composites produced on a large scale.....	299
Figure 176. Antibacterial activity of synthesised pure KC, KC/Chitosan, KC/Cloisite Na ⁺ and KC/SWN composites against MRSA.....	300
Figure 177. Antibacterial activity of synthesised pure KC, KC/Chitosan, KC/Cloisite Na ⁺ and KC/SWN composites against <i>E. coli</i>	301
Figure 178. Antibacterial activity of synthesised pure KC, KC/Chitosan, KC/Cloisite Na ⁺ and KC/SWN composites against <i>P. aeruginosa</i>	302

List of Tables

Table 1. The comparison of MTT reduction in cells under different treatment after 24, 48 and 72 hours..	147
Table 2. Effect of BC-based materials on 3t3 cells after 24, 48 and 72 hours.	186
Table 3. Properties and structure of commercially available organoclay layered silicates supplied by Southern Clay Products, Inc ^[92]	188
Table 4. The antibacterial activity of all tested materials against MRSA, <i>E. coli</i> and <i>P. aeruginosa</i>	306

Chapter 1. Introduction

The introduction covers the current state-of-the-art progress in the synthesis of BC-based composites with antibacterial properties. The first Section will review the fundamental knowledge on BC structure, properties and applications, including modification and examples of BC-based composites with various antibacterial agents. Since clays were used as antibacterial agents in this project, the second Section will focus specifically on clay and BC/clay composites with antibacterial properties and their applications in wound healing. Thereafter, the third Section will be based on chitosan, which has also been used as an antibacterial agent in this current study, its antibacterial properties and potential for antibacterial BC/chitosan composites. The next part will review the progress in Kombucha cellulose as an alternative for conventional BC. The last Section will summarise the literature review, explain the need for the research, the hypothesis and experimental aim.

1.1. Bacterial cellulose

1.1.1. Structure of bacterial cellulose

Cellulose ($C_6H_{10}O_5$)_n is a homopolysaccharide formed by a linear chain of monosaccharide β -d-glucose residues linked by $\beta(1 \rightarrow 4)$ bonds to form β -1,4 glucan chains^[1, 2]. Linear β -1,4-glucan chains are secreted outside the cells through a linear row of pores located on the bacterial outer membrane^[3]. In addition to β -1,4 covalent bonds, each *d*-glucose subunit also has hydrogen bonds between *d*-glucose monomers^[1]. The glucan chains are held together by inter- and intra-hydrogen bonding (Fig. 1)^[1]. The interchain hydrogen bonding is located between the exposed hydroxyl groups of the aligned chains.

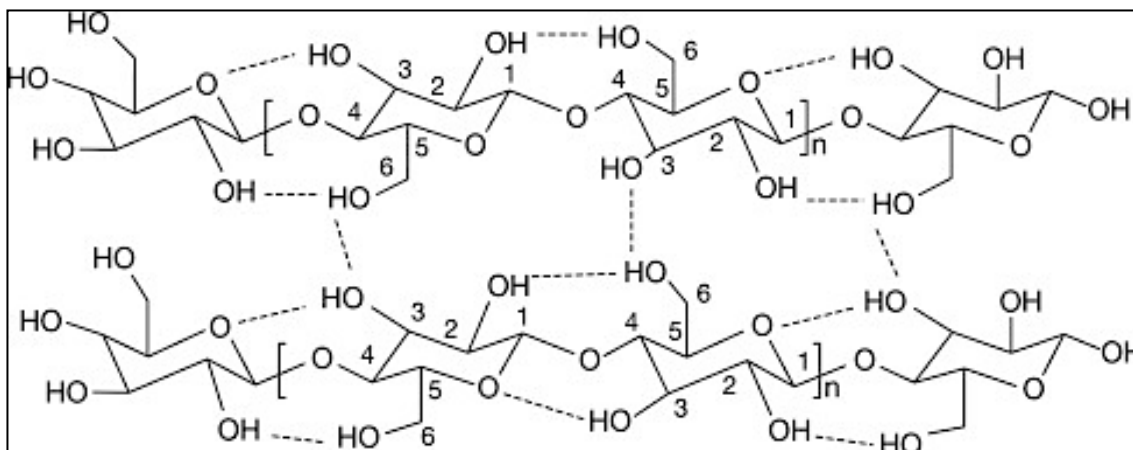


Figure 1. Inter- and intra-hydrogen bonding of bacterial cellulose^[1].

In BC, each glucose residue has one intermolecular ($O_6-H \cdots O_3$) and two intramolecular hydrogen bonds ($O_6 \cdots H-O_2$) and ($O_3-H \cdots O$ ring).

The subsequent assembly of the β -1,4-glucan chains leads to the formation of sub-fibrils. Each sub-fibril consists of 10–15 nascent β -1,4-glucan chains and has a width of approximately 1.5 nm^[1, 4]. Sub-fibrils are crystallised into microfibrils that then form bundles and ribbons. The ribbon is composed of approximately 1000 individual glucan chains^[1]. This process results in the formation of a thick, porous membrane in static culture conditions (Fig. 2). The matrix of BC consists of uniaxially orientated fibres with a diameter of 3-8 nm^[1].

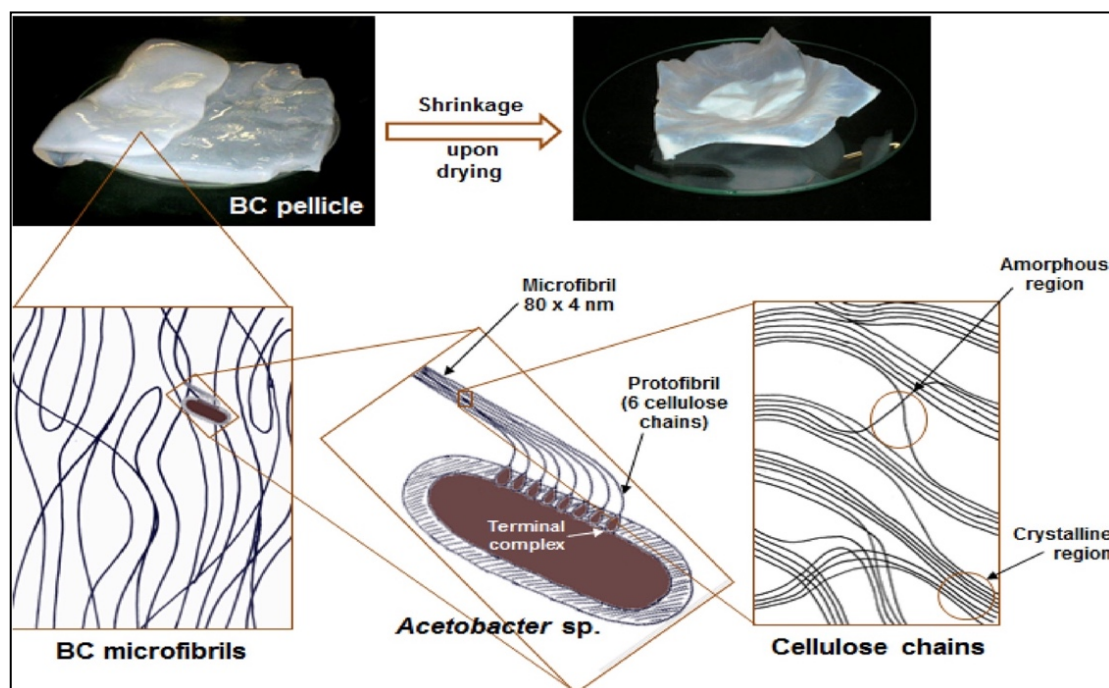


Figure 2. Schematic representation of bacterial cellulose organisation^[4].

1.1.2. Synthesis of bacterial cellulose

BC is synthesised mainly by two genera of acetic acid bacteria: *Acetobacter* and *Gluconacetobacter*^[5]. *Gluconacetobacter xylinus* (*G. xylinus*) is one of the most efficient cellulose producers^[5]. It can utilise different types of carbon sources such as glucose, galactose, fructose, sucrose, lactose, maltose, glycerol, dihydroxyacetone, pyruvate and dicarboxylic acids^[6]. During BC formation, glucose monomers are covalently attached to a linear chain by cellulose synthase enzymes^[1].

1.1.2.1. Acetic acid bacteria: genus *Gluconacetobacter*

Acetic acid bacteria are so named because of their ability to oxidise ethanol into acetic acid. The *Acetobacteraceae* family consists of strictly aerobic, Gram-negative acetic acid bacteria with the ability to oxidise alcohols, carbohydrates and sugar alcohol into acetic acid and other organic acids such as fumaric,

ketones, gluconic, citric and oxoacids^[5]. The genus *Gluconacetobacter* is one of the most efficient cellulose producers amongst acetic acid bacteria. *G. xylinus* is non-pathogenic bacterium, which is a common contaminant of beer and wine and is found on the surface of leaves, flowers and fruits^[1, 5]. The cellulose produced by *G. xylinus* protects bacteria from harsh environmental conditions such as toxins, including antibiotics and UV radiation, and helps to retain moisture^[5]. For example, the biofilm produced by *G. xylinum* promotes bacterial colonisation while inhibiting colonisation of competing organisms on fruits^[5]. In addition, cellulose, which is produced in liquid environments, floats and allows the bacteria to stay near the oxygen-rich surface. However, in a natural environment, the cellulose does not reach the same thickness of the fibres as those obtained on the surface of liquid broth in a laboratory environment^[1].

1.1.3. The process of BC biosynthesis

The biosynthesis of cellulose is a multi-step reaction, which contains four key enzymatic steps (Fig. 3):

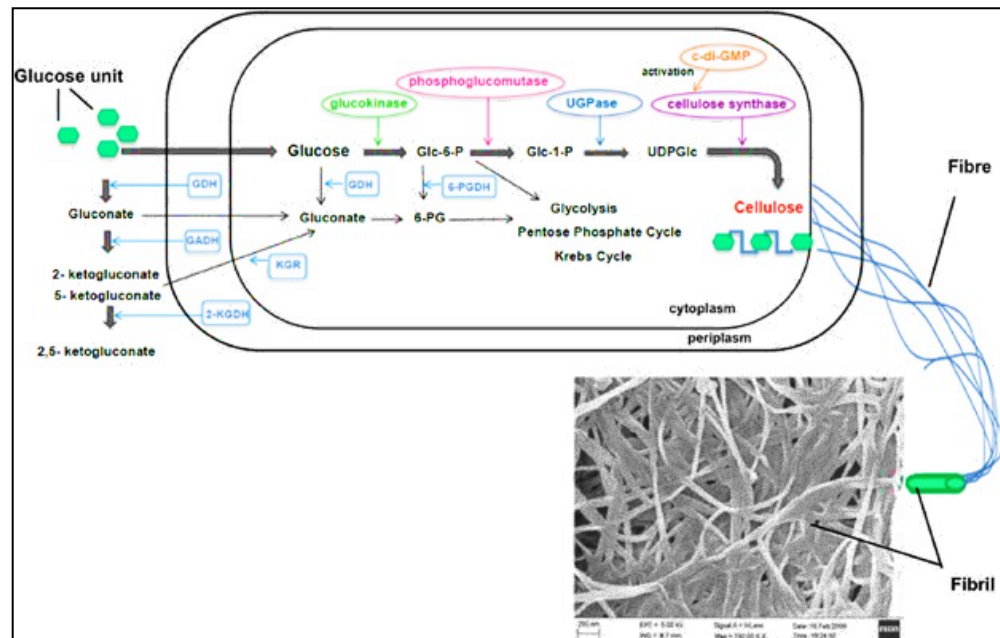


Figure 3. A schematic representation of the biosynthesis of cellulose by *Acetobacter xylinus*^[7].

The first step is phosphorylation of glucose to glucose-6-phosphate (Glc-6-P) by enzyme glucokinase^[7]. This is followed by the isomerisation of glucose-6-phosphate to glucose-1-phosphate (Glc-1-P) by phosphoglucomutase^[7]. Glc-1-P is then converted to UDP- glucose by UDPG-pyrophosphorylase (UGPase)^[7]. UPD-glucose monomers subsequently bind with each other to form cellulose, further forming a linear chain^[1]. Thus, bacterial cellulose is a polymer synthesised from UDP-glucose monomers^[1]. Cellulose synthase is the key enzyme involved in the formation of cellulose because it catalyses the covalent attachment of glucose monomers into a linear chain^[1]. This enzyme is encoded by the genes of the bacterial cellulose synthase (*bcs* or *axcs*) operon^[5]. Cellulose synthase operates with endo-b-1,4-glucanase (CMCAx), cellulose complementing factor (CcpAx) and b-glucosidase (BglAx). Their genes are located in the operon flanking regions. This operon comprises three (*bcsAB*, *bcsC*, and *bcsD*) or four (*bcsA*, *bcsB*, *bcsC*, and *bcsD*) genes, encoding the subunits BcsA, BcsB, BcsC, and BcsD (Fig.4)^[5].

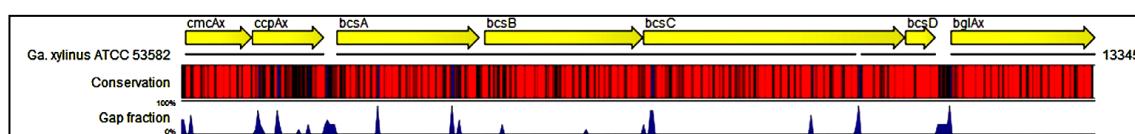


Figure 4. Organisation of cellulose synthase operon of the genus *Gluconacetobacter*^[3].

BcsA, *bcsB*, and *bcsC* genes of the *bcs* operon are characteristic of known microorganisms that produce cellulose. Regarding *Gluconacetobacter*, the most conserved gene is *bcsD*, followed by *bcsA* and *bcsB*, whereas the *bcsC* sequence contains the greatest number of mutations^[5]. BC is formed between the cytoplasm and outer membranes of the cell. The cellulose molecules, which are synthesised inside the bacteria, are then spun through cellulose export components, forming protofibrils.

1.1.4. Transport of cellulose through the membrane

The synthesis and transport of cellulose through the membrane is mediated by the cellulose synthase complex that contains a membrane-integrated catalytic BcsA subunit and a periplasmic, membrane-anchored BcsB domain (Fig. 5)^[8].

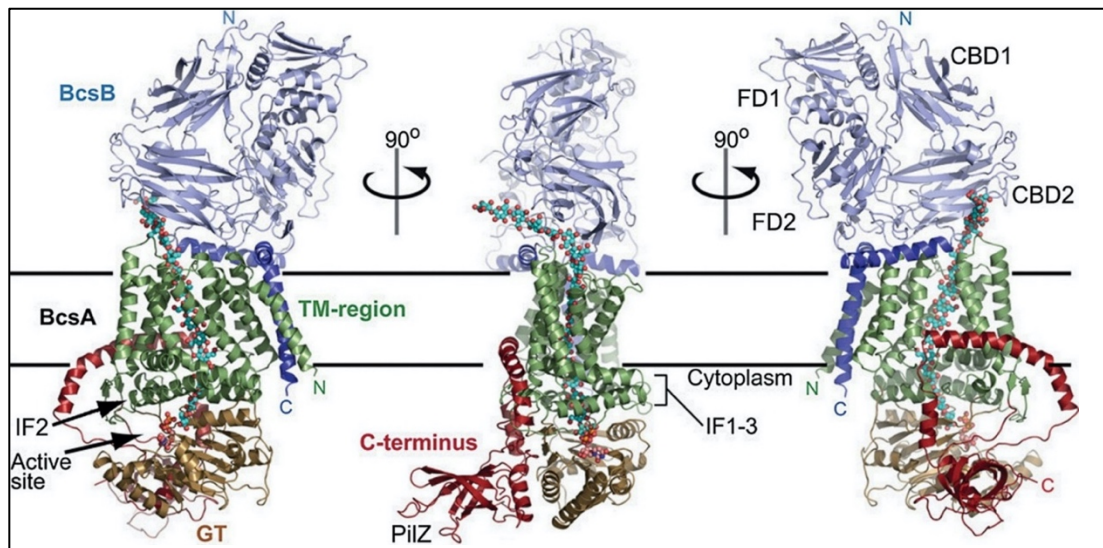


Figure 5. BcsA-BcsB complex^[9].

The membrane-integrated BcsA subunit, which is located on the inner membrane, is the catalytically active protein. BcsA subunit mediates both transport and synthesis of cellulose through the inner membrane^[8]. The subunit is connected to the cytoplasmic membrane by 8 transmembrane (TM) helices, which are flanked by 3 amphipathic helices (IF1-3) that are located at the cytosolic water-lipid interface parallel to the membrane^[9]. The cytoplasmic region of the BcsA subunit consists of a catalytic domain with glucosyltransferase (GT) activity that uses UDP-glucose as a precursor of the β -1,4-glucan chain and a PilZ regulatory domain that binds a specific allosteric activator to the c-di-GMP molecule^[9].

BcsB is the periplasmic domain that is anchored to the inner membrane by a single, carboxy-terminal transmembrane helix. BcsB consists of two periplasmic carbohydrate-binding domains that are connected to two α/β -domains (FD1 and

FD2) (Fig.5)^[10]. BcsB domain transports a newly synthesised β -1,4-glucan chain from the cytoplasm through the periplasmic space^[10]. The BcsA subunit and BcsB domain form the core of the cellulose synthase complex^[9]. This complex is crucial for the synthesis of BC both *in vitro* and *in vivo*.

The exact mechanism of cellulose translocation is currently unknown^[11]. However, a model of cellulose transport was proposed by Morgan *et al.*^[10]. In this model, the newly added glucose molecule might rotate around the acetal linkage to align with the glucan in the channel, where the allosteric interactions could guide the direction of the rotation^[10]. This might lead to the formation of the β -1,4 glucan with an intramolecular O3-H••O5 hydrogen bond. Moreover, the glucan might translocate into the channel during a relaxation^[11]. This process can be repeated in a second for UDP-glucose, but the rotation would be in the opposite direction due to steric constraints^[10].

Cellulose might be moved by one glucose unit each round of catalysis *via* the cellulose synthase complex: thus, newly added glucose unit can be positioned to become an acceptor in the subsequent reaction. Therefore, the translocation can be coupled with conformational changes at the active site followed by relaxation of the newly added glucose into the plane of the cellulose^[11]. Interaction of the cellulose subunits should be dynamic allowing either the protein to slide along rigid cellulose fibres or isolation of glucan chains to pass through pores^[11].

Furthermore, the BcsC subunit is predicted to form an 18-stranded β -barrel in the outer membrane^[11]. The BcsC subunit is followed by a large periplasmic domain that contains tetratricopeptide repeats that might be involved in the complex assembly. This subunit is required for the synthesis of cellulose *in vivo*, but not *in vitro*. Furthermore, BcsC might create pores in the outer cell membrane and be involved in the export of synthesised polysaccharides outside the cell^[11]. An interaction of the inner BcsA subunit and BcsB domain with the outer membrane

BcsC subunit is still unknown^[11]. It is also unknown how cellulose enters the channels in the outer membrane^[11].

Bacteria usually contain an additional BcsD subunit, which is a small periplasmic protein with approximately 160 residues^[11]. BcsD is located in the periplasm between BcsA and BcsB units^[11]. BcsD might be responsible for the formation of crystalline regions of the cellulose chain by facilitating a formation of hydrogen bonds between the four newly established chains of β -1,4-glucan^[9]. However, the exact function of this subunit is unknown^[11]. A direct interaction between BcsD and the membrane-associated BcsA and BcsB subunits has not yet been demonstrated^[11].

1.1.5. The comparison of BC and cotton fibres

BC can be compared to cotton fibres (CFs) that are made up of nearly 90% cellulose^[12]. The cellulose in both BC and CF cellulose is chemically identical, as both are type I cellulose (insoluble in both water and the most common organic solvents)^[13]. However, at a macroscopic level, they differ, as BC is rich in triclinic structure I_a whereas CFs are predominantly monoclinic structure I_b ^[14].

BC is synthesised in a pure state and found external to the bacteria^[13]. Fibres of BC are uniaxially orientated and create a well-separated, highly porous matrix^[15] (Fig. 6).

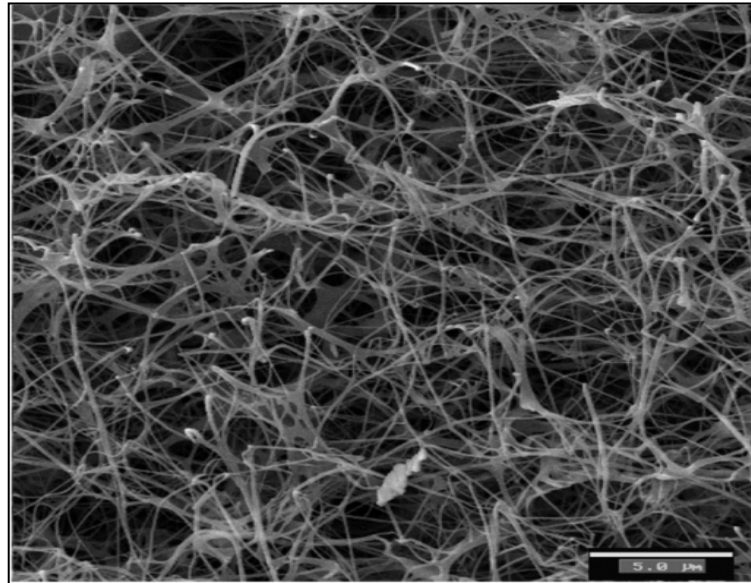


Figure 6. SEM image showing a coherent 3-D network of BC^[16].

CFs are found in both primary and secondary plant cell walls. A primary cell wall includes cellulose in addition to proteins (1.0–1.9%), waxes (0.4–1.2%), pectins (0.4–1.2%), inorganics (0.7–1.6%) and other substances (0.5–8.0%)^[12, 17]. The secondary cell wall contains fewer non-cellulose constituents^[12]. Fig. 7 shows SEM image of CFs.

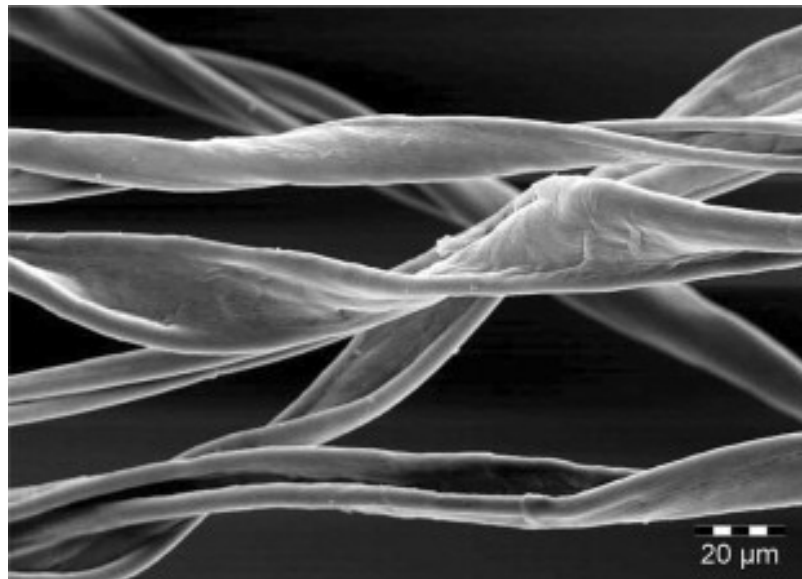


Figure 7. SEM image of cotton fibres^[12].

Both BC and cotton fibres show a high crystallinity, 89% and 70-80%, respectively, suggesting a similarly packed fibre structure^[13, 18, 19]. Both BC and CFs have a porous matrix. However, the porosity of BC is 28.3% whereas the porosity of CFs has been found to be 11.36%^[3, 17]. Porosity greatly affects the water absorption capacity of cellulose. The water holding capacity of BC is 142%, which is far greater than the 9.5% of CFs^[16, 18]. According to the aforementioned differences, BC seems to be more promising material than CFs for a variety of applications that are detailed below.

1.1.6. Applications of bacterial cellulose

Due to high *in vivo* biocompatibility, the ability to provide a three-dimensional substrate for the attachment of cells as well as flexibility, high water-holding capacity and gas exchange, BC has a wide range of applications. For example, BC can be used in the food industry as a thickening agent in pastry condiments, gelation agent in tofu and stabilising agent in ice creams^[20]. A product containing BC as a stabilising agent may retain its moisture for at least a month during storage as well as keep its shape^[21]. Adding BC to ice cream can make the shape of ice cream remain the same for at least 60 minutes after removing it from a freezer^[21]. As a gelling agent, BC significantly increases the strength of tofu by 0.2–0.3% and provides better texture and firmness^[21]. Additionally, BC helps to produce low-cholesterol and low-calorie food ingredients. Introducing BC to monascus, which is a natural red pigment, leads to the formation of a dietary complex with meat flavour^[21]. Moreover, BC is used in food packaging. The addition of BC increases transparency and thermostability and reduces the diffusion of gases^[20]. For example, a BC-reinforced PLA composite results in improved transparency and mechanical properties that might be ideal for food packaging applications^[20].

Due to high purity, BC has a low endotoxin unit (EU) level (<20 EU/g), which is required by the Food and Drug Administration (FDA)^[22]. Endotoxins are

lipopolysaccharides, which are potential inducers of inflammation. The endotoxin values measured on the purified BC membrane have been shown to be 0.3-3 EU/g^[23, 24]. In contrast, cellulose obtained from wood and ultrapure cellulose nanofibrils (CNF) have endotoxins level of around 100 EU/g and 50 EU/g, respectively^[25]. Because of its non-toxicity, BC has the potential to be used as artificial skin, *in vivo* implants and artificial blood vessels^[22]. Furthermore, BC can be produced in different sizes and shapes without significantly affecting its properties. BC consists of a number of almost parallel, thin cellulose layers^[1]. Each new layer is formed at the upper film surface, resulting in increased thickness over time^[1]. Therefore, it is possible to reform the pellicles into a desirable shape. Nimeskern *et al.* have designed an implant for the replacement of ear cartilage using BC^[26]. Fig. 8 shows different shapes of BC produced for a variety of applications, such as vascular graft, burn dressing material and a meniscus implant^[1].

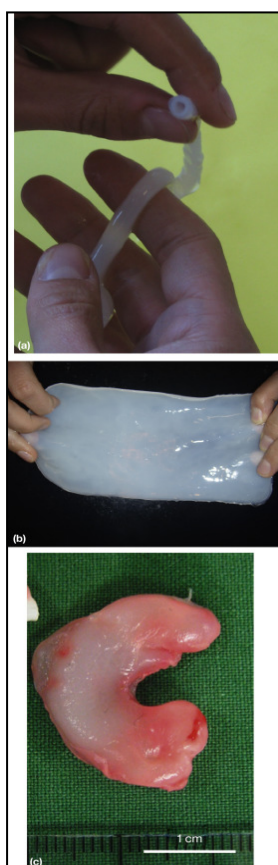


Figure 8. BC produced in various shapes. Tube to be used as a vascular graft (a), membrane to be used as burn dressing (b), and meniscus implant (c)^[1].

Due to the extracellular production of BC and the fact that it can be extracted without lipopolysaccharide (endotoxin) contamination, bacterial cellulose can be used *in vivo* as blood vessels. Scherner *et al.* investigated the possibility of using BC tubes as *in vivo* replacements of blood vessels in ten sheep for three months^[27]. In this study, BC showed good blood compatibility, no changes in blood cells and minimal inflammatory response compared to the control group^[27]. Furthermore, BC has the potential to be used as a scaffold in tissue engineering due to biocompatibility, which is a crucial property for implantation. The biocompatibility of BC was evaluated using Wistar rats by Helenius *et al.*^[28]. In this study, BC was implanted in rats for one, four and 12 weeks, respectively. By the end of the experiment, there were no microscopic signs of inflammation and an absence of fibrotic or giant cells^[28].

BC is widely used as a wound-healing material. Wound healing is a biological process, which consists of four basic phases: hemostasis, inflammation, proliferation and maturation^[29]. Wounds secrete exudate, which is liquid produced from wounds and released during the inflammation and proliferation phases, providing moisture to a wound, which leads to a healing process^[30]. However, a high level of exudate decreases the concentration of proteinase inhibitors and growth factors, which subsequently results in the degradation of tissue and retards the healing process^[29, 30]. Generation of a moist environment is crucial for controlling the level of exudates and, therefore, is beneficial for enhancing re-epithelialisation and reducing scar formation^[30]. Hence BC, as a wound dressing system can provide a moist environment, absorb excessive exudates, offer transparency for a wound inspection, provide mechanical strength and prevent fluid loss. BC can also improve the interaction of living cells with moisture and support cell migration, which results in the replacement of lost tissue in burn surgery^[29]. Due to its high water-holding capacity, BC increases healing rates and reduces pain^[29]. Its ability to retain a moist environment can also prevent wounds from drying as well as sticking to wound dressings. In addition,

its water-absorption and -holding capacities may be beneficial when incorporating drugs or bioactive components^[29].

However, the major drawback of BC as a wound-healing material is the lack of a barrier between a wound and infections. Long-term chronic wounds can be contaminated by foreign bodies, such as bacteria, which induce inflammatory responses^[29]. As a consequence, more than 50% of diabetic chronic ulcers become infected^[29]. The infections are one of the most challenging issues in burn recovery as they can delay the healing process due to patient's adversely affected immune system together with the extensive disruption of the physical skin barrier. In order to prevent an infection, BC can be modified using different materials with antimicrobial properties. Application in other areas is becoming more popular, while its use in even broader areas may be possibly the enhancement of its properties in the future.

1.2. Bacterial cellulose-based composites

1.2.1. Modification of BC

BC is typically modified to improve its properties, usually to introduce antimicrobial properties and enhance biocompatibility and its liquid-holding and -realising capacities. Modification of BC can be achieved through an adjustment of the BC structure during the biosynthesis process (*in situ*) or post-synthesis (*ex situ*) (Fig. 9).

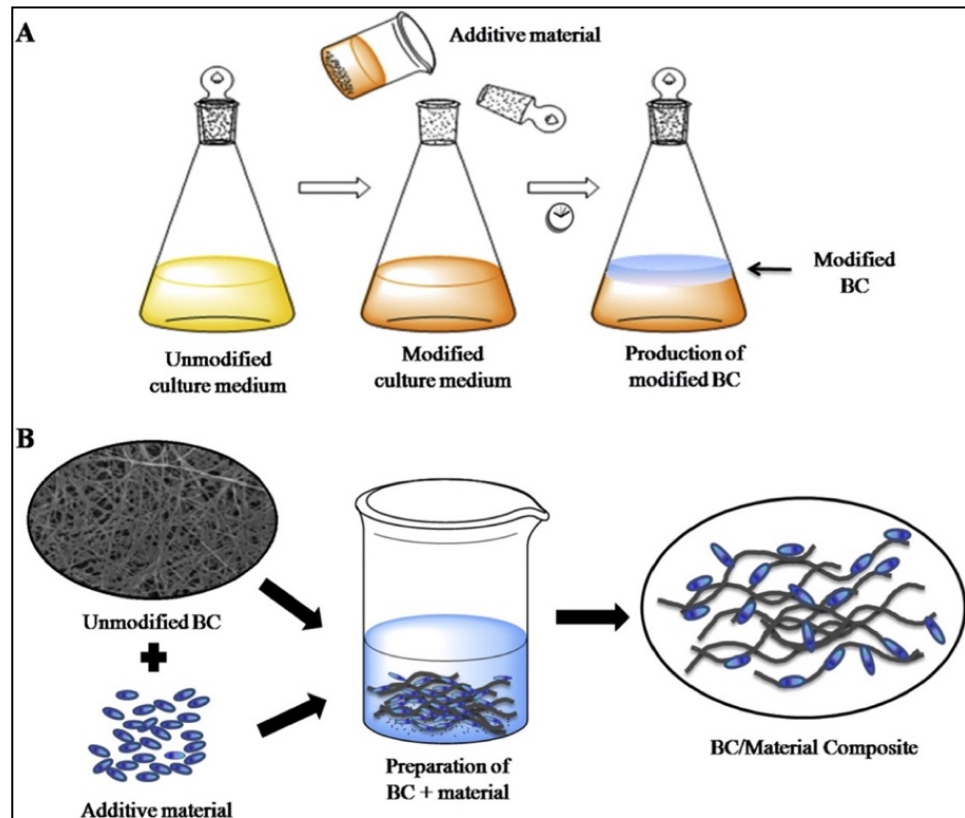


Figure 9. Schematic representation of BC modification methods. (a) *In situ* modification of BC, where additive/reinforcement material is added directly into the culture medium. (b) *Ex situ* modification, where BC is modified by chemical treatment or absorption of other materials (immersion)^[2].

Various BC-based composites have been designed to introduce different properties into BC, such as antibacterial properties, and to improve mechanical properties in different biomedical applications. Fig. 10 summarises a range of biomedical applications of BC-based composites.

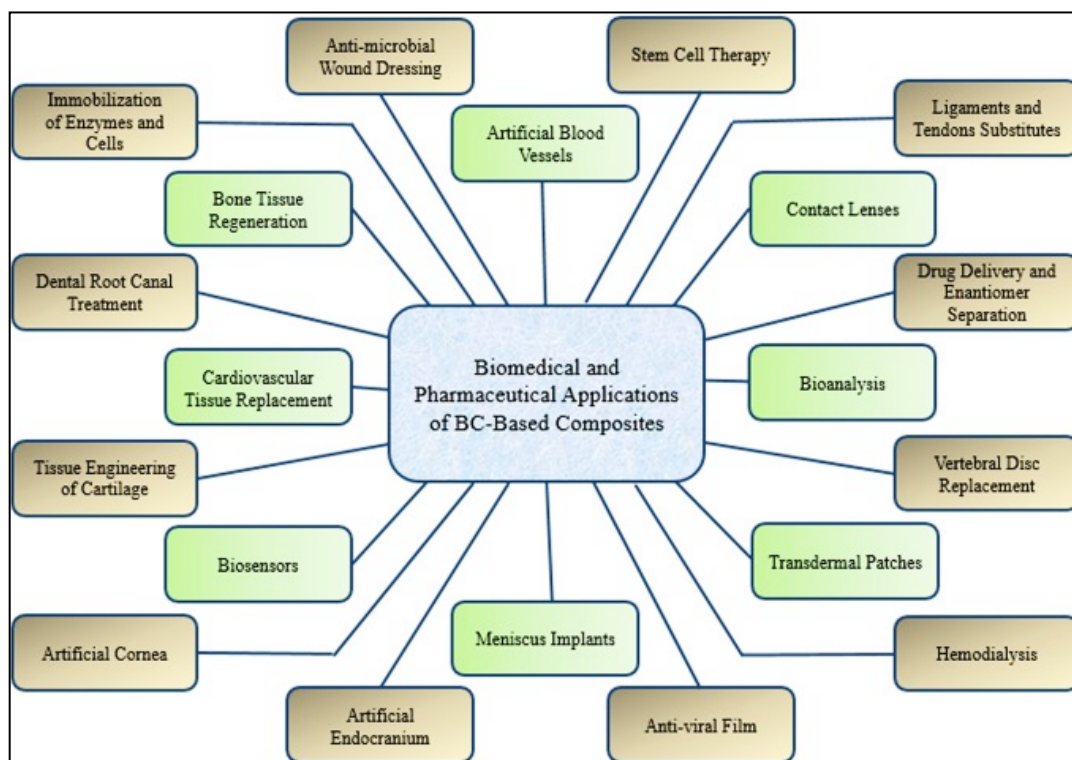


Figure 10. Summary of various biomedical and pharmaceutical applications of BC-based nanocomposites^[29].

Thus, BC-based nanocomposites can be used as antimicrobial/antiviral films and in wound dressing systems, bioengineering, drug delivery systems, ophthalmic and skeletal systems and cardiovascular system^[29].

1.2.2. Overview of *in situ* modification of BC

The *in situ* methods are based on the utilisation of additive material in medium at the beginning of bacterial cultivation. This material can be added directly to the culture medium prior to or during the synthesis of cellulose to generate BC with novel properties by modifying the intrinsic biophysical properties. These additives then become a part of the BC nano- or micro-fibril networks, usually by interacting with -OH moieties of glucose and subsequently building new interconnected hydrogen bridges^[20]. Hydrophilic and water-soluble materials are mainly chosen for such a modification. For example, in order to improve the rehydration ability of BC, 1% of hydroxypropylmethyl cellulose (HPMC) is added to the culture

medium^[31]. As a result, the rehydration ratio increases twice compare to the original BC. Another example is the synthesis of BC with carboxymethyl cellulose (CMC) for the biofiltration of blood proteins^[32]. BC produced in a CMC environment shows reduced irreversible structural changes of the network during the process of drying^[20, 32].

BC has also been modified specifically for bone tissue engineering applications^[33, 34]. In order to enhance the porosity of BC and prepare a BC scaffold for bone regeneration, paraffin microspheres were added into the culture medium^[35]. The research showed that the synthesised BC scaffold significantly enhanced cell infiltration^[35]. In another example, hydroxyapatite nanoparticles (HA - $\text{Ca}_5(\text{PO}_4)_3(\text{OH})$) were added into the BC culture medium for the fabrication of scaffolds for bone regeneration^[2, 36, 37]. The results of the Stumpf *et al.* study showed a lack of inflammatory reaction, as well as bone defects filled with new bone tissues after four weeks^[2]. Barreiro *et al.* added a sand dollar skeleton (from *Clypeaster subdepressus*), composed of $\text{CaMg}(\text{CO}_3)_2$, into *Gluconacetobacter hansenii* culture medium^[38]. The resulting material had 3.6 ± 0.8 MPa compressive strength and apatite particles deposited over the BC surface^[38].

Materials with antibacterial properties have also been used for *in situ* BC modification. Danuta Ciechańska added chitosan acetate and chitosan lactate into the culture medium^[39]. The developed BC/chitosan composites, which had *N*-acetylglucosamine and glucosamine units, showed antibacterial activity against *E. coli* and *Staphylococcus aureus* (*S. aureus*)^[39]. Moreover, 0.5% concentration of poly (vinyl alcohol) (PVA) compounded with chitosan can improve the mechanical properties of BC as well as introduce additional antimicrobial properties^[29]. This BC composite showed antibacterial activity against *E. coli*. Another example is the study by Yang *et al.*, where silver nanoparticles were added into the culture medium with different carbon sources such as glucose, maltose and sucrose. The results showed that sucrose-derived BC possessed the lowest crystallinity and exhibited the highest silver content,

whereas maltose-derived BC showed more than 99.99% antibacterial activity against *E. coli* after 18 hours^[40].

1.2.3. *Ex situ* modification of BC with antibacterial metal particles

BC can also be modified after the synthesis. This type of modification is called *ex situ* modification. *Ex situ* modification is based on adding materials once the BC has been produced and purified^[20, 22]. This type of modification might be beneficial in the cases that there is a need to keep the original BC structure. There are several ways of achieving BC *ex situ* modification. One of the common methods is an immersion of purified BC into a solution or suspension, where BC can interact with exogenous molecules (also known as accessory materials)^[20]. Secondly, BC may also be stirred with an accessory material. The third method is the incorporation of an accessory material inside the BC network using laser or vacuum^[41]. For instance, Dinca *et al.* incorporated ZnO nanoparticles into BC using the matrix-assisted pulsed laser evaporation (MAPLE) method with a laser wavelength of 266 nm, 6 ns pulse duration and 10 Hz repetition rate^[41].

Due to the lack of antimicrobial activity, BC alone does not provide a barrier between a wound and infection. This means that introducing antimicrobial properties to BC can increase the material's diabetic efficiency in the treatment of extremely severe cases such as chronic wounds, ulcers and burns. Therefore, it would be useful to synthesise BC-based composites with antimicrobial properties. For example, metal nanoparticles such as ZnO, gold, silver and copper can be incorporated into BC and provide antimicrobial activity to the synthesised composite^[22, 41, 42].

1.2.3.1. Gram-positive and Gram-negative bacteria

Most bacteria can be divided into two groups based on their stainability: Gram-positive and Gram-negative bacteria. A difference in stainability between these groups is based on the structure of their cell walls. Gram-positive bacteria have just one cell wall, whereas Gram-negative bacteria have an additional outer membrane^[43]. Cell walls of both Gram-positive and Gram-negative bacteria contain peptidoglycan. Peptidoglycan is composed of a glycan backbone of N-acetylglucosamine and N-acetylmuramic acid that form long chains^[43]. The layers of peptidoglycan represent a cross-linked matrix consisting of linear glucan chains that are linked *via* covalent bonds^[43].

The chains of glucan are highly cross-linked by bridges of tetra-peptides in Gram-positive bacteria (for instance, *Staphylococcus aureus*) or partially cross-linked in Gram-negative bacteria (for example, *Escherichia coli*)^[43]. However, the layer of peptidoglycan in Gram-positive bacteria is much thicker than that in the Gram-negative bacteria. For instance, approximately 50% of the cell wall of Gram-positive bacteria is composed of peptidoglycan^[44]. Due to the lack of the outer membrane, cell walls of Gram-positive bacteria are much more penetrable than those of Gram-negative bacteria^[44]. The structure of the cell walls of both Gram-positive and Gram-negative bacteria is shown in Fig. 11^[44]. As seen in Fig. 11, the cell wall of Gram-positive bacteria has several layers of peptidoglycan. The thick layers of peptidoglycan help to support the cell and result in retaining most of the crystal violet dye after Gram staining, causing bacteria to appear purple.

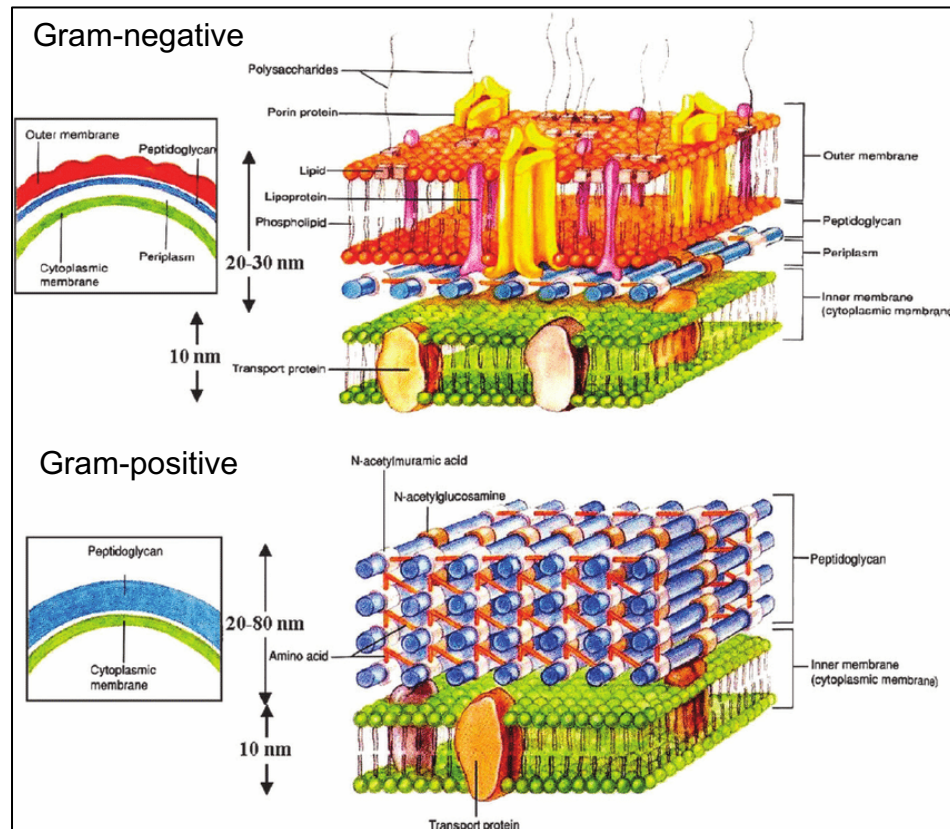


Figure 11. The structure of the cell walls of Gram-negative (top) and Gram-positive (bottom) bacteria^[44].

The remaining 50% of the cell wall of Gram-positive bacteria is composed of a variety of polymers such as teichoic acids^[44]. Teichoic acids are polyol phosphate polymers consisting of small repeating units of glycerol phosphate, glucosyl phosphate or ribitol phosphate that are linked *via* phosphodiester bonds^[43]. Teichoic acids are extended from the plasma membrane through a layer of peptidoglycan^[45]. There are two main groups of teichoic acids: lipoteichoic acids (LTA), which are anchored in a membrane *via* a glycolipid, and wall teichoic acids (WTA) that are covalently linked to peptidoglycan^[45]. WTA consist of a chain polymer of phosphodiester-linked polyol repeat units and a disaccharide linkage unit. The phosphodiester-linked polyol repeat units of WTA are extended from the glycerol-3-phosphate end of the linkage unit^[45]. One or two glycerol-3-phosphate units are attached to the C4 oxygen^[45]. The disaccharide linkage unit is composed of N-acetylmannosamine ($\beta 1 \rightarrow 4$) N-acetylglucosamine-1-phosphate^[45]. The anomeric phosphate of the linkage unit is covalently attached

to peptidoglycan through a phosphodiester bond. Teichoic acids are present just in the cell wall of Gram-positive bacteria and help the cell to maintain its shape, play a role in cell division as well as to infect and cause disease^[43].

Gram-negative bacteria have a thin layer of peptidoglycan (10-20%) in their cell walls that is surrounded by an outer membrane containing lipopolysaccharides (LPS), which are not found in Gram-positive bacteria^[44]. Each LPS is a complex molecule consisting of a polysaccharide core, a lipid A and chains of carbohydrates. Lipid A is composed of fatty acids and anchors the LPS structure to the membrane^[43]. Core carbohydrates, which are connected to lipid A, consist of octanoic and ketodeoxytonic acids as well as heptose^[43]. Core carbohydrates may also represent up to 40 sugars and cover the surface of the cell wall^[43].

Furthermore, in Gram-negative bacteria, the outer membrane involves two classes of proteins such as β -barrel proteins and lipoproteins. β -barrel proteins (porins) represent β sheets that are wrapped into cylinders^[46]. In order to allow low molecular weight compounds to pass through a cell wall *via* slow diffusion, several porins or proteins are located on the membrane^[43]. For instance, the function of OmpF and OmpC porins is to allow the passive diffusion of small molecules such as amino acids, mono- and disaccharides across the outer membrane^[43]. LamB and PhoE porins allow the diffusion of maltose, anions and maltodextrins^[43]. These porins have 16 transmembrane β strands^[43]. Furthermore, lipoproteins consist of lipid moieties that embed lipoproteins in the leaf of the outer membrane through the attachment to the amine terminal cysteine residue^[43]. For instance, the cells of *Escherichia coli* (*E. coli*), have about 100 lipoproteins in their outer membrane^[43]. Therefore, the structure of the outer membrane of Gram-negative bacteria may show a greater resistance to antibiotics than the cell wall of Gram-positive bacteria^[47].

1.2.3.2. Antibacterial activity against Gram-positive and Gram-negative bacteria

Due to the difference in structures of cell walls, antibacterial agents might affect Gram-positive and Gram-negative bacteria in different ways. Antibacterial agents such as amine groups, nanoparticles and quaternary ammonium compounds (QAC) can influence the permeability of a cell wall, penetrate into the cytoplasm and/or affect bacterial DNA^[47]. The antibacterial action of nanoparticles against a bacterial cell is shown in Fig. 12^[47].

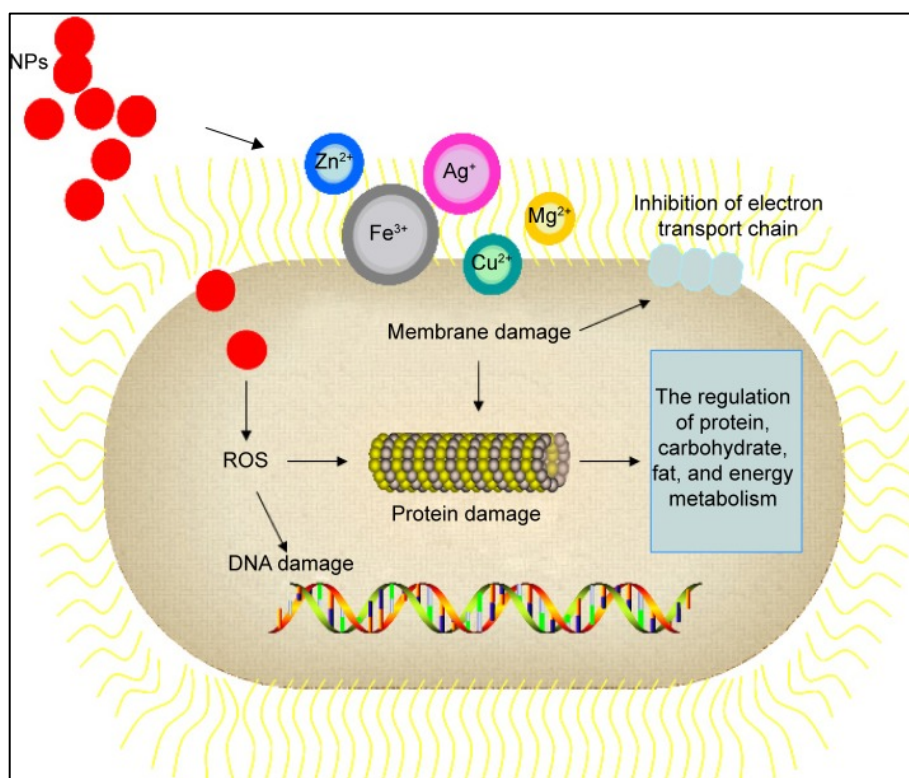


Figure 12. The mechanism of antibacterial action of nanoparticles^[47].

As shown in Fig. 12, nanoparticles can interact with a cell wall, penetrate it and affect DNA and proteins. The interaction of nanoparticles with ribosomes, lysosomes and enzymes can lead to oxidative stress, enzyme inhibition, disruption of electrolyte balance and deactivation of proteins^[47].

The mechanism of antibacterial action is mainly based on electrostatic interactions^[48]. In order to possess antibacterial activity, nanoparticles need to be in contact with a bacterial cell wall. Nanoparticles and other antibacterial agents can electrostatically bind to negatively charged components on a bacterial cell wall and, as a result, change the penetrability of the cell wall. The antibacterial effect of different nanoparticles may vary among Gram-positive and Gram-negative bacteria. Surface charge, hydrophobicity, molecular weight and size of nanoparticles can affect their antibacterial activity^[49]. Both LPS in Gram-negative bacteria and teichoic acids in Gram-positive bacteria are negatively charged, whereas most of antibacterial agents are positively charged^[50-52].

The cell wall of Gram-positive bacteria consists of layers of peptidoglycan and teichoic acid as well as abundant pores that allow foreign molecules to penetrate and cause damage^[47]. A number of studies have reported that nanoparticles possess a greater antibacterial activity against Gram-positive bacteria than against Gram-negative bacteria due to the presence of an additional outer membrane in Gram-negative bacteria that is composed of LPS, phospholipids, porins and lipoproteins and forms a penetration barrier, which allows the entrance of only macromolecules^[47, 50-52]. For instance, hydroxyapatite whisker/nano-zinc oxide showed a stronger antibacterial activity against Gram-positive *S. mutans* and *S. aureus* than Gram-negative *E. coli* ^[47]. Moreover, LPS, phospholipids and lipoproteins are connected with divalent cations that are required to stabilise the outer membrane of Gram-negative bacteria by electrostatic interactions^[53]. The packing of LPS molecules is tight and, therefore, LPS could provide an effective permeability barrier^[54]. For example, the outer membrane of *E. coli* contains from hundreds to thousands of LPS molecules^[54]. This LPS barrier might, however, not be effective against amine groups. Amine groups can bind to negatively charged O-specific oligosaccharide units of LPS and, thus, disturb the integrity of the outer membrane^[53]. Furthermore, amine groups that bind either to lipid A or divalent cations could also increase the permeability of the outer membrane^[53]. In addition, Amro *et al.* showed that the depletion of metal can cause the

formation of irregular-shaped pits in the outer membrane followed by changing the permeability of the membrane and, subsequently, a progressive release of LPS molecules and membrane proteins^[54, 55]. Moreover, in Gram-negative bacteria, Al₂O₃ nanoparticles may interact with LPS through hydrogen bonding and ligand exchange. As a result, such structural changes might lead to the loss of molecules, destruction of the cell wall and cytoplasmic leakage^[47].

The charge of a bacterial cell wall also plays a crucial role in the antibacterial activity. For instance, the cell wall of *Listeria innocua* contains lysine-derived phospholipids that do not possess a strong net negative charge with zeta-potential being around -20 mV^[47, 56]. Whereas, the zeta potential of *E. coli* could be around -44.2 mV^[57]. The difference in the zeta potential may be due to the additional layer of negatively charged LPS in the cell wall of *E. coli*. This could make the cell wall of Gram-positive bacteria such as *L. innocua* more permeable than Gram-negative *E. coli* ^[47].

Another possible reason for different sensitivities of bacteria to antibacterial agents is the thickness of the bacterial cell wall. For example, polymyxin polypeptides may affect LPS in Gram-negative bacteria followed by changing the structure of the cell wall and disruption of the osmotic balance^[58]. Furthermore, polymyxin can increase water uptake and discharge molecules from the interior of the cell^[58]. However, polymyxin does not affect the cell walls of Gram-positive bacteria, because their cell wall is too thick due to layers of peptidoglycan^[58].

Porins, which allow diffusion of molecules smaller than 600 Da, are the main channels for the movement of foreign molecules into and out of a bacterial cell wall^[47]. Hydrophilic antibiotics (β -lactams and fluoroquinolones) might enter Gram-negative bacteria *via* porin channels^[59]. However, bacteria such as *Pseudomonas* and *Acinetobacter* exhibit a low membrane permeability due to a different structure of their porins. For example, OprF is the major outer membrane porin of *Pseudomonas aeruginosa* (*P. aeruginosa*)^[50]. The diffusion of different

molecules through this channel is approximately two orders of magnitude slower than through the OmpA porin of *E. coli* [50]. This is one reason why *Pseudomonas* shows higher intrinsic resistance to many antibacterial agents [60].

One of the crucial functions of a cell wall is the respiratory activity of bacteria [47]. Nanoparticles can disrupt the respiratory activity of a bacterial cell wall, which might be analysed by detecting a reduction in 2,3,5-triphenyltetrazolium chloride or O₂ [47]. TiO₂ nanoparticles might adhere to the surface of a bacterial cell and produce reactive oxygen species (ROS) followed by damaging the structure, composition of a cell wall and leakage of cellular contents [47]. ROS are chemically reactive species that have a strong positive redox potential [47]. Therefore, the oxidative stress can be one of the key contributors to altered permeability of the cell wall [47]. Moreover, the binding of TiO₂ to DNA could lead to DNA degeneration, compression and fragmentation [47].

Metal ions, which can be released slowly from a metal oxide, might be absorbed through the cell wall [55]. This leads to the direct interaction of ions with functional groups of nucleic acids and proteins followed by changing the structure of cells, damaging enzyme activity, affecting the normal physiological processes and ultimately inhibiting the growth of microorganisms [55]. MRSA might be inactivated by the generation of a large amount of hydroxyl radicals and diffusion of graphene oxide or iron oxide nanoparticles [47]. Both hydroxyl radicals and hydrogen peroxide can penetrate cell walls [47].

Many antibacterial agents can inhibit the growth of both Gram-positive and Gram-negative bacteria. Silver is one of the most studied materials for introducing antimicrobial properties against a wide spectrum of pathogens such as *S. aureus*, *Bacillus subtilis* (*B. subtilis*), *Klebsiella pneumoniae* (*K. pneumoniae*), *P. aeruginosa* and *E. coli* as well as fungi and viruses [22, 41]. For instance, silver ions can bind to the bacterial cell wall, damage proteins, alter the function of bacteria by interacting with the thiol groups of enzymes or affect bacterial cells from the inside [61]. Silver ions can inhibit the growth of both *S. aureus* and *E. coli* by

binding to functional groups of enzymes, causing the release of K^+ ions^[62]. For example, Thawatchai *et al.* have introduced antimicrobial properties into BC by incorporating silver nanoparticles through immersion^[63]. The material produced showed antibacterial activity against both *E. coli* and *S. aureus*^[63]. Tabaii *et al.* have also synthesised BC/silver composites through immersion that inhibited *E. coli* and *S. aureus* by 100% and 99.99%, respectively^[64]. Additionally, BC/sodium alginate with silver sulfadiazine composites showed strong antimicrobial properties against *E. coli* and *S. aureus* bacteria as well as *Candida albicans* (*C. albicans*) yeast^[65]. In Gram-negative *E. coli*, nanosized silver particles can cause both structural changes and death^[55]. After contact with silver nanoparticles, the cell walls of *E. coli* exhibited a significant increase in permeability, impaired transport regulation through the walls followed by cell death^[66]. Bacterial cell walls appeared to shrink and were separated from the cell followed by cell degradation^[62]. Silver ions can penetrate the cell wall of Gram-positive bacteria and bind to DNA, which then loses its replication ability, cellular and functional proteins followed by protein denaturation^[55]. Furthermore, small size silver nanoparticles (<10 nm) might pass through pores in the cell membrane^[47]. Silver nanoparticles could be involved in a species-specific mechanism of upregulation of several antioxidant genes and genes coding for proteins involved in metal transport, metal reduction and ATPase pumps^[47].

ZnO, CuO and FeO might be more effective against Gram-positive bacteria *B. subtilis* and *S. aureus* than Gram-negative bacterial strains of *E. coli* and *P. aeruginosa*^[67]. ZnO nanoparticles may possess antibacterial activity through releasing Zn ions in a manner that disrupts transport of amino acids, metabolism and causes disruption of an enzyme system in both *S. aureus* and *Saccharomyces cerevisiae*^[68]. ZnO might affect the cell wall of Gram-negative bacteria externally due to particle size that could penetrate neither the cell membrane nor cell wall^[68, 69]. Furthermore, ZnO nanoparticles can also be incorporated in BC and provide antimicrobial activity against *K. pneumoniae* and *S. aureus*^[41]. In addition, copper exhibits antibacterial activity against

Salmonella typhimurium (*S. typhimurium*), *Listeria monocytogenes* (*L. monocytogenes*), *Salmonella enterica* (*S. enterica*) and *Campylobacter jejuni* (*C. jejuni*)^[42]. Araujo *et al.* reported that BC synthesised with copper and copper alloy (Cu_xO_y) nanoparticles by immersion possessed antimicrobial activity against *E. coli*, *S. aureus*, *S. enterica* and *C. albicans*^[42].

Bacterial resistance can be developed against different antibacterial effects. Mechanisms of resistance can include expression of enzymes that might degrade or modify antibiotics^[47]. However, most of mechanisms of resistance could be irrelevant to nanoparticles, because most nanoparticles might affect bacterial growth externally, without penetrating the cell wall^[47].

1.2.4. Limitations of the current BC modification techniques

There are a number of limitations of the current BC modification techniques. One of the main challenges is controlling the amount of incorporated material into BC. For instance, the study by Grade *et al.* showed that 22% of hydroxyapatite was not integrated into the final *in situ* synthesised BC/hydroxyapatite composite^[37]. Another study by Thawatchai *et al.* showed that both the size and amount of silver nanoparticles inside BC increased after the *ex situ* incorporation^[63]. In addition, the incorporation of nanoparticles into BC can result in non-uniform distribution or accumulation of particles on the surface^[63]. The study by Lvov *et al.* used raw halloysite clay nanotubes added directly into the culture medium. The results showed that clay particles were aggregated and subsequently settled at the bottom of the medium after cultivation^[70]. This variation of concentration of nanoparticles within the BC matrix means that a varied dose of an antibacterial agent will be encountered by bacteria.

Excessive use of the same antibacterial agent may lead to bacterial mutations. There is evidence that bacteria can mutate and develop resistance to an antibacterial agent^[61]. These mutations can occur in normal cellular genes,

plasmids or transposons^[61]. For instance, plasmid-mediated biocide resistance to silver was documented in *S. aureus* and members of *Enterobacteriaceae* and *Pseudomonas*^[61]. This means that excessive and uncontrolled use of silver might result in more bacterial resistance.

Besides strong antibacterial activity, some metal nanoparticles such as silver and copper might have adverse effects on human health. For example, silver nanoparticles can inhibit cell viability, increase reactive oxygen species (ROS) in mitochondria and lactate dehydrogenase release activity^[71]. Silver ions might result in a number of negative effects on human health such as genotoxicity, cytotoxicity, immunological responses and cell death^[71-73]. Silver ions may also pass through tissues, such as the blood-brain barrier^[71]. Moreover, one study showed that 30% of patients with burns who were treated with silver nanoparticles experienced the reversible hepatotoxicity and argyria-like symptoms^[29]. Cu nanoparticles can also release toxicity on somatosensory neurons of rats and livers of juvenile fish^[29]. Another example is that titanium dioxide (TiO₂) may induce ROS and initiate lipid peroxidation, DNA degradation and protein disruption in the mouse brain^[71, 74].

Different size and shapes of metal nanoparticles can exhibit different levels of cytotoxicity on mammalian cell lines. Dermal toxicity and irritation might be worse with smaller size particles, because smaller gold and silver particles penetrate deeper, while the larger ones accumulate in the superficial epidermis or dermis^[29]. The results of Carlson *et al.* showed that 15 nm hydrocarbon-coated silver nanoparticles induced more ROS generation than 55 nm in macrophage cell lines^[75]. Another study by Liu *et al.* was focused on using 5 nm, 20 nm and 50 nm silver nanoparticles and four different cell lines, A549, HepG2, MCF-7, SGC-7901^[76]. The results showed that 5 nm silver nanoparticles exhibited more cytotoxicity than the 20 nm and 50 nm particles^[76]. Moreover, Wang *et al.* reported that 20 nm citrate-coated silver nanoparticles showed greater cytotoxicity followed by neutrophilic inflammation in the lungs of mice than 110

nm silver nanoparticles^[71, 77]. However, Kaba *et al.* showed that smaller silver particles have not affected the viability of HeLa and U937 tumour cells^[71, 78]. Therefore, small silver nanoparticles can inhibit cytotoxicity in specific cell types.

The shape of nanoparticles can also influence cytotoxicity parameters. For instance, spherical silver particles do not show a cytotoxicity effect on A549 cells, whereas wires have been shown to be toxic^[71]. Due to a variety of cell lines, which are sensitive to specific morphological characteristics of nanoparticles, the overall toxicity examination system was developed. This system is called the toxicity threshold (TT)^[71]. TT is the minimum dose of any material that starts to result in cytotoxicity^[71]. TT can vary even within the same cell line. For instance, TT value of silver nanoparticles in an A431 cell line is between 1.51 µg/ml and 50 µg/ml, but the TT value in A549 cells is from 0.5 µg/ml to 50 µg/ml^[71].

Based on the above-mentioned evidence, there is a need to develop a BC-based composite combining both antibacterial and healing properties. The ideal material will possess all crucial features of BC and include additional antibacterial activity but not be toxic to mammalian cells. Such material will be suitable for medical applications such as wound and burns therapy. In order to synthesise such a BC-based composite, non-toxic materials need to be chosen. In order to do so, this research is focused on natural and organically modified clay and chitosan. Therefore, clay and chitosan will be reviewed further.

1.3. Bacterial cellulose composites with clay particles and their applications

1.3.1. Smectite clay

Clay can be described as fine-grained rocks and soil components. Clay minerals are small, hydrated silicate sheets. Most clay minerals are made by a stack of tetrahedral (T) and octahedral (O) sheets. The main types of clay can be discerned by the arrangement of these layers. For instance, the structure of

kaolinite and serpentine clay is represented by a combination of a tetrahedral and an octahedral sheet (TO or 1:1 combination)^[79]. Smectite, vermiculite and illite groups have TOT or 2:1 structure, whereas chlorite has a TOTO structure^[79, 80]. Different types of clay have different properties and applications. Kaolinite is used in ceramic applications, whereas the serpentine group is used as a source of magnesium and asbestos as well as decorative stone^[80]. Smectites are applied in foundry, oil well drilling, wine and feed pelletising industries^[81]. Clay can also be used as antibacterial and sterilising agents as well as for adsorption of toxins and membrane coating^[79].

Smectites have TOT or 2:1 structure with a single octahedral and two tetrahedral sheets. The net positive charge deficiency is balanced by exchangeable cations that are absorbed between the unit layers and on the edges^[82].

1.3.1.1. Montmorillonite (MMT) clay

Montmorillonite (MMT) clay was named after the Montmorillon region in France where the clay was discovered^[83]. Sodium MMT clay is obtained from glassy igneous material such as volcanic ash or tuff.

The structure of MMT consists of two building blocks: the tetrahedral sheet, which is composed of siloxane ($\text{Si}_2\text{O}_5^{-2}$), and octahedral sheet, which consists of alumina ($\text{Al}(\text{OH})_6^{-3}$), as shown in Fig.13^[83].

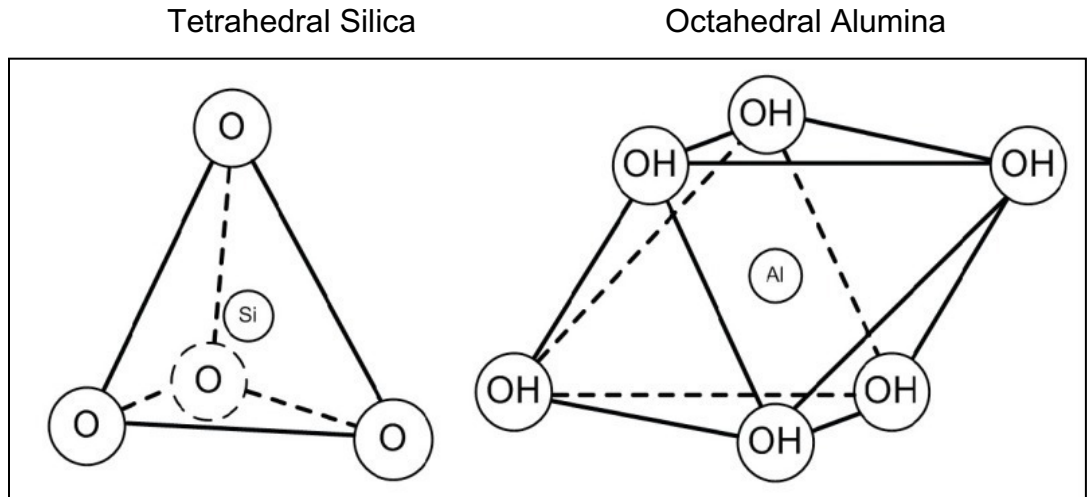


Figure 13. Schematic presentation of silica tetrahedron and alumina octahedron. A silicon atom bonds four oxygen atoms in the tetrahedral sheets, whereas in an octahedral sheet, an alumina atom bonds six oxygen atoms^[83].

Octahedral layers are constituted by six OH groups, whereas OH groups are replaced with the apical oxygen atoms in tetrahedrons^[84]. Tetrahedra link to neighbouring tetrahedra by sharing three corners with oxygen, resulting in a hexagonal network (Fig. 14)^[85]. The fourth corner with oxygen is then adjusted to an octahedral sheet.

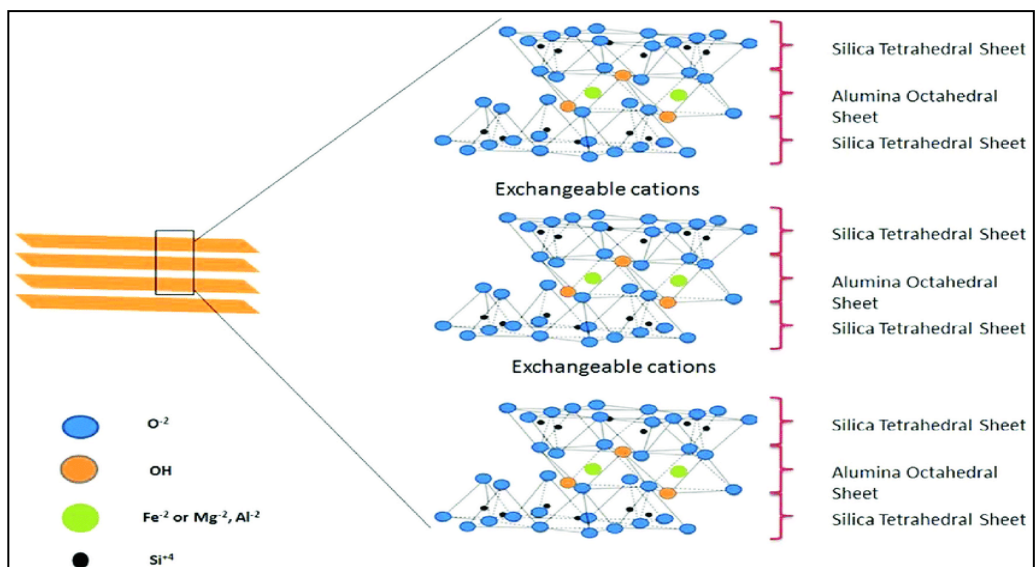


Figure 14. Chemical structure of montmorillonite^[85].

Each layer is 50-200 nm long (Fig. 15)^[83]. The space between TOT layers is called the interlayer spacing or gallery^[79]. The thickness of each clay layer with interlayer spacing is known as the d-spacing (d_{001}) or basal spacing.

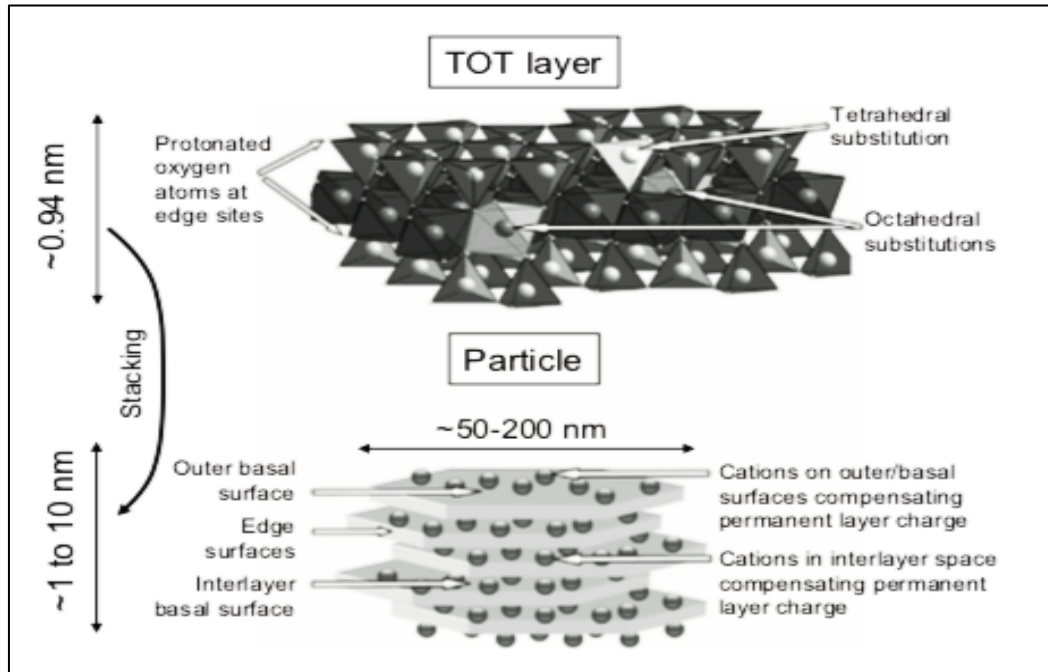


Figure 15. The structure of MMT. Figure showing the size of the layers^[83].

While the sheets together form a single layer, several layers can also be joined by interlayer cations and van der Waals force^[82]. Each layer has an excess negative charge due to the isomorphous substitution of Si^{4+} by Al^{3+} in the tetrahedral sheet and of Al^{3+} by Mg^{2+} ions in the octahedral sheet^[83]. The charge imbalance in smectite is about 0.66 per unit cell^[82]. The negative charge is compensated by counter-cations, which can be located either in the interlayer space or on the outer basal surfaces (Fig. 14). The interlayer cations are called exchangeable cations due to their ability to be replaced with other materials^[82]. Cation exchange capacity (CEC) is a parameter used to measure the ability of clay to exchange its interlayer cations. It is inhibited in milliequivalents per 100 g of calcined clay^[79]. CEC of NaMMT is 92.6 meq/100 g^[86]. The CEC is one of the essential parameters for a modification of natural clay.

MMT clay can be organically modified with quaternary ammonium salts^[87]. For instance, the quaternary ammonium salt in Cloisite 30B clay is methyl tallow bis-2-hydroxyethyl quaternary ammonium chloride^[86, 87]. The size of organic cations is larger than compensating cations due to the presence of a long alkyl chain^[87]. This results in an increase in the basal distance in organically modified clay (organoclay)^[84, 88]. For example, $d(001)$ spacing in NaMMT is 1.17 nm, whereas $d(001)$ spacing in Cloisite 15A can reach 3.15 nm^[86]. Regarding Cloisite 30B, the surface modifier is quaternary ammonium salt consisting of hydroxyl groups, which allows hydrogen bonding with carbonyl groups^[89]. The enhancement of the interlayer space results in hydrophobicity^[87].

1.3.2. Properties of MMT

1.3.2.1. Physical properties of MMT

Smectites have reactive edges on individual layers and an ability to interact with a wide range of natural and synthetic organic compounds^[90]. The large surface area of MMT clay is effective for the absorption of organic compounds. For example, the surface area of MMT clay is 650–800 m²/g^[91]. Organic compounds, which react with clay, have access to tetrahedral and octahedral sheets as well as metal ions inside interlayer spaces. As a result, clay may rearrange or swell^[90]. MMT is hydrophilic clay, possessing high swelling behaviour in water. The ability of clay to absorb a large amount of water and swell can be caused by two factors. The first factor is a large number of hydrophilic-compensating cations on the large surface area. The second is the flexibility of sheets, which creates pores within sheets, particles and aggregates^[91]. Porosity in smectite clay can be modulated by a variety of shapes, sizes and concentrations of intercalated materials as well as by partial exchange of inorganic cations or by modifying the interlayer charge density^[91].

Clay also have high fracture toughness, high modulus and fire resistance^[92]. These properties allow clay to be used as an enhancement material in developing polymer/clay composites.

1.3.2.2. Antimicrobial properties of MMT

Natural unmodified MMT clay does not show any antimicrobial activity, but organic modification of MMT results in antibacterial and antifungal properties being introduced^[88, 93-95]. For instance, organoclays that are quaternary ammonium surfactant-based can show antimicrobial activity against both Gram-positive and Gram-negative bacteria^[88, 94, 96]. The interaction of a quaternary ammonium group of organoclay with bacterial cells can disrupt cell membranes and cause death^[97]. Quaternary ammonium compounds disturb the structure of cell membrane through physical interaction with the membrane components, allowing vital cell content to be released^[98, 99]. For instance, the alkyl chain of quaternary ammonium compounds reacts with fatty acid chains of membrane lipids and destabilises interactions between phospholipids and proteins^[98]. Due to their organophilic nature, organoclays can also penetrate the membrane of bacteria. A low concentration of quaternary ammonium compounds leads to membrane damage and leakage of cytoplasmic constituents, whereas high concentrations cause coagulation of the cytoplasm, presumably through denaturation of proteins^[98]. For example, Cloisite 20A and Cloisite 30B have been shown to have strong antibacterial activity against Gram-positive *S. aureus* and *L. monocytogenes* and Gram-negative and *E. coli* and *S. typhimurium*^[97]. Moreover, Cloisite 10A and 15A have also shown antibacterial activity against *S. aureus*^[100]. In addition, quaternary ammonium compounds can disorganise the plasma membrane in yeast membranes^[98].

1.3.3. Mammalian toxicity of MMT clay

The cytotoxicity of MMT has been investigated by a number of cell research groups, but results vary significantly due to factors such as clay concentration, type of cells and composition of culture medium. Thus, the concentration up to 31 µg/ml of natural NaMMT did not show any cytotoxicity for Caco-2 and HepG2 (liver) cell lines in previous studies^[101-103]. Maisanaba *et al.* reported no cytotoxicity effect of NaMMT at 31.25 µg/ml concentration on Caco-2 cells^[78]. However, cell viability decreased with a higher concentration of NaMMT (31.25–125 µg/ml)^[78]. Maisanaba *et al.* tested the viability of human umbilical vein endothelial cells (HUVEC) in the presence of 0-125 µg/ml ultrasound-treated NaMMT suspension^[104]. The results showed that NaMMT did not exhibit any cytotoxicity^[104]. Furthermore, Lordan *et al.* reported that NaMMT inhibited HepG2 cell growth, which then resulted in cell necrosis at all used concentrations from 1 to 1000 µg/mL^[105]. However, Maisanaba *et al.* had completely opposite results, where NaMMT suspension did not exhibit any cytotoxicity towards HepG2 cells at 0-62.5 µg/mL concentration^[78]. One of the main differences between these two studies was medium type. Lordan *et al.* used DMEM with 10% fetal bovine serum (FBS), whilst Maisanaba *et al.* used EMEM with 10% FBS^[80, 105]. Therefore, the composition of tissue culture medium might also influence a cytotoxicity assay. Lordan *et al.* analysed the effect of different fetal calf serum (FCS) serum concentrations along with 1 mg/ml NaMMT on human monocytic U937 cells^[106]. The results showed that NaMMT suspension had a detrimental effect on the cells in serum-free medium, whereas clay did not inhibit any cytotoxicity in medium with 5% and 2.5% of FCS^[106]. This might be due to clay particle agglomeration in the medium-containing serum, but the dispersion of particles in serum-free medium^[106]. Moreover, 1 mg/ml may also be a very high concentration, which could affect the viscosity of the medium and subsequent penetration of oxygen.

The cytotoxicity of different concentrations of organoclay has also been investigated. For example, Cloisite 20A at a concentration ranging from 0 to 65

$\mu\text{g/ml}$ of did not show any cytotoxicity for Caco-2 and HepG2 cell lines after 24 and 48 hours, respectively^[101]. In contrast, Cloisite 30B can damage DNA of Caco-2 cells at concentration 170 $\mu\text{g/ml}$ after 24 hours^[102, 104]. Furthermore, Cloisite 30B showed cytotoxicity at 125 $\mu\text{g/ml}$ against HepG2^[102]. The study by Sharma *et al.* showed that a 226 $\mu\text{g/ml}$ concentration of Cloisite 30B induced 40% cytotoxicity in Caco-2 cells^[102]. In addition, 250 $\mu\text{g/ml}$ of Cloisite 30B was toxic for HUVEC cells^[104]. Cloisite 93A reduced the viability of HepG2 cells to 37% at 1000 $\mu\text{g/mL}$ concentration^[105]. The toxicity of organoclay can also be caused by the surfactants. However, organo-modifiers such as amine or carboxyl groups have shown low cytotoxicity and DNA damage^[104]. Thus, the type of the cell line and the modifier plays a crucial role in toxicity testing.

The toxicity of MMT on animal organs and the whole body has also been analysed. For instance, Mitchell *et al.* tested the toxicity effect of 0.75-1.5 grams of solid MMT particles, which were applied directly on to rabbit eyes^[107]. The results showed no damage to the organ^[107]. MMT was also injected and orally tested using Wistar rats as an *in vivo* model for 72 hours^[108]. The results showed a lack of MMT toxicity on healthy rats, but there was toxicity on the rats with cardio-vascular diseases^[108]. This might be due to the penetration of particles into already clogged blood vessels, which caused additional blockage. Furthermore, Lee *et al.* reported non-toxic behaviour of MMT after oral administration in rats^[108]. In addition, Wiles *et al.* orally tested MMT clay on pregnant Sprague-Dawley rats for 16 days^[109]. The results showed an absence of any negative effects on rats or embryos as well as on normal tissue weights and maternal body gain^[109]. Mitchell *et al.* confirmed that 1.5 g/day oral dose of purified CaMMT is safe for children at least for a period of 14 days^[107]. Furthermore, 5 wt.% of NaMMT per day is considered safe and can act positively on bone mineralisation in pigs^[110].

1.3.4. Current progress on BC/MMT composites

Due to the presence of active functional hydroxyl groups, BC can be combined with inorganic nanoparticles such as clay^[111]. The porous matrix of BC is beneficial for the synthesis of nanocomposites due to its biodegradability and considerable mechanical properties. The mechanical properties of BC can also be further modified *via* incorporation of different fillers such as clay. The addition of well-exfoliated MMT nanoparticles can improve thermostability and the mechanical, barrier and antimicrobial properties of BC^[112]. For example, MMT can improve the mechanical properties of composites up to 10 times^[112]. Another advantage is that BC/MMT composites can be synthesised without any toxic and expensive organic solvents. As with other additive materials, MMT clay particles can be introduced to BC by *in situ* or *ex situ* methods (Section 1.2).

Using *in situ* modification, the structure, shape and properties of BC/MMT composites can be easily adjusted^[113]. The BC/MMT *in situ* growth conditions can be either static or agitated, which may influence the structure and crystallinity of the composite as well as dispersion of particles during biosynthesis^[113]. Non-exfoliated particles might not fully attach to BC fibres during the static cultivation due to settling, whereas formation of BC occurs on the top of the medium^[114]. Alternatively, BC/MMT can be synthesised in agitated culture, where the movement of medium lets particles penetrate into the BC^[113]. However, the continuous movement of the medium might affect the structure and porosity of BC.

The *ex situ* method allows incorporation of particles into BC without affecting its initial structure. The *ex situ* method is usually performed using the solution impregnation technique, which is the immersion of BC matrix into a clay suspension^[113]. This immersion method also has limitations. Firstly, due to the hydrophilic nature of BC, the incorporation of organophilic oil-dispersible clay is a challenge. Secondly, only submicron and nano-sized particles can penetrate

the BC matrix, because the size of the largest pores of BC can vary from 4 to 1000 μm in diameter^[115]. Therefore, exfoliation state and concentration of clay are crucial factors for achieving desirable properties in the final BC/MMT composites. A high concentration of clay can lead to particle agglomeration, which can adversely affect the composite properties^[116]. For instance, UI-Islam *et al.* 2012 stirred BC with 1 wt.%, 2 wt.% and 4 wt.% MTT clay suspensions, respectively, for 24 hours at 150 rpm^[112]. The results showed that the number of particles absorbed by BC increased with increasing clay concentrations^[112]. Thus, 25.72%, 40.36% and 45.06% of MMT particles from 1 wt.%, 2 wt.% and 4 wt.% concentrations were absorbed by BC, respectively^[112]. However, the final weight of BC/MMT composites was not significantly increased from the 2 wt.% to 4 wt.% of clay concentration^[112]. This might be due to particle agglomeration and subsequent lack of proper binding to BC fibres, which then resulted in clay leaching.

1.3.5. BC/MMT composites for wound healing applications

MMT clay has been used in therapeutic applications including wound healing due to its ability to inhibit bacterial growth, protect the skin, improve blood clotting and control haemorrhage in trauma patients^[112, 117]. The possible mechanism triggering clay antibacterial activity may be the destruction of the cell membranes, enzyme inhibition, physical adsorption of bacteria or cation release from the clay^[111, 118, 119]. The common bacterial species that cause wound infections are *S. aureus*, *P. aeruginosa* and methicillin-resistant *S. aureus* (MRSA)^[120]. Thus, different BC/MMT composites such as BC/NaMMT, BC/CaMMT and BC/CuMMT have been tested against these species. The antibacterial activity of different freeze-dried BC/MMT composites was analysed by zone inhibition assay. For instance, UI-Islam *et al.* immersed BC into 2 wt.% and 4 wt.% of NaMMT, CaMMT and CuMMT suspensions, respectively, in order to develop films with potential antibacterial activity^[118]. Freeze-dried BC/CuMMT composites, which were placed directly on the TSA agar, showed 20 mm inhibition zones against *E. coli*

and 9 nm against *S. aureus*^[118]. Sajjad *et al.* tested the antibacterial activity of *ex situ* synthesised BC/NaMMT, BC/CuMMT and BC/CaMMT composites against MRSA, *S. aureus*, *E. coli*, *P. aeruginosa*, *S. typhimurium* and *Citrus freundii* (*C. freundii*)^[94]. The results showed that BC/NaMMT composite produced a 43.6 mm zone against *E. coli* and 34 mm zone against both MRSA and *S. aureus*^[94]. There was no antibacterial activity of BC/NaMMT against *P. aeruginosa*, *S. typhimurium* and *C. freundii* ^[94]. Furthermore, BC/CaMMT resulted in 30, 25, 22 mm zones against *S. aureus*, *E. coli* and *C. freundii*, respectively^[94]. The zones of inhibition for *S. typhimurium*, *E. coli*, *S. aureus* were 34, 33 and 36 mm, respectively, using freeze-dried BC/CuMMT^[94].

However, while zone assays can give preliminary information about the antibacterial activity of composites, the determination of the viability of bacteria could be more accurately assessed in terms of efficiency of concentration and time. For instance, freeze-dried BC/NaMMT, BC/CaMMT, BC/CuMMT composites prepared *ex situ* with 2 wt.% of clay suspension showed a reduction of *E. coli* to 85, 80 and 22%, respectively, after 24 hours^[118]. Furthermore, BC/NaMMT, BC/CaMMT, BC/CuMMT composites prepared with 4 wt.% clay suspensions reduced the viability of *E. coli* to 81, 75 and 1% and *S. aureus* to 84, 80 and 20% after 24 hours, respectively^[118].

Although copper itself has proven antibacterial properties, the mechanism behind the antibacterial activity of BC/NaMMT and BC/CaMMT is still uncertain^[121]. According to Cabezas-Pizarro *et al.*, sodium salts destabilise the permeability of the cytoplasmic membrane and inhibit enzymes, which can lead to the death of *Salmonella enteritidis* (*S. enteritidis*), *P. aeruginosa*, *Enterococcus faecalis* (*E. faecalis*) and *C. albicans*^[121]. Sodium cations can bind to the negatively charged lipopolysaccharides (LPS) in Gram-negative bacteria^[122]. Moreover, Jantsch *et al.* noticed that infected areas in a wound display remarkable Na⁺ accumulation, which reduces after antibiotic treatment^[123]. Sodium cations can be stored inside or directly under the epidermis and generate osmotic conditions in healthy

tissues. Results showed that osmotic stress within Na⁺ cation loaded interstitial fluid boosts the host's defence against bacteria and, therefore, strengthens the anti-infectious barrier function of the skin^[123].

The antibacterial activity of different BC/MMT composites can also be stronger than other BC/metal particles composites. For instance, BC/NaMMT and BC/CaMMT composites showed antibacterial activity against MRSA and, in case of BC/CuMMT, against *S. typhimurium*, whereas BC/ZnO nanocomposites did not exhibit any antibacterial activity against these pathogens^[94, 124]. According to Agnihotri *et al.*, *S. aureus* and *C. freundii* are the most common pathogens associated with burns^[125]. Therefore, modified BC/MMT composites may perhaps be used to control infections caused by these pathogens.

Tissue regeneration properties of BC along with healing capabilities of MMT can also be exploited for developing materials for treating burn wounds. In the study by Sajjad *et al.*, BC/NaMMT, BC/CuMMT and BC/CaMMT composites were used to treat wounds in 35 mice, which were divided into five groups including groups with pure BC and positive control with silver sulfadiazine (standard topical cream)^[94]. The results showed that the best healing rate was observed with silver cream (76%) and BC/CuMMT (75%), then BC/NaMMT (64%), BC/CaMMT (55%) and pure BC (38%) (Fig. 16)^[94].

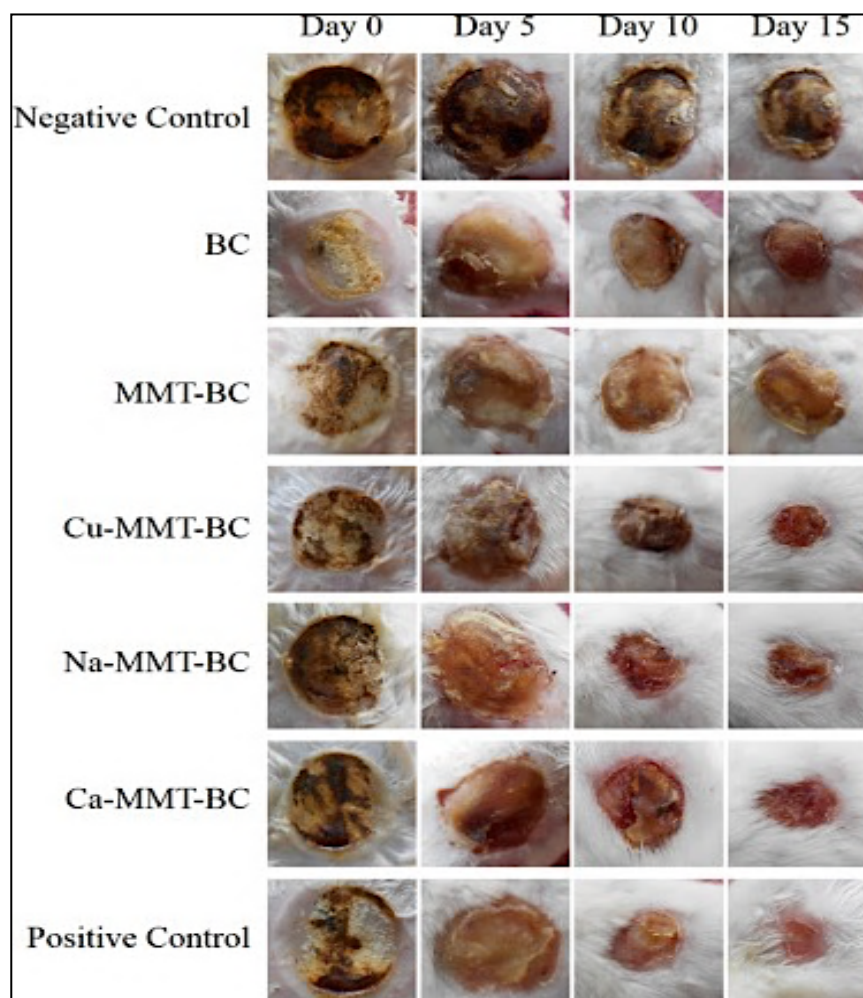


Figure 16. Representative wound photographs of BC/CuMMT, BC/NaMMTC and BC/CaMMT treated group, negative control (without BC), pure BC, unmodified MMT-BC group and positive control group (silver sulfadiazine) during the course of treatment^[94].

As shown in Fig. 13, BC/CuMMT showed the highest healing rate among the other composites. Copper and copper oxide can play an important role in the inhibition of extracellular matrix proteins and promotion of angiogenic factors^[94]. Borkow *et al.* found enhanced healing and wound closure in diabetic mice using copper^[126]. However, copper can also be toxic to mammalian cells. For instance, Assadian *et al.* reported that CuO nanoparticles affected the mitochondrial membrane and resulted in lysosome leakiness of human blood lymphocytes at 382 μM concentration^[127]. On the other hand, BC/NaMMT composite, which showed 64% healing rate, did not exhibit any cytotoxicity to mammalian cells^[94].

According to Sajjad *et al.*, BC/NaMMT composites showed smooth healing of the wound without obvious signs of infection.

The healing effect of BC/NaMMT composites was also investigated using haematoxylin and eosin (H&E) histological stains of tissues. Tissue groups treated with BC/NaMMT showed better wound healing with healthy re-epithelisation than the control group without any treatments^[94]. Similarly, Ji *et al.* showed that sodium humate composites promote wound healing in the rat model due to the acceleration of wound contraction and increasing hydroxyproline content^[128]. As the skin epidermis plays a crucial role in preventing transepidermal water loss, active transport of Na⁺ cations can create a physiological fluid as the additional barrier. Thus, the increased concentration of Na⁺ cations can promote the healing of the wounds^[123].

1.4. BC/chitosan composites

1.4.1. Chitosan overview

1.4.1.1. Chitosan as chitin derivative

Chitosan is a natural, linear polysaccharide, which can be obtained from partial or full deacetylation of chitin^[129]. Chitin, which is poly(β -(1 \rightarrow 4)-N-acetyl-d-glucosamine), is the second most abundant polymer after cellulose^[130]. In nature, chitin occurs as ordered crystalline microfibrils that form structural components in the cell walls of fungi, yeast and in the exoskeleton of arthropods^[131]. The main commercial sources of chitin are crab and shrimp waste shells^[132]. Chitin shows low toxicity to mammalian cells, is biodegradable and has antibacterial properties^[133]. For example, chitin can inhibit the growth of *E. coli* and suppress the growth of tumour cells in mice^[133]. Moreover, chitin may also accelerate wound healing^[133]. However, the major drawback of chitin is its insolubility in water and other organic solvents, therefore the applications of chitin are limited^[133].

In order to achieve solubility, chitin can be deacetylated to chitosan. Firstly, chitin is extracted from crustaceans by using acids in order to dissolve the calcium carbonate^[134]. The acid treatment is followed by solubilising the proteins under an alkaline wash. Partial deacetylation with concentrated NaOH or enzymatic hydrolysis leads to the final product, which is chitosan^[131]. Deacetylation results in the removal of the acetyl group of the glucosamine unit and the formation of the amino group^{[132], [135]} (Fig. 17).

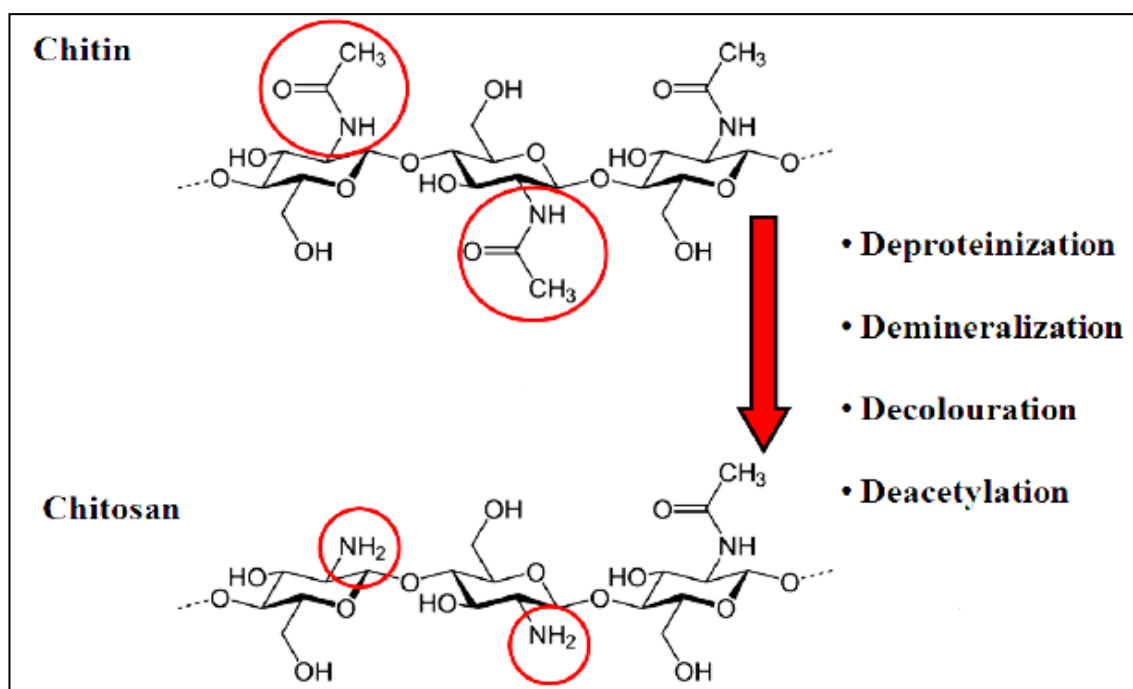


Figure 17. Effect of conversion of chitin into chitosan on the molecular structure through four steps: deproteinisation, demineralisation, decolourisation, deacetylation^[135].

Chitin can undergo additional steps for final removal of residual proteins and pigments that could cause problems in biomedical applications.

Thus, the polymer is called chitosan when the fraction of glucosamine units is greater than 50%, whereas chitin has greater than 50% of the fraction of N-acetyl glucosamine^[136]. The number of glucosamine units reflecting the degree of deacetylation (DDA), while the N-acetyl glucosamine units indicated the degree of acetylation (DA)^[136].

1.4.2. Structure and properties of chitosan

Chitosan consists of β -(1–4)-2-acetamido-2-deoxy-D-glucose and β -(1–4)-2-amido-D-glucose units linked by β -(1→4) glycosidic bonds (Fig. 18)^[129, 136]. β -(1–4)-2-acetamido-2-deoxy-D-glucose is the sugar unit GlcNAc (N-acetyl-D-glucosamine unit) or A-unit, whereas 2-amino-2-deoxy-D-glucose is the positively charged sugar unit GlcN (deacetylated D-glucosamine) or D-unit^[137, 138]. Chitosan varies in the wide range of A-unit fractions (F_A) and chain lengths^[137]. The value of F_A units can vary from ca. 0.7 (70% acetylated) to 0 (0% acetylated, which means that all units are charged). Chitosan can be considered to be an ampholyte due to enrichment in A-unit fractions^[137]. The amino-groups of D-unit are predominantly positively charged at pH-values lower than 6.5. A- and D-units are randomly distributed along the chitosan chain^[139].

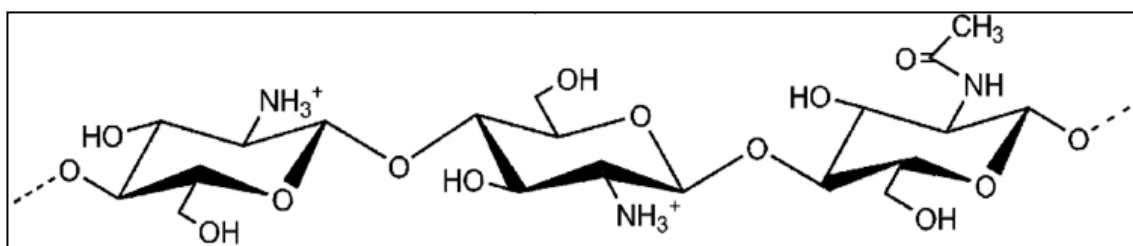


Figure 18. Schematic molecular structure of chitosan^[137].

The semi-crystalline polymer structure of chitosan results in strong inter- and intra-molecular hydrogen bonds^[140]. Chitosan can be described in terms of the DDA and average molecular weight (MW)^[141]. As was mentioned above, DDA is the percentage of N-glucosamine^[142, 143].

Depending on the preparation procedure and a source, MW of chitosan may vary up to 1000 kD with DDA from 30 to 95%^[144]. Chitosan with MW of 8.6 kDa or more along with DDA of 75-88% has shown the highest aggregation of whole blood, washed platelets and erythrocytes in platelet-rich plasma^[145]. Furthermore, a high concentration of high MW of chitosan (for example, 247 kDa) may cause

the aggregation of whole blood, PRP and washed erythrocytes^[145]. However, MW of chitosan can be modified by chemical, enzymatic or mechanical degradation methods such as shearing, ultrasound and microfluidisation^[146].

Chitosan has three types of reactive functional groups: an amine group, and a primary and secondary hydroxyl group^[140, 144]. These groups allow modification of chitosan for specific applications such as covalent, ionic modifications for mechanical and biological properties.

1.4.2.1. Solubility of chitosan

Due to a semi-crystalline structure, which is derived mainly from intra- and intermolecular hydrogen bonds, chitosan becomes soluble only at pH lower than 6 in aqueous acidic environment made of acetic, formic, lactic and hydrochloric acids^[140]. In such an environment, amine groups of chitosan can be protonated^[140]. Once the amine groups get protonated, they become positively charged and facilitate the solubility of chitosan in diluted acids that makes chitosan a water-soluble cationic polyelectrolyte^[144]. If pH increases above 6, amine groups become deprotonated, therefore, chitosan loses its charge and becomes insoluble^[147]. A transition state between soluble and insoluble chitosan occurs at pH between 6 and 6.5^[147]. The concentration of ions can also affect the form of chitosan in solution^[148].

The following equilibrium reaction describes the state of ionisation, when chitosan is dispersed in an acetic acid solution:

1. $CH_3COOH + H_2O \leftrightarrow CH_3COO^- + H_3O^+$
2. $Chitosan - NH_2 + H_3O^+ \leftrightarrow Chitosan - NH_3^+ + H_2O$ ^[148]

The concentration of hydrogen ions in the solution is determined by acetic acid. Once chitosan is dispersed in the acid solution, free amine groups start to bind

hydrogen ions to form cations^[148]. A solubilisation occurs when approximately 50% of all glucosamine units are protonated^[148].

The solubility of chitosan may be associated with the degree of deacetylation (DDA)^[140]. A structure with a DDA value of less than 60% (chitin) is insoluble in acidic solutions, whereas DDA at over 60% is defined as chitosan and can be water-soluble^[149]. The condensation of protonated charge occurs in a chitosan solution with DDA over 75% due to a large charge density that leads to both high solubility and electrostatic repulsion^[149]. A decrease of DDA (<50%) shows the largest number of N-acetyl-d-glucosamine units and leads to the hydrophobic nature of the polymer chains^[149]. Therefore, the fraction of N-acetyl-d-glucosamine units have a high influence on the solubility of chitosan^[149].

In addition to DDA and pH, molecular weight (MW) can also affect the solubility of chitosan. Chitosan with lower MW is more soluble in the acidic medium than chitosan with a higher MW^[150]. High MW chitosan (MW <300 kDa) might promote the formation of aggregations^[149]. Such aggregations may occur due to both reduction of hydrogen bonds between macromolecules and lack of free amine groups for the formation of intermolecular hydrogen bonds^[149]. Furthermore, aggregation could appear by a loss of conformational entropy due to the arrangement of the molecular chains in a regular crystalline array^[149]. This loss of entropy is compensated by the release of water during the aggregation of a chain.

1.4.3. Antimicrobial properties of chitosan

Chitosan can possess antibacterial properties against both Gram-positive and Gram-negative bacteria. However, the mode of antibacterial action of chitosan may vary between Gram-positive and Gram-negative bacteria due to the difference in the structures of their cell walls (Section 1.2.3.1)^[151].

1.4.3.1. Mechanism of antibacterial action of chitosan

The antibacterial activity of chitosan occurs due to the presence of the amine groups. The antibacterial mechanism of chitosan is not well understood; however, several theories have been proposed^[53, 152]. The most accepted theory is based on a mechanism involving electrostatic interaction between positively charged chitosan and the negatively charged bacterial cell wall, which leads to the alteration of cell permeability and lysis. As described in Section 1.4.2.1, chitosan becomes soluble in an acid aqueous environment, where the amine groups get protonated and, therefore, are positively charged. This means that the $-NH_2$ groups are converted to a soluble protonated form $-NH_3^+$ ^[46]. The structure of Gram-positive bacteria carries a large net negative charge due to phosphate groups in teichoic acids, whereas LPS are negatively charged in the outer membrane of Gram-negative bacteria^[43]. Fig. 19 shows a schematic representation of how chitosan binds to the cell walls of Gram-positive and Gram-negative bacteria.

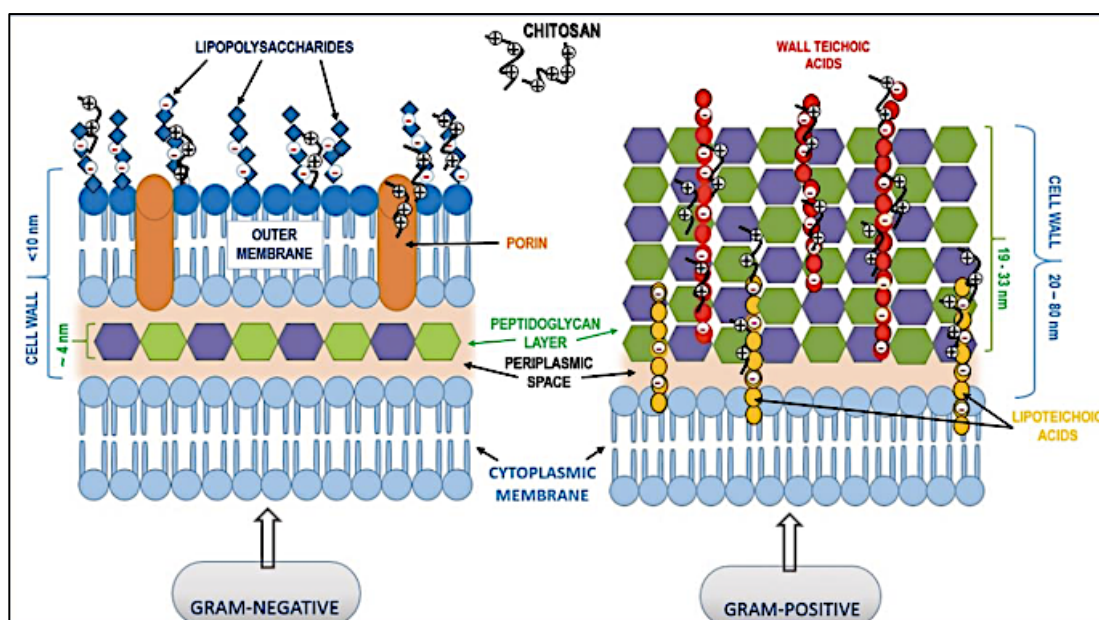


Figure 19. Interactions between bacterial cell walls and chitosan^[46].

For example, the interaction of chitosan and Gram-positive bacteria, such as *S. aureus*, can result in electrostatic binding to the negatively charged teichoic acids

and approximately 100% inhibition of bacterial growth^[151]. Tantala *et al.* showed the alteration of the cell wall of *Listeria innocua* (*L. innocua*) bacteria treated with 0.25 and 0.5 wt.% of high MW chitosan, respectively^[152]. The accumulation of chitosan around the cell walls of *L. innocua* was observed by transmission electron microscopy (TEM)^[152]. TEM results showed that the cell walls of *L. innocua* were covered with chitosan^[152]. This might be due to the high MW of chitosan making it unable to penetrate the cell walls.

The ability of chitosan to interact with LPS caused changes in the permeability of the bacterial membrane, therefore enhancing both non-protein nitrogenous substance uptake and release of LPS from the cell surface^[131, 151]. The binding of chitosan to the outer membrane of Gram-negative bacteria leads to a vesicular structure on the cell surface, disruption of the outer membrane and, subsequently, results in the loss of cell membrane barrier properties^[53, 152].

In Gram-negative bacteria, proteins and LPS are held together by electrostatic interactions with divalent cations in order to stabilise the outer membrane. Replacement of Mg^{2+} and Ca^{2+} ions present in the cell wall may disrupt the integrity of the cell wall or influence the activity of degradative enzymes. Chitosan may bind to metal ions such as Ni^{2+} , Fe^{2+} or Cu^{2+} that are present in the cell and play an essential role in cell viability and, therefore, can also inhibit the cell growth^[132]. The metal-binding capacities of chitosan are stronger at a lower pH (below 6.0)^[46]. Li *et al.* reported FTIR spectra and kinetic traces results showing that chitosan rapidly attacks the cell wall of *E. coli* ^[53]. The cell wall was damaged^[53]. The leakage of cytoplasm as well as release of DNA and proteins were measured by absorbance at 260 nm and 280 nm^[53]. Furthermore, TEM results showed an alteration of the outer membrane that was coupled with the coagulation of cytosolic components after 24 hours^[53]. In addition, porins, which are located inside the cell wall of Gram-negative bacteria and responsible for the uptake of nutrients, could interact with the amine groups thus leading to blockage

of nutrients exchange due to the formation a polymer layer over the surface of bacterial cells^[46].

In Gram-positive bacteria, teichoic acids along with Mg^{2+} and Ca^{2+} cations help to maintain the integrity and enzymatic functions of the cell wall^[46]. The absence of these divalent cations could lead to the sensitivity of the cell wall to chemical and antibacterial components^[46]. Raafat *et al.* reported ultrastructural changes in *S. simulans* that were exposed to chitosan^[131]. It was possible to identify chitosan molecules attached to the cell walls using TEM^[131]. In addition, Mansilla *et al.* added Mg^{2+} and Ca^{2+} cations to the medium and showed an increase in a positive charge of the bacterial cell wall that subsequently weakened the antibacterial activity of chitosan^[46, 131].

To summarise the comments made above, the interaction between chitosan and a bacterial cell wall can cause chelation of trace metal cations, which are necessary for the growth of bacteria, breaking down the bacterial cell wall followed by the leakage of proteinaceous and other intracellular constituents of the cytoplasm^[132, 153, 154]. Furthermore, the electrostatic interaction between chitosan and the bacterial cell may result in an imbalance of internal osmosis and consequently inhibit the growth of microorganisms^[131]. In addition, chitosan can form a layer over the cell that can subsequently affect the absorption of nutrients^[53, 132].

Another proposed theory is based on an intracellular mode of antibacterial action of chitosan. Chitosan might penetrate a bacterial cell wall and bind to DNA, which is negatively charged due to the presence of phosphate groups^[155]. However, the mechanism of interaction of chitosan with bacterial DNA is not well understood^[155]. Due to the cationic nature of chitosan and anionic nature of DNA, such a binding interaction might be pH dependent and, thus, stronger at a lower pH^[156]. Chitosan is capable of forming hydrogen bonds with A-T base pairs that might lead to a breakage of the Watson Crick hydrogen bonds, whereas the

Watson Crick hydrogen bonds between G-C nucleotides could exhibit a higher stability and restrain diffusion of chitosan^[156]. The binding of chitosan to bacterial DNA can prevent DNA transcription, mRNA synthesis and interrupts protein synthesis^[131]. For example, chitosan oligomers were found inside *E. coli* using a confocal laser microscope and caused the prevention of DNA transcription^[53]. Moreover, chitosan may cause both restraining of motion and structural distortions of DNA that could lead to a transformation of DNA into a compact structure^[156]. It is still unknown whether chitosan interacts with DNA in a specific binding manner^[156]. However, it might be difficult for chitosan to pass through the outer membrane of Gram-negative bacteria^[53]. It has been concluded that chitosan reacts mostly with the cell walls and proteinaceous content rather than DNA or RNA^[53]. It has been stated that even though this mechanism is accepted, the probability of chitosan passing through cell walls and bind DNA is rather low^[53, 131]. Therefore, explaining these mechanisms is another aspect that has become an important and a great challenge.

1.4.3.2. Effect of DDA of chitosan on antibacterial activity

The ability of chitosan to penetrate a bacterial cell wall depends on DDA and MW. The DDA of chitosan might affect the antimicrobial properties due to a number of amine groups, which are directly involved in at least one of the proposed antibacterial mechanisms (Section 1.4.3.1.)^[132]. An increase in DDA was reported to result in a stronger antimicrobial activity due to the presence of the free amine groups^[132]. Moreover, the binding activity of chitosan is also stronger at a higher DDA^[156]. For example, higher DDA showed a stronger DNA binding capacity and ability to cause condensation^[156]. Furthermore, high DDA could restrain the global motion of DNA^[156]. Once DNA binds with chitosan, its surface collapses which might subsequently lead to a dehydration of DNA^[156]. Chitosan with higher DDA showed a quicker ability to form a stable complex than low DDA^[156]. In addition, the Coulombic energy between chitosan and DNA becomes weaker when DDA decreases^[156].

Li *et al.* found that minimal inhibitory concentration (MIC) of chitosan (DDA 51% and 61%, MW > 1000 kDa) was 0.25% against both *E. coli* and *S. aureus*, whereas increasing DDA to 76.98% resulted in a decrease of MIC to 0.1250%^[157]. Chitosan with 82% and 100% DDA showed a MIC of 0.0625% and 0.0313% against both *E. coli* and *S. aureus*, respectively, after 24 hours^[157]. According to Li *et al.*, the bacterial activity increased as DDA increased from 51% to 81% but remained stable after further increasing of DDA^[157]. Moreover, Chung *et al.* reported that increasing DDA of chitosan from 75% to 95% leads to increased antimicrobial activity against *S. aureus* and *E. coli* through nucleotide leakage^[158]. Similarly, Takahashi *et al.* showed that 2 wt.% low MW chitosan with increased DDA from 89% to 92% could enhance antibacterial properties and fully inhibit the growth of both *E. coli* and *S. aureus*^[159].

1.4.3.3. Effect of molecular weight on antibacterial activity

There are different molecular weights (MW) of chitosan. Low MW chitosan has MW < 190 kDa, medium MW is 190-310 kDa and high MW > 310 kDa^[160]. The exact antibacterial mechanism of different molecular weights of chitosan against both Gram-positive and Gram-negative bacteria is still unknown^[161]. Low MW chitosan might penetrate bacterial cell walls and enter bacterial cells^[161]. As Gram-positive bacteria have a thicker layer of peptidoglycan (20-80 nm), chitosan might not be able to penetrate the cell wall, but could form a bilayer over the surface of a cell^[132, 162]. However, low MW chitosan might penetrate the outer membrane of Gram-negative bacteria, which is the relatively thin (7-8 nm)^[162]. Therefore, the thickness of peptidoglycan might play an important role in penetration of chitosan into the cell^[161, 163]. The studies reported that low MW chitosan possessed higher antibacterial activity against Gram-negative bacteria than Gram-positive bacteria^[164]. Low molecular weight chitosan was found to be more effective for *E. coli*, *K. pneumoniae* and *P. aeruginosa*, whereas high molecular weight chitosan was more effective against Gram-positive bacteria^[165].

It has also been reported that chitosan with high MW might show reduced antibacterial activity against *E. coli* due to the formation of intramolecular hydrogen bonds that prevents amine groups from being available to attach to bacterial cells or blocks the entry of chitosan^[151]. Such a trend was not observed with Gram-positive bacteria, where MW of chitosan higher than 100kDa might form a film that inhibits the absorption of nutrients^[151].

Furthermore, it has been demonstrated that hydrophilicity of Gram-positive bacteria is lower than in Gram-negative, which makes the latter more sensitive to chitosan. As MW decreases chitosan can pass through the channels into cell^[166]. Low molecular weight chitosan might also bind to DNA and inhibit RNA replication^[46]. Inside a bacterial cell, low MW chitosan may affect the mobility of nucleic acids^[132, 162]. Xing *et al.* showed the interaction of the positively charged amine groups in oleoyl-chitosan nanoparticles at a concentration of 1 g/l with the negatively charged phosphate groups in the chains of nucleic acids such as DNA and RNA of *E. coli* ^[46]. Li *et al.* tested different MW of chitosan using OD₆₁₀ and reported that MW of 50kDa showed higher inhibitory activity than MW of 1000kDa^[53]. Another method of testing was based on measuring the leaching of DNA and RNA from the cells at OD₂₆₀ and OD₂₈₀^[53]. MW of 50 kDa resulted in the highest release of nucleic acids after 40 minutes^[53]. Furthermore, the cell wall of *E. coli* appeared to be more damaged with low MW chitosan than with high MW chitosan^[53]. TEM analysis showed that the cell walls of *E. coli* treated with low MW chitosan was disrupted after 24 hours^[53]. The cytoplasmic membrane was separated from the cell envelope followed by lysis^[53]. According to the study, low MW chitosan caused disruption of the outer membrane and separation of the cytoplasmic membrane, which resulted in a disruption of function, permeability of cell walls and leakage of intracellular components followed by the ultimate lysis of the cells^[53].

However, too low MW chitosan could also negatively affect the antibacterial activity. For instance, MW below 40kDa showed a weak antibacterial activity

against both *E. coli* and *S. aureus*^[164]. Jeon *et al.* reported that MW of chitosan should be higher than 10kDa for an effective inhibition of bacterial growth^[167].

As was stated previously, high MW chitosan may form a dense polymer film on the cell surface and prevent nutrients and oxygen from passing through the wall. This might inhibit the growth of aerobic bacteria^[46]. A number of research studies observed bacterial cells such as *E. coli* and *S. typhimurium* covered with chitosan using electron, fluorescence and transmission microscopes^[46, 168]. Cell walls appeared thicker due to being coated with chitosan^[46]. However, the effect of chitosan might also depend on the type of bacteria. For instance, low MW chitosan (50 kDa) was effective against Gram-negative *E. coli*, *E. coli* O-157, *Salmonella enterica*, *Bacillus cereus*, *B. subtilis*, *Listeria monocytogenes*, *Klebsiella pneumoniae* and *S. typhi*, but not *P. aeruginosa*^[131, 167]. *P. aeruginosa* appeared to be the most resistant microorganism to low MW chitosan in the research obtained elsewhere^[165]. Furthermore, *Streptococcus sobrinus* was sensitive to both high and low MW chitosan, whereas high molecular weight chitosan showed higher antibacterial activity against *S. mutans*^[169]. Therefore, the modes of action of different MW chitosan against both Gram-positive and Gram-negative bacteria need to be investigated further.

Zheng *et al.* showed that decreasing the molecular weight of chitosan (MW <5 kDa, DDA 75-85%) using 0.25 wt.% concentration enhances antibacterial activity by 50% against *E. coli* after 20 hours^[162]. Cruz-Romero *et al.* reported that 1 wt.% of both low and medium MW chitosan fully inhibited the growth of *Bacillus cereus*, *S. aureus*, *Pseudomonas fluorescens* and *E. coli* at 0.010 and 0.015 wt.% chitosan concentration, respectively, after 20 hours^[170]. Therefore, low MW chitosan has shown higher antibacterial activity than both medium and high MW chitosan^[170].

Liu *et al.* have reported that MW lower than 500 kDa of chitosan along with 80% DDA has been effective in the inhibition of growth of *E. coli* ^[171]. According to

Benhabiles *et al.*, the minimum inhibitory concentration using low MW chitosan (12 kDa, DDA 80%) at 0.1 wt.% concentration showed complete antibacterial activity against *E. coli* and *B. subtilis*, whereas 0.3 wt.% was effective against *S. typhimurium* and *S. aureus*^[172]. The concentration 0.5 wt.% of low MW chitosan inhibited the growth of *P. aeruginosa* after 4 hours^[172]. Moreover, Jeon *et al.* showed that 1 wt.% of chitosan (MW >10 kDa) caused 100% bacterial growth reduction of *Streptococcus mutans*, *S. aureus*, *Lactobacillus bulgaricus*, *Lactobacillus fermentum* and *Streptococcus faecalis* and 99% against *E. coli*, *E. coli O-157*, *Salmonella typhi* and *Staphylococcus epidermidis*, respectively^[167]. In addition, 40 kDa MW chitosan could inhibit 90% of *S. aureus* and *E. coli* at a concentration of 0.5 wt.%^[162]. Jeon *et al.* has claimed that increasing MW of chitosan to MW > 10 kDa is more effective against *E. coli* than MW <10 kDa^[167]. However, it was found that 305 kDa MW chitosan at 0.25 wt.% concentration shows 99% antimicrobial activity against *S. aureus* after 20 hours^[162]. According to Zheng *et al.*, the antibacterial activity against Gram-positive bacteria such as *S. aureus* can increase with increasing molecular weight, whereas decreasing the MW of chitosan can enhance antibacterial properties against Gram-negative bacteria such as *E. coli* ^[164].

The pH of the chitosan solution can also affect the antibacterial assay. According to Li *et al.*, the bactericidal effect of chitosan against *E. coli* and *S. aureus* was stronger in an acidic solution than in neutral and alkaline solutions^[157]. The reason for this may be due to the solubility of chitosan in an acidic environment, where the amine group of chitosan may be changed to $-NH_3^+$ and therefore have cationic characteristics. Li *et al.* reported that pH6 is optimal for the investigation of the antibacterial activity because bactericidal activity using chitosan solution at a pH below or above pH5 might also come from the effects of acids and alkali^[157]. For example, Chang *et al.* used fixed MW chitosan (MW 300 kDa, DDA 95%) against both *E. coli* and *S. aureus* for 24 hours, but at pH5 and pH6, respectively^[173]. The results showed that bacterial response and inhibition of

bacterial growth was increased at pH5, which might be due to either released amine groups or acidic stress^[173].

Chitosan also possesses antifungal properties. The interaction between the cation chain of chitosan and negatively charged macromolecules on the fungal cell membrane leads to leakage of intercellular electrolytes and other constituents^[132]. Furthermore, chitosan can affect the morphogenesis of the chitin cell wall by acting with enzymes responsible for fungal growth. For instance, low MW chitosan can penetrate the hyphae of *Fulvia fulva*, resulting in growth inhibition^[132]. Chitosan with MW of 7.6 kDa has been shown to be more effective than MW 700 kDa against *Botrytis cinerea* and *Colletotrichum lagenarium*, respectively^[174]. This might be due to the ability of lower molecular weight chitosan to penetrate the fungal cell more easily than medium or high MW chitosan. Moreover, Marquez *et al.* showed the membrane disruptive ability of low MW chitosan (75-85% DDA) on 31% of haploid deletion mutants of *Saccharomyces cerevisiae*^[175]. In addition, Hernandez-Lauzardo *et al.* showed the antifungal effect of different MW chitosan (17-30 kDa) against *Rhizopus stolonifer* in various stages of fungal development^[176]. The results show that chitosan with MW of 17 kDa is more effective in the inhibition of mycelial growth, whereas chitosan with MW of 30 kDa influenced sporulation and germination^[176]. Therefore, chitosan can be beneficial for introducing antimicrobial properties into BC for a number of potential wound healing applications.

1.4.4. BC/chitosan composites for wound dressing applications

The presence of O-H and N-H groups in chitosan may lead to strong chemical binding to BC^[177]. As chitosan can be beneficial in wound healing systems due to its antimicrobial properties, ability to absorb the wound exudates and lack of mammalian cytotoxicity, the possibility of incorporation of chitosan into BC for wound healing properties has been investigated.

In one case study, 0.1 wt.% chitosan (MW 30 and 80 kDa, DDA 85%) was added to coconut water, which contained 5 wt.% sucrose, in order to produce *in situ* a BC/chitosan composite. The composite was incubated for 5 days at 30°C. The results showed that the addition of chitosan to the medium inhibits the growth of BC^[138]. The final BC/chitosan composite had a denser fibre structure and smaller pore diameter than pure BC^[138]. Wahid *et al.* synthesised *ex situ* semi-interpenetrating BC/chitosan hydrogels with antibacterial properties against *E. coli* and *S. aureus*^[178]. In order to prepare the composite, BC was incubated using HS medium for 7 days at 30°C^[178]. Then, 1% of homogenised BC was mixed with both 2 wt.% of low MW chitosan solution and 2% glutaraldehyde as a cross-linking agent at 80 °C for 4 hours^[178]. The antibacterial properties were analysed through the colony-forming unit (CFU) method. BC/chitosan hydrogel reduced the population of *S. aureus* and *E. coli* by 88% and 98%, respectively^[178]. A similar antibacterial effect was observed by Wu *et al.*, where chitosan and synthesised BC were dissolved in 2 vol.% acetic acid and then mixed at ratio 1:1, 1:3 (1 part chitosan to 3 BC) and 3:1 (3 parts chitosan to 1 BC)^[179]. Then, all BC samples were placed in 24-well plates with bacteria, respectively, for 1, 2, 3 and 4 hours^[179]. After incubation, both BC and bacteria were sonicated for 75 seconds at 64 kHz^[179]. The bacteria were then plated on agar plates for 24 hours at 37°C^[179]. The results showed full inhibition of *E. coli* growth using 3:1 BC and 1:1 ratio, whereas the viability of bacteria was 5% with 1:3 ratio composite^[179]. The most effective ratio for inhibition of *S. aureus* growth was 3:1 (98%), then 1:1 (95%). Least effective was 1:3 (40% of bacterial viability)^[179]. Lin *et al.* immersed BC into 0.6 wt.% chitosan solution for 12 hours and then freeze-dried the composite for antibacterial agar diffusion assay^[180]. The results showed 99% reduction of both *E. coli* and *S. aureus* growth^[180].

1.4.4.1. Mammalian toxicity of BC/chitosan composites

The cytotoxicity of BC/chitosan composites has also been investigated. The cytotoxicity of the BC/0.6 wt.% chitosan composites, which were synthesised by

the immersion, were analysed using mouse skin fibroblast cells (L929) in the presence of DMEM and 10% FBS medium^[180]. The results showed that BC/chitosan composites do not affect cell viability^[180]. Similarly, Kingkaew *et al.* showed no cytotoxicity of BC/chitosan composite, which was synthesised by immersion of BC into 1 wt.% chitosan (MW 30 and 80 kDA)^[181]. Even though the growth of human skin keratinocytes and fibroblasts was similar within pure BC and the BC/chitosan composite, cell adhesion and spreading were improved within BC/chitosan material^[181]. Moreover, the results did not show any differences in cytotoxicity to fibroblasts between 30 kDA and 80 kDA MW chitosan in BC/chitosan composites on the cytotoxicity^[181].

Another investigation of the cytotoxicity of BC/chitosan composite used 1 wt.% chitosan solution that was mixed with 1g of BC in order to synthesise BC/chitosan composites at 1:1 ratio^[182]. The composite was air-dried and applied to L929 cells, which were maintained in DMEM medium for 24 hours. The results showed that cell viability using BC/chitosan composite was 90% compared to the control after 24 hours^[182]. Kim *et al.* compared 3t3 fibroblasts cell attachment to the fibres of pure BC and BC/chitosan composite, which was produced by immersion of BC into 1 wt.% chitosan solution, by seeding the cells on the surface of cellulose in DMEM for 48 hours^[183]. The results showed that cells that were attached to pure BC remained round-shaped, but the cells that were attached to BC/chitosan adhered with many pseudopodia, proliferated and almost completely spread over the surface^[183]. This might be due to better biocompatibility of BC/chitosan composite than pure BC.

The synthesised BC/chitosan composite has also been tested as a wound healing material on 18 8-weeks-old male Sprague Dawley rats, where pure BC and BC/chitosan dressings were compared to the commercial Tegaderm™^[180]. According to Lin *et al.*, both BC membranes showed rapid healing and 85% wound closure on the 8th day followed by complete healing on the 13th day, whereas Tegaderm™ showed lower epithelisation rate and complete healing on

the 14th day^[180]. Moreover, the average contraction of the wound was greater with BC/chitosan than pure BC. Furthermore, the keratin production was more integrated with BC/chitosan composite than pure BC on day 7^[180]. Due to the generation of type IV collagen, the epidermis and dermis were anchored tightly in the wounds treated with BC/chitosan^[180]. Chitosan can also increase the production of collagen type III. For example, in one study, 15-month old female beagles, weighing 8-10 kg, were wounded; one group was treated with 0.5 wt.% chitosan fibres for 15 days (MW 30kDA, DDA 18%)^[184]. It was found that chitosan promotes the granulation phase of healing by increasing the production of collagen type III^[184]. The chitosan-treated wounds showed major infiltration of polymorphonuclear leukocytes compare to the control group on the 3rd day^[184]. The increase of polymorphonuclear leukocytes led to the production of osteopontin, which is a glycosylated phosphoprotein that promotes the attachment and spread of cells^[185].

Chitosan can also accelerate the migration of macrophages. As chitosan consists of GlcN and GlcNA units, macrophages can inhibit the receptors for mannose- and GlcNA-glycoproteins, which then mediate the uptake of glycoprotein into macrophages^[185]. Therefore, GlcNA units of chitosan can bind to macrophage-specific receptors, which then leads to the release of various biological mediators and fast wound healing^[185]. In addition, chitosan can degrade *in vivo* mainly by enzymatic hydrolysis^[144]. Highly deacetylated chitosan (DDA > 85%) possesses a low degradation rate *in vivo*, which may last for several months, whereas lower DDA degrades more rapidly^[144]. Moreover, chitosan can also evoke a minimal foreign body reaction, which is beneficial for wound healing applications^[144].

1.5. Kombucha as an alternative to conventional BC

Another type of bacterial cellulose is Kombucha cellulose (KC). Similar to conventional BC, cellulose pellicles of KC are formed on the top of the growth medium, which is usually black tea, due to the presence of *Acetobacteraceae*.

1.5.1. The structure of Kombucha cellulose

The structure of KC is similar to conventional BC. The fibres of KC are less than 100 nm in diameter and composed of ribbon-like fibre bundles, which are 20–70 nm in width (Fig. 20)^[162]. These fibre bundles consist of 3–10 fibrils with a diameter of approximately 7-10 nm^[162].

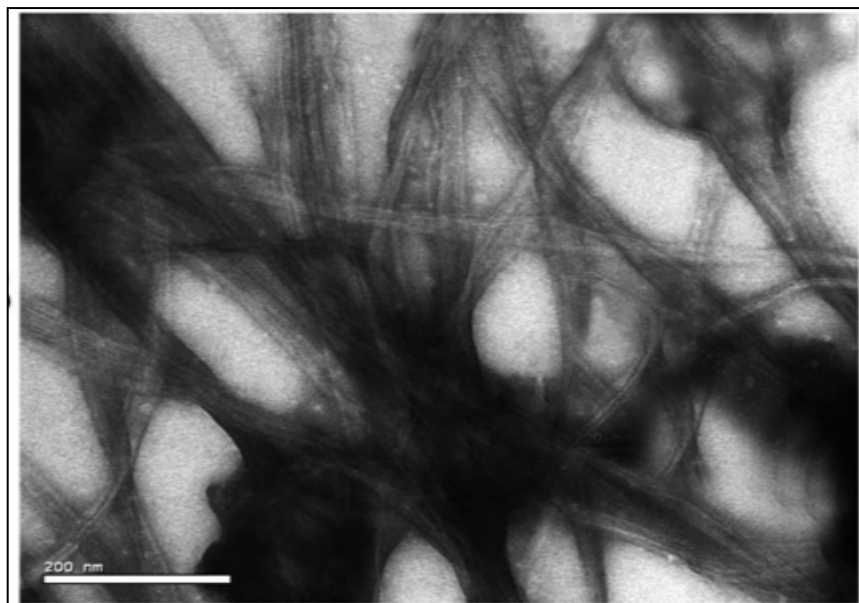


Figure 20. TEM image showing the structure of the KC matrix and fibres^[162].

As shown in Fig. 21, the 3-D matrix of KC is translucent, with numerous pores of different sizes^[162].

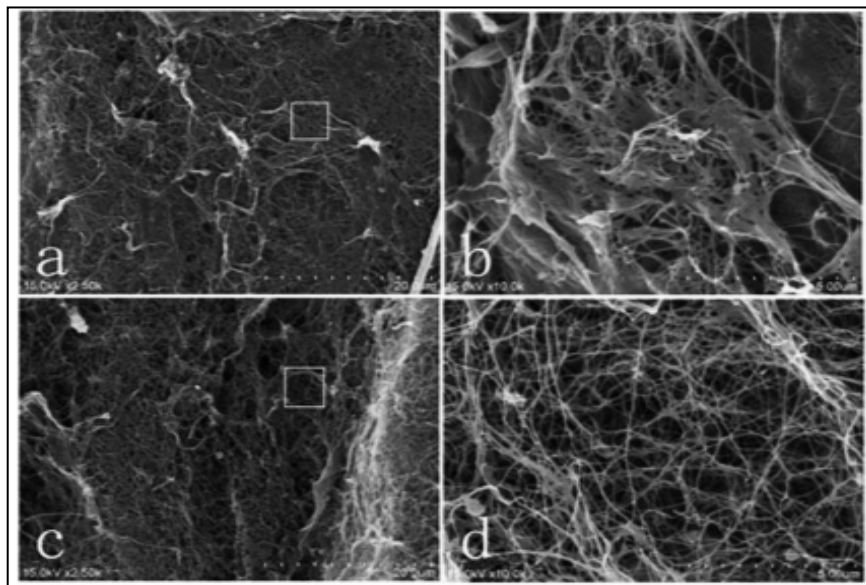


Figure 21. SEM images showing the structure KC matrix. A and c demonstrate the dense surface, whereas b and d show the enlarged porous matrix ^[162].

Therefore, KC and conventional BC have a similar 3-D structure, which suggests that KC can be used as an alternative due to the simpler fermentation process, which involves mainly microorganisms such as bacteria and yeasts, tea and sugar.

1.5.2. Microbial composition of Kombucha

Kombucha is a beverage prepared by fermenting mainly black tea and sugar along with a symbiotic culture of bacterial and yeast (SCOBY)^[186]. The SCOBY is a composition of microorganisms resembling a mushroom cap, which then starts the brew. The SCOBY consists of various acetic acid bacteria such as *G. xylinus*, *Acetobacter pasteurianus*, *Gluconobacter oxydans* and *Acetobacter aceti* and yeast such as *Saccharomyces* species, *Zygosaccharomyces kombuchaensis* and *Zygosaccharomyces bailii* ^[186, 187]. De Filippis *et al.* reported that the concentration of acetic acid bacteria (AAB) increased to 1.5 log and 5.5 log CFU/ml after 7 and 21 days, respectively, of cultivation at 20°C, whereas the initial concentration of AAB increased to 8.5 log CFU/g during the same period of time at 30°C^[188]. In addition, the genus *Gluconacetobacter* reached 90% in total

among all bacterial population after 7 days, while *Acetobacter* decreased to 3-5% after 21 days^[188]. Therefore, *Gluconacetobacter* is found to be the prevalent genus for production of Kombucha.

1.5.3. Fermentation of Kombucha cellulose

Kombucha cultivation can be achieved by placing SCOBY into a sugared tea broth. Fermented Kombucha beverage (KB) can consist of sugars, tea polyphenols, fibre, ethanol, acids such as acetic, glucuronic, lactic and gluconic, Ni, Mn, Fe, Cu, vitamins such as C and B, hydrolytic enzymes and carbon dioxide after fermentation^[189, 190]. For example, Kombucha that has been fermented for 14 days, has the concentration of 6.38 mg/ml and 1.34 mg/ml of gluconic acid and d-saccharic acid-1,4-lactone (DLS), respectively^[191, 192]. Furthermore, the concentration of ethanol increased within the time and reached 0.28 ± 0.014 g/L on the 7th day of fermentation, which then decreased to about 0.073 ± 0.003 g/L after 21 days of fermentation^[193]. This might be due to the utilisation of ethanol by AAB in order to produce acetic acid.

1.5.4. Benefits of Kombucha beverage

The FDA has not found any pathogenic organisms in Kombucha cellulose and Kombucha tea^[191]. Therefore, Kombucha is a safe product, which has been already commercially available. Kombucha has not shown any toxic signs in albino Wistar rats after feeding them orally with Kombucha at 2.5 ml/kg of their body weight for 60 days^[192]. Furthermore, Kombucha tea at a mass of 60 µg has not shown any cytotoxicity against hepatocytes liver cells after 24 hours maintained in DMEM^[194]. Due to antioxidant activity, Kombucha tea can modulate the oxidative stress in hepatocytes *via* mitochondrial-dependent pathways^[194]. This might be beneficial against liver diseases.

Kombucha components such as tea polyphenols, acids such as ascorbic and vitamins might result in the antioxidant potential of KB. Due to the benefits of such components on health, Kombucha can also reduce cholesterol level, blood pressure and inflammation, provide an antibiotic effect and generally enhance metabolism^[189]. The antioxidant properties of black tea have been compared to KB. Four-weeks-old Swiss albino male rats, weighing approximately 180-200 grams, were, in addition to their normal diet, fed with 150 mg/kg black tea and Kombucha, respectively, for 14 days^[191]. In this study, Kombucha was brewed with black tea containing 10 vol.% sucrose for 14 days. The results showed that the total phenol and flavonoid content, which contained a high level of antioxidants, owing to their ability to scavenge free radicals, increased in Kombucha by 27.2% and 75%, respectively, compared to black tea^[191]. The reason for this might be the presence of enzymes and other components such as organic acids, which are produced by bacteria and yeasts during Kombucha fermentation.

1.5.5. Antimicrobial properties of Kombucha beverage

The KB can exhibit antimicrobial activity against bacteria such as *E. coli*, *S. aureus*, *S. typhi*, *S. epidermis* ^[195-197]. The antibacterial activity of KB may be inhibited by the presence of acids such as acetic acid inside the Kombucha broth. During fermentation, the pH of KB can go from initial 5 to 2-3 on the 7th day of fermentation^[198, 199]. The decrease of pH was not continuous and went down to maximum pH 2-1.88 by the 21st day^[188].

An accurate antibacterial analysis can be obtained at a fixed pH. For example, Battikh *et al.* reported antibacterial properties of KB with pH was fixed at pH 2, which had been brewed in black tea containing 20 g/L sucrose for 21 days, against *S. epidermis*, *S. aureus*, *Micrococcus luteus* (*M. luteus*), *S. typhimurium*, *L. monocytogenes*, *E. coli* and *P. aeruginosa* ^[198]. The results showed that the largest inhibition zones were 18.5 ± 2.1 mm diameter for *S. epidermis* and 19.0

± 1.4 mm for *P. aeruginosa*, followed by 14.5 ± 2.1 mm for *S. aureus*, 16.5 ± 0.7 mm for *M. luteus* and 14.0 ± 1.4 mm for *S. typhimurium*^[198]. The smallest zone of inhibition was 11.0 ± 1.4 mm for *E. coli*^[198].

Furthermore, the antibacterial activity of KB against *E. coli*, *S. typhi*, *P. aeruginosa*, *S. aureus*, *Shigella sonnei* (*S. sonnei*) and *Microsporum canis* (*M. canis*), was evaluated by Santos *et al.* The KB was prepared using 0.5 wt.% mate tea containing 35 wt.% sucrose^[199]. The antibacterial effect of KB in volume of 50 μ l, but at different fermentation times was evaluated at a fixed pH4^[199]. The results showed the antibacterial activity of KB against *M. canis* after 14 days of fermentation, where zones of inhibition were from 24 to 28 mm in diameter^[199]. Fermented KB inhibited the growth of *E. coli* in 12-16 mm zones after 14 days^[199]. KB showed antibacterial activity against *S. typhi* on the 21th day of the fermentation, where the zones of inhibition were 30 mm in diameter^[199]. However, KB did not show any antibacterial activity against *P. aeruginosa*, *S. aureus* or *S. sonnei*^[199].

The antibacterial properties of KB prepared with black tea and 100 g/L sucrose for 9 days were also analysed against *S. aureus*, *E. coli*, *B. cereus*, *Salmonella choleraesuis* (*S. choleraesuis*) and *C. albicans*^[200]. In this research, KB pH was fixed at 7, subsequently absorbed by the sterile cotton pad and placed on the top of agar with freshly spread bacteria^[200]. Zones of inhibition for *S. aureus* were 1.2-1.4 mm, 1.5-1.6 mm for *E. coli* and 0.3-0.4 mm for *B. cereus*^[200]. Moreover, 1.2-1.5 mm zones were observed for *S. choleraesuis*, whereas *C. albicans* did not show any zones of inhibition^[200].

In addition, Ashrafi *et al.* mixed from 1 vol.% to 3 vol.% of KB that was produced in black tea containing 100 g/L sucrose for 18 days with 0.5 wt.% chitosan solution (MW 310-375 kDa, DDA 75-85%). The composite was then air-dried, cut into 1 x 4 cm strips and subsequently placed on the top of agar plates containing bacteria^[201]. The results from antibacterial assay showed that inhibitory zones for

S. aureus were 13.2 mm, 15.2 mm and 17.6 mm using chitosan/1 vol.% KB, chitosan/2 vol.% KB and chitosan/3 vol.% KB, respectively^[201]. The inhibitory zones using chitosan itself were 8.66 mm in diameter for *S. aureus* and 6.21 mm for *E. coli*^[201]. Chitosan/1 vol.% KB, chitosan/2 vol.% KB and chitosan/3 vol.% KB showed 15.3, 20.1, 20.1 mm in diameter zones of inhibition against *E. coli*, respectively^[201]. While untreated KB has antibacterial properties, treated KC did not show any bactericidal activity^[202].

1.6. Need for the research

There are limitations associated with biomedical applications of BC, especially in wound and burn surgeries. One of the major drawbacks of BC is the lack of innate antibacterial properties. The presence of antibacterial activity in BC is crucial, because infections are one of the most challenging issues in burn recovery, as they can delay the healing process by adversely affecting the patient's immune system and extensively disrupting the physical skin barrier. In order to prevent infections, BC can be modified using different materials with antimicrobial properties. However, another drawback is that most of antibacterial agents, such as silver, copper or TiO₂ might have adverse effects on human health^[71]. In addition, due to toxicity of those antibacterial agents, there is a challenge in controlling the amount of incorporated material into BC. The incorporation of antibacterial compounds into BC can result in a non-uniform distribution or accumulation of particles on its surface^[63]. This variation of concentration of nanoparticles within the BC matrix means that a varied dose of an antibacterial agent will be encountered by bacteria. The uncontrolled leaching of toxic additives can lead to relatively strong adverse effects on human health.

Based on the above-mentioned limitations, there is a need to develop a BC-based composite with permanent antibacterial and non-toxic to mammalian cells properties. This material might be suitable for medical applications such as wound and burns therapies. In order to fill the need, the current research is

focused on the use of BC and its derived soft gels with smectite clay and chitosan, to develop an antibacterial film that is non-toxic to mammalian cells and exhibits low levels of biocide leaching.

1.7. Aim and objectives of the study

The overall aim of the project is to use nanofillers to develop BC-based gels with permanent antimicrobial properties without biocide leaching. Such a material would be ideal for wound dressing, artificial skin and cosmetic applications. The aim was achieved by introducing the antimicrobial, natural and non-toxic towards mammalian cells materials into BC. These natural biocides were incorporated into BC through both *in situ* and *ex situ* modification.

In order to achieve the objective, natural Cloisite Na⁺ and synthetic SWN (lithium magnesium sodium silicate) clays were exfoliated and incorporated *in situ* and *ex situ* into the BC matrix. Moreover, the novel BC-based material, which was named bacterial chitosan, was developed using chitosan as the main carbon source. The antibacterial activity of bacterial chitosan was investigated against both MRSA and *E. coli*. The solubility of bacterial chitosan was evaluated by immersion of the material into vinegar for 48 hours. Furthermore, the modification *ex situ* was carried out by introducing either clay or chitosan into already formed BC gels. The antimicrobial behaviour of a hybrid structure of chemically cross-linked chitosan hydrogel and BC hydrated gel was also investigated. The enhancement of the antibacterial activity of BC/chitosan hybrid hydro and hydrated gels was obtained by using exfoliated clay. Organoclays containing QAC, which exhibit antibacterial properties, were incorporated into BC. In addition, antibacterial activity was provided to Kombucha, which is a mixture of organisms, using natural biocides. This demonstrates that the new materials can be produced in domestic environments, which may offer potential for future commercialisation and the creation of new industries.

This thesis is divided into eleven parts. The next Section is an experimental methodology that covers the materials and techniques used during the project. The results and discussion are presented in chapters 3-8. The 9th Section is the final discussion. The last two chapters conclude the results obtained and provide ideas for future work.

Chapter 2. Experimental Methodology

2.1. Materials used in the current study

Gluconacetobacter xylinus (*G. xylinus*) (ATCC 53524), which was used for the synthesis of BC, was supplied by LGC Ltd. Chosen bacteria for the antibacterial assay were methicillin-resistant *Staphylococcus aureus* (MRSA) NCTC 10418 and *Escherichia coli* (*E. coli*) NCTC 12493 that were obtained from the National Collection of Types Culture (NCTC). *Pseudomonas aeruginosa* (*P. aeruginosa*) ATCC 15442 was supplied by American Type Culture Collection (ATCC).

Bacteriological peptone (code 70175), citric acid (code 251275), disodium phosphate (code S7907), yeast extract (code Y1625), microbiology agar #3 (code A5306), D-(+)-glucose (code G8270), skimmed milk powder (code 70166), tryptic soy agar (TSA, code 22091), tryptic soy broth (TSB, code 22092) and phosphate buffered saline (PBS, code P4417) were purchased from Sigma Aldrich.

NIH 3t3 Swiss mouse embryo fibroblast cells (code 93061524) were purchased from Sigma Aldrich and used for the mammalian cytotoxicity assay. Dulbecco's modified Eagle's medium (DMEM, code 11965084) containing both glucose and L-glutamine was purchased from ThermoFisher Scientific. Dimethyl sulfoxide (DMSO, code 10103483) and fetal bovine serum (FBS, code 11563397) were manufactured by Gibco and were obtained from ThermoFisher Scientific. MTT (3-(4,5-dimethylthiazol-2-yl)-2,5-diphenyltetrazolium bromide) with the product code of M6494 and penicillin-streptomycin (code 11548876) were purchased from ThermoFisher Scientific. Dulbecco's phosphate buffered saline (D8662) was purchased from Sigma Aldrich.

Black Yorkshire tea (code B07JXK2C7V) was produced by Taylors of Harrogate and obtained from Amazon. Kombucha SCOBY was supplied by Amazon with

the Amazon standard identification number (ASIN) of B00H9I80C6 and manufactured by Happy Kombucha.

Natural NaMMT (Cloisite Na⁺) and Cloisite 10A, Cloisite 15A, Cloisite 20A, Cloisite 30B and Cloisite 93A organoclay were purchased from Southern Clay Products, USA. Organoclay are MMT clay that were organically-modified by incorporating quaternary ammonium cations into the clay structure.

Lucentite™ (SWN) was obtained from COOP, Japan. SWN is a synthetic, commercial smectite clay. SWN is a lithium magnesium sodium silicate and has a TOT structure similar to natural MMT. Si ions are located in tetrahedral sheets, whereas Mg ions can remain or be replaced with Li in an octahedral sheet (Fig. 22). SWN consists of silicate nanolayers with the dimension of height to length approximately 1:300 nm^[204]. The silicate nanolayers have diameter of 25 cm and thickness of 1 nm^[204]. This means that even SWN and Cloisite Na⁺ have similar structure, but the aspect ratio is smaller in SWN clay.

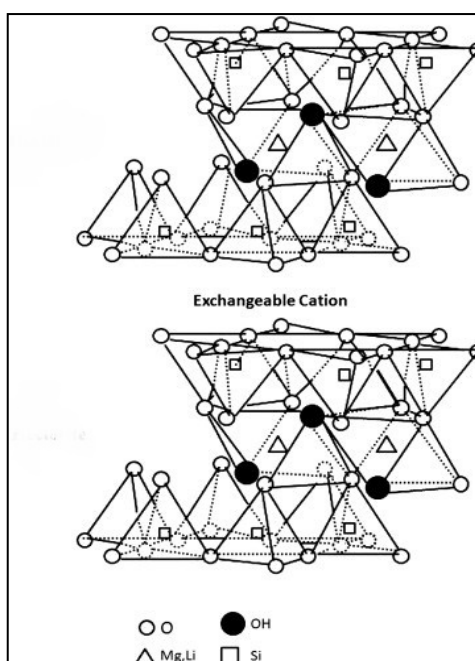


Figure 22. Schematic structure of synthetic SWN clay^[205].

Low molecular weight (MW) chitosan (product code 448869) with MW of 50-190 kDa and 75-85% degree of deacetylation (DDA). It was purchased from Sigma Aldrich. Medium MW chitosan (code 448877) with MW of 190-310 kDa and 75-85% DDA was also obtained from Sigma Aldrich. Widely-available (WA) chitosan with the Amazon standard identification number (ASIN) of B008TO725K was purchased from Amazon and produced by BioOrigins. Sodium metaperiodate (product code S878), which was used for the oxidation of BC, was obtained from Sigma Aldrich.

All materials were sterilised by either autoclaving at 121°C for 15 min at 100 kPa (15 psi) pressure or passing through 0.2 µm pore size filters (Fisher Scientific).

2.2. Synthesis of BC

2.2.1. Maintenance of bacterial species

For long-term storage, colonies from agar plates with *G. xylinus* were re-suspended in the solution that consisted of 3 grams of TSB, 2 grams of biology purpose skimmed milk powder, 0.5 grams of glucose powder, 4 ml of glycerol made up to 100 ml in total before sterilising. The bacteria were then stored at -80°C.

Hestrin Schramm (HS) medium was used for the growth of *G. xylinus* either on agar plates or in liquid broth. The medium consisted of 5 grams of bacteriological peptone, 5 grams of yeast extract, 1.15 grams of citric acid, 2.7 grams of disodium phosphate. If agar was required, 15 grams of microbiology agar #3 was added at this point. The medium was, then, adjusted to pH5 using 0.1M of hydrochloric acid and filled up to 960 ml by adding distilled water. The medium was then sterilised in an autoclave. Subsequently, 40 ml of 50 wt.% glucose solution, which was sterilised by the filter pore size of 0.2 µm, was added to either broth or agar after autoclaving to give a final concentration of 2 wt.%.

Prior to any experiment, bacteria were streaked from the frozen culture to HS agar and incubated for 48 hours at 30°C. These bacteria could then be stored for up to 2 weeks at 4-8°C.

2.2.2. Incubation of bacteria in liquid medium

Bacteria, that had been incubated on HS agar for 48 hours at 30°C, were aseptically re-suspended in sterile PBS. This bacterial solution was added to HS medium and inoculated on either small or large scale. For the small scale production, the bacterial suspension was adjusted to 0.1 OD₆₀₀ and then inoculated into 3 ml of HS medium. This small scale production continued by subsequent incubation of the bacteria in 6 well sterile polystyrene plates (Sarstedt, 3.5 cm diameter x 2 cm depth) statically at 30°C for up to 72 hours.

The large scale production was carried out by the diluting the bacterial suspension into 200 ml of HS medium. The bacteria were incubated statically inside sterile pyrex dishes (27 cm height x 35 cm width x 6 cm depth), which were sealed with aluminium foil, at 30°C for up to 96 hours.

The temperature, duration of incubation, medium type and carbon sources varied as detailed in subsequent experiments.

2.2.3. Treatment of BC after incubation

The synthesised BC was treated by submerging statically within 0.1M NaOH at 80°C for an hour, and then, washed with distilled water until pH reached 7. A sterility check by incubation of a portion of BC after the treatment was carried out in both HS and tissue culture medium. If no contamination was observed, BC was then termed as pure BC, which was the basis for further treatments and characterisation.

2.3. Optimisation of BC growing conditions

The growing conditions of BC were optimised on both small and large scales. The effect of temperature, time and concentration of a carbon source were analysed.

2.3.1 The effect of optical density

The effect of optical density on the synthesis of BC was investigated by inoculation of *G. xylinus* at 0.001-0.5 OD₆₀₀ with 3 ml of HS medium, respectively, at 30°C for 48 hours. The experiment was carried out on a small scale in 6 well sterile polystyrene plates (Sarstedt, 3.5 cm diameter x 2 cm depth). The produced BC was dried for 48 hours at 37°C. The growth of BC was evaluated by the mass yield of dried BC.

2.3.2 The effect of temperature

In order to investigate the optimal temperature for BC growth, 0.1 OD₆₀₀ of PBS-resuspended bacteria were inoculated with 3 ml of HS medium at 25°C, 30°C and 37°C, respectively, for 48 hours. The experiment was carried out on a small scale in 6 well sterile polystyrene plates (Sarstedt, 3.5 cm diameter x 2 cm depth). The growth of BC was evaluated by the mass yield of wet and dried BC. The wet mass was obtained by placing the produced wet BC into a centrifuge tube and sedimentation at 150xg followed by discarding the supernatant. This process was repeated three times. The dried mass was obtained by drying centrifuged BC pellet for 48 hours at 37°C.

2.3.3 The duration of incubation

The duration of incubation on the synthesis of BC was investigated by inoculation of *G. xylinus* at a concentration of 0.1 OD₆₀₀ for 24, 48 and 72 hours, respectively,

on a small scale at 30°C. The bacteria were also inoculated for 24, 48, 72 and 96 hours at 30°C on a large scale in sterile pyrex dishes (27 cm height x 35 cm width x 6 cm depth). The growth of BC was evaluated by the mass yield of wet and dried BC. The wet mass was obtained by placing the produced wet BC into a centrifuge tube and spinning the tube at 150xg followed by discarding of the liquid. This process was repeated three times. The dried mass was obtained by drying centrifuged BC pellet for 48 hours at 37°C.

2.3.4 The effect of carbon source

The effect of a reduction of a carbon source on the production of BC was investigated on a small scale in 6 well sterile polystyrene plates (Sarstedt, 3.5 cm diameter x 2cm depth). The bacteria at a concentration of 0.1 OD₆₀₀ were inoculated with 3 ml of HS medium containing from 2 wt.% (standard) to 1 wt.% glucose. The incubation was carried out for 48 hours at 30°C. The BC produced was then dried for 48 hours at 37°C. The growth of BC was evaluated by the mass yield of dried BC.

2.4. The growth of BC in a clay environment

Exfoliated and non-exfoliated Cloisite Na⁺ and SWN clay suspensions were mixed with HS medium at concentrations from 0.09 mg/ml to 3 mg/ml, respectively. The bacteria at the concentration of 0.1 OD₆₀₀ was added to HS/clay suspensions and inoculated on a small scale for 48 hours at 30°C. For the large scale production, both exfoliated and non-exfoliated Cloisite Na⁺ and SWN clay suspensions were used at the concentration of 3 mg/ml, respectively.

2.4.1. Preparation of clay suspensions

A stock solution containing 6 mg/ml of either Cloisite Na⁺ or SWN suspensions was prepared in a total of 100 ml by mixing the clay powder in distilled water,

respectively, and defined as non-exfoliated. Exfoliated suspensions were obtained using a blender (Tefal Fruit Sensation blender) for 16 minutes (for Cloisite Na⁺) and 10 minutes (for SWN) at speed 1, respectively. All clay suspensions were sterilised through autoclaving at 121°C for 15 minutes.

2.4.1.1. Exfoliation of clay suspensions

Both Cloisite Na⁺ and SWN clay suspensions were treated using ultrasound, magnetic stir and the Tefal blender, respectively. The treatment was based on disassociating of clay particles in 100 ml of each stock of clay suspensions for 16 minutes for Cloisite Na⁺ and 10 minutes for SWN, respectively.

In order to treat the clay using ultrasound, 100 ml of aqueous Cloisite Na⁺ and SWN clay suspensions were sonicated (Missonix) at 85% amplitude for 16 and 10 minutes, respectively. In order to prevent overheating of solutions, sonication occurred at intervals of 5 minutes, followed by a minute cooling period at 25°C. Cloisite Na⁺ and SWN suspensions at the concentration of 6 mg/ml in the volume of 100 ml being stirred using plastic covered stir bar for 16 and 10 minutes, respectively, at 800 rpm speed and at 25°C.

Aqueous suspensions of Cloisite Na⁺ and SWN clay were also exfoliated using the Tefal blender for 16 and 10 minutes, respectively, at speed 1. The effect of the coffee grinder and chopper blades on the exfoliation of the clay were investigated.

All suspensions were stored at 25°C for no longer than a day until incorporation into BC or further characterisation. The characterisation of the exfoliation state of the suspensions was carried out using dynamic laser scattering (DLS).

2.4.1.2. Characterisation of exfoliation state of the clay suspensions using dynamic laser scattering

Measurements of size, volume and number distribution of clay particles or aggregations were carried out using dynamic laser light scattering (DLS, supplied by Malvern N4). A cuvette containing 1 ml of each suspension was analysed at 25°C using a 90-degree beam angle and 5 minute equilibration time. The data obtained were observed by three mean parameters: numbers, volume and intensity. The measurements were repeated up to four times.

2.4.2. The rheological characterisation of gel formation

Non-exfoliated and exfoliated by the Tefal blender as described in Section 2.4.1.1. Cloisite Na⁺ and SWN suspensions at the concentration of 3 mg/ml were mixed with HS medium, respectively. The gel formation measurements were carried out at 0 and 48 hours, respectively, using a rheometer (supplied by Bohlin Instruments). Each sample with volume of 1.2 ml was sandwiched between the plates. The measurements carried out by rotating an upper plate and a fixed lower plate with the sample present between them. The working gap between the plates was 400 µm. The type of the upper plate used was PP40. The measurements of both viscous and elastic modulus were carried out at the frequency ranging from 0.01 to 10Hz for 21 minutes at 25°C. After 0 hours measurement, the samples were stored for 48 hours at 30°C incubator.

2.4.3. Inoculation of *G. xylinus* with clay suspensions on a small scale

The small scale production was carried out by the adding exfoliated and non-exfoliated Cloisite Na⁺ and SWN clay suspensions to HS medium with a final concentration of the clay ranging between 0.09-3 mg/ml, respectively. Inoculation of bacteria was carried out by adding 100 µl of 0.1 OD₆₀₀ PBS re-suspended bacteria to 3 ml of HS/Clay suspensions. The inoculum was incubated in 6 well plates (Sarstedt, 3.5 cm diameter x 2 cm depth) at 30°C for 48 hours. The BC

produced was dried for 48 hours at 37°C. The growth of BC was evaluated by the mass yield of dried BC.

2.4.4. Inoculation of *G. xylinus* with clay suspensions on a large scale

The large scale production was carried out by adding exfoliated and non-exfoliated Cloisite Na⁺ and SWN clay suspensions to HS medium to a final concentration of clay of 3 mg/ml, respectively. Then, 200 ml of HS/Clay medium was aseptically poured into sterile pyrex dishes (27 cm height x 35 cm width x 6 cm depth). The bacteria in the volume of 50 ml of 0.1 OD₆₀₀ was added to HS/clay medium, sealed with a foil and incubated at 30°C for 48 hours. Subsequently, the wet mass was obtained by placing the produced wet BC/clay composite into a centrifuge tube and spinning the tube at 150xg followed by discarding of the liquid. This process was repeated three times. The growth of BC was evaluated by the mass yield of wet and centrifuged BC.

2.4.5. Investigation of leaching behaviour

The leaching behaviour of clay from BC/clay composite produced *in situ* started with obtaining the calibration curves measuring the absorbances of different concentrations of Cloisite Na⁺ and SWN clay, respectively. For this, the stock clay suspensions were diluted to the concentration ranging from 0.6 to 0.0019 mg/ml. The absorption values of the characteristic peak at the wavelength of 211 nm of each concentration were measured. Then, the graph showing the absorption versus the concentration was obtained.

BC/Cloisite Na⁺ and BC/SWN composites produced *in situ* using the large scale method were placed into a centrifuge tube containing 20 ml of distilled water, respectively. The tubes were shaken using the plate shaker at the speed of 140 rpm for 24 hours. The measurements were taken from 0 to 24 hours.

2.5. Growth of BC in chitosan environment

There were two ways to grow BC *in situ* with chitosan. Firstly, 0.5 wt.% of WA chitosan solution was added to HS medium, which already had 2 wt.% of glucose. Secondly, glucose was replaced with 0.5 wt.% of WA chitosan solution, which was then used as the main carbon source.

2.5.1. Preparation of chitosan solutions

The stock of 0.5 wt.% of chitosan solution was prepared in either 0.1M of acetic acid or in 10 vol.% of vinegar (obtained from Morrison's) both adjusted to pH3. Chitosan solution was stirred (Stuart US152) at 880 rpm and 25°C for 24 hours to ensure full dissolution. Prior to the addition to the medium, chitosan solutions were filter-sterilised by passing through 0.2 µm pore size filter.

2.5.2. Replacing glucose with a chitosan solution in HS medium

HS medium was produced and sterilised as described previously, but the sterile glucose solution was replaced with an equal volume of filter-sterilised chitosan solution, which was prepared using 0.1M of acetic acid, to giving a final concentration of chitosan inside HS medium of 0.25%.

2.5.2.1. Inoculation of *G. xylinus* with modified HS medium

The bacteria inoculum at a concentration of 0.1 OD₆₀₀ was added to either HS medium containing both glucose and 0.5 wt.% of WA chitosan solutions, or to the modified HS medium that consisted of 0.5 wt.% WA chitosan as the main carbon source. The inoculation was carried out on a large scale at pH5 for 48 hours at 30°C. The produced material was then called bacterial chitosan (BC-CH).

For the incubation of bacteria with WA chitosan as the main carbon source, the variety of pH ranging from 6 to 2 was adjusted using either sterile 0.1M sodium hydroxide or 0.1M acetic acid in order to increase or decrease the pH, respectively.

2.5.2.2. Investigation of leaching behaviour of BC/chitosan composites

The leaching behaviour of chitosan from the BC/chitosan composite, which was produced *in situ* using both chitosan and glucose, started with obtaining a calibration curve for chitosan. The chitosan solution was diluted to the concentration ranging from 0.5 to 0.0019 mg/ml. The absorption values of the characteristic peak at wavelength of 325 nm for each concentration were measured. Then, the graph showing the absorption versus the concentration was obtained.

Then, the BC/chitosan composite was placed into a centrifuge tube containing 20 ml of distilled water. The tubes were shaken using the plate shaker at the speed 140 rpm for 80 hours. Measurements of absorbances at 325 nm were taken from 1 to 80 hours.

2.5.3. Investigation of solubility of BC-CH

In order to investigate the solubility of BC-CH, 3 grams of the material were placed into the centrifuge tube containing 20 ml of vinegar at pH2. The tube was then shaken using the shaking plate at a speed of 140 rpm for 48 hours. After 48 hours, 1 ml of washing vinegar from the tube was measured using UV-VIS. The peaks of the washing vinegar were compared to pure chitosan and vinegar.

2.6. *Ex situ* modification of BC

Pure BC was modified *ex situ* using clay suspensions, chitosan solutions and chitosan/genipin hydrogel, respectively. The modification of BC was carried out by either immersion or vacuum self-assembly methods.

2.6.1. Oxidation of BC

In order to improve the attachment of chitosan to BC, 6 grams of pure BC were immersed into 100 ml of the oxidising solution that consisted of 0.5 wt.% of sodium metaperiodate for 20 minutes at 25°C. The beaker was covered with aluminium foil to allow sufficient oxidation to occur without significant effects on the crystallinity. Subsequently, oxidised BC was rinsed with distilled water to remove excess oxidant and then dried for 24 hours at 25°C before placing on Buchner funnel and treated as described Section 2.6.3.1.

2.6.2. Preparation of additive materials

2.6.2.1. Preparation of clay suspensions

Non-exfoliated and exfoliated by the Tefal blender SWN and Cloisite Na⁺ clay suspensions at a concentration of 6 mg/ml were prepared as described in Section 2.4.1.

Cloisite 10A, 15A, 20A, 30B and 93A organoclay with the concentration of 6 mg/ml were mixed in acetone and treated in the same way as the other non-exfoliated suspensions. Each of the clay suspensions was then incorporated into BC matrix by applying the vacuum self-assembly technique (Section 2.6.3.1).

2.6.2.2. Preparation of chitosan solutions

Each type of chitosan of low, medium molecular weight and WA chitosan were prepared with at 0.1M acetic acid as described in Section 2.5.1. WA chitosan was also dissolved in 10 vol.% of vinegar at a final pH3 using the same method as detailed in Section 2.5.1. All chitosan solutions were stored at 25°C until used.

2.6.2.3. Preparation of chitosan hydrogels

Once 0.5 wt.% of WA chitosan was dissolved in 100 ml of distilled water containing 10 vol.% of vinegar at pH3, 5.5 mg of genipin was added into the solution. Subsequently, the solution was stirred at 880 rpm speed for an hour. The solution was pumped through pure BC to allow hydrogel to form the matrix of BC (Section 2.6.3.1).

2.6.2.4. Introducing exfoliated Cloisite Na⁺ clay to chitosan hydrogels

After dissolving 0.5 wt.% of WA chitosan in 100 ml of distilled water containing 10 vol.% of vinegar at pH3, 50 ml of the chitosan solution were mixed with 50 ml of exfoliated by the Tefal blender for 16 minutes Cloisite Na⁺ clay suspension at a concentration of 3 mg/ml at ration 1:1. Then, 5.5 mg of genipin was added into the chitosan/clay mixture. Subsequently, the solution was stirred at 880 rpm for an hour. The solution was pumped through pure BC to allow hydrogel formed within the matrix of BC (Section 2.6.3.1).

2.6.3. Incorporation of additive materials into pure BC

The clay suspensions and chitosan hydrogel were incorporated into the matrix of BC by using vacuum self-assembly method, respectively. All chitosan solutions were incorporated into non-oxidised and oxidised BC using immersion and vacuum self-assembly techniques, respectively.

2.6.3.1. Vacuum self-assembly method

The following method allowed incorporation of a range of additives into already produced pure BC. These additives were: SWN, Cloisite Na⁺, Cloisites 10A, 15A, 20A, 30B and 93A organoclay, low, medium MW and WA chitosan solutions, chitosan/genipin and chitosan/genipin/clay hydrogels.

Pure bacterial cellulose was produced on a large scale and treated as described in Sections 2.2.2 and 2.2.3. A circle of pure BC measured 10 cm diameter, weighing approximately 6 grams, was aseptically cut and placed onto the wetted filter paper in a Buchner funnel to ensure equal absorption of the treatments into BC. Firstly, the circle was rinsed with 10 ml of distilled water. Then, clay suspensions, chitosan solutions, chitosan/genipin and chitosan/genipin/clay hydrogels were slowly passed through the BC matrix, respectively, under a vacuum. Genipin, 10 vol.% of vinegar, 0.1M of acetic acid and acetone were also passed through the BC, respectively. Once all the solutions or suspensions went through, the BC was rinsed with 10 ml of distilled water. Synthesised BC composites were aseptically cut into 2x2 cm squares and sterilised by autoclaving.

2.6.3.2. The immersion method

Samples of oxidised and non-oxidised BC were immersed into each type of 0.5 wt.% chitosan solution, respectively, for 30 minutes to allow chitosan to penetrate BC matrix. BC was removed from the solutions and gently washed with 10 ml of distilled water for either antibacterial assay experiment or left to dry for 24 hours at 25°C for further characterisation.

2.7. Antibacterial activity of modified bacterial cellulose

2.7.1. Bacterial strains used in antibacterial assays

A total of three isolates were used to test the antibacterial properties of all synthesised BC materials. These were methicillin-resistant *Staphylococcus aureus* (MRSA), *Escherichia coli* (*E. coli*) and *Pseudomonas aeruginosa* (*P. aeruginosa*). The experiments also included analysis of pure BC and oxidised BC as well as BC treated with 0.1M acetic acid, 10 vol.% vinegar and acetone, respectively, in order to investigate any antibacterial effect of different solvents, which were used to dissolve chitosan and disperse organoclay.

2.7.2. Production of bacterial lawns

Frozen culture of *E. coli*, MRSA and *P. aeruginosa* were maintained as described in Section 2.2.1. In order to produce the population for the experiments, the isolates were incubated from the frozen state onto TSA for 24 hours at 37°C. The obtained colonies were re-suspended in 10 ml of TSB. The bacterial suspensions were subsequently incubated by shaking (at 150 rpm) for 16-20 hours at 37°C. These overnight cultures were then diluted in phosphate buffered saline to a concentration of 0.1 OD₆₀₀ for all further experiments.

2.7.3. Antibacterial assay of the components incorporated into BC

The antibacterial activity of Cloisite Na⁺, SWN and WA chitosan alone was investigated against *E. coli* and MRSA, respectively. Due to their organophilic nature, organoclay cannot be dispersed in water. Therefore, the antibacterial properties of Cloisite 10A, Cloisite 15A, Cloisite 20A, Cloisite 30B and Cloisite 93A organoclay were studied against *E. coli*, MRSA and *P. aeruginosa*, respectively, using the pressed discs method^[206].

2.7.3.1. Antibacterial assay using clay suspensions

Once the overnight cultures of MRSA and *E. coli* were prepared as detailed in Section 2.7.2. The bacteria were re-suspended in PBS at a final concentration of 0.1 OD₆₀₀. Both sterile non-exfoliated and exfoliated by the Tefal blender Cloisite Na⁺ and SWN clay suspensions were added to the wells of a 96-well plate in the volume of 75 µl, respectively. Then, 75 µl of PBS-resuspended MRSA or *E. coli* were mixed with 75 µl of each type of clay. The final concentration of Cloisite Na⁺ and SWN within the bacterial suspension was 3 mg/ml, respectively. The control MRSA and *E. coli* in a total volume of 150 µl were added, respectively, into separate wells. Then, the controls and clay/bacteria suspensions were serially diluted in sterile PBS and incubated for 24 hours at 37°C temperature. After 24 hours, an amount of 20 µl of each dilution was placed on the surface of a TSA plate in triplicate and incubated at 37°C temperature for 24 hours. After 24 hours, a number of colonies were calculated in each dilution Section. In order to calculate CFU, the number of colonies obtained was multiplied by both the dilution factor and by 50 and, subsequently converted to percentage.

2.7.3.2. The disc diffusion method using compressed powder handmade discs

This method focused on using organoclay clay powder as discs due to the high organophilic nature of the clay. Powders of Cloisites 10A, 15A, 20A, 30B and 93A organoclay were pressed into discs by a hydraulic press (Specac's Atlas Series Manual Hydraulic Press) using 5-ton load configurations and subsequently stored at 25°C. The discs, which contained 2 grams of each type of clay, were subsequently sterilised using dry heat at 120°C for 15 minutes. Bacterial lawns were produced as described in Section 2.7.2. Each disc was aseptically placed on each TSA plate containing bacteria. The plates were incubated for 24 hours at 37°C. The zones of inhibition were subsequently determined.

2.7.3.3. Antibacterial activity of chitosan

WA chitosan solution at a concentration of 0.5 wt.% was prepared using 10 vol.% of vinegar as detailed in Section 2.5.1. Sterile glass cover slips were coated with the chitosan solution and air-dried for 24 hours at 25°C to allow acetic acid from the vinegar to evaporate. Subsequently, the cover slip coated with chitosan was further dried and sterilised using UV-Ozone (supplied by BioForce nanosciences) for an hour. Each cover slip was placed inside an empty petri dish.

Overnight bacterial cultures were obtained as described in Section 2.7.2. Overnight cultures of MRSA and *E. coli* (100 µl) were placed on the surface of the cover slip and covered with 2 × 2 cm sterile plastic lid, respectively. The lid was sterilised prior to the experiment by immersion into 100 vol.% ethanol for an hour and subsequently dried inside the plate drier at “full” power. For the control, a sample of each type of the bacterium in a volume of 100 µl was placed on the surface of an empty sterile cover slip and covered with the lid. Then, the petri dishes with all cover slips were stationary incubated in a humid environment in a sterile pyrex glass dish, which was covered with aluminium foil for 24 hours at 37°C. After 24 hours, the bacteria were washed from the cover slips using 3 ml of sterile PBS and serially diluted. An amount of 20 µl of each dilution was placed on the surface of a TSA plate in triplicate and incubated at 37°C temperature for 24 hours. After 24 hours, a number of colonies were calculated in each dilution Section. In order to calculate CFU, the number of colonies obtained was multiplied by both the dilution factor and by 50 and, subsequently converted to percentage. In each case, the number of the pre-treatment bacteria was determined in CFU/ml concentration.

2.7.4. Antibacterial activity of synthesised BC-based materials

Sterile 2 cm × 2 cm squares of both *in situ* and *ex situ* modified BC were placed into empty, without agar sterile petri dishes. The bacterial culture produced as

described in Section 2.7.2 in a volume of 100 μ l were gently placed on the surface of cellulose and covered with a 2 cm \times 2 cm plastic lid, which was sterilised by ethanol prior to the experiment. The control bacteria in the same volume of 100 μ l were placed on the surface of the empty, without agar petri dish and covered with the lid. All petri dishes were stationary located in a humid environment in a sterile pyrex glass dish, which was covered with aluminium foil. The dishes were stored at 37°C for 24 hours.

After 24 hours, petri dishes containing bacteria and cellulose were then washed by adding 3 ml of PBS. Subsequently, bacterial culture, cellulose and the lids were placed into a sterile stomacher bag and mixed by Stomacher (Seward) at “normal setting” for a minute. Bacterial suspensions from the stomacher bag were then serially diluted in fresh PBS in 1:10 fold dilution. Then, the bacterial suspensions from each dilution was placed on a surface of a TSA plate in a volume of 20 μ l and incubated at 37°C temperature for 24 hours. After 24 hours, a number of colonies were calculated in each dilution Section. In order to calculate CFU, the number of colonies obtained was multiplied by both the dilution factor and by 50 and, subsequently converted to percentage. In each case, the number of the pre-treatment bacteria was determined.

2.8. Synthesis of Kombucha cellulose

The washed culture was derived from Kombucha by placing 6 grams of SCOBY into a sterile stomacher bag and mixed by Stomacher (Seward) at “normal setting” for a minute. The washed isolated culture of microorganisms (IM) was used for the growth of Kombucha cellulose (KC) in further experiments.

2.8.1. Optimisation of KC growing conditions

The growing conditions of KC were optimised in both small and large scales. The small scale experiments were carried out using 24 well plates (Sarstedt, 1.55 mm diameter). Sterile pyrex dishes (27 cm height \times 35 cm width \times 6 cm depth) were

used for the large scale production. The effect of optical density, temperature, concentration of tea and type of a carbon source on the production of KC were analysed.

2.8.2. Preparation of tea

A teabag of Yorkshire tea was added to 200 ml of boiling water for 6 minutes. Tea was quantified by pH, ultraviolet-visible spectrophotometry (UV-VIS) and optical reflective index. Prepared tea was then autoclaved at 121°C for 15 minutes before mixing with either glucose or chitosan solution. After the addition of carbon source, tea was then called the tea broth.

2.8.3. Effect of OD on the growth of KC

The effect of optical density on the growth of KC was investigated by inoculation of IM at 0.1-2 OD₆₀₀ concentration with 1 ml of the tea broth containing 2 wt.% of glucose solution, respectively, at 25°C for 48 hours. The experiment was carried out on a small scale. Produced KC was centrifuged tube at 150xg followed by discarding of the excess liquid. This was repeated three times. The growth of KC was evaluated by the mass yield of wet and centrifuged produced KC.

2.8.4. The effect of temperature on the growth of KC

The effect of temperature on the synthesis of KC was investigated using IM at concentration of 2 OD₆₀₀. The IM suspension was inoculated with tea containing 2 wt.% of glucose solution at 25°C, 30°C and 37°C for 48 hours. The experiment was carried out on a small scale in 24 (1.55 mm diameter) sterile polystyrene plates. The growth of KC was evaluated by the mass yield of produced wet and centrifuged KC.

2.8.5. Effect of tea concentration on the growth of KC

Black tea was prepared as described in Section 2.8.2. The tea stock was diluted from 100 vol.% to 0 vol.% with sterile distilled water. Subsequently, 2 wt.% of glucose was added into each dilution. IM at a concentration of 2 OD₆₀₀ was inoculated with each tea concentration on a small scale for 48 hours at 25°C. The growth of KC was evaluated by the mass yield of produced wet and centrifuged KC.

For the large scale production, 50 ml of 2 OD₆₀₀ PBS re-suspended IM was mixed with 200 ml of either 75% of the tea broth or sterile distilled water. The dishes were subsequently covered with aluminium foil and incubated statically at 25°C for 48 hours.

2.8.6. Effect of pH on the growth of KC

The effect of pH on the synthesis of KC was investigated using IM at concentration of 2 OD₆₀₀. The IM suspension was inoculated with the tea broth containing 2 wt.% of glucose solution at pH ranging from 6 to 2, which were adjusted using either sterile 0.1M NaOH or 10 vol.% of filter-sterilised vinegar solution, at 25°C for 48 hours on a small scale. The growth of KC was evaluated by the mass yield of wet and centrifuged KC.

2.8.7. Effect of carbon source

IM at concentration of 2 OD₆₀₀ was inoculated into 75% of the tea broth containing either 2 wt.% of filter sterilised glucose or 0.5 wt.% of WA chitosan solutions, respectively. The inoculation of IM was carried out on both small and large scales. The plates were covered either with filter paper or the foil for the small or large scale experiments, respectively, and incubated for up to 48 hours at 25°C. The growth of KC was evaluated by the mass yield of wet and centrifuged KC.

2.8.8. Treatment of KC after incubation

KC produced on a small and large scales was treated by submerging statically within 0.1M NaOH at 80°C for an hour, and then, washed with distilled water until pH reached 7.

2.9. Growth of Kombucha in clay environment

The growth of KC in a clay environment was carried out using 75% of the tea broth containing either 2 wt.% of glucose or 0.5 wt.% of chitosan solutions as the main carbon sources. Each type of the tea broth was mixed with either non-exfoliated or exfoliated Cloisite Na⁺ or SWN suspensions at clay concentration of 3 mg/ml, respectively. IM at concentration of 2 OD₆₀₀ were inoculated with the tea broths, respectively, for 48 hours at 25°C in both small and large scales.

2.9.1. Inoculation of Kombucha with clay suspensions on a small scale

Each type of non-exfoliated and exfoliated clay suspensions at a final concentration of 3 mg/ml was mixed with the tea broth. Inoculation of IM was carried out by adding 100 µl of PBS re-suspended IM at 2 OD₆₀₀ to 3 ml of tea/clay suspensions. The inoculation was carried out in 24 well plates at 25°C for 48 hours. The growth of KC/clay composite was evaluated by the mass yield of wet and centrifuged material.

2.9.2. Inoculation of Kombucha with clay suspensions on a large scale

The large scale production was carried out by mixing a non-exfoliated suspension and the suspension exfoliated by the Tefal blender of Cloisite Na⁺ and SWN clay with 200 ml of the tea broth, respectively, at a final concentration of clay of 3 mg/ml. Inoculation of IM was carried out by adding 50ml of 2 OD₆₀₀ PBS re-suspended IM to the tea/clay suspensions and incubating into sterile pyrex dishes

(27 cm height x 35 cm width x 6 cm depth) that were sealed by aluminium foil at 25°C for 48 hours. The growth of KC/clay composite was evaluated by the mass yield of wet and centrifuged material.

2.9.3. Antibacterial activity of synthesised KC-based materials

The antibacterial activity of synthesised pure KC, KC/chitosan, KC/clay, KC/chitosan/clay composites were investigated against MRSA, *E. coli* and *P. aeruginosa*, respectively, as described in Section 2.7.3.

2.10. Characterisation of developed materials

2.10.1. Surface energy measurement

In order to determine surface energy, hydrophilic or hydrophobic nature and, therefore, leaching behaviour of pressed organoclay discs using for antibacterial assay (Section 2.7.3.2.), the contact angle of each material was investigated using sessile drop method by drop shape analyser (DSA, supplied by Kruss). Each pressed disc was placed on a stage of DSA. A drop with 4 µl of distilled water was added to the surface on the discs. The dynamic contact angle was recorded for 100 seconds. The experiment was carried out once.

2.10.2. Characterisation of chemical structure using Fourier Transform-Infrared spectroscopy (FT-IR)

The FT-IR equipment (Agilent Technologies, USA) was used to determine functional groups in the solid samples as well as to provide qualitative analysis of the presence of the additive material inside the final composites (Wavenumber region 650-4000 cm⁻¹). Each experiment started with the baseline correction. Dried solid samples were then suspended on the equipment surface for analysis. The analysis was repeated two times.

2.10.3. Powder X-Ray diffraction analysis

X-ray diffraction analysis (PANalytical, UK) was used to characterise the crystal structure of pure BC, BC-CH and chitosan powder. Operating conditions for each test were 40kV volts (X-ray beam), 35 mA current and 0° - 120° scanning angle range with a step of 0.0167. Prior to the experiment, samples were dried for 24 hours at 25°C and then compressed into plate holders, suspended on a stage and analysed with the powder diffractometer. The analysis was done once.

2.10.4. Solid state UV-VIS-NIR spectroscopy

The solid-state UV-VIS equipment (Jasco V, model V-670, serial number A018261154) used to determine the change in chemical structure in various samples in the region of 190-2500 nm. Solid materials were dried for 24 hours at 25°C and then placed inside the sample holder, which was closed tightly, and analysed. The experiment conditions included baseline correction with scanning speed of 1000 nm/min. The analysis was repeated three times.

2.10.5. Scanning electron microscopy

The microstructure and morphology of nanoparticles, BC, KC and their composites were investigated using scanning electron microscopy (SEM, JEOL). Samples were placed in a freeze dryer (Modulyo) submerged in liquid nitrogen and exposed to a vacuum pressure 4 atmospheres for up to 3 days (72 hours). Each freeze-dried sample was subsequently coated with 10 nm gold. The samples were analysed at different working distance from 10 mm to 4 mm. The experimental conditions included 6.5 mm working distance and 10.0 kV of accelerating voltage.

2.11. Investigation of mammalian cell cytotoxicity of developed materials

The mammalian cytotoxicity of non-exfoliated and exfoliated Cloisite Na⁺ and SWN suspensions, organoclay, chitosan and BC-based materials was investigated using NIH 3t3 cells. The MTT (3-(4,5-dimethylthiazol-2-yl)-2,5-diphenyltetrazolium bromide) tetrazolium reduction assay was the main cytotoxicity assay. The MTT assay is a colorimetric assay that measures the metabolic activity of cells^[207]. The assay is based on the ability of nicotine adenine dinucleotide (NADPH)-dependent cellular oxidoreductase enzymes to reduce the tetrazolium dye MTT to its insoluble formazan (Fig. 23)^[207].

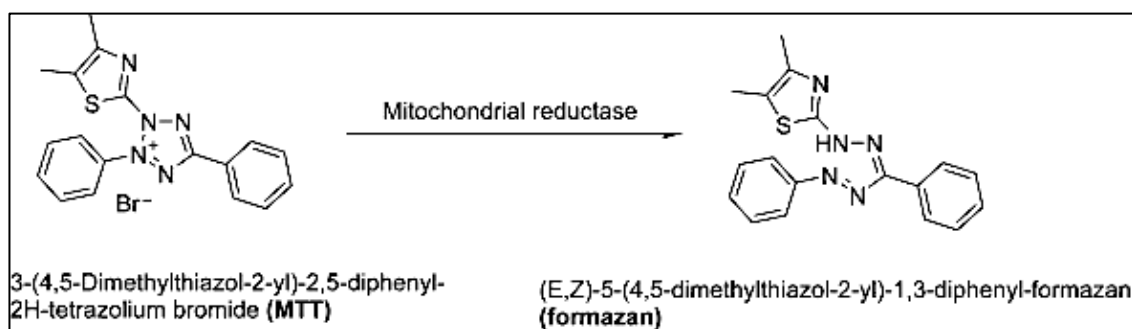


Figure 23. Reduction of MTT to formazan^[207].

During the assay, MTT enters the cells and becomes reduced by mitochondrial enzymes and lysosomal/endosomal compartments^[208]. Subsequently, MTT is transported to the surfaces of the cells to form needle-like MTT formazans^[207]. The quantity of formazan can be measured by the absorbance at 570 nm using a plate reading spectrophotometer^[207]. Dead cells lose their ability to convert MTT into formazan, therefore a difference in colour might be an indicator of the altered metabolic activity of cells. Metabolic active cells had dark purple colour, whereas non-active cells were colourless^[208]. However, the MTT reduction assay reflects the metabolism of viable cells, and is not direct measure of cell proliferation.

2.11.1. Maintenance of NIH 3t3 cells

The short-term storage of 3t3 cells was performed at -80°C . The cell pellets that were produced by centrifugation for 5 minutes at 150xg were re-suspended into 1 ml of the solution consisting of 900 μl of fetal bovine serum (FBS) and 100 μl of dimethyl sulfoxide (DMSO).

Dulbecco's modified medium (DMEM) was used to maintain 3t3 cells. DMEM was supplemented with a mixture of fetal bovine serum and penicillin-streptomycin antibiotic to give a final concentration of 10 vol.% and 1 vol.%, respectively.

2.11.2. Reviving 3t3 cells from frozen

Frozen 3t3 cells were thawed and diluted to 1:10 using the growth medium (DMEM). The cells were subsequently centrifuged at 150xg for 5 minutes. After centrifugation, cell pellets were re-suspended into 1 ml of fresh DMEM and then diluted to 1:6 using fresh DMEM. The cells were incubated in 25 cm^2 tissue culture flasks for up to 72 hours at 37°C .

2.11.3. Passaging of 3t3 cells

The passaging of 3t3 cells started with discarding the spent medium from flasks. Cells were subsequently washed once with sterile PBS and 1 ml of trypsin was added into the flask. The cells were then incubated for 5 minutes at 37°C . After 5 minutes of incubation, 9 ml of fresh DMEM was transferred into the flask. The cells were centrifuged at 150xg for 5 minutes. Cell pellets were re-suspended into 1 ml of fresh DMEM. Further passaging was carried out by diluting cells to 1:6 in fresh DMEM and incubating at 37°C .

Prior to the experiments, 3t3 cells were counted using a haemocytometer directly after centrifugation and re-suspension of cell pellets into 1 ml of fresh DMEM, but

before the passaging. After counting, the cells were seeded into sterile plasticware at appropriate concentrations, where 25,000 cell/ml was used for experiments in both 96-well plates and 24-well plates, respectively, whereas 350,000 cells/ml was used for the experiments in 6-well plates.

All biological waste was treated with 5 vol.% Trigene for 24 hours before autoclaving.

2.12. Mammalian cell cytotoxicity

2.12.1. MTT reduction assay

The metabolic activity of cells was determined by MTT reduction assay^[209]. MTT (3-(4,5-Dimethylthiazol-2-yl)-2,5-Diphenyltetrazolium Bromide) reagent was added to cells to a final concentration of 0.5 mg/ml. Cells were incubated for an hour at 37°C. Medium with MTT was then replaced with dimethyl sulfoxide (DMSO). Absorbance was measured using Gen5 plate reader and Gen5 software at 570 nm absorbance. Metabolically active cells were purple, whereas metabolically non-active cells were colourless. Therefore, this assay measures cell viability in terms of reduction of MTT as enzymatic conversion of the tetrazolium compound to formazan by dehydrogenases that occurs in the mitochondria of living cells^[208].

2.12.2. Effect of non-exfoliated clay suspensions on NIH 3t3 cells

NIH 3t3 cells were seeded at a concentration of 25,000 cells/ml in a volume of 100 µl per well in 96 well plates. Sterile 10A, 15A, 20A, 30B, 93A, SWN and Cloisite Na⁺ clay powders were added directly to the medium at a concentration from 0.09 to 6 mg/ml. The cells were incubated at 37°C for 24, 48 and 72 hours. The control without any treatments was also set up for each time frame. Metabolic activity of cells was measured by MTT reduction assay.

2.12.3. Effect of exfoliated clay suspensions on MTT reduction in 3T3 cells

Medium was mixed with Cloisite Na⁺ and SWN exfoliated clay suspensions in a volume of 100 µl per well at final concentrations of clay from 0.09 to 3 mg/ml, respectively. NIH 3t3 cells were seeded at a concentration of 25,000 cells/ml in 96-well plates. Cells were then incubated for up to 72 hours at 37°C. The metabolic activity of 3t3 cells was determined every 24 hours by MTT reduction assay and compared to untreated cells. Medium containing clay suspensions alone without the cells was also examined by the plate reader spectrometer. The effect of medium reduction on the MTT reduction of cells was measured by replacing medium with sterile PBS at the same dilution as with clay suspensions.

2.12.4. Effect of nanoparticles on 3T3 cell using coated slides

Glass coverslips were coated with 6 mg/ml of Cloisite 10A, 15A, 20A, 30B, 93A clay, respectively, and dried following sterilisation using UV-Ozone. Each coated slide was placed into each well of 6-well plates. A volume of 1 ml of NIH 3t3 cells at concentration 350,000 cells/ml were placed on the top of the cover slips and covered with 3 ml of fresh medium. Cells were incubated for 24 hours at 37°C. The metabolic activity of cells was measured by MTT reduction assay after 24 hours. The control was obtained by seeding the cells inside the empty wells of 6 well plates. The cells were also seeded on the top of the clear untreated cover glass.

2.12.5. Effect of chitosan on 3t3 cells

2.12.5.1. Addition of chitosan to culture medium

NIH 3t3 cells were seeded at a concentration of 25,000 cells/ml in a volume of 100 µl per well in 96 well plates. Sterile WA chitosan powder was added directly to the medium at a concentration of 5 mg/ml. The cells were incubated for 24 and 48 hours. Metabolic activity of the cells was measured by MTT reduction assay.

2.12.5.2. Effect of chitosan on 3T3 cell using coated slides

Cover slips were coated with 2 ml of 0.5 wt.% of WA chitosan solution, air-dried for 24 hours at 25°C and then dried for additional 6 hours using UV-Ozone (supplied by BioForce nanosciences). The cells were incubated with the coated cover slips for 24 and 48 hours at 37°C. The metabolic activity of cells was measured using MTT assay every 24 hours. The control was obtained by seeding the cells on the top of the clear untreated cover glass.

2.12.6. Effect of pure and modified BC on 3T3 cells

Sterile 1x1 cm squares of sterile pure BC and BC composites were soaked in 1 ml of fresh medium in 24 well plates for 24 hours prior to the actual experiment. Then, the medium was replaced with 1 ml per well of fresh medium containing 25, 000 cell/ml of 3t3 cells and incubated for up to 72 hours. The control was obtained by seeding the cells without any treatments. A metabolic activity of cells was measured by the MTT reduction assay every 24 hours.

2.13. Statistical analysis

Data were statistically analysed using Minitab software (Minitab, LLC, State College, Pennsylvania, USA; version 19.2.0.0). Statistical analysis was performed using either one-way ANOVA and Tukey test or a two-way ANOVA. A *P*-value of <0.05 was considered as statistically significant. Data represent the mean of experiments ± standard deviation.

Chapter 3. The growth of BC in clay environment

BC/clay composites were synthesised *in situ* by inoculating *Gluconacetobacter xylinus* (*G. xylinus*) ACCT53524 into HS medium containing one of two types of clay: Cloisite Na⁺ and SWN, respectively. Firstly, the growth conditions of pure BC were optimised on a small and large scales as described in Section 2.3. Then, exfoliated and non-exfoliated clay suspensions were added into the medium, respectively, inoculated with bacteria and incubated for 48 hours at 30°C. The synthesised BC/clay composites were investigated by the mass yield and UV-VIS-NIR (near IR) spectroscopy. The antibacterial activities of clay and BC/clay composites were studied against MRSA and *E. coli* (NCTC 12493). The cytotoxicity of clay and the composites were investigated using 3t3 fibroblast cells.

3.1. Results

3.1.1. Optimisation of BC growing conditions on a small scale

The first stage of synthesis of BC was the optimisation of initial bacterial inoculum. In order to achieve this, the bacteria were diluted in a range from 0.1 to 1.9 OD₆₀₀ of *G. xylinus* using PBS and streaked onto on HS agar plates. The bacterial colonies started to appear on the agar after 48 hours. Subsequently, the concentration of bacteria was calculated. A calibration curve was obtained (Fig. 24). The purpose of the calibration curve was to quantify the concentration of bacteria and to obtain the reproducible data. R² was 96%, which means that the relatively good linear relationships were obtained. This curve was used for the subsequent experiments to determine bacterial concentration.

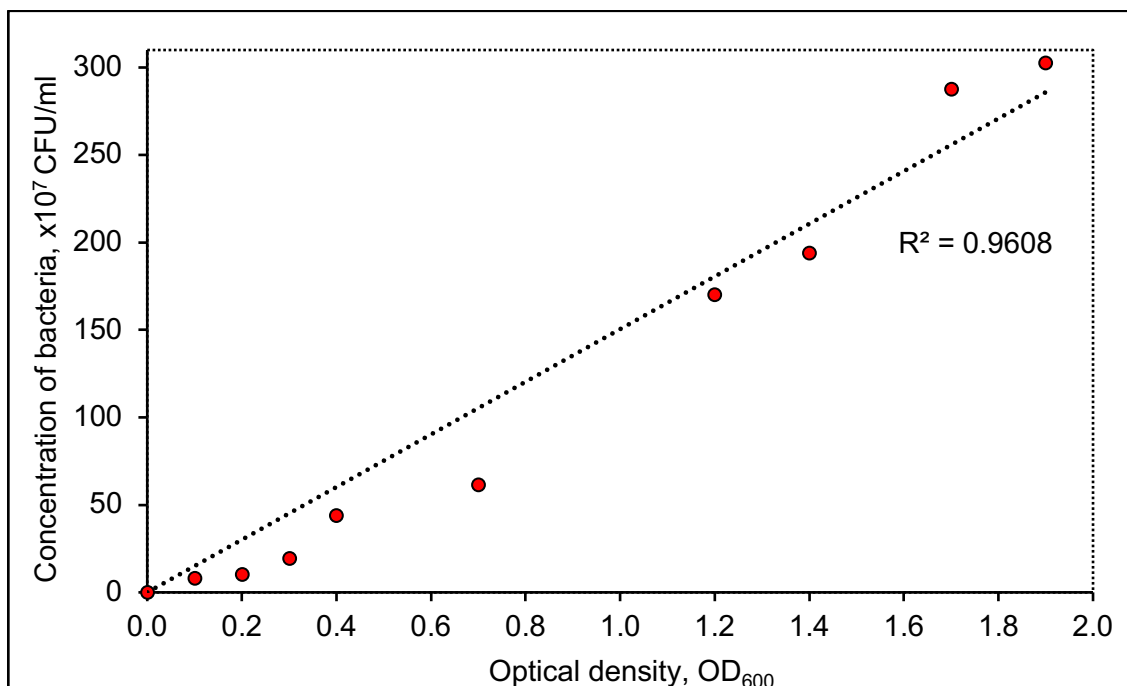


Figure 24. The relationship between OD₆₀₀ and concentration of *Gluconacetobacter xylinus*. The bacteria were incubated on HS plates for 48 hours at 30°C.

The wavelength of 600 nm of optical density was chosen because this wavelength is a relatively safe for bacterial cells^[210]. Due to the limited space of the 6-well plate and the concentration of nutrients, a relatively high bacterial number could have a negative effect on BC growth. An increase in the population of bacteria can lead to depletion of nutrients with time. It has been reported that the bacteria exhibited chemotactic behaviour and started to move towards the regions with higher nutrient concentration, which were observed to be at the edges of the medium, leaving the dead or dying cells behind in the centre^[211]. Because of this, the range from 0.001 to 0.5 OD₆₀₀ of *G. xylinus* was chosen for further investigation.

The synthesis of BC was carried out for 48 hours at 30°C. After the synthesis, BC (a pellicle) was aseptically transferred into plastic weighing boats and dried for 48 hours at 37°C. Fig. 25 shows the samples of BC in both wet and dry states, respectively.

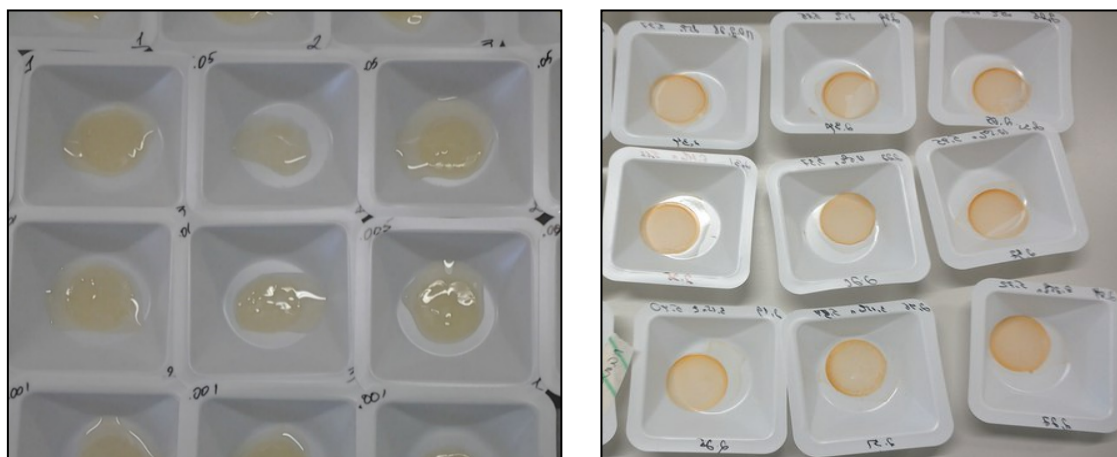
**Wet BC produced on a small scale****Dried BC produced on a small scale**

Figure 25. Images of wet (left) and dried (right) BC. BC was produced using an inoculum of 7.9×10^7 CFU/ml bacterial concentration at 30°C on a small scale for 48 hours.

The mass of dried BC at concentrations ranging from 0.001 to 0.5 OD_{600} was measured with the results shown in Fig. 26. There was little change in cellulose production from 0.001 to 0.005 OD_{600} , where the mass of synthesised BC was 0.06 grams. However, starting from 0.1 OD_{600} , the mass of BC increased. The mass of dried BC was greater for 0.1 and 0.5 OD_{600} and corresponded to 0.7 and 0.8 grams, respectively. In order to be conservative and avoid overpopulation of the bacteria in further experiments, the optical density of 0.1 OD_{600} , which corresponded to approximately 7.9×10^7 CFU/ml, was chosen.

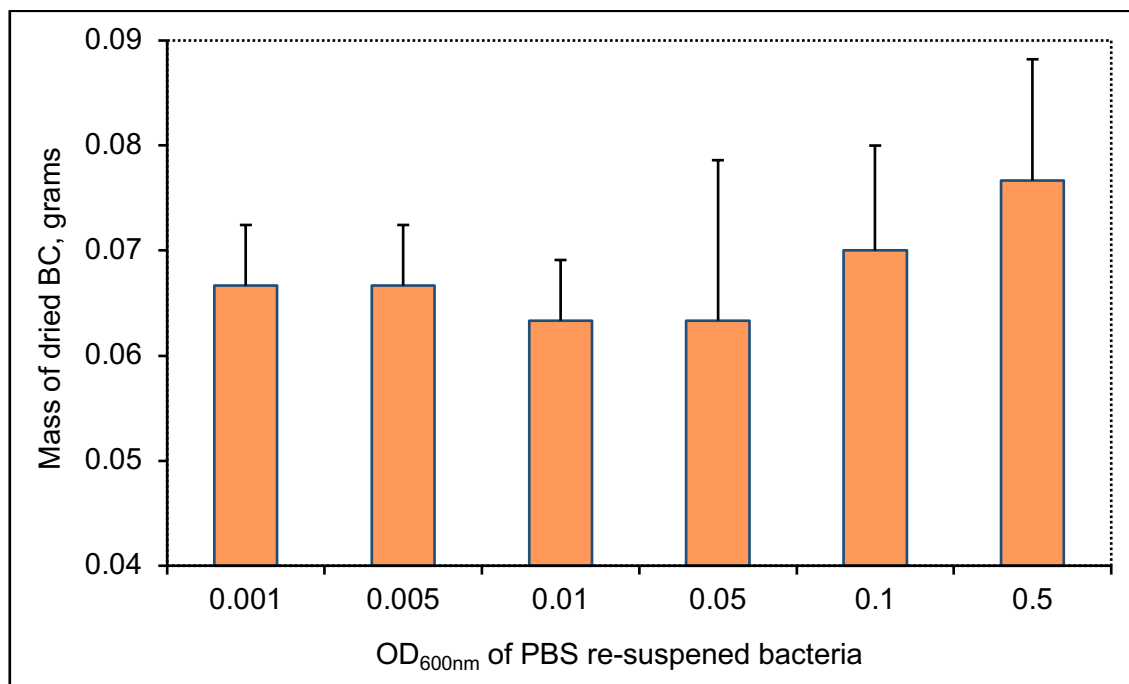


Figure 26. The effect of bacterial density on BC growth. The suspension of *G. xylinus* at 0.5-0.001 OD₆₀₀ was incubated in HS medium on a small scale for 48 hours at 30°C. Data shown represent the mean of three independent experiments with error bars of standard deviation. The mass obtained using 0.001 OD bacterial suspensions was compared to other OD. There is no statistically significant difference in data presented.

The effect of temperature on BC growth was investigated. *G. xylinus* was inoculated at a concentration of approximately 7.9×10^7 CFU/ml on a small scale at 25°C, 30°C and 37°C temperature. The BC produced was measured at both wet and dried states (Figs. 27-28). According to Fig. 27, the most effective temperature for BC growth was 30°C with the mass reaching 2.7 grams. Whereas, the mass of wet BC produced at 25°C and the 37°C temperature was 1.9 grams and 1.4 grams, respectively.

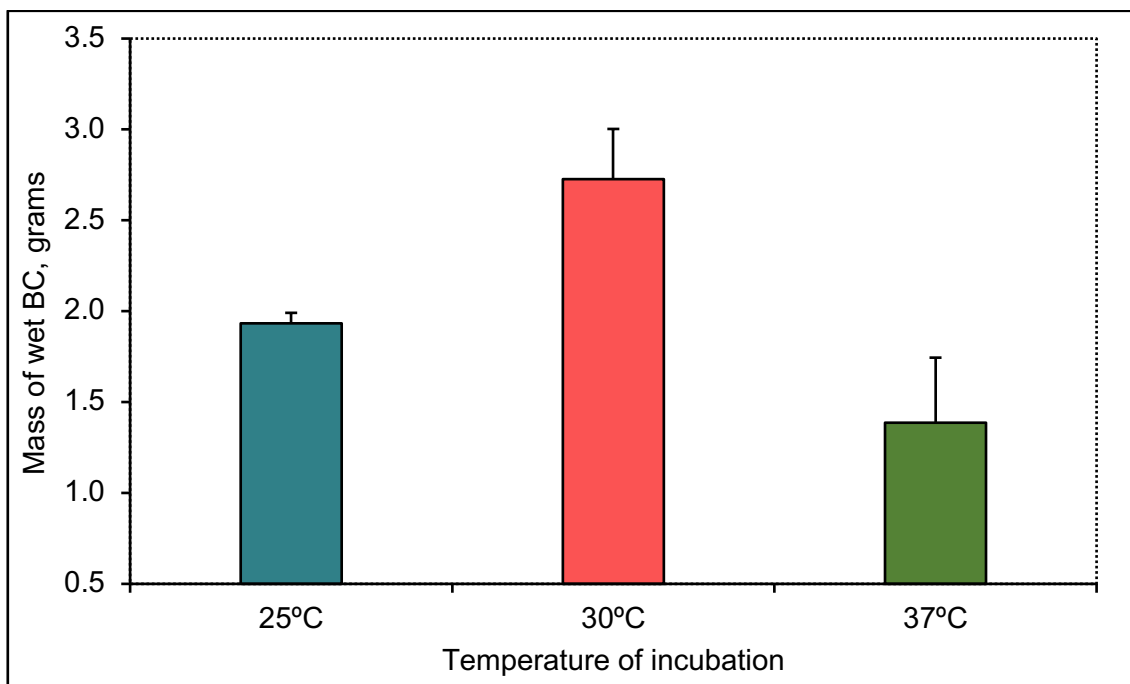


Figure 27. The mass of wet BC produced at 25°C, 30°C and 37°C temperature on a small scale. BC was produced using an inoculum of approximately 7.9×10^7 CFU/ml bacterial concentration. The bacteria were incubated for 48 hours on a small scale. Data shown represent the mean of three independent experiments with error bars of standard deviation. Temperature of 25°C was compared to either 30°C or 37°C. There is no significant difference between the temperatures.

The mass of dried BC produced at 25°C, 30°C and 37°C temperature is shown in Fig. 28. Similar to wet BC, the mass of dried BC produced at 30°C was the heaviest and reached 0.07 grams. Whereas the mass of BC synthesised at 25°C and 37°C was 0.023 grams and 0.056 grams, respectively. Therefore, the optimum temperature for BC growth was found to be 30°C. The temperature of 25°C has less extent of decrease in the mass of synthesised BC, whereas increasing the temperature to 37°C has pronounced negative effect on the growth of cellulose. Henceforth, bacteria at a concentration of approximately 7.9×10^7 CFU/ml were inoculated at 30°C in further experiments.

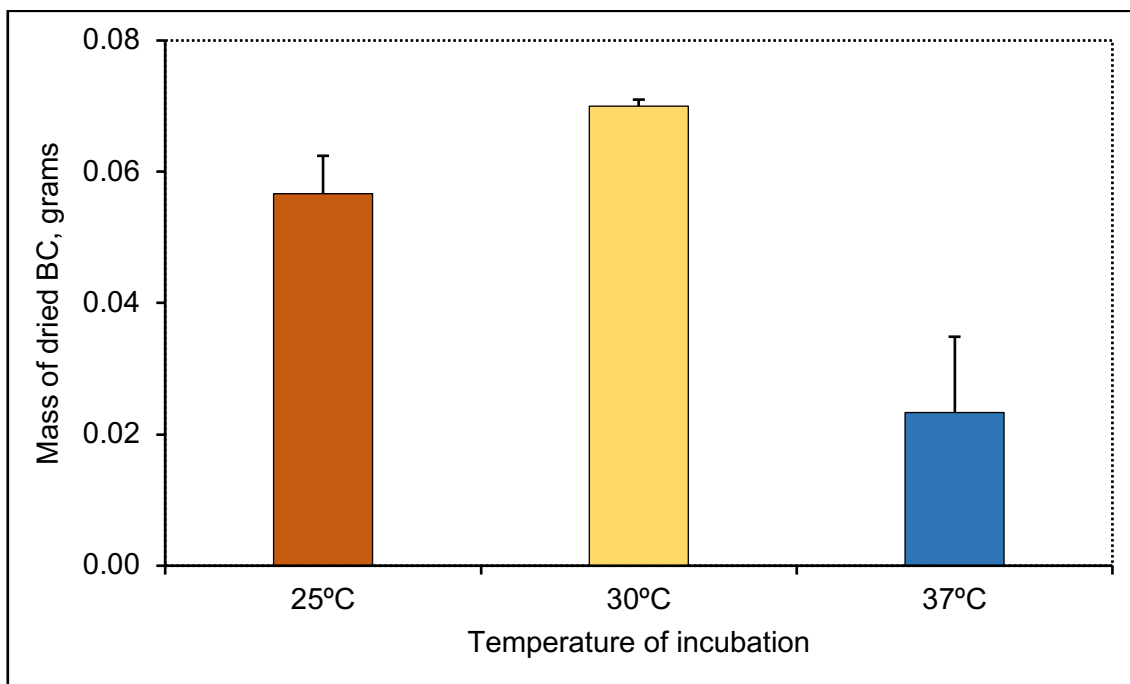


Figure 28. The effect of temperature on the mass of dried BC. BC was produced using an inoculum of approximately 7.9×10^7 CFU/ml bacterial concentration. The bacteria were incubated for 48 hours on a small scale. Data shown represent the mean of three independent experiments with error bars of standard deviation. The data of either 30°C or 37°C was compared to 25 °C. Data obtained at 30°C and 37°C are significantly different from 25 °C (P -value < 0.01).

The effect of time of incubation on the synthesis of BC was also investigated. The bacteria at a concentration of 7.9×10^7 CFU/ml were inoculated at 30°C for 24, 48 and 72 hours. The mass of wet and dried BC was measured in different times (Figs. 29-30). As shown in Fig. 29, the heaviest mass of wet BC was 2.43 grams after 48 hours. The lightest mass of BC was 2.08 grams after 24 hours. The mass of produced cellulose slightly reduced to 2.33 grams after 72 hours.

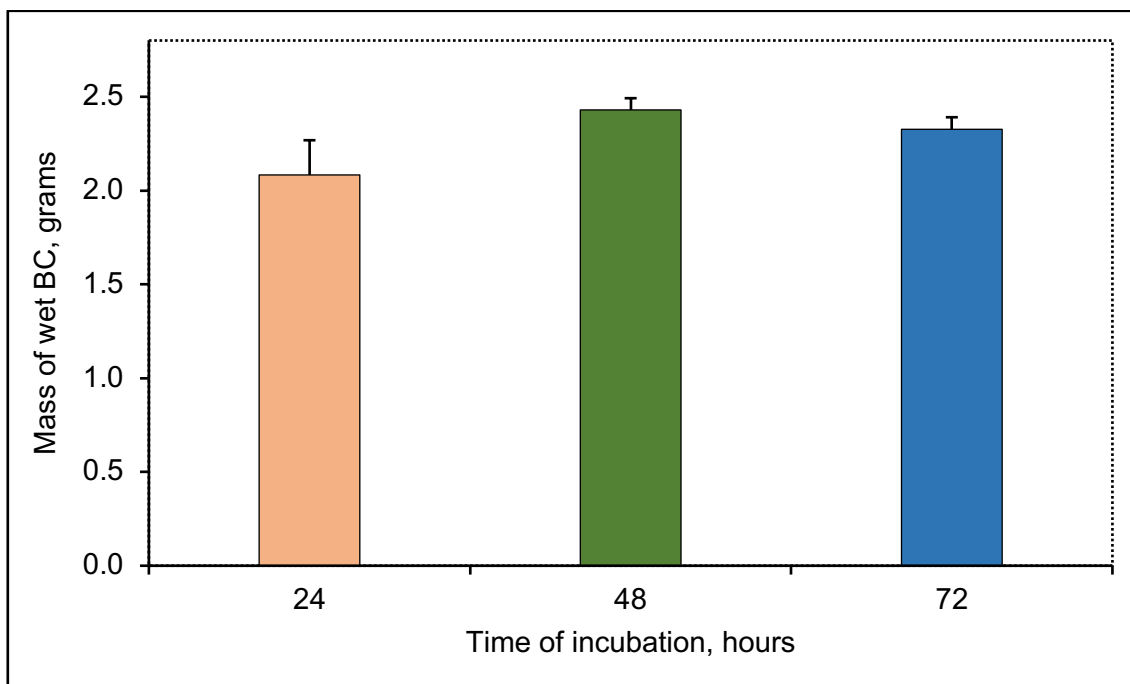


Figure 29. The mass of wet BC produced after 24, 48 and 72 hours on a small scale. BC was produced using an inoculum of approximately 7.9×10^7 CFU/ml at 30°C . Data shown represent the mean of three independent experiments with error bars of standard deviation. The mass obtained after 24 hours was compared to mass produced after either 48 or 72 hours. The data are not significantly different.

As shown in Fig. 30 of the dried samples, the mass of dried BC was 0.06 grams after 24 hours. The mass increased to 0.07 grams after 48 hours and remained almost unchanged for 72 hours. Therefore, the minimum mass of BC was observed after 24 hours, which might be due to the growth process not yet being completed. The synthesis of BC on a small scale was most productive after 48 hours. However, the formation of BC stopped after 48 hours due to the fact that there was no further increase in dried mass at 72 hours. Therefore, 48 hours of incubation was chosen for the synthesis of BC on a small scale in the subsequent studies.

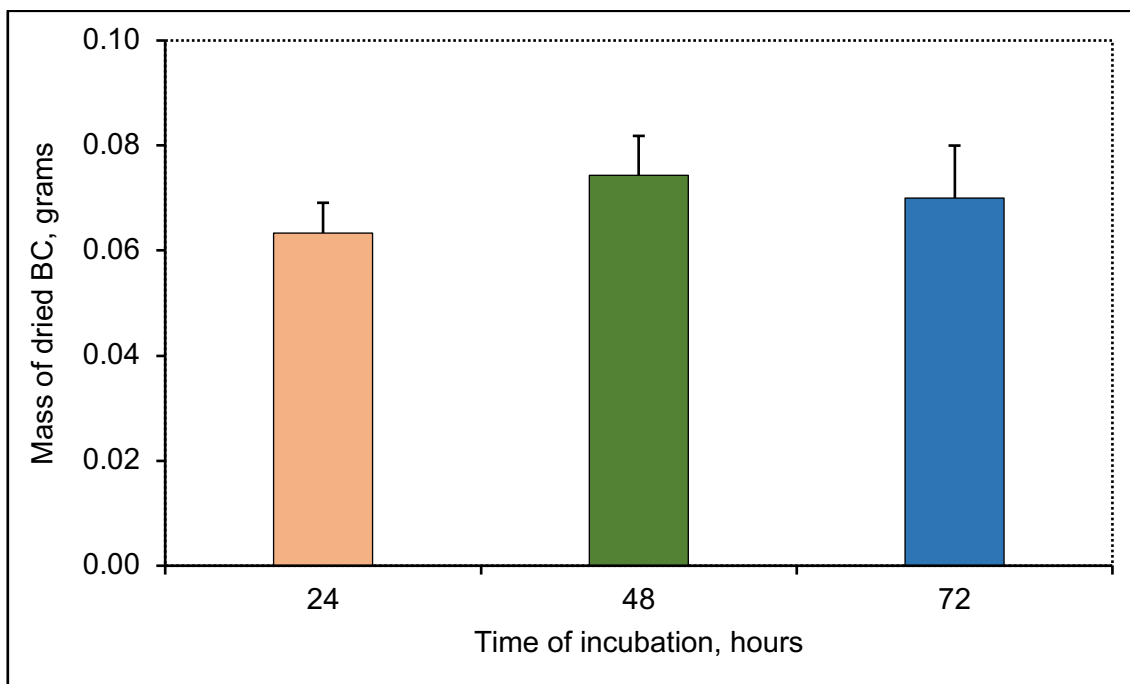


Figure 30. The mass of dried BC produced after 24, 48 and 72 hours on a small scale. BC was produced using an inoculum of approximately 7.9×10^7 CFU/ml at 30°C . The data shown represent the mean of three independent experiments. Data shown represent the mean of three independent experiments with error bars of standard deviation. The mass obtained after 24 hours was compared to mass produced after either 48 or 72 hours. The data are not significantly different.

Due to the variation of the standard carbon source in the subsequent experiments, the effect of concentration of glucose on the formation of BC was studied by replacing it with distilled water. As standard medium contains 2 wt.% of glucose, this concentration was chosen as the control. According to Fig. 31, the reduction of concentration of carbon source to 50%, which was corresponded to 1 wt.% of glucose inside the medium, has affected the BC growth. The formation of BC decreased rapidly within the reduction of concentration of carbon source under the constant amount of nitrogen source. As shown in Fig. 26, the reduction of glucose to 1.94 wt.% has not affected the biosynthesis of BC. The concentration of 1 wt.% of glucose resulted in a reduction of a mass of a pellicle from the control of 0.07 grams to 0.02 grams. This confirms the results obtained in Figs. 29-30, in which the growth of BC has stopped after 48 hours. The lack of sufficient carbon source appears to be the main reason for un-effective BC growth after 48 hours.

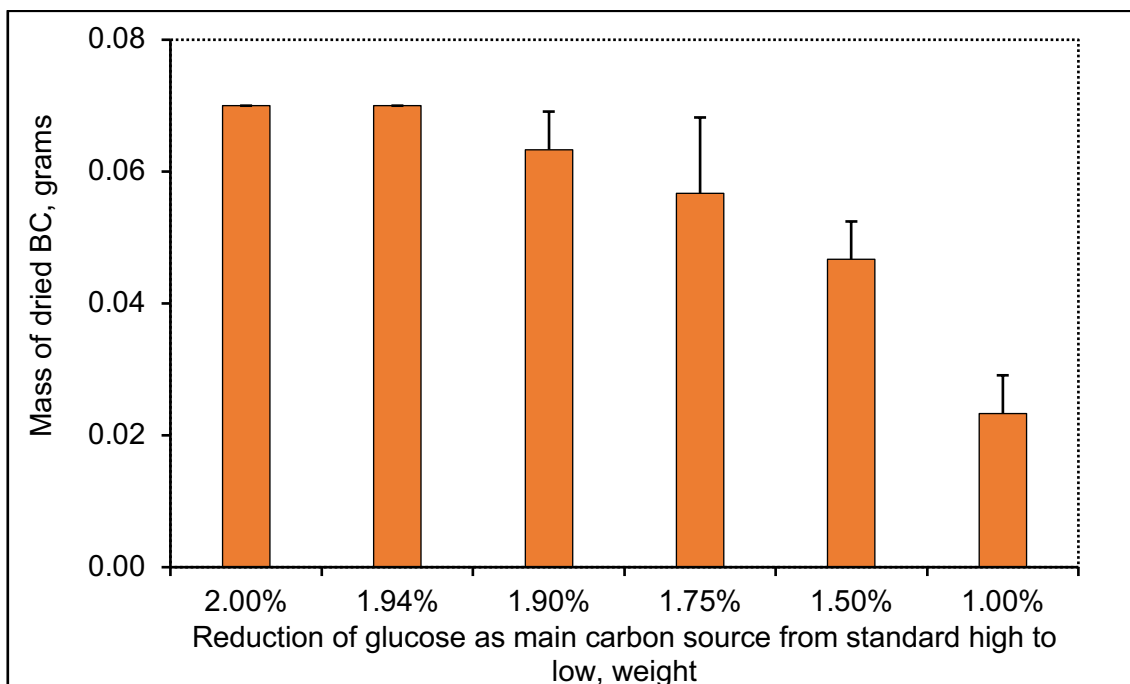


Figure 31. Effect of glucose on BC growth. Glucose was reduced from 2 wt.% of the standard (control) to 1 wt.%. Bacteria were incubated on a small scale using 7×10^7 CFU/ml inoculum concentration at 30°C for 48 hours. Data shown represent the mean of three independent experiments with error bars of standard deviation. The control (2 wt.%) is significantly different to both 1.5% and 1% treatments with P -value < 0.01, respectively.

The parameters for the synthesis of BC were optimised in small scale experiments. The chosen bacterial concentration was 7.9×10^7 CFU/ml. The incubation parameters were: 30°C temperature, 48 hours of incubation and HS medium containing 2 wt.% glucose. Based on the obtained results, the concentration of glucose for the synthesis of the original BC was chosen to be 2 wt.% for further experiments.

3.1.2. Synthesis of BC on a large scale

The effect of 24, 48, 72 and 96 hours of incubation on the growth of BC was investigated on a large scale using fixed parameters such as approximately 7.9×10^7 CFU/ml bacterial concentration, 30°C temperature and HS medium with

2 wt.% of glucose. As shown in Fig. 32, the BC yield increased from 24 to 96 hours. The pellicle, which was produced within 24 hours, was thin and did not cover the whole surface. The structure of cellulose was not robust enough after 24 hours. Starting from 48 hours, BC reached sufficient thickness. BC was much denser and thicker compared to others after 96 hours.

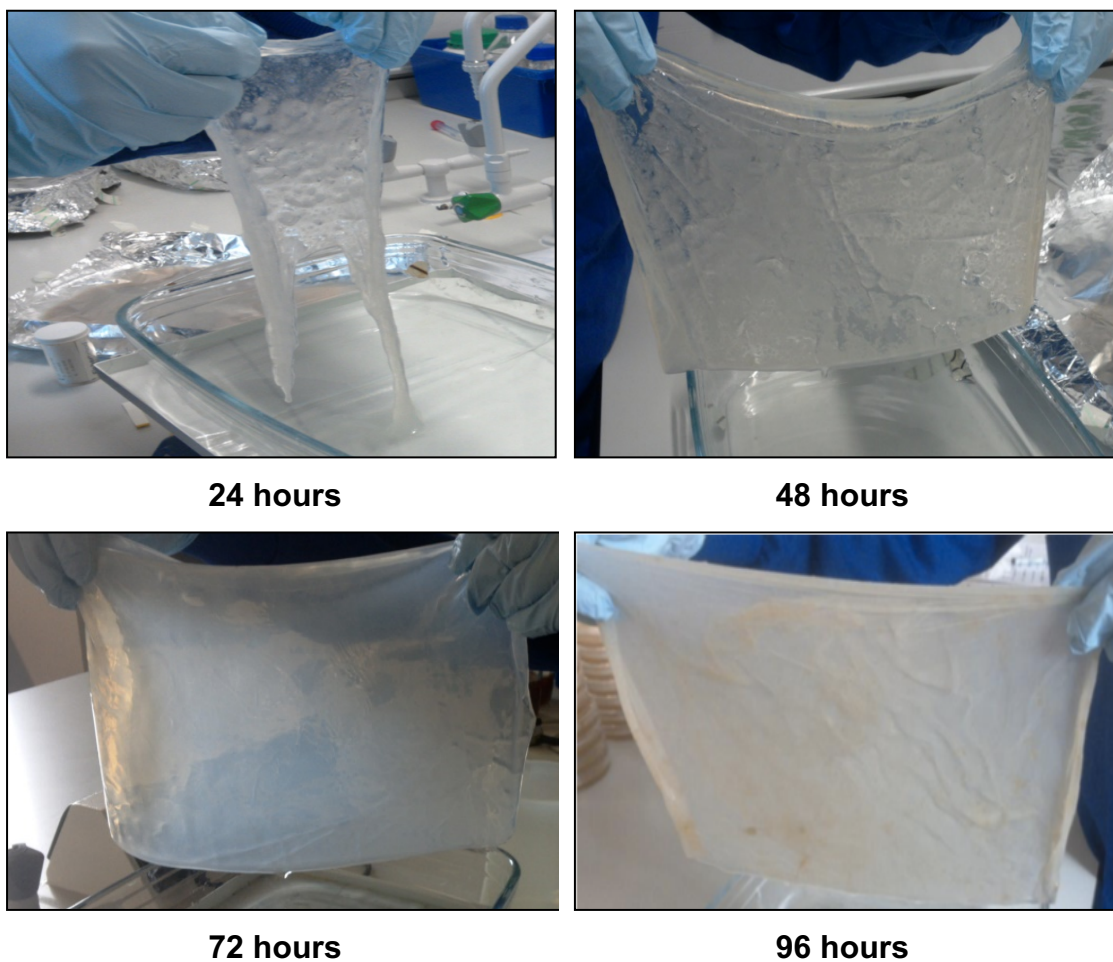


Figure 32. The effect of the time of incubation on the synthesis of BC on a large scale using 7.9×10^7 CFU/ml bacterial concentration at 30°C.

The yield of wet BC was measured. As shown in Fig. 33, the mass of wet BC was 140 grams after 48 hours, then increased to 182 grams and 196 grams after 72 and 96 hours, respectively.

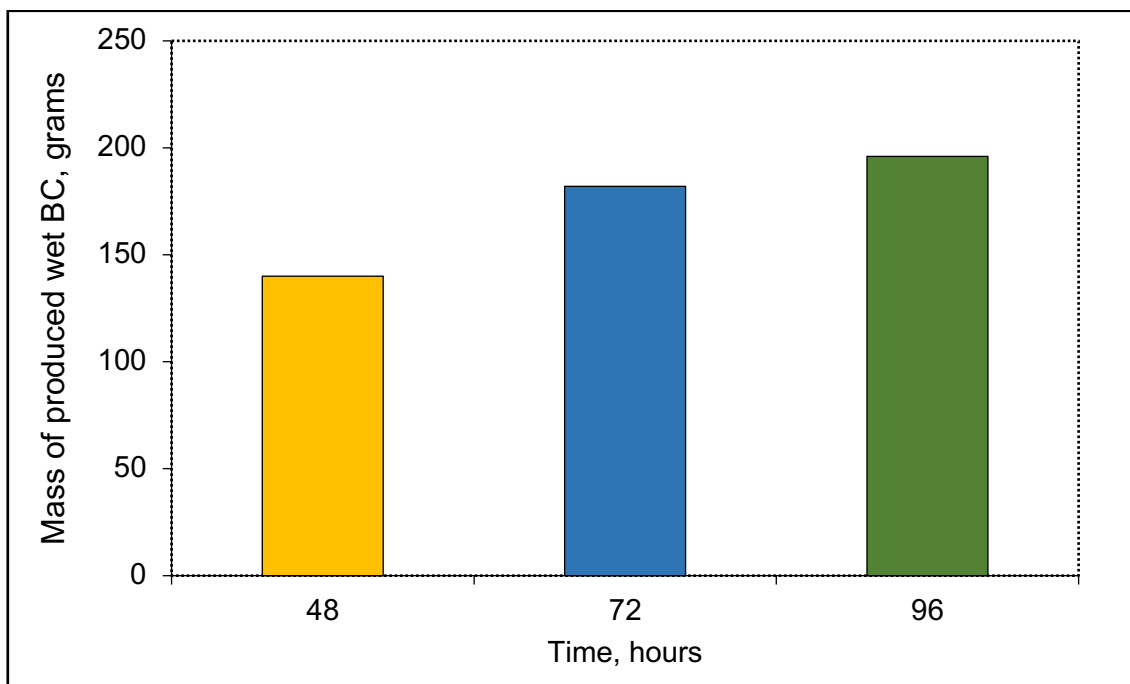


Figure 33. The effect of incubation time on the mass of wet BC on a large scale. BC was produced using an inoculum of 7.9×10^7 CFU/ml at 30°C for 48, 72 and 96 hours. Data shown represent the mean of a single experiment.

3.1.3. Investigation of clay suspensions for *in situ* modification of BC

Both Cloisite Na^+ and SWN clay suspensions were used for *in situ* modification of BC. Each suspension contained 6 mg/ml of a clay. The suspensions were used at either non-exfoliated or exfoliated states. In order to obtain a uniform exfoliated suspension, clay exfoliation was investigated using magnetic stirring, ultrasonication and blending techniques, respectively.

3.1.3.1. The morphology of the clay

The morphology of Cloisite Na^+ and SWN were studied using SEM as detailed in Section 2.10.5. Fig. 34 shows SEM images of dispersed and then freeze-dried clay particles. Both clays had similar layered structure, but different in aspect ratio. SWN has a smaller aspect ratio than Cloisite Na^+ .

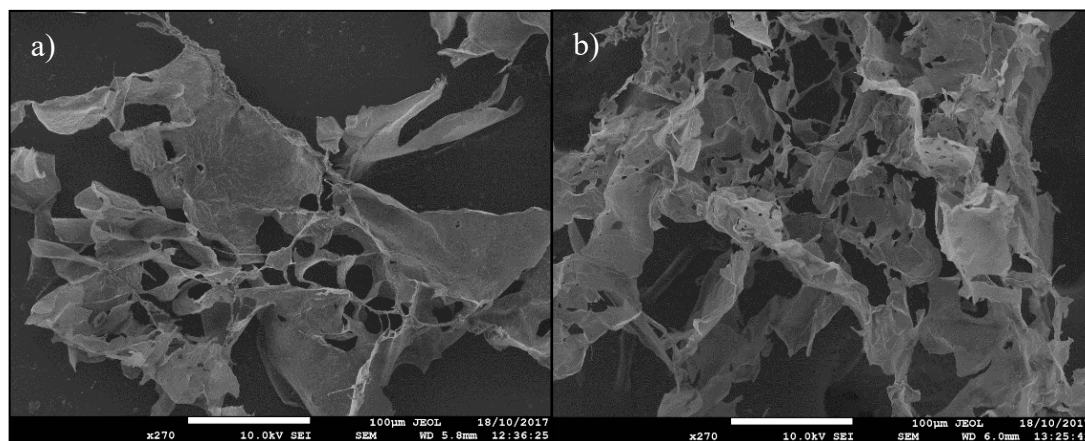


Figure 34. SEM images of a) Cloisite Na⁺ and b) SWN clay. The bars represent a distance in 100 µm.

3.1.3.2. Exfoliation of Cloisite Na⁺ clay suspensions

The process of exfoliation was based on disassociating aggregates of clay particles followed by breaking van der Waals and electrostatic forces between the layered structure in order to obtain individual delaminated silicate layers. Cloisite Na⁺ clay suspensions at a fixed concentration of 6 mg/ml were investigated using mechanical exfoliation methods by applying magnetic stirring, ultrasound and a Tefal blender, respectively. The extent of clay exfoliation was studied by DLS (Dynamic Laser Scattering). The success of these techniques on achieving the exfoliated state of the suspension was evaluated.

3.1.3.2.1. Analysis of Cloisite Na⁺ clay suspensions without exfoliation treatment

The exfoliation of Cloisite Na⁺ suspensions started with an analysis of the non-exfoliated state of the clay, which was prepared as described in Section 2.4.1. This allowed the comparison of the efficiency of different exfoliating techniques. Fig. 35 shows DLS results of Cloisite Na⁺ clay suspension without exfoliation treatment. The 43% and 42% of the total volume of particles were in 1584 and 1165 nm size range, respectively. The results indicated that the suspension was

non-uniform with extensive aggregation of micro-sized particles. An aggregation is a cluster of particles.

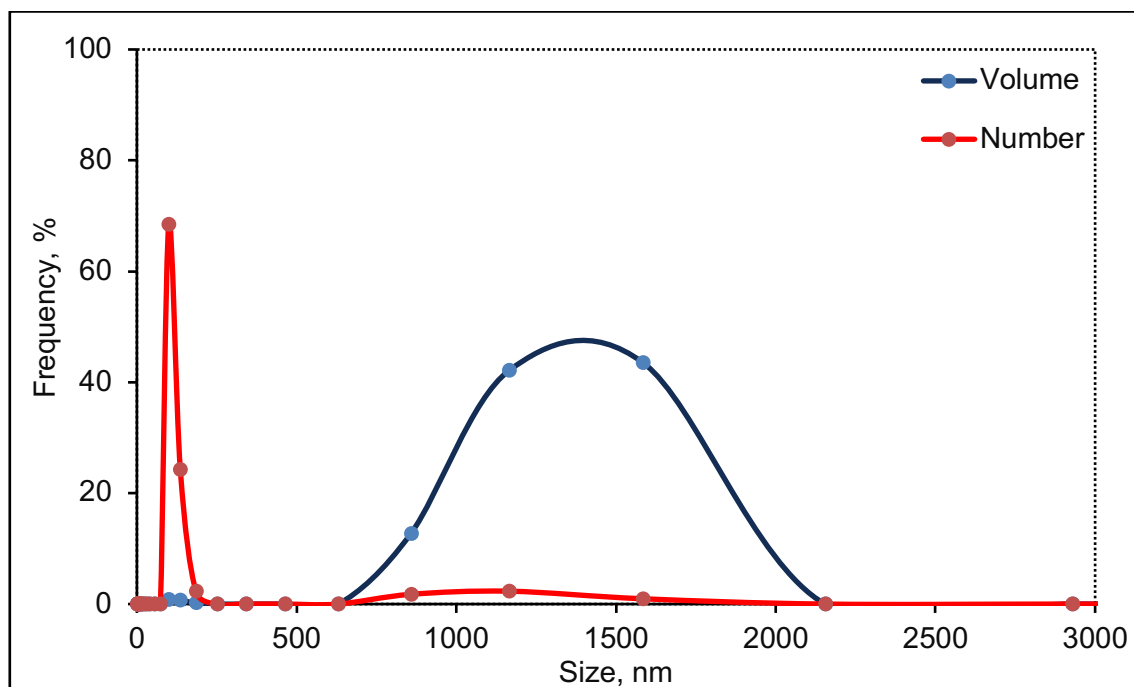


Figure 35. The particle size distribution of Cloisite Na⁺ clay suspension at concentration of 6 mg/ml without exfoliation treatment.

3.1.3.2.2. Exfoliation of Cloisite Na⁺ suspension through magnetic stirring

The suspension was then stirred for 16 minutes using magnetic stirring at speed of 880 rpm. As shown in Fig. 36, the differences in number and volume frequency became less broad compared to the control (Fig. 35). The number and volume distribution were similar range close to 857 nm. This means that micro-sized clay particle aggregations have disappeared. The suspension was more homogenous than the control, but it was not exfoliated.

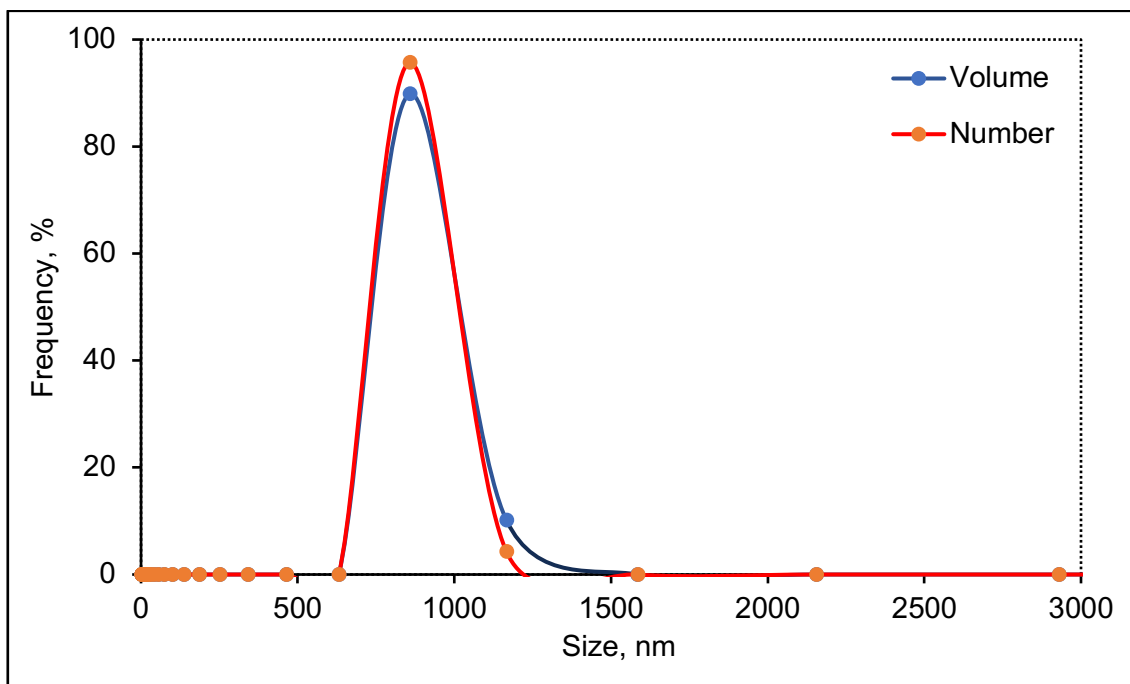


Figure 36. The particle size distribution of Cloisite Na⁺ suspension exfoliated using magnetic stirring. The suspension at 6 mg/ml concentration of clay was stirred at 880 rpm for 16 minutes at 25°C.

3.1.3.2.3. Exfoliation of Cloisite Na⁺ suspension through high power sonication

The next technique applied was ultrasonication of the initial suspension for 16 minutes using the amplitude of 85%. The process of ultrasonication was based on cavitation, which may break the layered structure of nanoparticles. As shown in Fig. 37, there were two peaks in volume distribution, second of which indicated the presence of micro-sized clay particle aggregations ranging from 1164 and 1584 nm. The results showed that number distribution of particles has significantly reduced compared to the control. However, the suspension was not only non-exfoliated, but contained large quantity of micro-sized particle aggregations.

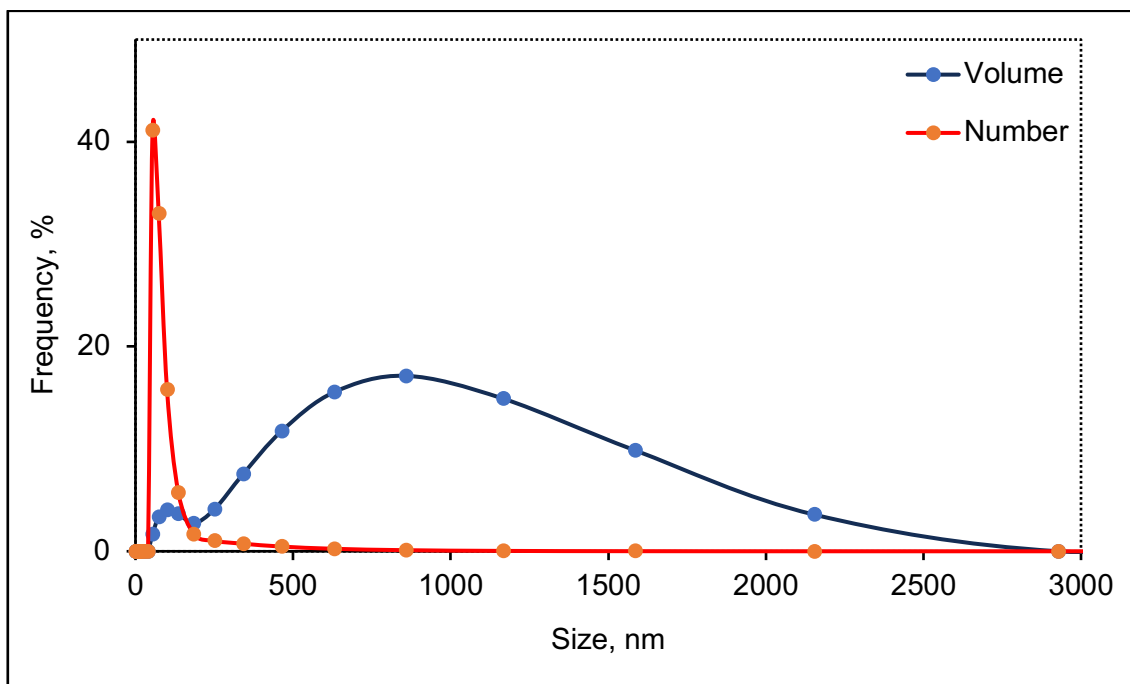


Figure 37. The particle size distribution of Cloisite Na⁺ suspension exfoliated using ultrasound. The suspension at 6 mg/ml concentration of clay was sonicated for 16 minutes.

3.1.3.2.4. Exfoliation of Cloisite Na⁺ suspension through blender

Cloisite Na⁺ suspensions were exfoliated using a Tefal blender as described in Section 2.4.1.1. The Tefal blender came with several attachable grinders. In the current research, two types of grinder were used: a chopper grinder (red) and coffee grinder (brown) (Fig. 38). The coffee grinder had the double-pronged blade at the bottom, whereas the chopper's blade had horizontal Z-shape. The efficiency in clay exfoliation of both grinders was investigated.

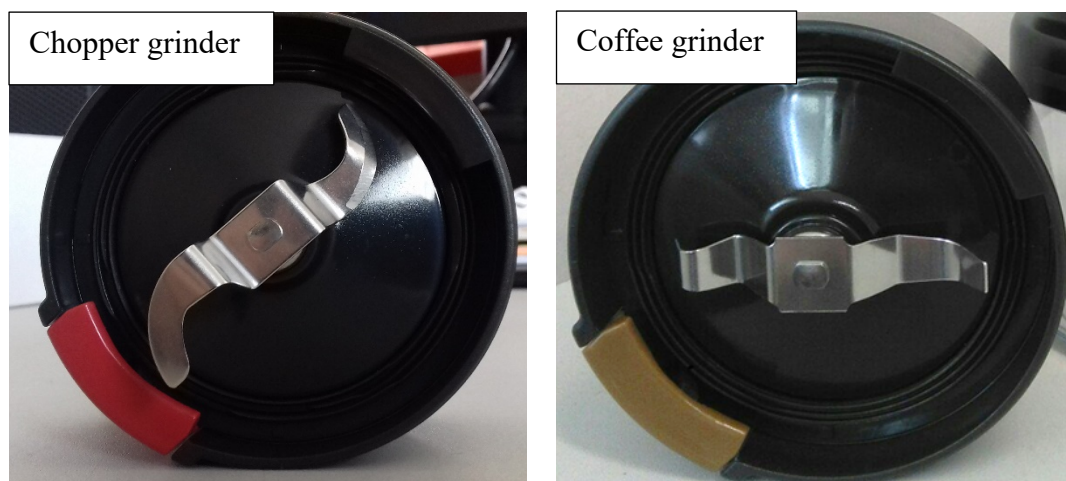


Figure 38. The structure of blades of the chopper grinder (red; left picture) and coffee grinder (brown; right picture).

Firstly, the clay suspension was treated using the red chopper grinder. As shown in Fig. 39, the total number of particles were in the range from 135 nm to 1165 nm. The total volume consisted of particles of size from 185 nm to 1165 nm. This means that the suspension contained micro-particle aggregations.

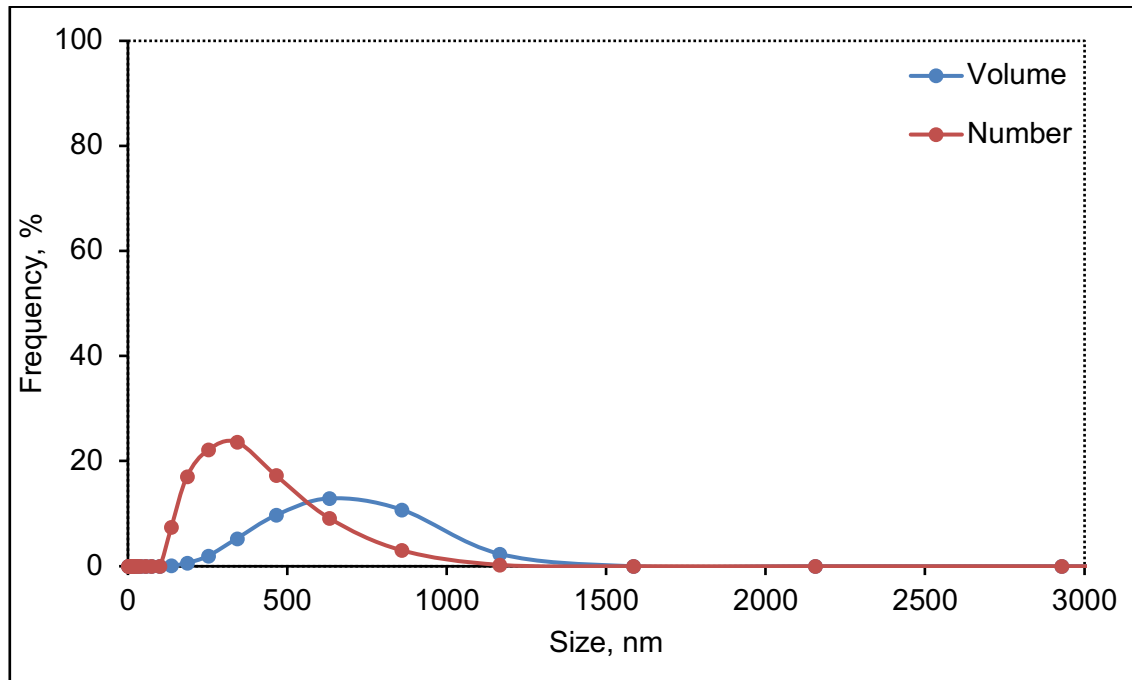


Figure 39. The particle size distribution of Cloisite Na⁺ suspension exfoliated using Tefal blender. The suspension at 6 mg/ml concentration of clay was blended for 16 minutes at speed 1.

The effect of the coffee grinder on exfoliation of the clay was studied. Figs. 40a and 40b shows the same DLS result of Cloisite Na⁺ suspension treated with the coffee grinder for 16 minutes at speed 1. As shown in Fig. 35b, 16 minutes was enough in order to achieve the uniformly exfoliated suspension, where 85.3% of the total volume consisted of particles at a size of 2.5 nm. The results showed that micro-sized clay particle aggregations have disappeared. The suspension was fully exfoliated. According to Figs. 39 and 40, the coffee grinder was more effective in exfoliation of the clay than the chopper.

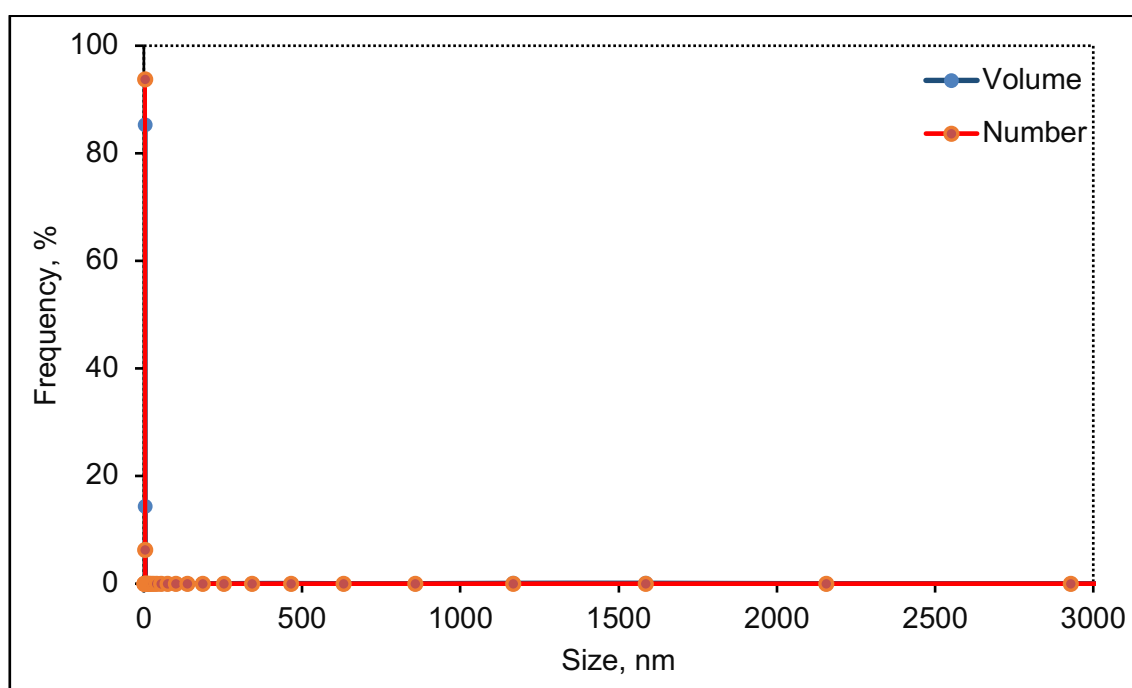


Figure 40a. The particle size distribution of Cloisite Na⁺ suspension exfoliated by using the coffee grinder. The suspension at 6 mg/ml concentration of clay was blended for 16 minutes at speed 1. The graph shows x-axis from 0 to 3000 nm size.

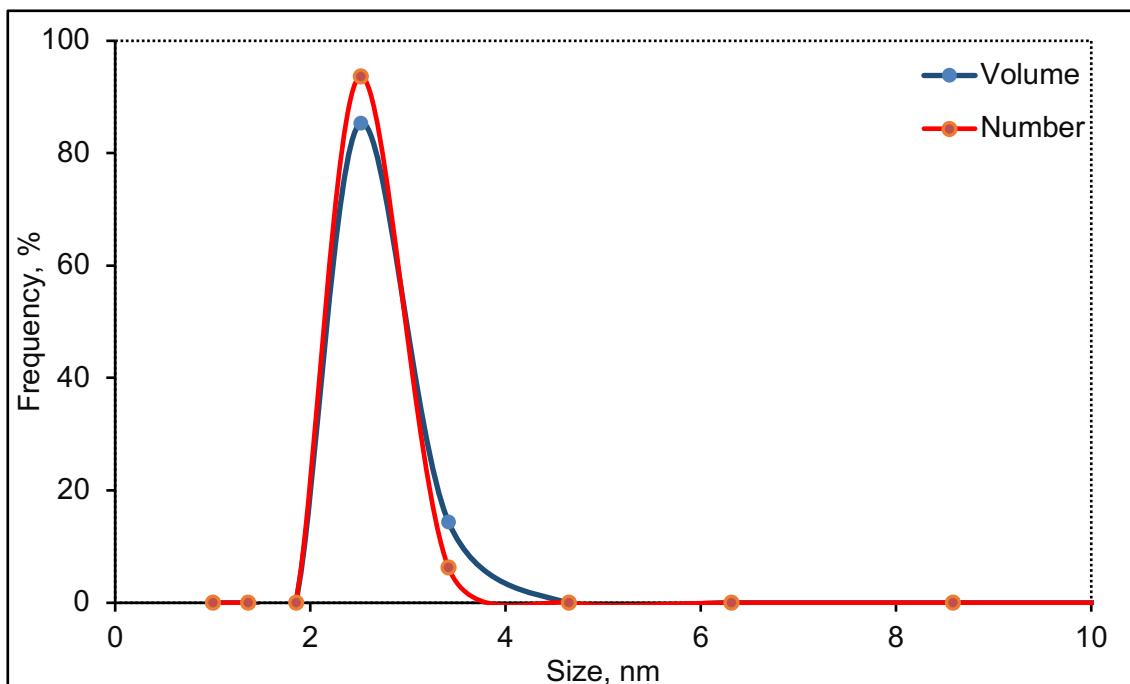


Figure 40b. The particle size distribution of Cloisite Na⁺ suspension exfoliated by using the coffee grinder. The suspension at 6 mg/ml concentration of clay was blended for 16 minutes at speed 1. The graph shows x-axis from 0 to 10 nm size.

3.1.3.3. Exfoliation of SWN clay suspensions

Similar to Cloisite Na⁺ clay suspension, exfoliation of SWN suspensions at a concentration of 6 mg/ml were investigated using magnetic stir, ultrasound and the Tefal blender. The comparison of these methods for achieving the exfoliation was made based on the results of DLS. Due to the exfoliation of SWN obtained by the Tefal blender after 10 minutes, this time was chosen for the comparison of the techniques.

3.1.3.3.1. Analysis of SWN suspension without exfoliation treatment

Prior to the actual exfoliation, SWN suspension without exfoliation treatment was analysed. The non-exfoliated SWN suspension was prepared as described in Section 2.4.1. Figs. 41a and 41b show the same DLS results of the particle size distribution of the SWN suspension without exfoliated treatment. According to Figs. 35 and 41a, the size of particles within the initial SWN suspension was

smaller than the size of Cloisite Na⁺ due to the smaller aspect ratio. As shown in Fig. 41b, there were two broad peaks of volume distribution indicating particle aggregations in a range from 4 to 39 nm. This means that particle aggregations were present.

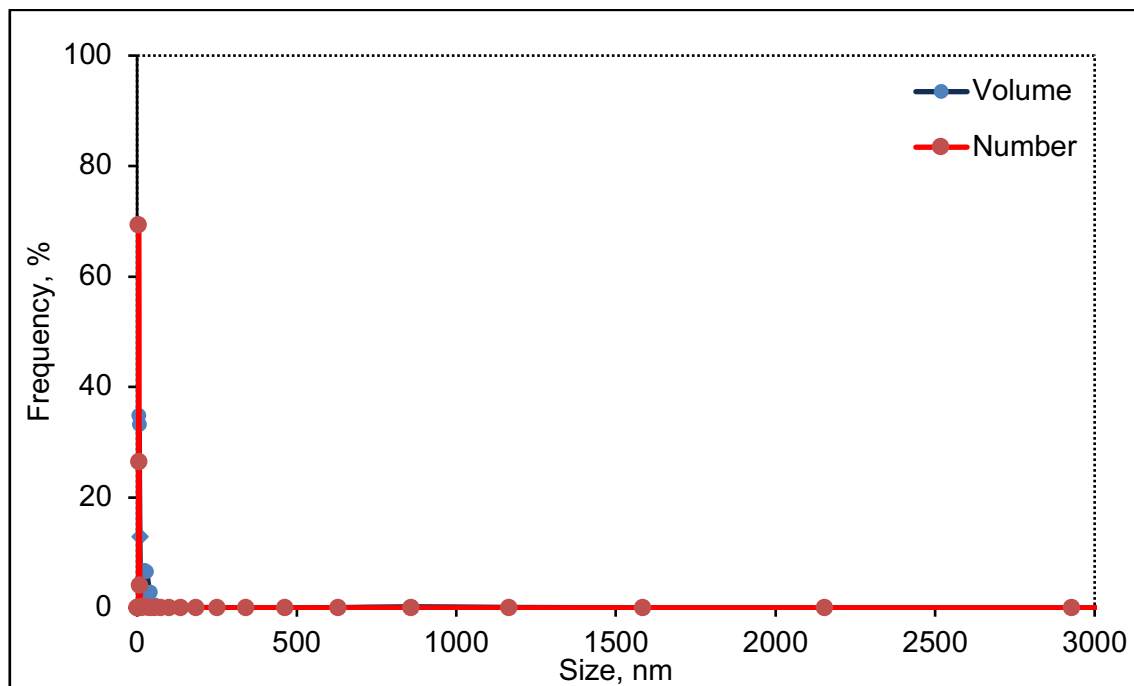


Figure 41a. The particle size distribution of non-exfoliated SWN suspension. A concentration of SWN in the suspension was 6 mg/ml. The graph shows x-axis from 0 to 3000 nm size.

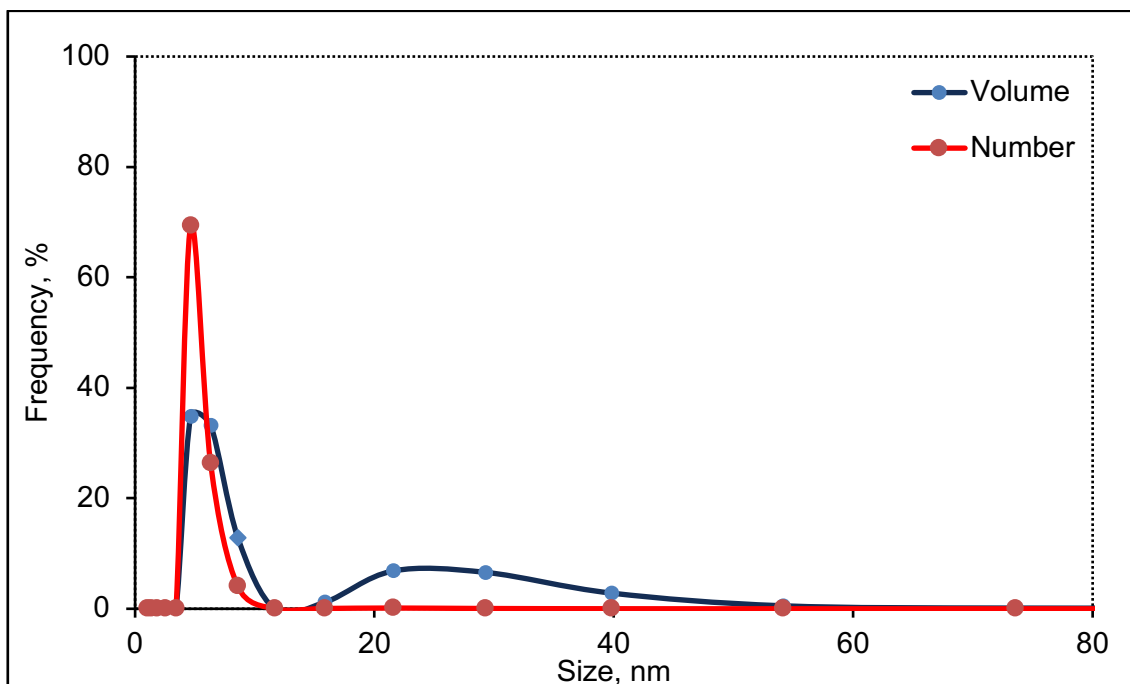


Figure 41b. The particle size distribution of non-exfoliated SWN suspension. A concentration of SWN in the suspension was 6 mg/ml. The graph shows x-axis from 0 to 80 nm size.

3.1.3.3.2. Exfoliation of SWN suspension through magnetic stirring

SWN suspension was stirred using the magnetic stir for 10 minutes at 880 rpm speed (Figs. 42a and 42b). As shown in Fig. 42a, there were no micro-size particles due to smaller aspect ratio. However, there were two broad peaks of volume ranging from 3 to 29 nm particle size, which indicated aggregation (Fig. 42b). In addition, there were differences in number and volume frequency. A possible reason behind this might be the non-sufficient shear stress applied for exfoliation. This means that the suspension was not fully exfoliated.

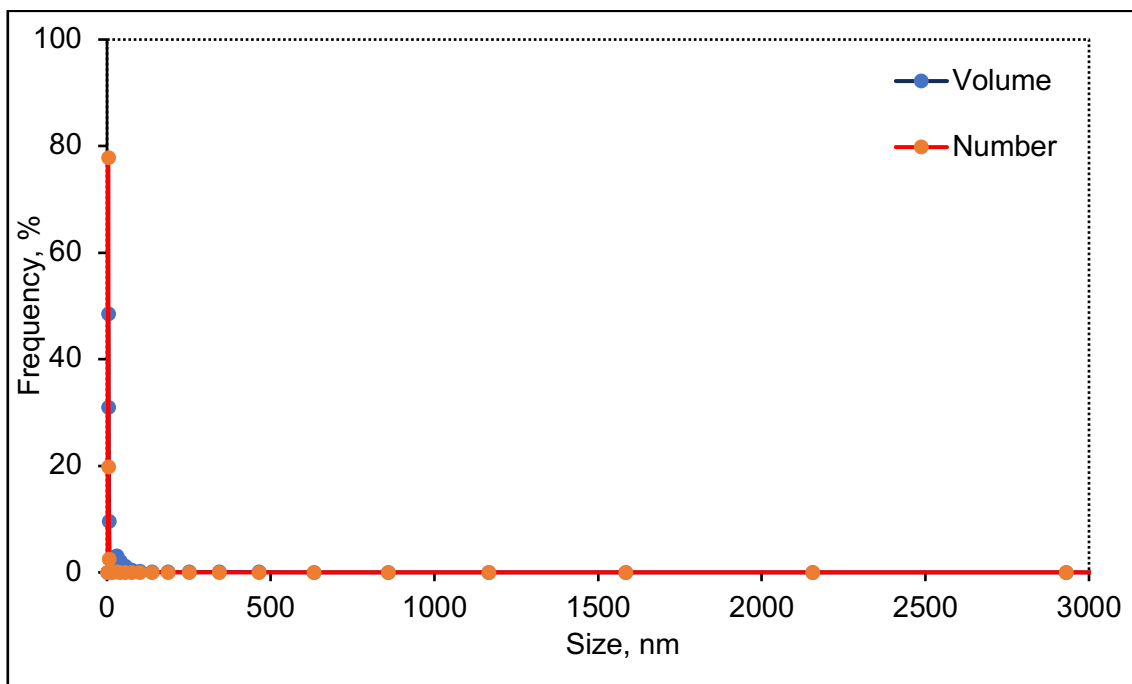


Figure 42a. The particle size distribution of SWN suspension exfoliated using magnetic stirring (Stuard). The suspension at a concentration of 6mg/ml of clay was stirred at 880 rpm for 10 minutes at 25°C. The graph shows x-axis from 0 to 3000 nm size.

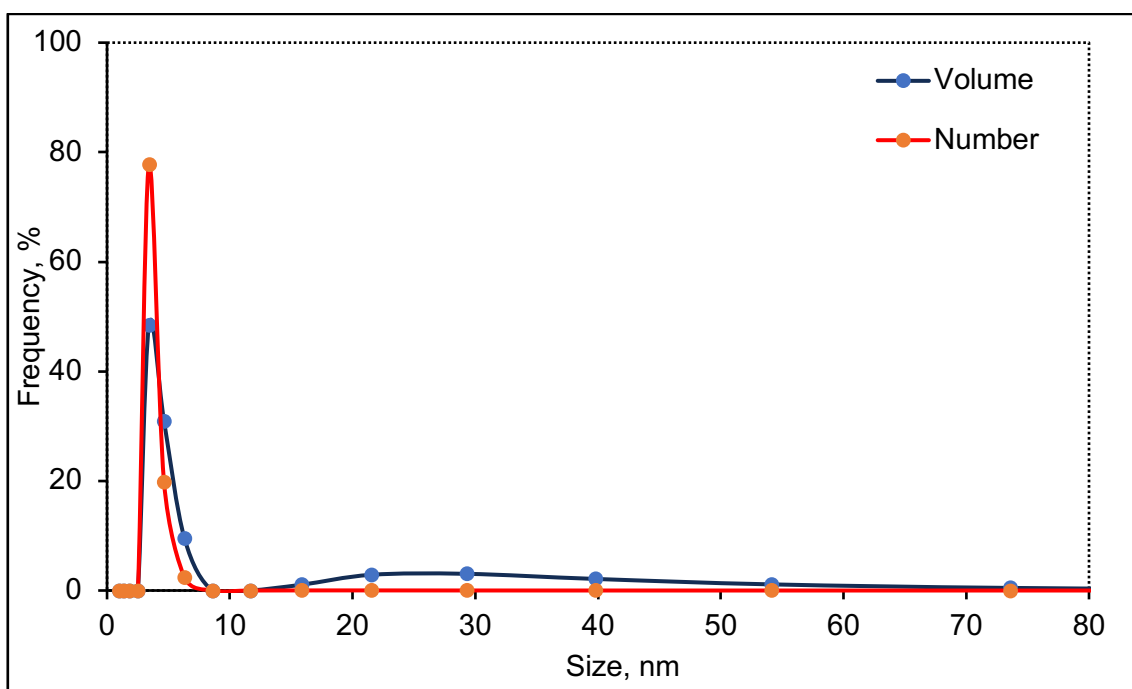


Figure 42b. The particle size distribution of SWN suspension exfoliated using magnetic stirring (Stuard). The suspension at a concentration of 6mg/ml of clay was stirred at 880 rpm for 10 minutes at 25°C. The graph shows x-axis from 0 to 80 nm size.

3.1.3.3.3. Exfoliation of SWN suspension through high power sonication

The next method of exfoliation of SWN suspension was ultrasonication for 10 minutes. As shown in Figs. 43a and 43b, there were no micro-size particle aggregation, but volume distribution was more broad compare to the non-exfoliated suspension (Fig. 43). The large volume of particles ranging from 8 to 54 nm indicated aggregations of particles. This means that the suspension was not exfoliated.

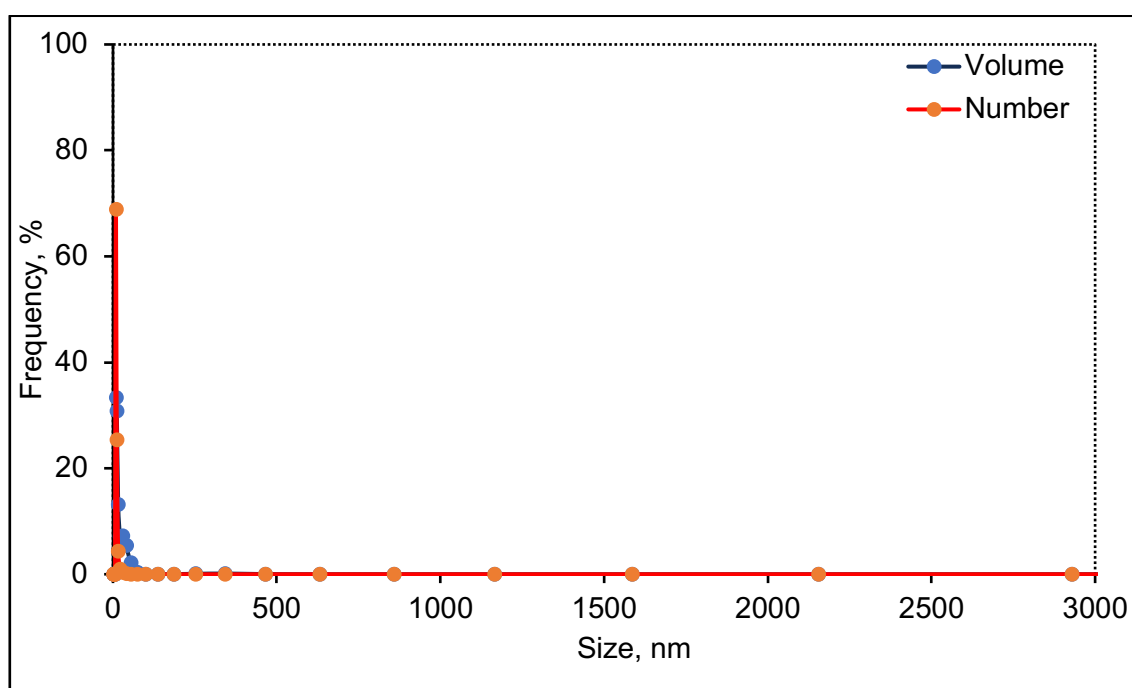


Figure 43a. The particle size distribution of SWN suspension exfoliated using ultrasound. The suspension at a concentration of 6 mg/ml of clay was sonicated at amplitude of 85% for 10 minutes. The graph shows x-axis from 0 to 3000 nm size.

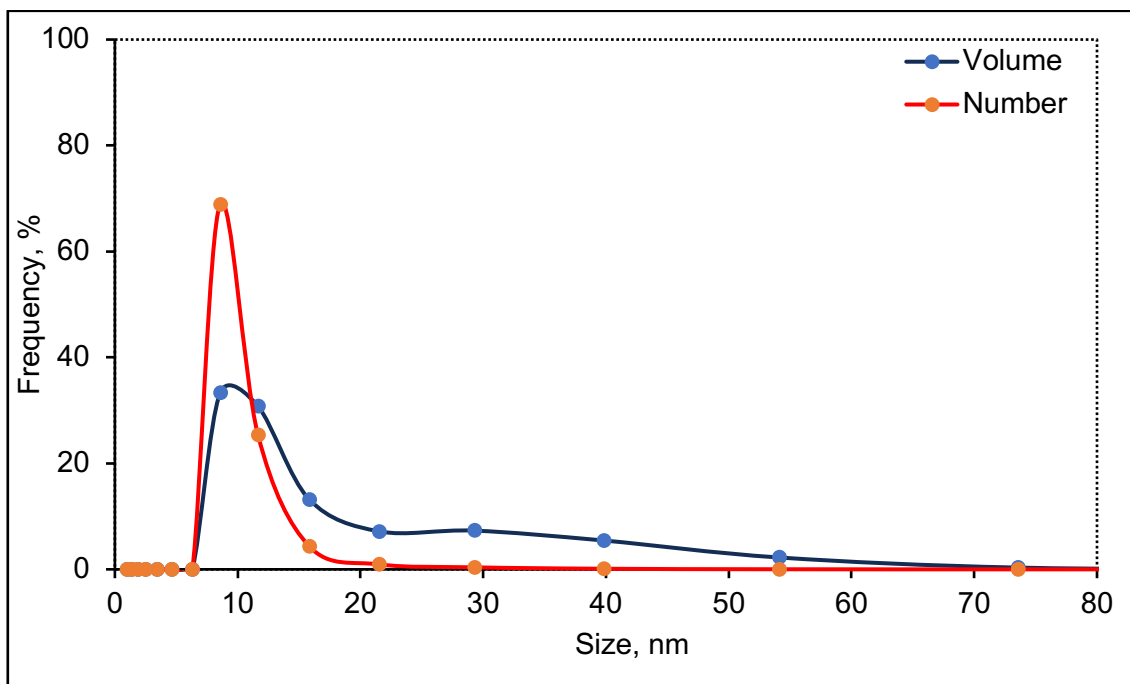


Figure 43b. The particle size distribution of SWN suspension exfoliated using ultrasound. The suspension at a concentration of 6 mg/ml of clay was sonicated at amplitude of 85% for 10 minutes. The graph shows x-axis from 0 to 80 nm size.

3.1.3.3.4. Exfoliation of SWN suspension through blending

SWN suspension was treated using the Tefal blender. The uniform and exfoliated SWN suspension was achieved by using the blade of the coffee grinder at speed 1 for 10 minutes. As shown in Figs. 44a and 44b, there was one peak of each volume and number distribution, where 90% of particles were 2.5 nm, which represent 79% of the total volume. This means that the Tefal blending technique was the successful way to exfoliate SWN suspension.

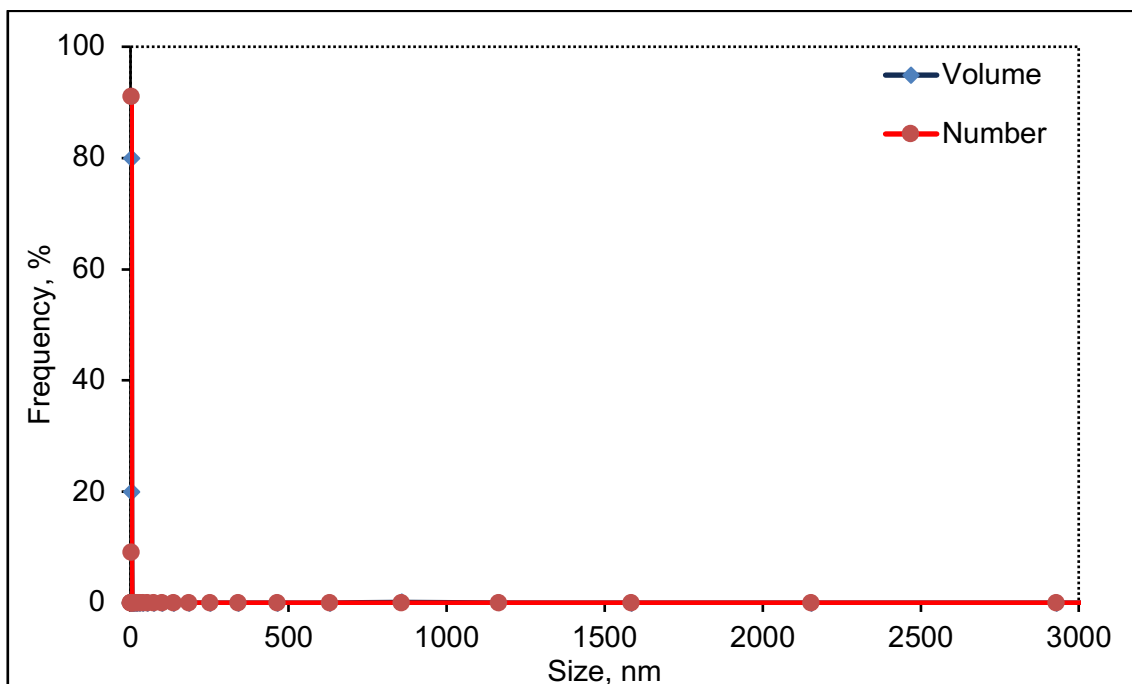


Figure 44a. The particle size distribution of SWN suspension exfoliated using the coffee grinder. The suspension at a concentration of 6 mg/ml of clay was blended using the coffee grinder of the Tefal blender for 10 minutes at speed 1. The graph shows x-axis from 0 to 3000 nm size.

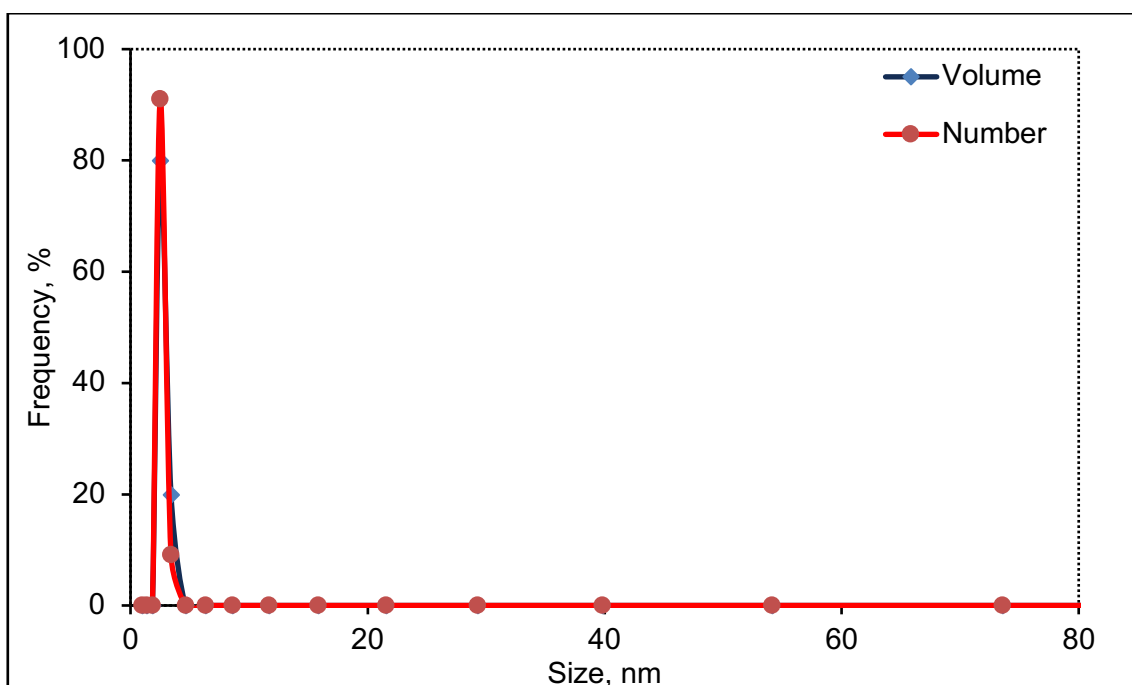


Figure 44b. The particle size distribution of SWN suspension exfoliated using the coffee grinder. The suspension at a concentration of 6 mg/ml of clay was blended using the

coffee grinder of the Tefal blender for 10 minutes at speed 1. The graph shows x-axis from 0 to 80 nm size.

3.1.4. Effect of exfoliation of clay on BC growth on a small scale

The effect of exfoliation of clay on BC growth was studied on a small scale as described in Section 2.4.3. Non-exfoliated and exfoliated Cloisite Na⁺ and SWN clay suspensions produced by the Tefal blender were added into HS medium prior to the inoculation of bacteria. Clay concentration inside the medium was ranging from 0 (no particles) to 3 mg/ml. *G. xylinus* at a concentration of 7.9×10^7 CFU/ml was inoculated using HS medium with and without particles at 30°C for 48 hours. Fig. 45 shows the mass of dried BC produced with non-exfoliated Cloisite Na⁺ and SWN suspensions, respectively, on a small scale. As shown in Fig. 45, non-exfoliated Cloisite Na⁺ clay suspension at a concentration of 1.5 and 3 mg/ml has reduced the growth of BC, the dried mass of which dropped to 0.01 and 0.02 grams, respectively. The mass of dried BC decreased to 0.01 grams using 1.5 mg/ml concentration of non-exfoliated SWN clay suspension. In addition, there was no synthesis of cellulose using 3 mg/ml concentration of non-exfoliated SWN.

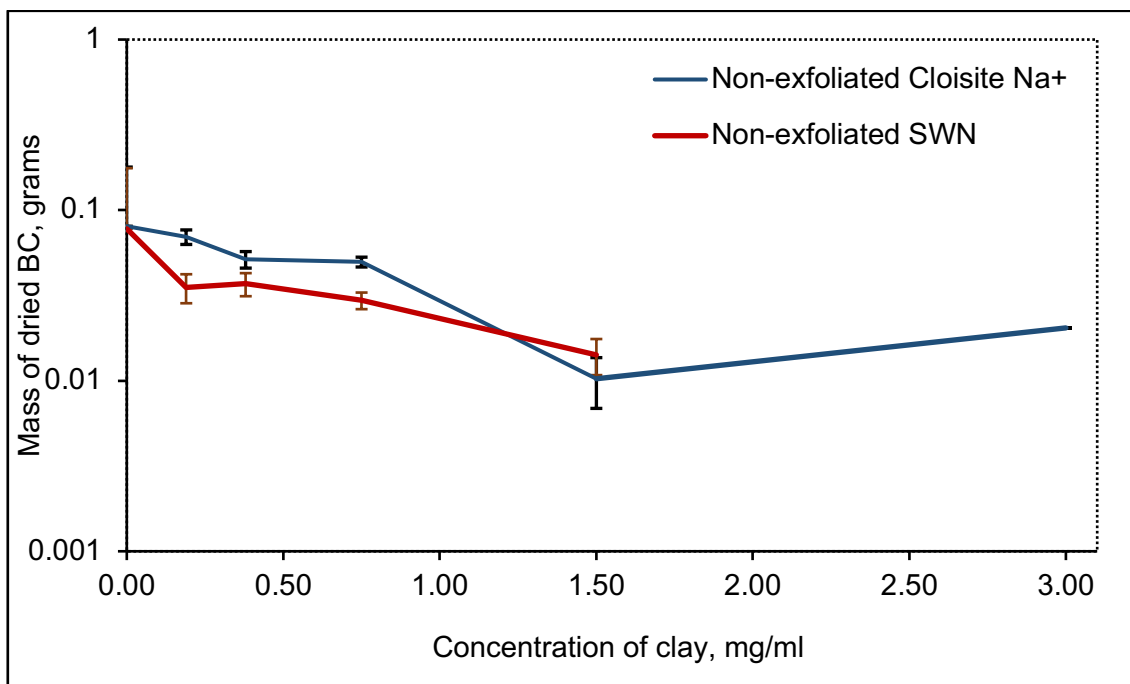


Figure 45. Effect of non-exfoliated Cloisite Na⁺ and SWN clay suspensions on the growth of BC on a small scale. Bacteria were inoculated at 7.9×10^7 CFU/ml concentration in HS medium containing clay at a final concentration from 0 to 3 mg/ml and incubated for 48 hours at 30°C. Data shown represent the mean of three experiments with error bars of standard deviation. The treatments were compared to the controls (0 mg/ml of clay). The data are not significantly different.

The effect of 16 minutes exfoliated Cloisite Na⁺ and 10 minutes exfoliated SWN suspensions produced by the Tefal blender on BC growth was analysed, respectively (Fig. 46). As shown in Fig. 46, the mass of dried BC formed with exfoliated Cloisite Na⁺ clay suspension decreased to 0.3 grams at clay concentrations ranging from 0.38 to 1.5 mg/ml. It was possible to obtain the pellicle in the presence of exfoliated SWN suspension at concentration of 3 mg/ml with the mass of dried BC being 0.007 grams.

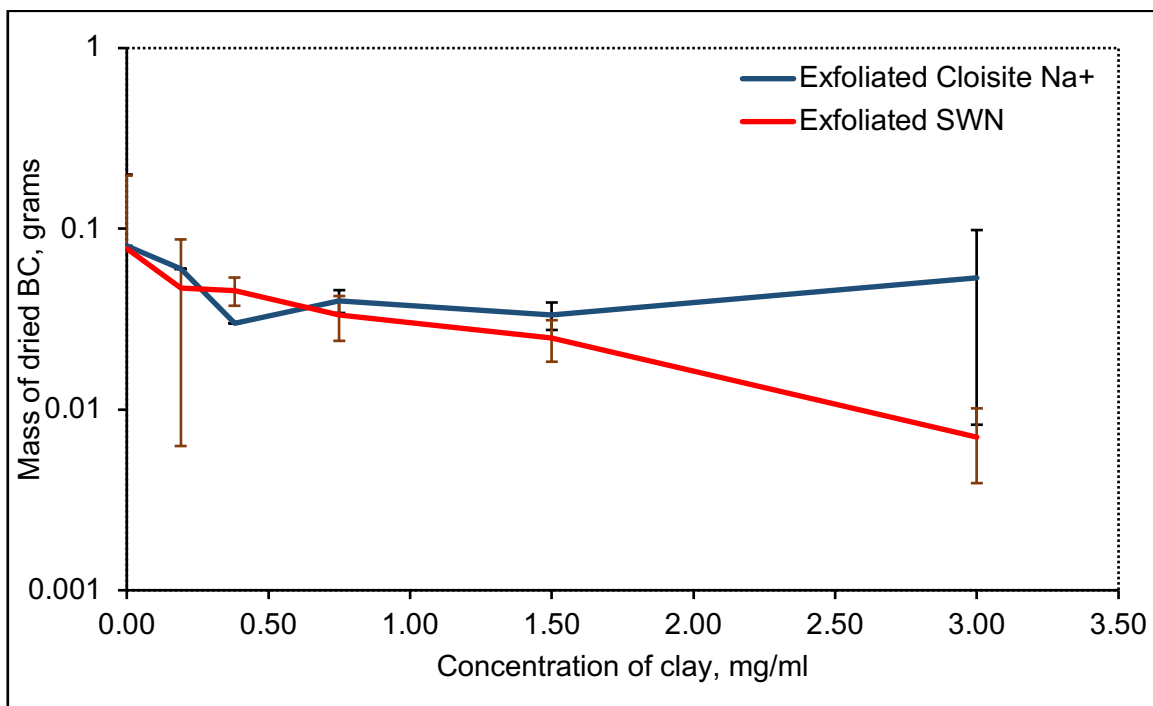


Figure 46. Effect of exfoliated Cloisite Na⁺ and SWN clay suspensions on the growth of BC on a small scale. Bacteria were inoculated at 7.9×10^7 CFU/ml concentration in HS medium containing clay at a final concentration from 0 to 3 mg/ml and incubated for 48 hours at 30°C. Data shown represent the mean of three experiments with error bars of standard deviation. The treatments were compared to the controls. The data are not significantly different.

Consequently, the exfoliation and concentration of the clay suspensions could affect the synthesis of cellulose, but the difference in mass was not statistically significant. Non-exfoliated suspensions of both types of the clay reduced the mass of dried BC at concentration of 3 mg/ml. A possible reason behind this might be ability of the clay to form physically self-cross-linked gel structures. The images of BC formation with non-exfoliated and exfoliated Cloisite Na⁺ and SWN suspensions at clay concentration of 3 mg/ml, respectively, are shown in Fig. 47.

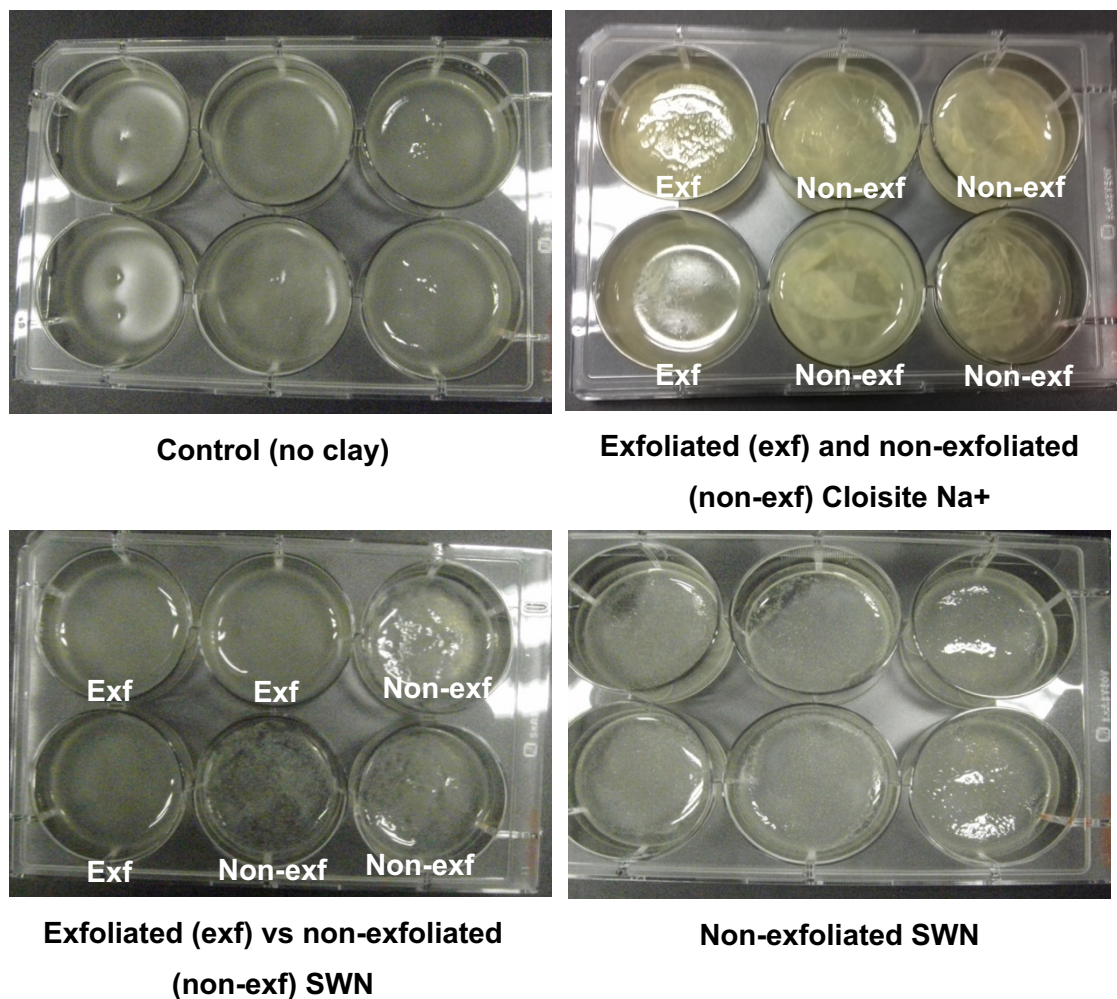


Figure 47. Images of BC synthesised under different treatments. The clay was used at concentration of 3 mg/ml at either non-exfoliated or exfoliated state for 48 hours at 30°C.

The gel formed by SWN clay can be detected by comparing the surface of the suspension to the control. In addition, a smaller yield of cellulose was obtained using non-exfoliated Cloisite Na⁺ compare to the control.

A gel formation of non-exfoliated and exfoliated Cloisite Na⁺ and SWN suspensions was investigated using a rheometer as described in Section 2.4.2. Clay suspensions were mixed with HS medium at concentration of 3 mg/ml, respectively. The viscoelastic properties of clay/medium suspensions were studied at 0 and 48 hours (Figs. 48-49). As shown in Figs. 48-49, SWN showed higher elastic and viscous modulus compare to Cloisite Na⁺ after 48 hours. The elastic modulus of non-exfoliated SWN significantly increased to 13Pa after 48.

The viscosity of non-exfoliated SWN increased from 0.2 to 1Pa after 0 and 48 hours, respectively. Exfoliated SWN showed relatively high elastic (13Pa) and viscous (1Pa) modulus at both 0 and 48 hours. Whereas, Cloisite Na⁺ had relatively low elastic and viscous modulus after 48 hours. The elastic modulus of non-exfoliated and exfoliated Cloisite Na⁺ was 5Pa and 6Pa, respectively, with the viscosity being 0.07Pa and 0.05Pa, respectively. This means that no gel formation of Cloisite Na⁺ occurred after 48 hours.

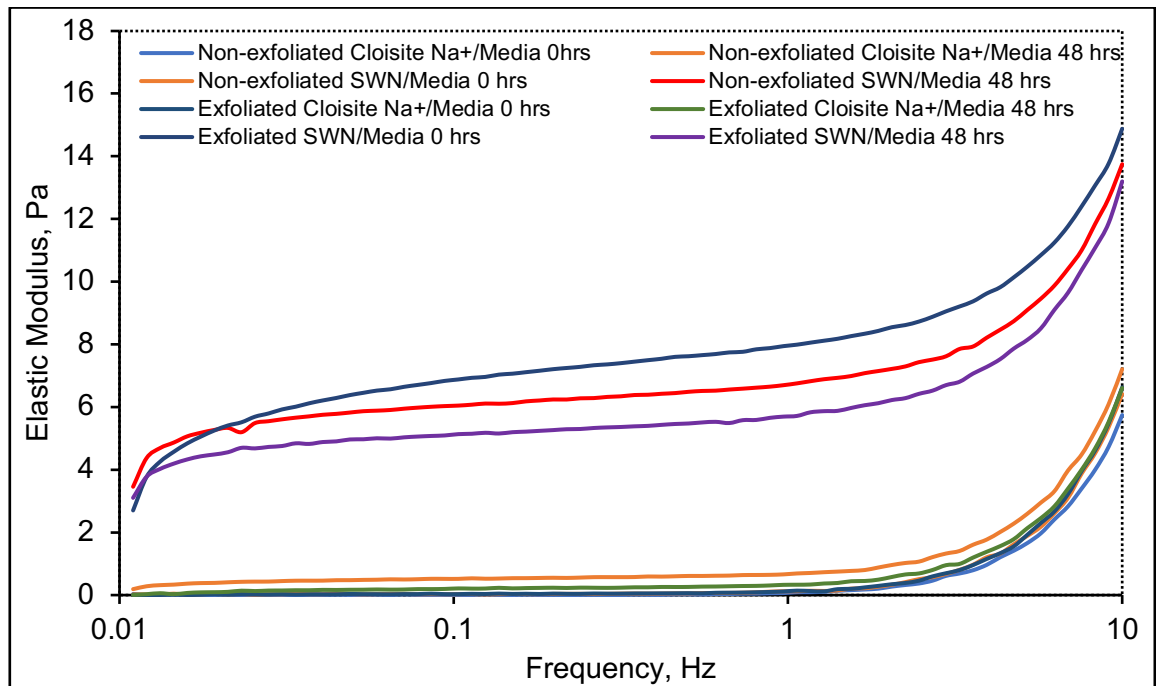


Figure 48. Elastic modulus of non-exfoliated and exfoliated Cloisite Na⁺/medium and SWN/medium suspensions after 0 and 48 hours.

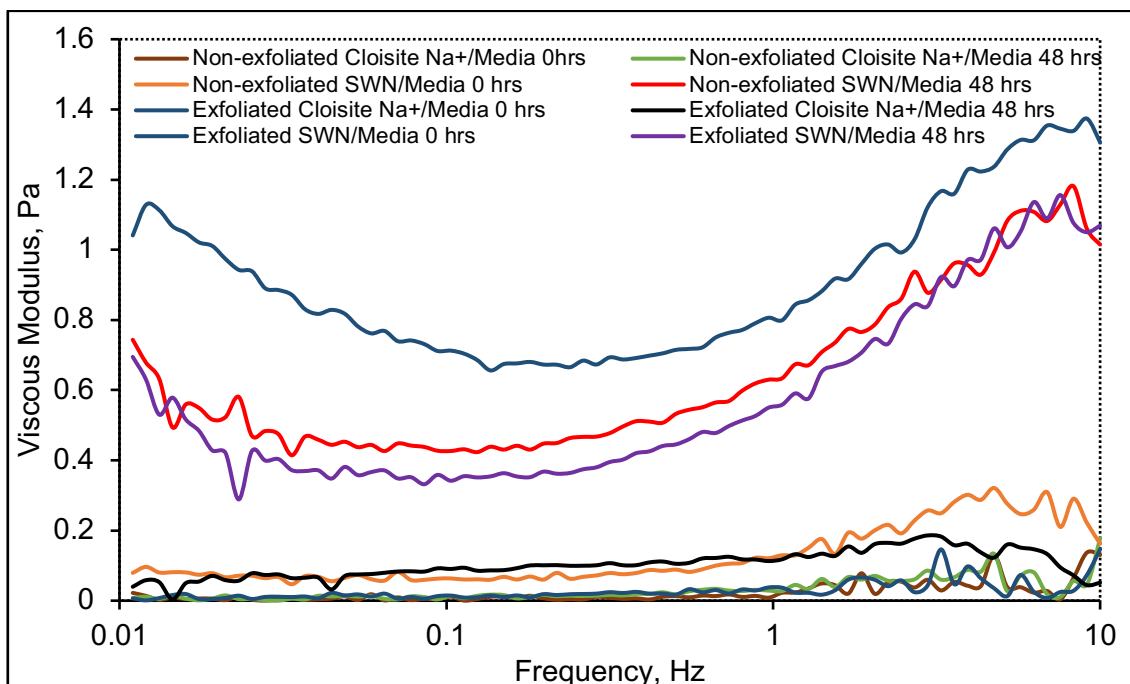


Figure 49. Viscous modulus of non-exfoliated and exfoliated Cloisite Na⁺/medium and SWN/medium suspensions after 0 and 48 hours.

This means that a physical self-cross-linked gel of SWN might result. A gelation could occur through the formation of micro-flocculation, where individual particles of clay can aggregate into clot-like masses due to the electrostatic attraction between the negatively charged parts of particles and the positively charged edges^[212].

3.1.5. Synthesis of BC in clay environment on a large scale

The effect of exfoliated and non-exfoliated Cloisite Na⁺ and SWN clay on the growth of BC was analysed on a large scale as described in Section 2.4.4. There was no growth of BC using 3 mg/ml concentration of non-exfoliated SWN suspension. Nonetheless, it was possible to synthesis BC with 3 mg/ml of non-exfoliated Cloisite Na⁺ suspension. The pellicle was weak and falling apart (Fig. 50).



Figure 50. The synthesised BC with 3 mg/ml of non-exfoliated Cloisite Na⁺ clay suspension. Bacteria was inoculated at a concentration of 7.9×10^7 CFU/ml and incubated at 30°C for 48 hours.

It was possible to synthesise BC with both exfoliated Cloisite Na⁺ and SWN at 3 mg/ml concentration of the clay. Fig. 51 shows wet BC produced on a large scale using exfoliated Cloisite Na⁺ (a) and SWN (b) suspensions. As shown in Fig. 51, BC/Cloisite Na⁺ composite was denser compare to BC/SWN.

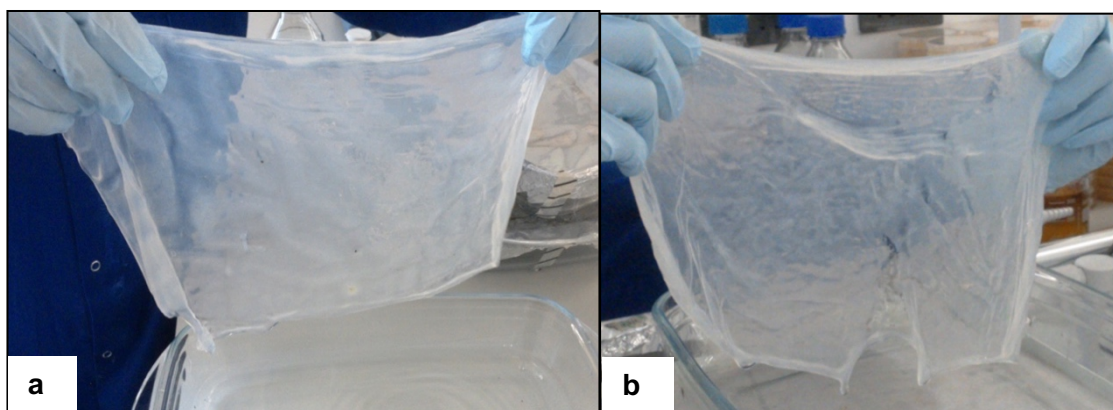


Figure 51. The synthesised BC in the presence of 3 mg/ml of exfoliated Cloisite Na⁺ (a) and SWN (b) clay suspensions. Bacteria was inoculated at a concentration of 7.9×10^7 CFU/ml and incubated at 30°C for 48 hours.

As shown in Fig. 52, the mass of wet pure BC was 74.89 grams, whereas the mass of BC/Cloisite Na⁺ was 87.22 grams. However, the lightest cellulose was BC/SWN composite with a mass of 29.87 grams. The mass of wet BC/Cloisite Na⁺ composite was heavier than both pure BC and BC/SWN.

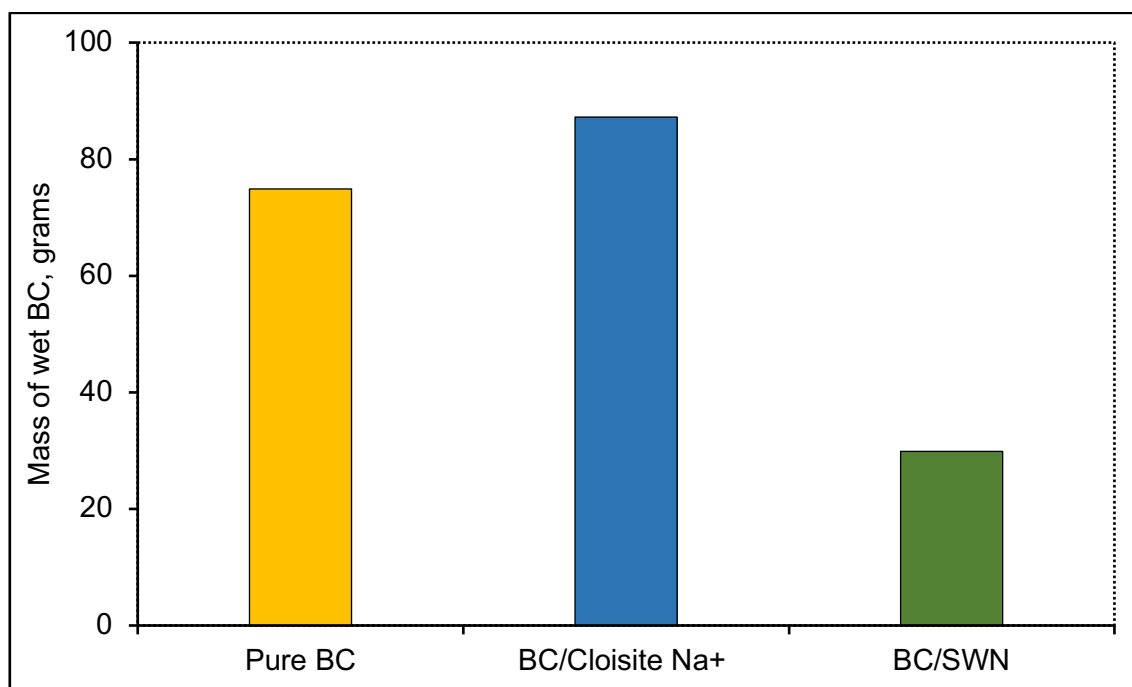


Figure 52. Mass of wet, centrifuged pure BC, BC/Cloisite Na⁺ and BC/SWN produced with exfoliated clay, respectively. The BC was produced using an inoculum of approximately 7.9×10^7 CFU/ml and HS medium containing exfoliated Cloisite Na⁺ and SWN suspensions, respectively, at a concentration of 3 mg/ml. The bacteria were incubated for 48 hours at 30°C. Data shown represent the mean of a single experiment.

The large volume of the medium and sufficient depth of the dish for incubation could be beneficial for the synthesis of BC. Furthermore, the results obtained on the large scale clearly shown that the synthesis of BC/clay composite was dependent on the exfoliation state of the clay, clay type and aspect ratio.

3.1.6. Leaching behaviour of clay

The leaching behaviour of clay was investigated as described in Section 2.4.5. Prior to the experiment, the calibration curves of Cloisite Na⁺ and SWN clay,

respectively, were obtained (Figs. 53-54). The purpose of the calibration curves was to quantify the concentration of clay leached from the composite during the washing process. As shown in Figs. 48-49, R^2 was 99%, which means that the almost ideal linear relationships were obtained.

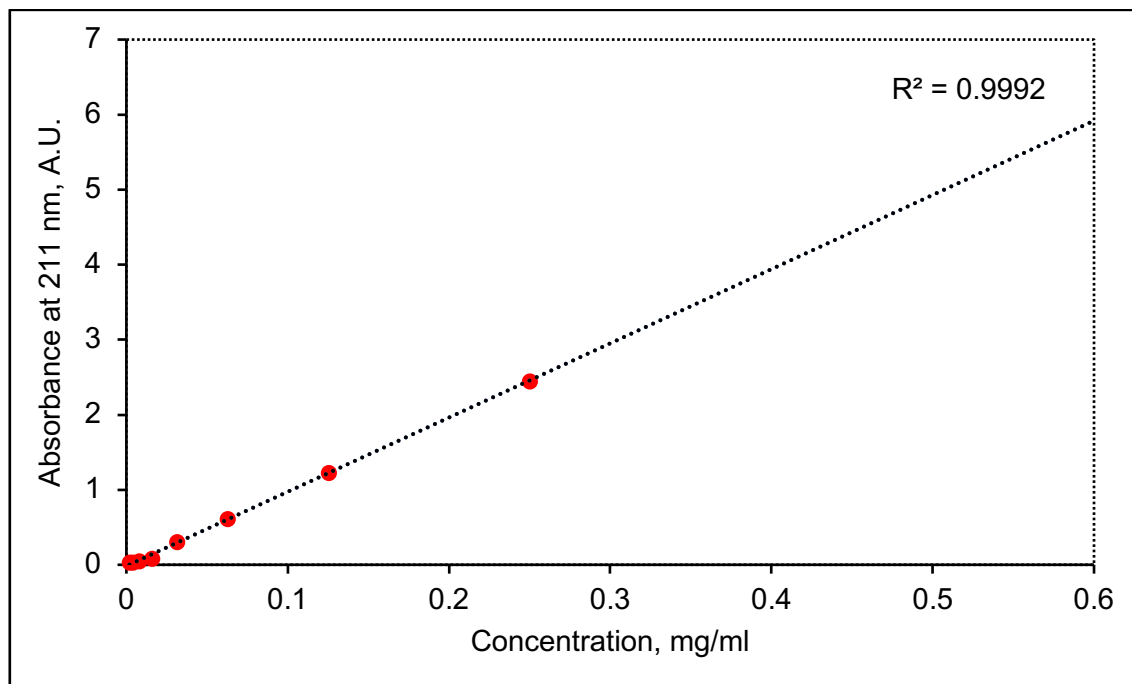


Figure 53. The relationship between absorbance and concentration of Cloisite Na⁺ suspension. The absorbance was measured at wavelength of 211 nm.

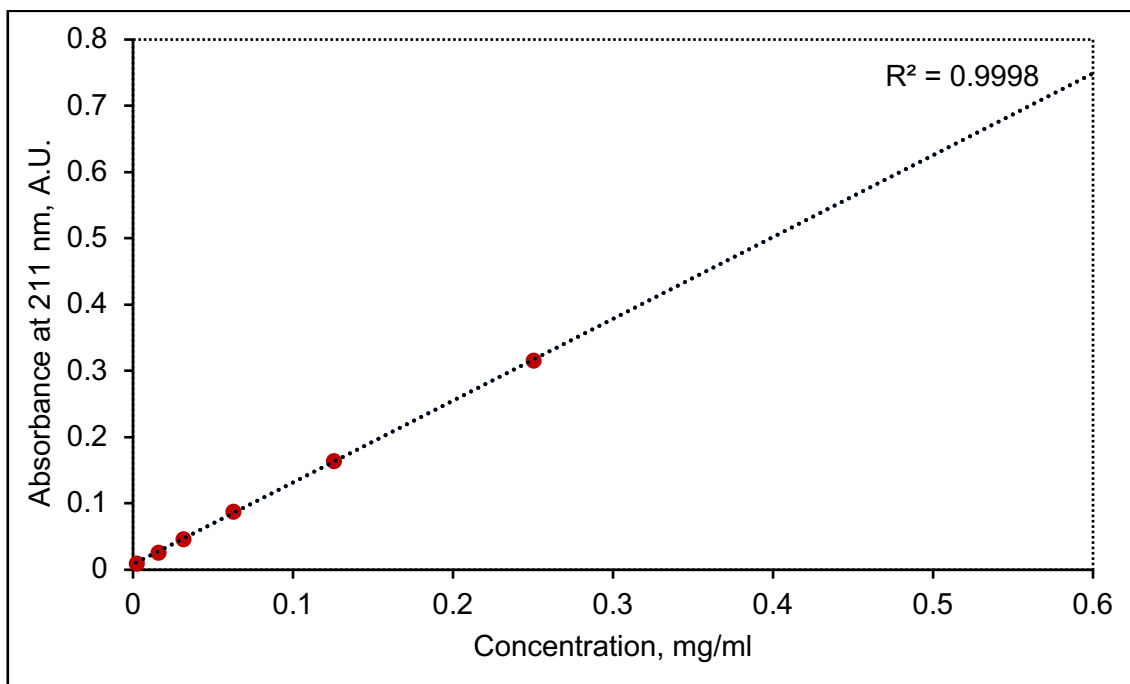


Figure 54. The relationship between absorbance and concentration of SWN suspension. The absorbance was measured at wavelength of 211 nm.

The concentration of leached Cloisite Na⁺ and SWN clay from BC/Cloisite Na⁺ and BC/SWN composites was calculated, respectively, using the calibration curves. BC/Cloisite Na⁺ and BC/SWN composites were washed with 20 ml of distilled water for 24 hours as described in Section 2.4.5. Fig. 55 shows the concentration of each clay leached from the composites from 0 to 24 hours. As shown in Fig. 55, Cloisite Na⁺ started to leach after 3 hours of washing. The concentration of Cloisite Na⁺ leached was 0.1 mg/ml after 24 hours. SWN clay started to leach after an hour of the washing. The concentration of SWN leached was 2.5 mg/ml after 24 hours.

SWN started to leach faster with the concentration leached being higher than Cloisite Na⁺. This might be due to smaller aspect ratio, which resulted in weaker attachment of clay particles to BC fibres, whereas high aspect ratio of Cloisite Na⁺ lead to stronger binding to BC.

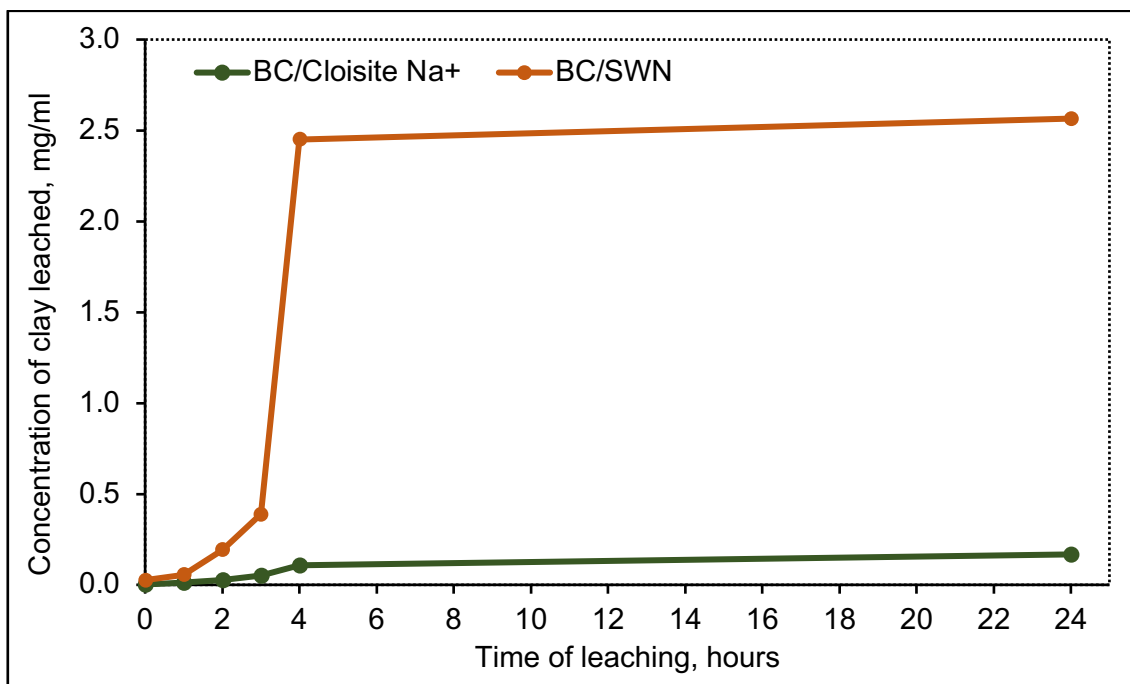


Figure 55. The concentration of leached clay of BC/Cloisite Na⁺ and BC/SWN, respectively, from 0 to 24 hours.

3.1.7. Characterisation of *in situ* synthesised BC/clay composites

In order to evaluate the incorporation of exfoliated particles into BC, BC/clay composites were analysed using UV-VIS-NIR spectroscopy after the washing. The ultraviolet region covers the range from 200 to 400 nm of the electromagnetic spectrum, whereas the visible region is from 400 to 700 nm^[213]. The used spectrometer was also able to detect peaks in near IR (NIR) region from 800-2500 nm. The evaluation of incorporation was based on the detection of the characteristic peaks of clay.

3.1.7.1. UV-VIS-NIR analysis of BC/Cloisite Na⁺ composites

UV-VIS-NIR spectrum of BC/Cloisite Na⁺ composites, which were synthesised *in situ* using the exfoliated clay, were compared to the spectra of both pure BC and Cloisite Na⁺ (Figs. 56-57). The peaks of Cloisite Na⁺ clay was at 211 nm and 250

nm, whereas both the composite and pure BC had peaks at 215, 263 and 283 nm^[214]. According to Fig. 56, the composite showed the spectrum similar to pure BC. The peak of the clay was not detected inside the composite. The reason for this might be the reflective nature of the equipment, where the light reflected from the surface. Clay may not be present on the surface after the washing process, but it may remain inside BC. In this case the equipment cannot detect clay in the samples.

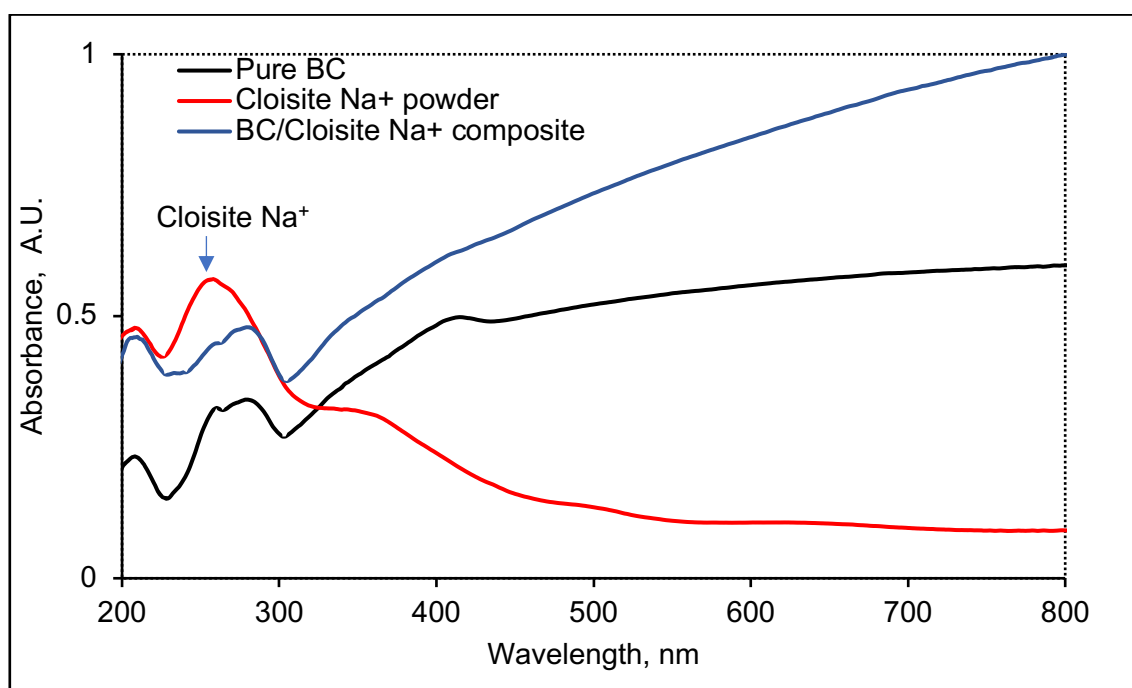


Figure 56. UV-VIS spectra of BC/Cloisite Na⁺ composite, pure BC and Cloisite Na⁺.

The presence of the clay, however, was detected in the composite in NIR spectra (Fig. 57). As shown in Fig. 57, BC/Cloisite Na⁺ composite had the characteristic peak of Cloisite Na⁺ clay at 1041 and 1426 nm due to the Si-O. Pure BC and BC/Cloisite Na⁺ showed a similar peak of the cellulose at 1921 nm^[214].

According to Figs. 56-57, the composite showed predominant cellulose structure. However, the presence of the characteristic peak of the clay at 1426 nm indicated that Cloisite Na⁺ clay particles were successfully incorporated into BC matrix.

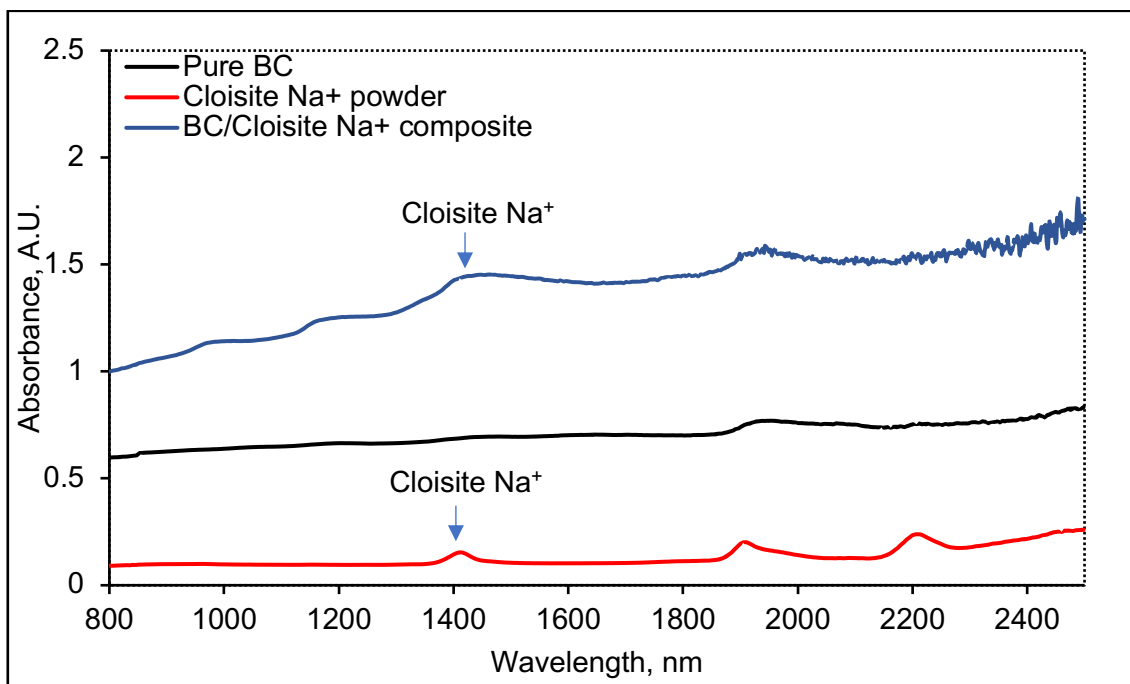


Figure 57. NIR spectra of BC/Cloisite Na⁺ composite, pure BC and Cloisite Na⁺.

3.1.7.2. UV-VIS-NIR analysis of BC/SWN composites

UV-VIS-NIR spectrum of BC/SWN composite was compared to spectra of pure BC and SWN clay (Figs. 58-59). As shown in Fig. 58, the composite had predominant BC peaks at 263 and 281 nm. BC/SWN composite had the broad peak at 211-215 nm, which made the detection of the clay difficult in UV region. The second peak of SWN at 256 nm was not observed in the composite.

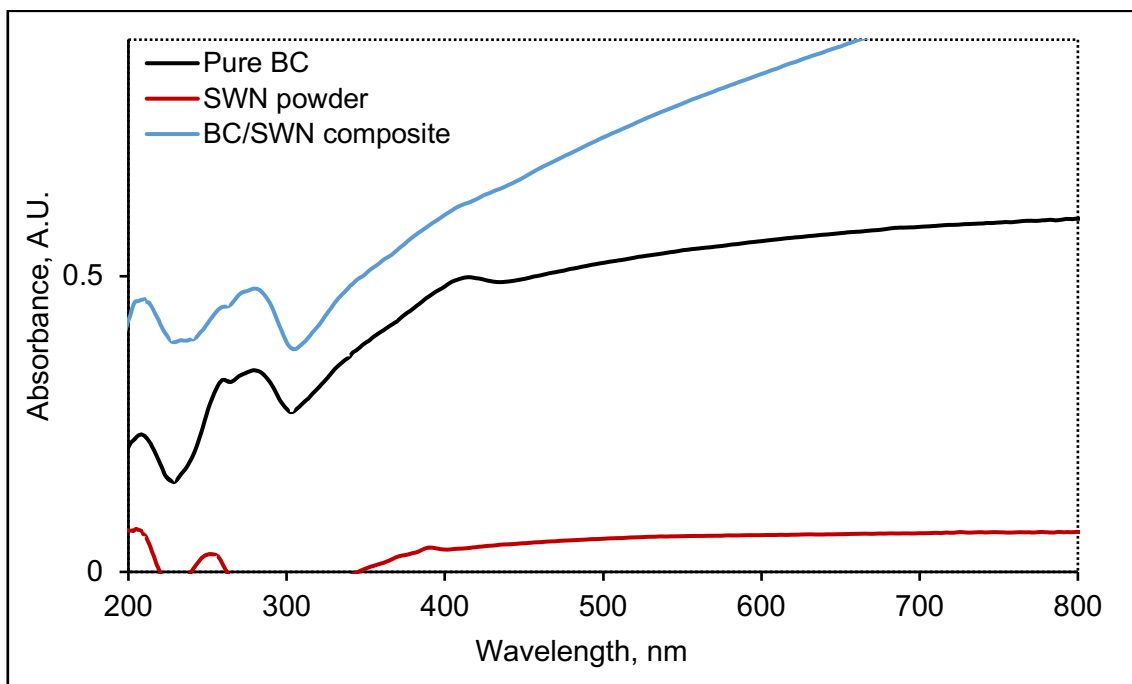


Figure 58. UV-VIS spectra of BC/SWN, pure BC and SWN clay powder.

The NIR spectrum of the BC/SWN composite was compared to SWN clay and pure BC (Fig. 59).

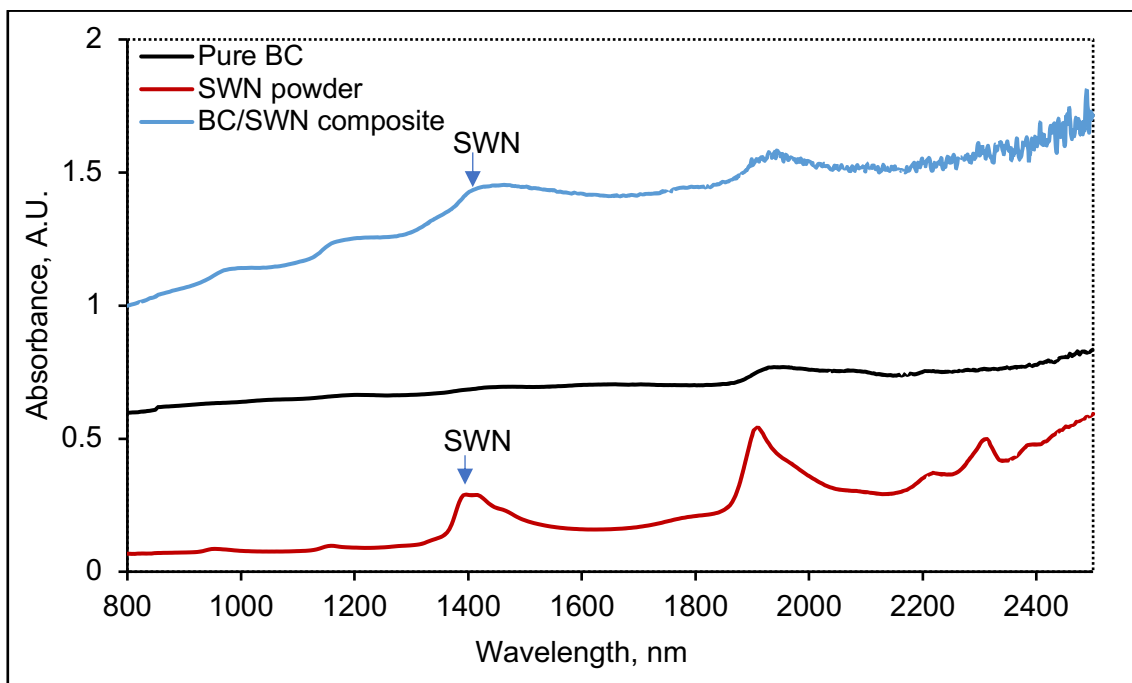


Figure 59. NIR spectra of BC/SWN composite, pure BC and SWN clay powder.

The characteristic peak of SWN at around 1400 nm was clearly visible inside the composite. This result indicated that SWN was incorporated into BC matrix during *in situ* synthesis of the composite. In addition, the peak of the cellulose was observed inside BC/SWN composite at 1950 nm.

3.1.8. Antibacterial activity of non-exfoliated clay suspensions

The antibacterial activity of non-exfoliated Cloisite Na⁺ and SWN suspensions at a concentration of 3 mg/ml against MRSA (NCTC 10418) and *E. coli* (NCTC 12493), respectively, was investigated as described in Section 2.7.3.1. Fig. 60 shows the antibacterial effect of non-exfoliated clay against MRSA. The control was PBS-resuspended MRSA without any treatment.

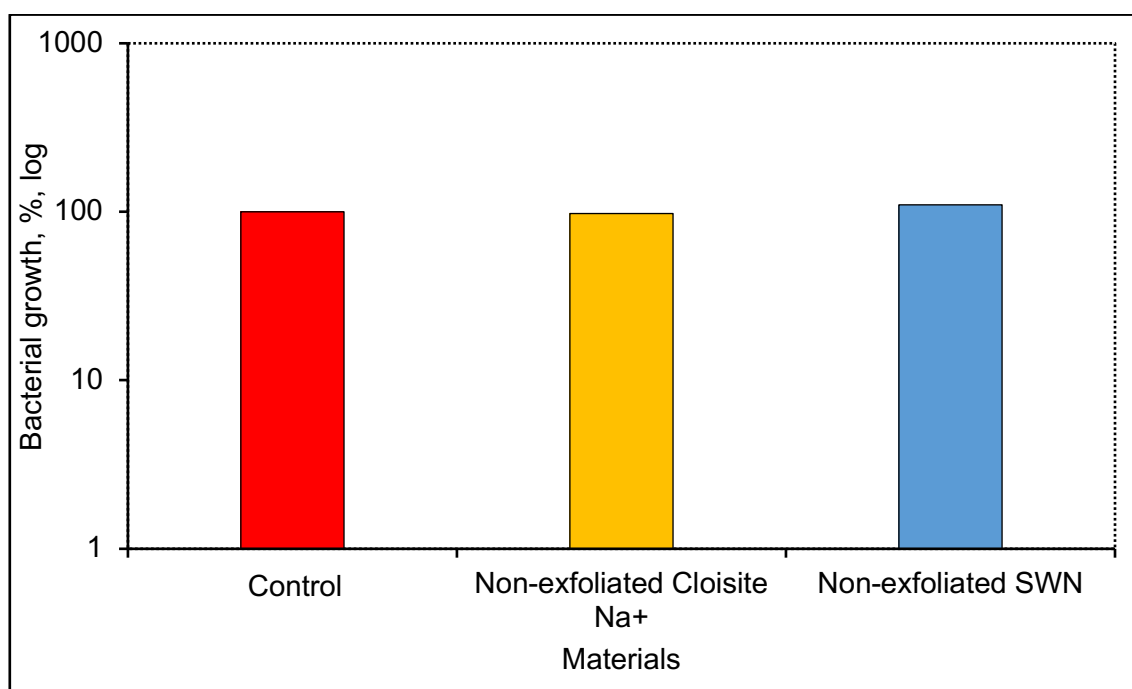


Figure 60. Antibacterial activity of non-exfoliated Cloisite Na⁺ and SWN suspensions against MRSA (NCTC 10418). The bacteria were incubated with Cloisite Na⁺ and SWN suspensions at 3 mg/ml concentration of clay, respectively, for 24 hours at 37°C. The control was PBS-resuspended MRSA without any treatments. Data shown represent the mean of a single experiment.

As shown in Fig. 60, there was a little reduction of bacterial growth to 97% of control values using non-exfoliated Cloisite Na⁺, whereas non-exfoliated SWN clay increased the growth of MRSA to 109%.

Fig. 61 shows the antibacterial activity of non-exfoliated Cloisite Na⁺ and SWN suspensions at a concentration of 3 mg/ml against *E. coli*. The control was PBS-resuspended *E. coli* without any treatment. Both non-exfoliated Cloisite Na⁺ and SWN clay did not show any antibacterial activity. The growth of *E. coli* increased to 129% and 115% of control values using Cloisite Na⁺ and SWN clay suspensions, respectively.

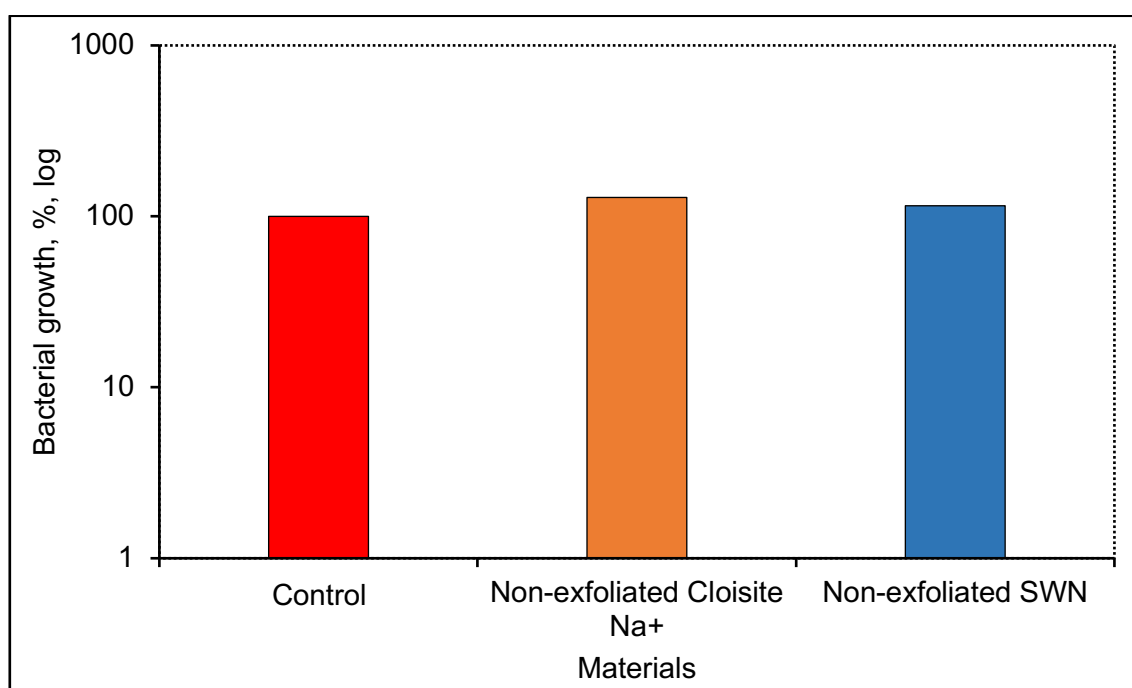


Figure 61. Antibacterial activity of non-exfoliated Cloisite Na⁺ and SWN suspensions against *E. coli* (NCTC 12493). The bacteria were incubated with Cloisite Na⁺ and SWN suspensions at 3 mg/ml concentration of clay, respectively, for 24 hours at 37°C. The control was PBS-resuspended *E. coli* without any treatments. Data shown represent the mean of a single experiment.

It has been reported that natural unmodified MMT clay does not show any antimicrobial activity^[88, 93-95]. The data obtained in Figs. 60-61 agreed that non-

exfoliated clay did not possess any antibacterial activity against either MRSA or *E. coli*.

3.1.9. Antibacterial activity of exfoliated clay suspensions

The antibacterial activity of exfoliated Cloisite Na⁺ and SWN clay suspensions at a concentration of 3 mg/ml was investigated against MRSA and *E. coli* as described in Section 2.7.3.1. As shown in Fig. 62, Cloisite Na⁺ possessed antibacterial activity against MRSA. The bacterial growth was reduced to 27.8% compare to the control, whereas SWN reduced the control values to 80%. SWN showed the highest antibacterial activity against *E. coli*, where the growth of bacteria decreased to 5% of control values (Fig. 63). Cloisite Na⁺ reduced the control values of *E. coli* to 29%.

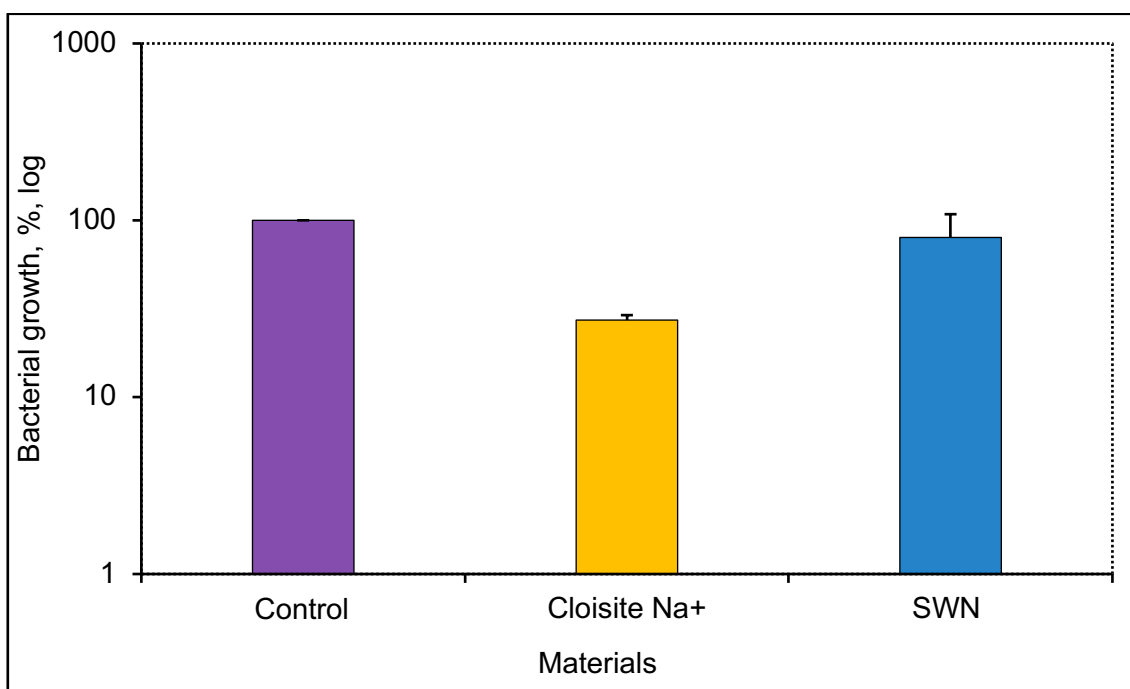


Figure 62. Antibacterial activity of exfoliated Cloisite Na⁺ and SWN suspensions against MRSA (NCTC 10418). The bacteria were incubated with Cloisite Na⁺ and SWN suspensions at 3 mg/ml concentration of clay, respectively, for 24 hours at 37°C. The control was PBS-resuspended MRSA without any treatments. Data shown represent the mean of two independent experiments with error bars of standard deviation.

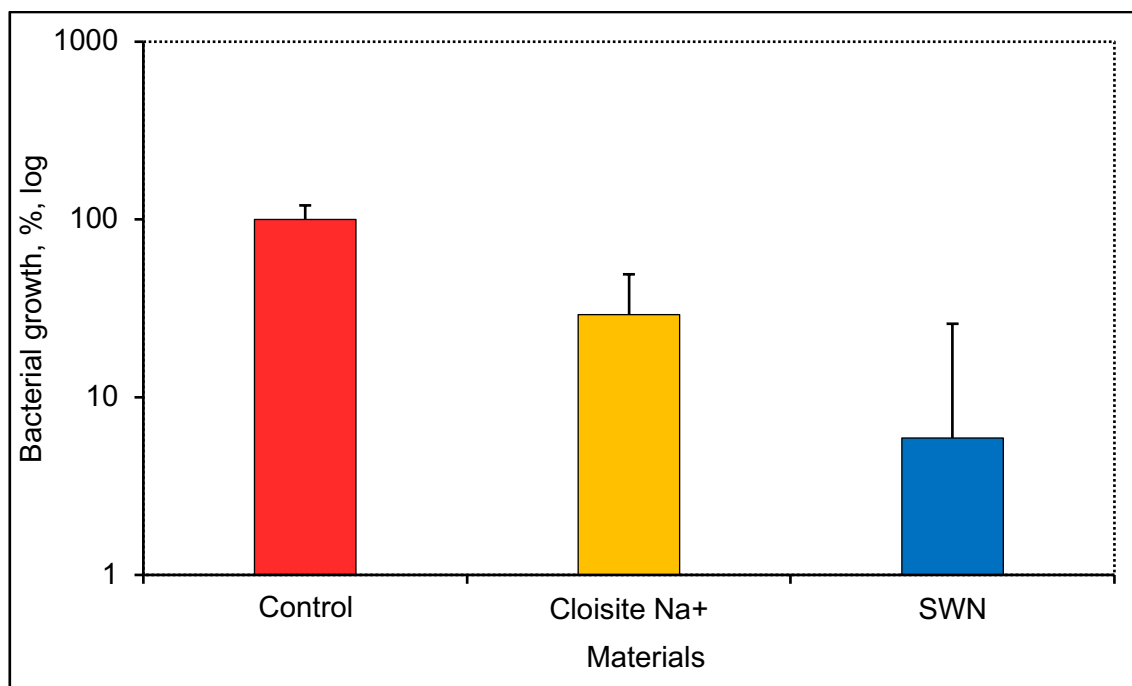


Figure 63. Antibacterial activity of exfoliated Cloisite Na⁺ and SWN suspensions against *E. coli* (NCTC 12493). The bacteria were incubated with Cloisite Na⁺ and SWN suspensions at 3 mg/ml concentration of clay, respectively, for 24 hours at 37°C. The control was PBS-resuspended *E. coli* without any treatments. Data shown represent the mean of two independent experiments with error bars of standard deviation.

According to Figs. 62-63, SWN showed stronger antibacterial activity against *E. coli* than MRSA, whereas Cloisite Na⁺ was effective against both bacteria.

3.1.10. Antibacterial activity of *in situ* synthesised BC/clay composites

As exfoliated clay showed antibacterial activity, the effect of both BC/SWN and BC/Cloisite Na⁺ composites, which were produced on a large scale, was investigated using MRSA and *E. coli* as described in Section 2.7.3. Bacteria at a concentration of 0.1 OD₆₀₀ were added to the surface of either BC or BC/clay composites, covered with a sterile plastic lid and incubated for 24 hours at 37°C. The growth of bacteria without any treatments (control) was compared to the

growth of bacteria using pure BC and BC/clay composites, respectively. As shown in Figs. 64-65, pure BC did not possess any antibacterial activity. This indicated that pure BC as can also increase the growth of the bacteria, which causes infections of wounds. Moreover, pure BC promoted the growth of *E. coli*.

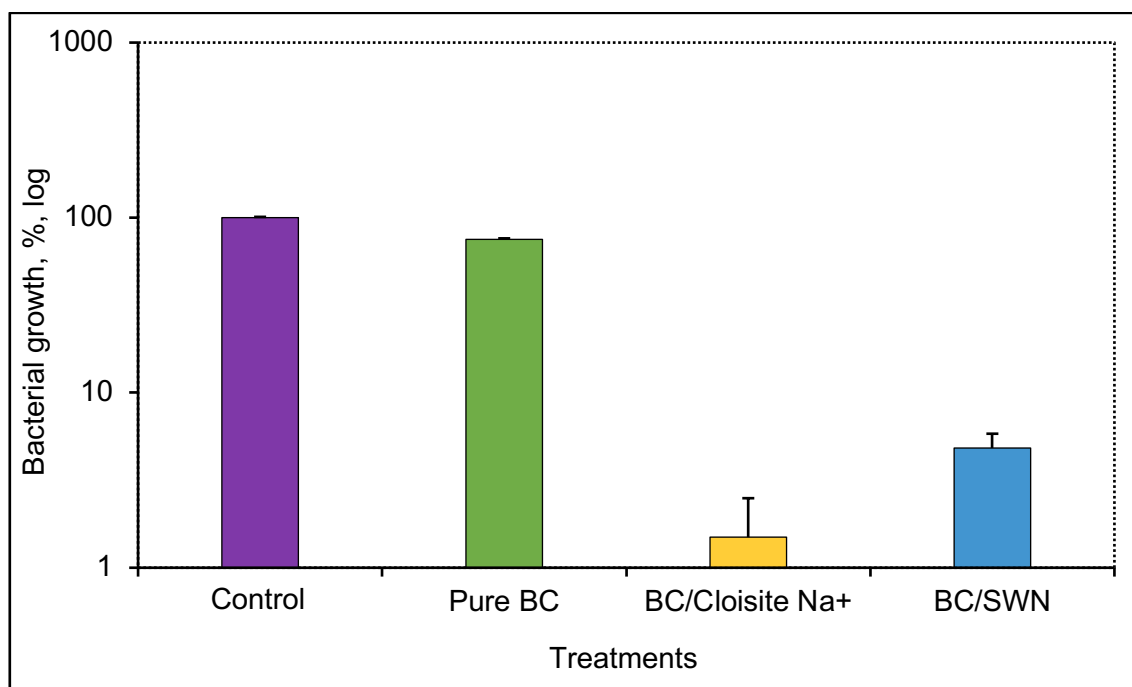


Figure 64. Antibacterial activity of BC/Cloisite Na⁺ and BC/SWN against MRSA. The control was PBS-resuspended MRSA without any treatments, which was placed on the surface of the empty petri dish and covered with a lid. The bacteria and different types of BC were incubated for 24 hours at 37°C. Data shown represent the mean of two experiments with error bars of standard deviation.

However, BC/Cloisite Na⁺ composite inhibited the growth of both MRSA and *E. coli*, where control values of bacteria were reduced to 1.4% and 14.6%, respectively. BC/SWN composites showed the reduction of the control values of MRSA to 4.8% and of *E. coli* to 16.8% respectively. Therefore, *in situ* synthesised BC/clay composites showed antibacterial activity against both MRSA and *E. coli* despite BC alone did not affect the bacteria. The antibacterial activity of the BC/clay composites was stronger against MRSA than *E. coli*. According to Figs. 62-65, the inhibition of bacterial growth by the clay was stronger inside the

composite. This might be due to a better interaction of bacteria and clay inside the matrix of BC rather than in aqueous PBS environment. According to *P*-value, there was no significant difference in the growth of bacteria.

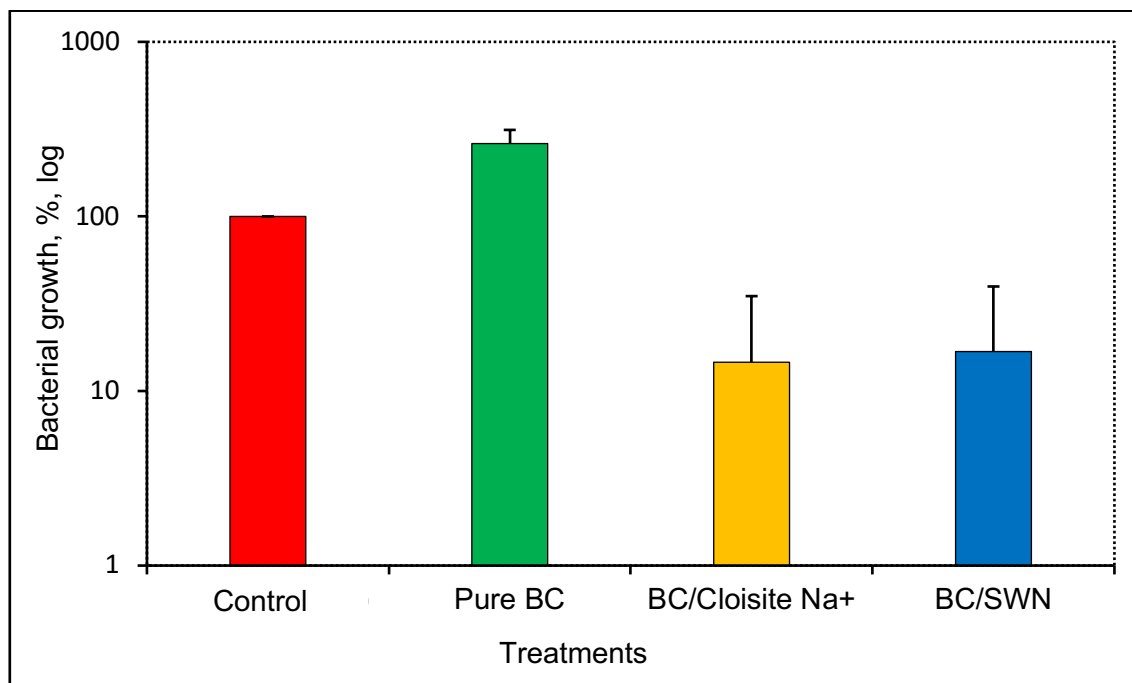


Figure 65. Antibacterial activity of BC/Cloisite Na⁺ and BC/SWN against *E. coli* (NCTC 12493). The control was PBS-resuspended *E. coli* without any treatments, which was placed on the surface of the empty petri dish and covered with a lid. The bacteria and different types of BC were incubated for 24 hours at 37°C. Data shown represent the mean of two independent experiments with error bars of standard deviation.

3.1.11. Cytotoxicity of Cloisite Na⁺ and SWN clay

The cytotoxicity of both Cloisite Na⁺ and SWN clay was investigated using non-exfoliated and exfoliated clay suspensions. Clay particles were either mixed with the tissue culture medium and were then considered as non-exfoliated or exfoliated using the Tefal blender as described in Section 2.4.1.1 prior to the cytotoxicity assay.

3.1.12. Cytotoxicity of non-exfoliated clay

Sterile Cloisite Na⁺ and SWN raw particles were mixed with the tissue culture medium at a concentration from 0.09 to 6 mg/ml. The suspensions were incubated with NIH 3t3 cells for up to 72 hours at 37°C.

3.1.12.1. Effect of non-exfoliated Cloisite Na⁺ clay on 3t3 cells

Fig. 66 shows the effect of non-exfoliated Cloisite Na⁺ clay suspensions on 3t3 fibroblast cells. As shown in Fig. 66, Cloisite Na⁺ affected the MTT reduction of the cells within first 24 hours. The highest percent of MTT reduced cells was 95%, which was observed using 0.19 mg/ml concentration of clay. The MMT reduction of 3t3 cells decreased with increasing the concentration of the clay and finally dropped to 40% using a concentration of 6 mg/ml. However, the overall MTT reduction of the cells increased after 48 hours. The level of MMT reduced cells raised over the control and reached 115% and 105% by using 0.09 and 0.19 mg/ml concentration of clay. In 48 hours, the percent of metabolically active cells decreased to 84% by using 1.5 mg/ml concentration of Cloisite Na⁺. Then, the level of MMT reduction of the cells continuously decreased to 46% by using 6 mg/ml concentration of the clay particles. After 72 hours, the overall percent of MMT reduced cells under the treatment reduced from a maximum of 57% to a minimum of 15% by using 0.09 and 6 mg/ml clay, respectively.

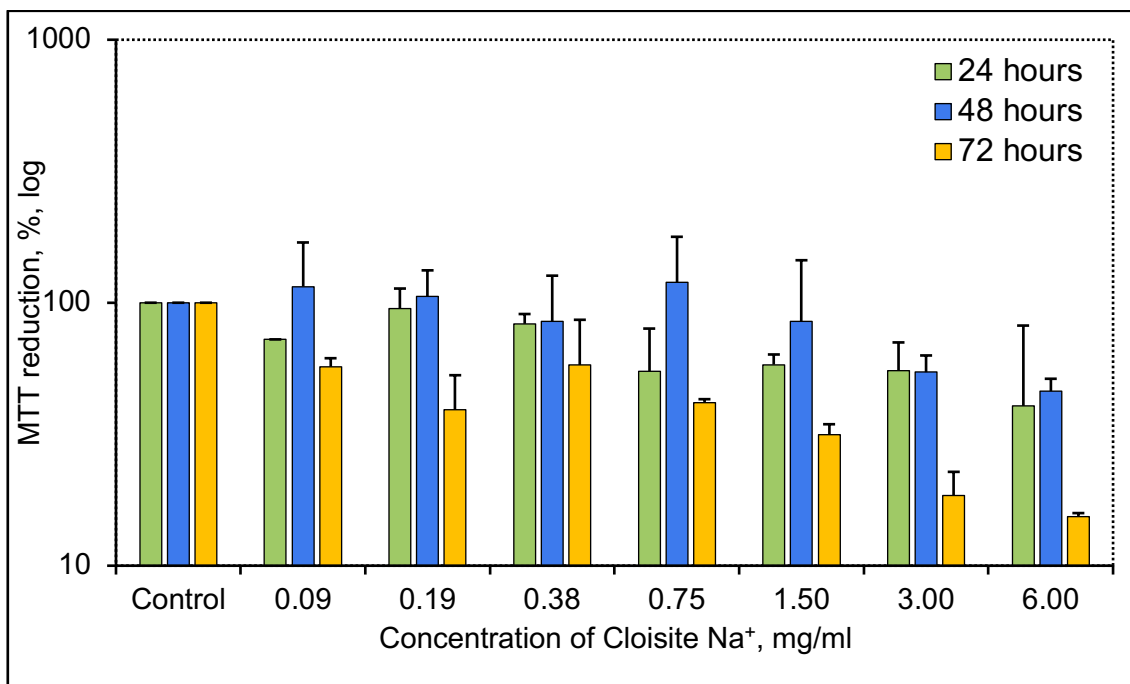


Figure 66. The effect of non-exfoliated Cloisite Na⁺ suspensions at 3t3 cells. Cloisite Na⁺ at a concentration of 0.09-6 mg/ml was incubated with NIH 3t3 cells for 24, 48 and 72 hours at 37°C. The control was the cells without any treatment at each tested time. Data shown represent the mean of two independent experiments of MTT assay with error bars of standard deviation. Treatments were compared to the controls. Regarding 24 hours of incubation, the data obtained after 24 and 48 hours using the concentration of 3 mg/ml are significantly different from the control with P -value <0.05 . After 72 hours, the treatments with concentrations of 0.09 and 0.38 mg/ml are different from the control (P -value <0.05), whilst 0.019, 0.075, 1.5, 3 and 6 mg/ml concentrations showed significant difference from the control with P -value <0.01 , respectively.

3.1.12.2. Effect of non-exfoliated SWN clay on 3t3 cells

Sterile SWN particles at concentrations from 0.09 to 6 mg/ml were incubated with 3t3 cells for 24, 48 and 72 hours at 37°C. According to Fig. 67, the level of MTT reduction of cells decreased within all treatments. Increasing the concentration of SWN in the medium led to a decrease in the MTT reduction of 3t3 cells from 93% to 32% using 0.09 and 6 mg/ml of the clay after 24 hours, respectively. Similarly, the MTT reduction decreased from 79% to 16% using the 0.09 and 6 mg/ml

concentration of clay, respectively, after 48 hours. However, the level of MTT reduction varied from 69% to 72% within 0.09 and 0.75 mg/ml after 72 hours. Starting from 1.5 mg/ml concentration of clay, MTT reduction of the cells significantly decreased to 34%. The lowest percent of MTT reduction obtained after 72 hours was detected to be 18% of control values at 6 mg/ml.

As shown in Fig. 67, SWN could inhibited the metabolic activity of 3t3 cells in a time- and concentration-dependent manner. This might be due to the ability of the particles to disrupt the cell membrane, which then leads to either apoptosis or necrosis^[215].

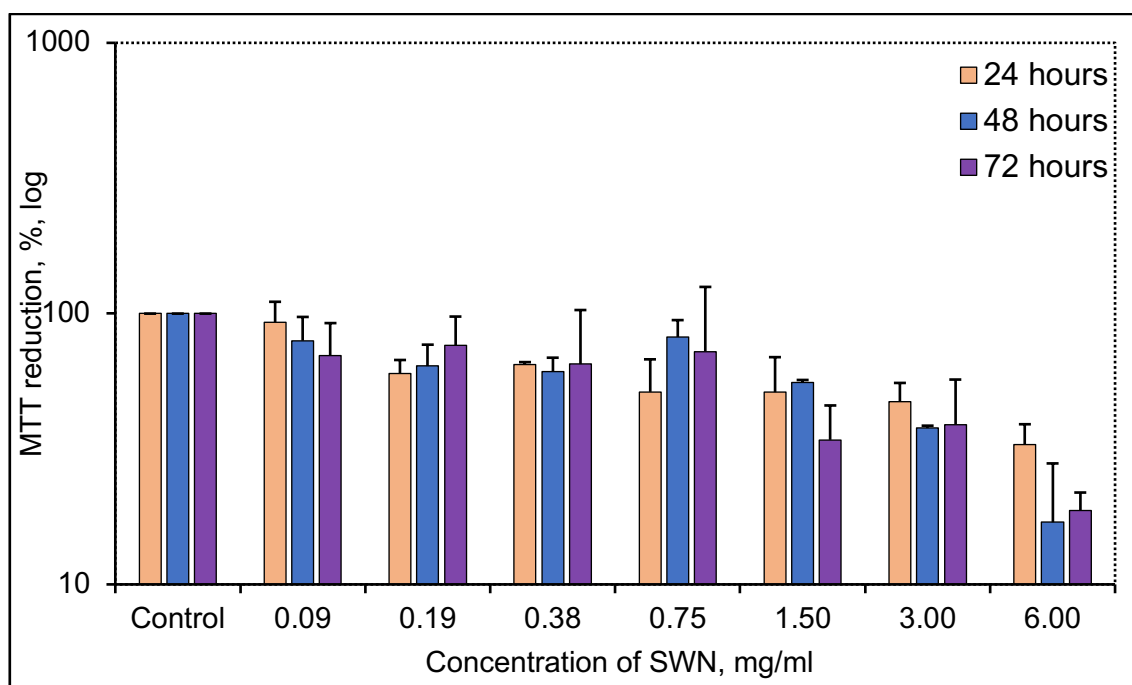


Figure 67. The effect of SWN/medium suspension on 3t3 cells. The suspension at a concentration of 0.09-6 mg/ml was inoculated with NIH 3t3 cells and incubated for 24, 48 and 72 hours at 37°C. The control was the cells without any treatment at each tested time. Data shown represent the mean of three independent experiments of MTT assay with error bars of standard deviation. Treatments were compared to the controls. Regarding 24 hours of incubation, the data obtained using the concentrations of 0.19, 0.38, 0.75, 1.5, 3 and 6 mg/ml are significantly different from the control with P -values <0.05, <0.001, <0.05, <0.01, <0.05 and <0.01, respectively. After 48 hours of incubation, the treatments with concentrations of 1.5 and 3 mg/ml showed significant difference from the control (P -value <0.01). The data obtained with concentrations of 1.5 and 3 mg/ml

are significantly different in comparison with the control after 72 hours (P -values are <0.05 and <0.001 , respectively).

3.1.13. Cytotoxicity of exfoliated suspensions

The cytotoxicity of exfoliated Cloisite Na⁺ and SWN clay suspensions was analysed using 3t3 cells, respectively. The cytotoxicity assay was carried out as described in Sections 2.12.1 and 2.12.3. The suspensions at a final concentration from 0 to 1.5 mg/ml were added to the tissue culture medium. The cells were incubated in the presence of the exfoliated clay suspensions for 24, 48 and 72 hours. As the medium was diluted and, therefore, the amount of the essential nutrients decreased, the effect of medium reduction on the metabolic activity of 3t3 cells was investigated prior to the experiment involving clay.

3.1.13.1. Effect of time on MTT reduction in 3t3 cells

The analysis of the cytotoxicity of the clay started with an investigation of levels of MTT reduction of 3t3 cells within different time frames. In order to achieve this, the cells were incubated for 24, 48 and 72 hours. The control was 24 hours. The effect of time on the MTT reduction of cells is shown in Fig. 68, the level of MTT reduction of 3t3 cells increased to 114% and 123% of the control values after 48 hours and 72 hours, respectively. Once the whole surface of the flask is covered, the growth of cells can decrease. This is called contact inhibition ^[216]. However, it was not the case in the current results. This specific cell line was identified by the supplier as transformed cells that continue proliferating even after they reach confluence.

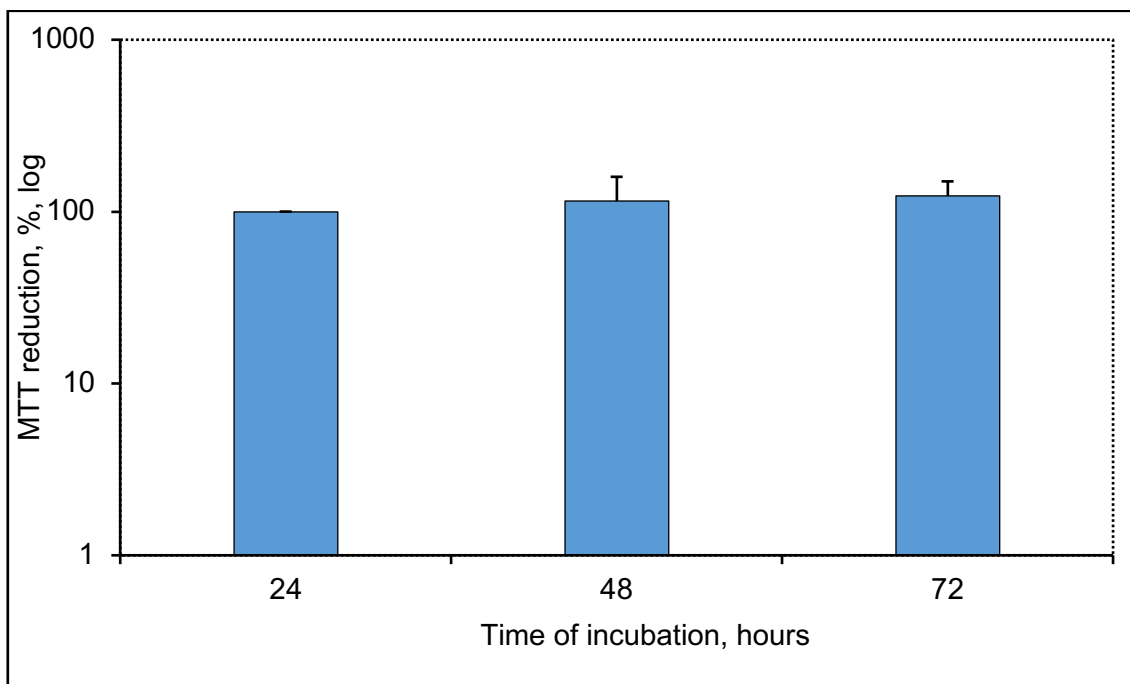


Figure 68. The effect of time of incubation on the MTT reduction in 3t3 cells after 24, 48 and 72 hours at 37°C. The control was obtained after 24 hours. Data shown represent the mean of three independent experiments of MTT assay with error bars of standard deviation.

3.1.13.2. The effect of the reduction of the medium on MTT reduction in 3t3 cells

Prior to the cytotoxicity assay with the clay suspensions, sterile PBS was used to dilute the medium from 100 to 75%, which corresponded to the volume of further added suspensions. The diluted medium was then incubated with the 3t3 cells from 24 to 72 hours at 37°C. As shown in Fig. 69, the MTT reduction of 3t3 cells gradually decreased from 100 to 61% by diluting medium from 99 to 75%, respectively, after 24 hours.

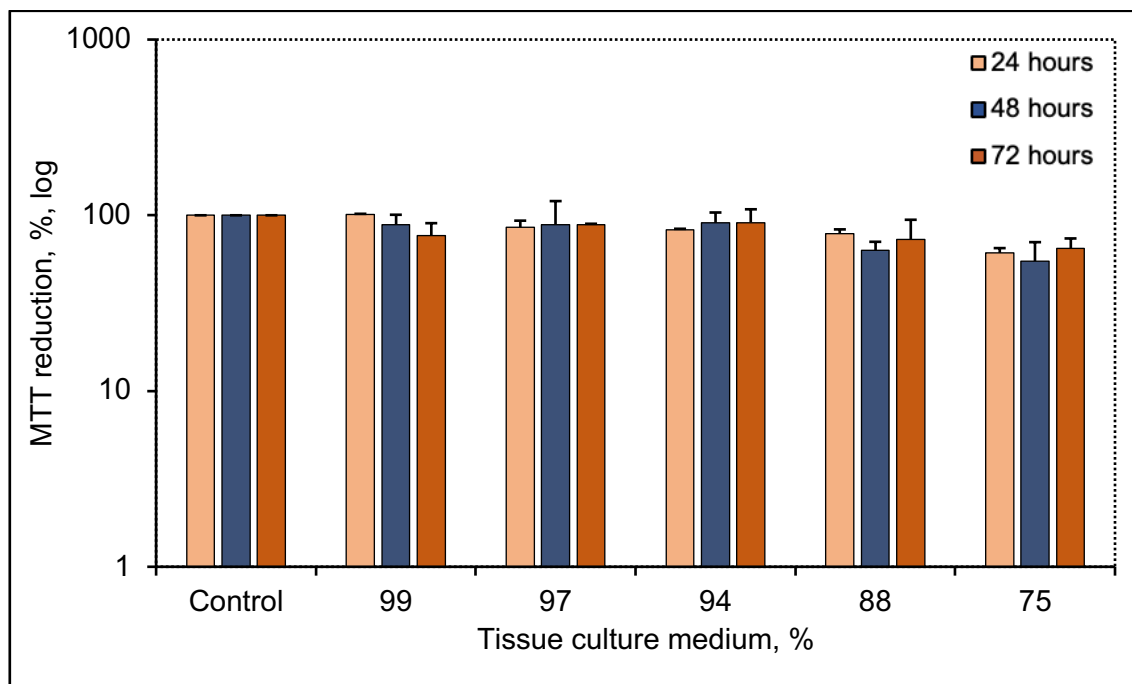


Figure 69. The effect of reduction of the medium on the MTT reduction in 3t3 cells. Culture medium was diluted with PBS from standard 100 to 75%. The control represented cells without any treatments after 24, 48 and 72 hours, respectively, at 37°C. Data shown represent the mean of three independent experiments of MTT assay with error bars of standard deviation. The treatments were compared to the controls. Values of 94% and 75% are significantly different from the control after 24 hours (P -value <0.05). After 48 hours, treatments of 88% and 75% are significantly different from the control (P -value <0.05), whereas 97% and 75% showed significant difference in comparison with the control after 72 hours with P -values <0.001 and <0.05 , respectively.

The level of MTT reduction of cells continuously decreased as medium was diluted. The lowest percentage of MTT reduction was observed using 75% of the medium after 48 hours, where the control values of the 3t3 cells significantly dropped to 54%. The level of MTT reduction of 3t3 cells slightly increased to 64% by diluting the medium to 75% after 72 hours. Such a decrease in MTT reduction would be taken into account when determining the effect of clay in further experiments.

3.1.13.3. Cytotoxicity of exfoliated Cloisite Na⁺ clay suspensions

The toxicity of exfoliated Cloisite Na⁺ clay suspensions, which were produced by 16 minutes of Tefal blending at a concentration from 0.09 to 1.5 mg/ml on 3t3 cells, was investigated after 24, 48 and 72 hours. A separate control was set up and inoculated within each time frame. As shown in Fig. 70, all clay concentrations increased the MTT reduction of cells. After 24 hours, the percent of MTT reduced cells reached a maximum of 139% using 0.09 mg/ml clay suspension. Then, there was a slight decrease to 100% using both 0.19 mg/ml and 0.38 mg/ml clay concentration. The level of MTT reduction increased again to 114% and 133% of control values by further increasing the concentration of Cloisite Na⁺ to 0.75 mg/ml and 1.5 mg/ml.

The MTT reduction in 3t3 cells firstly increased to 142% and 138% of control values by using 0.09 mg/ml and 0.19 mg/ml concentrations of the clay, respectively, after 48 hours. Then, there was a decrease of MTT reduced cells to 76%, 63% and 71% of control values using 0.38, 0.75 and 1.5 mg/ml of the clay, respectively. The percent of MTT reduced 3t3 cells went down to 22% at a clay concentration of 0.75 mg/ml after 72 hours. The decrease in MTT reduction could be due to the starvation of the cells.

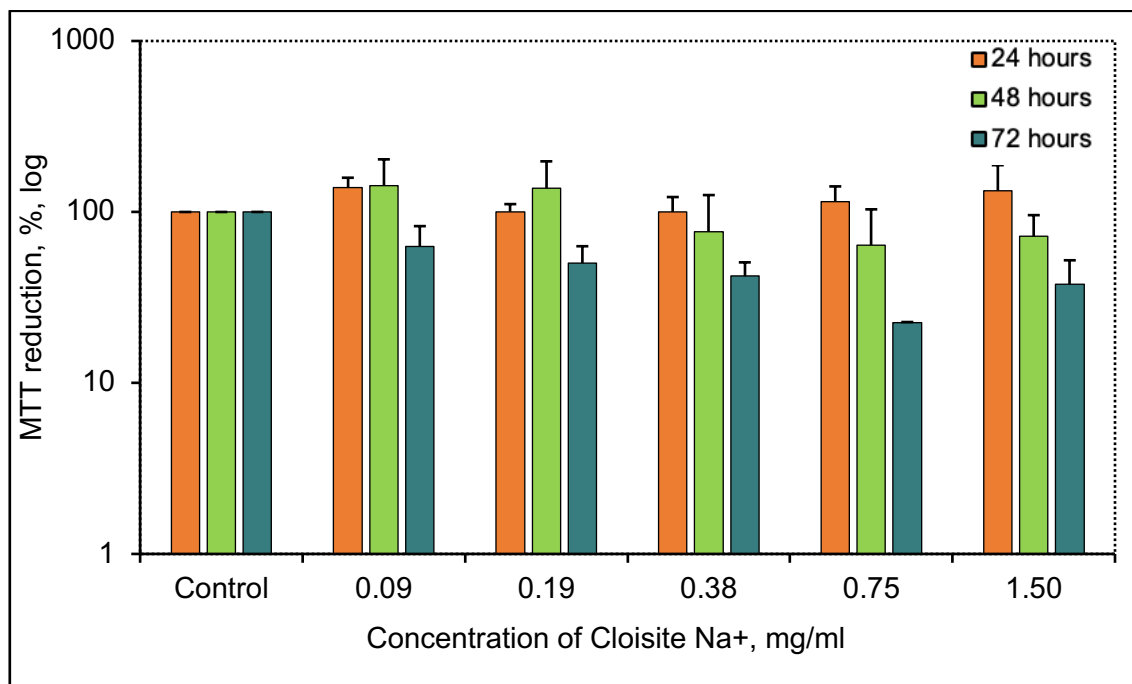


Figure 70. The effect of exfoliated Cloisite Na⁺ clay suspension on a level of MTT reduction in 3t3 cells. The cells were inoculated with clay suspensions at a concentration of 0.09-1.5 mg/ml and incubated for 24, 48 and 72 hours, respectively, at 37°C. The control the cells without any treatment after each time frame. Data represent the mean of two independent experiments of MTT assay with error bars of standard deviation. Controls were compared to the treatments obtained after 24, 48 and 72 hours. The data are not significantly different after both 24 and 48 hours. However, after 72 hours, the concentrations of 0.19, 0.38, 0.75 and 1.5 mg/ml are significantly different from the control with *P*-values <0.05, <0.01, <0.001 and <0.05, respectively.

Exfoliated Cloisite Na⁺ suspensions were not toxic for NIH 3t3 cells within 24 hours, whereas starting from 48 hours, the clay showed concentration-dependent toxicity on fibroblasts. However, such a decrease of the levels of MTT reduction of the cells was not statistically significant. It should also be noted that reducing the concentration of medium alone could result in the drop of metabolically active 3t3 cells.

3.1.13.4. Cytotoxicity of exfoliated SWN clay suspensions

The cytotoxicity of exfoliated SWN clay suspensions at the concentration from 0.09 to 1.5 mg/ml was also investigated using 3t3 cells (Fig. 71). As shown in Fig. 71, the level of MTT reduction of cells decreased from 105% to 56% of control values by using the concentration of SWN from 0.09 to 1.5 mg/ml, respectively, after 24 hours. In addition, 143% was the maximum percent of MTT reduced cells at 0.09 mg/ml concentration of the clay after 24 hours.

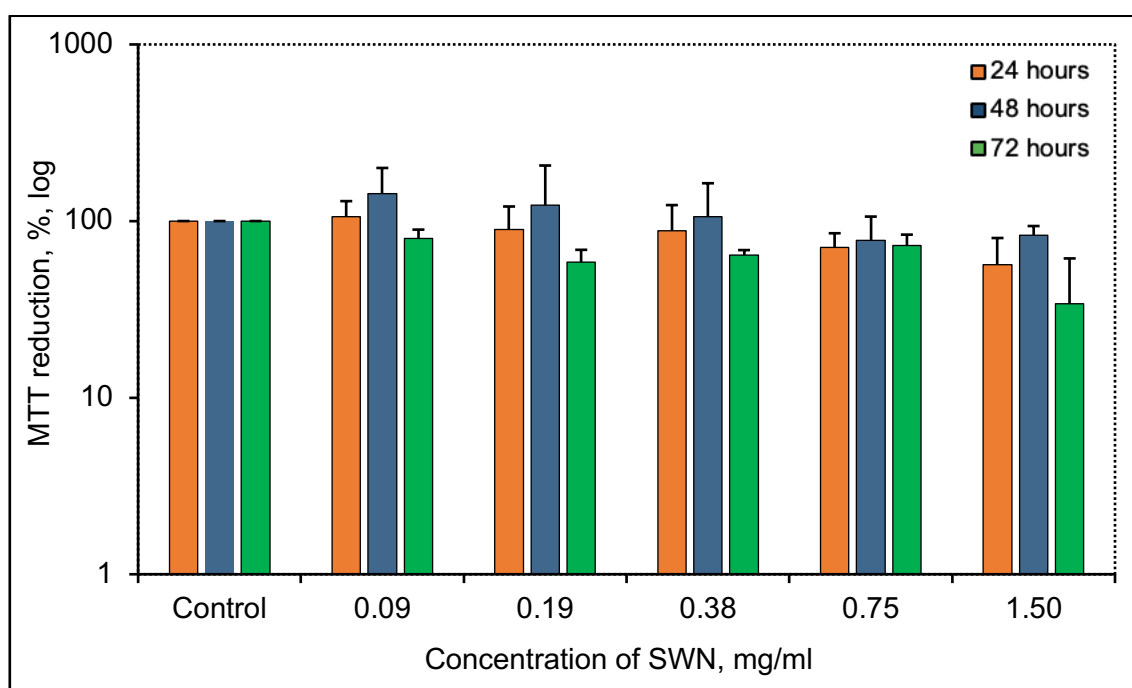


Figure 71. The effect of exfoliated SWN clay suspension on a level of MTT reduction in 3t3 cells. The cells were inoculated with clay suspension at a concentration of 0.09-1.5 mg/ml and incubated for 24 hours at 37°C. The control represented the cells without any treatment. Data represent the mean of two independent experiments of MTT assay with error bars of standard deviation. The treatments were compared to the controls. The concentration of 1.5 mg/ml is significantly different from the control after 72 hours (P -value <0.05).

The level of MTT reduction of cells at the concentration of 1.5 mg/ml of the clay increased from 56% to 83% after 48 hours. Similarly, the level of MTT reduced

cells dropped to a minimum of 34% of the control values at the highest concentration of the clay after 72 hours. The maximum number of MTT reduction was 80% at the lowest concentration of SWN after 72 hours.

Table 1 shows the level of MTT reduction of cells obtained after 24, 48 and 72 hours by using 75% diluted culture medium, Cloisite Na⁺ and SWN exfoliated suspensions at concentration of 1.5 mg/ml, respectively. As shown in Table 1, the levels of MTT reduction of the 3t3 cells was higher in the presence of clay after 24 and 48 hours, respectively. Then, the percent of MTT reduced cells decrease after 72 hours. Therefore, the clay was not toxic for the 3t3 cells within 48 hours. A possible reason behind the decrease of MTT reduced cells in a clay environment after 72 hours need to be further investigated.

Table 1. The comparison of MTT reduction in cells under different treatment after 24, 48 and 72 hours. Standard deviation is shown in the brackets.

Treatments at the highest used concentration/dilution	Time of incubation, hours		
	24	48	72
	MTT reduction in 3t3 cells (%)		
Medium diluted with PBS (75%)	61 (±23)	55 (±3)	65 (±13)
Exfoliated Cloisite Na ⁺ (1.5 mg/ml)	133 (±54)	71 (±23)	37 (±14)
Exfoliated SWN (1.5 mg/ml)	56 (±23)	83 (±10)	34 (±27)

3.2. Discussion

The optimal conditions for the growth of BC were investigated on both small and large scales. It was possible to introduce antibacterial activity to BC through synthesis *in situ* by using exfoliated Cloisite Na⁺ (NaMMT) and SWN suspensions. Non-exfoliated clays did not show any antibacterial activity against either MRSA or *E. coli*, whereas exfoliated clay reduced the growth of bacteria. The used concentration of clay of 3 mg/ml had no statistically significant effect on the MTT reduction in 3t3 cells.

3.2.1. Growth of pure BC in HS medium

There are factors that could affect the growth of pure BC. The formation of BC could be associated with a bacterial response to the temperatures studied. It has been reported elsewhere that temperatures below 20°C and above 35°C resulted in the lack of bacterial replication and, therefore, less extent of growth^[217]. Furthermore, the temperature over 35°C could lead to a reduction in bacterial multiplication through damaging the proteins in the cell wall^[217]. A number of studies stated that the highest yield of BC was observed in the range of 28-30°C^[218, 219]. This agrees with the results obtained in the current study. Moreover, the synthesis of BC did not decrease beyond 48 hours on a large scale as was observed on a small scale. A possible reason might be the effect of the volume of the medium as well as the size of the trays used. As the bacterial growth increases, and, therefore, the number of cells increase, a suitable depth of the medium might be beneficial for the growth of thick cellulose. Another study has observed the limit of BC formation on a large scale after 14 days, where the synthesis of BC was much faster within the first 7 days using a 250 ml flask with HS medium^[220]. This might be due to exhaustion of medium. Similar results were obtained by other researchers. It has been reported that the maximum bacterial growth at the log phase was observed to be after 48 hours, which then decreased after 72 hours using 24-well plates at 30°C^[221, 222].

Another possible reason for such a reduction in BC growth after 72 hours on a small scale might be insufficient amount of carbon and nitrogen sources left for bacterial survival after 48 hours. For instance, study elsewhere has continued to synthesise BC for 96 hours using 24-well plates at 30°C and stated that the growth of BC was completely stopped after 96 hours^[217]. Thus, the decrease in concentration of glucose could be another reason for poor BC formation. Glucose is utilised by bacteria in several ways. Glucose is used as an energy source as well as the cellulose precursor. The glucose is converted into (keto)gluconic acids, so that the concentration of glucose could decrease progressively during the fermentation process^[128]. In another study, the percentage of glucose used, and glucose converted into cellulose was found to be directly proportional to the production of BC^[217]. The yield of BC has been increased in parallel with increasing the initial glucose concentration^[128]. Therefore, exhaustion of the medium might be another reason why the growth of BC decreases after a long incubation period. Therefore, BC could require 48 hours in order to grow sufficiently for the subsequent experiments on both small and large scales.

3.2.2. Swelling and exfoliation of clays

As was described previously in Section 1.3.1.1, both Montmorillonite and SWN have 2:1 structure, where two tetrahedral sheets are sandwiching one octahedral sheet^[83]. These sheets are negatively charged and, thus, the charge is balanced by exchangeable cations such as Na⁺^[83]. In a dry state, the attractive interaction of both van der Waals and electrostatic forces can hold Na⁺ cations and clay sheets together^[83]. However, in the aqueous environment, exchangeable cations, which form a double layer between the particles, do not interact strongly and can flow independently^[223]. When the clay gets in contact with water, which enters the interlayer space, hydration of Na⁺ cations occurs^[224]. This leads to the swelling and delamination of particles. The exchangeable cations could attract water molecules in the interlayer space. As a result of the hydration, the exchangeable cations may expand in volume^[224]. The interaction between Na⁺

cations and water results in the formation of a solvation shell around the cations^[224]. This means that the interactions of Na^+ cations and the clay particles could decrease. It has been reported that Na^+ cations reside near the siloxane surface by moving to the middle plane of the interlayer space after hydration in the presence of 3 water molecules^[225]. This resulted in the opening of the interlayer space to 1.38\AA ^[225]. However, once Na^+ cations absorbed 5 molecules of water, the interlayer space increased to 15.35\AA ^[225]. This means that the hydration plays an important role in the exfoliation of Cloisite Na^+ . The simulation obtained elsewhere has shown that the hydration of Na^+ cations could lead to their relocation to the centre of the interlayer space of NaMMT in up to 200 picoseconds^[226, 227].

The shear force can increase the delamination of clay particles if just the interlayer space of clay is hydrated. Nanoparticles may be randomly delaminated from the stacks of initial clay. The delamination is a disconnection between layers followed by the deconstruction of chemical bonds, whereas the exfoliation means that chemical bonds between the clay layers are broken with the result that clay particles are completely separated^[223]. Fig. 72 illustrates an exfoliation of clay particles.

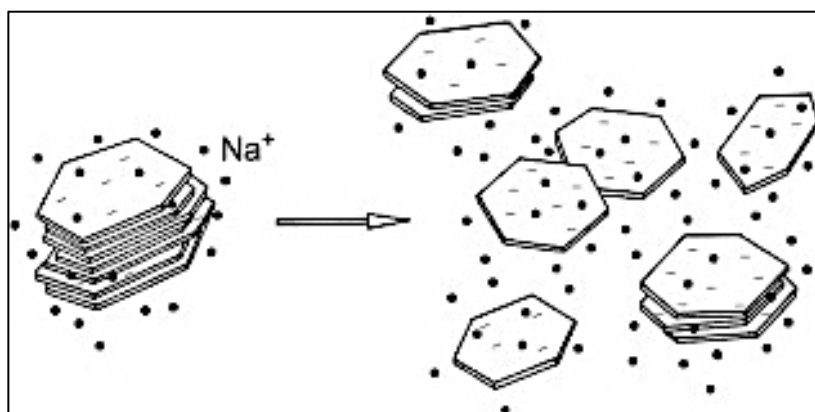


Figure 72. Schematic representation of exfoliation of clay particles^[223].

Magnetic stirring, ultrasonication and Tefal blending techniques were used for the exfoliation of both Cloisite Na^+ and SWN suspensions. However, the Tefal blending was the most successful technique for the exfoliation of clay. A possible

reason why magnetic stirring not being successful in exfoliation of both Cloisite Na⁺ and SWN suspensions might be the shear stress applied was insufficient for exfoliation. The mechanism of the magnetic stirring is based on the external magnetic field that rotates the magnetic bars inside the mixture, which results in a vortex effect and subsequent stirring of the suspension through the collision of particles^[228]. The turbulent flow of the stir could be enough to separate the aggregations of the micro-particles. However, the shear force might not be sufficient to fully exfoliate the clay and to separate the layers.

Furthermore, complete exfoliation was not achieved for either Cloisite Na⁺ or SWN suspensions using the ultrasound. A possible reason could be the duration of ultrasonication. It has been reported elsewhere that particles exposed to longer duration of sonication showed increased levels of breakage^[196]. As the ultrasonication was performed by an elongated tip, which was placed in the middle of the suspension, the size of particles at this location could be smaller than the size of particles located at the edges of the beaker. As another research study pointed out, the effective zone of dispersion of particles was observed near the tip^[196]. Furthermore, the volume of a suspension plays a crucial role in the exfoliation of clay. Increasing the volume of the suspension might lead to an increase in both final size of particles and time required for achieving the exfoliation^[196]. Another possible reason might be that the amplitude used could not be efficient for breaking all aggregations. It was found that at higher amplitudes more reduction in the size of particles was observed^[196]. Furthermore, the power of sonication influences the level of cavitation in the liquid^[196]. This means that high levels of power could increase the number of cavitation bubbles, which break the aggregations. However, the high power of ultrasonication could also damage the structure of nanosheets^[72]. Nevertheless, ultrasonication was found to be effective in exfoliation of most layers of the clay^[197], agglomerations of particles being observed even using the highest amplitude^[196]. However, it was clearly not the case in this study. In this particular case, the condition applied was

not only ineffective to exfoliate clay layers, but also failed to separate micro-particle aggregations.

The total Tefal blending method was the most effective technique for the exfoliation of clay. The mechanism of the blending could be based on the circular whirring motion that created a vortex. The vortex caused the blades to pull the particles towards the middle and then out to the sides. A combination of circulation, cavitation and shearing forces resulted in uniform exfoliation of the clay. The coffee grinder was more effective than the chopper for the exfoliation of the clay. Such a result might be due to the shape of the blades. A possible reason for the better exfoliation achieved using the coffee grinder could be narrow space between the flat blade and surface resulting in enhanced laminar flow. The shear stress in laminar flow might be much higher than in turbulent flow. Any particles that may possibly settle underneath the blade were pushed out to the sides by the vortex effect. Furthermore, such a structure could lead to the almost vertical tornado-like stirring of the suspensions. Oppositely, a distance between one side of the blade of the chopper was larger than another. This may result in slightly dislocated stirring towards one side of the bowl. Thereby, the best technique for the exfoliation of Cloisite Na⁺ was blending the suspension using the coffee grinder at speed 1 for 16 minutes.

The exfoliation of clay in aqueous liquid is currently a challenge^[229]. However, the exfoliation of clay was successfully achieved using the coffee grinder in this study. The result demonstrated that this method could be a simple and low-cost technique for the exfoliation of clay in an aqueous environment.

3.2.3. Growth of BC in clay environment

The increased viscosity of SWN seems to be a possible reason for the poor growth of BC/SWN composites. The viscosity could prevent bacteria from reaching oxygen and, therefore, it may be challenging for them to produce BC.

Aeration is one of the most important processes of the cultivation. As *G. xylinus* are highly aerobic bacteria, a suitable oxygen supply is crucial^[230]. The gel could block the access of oxygen and, therefore, lead to a reduction in the bacterial growth. The gel could also result in restriction of bacterial movement within the liquid. A possible reason behind the increased viscosity of SWN might be the ability of the clay to form physically self-cross-linked gel structures. This might be due to a disordered network of particles dispersed throughout its volume^[212]. It has been reported that the concentration of Laponite, which is a synthetic clay, above 1 wt.% might lead to blocking clay particles into a stable structure known as an equilibrium gel^[212]. It has been concluded elsewhere that a concentration of Laponite below 1 wt.% could lead to gel formation after a few months^[212]. However, the results showed that 0.3 wt.% of SWM started to form a gel after 24 hours. The gelation might occur through a formation of micro-flocculation, where individual particles of clay can aggregate into clot-like masses due to the electrostatic attraction between the negatively charged parts of particles and the positively charged edges^[212]. This can result in a card-house structure^[212].

Another reason for the poor synthesis of BC in a non-exfoliated clay environment might be pH. As the pH of the final medium/clay suspension was adjusted to pH5 prior to the experiment, the pH of the clay suspensions itself was not able to affect the synthesis of BC at the beginning. However, during the cultivation and formation of the cellulose, the bacteria produced gluconic acid, which resulted in a decrease to about pH4-3^[230]. It has been reported that a decrease in pH could lead to a decrease in negative zeta potential, which may affect the dispersion of particles^[231]. The dispersion of clay has been found to be better at alkaline rather than acidic pH^[232]. Therefore, clay may not be well-dispersed in an acidic environment created by the bacteria. In addition, as non-exfoliated clay had large aggregation of particles, these aggregations could even increase in a size during the growth of BC.

3.2.4. Antibacterial activity of natural clay

Natural dry clay did not show any antibacterial activity; however, clay might be antibacterial when it is hydrated^[233]. Exchangeable cations, which are located in the interlayer space could be released upon the hydration of the clay and affect growth of bacteria^[234]. The exact mechanism of the antibacterial action of natural exfoliated clay is not well understood^[234]. However, a mechanism of the antibacterial activity of exfoliated NaMMT has been proposed elsewhere (Fig. 73)^[234].

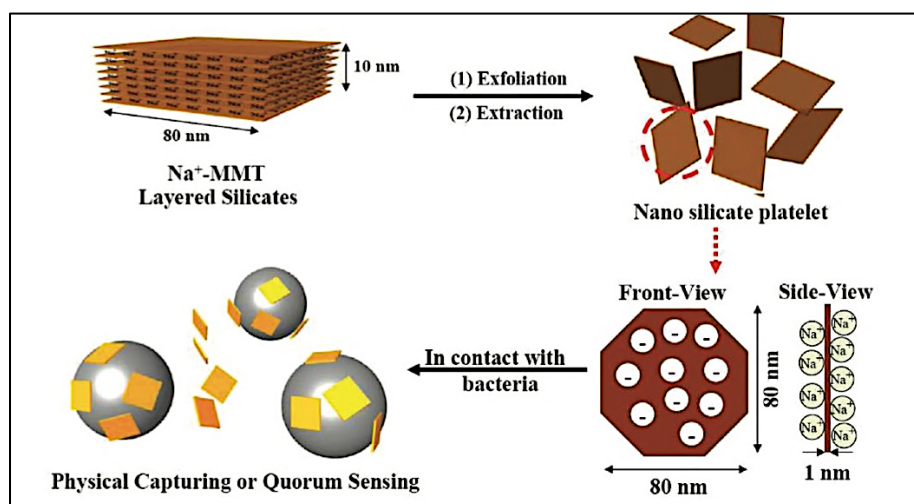


Figure 73. A proposed antibacterial mechanism of NaMMT^[234].

As shown in Figs. 72-73, during the exfoliation, Na⁺ cations, which are hidden between layers of the clay, could be exposed on the surface^[223, 224]. There are approximately 18, 000 ions per nanolayer^[235]. As was described in Section 1.2.3.1., the negative charge of Gram-negative bacteria such as *E. coli* appears due to the presence of phospholipids and LPS inside the outer membrane, whereas Gram-positive MRSA carries a negative charge due to the presence of teichoic acids^[236-238]. Thus, an electrostatic interaction between Na⁺ cations and the negatively charged membrane of bacteria could occur. This may lead to permeabilisation and burst release of the components of a bacterial cell wall^[239]. For instance, it has been reported elsewhere that the cell walls of *E. coli* were shrunk and degenerated after being in the exfoliated clay environment for 24

hours^[239]. Furthermore, ionic charges of nanoparticles could attract polar organic molecules and, subsequently, adhere to a bacterial cell wall followed by creating a “blockade effect”^[234]. It has been reported that the diameter of *E. coli* and *S. aureus* cells is about 1.5–2 μm and 0.5–1 μm , respectively, whereas the dimensions of a nanoparticle are about 100 nm \times 100 nm \times 1 nm^[240]. This means that the particles may cover the surface of bacteria. This might interfere with crucial biological functions such as sodium-ion transport and quorum sensing. Furthermore, such an attachment of the Na⁺ cations to a bacterial cell wall could affect osmosis and lead to the dehydration of bacterial cells. This might explain why non-exfoliated clays did not show any antibacterial activity against both MRSA and *E. coli*, whereas exfoliated clay reduced the growth of bacteria.

In the current study, the exfoliated Cloisite Na⁺ and SWN clay showed antibacterial activity against both MRSA and *E. coli*. It has been reported elsewhere that the exfoliated NaMMT nanoparticles decreased the growth of *E. coli* by 99% after 24 hours^[240]. SEM results have shown accumulation and association of exfoliated clay particles around the cell wall of *E. coli*, which appeared rough^[240]. In another study, *Salmonella* cells that were incubated with 0.1 wt.% of clay nanoparticles for 24 hours and tended to bind together that can be associated with the motion of their flagella^[234]. The surface of *Salmonella* cells appeared shrink and dehydrated after contacting clay for 24 and 48 hours^[234]. Furthermore, it has been reported that exfoliated nanoparticles of NaMMT at a concentration of 0.3 wt.% showed antibacterial effects against both *S. aureus* and *E. coli* after 24 hours, whereas non-exfoliated NaMMT clay did not possess any antibacterial activity^[240]. The results obtained in the current study are in agreement with these reports. SEM results elsewhere have shown that the nanoparticles covered the cell walls of both *S. aureus* and *E. coli* after 24 hours^[240]. Another study has concluded that nanosized silicate particles that were obtained from natural silicate clay minerals had antibacterial activity through physical trapping mechanism^[235]. This means that clay particles might exhibit antibacterial activity externally without penetrating a cell wall. Moreover, it has

been stated that nanoparticles could inhibit the growth of Gram-positive MRSA, *S. aureus* and *Streptococcus pyogenes* as well as Gram-negative *E. coli* and *P. aeruginosa* through generating ROS^[235]. In addition, it has also been concluded elsewhere that an increase in surface area by exfoliation might be a key factor in boosting antibacterial activity^[240].

The antibacterial effect of exfoliated nanoparticles could be time-dependent. As time of the incubation increased, some hollow spaces around particles were observed^[240]. This might mean that the bacteria could be dead. It has been reported that the overall count of *E. coli* decreased during the increasing time of incubation with 1 wt.% of nanoparticles from 24 hours, when the concentration of bacteria treated with clay was close to the control values, to 72 hours, when the CFU of treated bacteria reduced up to 50% compared to the control^[240]. Both duration of incubation and concentration of nanoparticles can affect the interaction between the anionic components of the cell walls and the positively charged exchangeable cations^[240].

In addition, no growth of *Salmonella typhimurium* strains was observed in the presence of exfoliated nanoparticles elsewhere^[241]. However, particles have not shown any effect on the mutagenicity in 5 different *Salmonella typhimurium* strains^[241]. Also, there was no increase in the frequency of micronuclei and no chromosomal damage after treatment with nanoparticles^[241]. This means that exfoliated nanoparticles might not be able to penetrate the cell wall of Gram-negative bacteria such as *Salmonella*. Another study, however, concluded there was no difference in inhibiting the growth of both Gram-positive and Gram-negative bacteria^[240].

The antibacterial activity could also be dose-dependent. It has been reported elsewhere that a concentration of 0.3 wt.% of nanoparticles inhibited 85% of the growth of *E. coli* in saline buffer^[235]. However, no antibacterial activity of nanoparticles has been observed in lysogeny broth^[235]. Furthermore, non-exfoliated NaMMT did not show any antibacterial activity at a concentration of 1

wt.% either in the saline solution or in lysogeny broth^[235]. In addition, another study has reported that showed that exfoliated clay inhibits the growth of bacteria just in a PBS environment, whereas no significant antibacterial activity was observed in the medium^[234]. This might be due to the polar interaction of nanoparticles with proteins in the medium, which prevents the adherence of particles on the surfaces of cells. This might explain why *G. xylinus* was able to synthesise BC in the exfoliated clay environment.

Some experiments have been performed with separated DNA and NaMMT clays elsewhere^[242, 243]. It has been reported that DNA could be absorbed by NaMMT and SWN through electrostatic interactions and ligand exchange, where phosphate groups at the end of a DNA molecule and hydroxyl groups of the ribose can be absorbed to the clay^[242, 243]. It has been found that NaMMT can intercalate single-stranded DNA to the interlayer space. However, the results elsewhere have shown that the binding of DNA to NaMMT was weak in water^[242, 243]. Thereby, the mechanism of antibacterial action of the exfoliated clay and possibility of particles to enter bacterial cells need to be further investigated.

3.2.5. Effect of clay on MTT reduction in 3t3 cells

Both Cloisite Na⁺ and SWN suspensions decreased the levels of MTT reduction in 3t3 cells in time- and concentration-dependent manners. It has been stated elsewhere that Cloisite Na⁺ could inhibit the proliferation of mammalian cells at high concentration and over long periods of exposure^[244]. A concentration of 6 mg/ml of the non-exfoliated SWN suspension significantly reduced the metabolic activity of 3t3 cells after 24 hours. Clay particles could bind to negatively charged components inside the membrane of cells and affect either cell proliferation or life cycle^[244]. For example, it has been reported elsewhere that particles of the clay could penetrate cells of the epithelium^[244]. Furthermore, in another study, particles of Cloisite Na⁺ have accumulated in the perinuclear region; however, they have not penetrated the nuclear membrane^[244]. Moreover, clay may diffuse, settle and eventually aggregate in solution. These processes can, thus, lead to

the development of physicochemical stress over the cells^[24]. An interaction of Cloisite Na⁺ clay with the growth medium could lead to either intercalation or absorption of substances that are present in the medium. These adsorbed molecules might attract the cells to adhere to the surface of Cloisite particles. A high concentration of clay might lead to intensive interaction between the negatively charged cell surface and positively charged cations between layers of the clay. Alternatively, negatively charged components of the medium could bind to the particles, which would possibly restrict access of the cells to nutrients after 72 hours. Following this reasoning, aggregates of the clay could settle down on the bottom of the wells, interact with the cells and, as a consequence, clay-cell compounds might be washed out during the MTT assay.

Furthermore, it has been reported elsewhere that small sized particles might enter mammalian cells, which may die after 24 hours^[215]. However, the data obtained in the current study showed that the level of MTT reduction by the cells increased after 48 hours. It has been stated elsewhere that exfoliated clay particles did not affect the MTT reduction in both human gingival fibroblasts and blood endothelial cells after 24 hours^[240]. Moreover, the MTT reduction in the blood endothelial cells treated with 0.3 wt.% of exfoliated silica nanoparticles was similar to the control after 72 hours^[240]. This experiment has been carried out elsewhere using 24-well plates, where the clay suspensions were added directly to the culture medium^[240]. The cells were incubated for 24, 48 and 72 hours and then monitored by MTT assay^[240].

A time-dependent uptake of the clay by cells might occur at doses over 1 mg/ml after 48-72 hours^[244, 245]. It has been observed elsewhere that concentrations over 1 mg/ml can change the viscosity of the medium and subsequent penetration of oxygen^[106]. This might explain why the levels of MTT reduction in 3t3 cells dropped after 48 and 72 hours using concentrations over 1 mg/ml of the clays. However, a concentration up to 31 µg/ml of non-exfoliated NaMMT suspension did not show any cytotoxicity towards Caco-2 and HepG2 (liver) cell

lines in previous studies^[101-103, 105]. The viability of human umbilical vein endothelial cells (HUVEC) in the presence of 0-125 µg/ml ultrasound-treated NaMMT suspension has been observed elsewhere^[104]. The results showed that NaMMT did not exhibit any cytotoxicity^[104]. It has also been reported that NaMMT inhibited HepG2 cell growth, which then resulted in cell necrosis at all used concentrations starting from 1 to 1000 µg/ml^[105].

Regarding exfoliated clay suspensions, one reason for low levels of MTT reduction in 3t3 cells could be exhaustion of the medium. The starvation of cells played a crucial role in the analysis of the toxicity of clay suspensions. The possibility of exhaustion of the medium was overcome by using non-exfoliated clay suspensions that were mixed with the culture medium. However, the main limitation of such a method is the swelling behaviour of the clay. As the clay was added in the form of powder, the interlayer space expanded and liquid from the medium started to penetrate between the layers. Furthermore, positively charged components of the medium and bioactive molecules could interact with the clay by ion exchange reactions. This means that the adsorption capacity of Cloisite clay might reduce the amount of nutrients available. Therefore, mammalian toxicity of clay should be investigated further.

Chapter 4. *Ex situ* synthesis of BC/clay composites

Another technique for the incorporation of clay into BC matrix was *ex situ* modification using the vacuum self-assembly method as described in Section 2.6.3.1. SWN, Cloisite Na⁺ and Cloisite 10A, 15A, 20A, 30B and 93A organoclay were impregnated *ex situ* into pure BC. The antibacterial activity of the BC/clay composites was investigated against MRSA, *E. coli* (NCTC 12493) and *P. aeruginosa*. The mammalian cytotoxicity behavior of organoclay and synthesised composites was analysed using 3t3 cells.

4.1. Results**4.1.1. *Ex situ* synthesised BC/Cloisite Na⁺ and BC/SWN composites**

Ex situ synthesised BC/Cloisite Na⁺ and BC/SWN composites were prepared through vacuum self-assembly method using 6 mg/ml of each exfoliated clay suspension, respectively, as described in Section 2.6.3.1. The composites were analysed for their antibacterial and cytotoxicity properties. The antibacterial activity of the BC/clay composites was investigated on MRSA, *E. coli* and *P. aeruginosa*.

4.1.2. Antibacterial activity of *ex situ* modified BC/SWN and BC/Cloisite Na⁺ composites

Fig. 74 shows the antibacterial activity of pure BC and *ex situ* modified BC/SWN and BC/Cloisite Na⁺ composites against MRSA. As shown in Fig. 74, pure BC did not possess any antibacterial activity and increase the growth of MRSA nine fold compare to the control values. This might be due to the water-holding capacity of BC. However, the BC/Cloisite Na⁺ composite showed antibacterial activity and decreased the growth of MRSA to 40% of the control values. The BC/SWN composite inhibited strong bacterial activity and significantly reduced the growth of MRSA to 6% of control values.

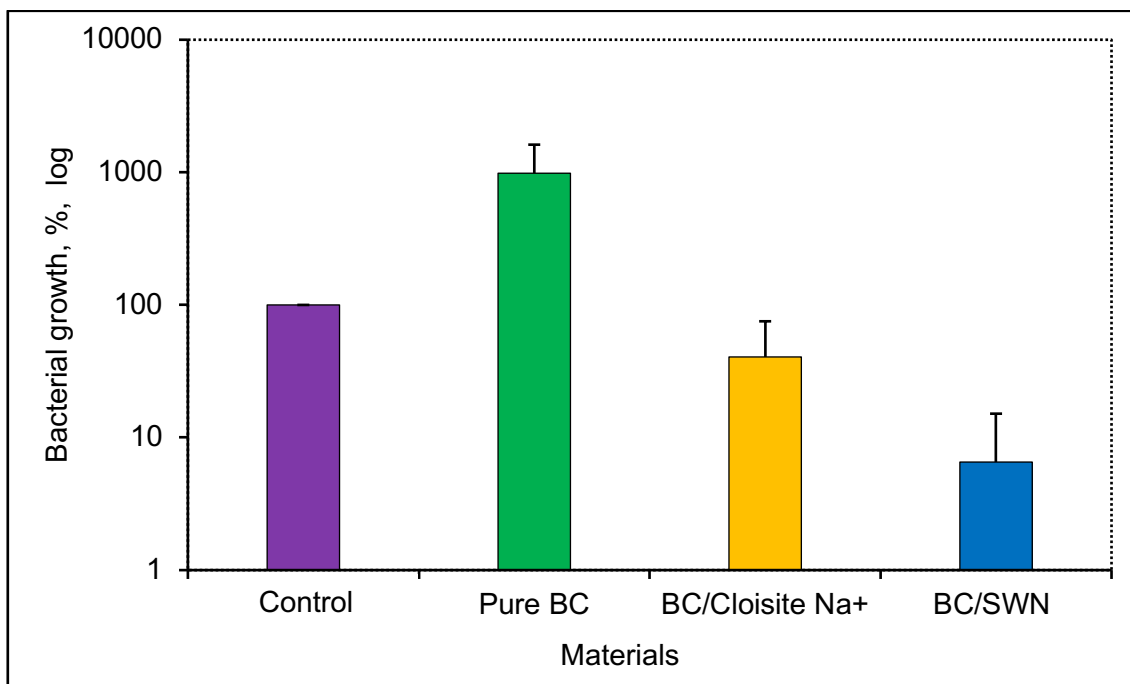


Figure 74. Antibacterial activity of pure BC, BC/Cloisite Na⁺ and BC/SWN against MRSA after 24 hours. The exfoliated clay at a concentration of 6 mg/ml was pumped inside the matrix of BC. The control was PBS-resuspended MRSA, which was placed on the surface of the empty petri dish and covered with a lid. Data represent the mean of four independent experiments with error bars of standard deviation. The treatments were compared to the control. Pure BC, BC/Cloisite Na⁺ and BC/SWN are significantly different from the control (P -value <0.01).

The antibacterial activity of *ex situ* synthesised BC/Cloisite Na⁺ and BC/SWN composites were investigated against *E. coli*. As shown in Fig. 75, both BC/Cloisite Na⁺ and BC/SWN possessed antibacterial activity against *E. coli* and reduced its growth to 15% and 13%, respectively.

According to Figs. 73 and 75, the antibacterial activity of *ex situ* and *in situ* synthesised BC/Cloisite Na⁺ and BC/SWN composites was similar against *E. coli*.

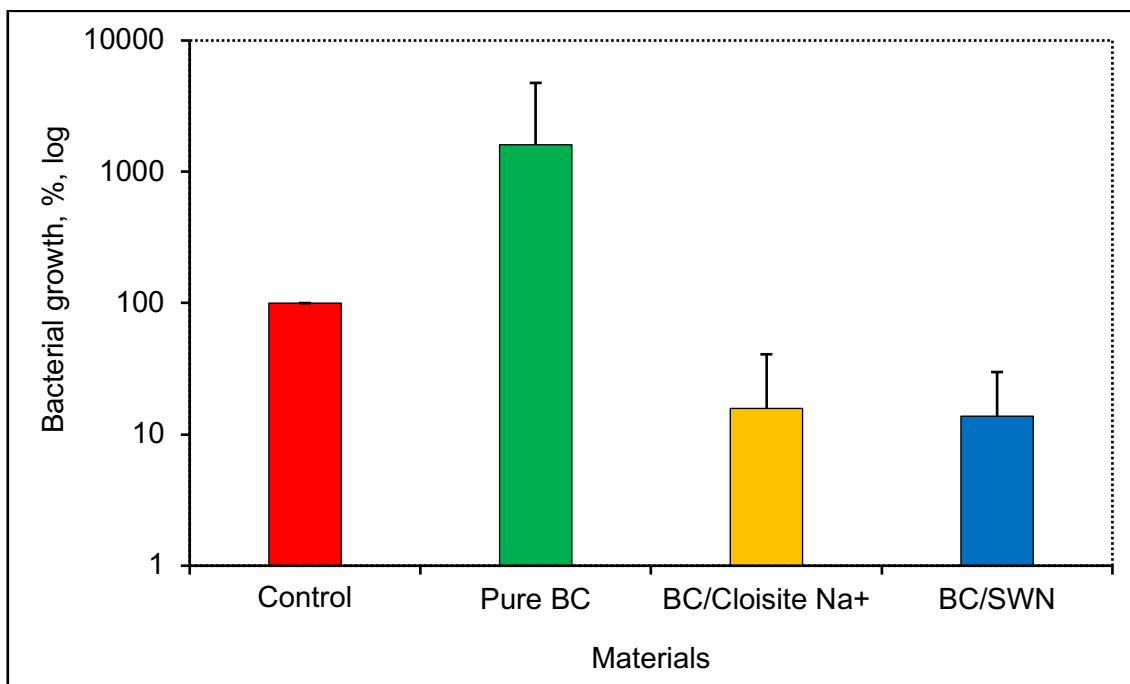


Figure 75. Antibacterial activity of BC/Cloisite Na⁺ and BC/SWN against *E. coli* after 24 hours. Each type of exfoliated clay at a concentration of 6 mg/ml was pumped inside the matrix of BC, respectively. The control was PBS-resuspended *E. coli*, which was placed on the surface of the empty petri dish and covered with a lid. Data represent the mean of six independent experiments with error bars of standard deviation. The treatments were compared to the control. All treatments outcomes are not significantly different from the control.

As shown in Fig. 76, BC/Cloisite Na⁺ were not effective against *P. aeruginosa*, which had the growth of 130% of the control values. However, BC/SWN reduced the control values of the bacteria to 58%.

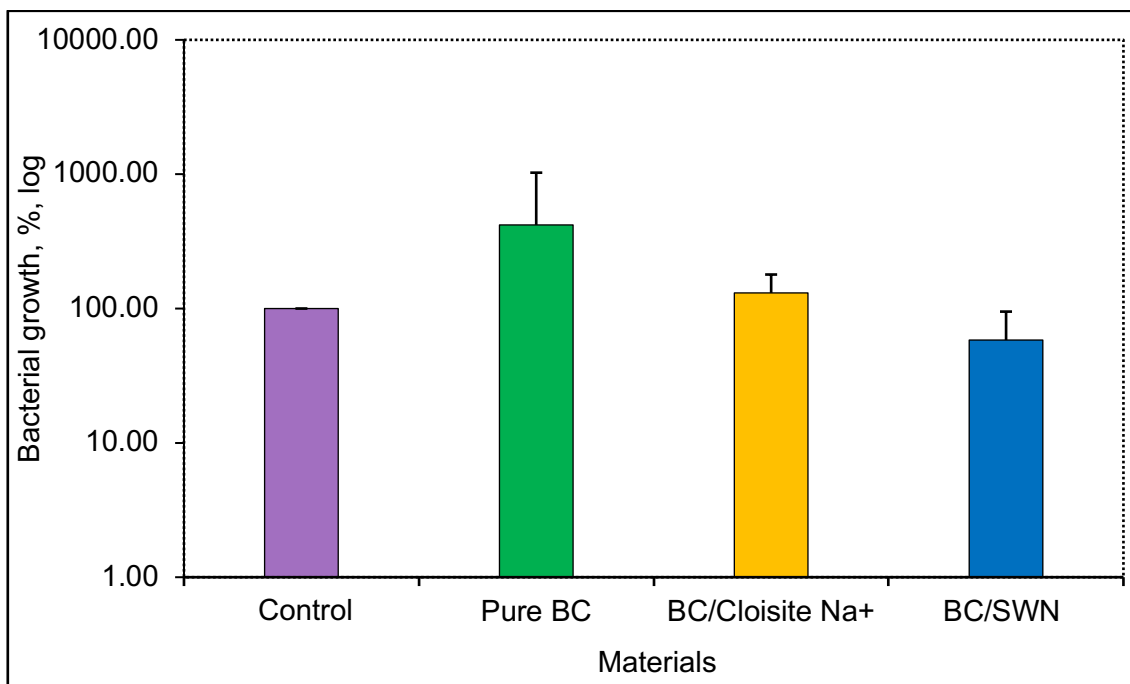


Figure 76. Antibacterial activity of BC/Cloisite Na⁺ and BC/SWN against *P. aeruginosa* after 24 hours. Each type of exfoliated clay at a concentration of 6 mg/ml was pumped inside the matrix of BC, respectively. The control was PBS-resuspended *P. aeruginosa*, which was placed on the surface of the empty petri dish and covered with a lid. Data represent the mean of three independent experiments with error bars of standard deviation. The treatments were compared to the control. All treatments outcomes are not significantly different from the control.

According to Figs. 74-76, BC/Cloisite Na⁺ was the most successful in inhibition of *E. coli*. However, this composite did not show any antibacterial activity against Gram-negative *P. aeruginosa*. Furthermore, pure BC promoted the growth of all tested bacteria.

4.1.3. Cytotoxicity of BC/clay composites

The mammalian cytotoxicity of *ex situ* synthesised BC/Cloisite Na⁺ and BC/SWN composites were investigated using 3t3 cells (Fig. 77). The cells were seeded on the top of each type of BC and incubated for 24 and 48 hours as described in Section 2.12.6. The control represented the cells without cellulose after each time

frame. As shown in Fig. 77, pure BC promoted the level of MTT reduction in cells to over 485% compare to the control values after 24 hours.

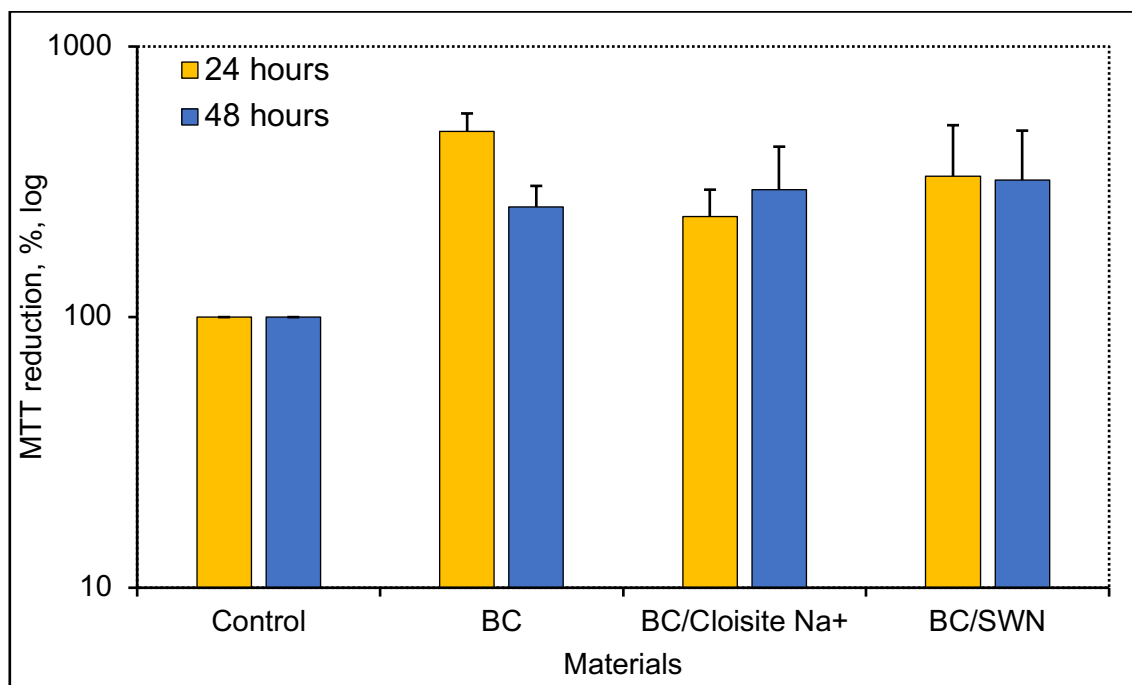


Figure 77. The effect of pure BC, BC/Cloisite Na⁺ and BC/SWN composites on MTT reduction in 3t3 cells. Cells at a concentration of 25×10^3 cells/ml were seeded on the top of the composites and incubated for 24 and 48 hours, respectively, at 37°C. The control showed the MTT reduction in cells without any treatment for each time frame. Data represent the mean of three independent experiments with error bars of standard deviation. The treatments were compared to the controls. All treatments were compared to the each of the control. Both BC and BC/Cloisite Na⁺ are different from the control after 24 hours with *P*-value being <0.01, respectively. After 48 hours, BC, BC/Cloisite Na⁺ and BC/SWN are different compared to the control (*P*-value <0.05), respectively.

This can be due to the healing properties of BC, which are based on the ability to keep and retain moisture. However, the levels of MTT reduction in cells with pure BC decreased from 485% to 255% after 48 hours.

The percent of MTT reduced cells was 235% using BC/Cloisite Na⁺ after 24 hours. This percent slightly increased to 295% after 48 hours. Furthermore, the

percent of MTT reduced cells reached 331% using BC/SWN composite after 24 hours. Then, the level of MTT reduction in cells with the composite decreased to 320% of control values after 48 hours.

4.1.4. *Ex situ* synthesised BC/organoclay composites

Cloisite 10A, Cloisite 15A, Cloisite 20A, Cloisite 30B and Cloisite 93A organoclay, at a concentration of 6 mg/ml were incorporated *ex situ* into pure BC using the vacuum self-assembly technique. The antibacterial activity of synthesised BC/organoclay composite was investigated against MRSA, *E. coli* and *P. aeruginosa*. The mammalian cytotoxicity of the composites was analysed using 3t3 cells after 24 and 48 hours.

4.1.4.1. Antibacterial activity of organoclay

The antibacterial activity of organoclay was investigated by zone inhibition assay due to their organophilic nature. This means that the organoclay could not be dispersed in water. Therefore, 2 grams of each type of organoclay were pressed into a disc, sterilised and placed on the top of TSA agar with freshly spread bacteria. As shown in Fig. 78, the largest zones of inhibition of 50, 40 and 45 mm were observed with Cloisite 10A against MRSA, *E. coli* and *P. aeruginosa*, respectively. Cloisite 30B had also shown 15 and 9 mm zones of inhibition against MRSA and *E. coli*, respectively. Cloisite 15A and 20A possessed stronger antibacterial activity against *E. coli* than other bacteria. However, the zone of inhibition of Cloisite 93A was 0.5 mm for all types of bacteria.

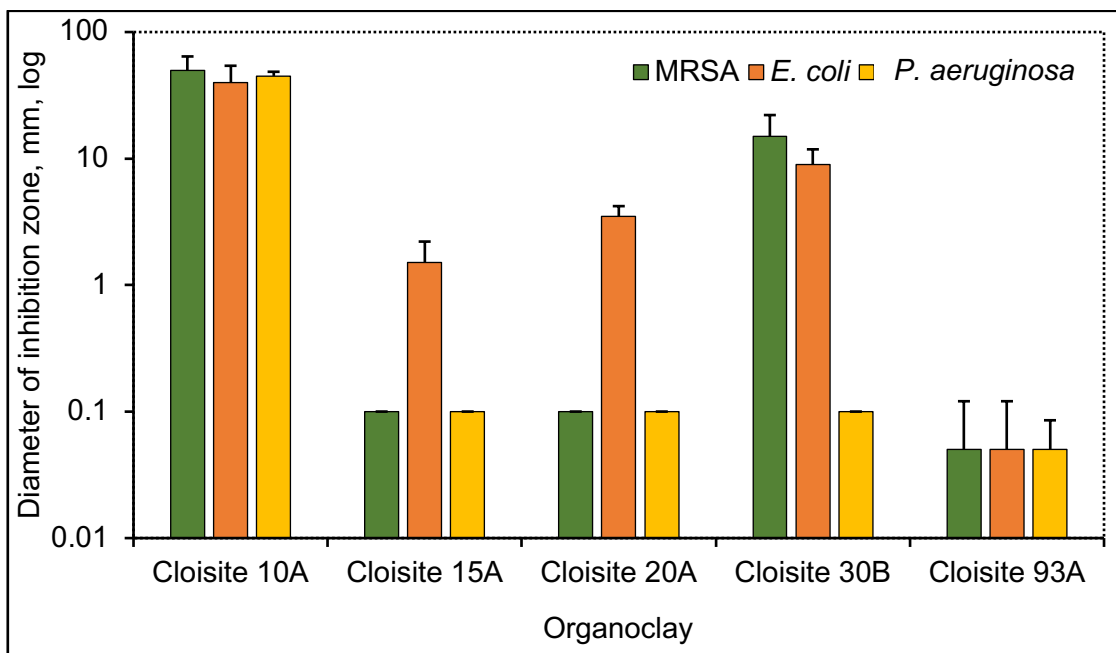


Figure 78. The zones of inhibition of Cloisite organoclay against MRSA, *E. coli* and *P. aeruginosa*. Data shown represent the mean of two independent experiments with error bars of standard deviation. The treatments were compared to the control (no zones of inhibition). Both 10A and 30B clays are significantly different from the MRSA control (P-value<0.001). Regarding *E. coli* and *P. aeruginosa*, just Cloisite 10A is significantly different in comparison with the control (P-value<0.001).

Leaching behaviour of organoclay could be a reason for the difference in antibacterial activity obtained in the zone of inhibition assay. Thereby, the leaching behaviour of organoclay was investigated using a drop shape analyser (DSA).

4.1.4.2. Investigation of leaching behaviour of organoclay

The leaching behaviour of organoclay was investigated using a DSA. Each type of organoclay in amounts of 2 grams were pressed into discs. The contact angle between the surface of organoclay and a drop, which contained 4 μ l of distilled water, was measured. Figs. 79-83 show the measurement of time-dependent contact angles for all organoclay. According to Fig. 79, Cloisite 10A did constantly leach, starting from 0 to 800 seconds, where the contact angle decreased from

71.6 θ to 60.4 θ . Regarding Cloisite 15A, the contact angle was unstable within the first 4 seconds and varied from 172 θ to 3 θ , but starting from 4 until 100 seconds, it was stable at 0 θ (Fig. 80).

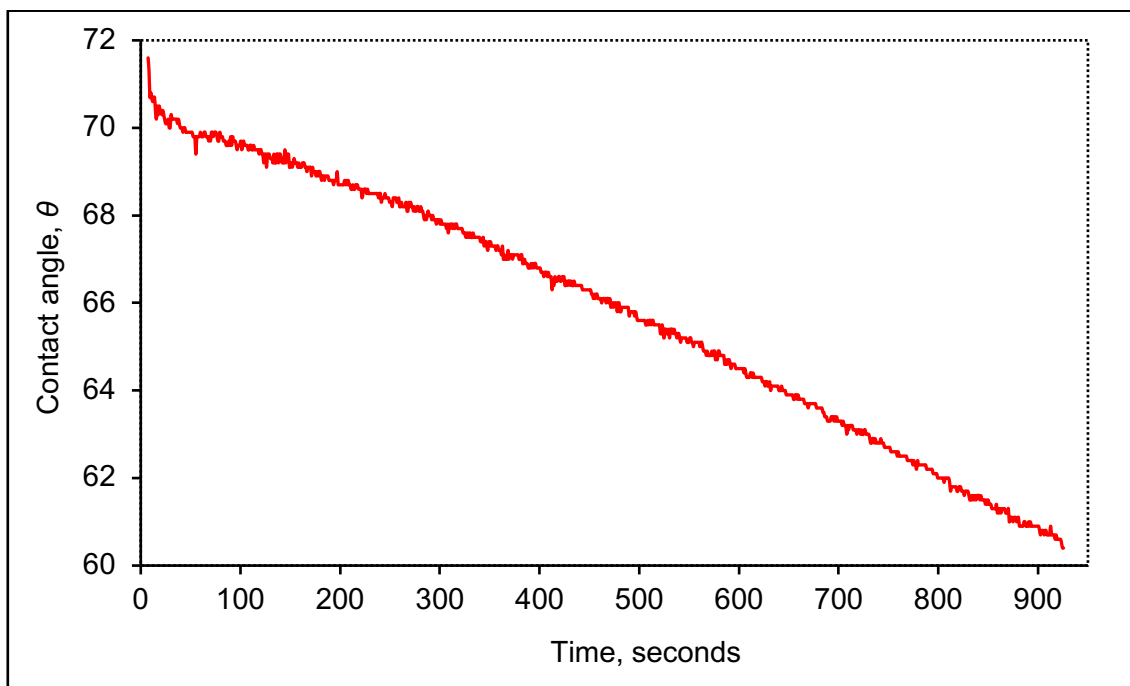


Figure 79. The time-dependent contact angle of Cloisite 10A. Distilled water in a volume of 4 μl was placed on a surface of hand-made Cloisite 10A discs.

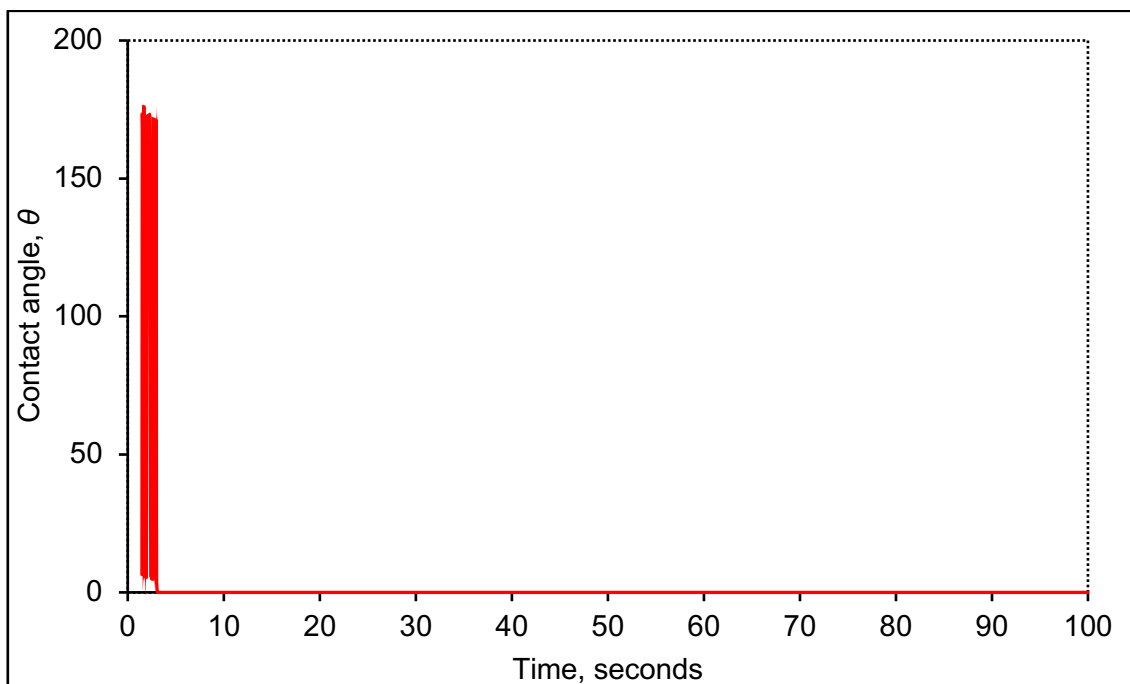


Figure 80. The time-dependent contact angle of Cloisite 15A. Distilled water in a volume of 4 μl was placed on a surface of hand-made Cloisite 15A discs.

As shown in Fig. 81, the contact angle of Cloisite 20A was similar to Cloisite 15A. Both Cloisite 20A and Cloisite 15A have the same organic modifier, therefore similar wettability was observed. According to Fig. 81, the contact angle went up to 180 θ within the first 2 seconds and then decreased to 0.1 θ after 3 seconds. The contact angle stabilised after 6 seconds at 77.3 θ and then remained the same until 100 seconds. The methyl groups of Cloisite 15A and 20A could make the clay leach less.

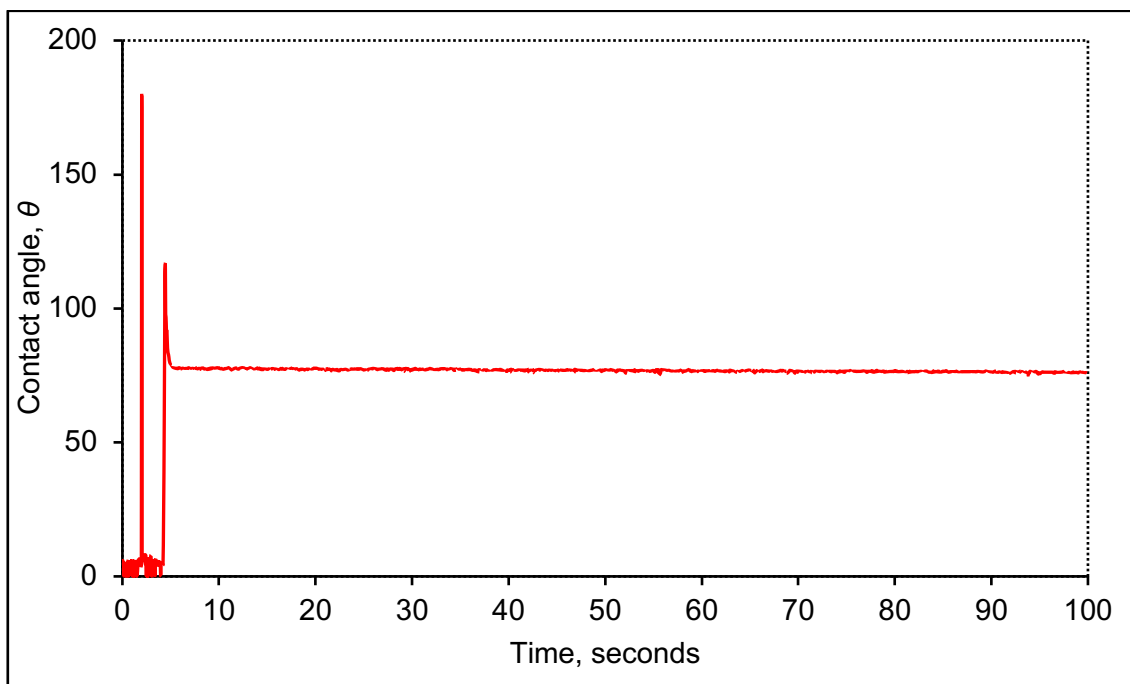


Figure 81. The time-dependent contact angle of Cloisite 20A. Distilled water in a volume of 4 μ l was placed on a surface of hand-made Cloisite 20A discs.

According to Fig. 82, Cloisite 30B had also leached within the first 6 seconds. Then, from 6 to 100 seconds, the contact angle was in the diapason of 68-63 θ . Cloisite 30B can be less organophilic than Cloisite 20A due to the presence of 2-hydroxyethyl groups.

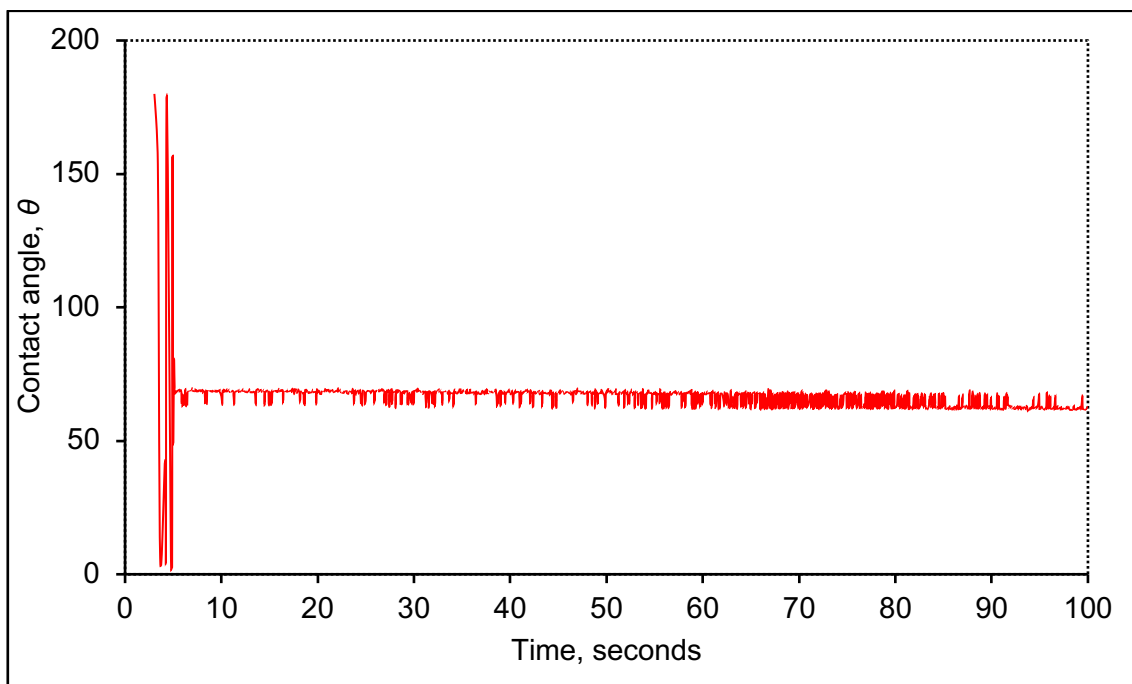


Figure 82. The time-dependent contact angle of Cloisite 30B. Distilled water in a volume of 4 μl was placed on a surface of hand-made Cloisite 30B discs.

Regarding Cloisite 93A, the contact angle went down from 140 θ to 74 θ within the first 6 seconds and remained stable until 100 seconds (Fig. 83).

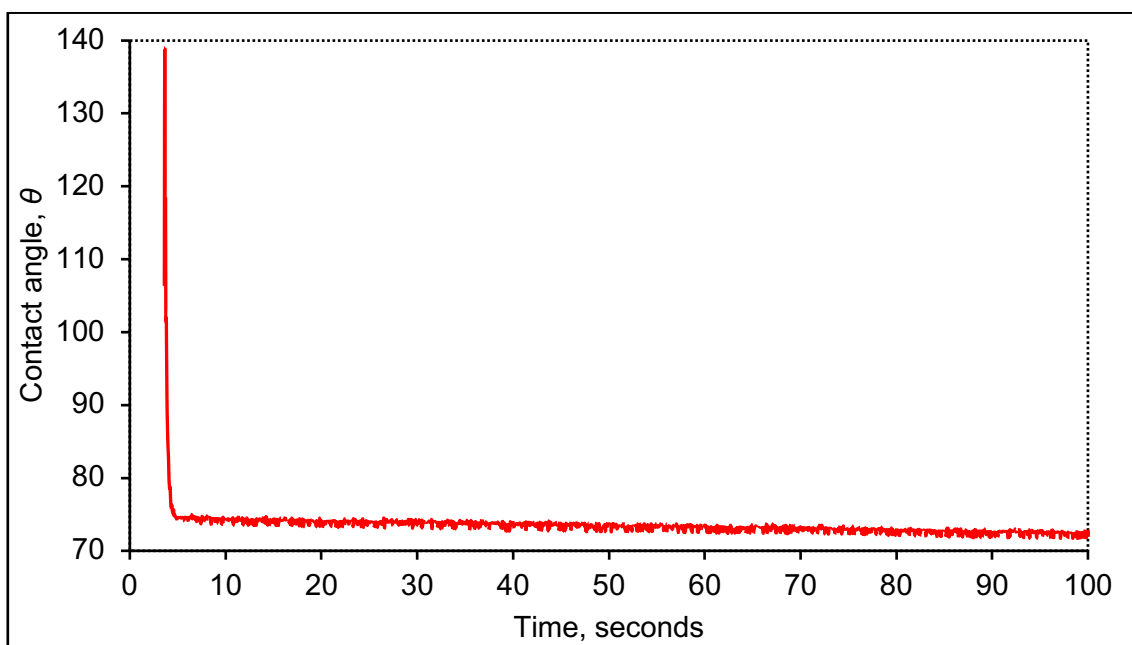


Figure 83. The time-dependent contact angle of Cloisite 93A. Distilled water in a volume of 4 μl was placed on a surface of hand-made Cloisite 93A discs.

As shown in Figs. 79-83, Cloisite 10A showed the highest leaching behaviour compared to other organoclay. Moreover, Cloisite 30B also showed the ability to leach, whereas Cloisite 93A had the lowest variation between contact angles and, thus, the strongest organophilic properties. This agrees with the results of the zone inhibition assay, where the largest inhibition zones were observed with both Cloisite 10A and Cloisite 30B clay.

4.1.5. Antibacterial activity of *ex situ* synthesised BC/clay composites

Clay were pumped through pure BC at a concentration of 6 mg/ml using a vacuum self-assembly method as described in Section 2.6.3.1. The antibacterial properties of *ex situ* synthesised BC/clay composites were analysed using Gram-positive MRSA and Gram-negative *E. coli* and *P. aeruginosa* (Figs. 84-87).

4.1.6. Antibacterial activity of *ex situ* synthesised BC/organoclay composites

As organoclay suspensions were prepared in acetone, acetone was pumped through pure BC and treated the same way as the other composites. According Fig. 84, BC treated with acetone did not show any antibacterial activity, whereas all of BC/organoclay composites showed an antibacterial effect. The most effective composites were BC/Cloisite 30B and BC/Cloisite 10A, where the growth of MRSA went down to 0.01% and 0.14% of control values, respectively. BC/Cloisite 15A and BC/Cloisite 20A possessed antibacterial activity and reduced the growth of MRSA to 1.8% and 45%, respectively, compare to the control. The least effective was BC/Cloisite 93A composite, which reduced MRSA to 69% of the control values.

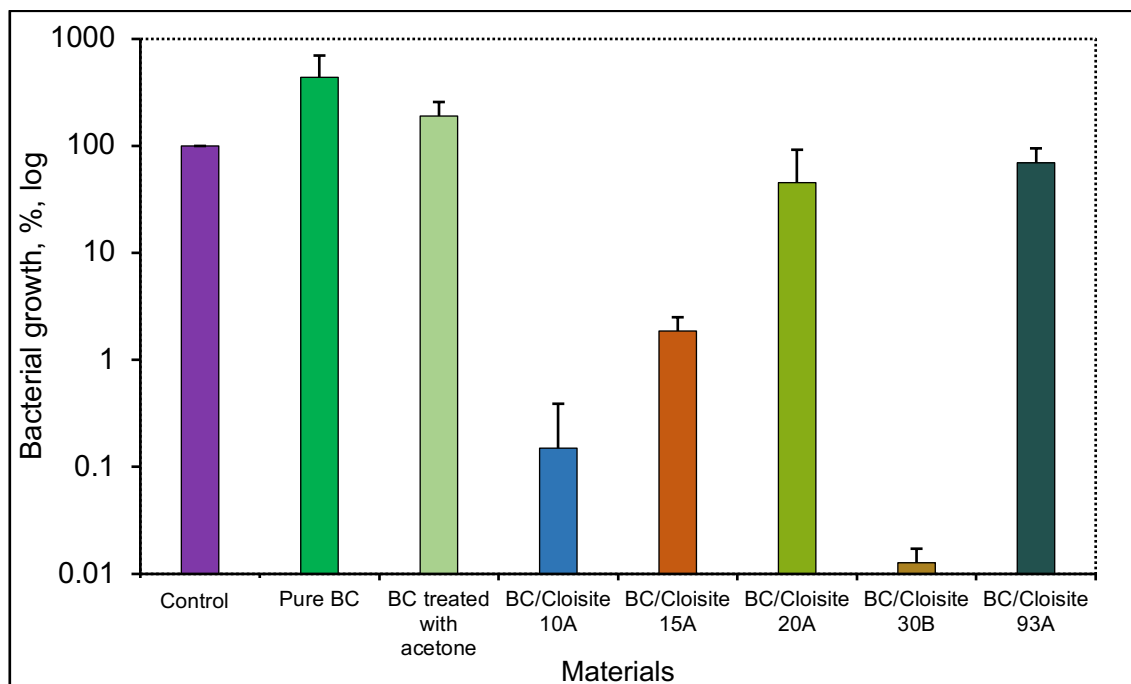


Figure 84. Antibacterial activity of BC/organoclay composites against MRSA. BC/organoclay composites were prepared by pumping 6 mg/ml of organoclay into BC matrix. Each BC/organoclay composite was placed on the surface of empty, without agar petri dish. PBS-resuspended MRSA was placed on the top of each BC/organoclay composite, covered with a lid and incubated for 24 hours at 37°C. The control was PBS-resuspended MRSA that was placed on the surface of empty, without agar petri dish. Data shown represent the mean of three independent experiments with error bars of standard deviation. Treatments were compared to the control. Pure BC, BC/Cloisite 10A, BC/Cloisite 15A and BC/Cloisite 30B are different from the control with P -value < 0.05, respectively.

As shown in Fig. 85, BC/Cloisite 10A, BC/Cloisite 15A and BC/Cloisite 30B showed antibacterial activity against *E. coli*, where the control values went down to 0.2%, 0.3% and 0.1%, respectively. However, BC/Cloisite 20A and BC/Cloisite 93A were not that effective. The growth of bacteria was not reduced and remained at 101% using BC/Cloisite 93A. Furthermore, BC/Cloisite 20A increased the control values of *E. coli* to 267%. In addition, both pure BC and BC treated with acetone promoted bacterial growth, which means that pumped acetone was completely washed out of BC.

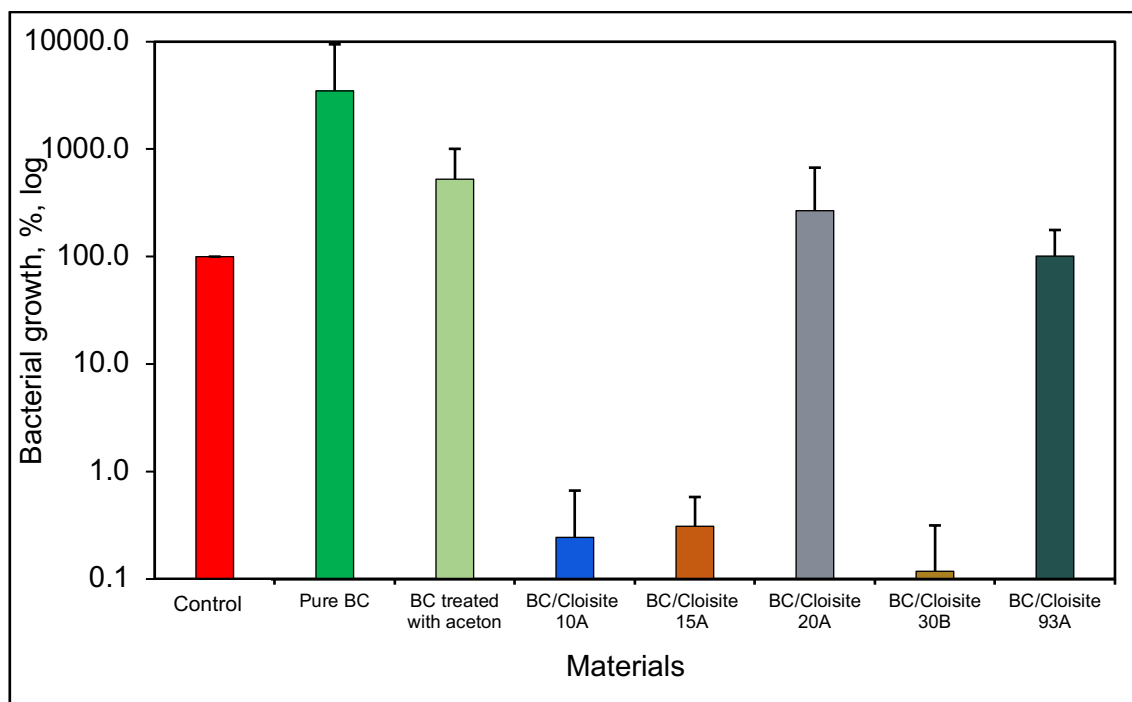


Figure 85. Antibacterial activity of BC/organoclay composites against *E. coli*. BC/organoclay composites were prepared by pumping 6 mg/ml of organoclay into BC matrix. Each BC/organoclay composite was placed on the surface of empty, without agar petri dish. PBS-resuspended *E. coli* was placed on the top of each BC/organoclay composite, covered with a lid and incubated for 24 hours at 37°C. The control was PBS-resuspended *E. coli* that was placed on the surface of empty, without agar petri dish. Data shown represent the mean of three independent experiments with error bars of standard deviation. Treatments were compared to the control. BC/Cloisite 10A, BC/Cloisite 15A and BC/Cloisite 30B are different from the control with P -value<0.001, respectively.

Pure BC increased the control values of *P. aeruginosa* to 419%, whereas BC treated with acetone decreased the growth of the cells to 45% (Fig. 86). This might be due to the non-complete washing of acetone from the matrix of the cellulose. Nonetheless, the control values of the bacteria reduced by remaining acetone inside BC, BC/organoclay composites showed a stronger reduction of the bacterial growth. As shown in Fig. 86, BC/Cloisite 10A, BC/Cloisite 15A, BC/Cloisite 20A and BC/Cloisite 30B composites reduced the control values of

P. aeruginosa to 1.1, 1.6, 1.4 and 0.4%, respectively. BC/Cloisite 93A increased the control values to 123%.

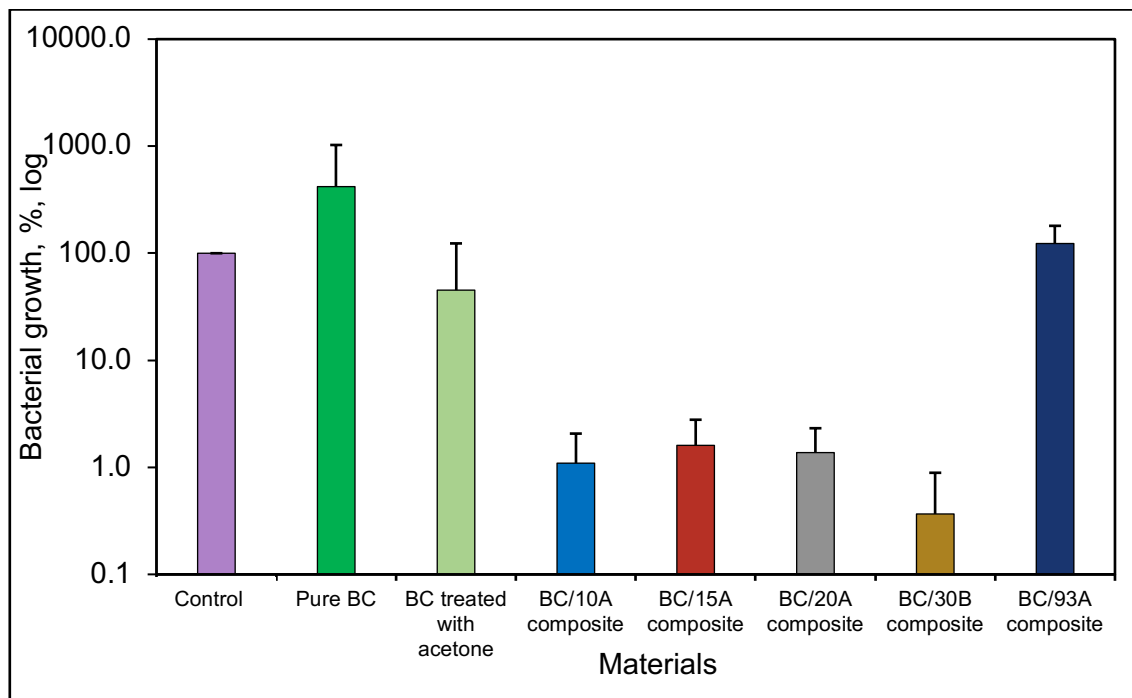


Figure 86. Antibacterial activity of BC/organoclay composites against *P. aeruginosa*. BC/organoclay composites were prepared by pumping 6 mg/ml of organoclay into BC matrix. Each BC/organoclay composite was placed on the surface of empty, without agar petri dish. PBS-resuspended *P. aeruginosa* was placed on the top of each BC/organoclay composite, covered with a lid and incubated for 24 hours at 37°C. The control was PBS-resuspended *P. aeruginosa* that was placed on the surface of empty, without agar petri dish. Data shown represent the mean of three independent experiments with error bars of standard deviation. Treatments were compared to the control. BC/Cloisite 10A, BC/Cloisite 15A, BC/Cloisite 20A and BC/Cloisite 30B are different from the control with P -value<0.001, respectively.

Consequently, the most effective composites against all three types of bacteria were BC/Cloisite 10A, BC/Cloisite 15A and BC/Cloisite 30B. This means that such BC/organoclay composites were effective against both Gram-positive and Gram-negative bacteria. This agrees with data obtained from the zone of inhibition assay.

4.1.7. Mammalian cytotoxicity of organoclay

The cytotoxicity assay of organoclay was carried out using the clay/medium suspensions as described in Section 2.12.2. Each type of organoclay such as Cloisite 10A, Cloisite 15A, Cloisite 20A, Cloisite 30B and Cloisite 93A at a concentration of 0.09 to 6 mg/ml was mixed tissue culture medium. The 3t3 cells were incubated with clay/medium suspensions for 24, 48 and 72 hours at 37°C.

Fig. 87 shows the MTT reduction in 3t3 cells in a presence of Cloisite 10A after 24, 48 and 72 hours. The control represented the percent of MTT reduction in the cells without any treatment at each time frame. As shown Fig. 87, maximum increase of control values was 174% using 0.09 mg/ml of Cloisite 10A, whereas the minimum percent of MTT reduction was 52% at 3 mg/ml concentration of the clay after 24 hours. The level of MTT reduction by cells then increased after 48 hours. The concentration of up to 0.75 mg/ml of Cloisite 10A promoted the level of MTT reduction in 3t3 cells to a maximum of 155% of control values after 48 hours. Starting from 1.5 mg/ml concentration, the percent of MTT reduction in the cells decreased to 60%. The drop to 37% in percent of MTT reduced cells was observed at 6 mg/ml of the clay. The level of MTT reduction by the cells increased to 132% of control values just in the treatment with 0.09 mg/ml of Cloisite 10A after 72 hours. The lowest percent of MTT reduction by cells was 36% of control values using 6 mg/ml of the clay after 72 hours. The concentration from 1.5 mg/ml of Cloisite 10A was detected to reduce the level of MTT reduction in cells after 48 hours. This might be the limit where the clay started to possess toxicity and affect the membranes of the cells.

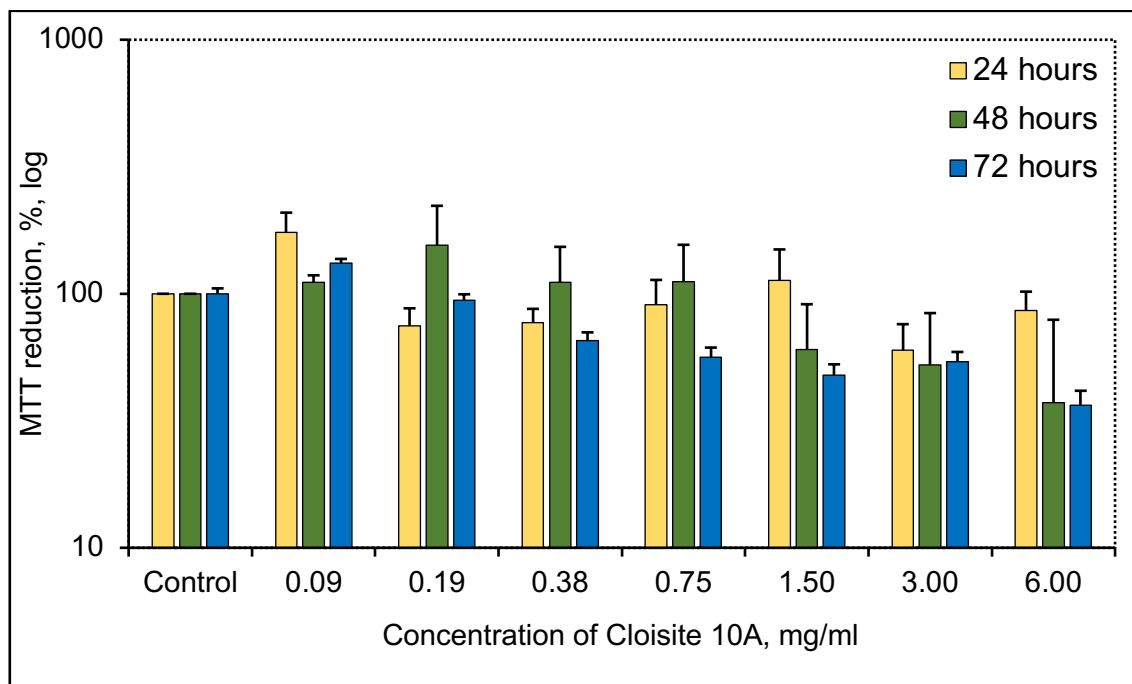


Figure 87. The effect of Cloisite 10A/medium suspension on the level of MTT reduction in 3t3 cells. Cloisite 10A at a concentration of 0.09-6 mg/ml was mixed with the culture medium. The cells were incubated with the medium for 24, 48 and 72 hours at 37°C. The control represented the MTT reduction in cells without any treatment for each time frame. Data shown represent the mean of three independent experiments of MTT assay with error bars of standard deviation. Treatments were compared to the controls. The data obtained using 3 mg/ml concentration of clay after 24 hours are significantly different in comparison with the control (P -value<0.5), whereas there is no significant difference between the treatments and the control after 48 hours. The treatments with a concentration of 6 mg/ml are significantly different from the control after 72 hours (P -value<0.05).

Fig. 88 shows the cytotoxicity results of Cloisite 15A/medium suspension at a concentration from 0.09 to 6 mg/ml on the MTT reduction in 3t3 cells at 24, 48 and 72 hours, respectively. The concentration of the clay at 0.09 and 0.19 mg/ml promoted the growth of 3t3 cells to 147% and 116% of the control values, respectively, after 24 hours. Then, the level of MTT reduction decreased from 83% to 60% by increasing the concentration of the clay from 0.38 to 3 mg/ml. The minimum percent of MTT reduction in cells was 38% of control values using 6 mg/ml concentration of the clay. The level of MTT reduction in 3t3 cells increased

after 48 hours using 0.09-1.5 mg/ml of the clay. The maximum percent of MTT reduction by the cells was 217% of control values at the lowest concentration of the clay, which then decreased to 51% by increasing the clay to 3 mg/ml. As shown in Fig. 88, the concentration of the Cloisite 15A at 6 mg/ml resulted in a drop of MTT reduction in the cells to 42% compare to the control values. The rise in MTT reduction was detected at both 0.09 and 0.75 mg/ml concentration, where the percent of the cells increased to 103% and 129% of the control values, respectively, after 72 hours. Starting from 1.5 mg/ml concentration of Cloisite 15A, the level of MTT reduction in 3t3 cells dropped to 75%. The percent of MTT reduction in the cells decreased to 43% and 14% of the control values using 3 and 6 mg/ml concentration of the clay, respectively, after 72 hours. Similar to Cloisite 10A, the lowest cytotoxicity of the clay was observed after 48 hours. A low limit for the cytotoxic concentration of Cloisite 15A could be 3 mg/ml.

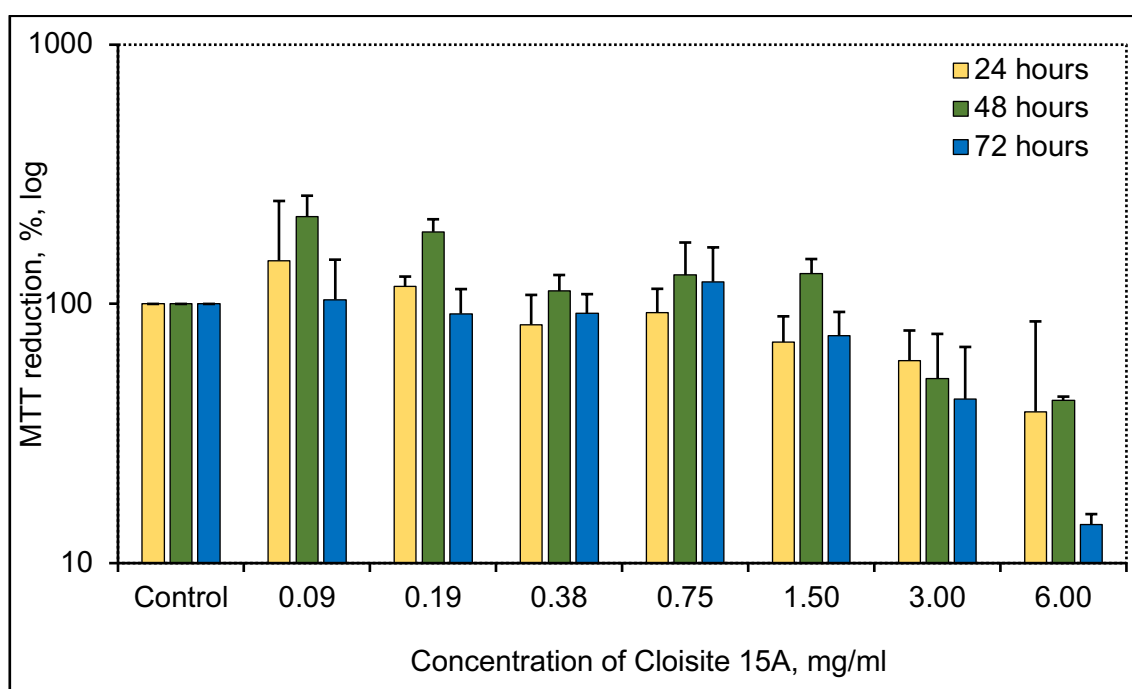


Figure 88. The effect of Cloisite 15A/medium suspension on the level of MTT reduction in 3t3 cells. Cloisite 15A at a concentration of 0.09-6 mg/ml was mixed with the culture medium. The cells were incubated with the medium for 24, 48 and 72 hours at 37°C. The control represented the MTT reduction in cells without any treatment for each time frame. Data shown represent the mean of three independent experiments of MTT assay with

error bars of standard deviation. The data obtained using 3 mg/ml concentration of clay after 24 hours are significantly different in comparison with the control (P -value <0.05). The treatments with a concentration of 6 mg/ml are significantly different from the control after 48 and 72 hours with P -values <0.05 and <0.001 , respectively.

The mammalian cytotoxicity of Cloisite 20A/medium suspensions at concentrations from 0.09 to 6 mg/ml was analysed (Fig. 89). As shown in Fig. 89, the lowest percentage of control value for MTT reduction in 3t3 cells was 93% at a concentration of 0.38 mg/ml of the clay after 24 hours. The maximum MTT reduction was 153% of using 0.09 mg/ml of Cloisite 20A. Furthermore, the drop in the level of MTT reduction in the cells was detected just at 0.75 mg/ml after 48 hours, where the percent of the cells decreased to 89% of the control values. After 72 hours, the MTT reduction by the cells was up to of 80%, 86% and 67% by using 0.38, 3 and 6 mg/ml of the clay, respectively. Cloisite 20A has not significantly affected the MTT reduction by the cells within 48 hours, whereas the maximum decrease of metabolically active cells was detected at 6 mg/ml of the clay after 72 hours. The results indicated that Cloisite 20A did not show strong cytotoxicity effects on 3t3 cells.

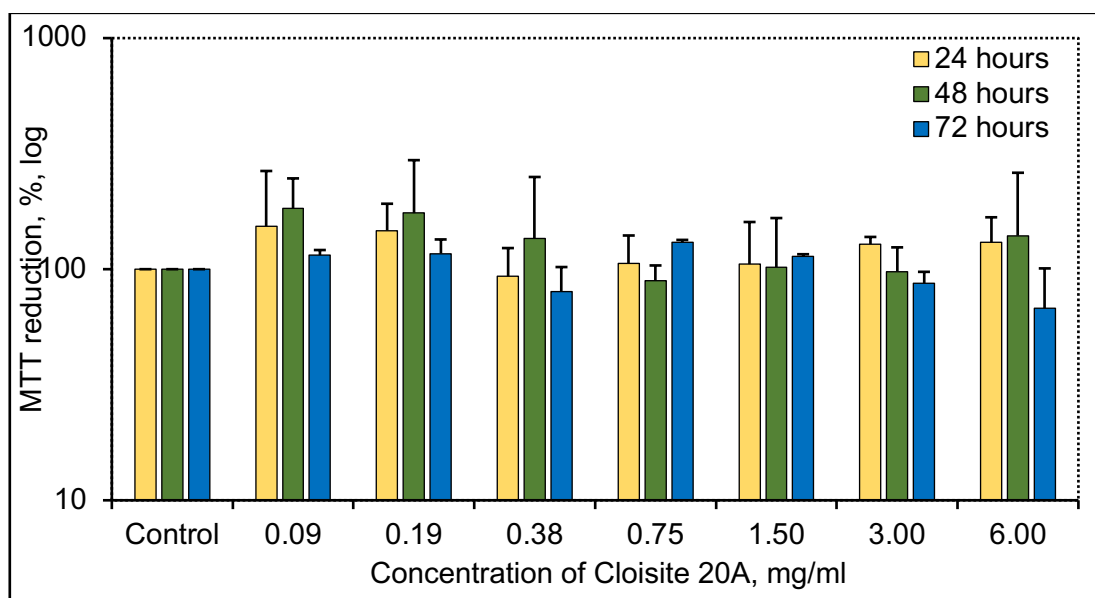


Figure 89. The effect of Cloisite 20A/medium suspension on the level of MTT reduction in 3t3 cells. Cloisite 20A at a concentration of 0.09-6 mg/ml was mixed with the culture

medium. The cells were incubated with the medium for 24, 48 and 72 hours at 37°C. The control represented the MTT reduction in cells without any treatment for each time frame. Data shown represent the mean of three independent experiments of MTT assay with error bars of standard deviation. The treatment outcomes are not significantly different in comparison with the controls.

Fig. 90 shows cytotoxicity of Cloisite 30B on 3t3 cells after 24, 48 and 72 hours. Cloisite 30B clay exhibit higher cytotoxicity than Cloisite 10A, 15A and 20A. The MTT reduction in cells did not go higher than 90% of control values at 1.5 mg/ml concentration within the first 24 hours. The lowest percent of MTT reduction in 3t3 cells was 30% at 6 mg/ml concentration of the clay. The percent of MTT reduction in the cells increased to 113% of control values at 0.09 mg/ml of the clay after 48 hours, whereas there was a drop in the percent of metabolically active cells compare to the control values starting from 0.38 to 1.5 mg/ml concentration of Cloisite 30B.

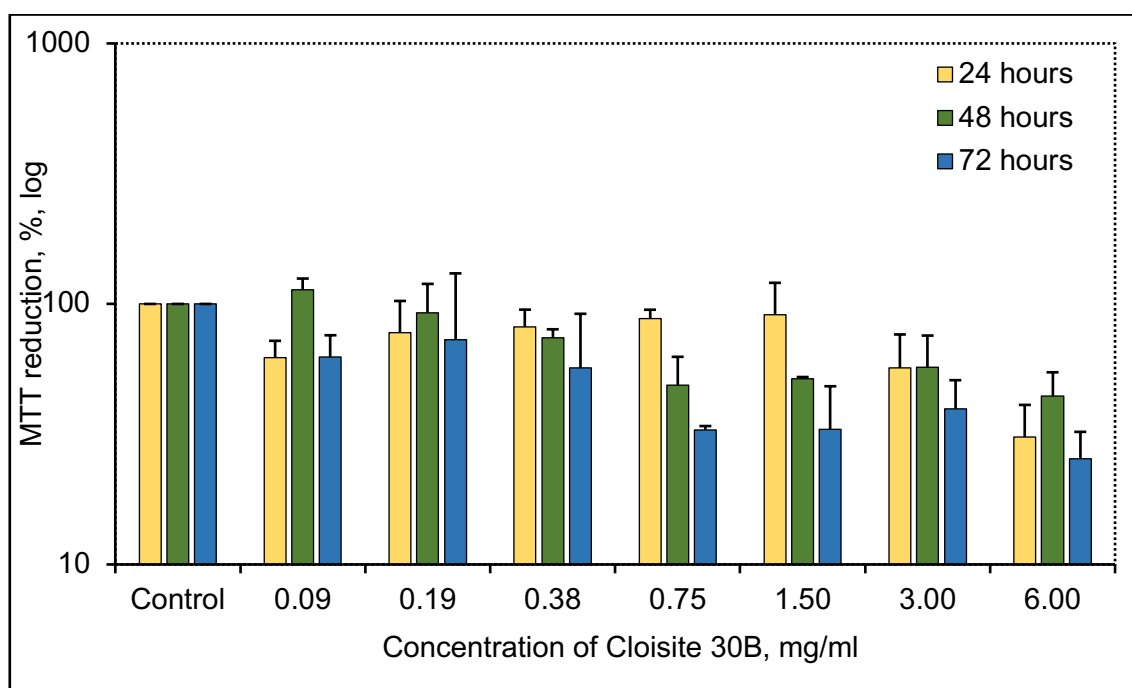


Figure 90. The effect of Cloisite 30B/medium suspension on the level of MTT reduction in 3t3 cells. Cloisite 30B at a concentration of 0.09-6 mg/ml was mixed with the culture medium. The cells were incubated with the medium for 24, 48 and 72 hours at 37°C. The

control represented the MTT reduction in cells without any treatment for each time frame. Data shown represent the mean of three independent experiments of MTT assay with error bars of standard deviation. The treatments were compared to the controls. After 24 hours, the treatments with concentrations of 0.09 and 6 mg/ml are different from the control (P -value <0.05). The data obtained using 0.38, 0.75 and 6 mg/ml concentrations of clay are significantly different in comparison with the control (P -value <0.05) after 48 hours. The treatments with concentration of 1.5 mg/ml are different from the control after 48 hours with P -value <0.001 . After 72 hours, concentrations of 0.75 and 6 mg/ml are different compared to the control with P -value <0.001 . Furthermore, 1.5 and 3 mg/ml concentrations are different from the control after 72 hours (P -value <0.05).

The level of MTT reduction in cells slightly increased from 56 to 57% within 48 hours using a concentration of 1.5 mg/ml of Cloisite 30B. The increase in the percent of MTT reduction was also observed in 6 mg/ml concentration of the treatment, where it increased to 44% of the control values after 48 hours. However, all concentration of the clay resulted in decreasing of levels of MTT reduction in the cells after 72 hours. The lowest percent of MTT reduction in the cells was 25% using 6 mg/ml concentration of Cloisite 30B.

The MTT reduction in cells increased to 166% of control values at 0.09 mg/ml concentration of Cloisite 93A clay within 24 hours (Fig. 91). The drop in the MTT reduction activity can be observed within all other concentrations after 24 hours of incubation. The lowest percent of MTT reduction activity in 3t3 cells was 35% using 6 mg/ml concentration of Cloisite 93A. However, the level of MTT reduction in cells increased to 155%, 170%, 118% and 121% of the control values at concentration of 0.09, 0.19, 0.38 and 1.5 mg/ml, respectively, after 48 hours. Cloisite 93A decreased the MTT reduction activity in the cells to 74% at a concentration of 0.75 and 3 mg/ml, respectively. The lowest concentration of Cloisite 93A did not affect the levels of MTT reduction in the cells, which remained 100% after 72 hours. However, the reduction of the MTT activity in cells could be observed within concentrations higher than 0.19 mg/ml. The lowest percent of the cells was 24% of the control values using 6 mg/ml of Cloisite 93A.

Consequently, the highest concentration of 6 mg/ml of Cloisite 93A was much less compared to other tested Cloisite clay.

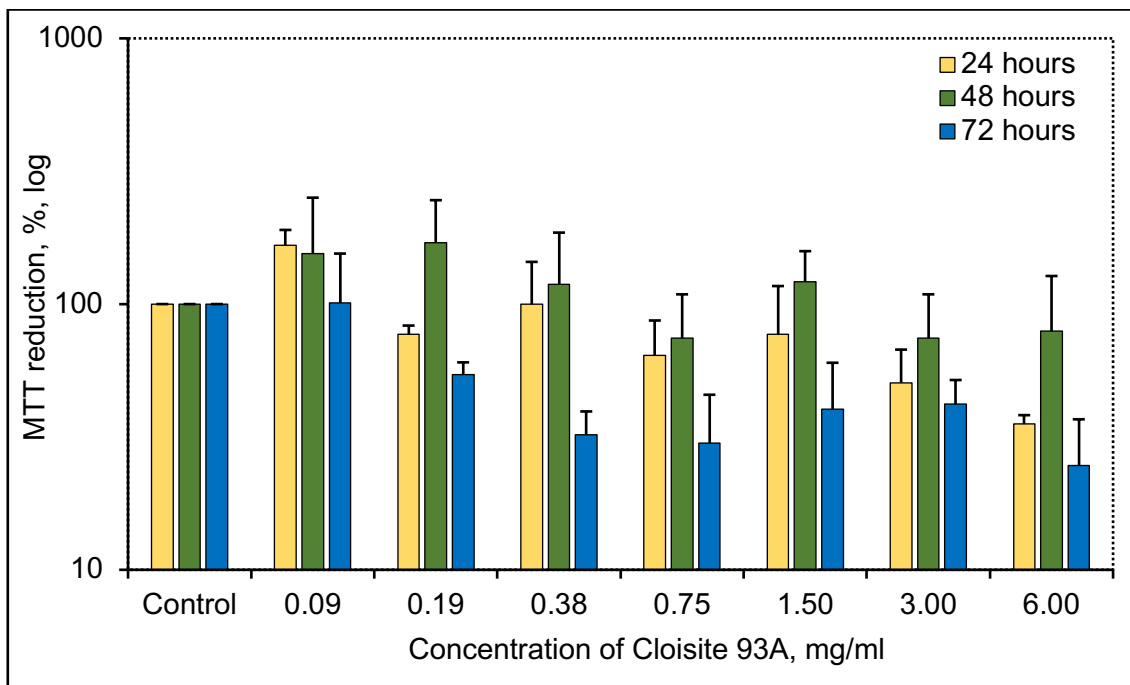


Figure 91. The effect of Cloisite 93A/medium suspension on the level of MTT reduction in 3t3 cells. Cloisite 93A at a concentration of 0.09-6 mg/ml was mixed with the culture medium. The cells were incubated with the medium for 24, 48 and 72 hours at 37°C. The control represented the MTT reduction in cells without any treatment for each time frame. Data shown represent the mean of three independent experiments of MTT assay with error bars of standard deviation. The treatments are not significantly different from the control after 48 hours. After 24 hours, treatments of 0.38 and 6 mg/ml clay concentrations are significantly different in comparison with the control (P -value<0.05). Regarding 72 hours of incubation, the treatments of 0.38 mg/ml clay concentration are significantly different from the control (P -value<0.05).

4.1.8. Cytotoxicity assays on 3t3 cells using clay coated cover glass

Due to their organophilic nature, organoclay were not fully dispersed in the medium. Therefore, another method for evaluation of mammalian cytotoxicity of the clay was proposed. The cytotoxicity of organoclay was investigated using a cover glass coated with organoclay that were pre-dispersed in acetone at a

concentration of 6 mg/ml and subsequently dried and sterilised using UV-Ozone as described in Section 2.12.4. The cells were seeded on the top of a dry sterile cover glass coated with the clay, covered with medium and incubated for 24 hours at 37°C. Fig. 92 shows the cytotoxicity effect of organoclay on 3t3 cells. The control represented the cells growing on the surface of the 6-well plate without any treatment. This control was compared to the cells that grew on the surface of the clean cover glass without the clay. As shown in Fig. 92, the MTT reduction in the cells on the clean cover glass reduced to 78% of the control values. The effect of Cloisite 30B on the cells was observed, where the level of MTT reduction in the cells significantly decreased to 22%. Cloisite 10A decreased the MTT reduction activity in the cells to 44%, whereas Cloisite 15A, 20A and 93A increased the percent to 290%, 173% and 128% of the control values, respectively. Therefore, Cloisite 10A and Cloisite 30B showed the strongest cytotoxicity than other organoclay. This supports the results, which were obtained in Section 4.1.9.

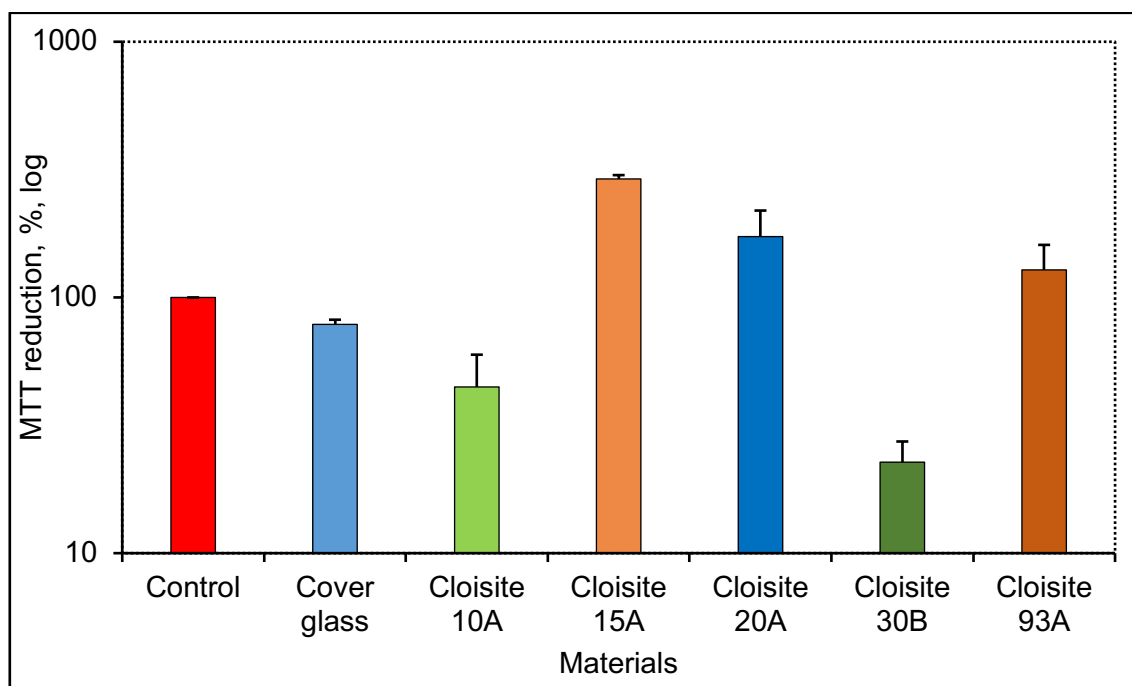


Figure 92. The effect of Cloisite 10A, 15A, 20A, 30B and 93A at a concentration of 6 mg/ml on 3t3 cells. The control represented the viability of cells without any treatment that grew on the surface of the 6-well plate. The cover slip glass was coated with each clay

suspension and dried by UV-Ozone. Cells were seeded on the top of each cover glass, covered with medium and incubated for 24 hours at 37°C. Data shown represent the mean of two independent experiments of MTT assay with error bars of standard deviation.

4.1.9. The mammalian toxicity of BC/organoclay composites

The cytotoxicity of synthesised *ex situ* BC/organoclay composites was investigated using NIH 3t3 cells after 24, 48 and 72 hours (Fig. 93). The cells were seeded on the top of pure BC and each of BC/clay composites and incubated at 37°C as described in Section 2.12.6. As shown in Fig. 92, both pure BC and BC/clay composites promoted the MTT reduction in 3t3 cells compare to the control values. The MTT reduction activity in the cells with pure BC increased to 357% of control values after 24 hours. Furthermore, the MTT reduction activity cells raised to 235%, 225%, 189%, 329% and 142% of the control values using BC/Cloisite 10A, BC/Cloisite 15A, BC/Cloisite 20A, BC/Cloisite 30B and BC/Cloisite 93A, respectively.

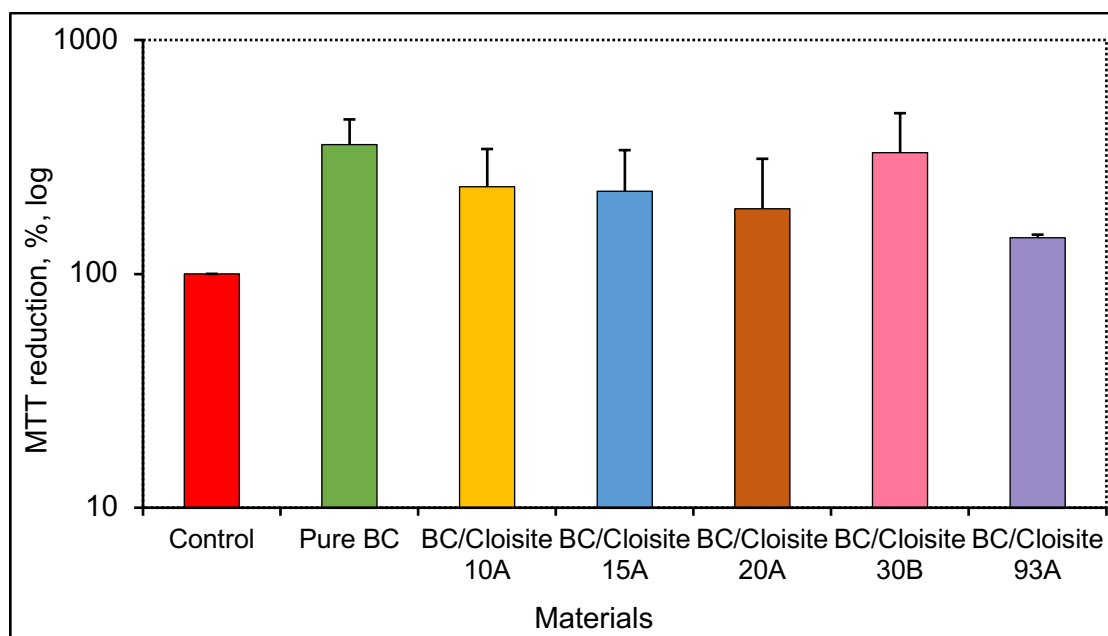


Figure 93. The effect of pure BC and BC/organoclay composites on 3t3 cells after 24 of incubation at 37°C. The control shows the MTT reduction of the cells without any

treatment. Data shown present the mean of three independent experiments of MTT assay with error bars of standard deviation. The treatments were compared to the control. Pure BC, BC/Cloisite 30B and BC/Cloisite 93A are significantly different in comparison with the control with P -values <0.01 , <0.05 and <0.01 , respectively.

The level of MTT reduction in 3t3 cells was higher than the control after 48 hours. Fig. 94 shows the cytotoxicity of pure BC and BC/organoclay composites after 48 hours. The control represented the MTT reduction in 3t3 cells without any treatments after 48 hours. According to Fig. 94, pure BC promoted the metabolic activity of the cells to 248% compare to the control. BC/Cloisite 10A, BC/Cloisite 15A, BC/Cloisite 20A, BC/Cloisite 30B and BC/Cloisite 93A have also increased the MTT reduction activity in 3t3 cells.

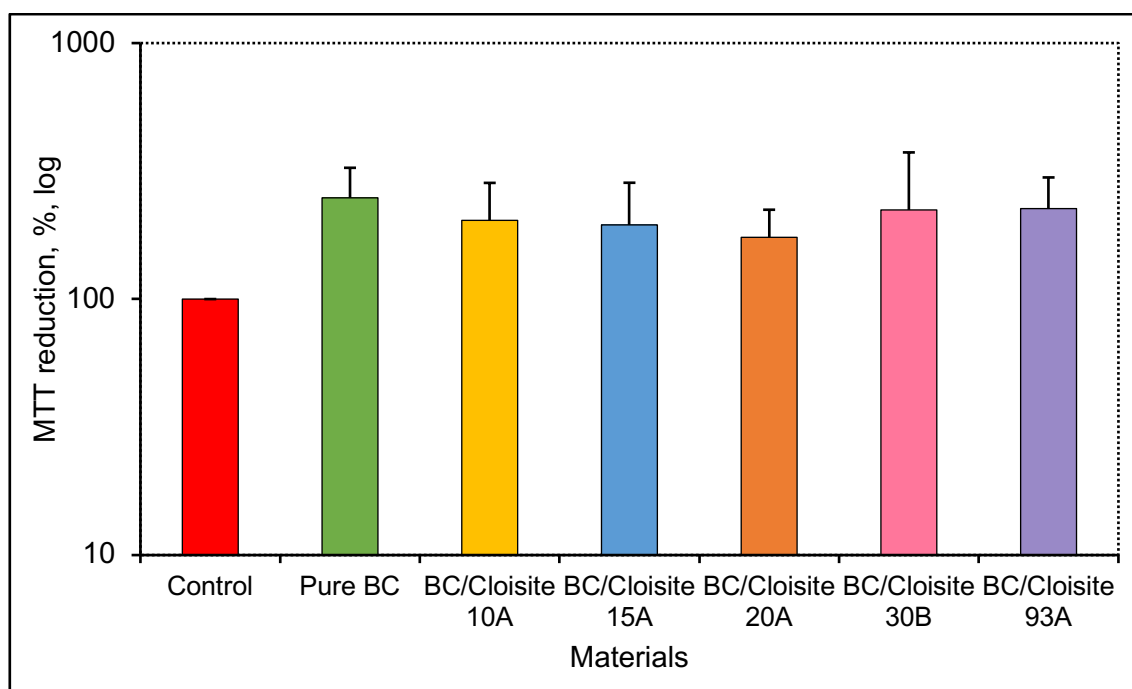


Figure 94. The effect of pure BC and BC/organoclay composites on 3t3 cells after 48 of incubation at 37°C. The control shows the MTT reduction in the cells without any treatment that grow on the glass. Data shown represent the mean of three independent experiments of MTT assay with error bars of standard deviation. Pure BC and BC/Cloisite 93A are significantly different in comparison with the control (P -value <0.05).

The MTT reduction activity of 3t3 cells reached 327% of control values using pure BC after 72 hours (Fig. 95). The percent of MTT reduction increased to 186%, 197%, 264%, 255% and 220% by using BC/Cloisite 10A, BC/Cloisite 15A, BC/Cloisite 20A, BC/Cloisite 30B and BC/Cloisite 93A composites, respectively.

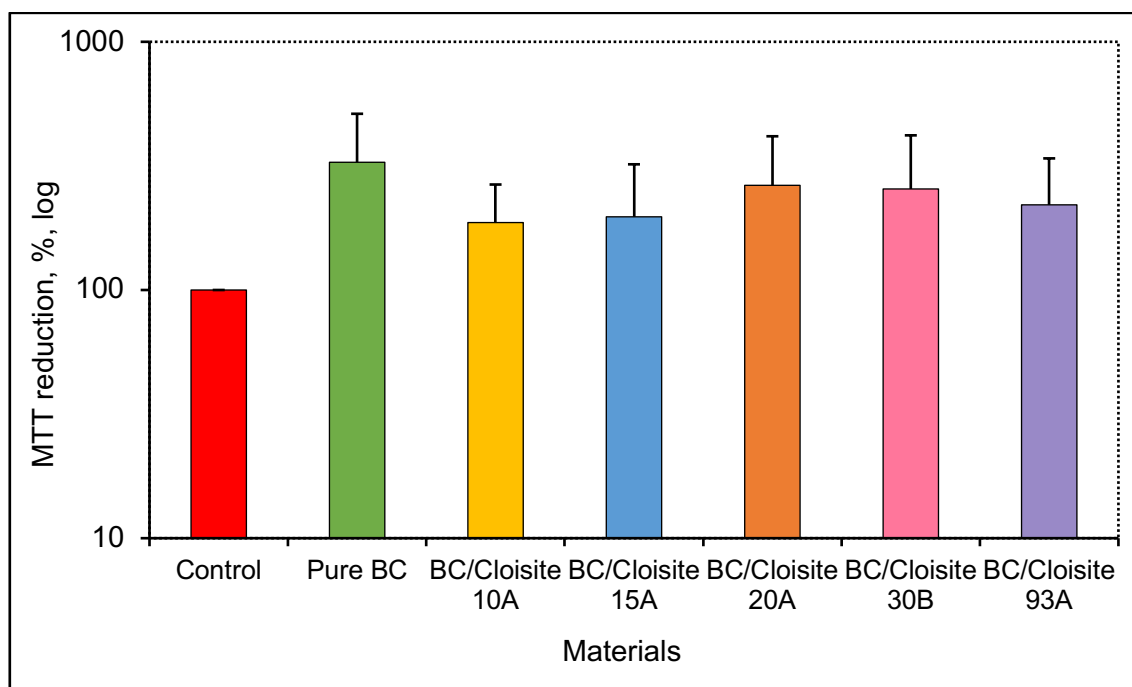


Figure 95. The effect of pure BC and BC/organoclay composites on 3t3 cells after 72 of incubation at 37°C. The control shows the MTT reduction in the cells without any treatment. Data shown represent the mean of three independent experiments of MTT assay with error bars of standard deviation. The treatments outcomes are not significantly different in comparison with the control.

The incorporation of organoclay into BC resulted in generation of antibacterial material with enhanced levels of MTT reduction in mammalian cells. Table 2 summaries the MTT reduction activity in the cells in the presence of synthesised BC-based materials obtained after 24, 48 and 72 hours.

Table 2. Effect of BC-based materials on 3t3 cells after 24, 48 and 72 hours.

Time, Hours	Pure BC	BC/Cloisite 10A	BC/Cloisite 15A	BC/Cloisite 20A	BC/Cloisite 30b	BC/Cloisite 93A
	MTT reduction, %					
24	357	235	225	189	329	142
48	248	203	194	174	222	225
72	327	186	197	264	255	220

4.2. Discussion

4.2.1. Attachment of clay to BC

Particles of Cloisite clay could penetrate a matrix of BC, fill empty spaces between BC fibres and physically attach to them. Moreover, it has been reported that an interaction of silicate particles with the OH groups of BC might also occur through a hydrogen bonding^[246]. This means that the presence of hydroxyl groups in both BC and NaMMT clay may lead to a weak organic-inorganic interaction^[112]. For instance, FTIR results, which have been reported elsewhere showed two sharp peaks in the OH stretching of BC/NaMMT composite, which could indicate hydrogen bonding between BC and both Mg(OH) and Al groups of NaMMT clay^[112]. In addition, the presence of merging bands of Si/MgO in MMT and OH groups in BC, respectively, has been observed elsewhere in FTIR spectra^[112]. Thus, the particles of Cloisite clay could be attached to BC through both *in situ* and *ex situ* synthesis. However, there might be a better penetration of the exfoliated clay particles into BC during the formation *in situ*, because forced incorporation of clay through the vacuum self-assembly method might result in both uneven penetration and distribution of clay particles followed by a leaching of clay out of BC. The presence of nanoparticles inside the matrix and on the surface of BC has been observed by SEM elsewhere^[112]. It has been concluded that the amount of absorbed NaMMT clay by both BC surface and matrix could increase with increasing a concentration of clay. However, a high concentration

of clay may lead to particle agglomeration that can adversely affect properties of the composite^[116]. Non-exfoliated clay particles might also result in insufficient load between the matrix and the nanofillers^[116]. For instance, the effect of 1 wt.%, 2 wt.% and 4 wt.% clay concentration has been studied in the synthesis of BC/NaMMT composites. The results showed that BC absorbed 25.72%, 40.36% and 45.06% of NaMMT suspension containing 1 wt.%, 2 wt.% and 4 wt.% clay concentration, respectively^[112]. However, the effect was reported to be more permanent with a clay concentration up to 2 wt.%^[112]. This might be due to particle agglomeration and subsequent lack of proper binding to BC fibres, which then resulted in a clay leaching.

4.2.2. Antibacterial activity of synthesised *ex situ* composites

There are a number of reasons for the antibacterial activity of organoclay. Firstly, the surfactant of organoclay has quaternary ammonium compounds (QAC) that can possess antibacterial activity^[87]. Due to the presence of the positively charged surfactants, organoclay has a positive zeta potential, whereas bacterial cells have a negative zeta potential^[247]. In order to express antibacterial activity, QAC need to be in a contact with a bacterial cell wall. Therefore, the leaching behaviour of organoclay could also play a crucial role in the inhibition of bacterial growth.

4.2.2.1. Quaternary ammonium compounds

The organic modifier of all organoclay used consists of QAC (Table 3).

Table 3. Properties and structure of commercially available organoclay layered silicates supplied by Southern Clay Products, Inc^[92].

Commercial Name	Organic Modifier	Molecular structure
Cloisite® 10A	Dimethyl benzyl hydrogenated tallow quaternary ammonium	$ \begin{array}{c} \text{CH}_3 \\ \\ \text{H}_3\text{C}-\text{N}^+-\text{CH}_2-\text{C}_6\text{H}_5 \\ \\ \text{HT} \end{array} $ <p style="text-align: right;">[248]</p>
Cloisite® 15A	Dimethyl dehydrogenated tallow quaternary ammonium	$ \begin{array}{c} \text{CH}_3 \\ \\ \text{CH}_3-\text{N}^+-\text{HT} \\ \\ \text{HT} \end{array} $ <p style="text-align: right;">[89]</p>
Cloisite® 20A	Dimethyl dehydrogenated tallow, quaternary ammonium	$ \begin{array}{c} \text{CH}_3 \\ \\ \text{CH}_3-\text{N}^+-\text{CH}_2\text{CH}(\text{CH}_2\text{CH}_2\text{CH}_2\text{CH}_3) \\ \\ \text{HT} \end{array} $ <p style="text-align: right;">[89]</p>
Cloisite® 30B	Methyl tallow bis-2-hydroxyethyl quaternary ammonium	$ \begin{array}{c} \text{CH}_2\text{CH}_2\text{OH} \\ \\ \text{CH}_3-\text{N}^+-\text{T} \\ \\ \text{CH}_2\text{CH}_2\text{OH} \end{array} $ <p style="text-align: right;">[87]</p>
Cloisite® 93A	Methyl dehydrogenated tallow ammonium	$ \begin{array}{c} \text{H} \\ \\ \text{CH}_3-\text{N}^+-\text{HT} \\ \\ \text{HT} \end{array} $ <p style="text-align: right;">[249]</p>

QAC are a major class of cationic surfactants, which have at least one hydrophobic hydrocarbon linked to a positively charged nitrogen atom. As shown in Table 3, QAC are composed of a charged nitrogen “head” bearing four bonds^[250]. A proposed mechanism for the antibacterial action of QAC is based

on the electrostatic interaction between QAC and bacterial cell walls that leads to the formation of surfactant-bacteria complexes^[251]. For instance, QAC could act by the cationic head groups, which face outwards and bind to the anionic head groups of acidic phospholipids in bacterial cell walls^[251]. Moreover, the hydrophobic tails of QAC may also be inserted into the lipid bilayers of a bacterial cell^[251]. QAC could interact with Gram-positive bacteria through binding to teichoic acids^[252]. An interaction of QAC with bacteria leads to increased permeability of the cell wall. Furthermore, QAC may form aggregates with the hydrophobic cell wall and solubilise it. For instance, an alkyl chain of QAC reacts with fatty acid chains of lipids of a cell wall and destabilises interactions between phospholipids and proteins^[98]. QAC might first pass the outer membrane of Gram-negative bacteria by lysis, interact with the inner cell wall and subsequently with intracellular components^[253]. After contact with QAC, bacterial cells have been found to exhibit progressive leakage of cytoplasmic materials^[251]. The lysis of cells could occur when the outer membrane of the cell is broken down or destroyed followed by a release of intracellular materials such as proteins, organelles, RNA and DNA^[253]. It has been reported that QAC might also affect DNA, which then loses its ability for multiplication^[253]. Contact between QAC and a cell wall can be identified by ATP leakage^[253]. Thereby, the mechanism of QAC involves absorption, disorganisation, disruption of cell walls, releasing of vital cell content, a possible penetration into a cell wall followed by intracellular degradation of nucleic acids^[98, 100, 253, 254].

Low concentrations of QAC could lead to both damage and leakage of cytoplasmic constituents, whereas high concentrations might cause coagulation of the cytoplasm presumably through denaturation of proteins^[98, 251]. Moreover, it has been found that the positively charged QAC may also prevent the formation of biofilms and impede the elongation that is necessary for the division of Gram-negative bacteria^[255]. It has been reported elsewhere that organoclays show antimicrobial activity against both Gram-positive and Gram-negative bacteria^[101, 103, 105]. In other studies, it was found that Cloisite 10A, Cloisite 15A, Cloisite 20A

and Cloisite 30B showed strong antibacterial activity against Gram-positive *S. aureus* and Gram-negative *E. coli* [97, 99]. *P. aeruginosa* could be less susceptible for QAC than other bacteria due to the presence of OprF membrane porin, because the diffusion of different molecules through this porin is approximately two orders of magnitude slower than through OmpA porin in *E. coli* [50]. However, the results in the current study showed that BC/Cloisite 10A, BC/Cloisite 15A, BC/Cloisite 20A and BC/Cloisite 30B successfully inhibited the growth of *P. aeruginosa*.

A strong correlation between the length of an alkyl chain and antibacterial activity was found elsewhere [252, 256]. Alkyl groups are mostly short-chain substituents such as methyl or benzyl groups [256]. It has been observed that alkyl chains that consist from 12 to 16 carbons could possess an optimal antibacterial activity [250]. For instance, the length of C16 of the hydrophobic tail was found to be more effective against Gram-negative bacteria than shorter-chain compounds due to a stronger interaction of C16 with the fatty acid portion of Lipid A in LPS [252]. The tested organoclay could be divided into two groups based on their molecular structure of QAC. Cloisite 10A and Cloisite 30B consist of a single long tail of hydrogenated tallow, whereas Cloisite 15A, Cloisite 20A and Cloisite 93A have two long tails of hydrogenated tallow (Table 3). It has been shown that the most effective antibacterial activity was observed using Cloisite 10A and Cloisite 30B organoclay, whereas the least was with Cloisite 93A [257]. The results obtained in the current study are in agreement with this report. Furthermore, it has been reported that cationic surfactants that contain one long tail can be more effective against bacteria than those QAC containing only short aliphatic tails [257]. This might explain why Cloisite 10A and Cloisite 30B showed stronger antibacterial activity than other organoclay.

In addition, the tested organoclay contains different amount of surfactants. For instance, even though Cloisite 15A and Cloisite 20A have the same cationic surfactant, Cloisite 15A, which exhibits stronger antibacterial activity, has a higher

concentration of the surfactant^[257]. This might be a reason why BC/Cloisite 15A showed stronger antibacterial activity against MRSA and *E. coli* than BC/Cloisite 20A.

4.2.2.2. Effect of zeta potential on the antibacterial activity of organoclay

Each layer of MMT clay has a net charge from 0.2 to 0.9 per formula unit due to isomorphous substitution such as Mg^{2+} for Al^{3+} in the octahedral sheet or Al^{3+} for Si^{4+} substitution in the tetrahedral sheet. In the octahedral sheet, the charge is delocalised on both top and bottom of the structure^[258]. The substitution in the tetrahedral sheet is more localised, where a charge is present only on one surface^[258]. The negative charge of clay particles is compensated by the exchangeable Na^+ cations^[258]. The zeta potential of MMT clay was found to be -39.0 mV, which means that the surface of the particles is negatively charged^[258].

The pH condition might affect the zeta potential of unmodified NaMMT clay. It has been reported that zeta potential was -28 mV at pH2 and became more negative as pH values increases^[259]. The replacement of Na^+ by H^+ can occur at a low pH and lead to an increase in the concentration of sodium, electrical conductivity of the suspension and numbers of H^+ on the surface^[259]. Furthermore, dissolution of MMT structure could arise through the breakage of bridging oxygen bonds (Si–O–Al) at a low pH. This leads to the release of Al and then Si atoms into the suspension. Al^{3+} might displace the Na^+ cations, reside between the layer and neutralise the negative surface more effectively than Na^+ . This then results in an increase in zeta potential. At pH10, zeta potential decreased to -48 mV and remained stable^[259]. The net negative charge of NaMMT could be associated with better dispersion of clay particles. A negative charge of a single particle might be greater than that of clay aggregates.

The zeta potential might also vary within different clay structures. The modification of MMT clay with cationic QAC leads to an increase in zeta potential

in a positive direction^[260]. It has been found that zeta potential for organoclay was higher than for unmodified clay due to the stronger binding of organic than inorganic cations to the clay layers^[260]. Furthermore, the addition of C16 leads to an increase in the charge of MMT, which becomes positive in acidic or neutral solution and decreases when the concentration of hydroxyl ions increases. Moreover, an increase in the length of alkylammonium cations might result in better absorption of cations outside the surfaces of the clay through cation exchange and hydrophobic binding^[261]. Thus, QAC with a benzyl group was found to have zeta potential around +22.7mV, whereas the zeta potential of MMT clay modified with other QAC was around +14.4 mV^[247]. Due to the organic cation saturation, Cloisite 10A is highly organophilic and not homogeneously dispersed in water^[262]. Therefore, it is challenging to measure zeta potential of organoclay consistently. The values of Cloisite 30B were found to be lower than Cloisite 15A, which means that Cloisite 30B suspension is more stable^[263].

The surface of a bacterial cell is negatively charged and is balanced by positively charged cations present in the surrounding medium. Zeta potential values of *S. aureus* have been found to be -35.6 mV, whereas that for *E. coli* was -44.2 mV^[57]. Another study reported zeta potential values of MRSA and *P. aeruginosa* being -17mV and -13.4mV, respectively^[264, 265]. It has been stated elsewhere that the neutralisation of the surface charge of a cell could lead to membrane permeability^[266]. The electrostatic interaction between various agents and the bacterial surface might affect zeta potential, which can, subsequently, cause not just greater permeability of the cell surface, but also might lead to cell death. In addition, the cationic compounds might interfere with membrane bound ATPase, which are responsible for membrane potential through the regulation of movements of H⁺ across the membrane, and disturb the ion transport^[266].

4.2.2.3. Leaching behaviour of organoclay

In order to inhibit antibacterial activity by contact, the cationic surfactant, which is located between the clay layers, needs to be exposed to the surface of a material.

Therefore, the leaching ability of organoclay could be another possible reason for the antibacterial activity. The leaching behaviour was analysed by measuring the contact angle between hand-made pressed discs of Cloisite 10A, Cloisite 15A, Cloisite 20A, Cloisite 30B and Cloisite 93A and a drop of water, respectively. The contact angle represents the tendency of a fluid to spread over the solid surfaces. Wettability refers to the degree of dispersion of fluids on the surface of solid materials. A contact angle that is less than 90° indicates that a solid has a wetting (hydrophilic) behaviour, whereas a contact angle, which is greater than 90° , shows that a solid has a non-wetting (hydrophobic) property^[267]. Therefore, an increase in a contact angle leads to increasing hydrophobicity of a material. The advancing contact angle is referred to a state when a drop touches the surface and spreads just after making contact. This angle is more sensitive to hydrophobic surfaces. The receding contact angle is the smallest state of the angle^[268]. Furthermore, the equilibrium contact angle is defined when the system has the absolute minimum free energy^[268]. The measurement of wettability might be challenging due to the liquid absorption and roughness of the hand-made discs. The porosity of hand-made discs could also influence contact angle measurements. It has been reported that the pore volume of NaMMT clay decreased from about 4 nm to about 3 nm after loading of surfactants of organoclay^[269]. Porous materials can be either partially-wetting or complete wetting. Regarding a partial-wetting process, once a drop of water touches a porous material, the contact angle decreases almost linearly from the initial to a static contact angle^[270]. During this stage, the base of a droplet does not move^[270]. Then, the contact angle remains stable. However, in the case of complete wetting, the contact between a droplet and a porous surface is initially stable, where the spreading of a droplet almost stops^[270]. Then, the droplet starts to soak into a porous material leading to a rapid decrease in a contact angle^[270]. According to the results obtained in the current study, the contact angle between Cloisite organoclay and the drops of water showed a pattern similar to partially-wetting porous materials. However, both Cloisite 10A and Cloisite 30B did not completely reach static contact angles after 900 and 100 seconds, respectively.

Due to the hydrophilicity of Cloisite Na⁺, the drop of water was not sufficiently stable to measure a contact angle.

An increase in the amount of an organic modifier leads to a change in the clay from being hydrophilic to organophilic^[259]. Organophilic property of organoclay could be influenced by the length of an alkyl chain, where the longer the chain is, the more organophilic is the clay^[271]. Depending on the surfactant, long carbon chains might be arranged as mono, bilayers or pseudotrimolecular layers between the clay sheets parallel to the clay surface^[262]. *D*-space increases with surfactants that contain two long tails. For instance, Cloisite 10A has a *d*-space of 19.13Å and a pseudotrimolecular orientation of alkylammonium cations in the interlayer space^[262]. Furthermore, benzyl substitute groups in QAC result in superhydrophobic surface and water non-wettability, whereas clay that is modified with QAC without benzyl substitute group becomes more hydrophilic and water-wettable^[247].

Moreover, the static angle was about 80° for both Cloisite 20A and Cloisite 93A. This might indicate a similar wettability of both clays. The contact angle of Cloisite 30B was not stable and had the values of 70° ± 10°. A study elsewhere has reported that the contact angle values for Cloisite 30B were 73°, 60° or 81°^[268]. These values are in agreement with the results obtained in the current study. Furthermore, it also has been stated that static contact angles for Cloisite 10A, Cloisite 20A and Cloisite 30B compacted discs were not different^[268]. However, in the current study, Cloisite 10A did not reach a static contact angle after 900 seconds where the values of the angle constantly dropped.

The measurements of contact angle elsewhere have shown that leaching of surfactants used for the preparation of Cloisite 10A and Cloisite 30B was quicker compared to Cloisite 15A, Cloisite 20A and Cloisite 93A^[257]. It was found that Cloisite 93A leached the least among others^[257]. These results agreed with the current study, where Cloisite 10A and Cloisite 30B leached the most, whereas the leaching behaviour of Cloisite 93A was the least pronounced compared to

other organoclays. Cloisite 15A contains the same type of surfactant as Cloisite 20A, but in a higher amount, which results in a smaller increase in *d*-spacing compared to Cloisite 20A^[257]. Therefore, a difference in leaching behaviour might occur.

Organophilic property of the clay could lead to the antibacterial activity by attracting the bacterial surfaces^[272]. It has been reported that *S. aureus* has hydrophobic characteristics with the contact angle of the cell wall being 72θ due to the presence of lipoteichoic acids^[272]. Hydrophobic cells might have a preference for hydrophobic surfaces, where bacteria may get attracted to organoclay and, subsequently, be inhibited by the free QAC surfactant^[272].

4.2.2.4. Comparison of antibacterial activity of BC/clay composites

Both QAC and leaching behaviour could be major reasons for the antibacterial activity of organoclay. The variation of CFU reduction could be explained by the leaching behaviour of tested organoclay. Cloisite 10A and Cloisite 30B showed greater leaching behaviour compared to others. Furthermore, BC/Cloisite 20A showed antibacterial properties against both MRSA and *P. aeruginosa*, but did not affect the growth of *E. coli*. As Cloisite 15A and Cloisite 20A are similar in chemical structure, Cloisite 20A would have also possessed antibacterial activity against *E. coli*. A possible reason for this might be an uneven distribution of either bacteria or Cloisite 20A within the matrix of BC. In addition, Cloisite 93A was the least effective composite in terms of antibacterial activity in both zone inhibition assay as well as inside the BC/Cloisite 93A composites. BC/Cloisite 93A reduced the growth of MRSA, but did not affect either *E. coli* or *P. aeruginosa*. As was observed from the experiments on the contact angle of Cloisite 93A, the leaching behaviour of the clay was less pronounced than the leaching activity of Cloisite 10A and Cloisite 30B. This might have an impact on the attachment of the bacteria to the clay and subsequent binding of the clay to the bacterial cell wall.

The antibacterial activity of organoclays, mainly Cloisite 10A and Cloisite 30B, was stronger than Cloisite Na⁺ and SWN clay without surfactants. It has been concluded elsewhere that both the charge and hydrophobic nature of organoclay could be associated with their antibacterial activity^[272]. The organoclays were more effective against *P. aeruginosa* compared to Cloisite Na⁺ and SWN clay. However, the antibacterial activity of organoclay was associated with the QAC and leaching behaviour, whereas the antibacterial activity of the natural clay was possibly due to the release of Na⁺ cations in the exfoliated state.

Similar results were obtained in another study, where BC/NaMMT, which was synthesised *ex situ* through immersion using 1 wt.% of clay, showed antibacterial activity against *S. aureus* and *E. coli*, but did not inhibit *P. aeruginosa*^[239]. Previous studies have reported a very slow release of ions from BC composites, which resulted in a strong antibacterial effect through physical attachment with bacteria^[125]. As a current method for the antibacterial assay is based on placing the bacteria inside the composite, such attachment might be successfully achieved. Furthermore, the bacterial death could be due to the destruction of the cell walls, change in cellular pathways or due to the ability of sodium to destabilise the permeability of the bacterial cell wall (Section 3.2.4). BC/SWN, however, showed antibacterial activity against three tested organisms and especially strong inhibition of growth was observed with MRSA. This might be due to the low aspect ratio, which allowed better dispersion within the BC matrix and, therefore, interaction with the bacterial cell walls with subsequent penetration of SWN inside the bacteria. Moreover, the stronger antibacterial activity of SWN against MRSA might be because Gram-positive bacteria have a single cell wall, whereas Gram-negative bacteria have the additional outer membrane as described in Section 1.2.3.1^[273].

Pure BC promoted the growth of all tested bacteria. This might lead to a spread of pathogens within the wounds. It has been reported elsewhere that common bacterial species that cause wound infections are *S. aureus*, *P. aeruginosa* and MRSA^[119, 120]. The incorporation of exfoliated clay resulted in the antibacterial

activity of BC, which might overcome the issues associated with wound infections.

4.2.3. Effect of organoclay on 3t3 cells

Both Cloisite 10A and 30B organoclays alone possessed cytotoxic behaviour; however, as shown in Table 2, all BC/organoclay composites increased the levels of MTT reduction in 3t3 cells. The level of MTT reduction of the cells was the highest in the presence of pure BC after 24 hours. The MTT reduction activity of the cells increased after 72 hours using BC/Cloisite 20A and BC/Cloisite 93A composites.

Nonetheless, the percent of metabolically active cells inside the matrix of pure BC was higher than inside the composites after 24 hours, the levels of MTT reduction in 3t3 cells dropped to about 50% less compared to the control values using pure BC after 48 hours. A possible reason behind this might be the reduction of nutrients, which could be consumed by a large number of cells, and, therefore, due to insufficient amount of nutrients after 48 hours cells exhibit low metabolic activity. Oppositely, BC/clay composites might stabilise the overpopulation of the cells. However, the MTT reduction activity of 3t3 cells decreased after 72 hours in the presence of BC/Cloisite 10A, BC/Cloisite 15A and BC/Cloisite 30B. This might be due to the leaching behaviour. Due to their organophilic nature, the clay might not be properly dispersed inside the tissue culture medium, which could lead to agglomeration of particles with subsequent settling down at the bottom of the wells. This might also influence the proliferation of cells. In order to evaluate the current method for analysis of cytotoxicity, a new method using a cover glass coated with the pre-suspended clay was proposed. Such a method allowed better interaction of the clay with the cells.

However, there was a variation of MTT reduction in 3t3 cells within three experiments at 6 mg/ml concentration of the clay after 24 hours. A possible reason for this might be that 6 mg/ml was too high a concentration, which could

negatively affect the proliferation of the cells. It has been reported that Cloisite 20A did not show any cytotoxicity towards Caco-2 and HepG2 cell lines at a concentration of up to 0.065 mg/ml after 24 and 48 hours^[101]. A concentration of Cloisite 30B over 0.19 mg/ml affected the MTT reduction in 3t3 cells. The damage of DNA of Caco-2 cells by Cloisite 30B at 0.17 mg/ml after 24 hours has been reported elsewhere^[102, 104]. Furthermore, Cloisite 30B has shown cytotoxicity at a concentration of 0.125 mg/ml against HepG2 cells^[102]. Another study has shown that a 0.226 mg/ml concentration of Cloisite 30B induced 40% cytotoxicity in Caco-2 cells^[102]. In addition, 0.250 mg/ml of Cloisite 30B has been reported as toxic for HUVEC cells^[104]. The lowest concentration of Cloisite 93A did not affect the metabolic activity of 3t3 cells, which remained at 100% of the control values after 72 hours. However, the decrease in the MTT reduction in the cells could be observed within concentrations higher than 0.19 mg/ml. The lowest percent of metabolically active cells was 24% of the control values using 6 mg/ml of Cloisite 93A. Consequently, the highest concentration of 6 mg/ml of Cloisite 93A affected MTT reduction in 3t3 cells much less compared to other tested Cloisite clay. This might be due to the highly organophilic nature of the clay. Similar results were obtained in another study, which stated that Cloisite 93A reduced the viability of human monocytic U937 cells at over 1 mg/ml concentration after 24 hours^[106].

A connection between antibacterial activity and cytotoxicity of the Cloisite clay used can be observed. Organoclay with a high ability to leach could exhibit cytotoxicity towards fibroblasts. Thereby, Cloisite 10A and Cloisite 30B clay, which showed the strongest antibacterial activity and leaching behaviour, also induced a decrease in MTT reduction in 3t3 cells. Whereas Cloisite 93A, which showed the weak antibacterial activity, was not as toxic as other clay to 3t3 cells even at the highest concentration. This might raise concerns regarding the use of Cloisite 10A and Cloisite 30B in wound healing systems. Both BC/organoclay and BC/natural clay without surfactants induced an increase in the metabolic activity of the 3t3 cells compared to the control values.

Chapter 5. Incorporation of chitosan into BC through synthesis *in situ*

Bacterial cellulose was synthesised *in situ* in the standard HS medium containing a solution of widely-available (WA) chitosan (MW 161 kDA, 90% DDA) as described in Section 2.5.2. The chitosan solution was prepared using 0.1M of acetic acid and 0.5 wt.% of chitosan followed by magnetic stirring for 24 hours. The solution was then added to the medium to a final concentration of 0.25 wt.%. The pH of the medium was adjusted to pH5. *G. xylinus* at an inoculum concentration of approximately 7.9×10^7 CFU/ml was mixed with HS medium, which already contained both 2 wt.% glucose and 0.25 wt.% of the chitosan solutions, and incubated for 48 hours at 30°C. The synthesised composite was then characterised by UV-VIS-NIR spectroscopy. The antibacterial properties of the composite were analysed using MRSA and *E. coli*. The cytotoxicity of chitosan was investigated using the 3t3 cell line.

5.1. Results**5.1.1. *In situ* synthesis of BC/chitosan composite involving glucose****5.1.1.1. Characterisation of *in situ* produced BC/chitosan composite**

The formation of the pellicle was observed using WA chitosan after 48 hours. Fig. 96 shows synthesised BC/chitosan composite. The composite was weak compare to the original BC. Similarly, another study reported inhibition of synthesis of BC in the presence of 0.1 wt.% of chitosan in the medium^[138]. A possible reason for this might be viscosity, which can increase in a higher concentration of chitosan. This appears due to the presence of ionic groups that result in expansion of the polymer chains and causing an increase in viscosity. However, during synthesis, chitosan can establish hydrogen bonds with BC and with water molecules^[180]. This might result in strong physical binding of chitosan to the matrix of BC.



Figure 96. A photograph of the synthesised BC/chitosan composite. BC was produced using inoculum of *G. xylinus* and HS medium containing both glucose solution and WA MW chitosan solution at 2 wt.% and 0.25 wt.%, respectively, at pH5 on a large scale. Bacteria was incubated for 48 hours at 30°C.

5.1.1.2. Leaching behaviour of BC/chitosan composite

The leaching behaviour of chitosan was investigated as described in Section 2.5.2.2. Prior to the experiment, the calibration curve of chitosan at characteristic peak at wavelength of the 325 nm^[274] was obtained (Fig. 97). The purpose of the calibration curve was to quantify the concentration of chitosan leached from the composite during the washing process. As shown in Fig. 97, R^2 was 99%, which means that the good linear relationships were obtained.

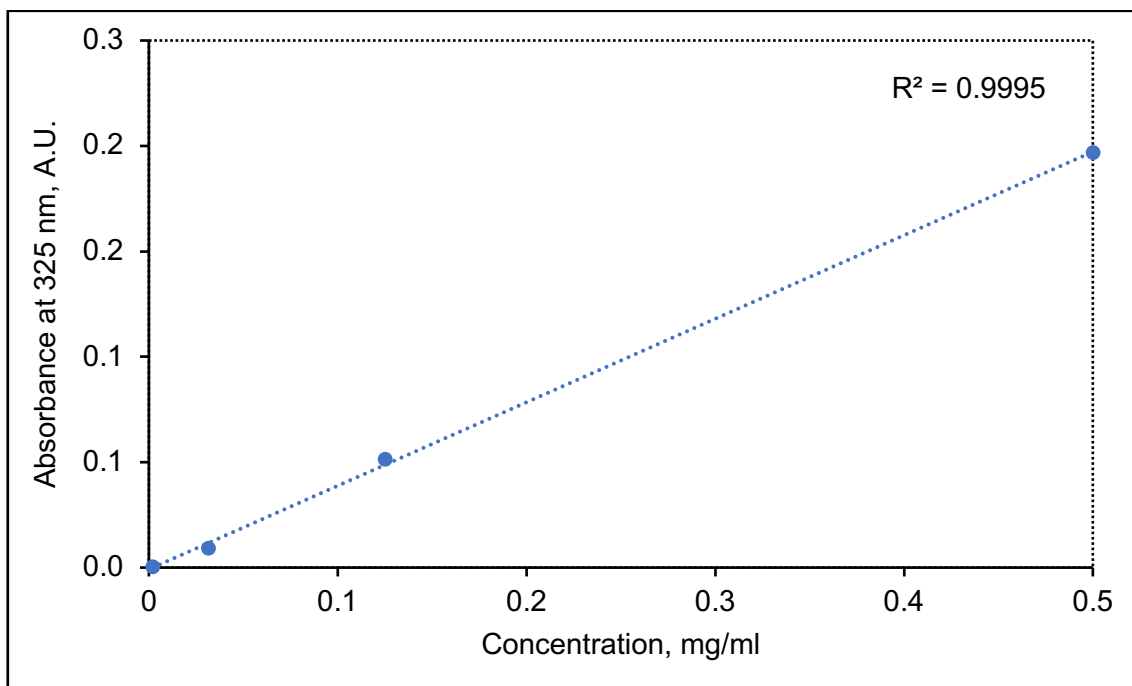


Figure 97. The relationship between absorbance at wavelength of 325 nm and concentration of chitosan.

BC/chitosan composite in amount of 6 grams was placed into a centrifuge tube containing 20 ml of distilled water and washed from 1 to 80 hours. The concentration of chitosan leached was determined by UV-VIS and calculated using the calibration curve. Fig. 98 shows the concentration of chitosan leached from BC/chitosan composite from 1 to 80 hours. As shown in Fig. 98, the concentration of chitosan leached within first 3 hours was 0.01, 0.04 and 0.05 mg/ml, respectively. Then, the leaching amount of chitosan increased to 0.85 mg/ml after 75 hours. BC/chitosan composite started to break and fall apart at this point. Therefore, other peaks after 75 hours might be due to the disturb structure of the cellulose.

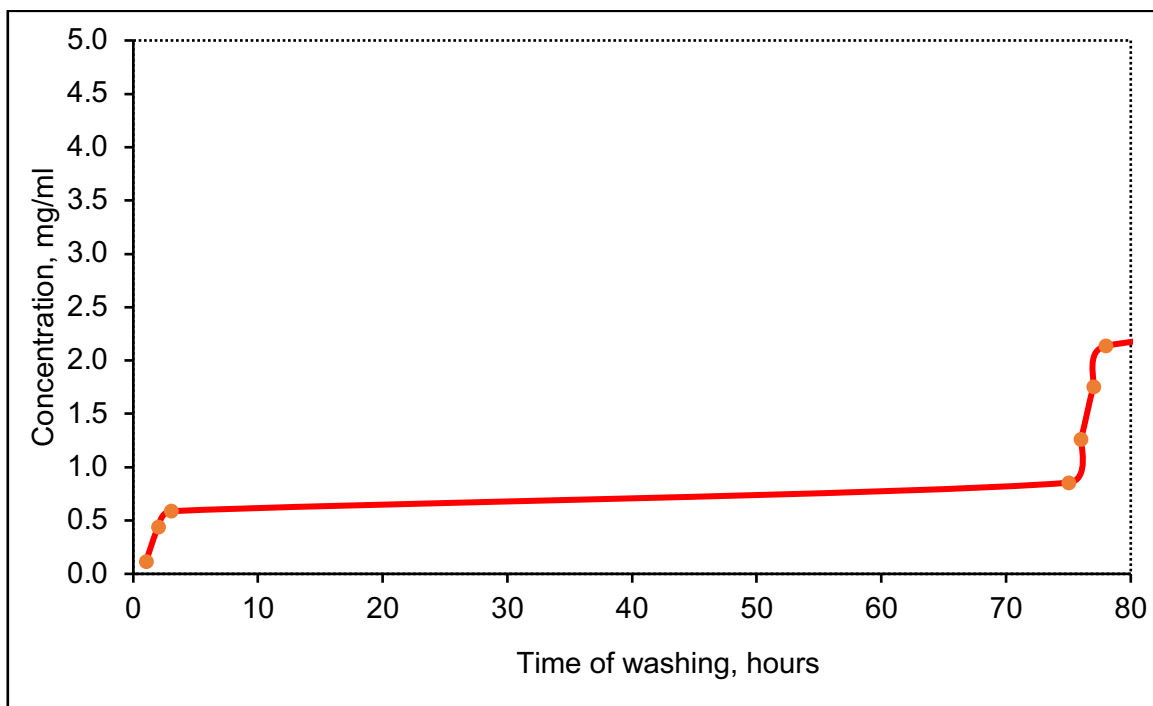


Figure 98. The concentration of chitosan leached from the composite during washing from 1 to 80 hours.

5.1.1.3. UV-VIS-NIR analysis of synthesised *in situ* BC/chitosan composite

After treatment with NaOH and washing, BC/chitosan composite was analysed by UV-VIS-NIR spectroscopy (Figs. 99-100). The UV-VIS-NIR spectrum of the composite was compared to those of both chitosan powder and pure BC.

As shown in Fig. 99, BC/chitosan composite had predominant peaks of BC. The characteristic peak of chitosan at 325 nm were not detected inside the composite^[274]. This might be due to either washing of chitosan out of BC/chitosan composite or the presence of chitosan inside the composite, but not on a surface of a material that made it hard to detect. However, the presence of chitosan inside the composite might be detected in the NIR spectrum, where both chitosan and BC/chitosan composite had peaks in a range of 1404-1660 nm (Fig. 100). Chitosan might remain inside BC after the washing. It may be that the presence

of O-H and N-H groups in chitosan leads to strong chemical binding to BC^[177]. This can result in broader peak at 1404-1660 nm, which included separate peaks of both BC and chitosan.

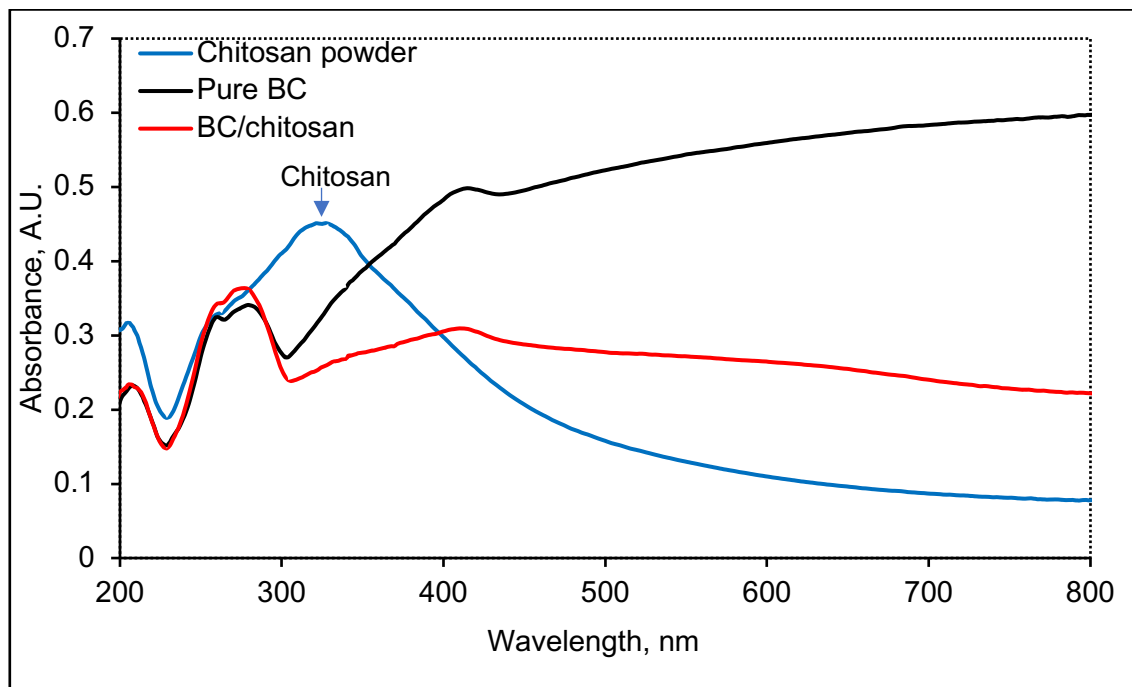


Figure 99. UV-VIS spectra of medium MW chitosan, pure BC and BC/chitosan composite.

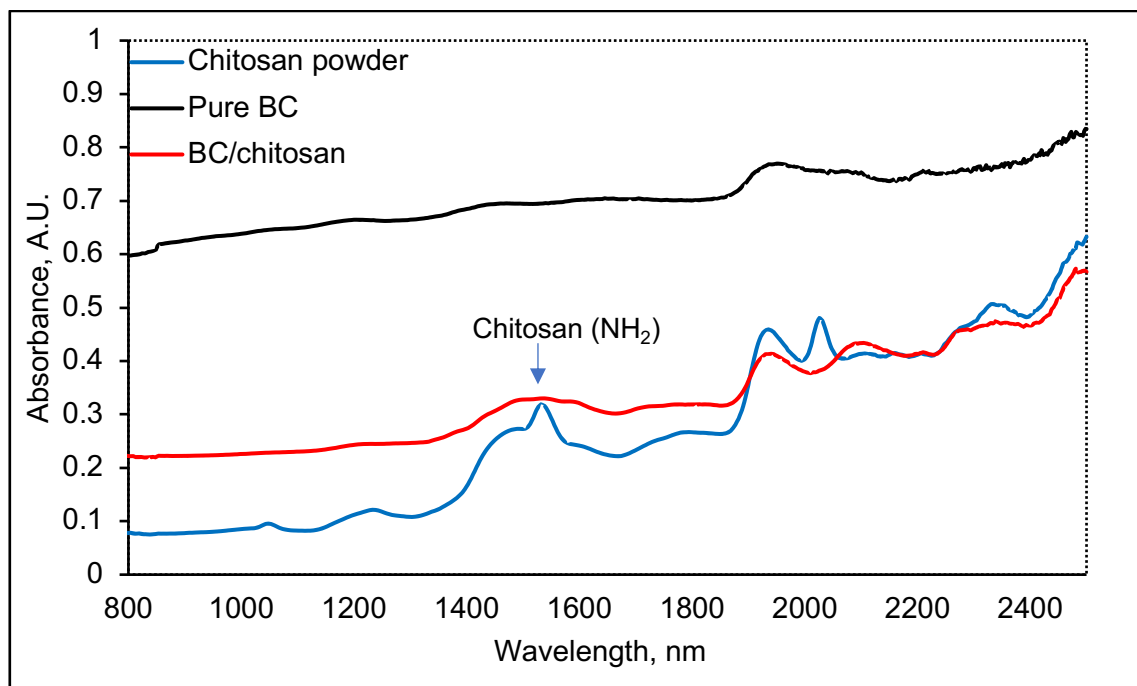


Figure 100. NIR spectra of MW chitosan, pure BC and BC/chitosan composite.

5.1.1.4. Antibacterial activity of chitosan

The effect of pure chitosan on a bacterial growth was investigated using MRSA and *E. coli* as described in Section 2.7.3.3. Figs. 101-102 show antibacterial activity of chitosan solution at a concentration of 0.5 wt.%. The control was PBS-resuspended either MRSA or *E. coli* without any treatment. According to Figs. 101-102, chitosan showed antibacterial activity against both tested bacteria. Chitosan reduced the control values of MRSA and *E. coli* to 1.7% and 4%, respectively.

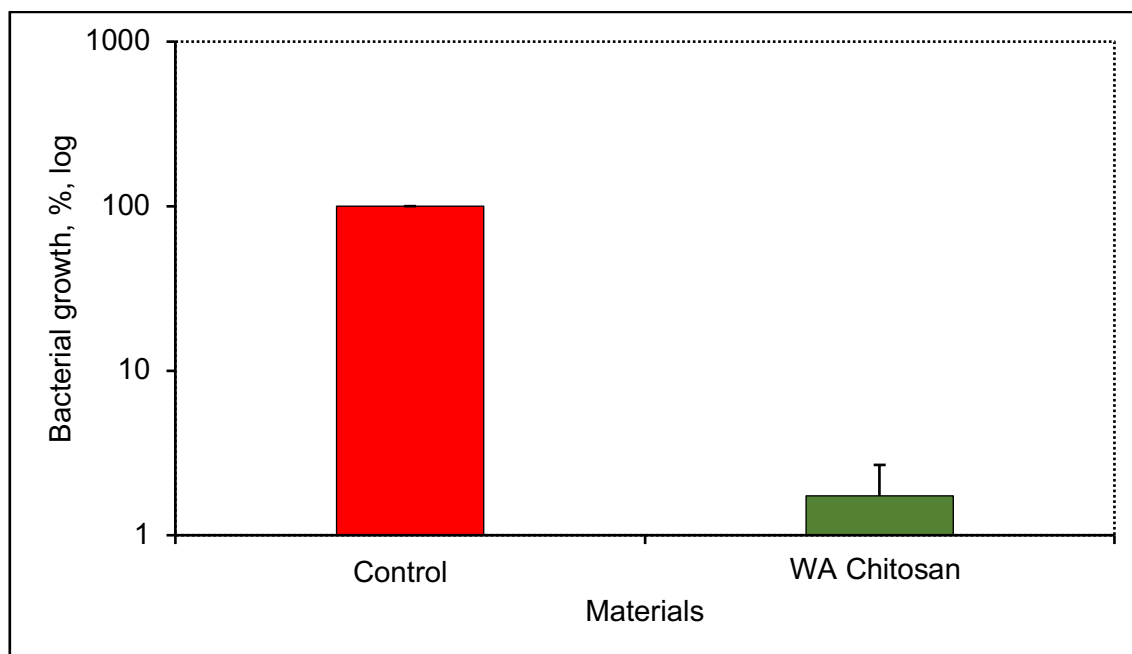


Figure 101. Antibacterial activity of chitosan against MRSA. The bacteria were incubated for 24 hours at 37°C. The control was MRSA without any treatment after 24 hours. Data represent the mean of two independent experiments with error bars of standard deviation. WA chitosan is significantly different in comparison with the control (P -value<0.01).

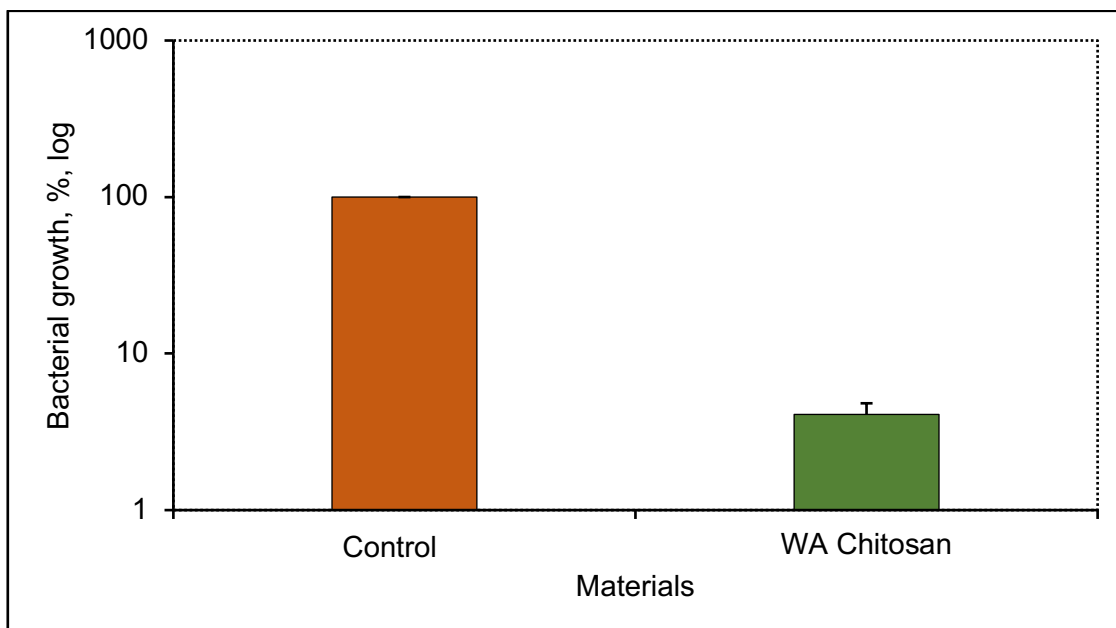


Figure 102. Antibacterial activity of chitosan against *E. coli*. The bacteria were incubated for 24 hours at 37°C. The control was *E. coli* without any treatment after 24 hours. Data shown represent the mean of two independent experiments with error bars of standard deviation. WA chitosan is significantly different in comparison with the control (P -value<0.01).

5.1.1.5. Antibacterial activity of BC/chitosan composite

The antibacterial activity of the BC/chitosan composite was investigated against MRSA, *E. coli* and *P. aeruginosa* as described in Section 2.7.3 (Fig. 103-105). The control for each experiment was PBS-resuspended MRSA, *E. coli* or *P. aeruginosa*, respectively, that was placed on the surface of the empty petri dish without agar and covered with the plastic lid. As shown in Fig. 103, pure BC did not show any antibacterial activity against MRSA, where the growth of the bacteria was the same as the control. Whereas the control values were significantly lower and decreased to 0.003% with BC/chitosan composite. This result indicated that chitosan was successfully incorporated into BC through biosynthesis *in situ*. BC/chitosan composite showed strong antibacterial activity against Gram-positive MRSA.

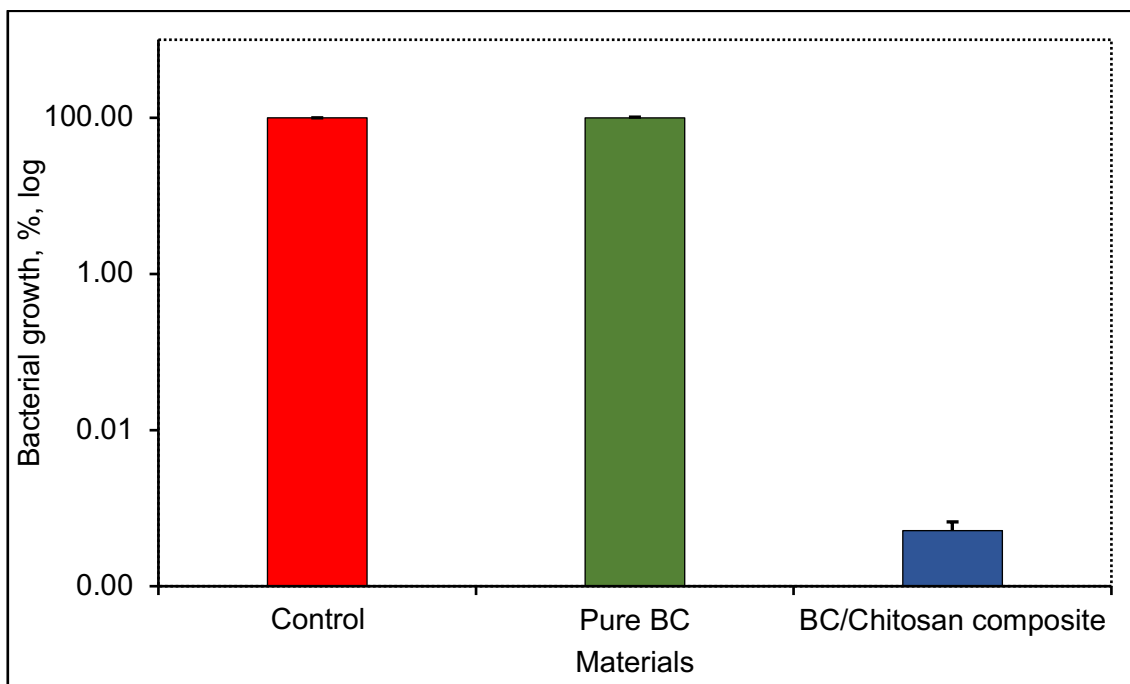


Figure 103. Antibacterial activity of BC/chitosan composite against. The control was PBS-resuspended MRSA, which was placed on the surface of the empty petri dish without agar and covered with a lid. The bacteria were incubated for 24 hours at 37°C. Data shown represent the mean of two independent experiments with error bars of standard deviation. BC/Chitosan composite is significantly different from the control (P -value<0.001).

Furthermore, pure BC promoted the growth of *E. coli* after 24 hours (Fig. 104). The control values increased to 151% with pure BC. However, BC/chitosan composite significantly decreased the growth of *E. coli* to 40% of control values. In addition, BC/chitosan composite did not show any antibacterial activity against *P. aeruginosa* (Fig. 105). As a consequence, the BC/chitosan composite was more effective against Gram-positive MRSA than Gram-negative *E. coli* and *P. aeruginosa*.

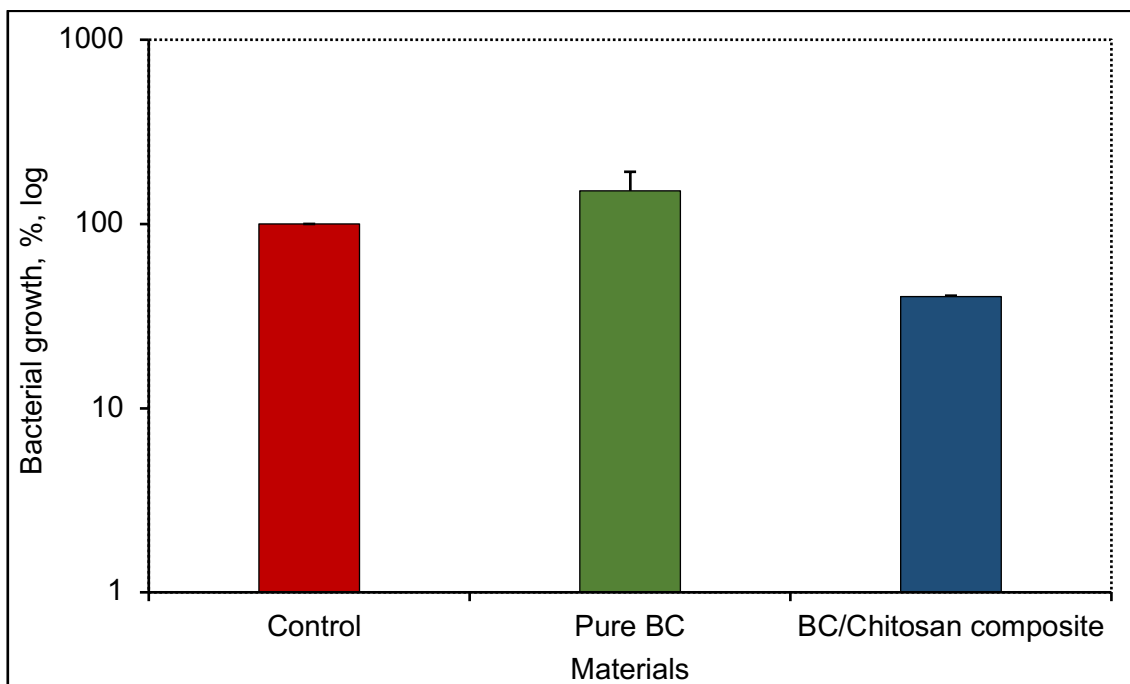


Figure 104. Antibacterial activity of BC/chitosan composite against *E. coli*. The bacteria were incubated for 24 hours at 37°C. The control was PBS-resuspended *E. coli*, which was placed on the surface of the empty petri dish without agar and covered with a lid. Data shown represent the mean of two independent experiments with error bars of standard deviation. BC/Chitosan composite is significantly different from the control (P -value<0.05).

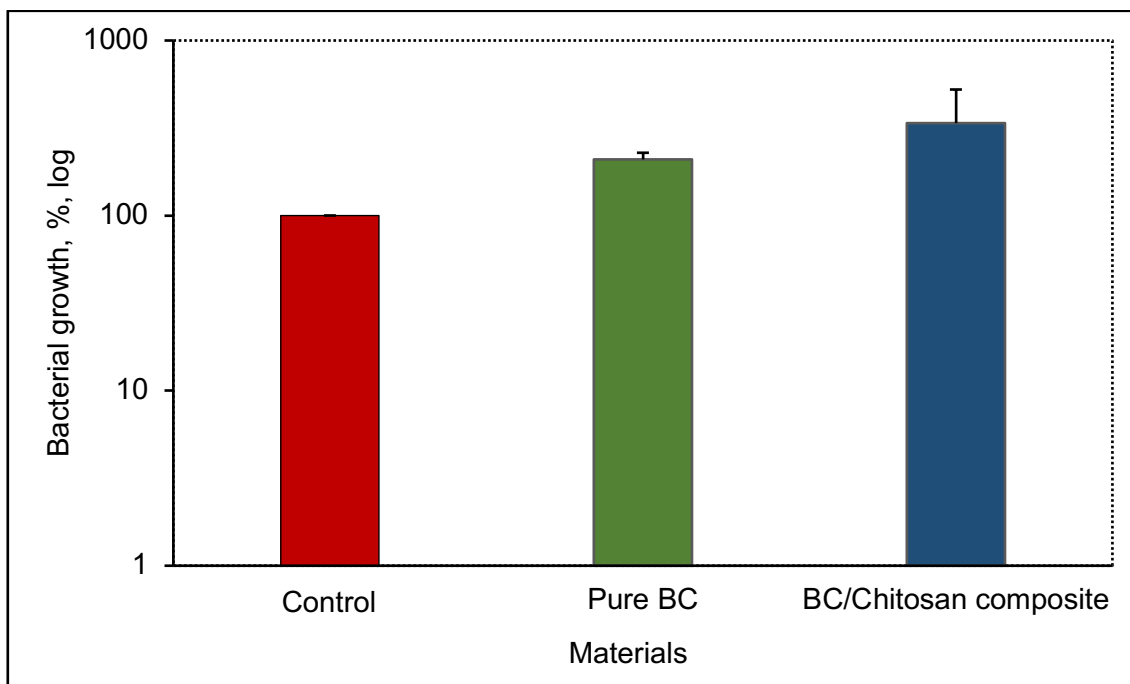


Figure 105. Antibacterial activity of BC/chitosan composite against *P. aeruginosa*. The bacteria were incubated for 24 hours at 37°C. The control was PBS-resuspended *P. aeruginosa*, which was placed on the surface of the empty petri dish without agar and covered with a lid. Data shown represent the mean of two independent experiments with error bars of standard deviation.

5.1.1.6. Mammalian cytotoxicity of chitosan

The cytotoxicity of chitosan on 3t3 cells was investigated using two methods as described in Section 2.12.5. Firstly, chitosan powder at a concentration of 5 mg/ml was mixed with the tissue culture medium and incubated with 3t3 cells for 24, 48 and 72 hours at 30°C. Secondly, a glass cover slip was coated with 0.5 wt.% chitosan solution that was dissolved at pH3, dried and sterilise by UV-Ozone. The cells were seeded on the top of both clean cover glass and the cover glass coated with the chitosan solution, covered with tissue culture medium and incubated for 24 and 48 hours, respectively, at 37°C.

5.1.1.6.1. Evaluation of toxicity of chitosan powder

The cytotoxicity of WA chitosan at a concentration of 5 mg/ml in the growth medium was investigated using 3t3 cells after 24, 48 and 72 hours (Fig. 106). The control represented the cells without any treatment after each time frame. WA chitosan was mixed with medium and incubated with cells at 37°C. As shown in Fig. 106, the level of MTT reduction by cells increased to 370% of control values by using chitosan after 24 hours. Then, the percent of MTT reduction decreased to 147% and 91% of control values after 48 and 72 hours, respectively.

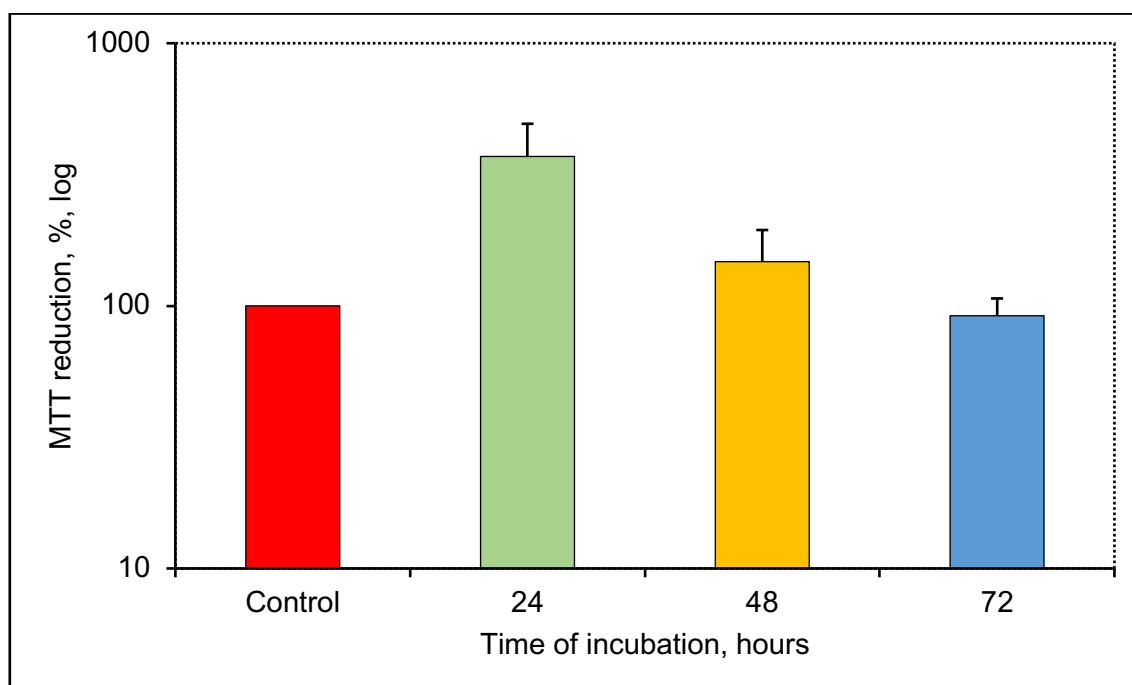


Figure 106. The effect of chitosan powder on 3t3 cells after 24, 48 and 72 hours. Chitosan at a concentration of 5 mg/ml was mixed with growth medium. Cells were incubation at 37°C. The control represented the cells without any treatment after each time frame. Data shown represent the mean of three independent experiments of MTT assay with error bars of standard deviation. Data obtained after 24 and 48 hours are significantly different to the control (P -value<0.001).

The main issue with this method was insolubility of chitosan at neutral pH. The pH of the tissue culture medium was pH7. This means that chitosan might not be

dissolved in the medium and, therefore, the interaction of chitosan with the cells could not occur. In order to overcome this issue, another method for evaluation of cytotoxicity of chitosan was proposed (Section 2.12.5.2).

5.1.1.6.2. Cytotoxicity assay using cover glass coated with chitosan

Another method for the evolution of cytotoxicity of chitosan was based on using the glass coverslip coated with 0.5 wt.% of WA chitosan solution as described in Section 2.12.5.2. The glass was subsequently dried and sterilised by UV-Ozone. The 3t3 cells were seeded on the top on it, covered with tissue culture medium and incubated for 24 and 48 hours at 37°C. As shown in Fig. 107, the level of MTT reduction of cells increased in the presence of chitosan. The level of MTT reduction was 332% and 249% of control values after 24 and 48 hours, respectively.

The data obtained using the glass coverslip coated with chitosan agreed with the results in Fig. 106. Chitosan increased level of MTT reduction in the cells. According to Figs. 106-107, MTT reduction in 3t3 cells was higher using the glass coverslip coated with chitosan rather than chitosan powder after 48 hours. This means that the proposed method can provide a better interaction of chitosan with the cells.

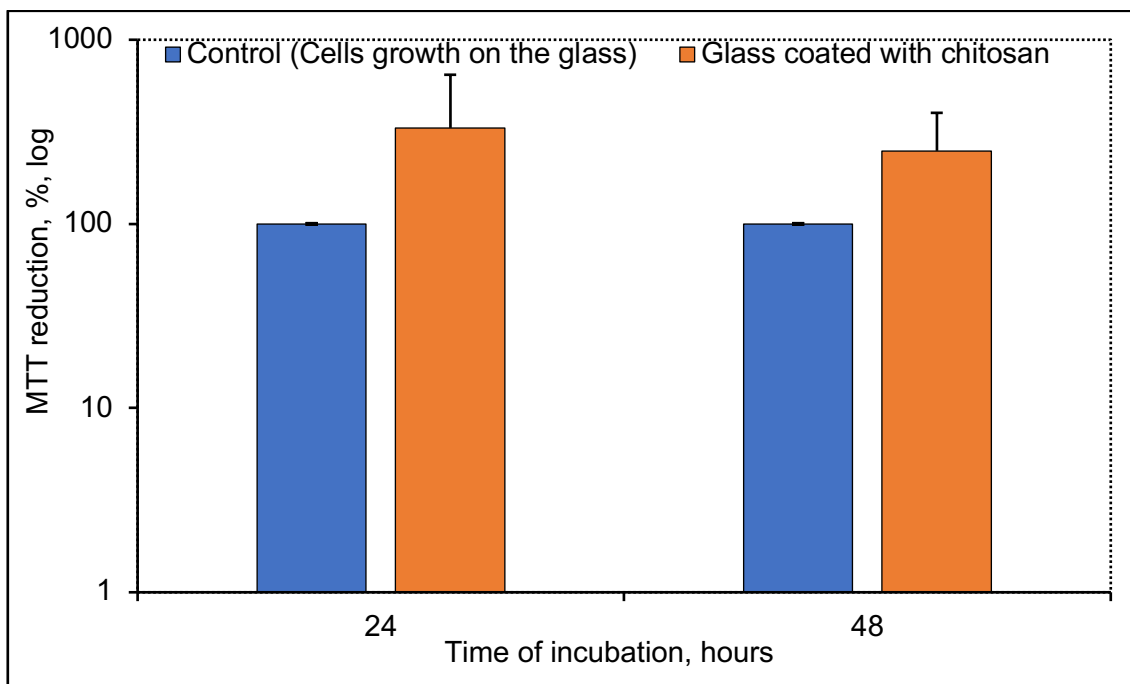


Figure 107. The effect of chitosan coated coverslips on MTT reduction in 3t3 cells. The cover slips were coated with 0.5 wt.% of WA chitosan solution and dried by UV-Ozone. Cells were seeded on the top of each cover glass, covered with medium and incubated for 24 and 48 hours at 37°C. Data shown represent the mean of two independent experiments of MTT assay with error bars of standard deviation.

5.1.2. *In situ* synthesis of BC-CH using chitosan as the main carbon source

Another method of synthesis *in situ* of BC was based on the complete replacement of the main carbon source. Glucose was replaced with 0.5 wt.% of WA chitosan solution, which was prepared using 10 vol.% distilled vinegar. *G. xylinus* was incubated in the modified medium for 48 hours at 30°C. The synthesised material is a completely new type of material and temporarily named as “bacterial chitosan” (BC-CH) before the chemical structure of the material is understood. The synthesis of BC-CH started with an investigation of pH on BC-CH growth. Then, BC-CH was characterised using UV-VIS-NIR, FT-IR and X-ray spectroscopy. The antibacterial activity of the material was investigated against MRSA and *E. coli*.

5.1.2.1. Effect of pH on the synthesis of BC-CH

As chitosan must be dissolved in an acidic environment, the modified medium was adjusted from pH6 to 2 using either 0.1M of sodium hydroxide in order to increase the pH or 0.1M of hydrochloric acid for decreasing the pH, as described in Section 2.5.2.1. Fig. 108 shows the images of the synthesised and treated BC-CH after 48 hours of incubation at different pH values from 6 to 4.



BC-CH produced at pH6 BC-CH produced at pH5 BC-CH produced at pH4

Figure 108. Photographs of BC-CH growth at pH6, 5 and 4 on a large scale. There was no BC-CH growth at pH 3 and 2.

Bacteria did not produce any BC-CH at pH3 and pH2. As shown in Fig. 108, the greater yield of BC-CH was obtained at pH5, which is the standard for the synthesis of BC. The material produced at pH4 was weaker than others. BC-CH synthesised at pH6 had a relatively high yield, but was not robust for further treatments.

Fig. 109 shows the mass yield of wet BC-CH produced at pH4-6 and centrifuged. The greater BC-CH yield was obtained at pH5 and reached 3.7 grams, whereas BC-CH produced at pH6 and pH4 was 3.5 grams and 1.5 grams, respectively.

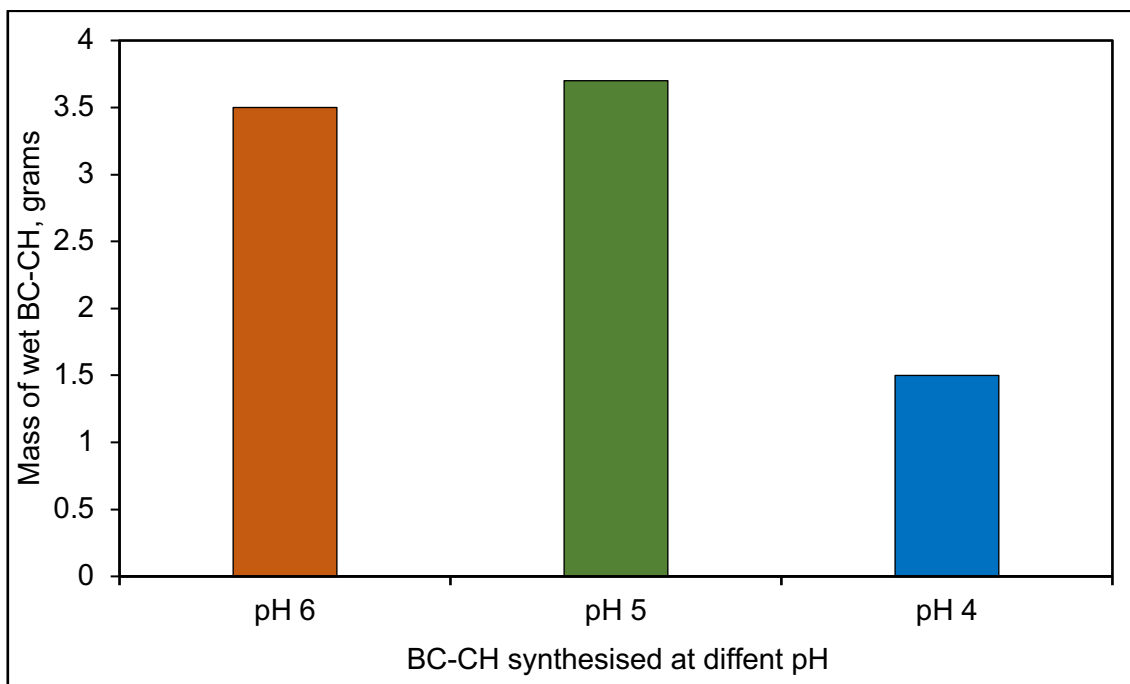


Figure 109. The mass of wet BC-CH produced *in situ*. BC-CH was produced with 0.5 wt.% WA MW chitosan as the main carbon source using approximately 7.9×10^7 CFU/ml bacterial concentration for 48 hours at 30°C in a large scale. Data shown represent the mean of a single experiment.

5.1.3. Understanding the structure of BC-CH

The characterisation of BC-CH started with the morphology of the synthesised BC-CH using SEM. As seen in Fig. 110, BC-CH showed a porous structure with randomly and ununiformly oriented fibres compare to BC. The size of the pores varied within the matrix.

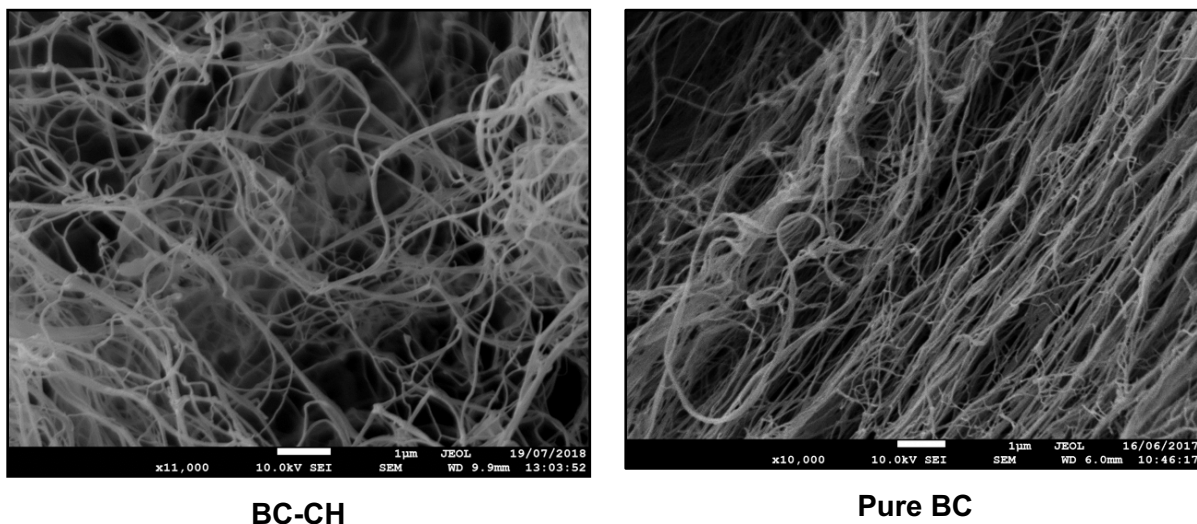


Figure 110. SEM micrograph of BC-CH (left image) and pure BC (right image). The bars represent a distance in 1 μm.

5.1.4. Solubility of BC-CH

Due to the fact that chitosan is soluble in acidic environments, the solubility of BC-CH was investigated. In order to study the solubility of the material, 3 grams of BC-CH were placed in 20 ml of pure vinegar at pH2 for 48 hours as described in Section 2.5.3. Fig. 111 shows the blue centrifuge tube with BC-CH inside the vinegar after 48 hours. As shown in Fig. 111, BC-CH visually remained the same structure.



Figure 111. The centrifuge tube containing 3 grams of BC-CH inside the pure vinegar at pH2 after 48 hours.

The vinegar liquid from the tube was then analysed by using UV-VIS for the presence of any chitosan that might possibly leach and dissolve from BC-CH after 48 hours (Fig. 112). If chitosan leaches and dissolves in vinegar, UV-VIS can detect the presence of it. As shown in Fig. 112, the washing vinegar, which was vinegar that contained BC-CH for 48 hours, did not show the characteristic peak of chitosan. This means that BC-CH not only did not leach, but also cannot be dissolved in acid.

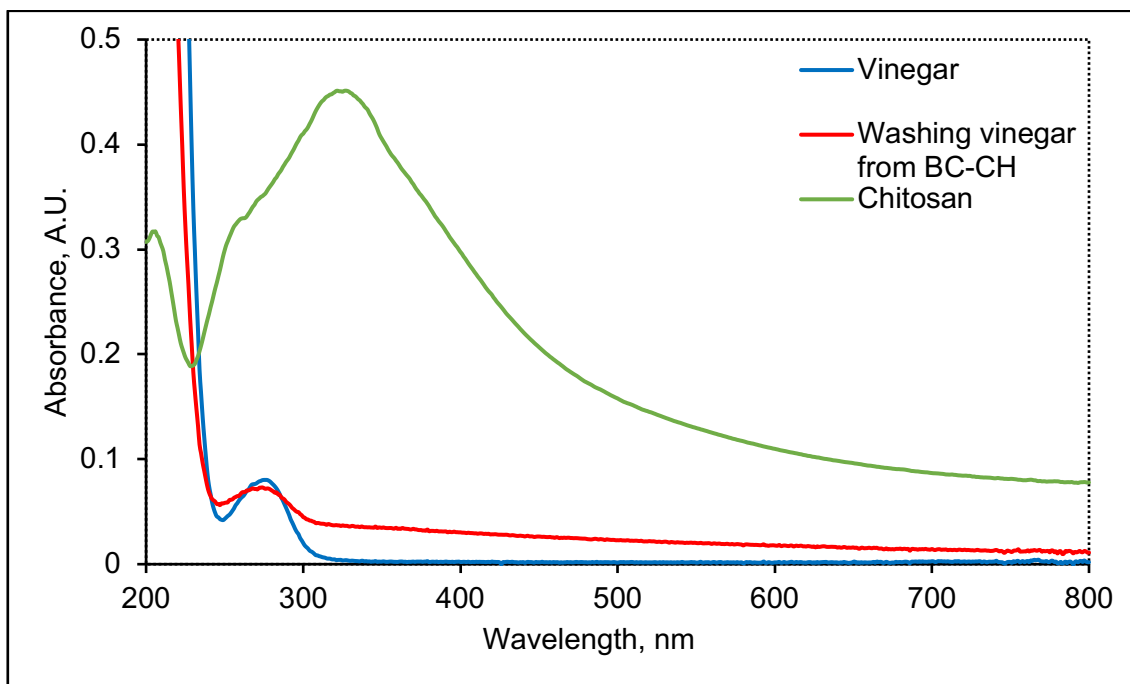


Figure 112. UV-VIS spectra of washing vinegar liquid, which contained BC-CH for 48 hours, chitosan and pure vinegar.

5.1.5. UV-VIS-NIR analysis of BC-CH

Synthesised BC-CH was compared to pure BC and chitosan powder using UV-VIS-NIR spectroscopy (Fig. 113). According to Fig. 113, chitosan powder, pure BC and BC-CH had peaks of 211, 216 and 220 nm, respectively. The characteristic peak of chitosan at 325 nm^[275] was slightly detectable inside BC-CH. Furthermore, BC-CH and chitosan shared the similar peaks of 1437 nm in NIR region. This might be evidence of the presence of NH₂ inside the BC-CH^[275]. In addition, the peak at around 2000 nm seems to be larger in the composite than inside pure BC.

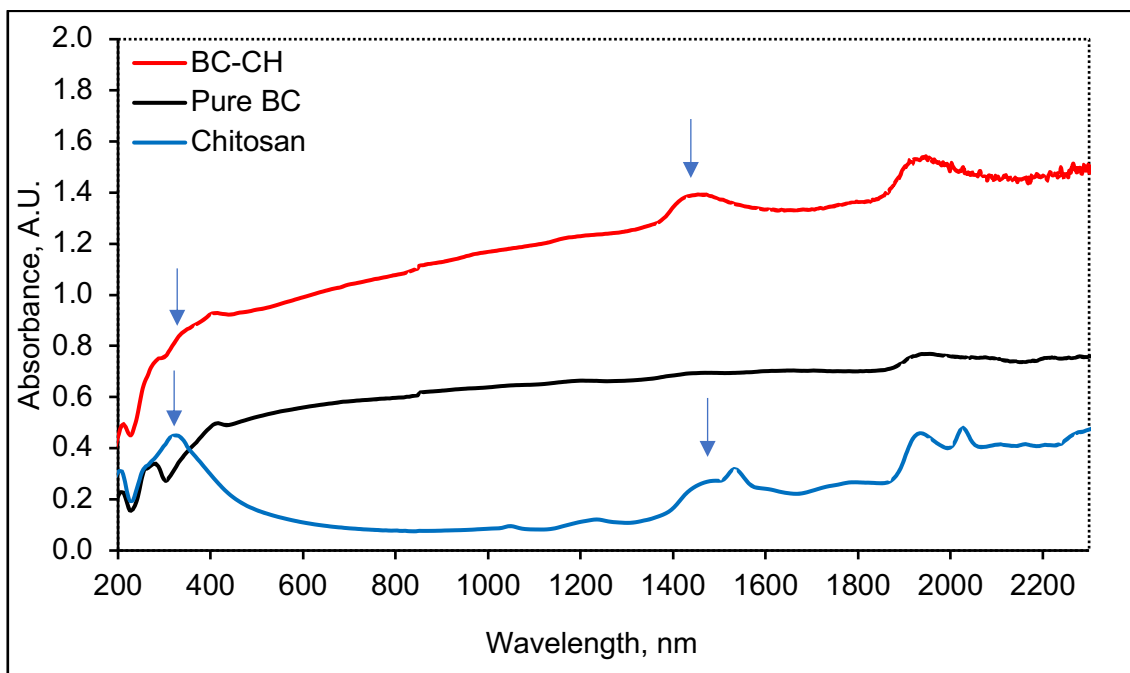


Figure 113. UV-VIS-NIR spectra of chitosan powder, pure BC and BC-CH. Arrows indicate characteristic peaks of chitosan.

5.1.6. Analysis of BC-CH using FT-IR

The structure of BC-CH was studied using infrared (IR) spectroscopy. According to Fig. 114, BC-CH had predominantly cellulose peaks. The peak at 1158 cm^{-1} is due to C-O-C stretching vibrations in pure BC matrix^[276]. The peak of 1643 cm^{-1} , which is corresponded to the glucose carbonyl, was similar to both BC-CH and pure BC. Chitosan had the peaks of around 1531 cm^{-1} , which showed N-H bending vibration of protonated amine groups^[277], 1640 cm^{-1} corresponded to C-O bending of the acetyl group^[275] and 3270 cm^{-1} that is corresponded to N-H stretch could be seen in BC-CH. The peaks of 2921 cm^{-1} and 2867 cm^{-1} are due to the C-H stretching in chitosan^[275]. Moreover, peaks at 1580 cm^{-1} and 1425 cm^{-1} are associated with stretching vibrations of CH and CH₂, respectively^[276].

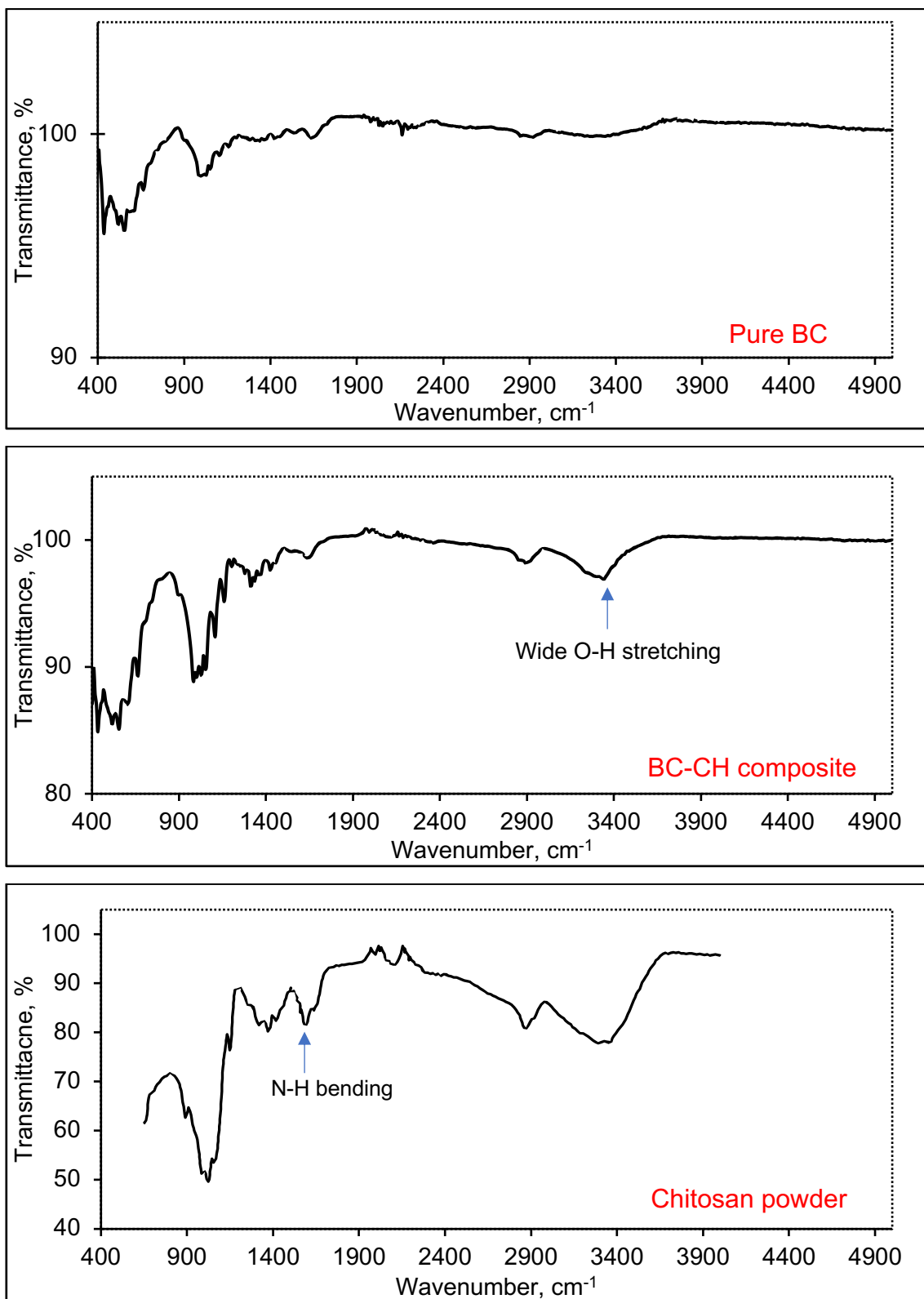


Figure 114. IR spectra of chitosan, pure BC and BC-CH using FT-IR spectroscopy.

The peak of 3350 cm^{-1} of BC-CH was similar to both BC and chitosan indicated O—H stretching^[276]. The widening of O-H stretching could be due to overlapping the N-H stretching $3500\text{-}3000\text{ cm}^{-1}$ of chitosan and O-H stretching vibration of cellulose^[180]. As BC-CH had predominantly the structure of BC, the peaks of chitosan could be overlap with the peaks of cellulose, and, therefore, were hardly detectable. However, due to the presence of two characteristic peaks of chitosan inside the composite, it might be possible to confirm the presence of chitosan inside BC-CH. However, the resolution of attenuated total reflection (ATR) FTIR might not give enough resolving powder to distinguish the difference in structure.

5.1.7. X-ray diffraction analysis of BC-CH

The XRD patterns of BC-CH, pure BC and chitosan are shown in Fig. 115. The purpose of X-ray was to investigate the crystalline structure of BC-CH. As shown in Fig. 115, synthesised BC-CH had two peaks at a 2θ angle of 14° and 22° corresponded to crystalline plane 110 and 002, respectively. These peaks of BC-CH were similar to pure BC indicating that BC-CH was cellulose type Ia^[113, 278]. The difference between BC-CH and pure BC peaks was the intensity. The intensity for BC-CH was higher with first peak being at 64 and the second at 86, respectively, whereas the intensity of the first and second peaks of pure BC was 34 and 55 counts, respectively.

Chitosan had two peaks at 10° and 20° , which correspond to the crystallographic planes (002) and (101), respectively. These data were in agreement with the results of other work^[279]. These peaks were not detected in BC-CH. This means that the presence of chitosan has not affected the crystalline morphology of BC.

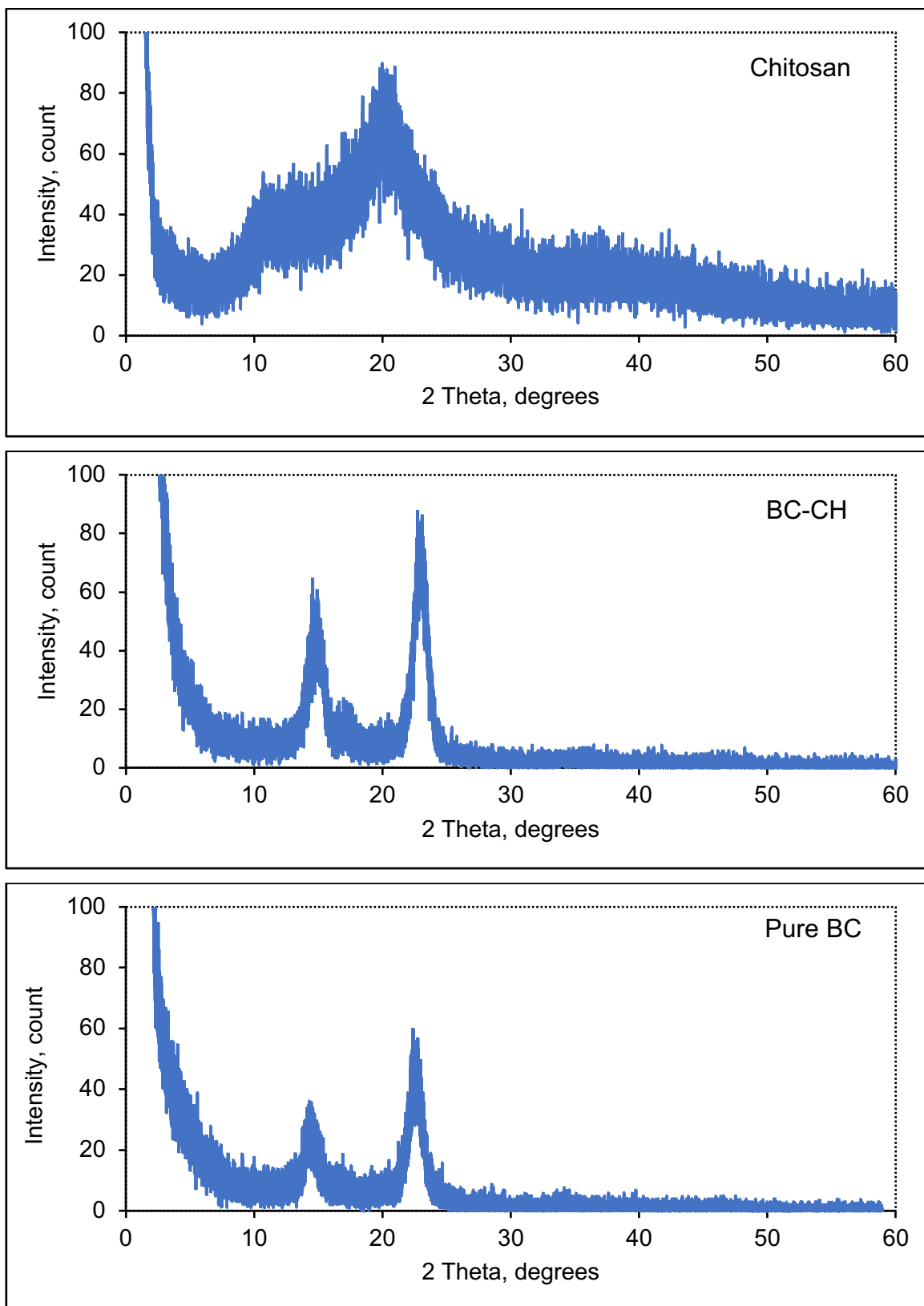


Figure 115. XRD patterns of chitosan, pure BC and BC-CH.

5.1.8. Antibacterial activity of BC-CH

Antibacterial activity of BC-CH was investigated against both MRSA and *E. coli*. As shown in Fig. 116, BC-CH showed significant antibacterial behaviour against MRSA and reduced the growth of the bacteria to 0.0003% of control values. BC-CH reduced the control values of *E. coli* to 1.7% (Fig. 117).

According to Figs. 101-102 and 116-117, BC-CH was more effective against both MRSA and *E. coli* than pure chitosan, which reduced the percent of the control values of MRSA and *E. coli* to 1.7% and 4% of control values, respectively. It may further indicate a new material has been formed that is different from both BC and chitosan.

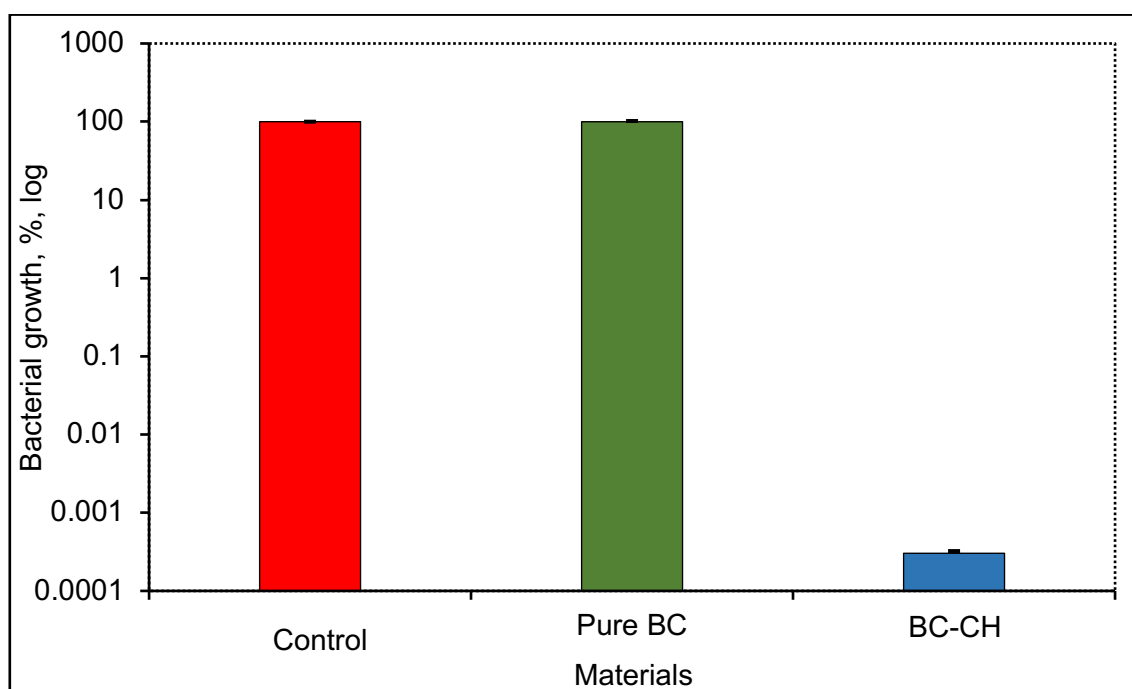


Figure 116. Antibacterial properties of BC-CH composite against MRSA. The bacteria were incubated for 24 hours at 37°C. The control was PBS-resuspended MRSA placed on the surface of the empty petri dish without agar and covered with a lid. Data shown represent the mean of two independent experiments with error bars of standard deviation.

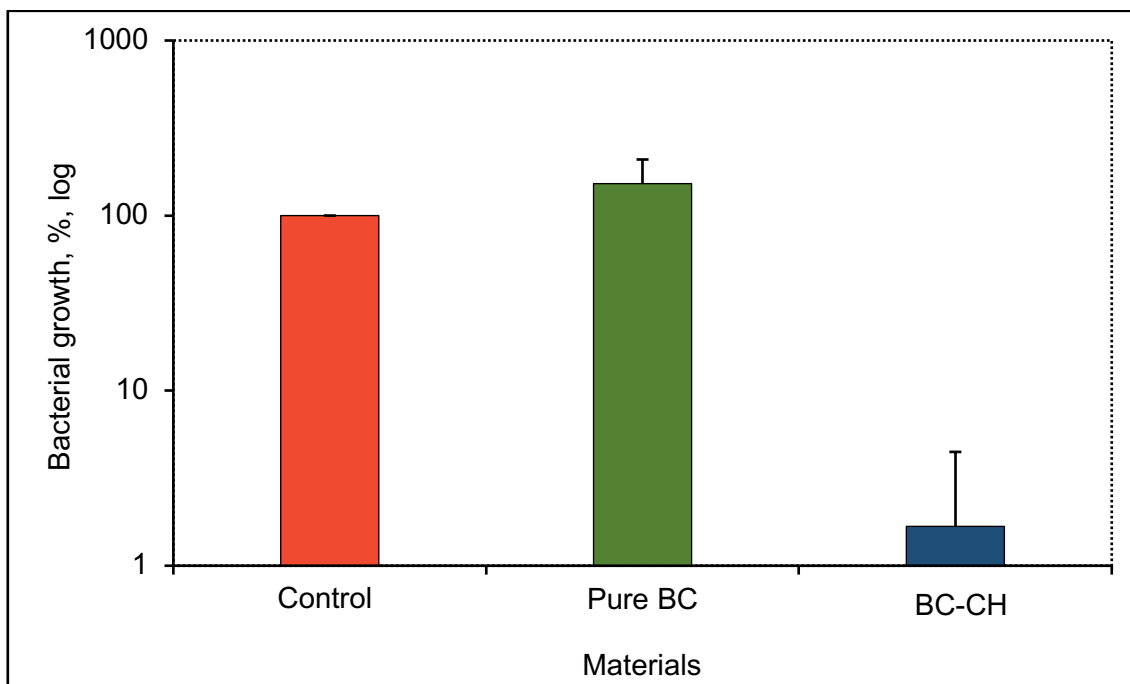


Figure 117. Antibacterial properties of BC-CH composite against *E. coli*. The bacteria were incubated for 24 hours at 37°C. The control was PBS-resuspended *E. coli* placed on the surface of the empty petri dish and covered with a lid. Data shown represent the mean of two independent experiments with error bars of standard deviation.

5.2. Discussion

It was possible to incorporate chitosan into BC through synthesis *in situ*. The novel BC-CH was synthesised by replacing glucose with chitosan in HS medium. UV-VIS-NIR and FT-IR analysis indicated the presence of chitosan inside BC-CH. Furthermore, BC-CH expressed strong antibacterial activity against both MRSA and *E. coli*, which was further evidence for the presence of chitosan inside BC-CH. However, X-ray diffraction showed the unchanged crystalline structure of the cellulose of BC-CH. There are two possible reasons behind the results obtained. First, bacteria that consumed chitosan can synthesise original BC, but with the physical attachment of chitosan to BC fibres. Alternatively, the bacteria synthesised BC with chemically attached chitosan. This would make chitosan permanently attached to the structure of cellulose.

5.2.1. Attachment of chitosan to BC

Chitosan could penetrate the pores of BC and, subsequently, interact with fibrils^[180]. The mechanism of attachment of chitosan has been described elsewhere. Both BC and chitosan have the similar structures with β -glycoside linkages^[280]. However, BC has hydroxyl groups, whereas chitosan has primary amine groups at the C2 position^[280]. Chitosan and BC might interact by hydrogen bonds that are formed between the functional groups. The intramolecular hydrogen bonds could be formed between the chemical groups in chitosan (-OH and NH₂) and BC (-OH). This may lead to restricting motions of the matrix and promote rigidity. It has been reported elsewhere that the intramolecular hydrogen bonds in BC could break down in order to form hydrogen bonding between BC and chitosan^[138, 140]. Therefore, the widening of -OH stretching, which was observed inside BC-CH could be evidence for the presence of chitosan in BC. Furthermore, chitosan could coat fibres of BC and, in this case, subsequently leach. BC/chitosan composite produced using both glucose and chitosan as carbon sources showed a leaching behaviour. This means that the attachment of chitosan to BC might not be permanent. In contrast, BC-CH did not exhibit leaching of chitosan even in vinegar. Therefore, BC-CH could not be dissolved in acid.

5.2.2. The dependence of microbial growth on medium

Microbial growth is referred to an increase in the number of cells. The microbial growth depends on factors such as temperature, pH, oxygen and the composition of the medium. Microbial growth undergoes several phases. Firstly, the lag phase can be characterised as a period of adjustment of cells to new conditions with little or no increase in population^[281]. The next phase of growth is a logarithmic (log) phase, where cells begin to divide followed by a period of rapid growth, where the number of cells produced is higher than the number of cells that die^[281]. The third phase is the stationary phase, during which a population of cells begins to stabilise, the cell number does not increase, and cell division starts to slow

down. The last phase is the decline or death phase. The “growth curves” have the following shape: no growth is detected at the lag phase followed by exponential growth, then the growth slows down and ends with a period of no net growth, which is the stationary phase^[282]. Slow bacterial growth can be due to poor nutrients present in medium. As a result, cells do not achieve the metabolic state that is necessary to allow exponential growth^[282]. Starvation of bacteria could result in a decrease in the size of the cells, which appear almost spherical. Such a reduction might improve the survival of cells^[282]. A condensation of cytoplasm could occur followed by an increase in the volume of periplasm as well as deposition and changes to subcellular compartments. In order to generate agglomeration, the membrane might become less permeable and more hydrophobic^[282].

The lag phase represents the beginning of the growth curve, where an inoculum is added to a fresh medium. During this phase, cells are metabolically active and synthesise proteins that are needed for cells to grow within a medium. The duration of this phase is determined by many factors including composition of the medium. There are different types of medium, which can serve a variety of purposes. The culture medium is a nutrient material that is prepared for microbial growth. Some media such as tryptic soy broth (TSB) is considered all-purpose media and can support a growth of a large variety of microorganisms including *S. aureus*, *E. coli* and *P. aeruginosa*^[283]. Bacterial growth is a process that includes a number of anabolic, for instance, synthesis of cell metabolites and constitutes as well as catabolic, which is breaking down cell constitutes and metabolites, reactions^[283]. These reactions result in a cell division. The log phase occurs when the cells are dividing actively by binary fission, thus, the number of cells increases exponentially^[283]. The bacterial growth refers to a large population of cells ($\geq 10^7$)^[283].

G. xylinus is a strictly aerobic, catalase-positive and oxidase-negative Gram-negative bacterium^[284]. HS medium is the optimal growth medium for *G. xylinus*. In order to grow, bacteria need a minimum of nutrients including water, carbon

source, nitrogen source and minerals^[285, 286]. Water plays a crucial role in hydrolysis reactions, transporting and solubilising nutrients^[285]. Carbon is essential for bacteria to produce carbon molecules such as carbohydrates, fats or organic sources such as alcohols and sugars^[285]. Nitrogen source is used by bacteria in the synthesis of their proteins^[285]. Phosphorus is required for nucleic acid, synthesis of phospholipids and ATP, whereas sulphur is crucial for amino acids and vitamins^[285]. Micronutrients such as K^+ , Mg^{2+} , Fe^{2+} and Ca^+ are needed for enzymes, to stabilise membrane, ribosomes and electron transport systems. However, the minimal medium cannot be enough for the growth of bacteria that need specific elements^[285]. Therefore, a medium may be supplied with additional elements. Thereby, enrichment medium is a medium for a growth of desired microorganisms in an inoculum. Growth factors, which are the elements that bacteria are unable to synthesise using just minimal medium, could be added to such an enrichment medium. For instance, purine and pyrimidine bases are necessary for nucleic acids, amino acids and synthesis of proteins and vitamins. There is also another type of medium, which is a selective medium that is used to grow specific bacteria from an inoculum. This medium can contain a variety of antibiotics, antiseptics, ethanol, etc^[285].

G. xylinus is a mesophilic organism with an optimum temperature for growth being 30°C and pH5-6.5, but the bacterium might grow at a lower pH^[284]. In the presence of oxygen, *G. xylinus* can oxidise sugars, alcohols, aldehydes or sugar alcohols by primary dehydrogenases that are located on the outer surface of the cytoplasmic membrane^[284]. Glucose is a preferred carbon source for the growth of *G. xylinus*^[287]. The effect of different carbon sources such as sucrose, glucose, fructose, lactose, xylose and glycerol on a growth of *G. xylinus* has been evaluated elsewhere. It has been reported that BC synthesised in the standard HS medium containing glucose can reach a concentration of 4.1 g/l, whereas the concentration of BC produced in a sucrose-based HS medium was 4.9 g/l^[286]. It has been found that lactose and xylose were not efficiently metabolised by *G. xylinus* resulted in low BC production with concentrations of 1.7 g/l and 1.6 g/l,

respectively^[286]. *G. xylinus* could oxidise xylose to *d*-xylonic acid, but this led to the accumulation of xylonate in the medium followed by lowering the pH that could subsequently inhibit the growth of bacteria and, therefore, BC production. Furthermore, *G. xylinus* does not have the gene that encodes the β -galactosidase enzyme, which is responsible for hydrolysis of lactose^[286]. It has been reported that BC produced in a fructose-based HS medium showed the highest concentration of BC of 5.65 g/l^[286]. Glycerol can also be used for the growth of *G. xylinus*, but the concentration of BC decreased to 3.4 g/L^[286].

As a result, products of oxidation could accumulate in the medium. There are two main phases of oxidation by *G. xylinus*. Firstly, *G. xylinus* can oxidise ethanol to acetic acid by two sequential catalytic reactions. Ethanol is oxidised to acetaldehyde, which is then catalysed by membrane-bound pyrroloquinoline quinone, and which depends on alcohol dehydrogenase (ADH)^[284]. The acetaldehyde is then oxidised to acetate by membrane-bound aldehyde dehydrogenase (ALDH), which is located near ADH^[284]. Both ALDH and ADH form a multienzyme complex in the bacterial cell wall with the function to produce acetic acid from ethanol. The acetic acid then released into the growth medium to a maximum of 10-20%^[284]. An exhaustion of acetate may be observed after this phase. This means that the medium needs to be supplemented with acetate for further growth of the bacteria. *G. xylinus* could be resistant to acetic acid due to the presence of specific proteins, which associate the protons and conjugate a base of the dissociated acid, which renders it in the undissociated form and, thus, decreases toxicity level^[284]. Therefore, the bacteria are able to adjust to the acidic condition of the medium. Furthermore, it has been found that a crystallite size of BC produced in the presence of acetic acid is lower than of BC produced in the original HS medium containing citric acid^[287]. The second phase is an assimilation of sugars^[288]. It has been reported that an increase in pH could be an indicator that the amount of glucose depletes. This could be accompanied by a major augmentation of the yield of BC in the medium^[289].

G. xylinus cells are able to form cellulose with acetate, but in the presence of sugars. The acid did not affect the sugar consumptions^[287]. It has been reported that the yield of BC produced without glucose, but with acetate decreased from 0.2 mg to 0.1 mg^[287]. It has been stated that HS medium containing acetic acid instead of the glucose showed a slight decrease in pH within first 10 hours of incubation^[287]. The results reported elsewhere stated that bacteria were able to grow without glucose by using other carbon sources such as citric acid, amino acids and vitamins that come from yeast extract and peptone^[287]. The growth of BC does not start immediately after the incubation of cells, because, at the beginning, bacteria may colonise the surface and start to change the physical properties of the air-broth interface. A primary cellulosic biofilm starts to appear at the air-broth interface by clustering biomass, fibrils of BC and other bioproducts at an early stage of incubation^[287].

Based on the above comments, a possible reason why pH5 was the best condition for the synthesis of BC-CH might be the nature of the acetic acid bacteria. *G. xylinus* needs acidic conditions for the growth and synthesis of cellulose, which it creates during the cultivation. During the cultivation and synthesis of BC, the bacteria secrete gluconic acid and 5-keto-gluconic acid, which results in a decrease in pH^[231]. However, an excessive amount of acidity could inhibit the growth of bacteria. Thus, the inoculation of the bacteria at pH3 or pH2, which then decreases during the cultivation, could lead to bacterial cell death. In addition, a decrease in pH during the cultivation might be beneficial due to the solubility of chitosan in an acidic environment (Section 1.4.2.1). As a consequence, the growth of BC-CH might be due to the presence of acetic acid in vinegar, to the composition of HS medium and/or to consumption of chitosan as a carbon source by the bacteria. Further investigation of the mechanism of production of BC-CH is needed.

5.2.3. Antibacterial activity of chitosan

BC-CH could inhibit the growth of Gram-positive MRSA and Gram-negative *E. coli*. The difference in antibacterial activity against Gram-positive and Gram-negative bacteria could be due to the different structures of the cell walls as described in Section 1.2.3.1.

The exact mechanism of chitosan as an antimicrobial agent is not well understood, although different hypotheses have been proposed^[152]. The proposed mechanisms of the antibacterial action of chitosan are described in Section 1.4.3.1. The most accepted theory is based on a mechanism involving electrostatic interaction between positively charged chitosan and negatively charged bacterial cell walls. The structure of Gram-positive bacteria carries a large net negative charge due to phosphate groups in teichoic acids, whereas LPS are negatively charged in the outer membrane of Gram-negative bacteria^[43]. The electrostatic interaction between chitosan and the bacterial cell wall could lead to either changes in the permeability of the bacterial cell wall followed by internal osmosis imbalance or hydrolysis of the peptidoglycan in walls, which could then lead to the leakage of intracellular components^[131].

Chitosan becomes soluble in an acidic aqueous environment, where the high cationic nature of the amine group is protonated and, therefore, is positively charged. This means that the $-NH_2$ groups are converted to a soluble protonated form $-NH_3^+$ ^[46]. The interaction of positively charged amine groups of chitosan and negatively charged teichoic acids of MRSA might result in the leakage of intracellular constituents^[132, 153, 154]. Furthermore, an imbalance in osmosis could be one reason behind the reduction of the growth of MRSA^[131]. Another reason might be the ability of chitosan to form a layer over a bacterial cell wall that may subsequently affect the absorption of nutrients^[132]. Moreover, cell walls of Gram-negative bacteria consist of LPS, phospholipids and lipoproteins that are connected by electrostatic interactions with divalent cations, which are required

to stabilise the outer membrane^[53]. Amine groups could bind to the negatively charged O-specific oligosaccharide units of LPS and, thus, disturbing the integrity of the outer membrane^[53]. A permeability barrier of the outer membrane of *E. coli* is formed by cross-bridging of lipid A molecules and divalent cations (calcium or/and magnesium). Amine groups could also bind either to lipid A or divalent cations^[53].

BC-CH showed stronger antibacterial activity against MRSA than *E. coli*. This might be due to the additional outer cell wall of Gram-negative bacteria. Chitosan may not cross the outer membrane of Gram-negative bacteria, but could affect *E. coli* externally^[168]. *P. aeruginosa* showed high resistance to the BC/chitosan composite. This might be due to the stronger outer membrane of this bacterium, which has porins different from *E. coli*.

5.2.4. Mammalian cytotoxicity of chitosan

Chitosan increased the level of MTT reduction compared to control values in 3t3 cells after 24, 48 and 72 hours. The increase in MTT reduction suggests that chitosan may increase the metabolic activity of 3t3 cells. This might be due to decomposition and release of N-acetyl- β -D-glucosamine from chitosan, which has been found to also increase the proliferation of fibroblasts^[290].

The effect of chitosan powder was evaluated. However, the main issue with this method was the insolubility of chitosan at neutral pH. The pH of the tissue culture medium was pH7. This means that chitosan might not be dissolved in the medium and, therefore, the interaction of chitosan with the cells could not occur. In order to overcome this issue, another method for evaluation of cytotoxicity of chitosan was proposed (Section 2.12.5.2). The results from the experiment which was based on using glass cover slips coated with 0.5 wt.% chitosan also suggests that chitosan increased the levels of MTT reduction in 3t3 cells.

The cytotoxicity of BC/chitosan composites has also been investigated elsewhere. The cytotoxicity of the BC/0.6 wt.% chitosan composites, which were synthesised by the immersion method, were analysed using mouse skin fibroblast cells (L929) in the presence of DMEM medium containing 10% FBS^[180]. It was reported that BC/chitosan composites did not affect the cell viability^[180]. It has been shown that the adhesion and spreading of fibroblasts cells on a BC/chitosan composite was better than on pure BC^[181]. Furthermore, the attachment of 3t3 cells to the fibres of both pure BC and BC/chitosan composite, which was produced by immersion of BC into 1 wt.% chitosan solution followed by seeding the cells on the surface of the composite in DMEM for 48 hours has been investigated elsewhere^[183]. The results of that study have shown that the cells attached to BC/chitosan proliferated and spread almost completely over the surface, whereas 3t3 cells remained round-shaped inside the matrix of pure BC^[183]. This might be due to better biocompatibility of BC/chitosan composite than pure BC. Therefore, BC-CH could be an ideal material for biomedical applications due to lack of cytotoxicity, strong antibacterial activity and cheaper synthesis compared to the pure BC.

Chapter 6. *Ex situ* integration of chitosan into BC matrix

Widely available (WA) (161 kDa, 90% DDA), low (50-190 kDa, 75-85%DDA) and medium (200-800 kDa, 75-85%DDA) molecular weight (MW) chitosan at a concentration of 0.5 wt.% was incorporated *ex situ* into non-oxidised (non-ox) BC and oxidised BC (ox BC), which was obtained by using sodium metaperiodate as described in Section 2.6.1. The incorporation *ex situ* of chitosan into BC was carried out through immersion and vacuum self-assembly methods. The immersion was based on placing pure oxidised and non-oxidised BC into 0.5 wt.% of each of WA, low and medium MW chitosan solutions, respectively, for an hour. Vacuum self-assembly method implied the forced incorporation of chitosan into BC using a vacuum pump. The synthesised BC/chitosan composites were analysed using UV-VIS-NIR and FT-IR. Antibacterial activity of synthesised composites was investigated against MRSA, *E. coli* and *P. aeruginosa*, respectively.

6.1. Results**6.1.1. Comparison of oxidised and non-oxidised BC**

BC was oxidised to dialdehyde cellulose by using sodium periodate. The mechanism of oxidation is described in Section 6.2.1. During the oxidation, aldehyde groups (-CHO) of the oxidised BC were grafted with amine groups of chitosan by a Schiff's base reaction^[291]. At the end of the oxidation reaction, the hydroxyl groups are replaced with aldehyde groups^[292].

The characterisation of the composites started with the comparison of oxidised (ox BC) and non-oxidised (non-ox) BC using UV-VIS-NIR and IR spectroscopies (Figs. 118-120). As shown in Fig. 118, non-ox and ox BC had similar peaks in regions of 203-215, 240-258 and 397-417 nm. However, ox BC showed an additional peak in the UV region at 356 nm wavelength, which was not present in original BC. Both types of BC had a significant peak at 1950 nm and a smaller peak at 2090 nm in NIR region. Ox BC differs from non-ox BC with a sharper

peak at 2096 nm, which suggest that oxidation led to minor differences in structure.

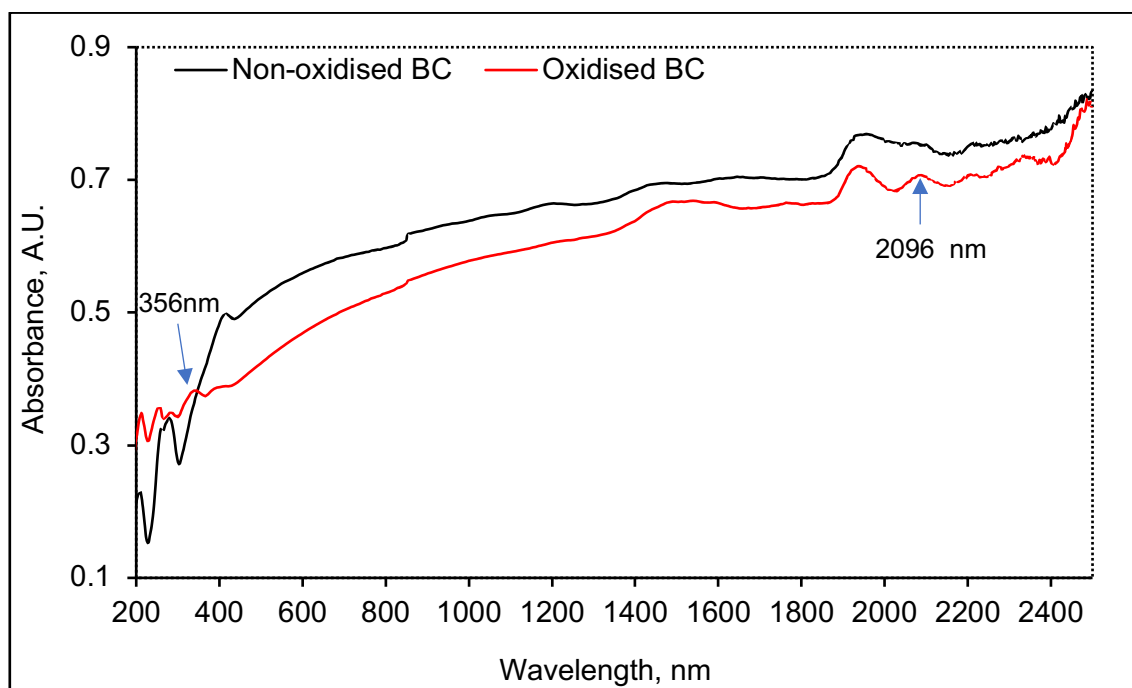


Figure 118. UV-VIS-NIR spectra of non-oxidised and oxidised BC. Arrows indicate additional peaks of ox BC.

FT-IR spectra obtained from non-ox and ox BC are shown in Figs. 119-120. It has been reported that the process of oxidation occurs in the bulk material^[292]. Therefore, the aldehyde groups could be detectable in FT-IR spectrum. It has been stated that a peak, which is corresponding to a symmetrical stretching of C=O bond, can be assigned to the aldehyde group that was inserted in the structure by the periodate oxidation process^[292]. The peak around 1738 cm^{-1} appeared in the oxidised cellulose due to the stretching vibration of C=O double bond of the aldehyde group^[291]. As shown in Figs. 119-120, this peak is much more intense in the spectrum of ox-BC than non-ox BC. This means that BC was successfully oxidised.

Regarding similarities, non-ox and ox BC shared peaks of 915-924, 1146 and 1192-1198 cm^{-1} that indicated the presence of the C-O-C chemical bonding. The peak at around 800 cm^{-1} is corresponded to out-of-plane bending of C-O-H in BC matrix^[276]. The peaks of 1351, 1410-1416 cm^{-1} showed the chemical bonding between carbon and hydrogen (C-H bonding)^[276]. Other peaks at 1086-1093, 1503-1509, 2048 and 3017 cm^{-1} were also present in both types of BC. The broad peaks of 3350 cm^{-1} and around 3400–3500 cm^{-1} indicated O-H stretching.

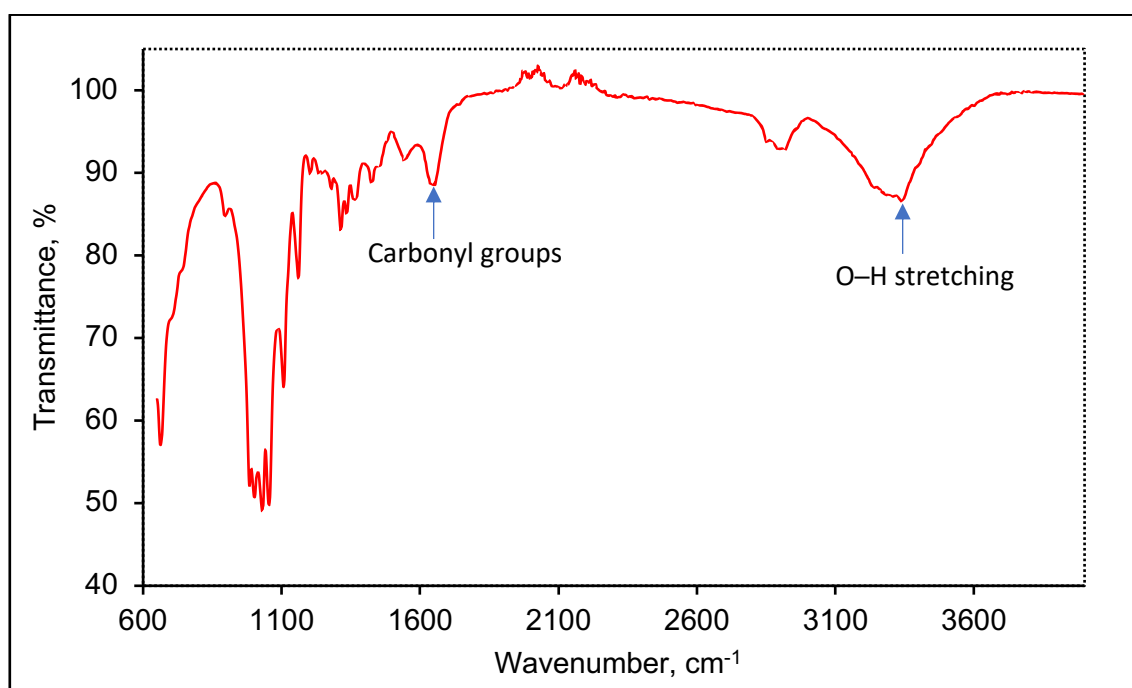


Figure 119. IR spectrum of non-oxidised BC.

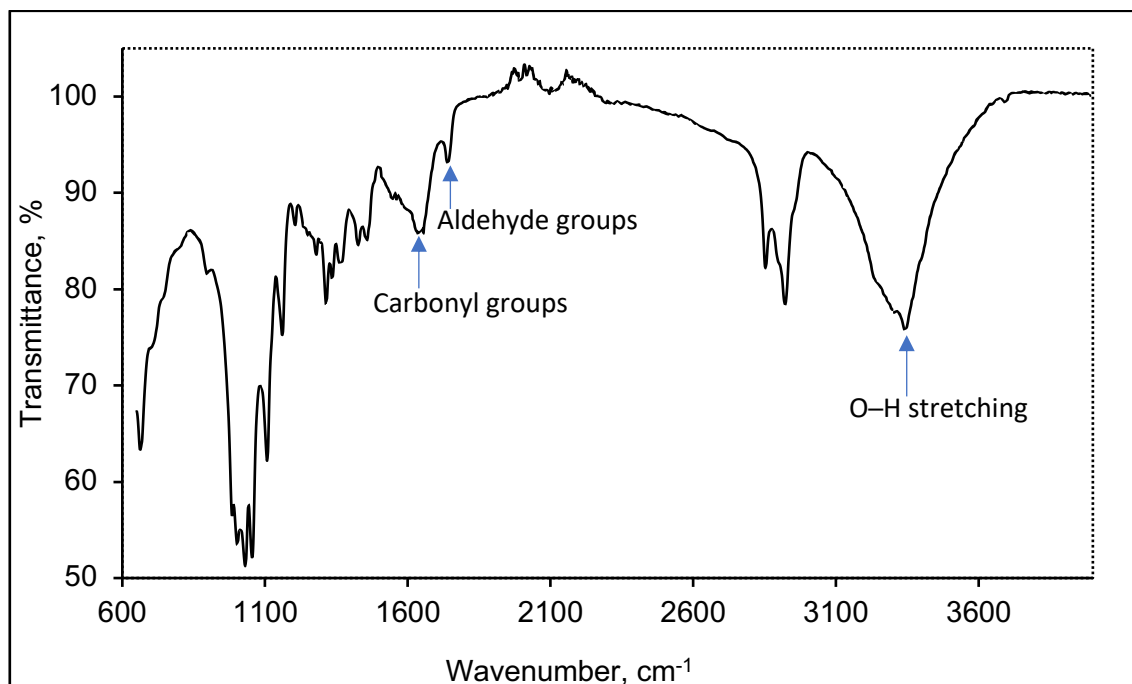


Figure 120. IR spectrum of oxidised BC.

6.1.2. Comparison of different types of chitosan

Once the differences between the two types of BC were observed, three types of chitosan powder were compared (Figs. 121-122). Firstly, chitosan low, medium and WA chitosan powder were analysed using UV-VIS-NIR. Fig. 123 shows that the spectra of the three types of chitosan powders were very similar. Chitosan had a characteristic peak at 325 nm^[275]. The characteristic peak of chitosan in UV region could also be observed inside all three spectra. Chitosan also showed characteristic peaks in a range of 1460-1540 nm in the near IR region due to the presence of NH₂, the other peaks unique to the chitosan powders were at 1953 and 2031 nm^[275]. Therefore, UV-VIS-NIR spectra was similar for WA, low and medium MW chitosan.

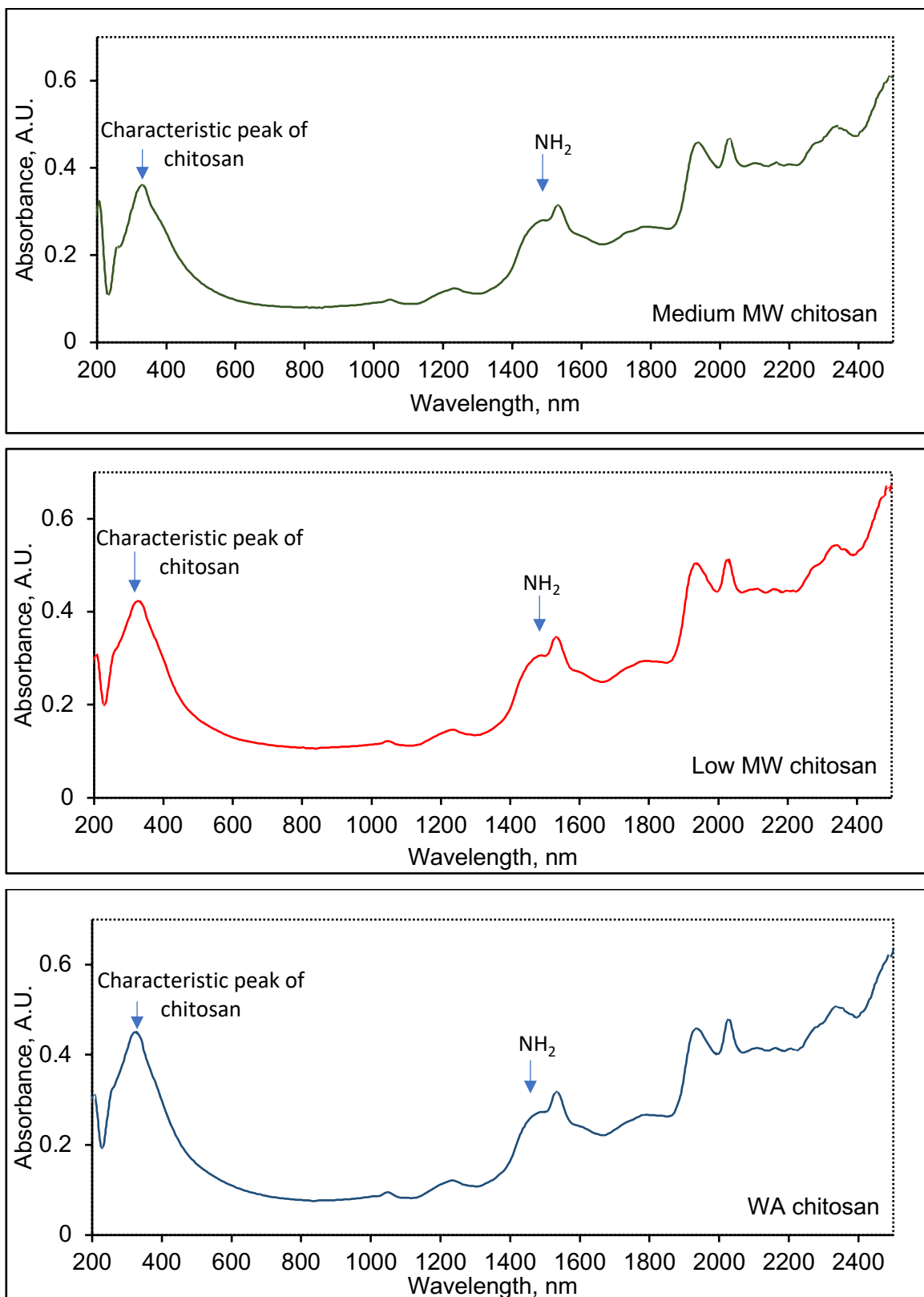


Figure 121. UV-VIS-NIR spectra of WA, low and medium MW chitosan.

Fig. 122 shows IR spectra of WA, low and medium MW chitosan. Three types of chitosan had similar IR spectra. Chitosan had the peaks between 3200 cm^{-1} and 3400 cm^{-1} that indicated N-H stretch. Furthermore, chitosan had the peaks of around 1580 cm^{-1} , which showed N-H bending vibration of protonated amine groups^[277, 293] and 1640 cm^{-1} corresponded to C-O bending of the acetyl group^[275]. The peaks of 2921 cm^{-1} and 2867 cm^{-1} are due to the C-H stretching in chitosan^[275, 276]. The characteristic peaks for chitosan are indicated by arrows in Fig. 122. Further assessment of BC/chitosan composites will be based on identification of these characteristic peaks of chitosan in BC/chitosan composites.

According to the results obtained from UV-VIS-NIR and FT-IR, the three types of chitosan had very similar structure. The main differences between these three types of chitosan were molecular weight and degree of deacetylation (DDA). Molecular weight of WA, low and medium chitosan was 161 kDA, 50-190 kDA and 190-310 kDA, respectively. WA chitosan had the highest degree of deacetylation at 90%, whereas low and medium MW chitosan had DDA at 75-85%.

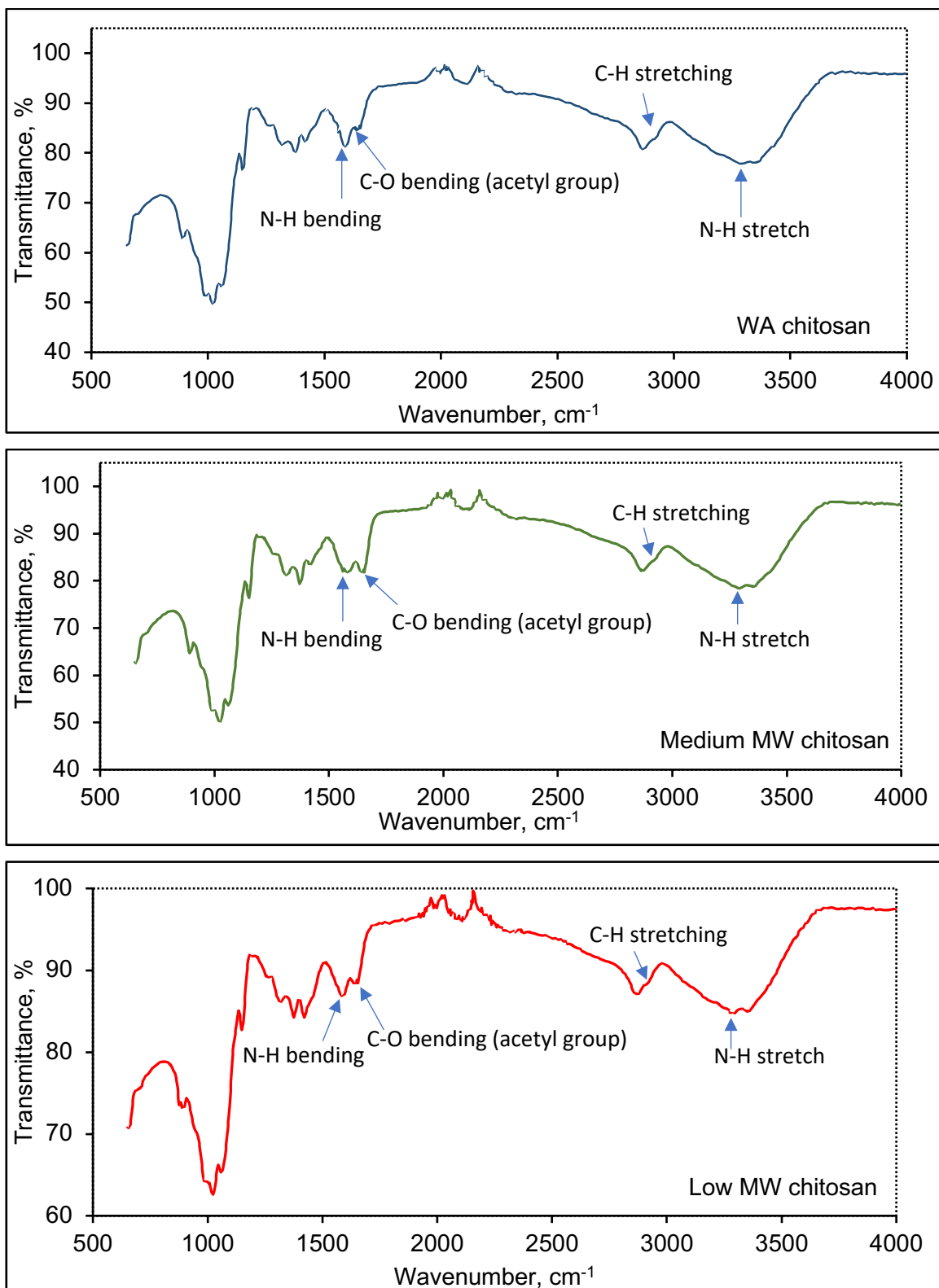


Figure 122. IR spectra of WA, low and medium MW chitosan.

6.1.3. Modification *ex situ* of BC through immersion

The modification of BC was obtained through immersion of non-ox and ox BC into each of 0.5 wt.% solution of WA, low and medium MW chitosan, respectively, for an hour. The materials were either air-dried for 24 hours at 25°C when analysed by UV-VIS-NIR and FT-IR or sterilised using autoclave at 121°C for 15 minutes and were used in the antibacterial assay experiments.

6.1.4. Non-oxidised BC/chitosan composites

Non-ox BC was immersed into 0.5 wt.% of WA, low and medium MW chitosan solutions, respectively, for 30 minutes at 25°C as described in Section 2.6.3.2. After air-drying, each type of synthesised non-ox BC/chitosan composite was firstly analysed by UV-VIS-NIR (Fig. 123). As shown in Fig. 123, the peaks of the composite were similar to pure BC. BC character was predominant in the UV-VIS-NIR spectrum, which might be due to overlapping of chitosan peaks.

The non-ox BC/WA and BC/Medium MW chitosan composites did not show the characteristic peak of chitosan at about 325-340 nm. Whereas BC/Low MW chitosan composite had a small peak around 347 nm. This might be due to the presence of chitosan inside the structure, but not on the surface of BC. Alternatively, chitosan might not be incorporated into BC.

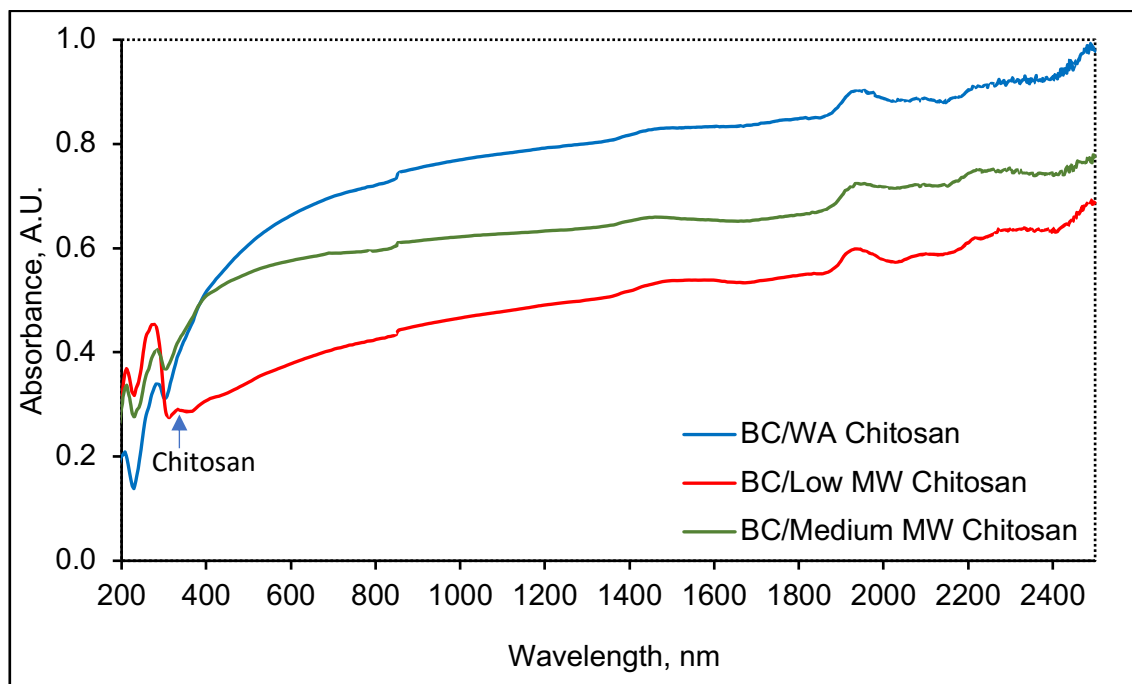


Figure 123. UV-VIS-NIR spectra of non-ox BC/WA, non-ox BC/Low and non-ox BC/Medium MW chitosan composites.

The composites were then compared to both non-ox BC and chitosan powder using FT-IR (Fig. 124). The O-H peak of BC can be seen at 3340 cm^{-1} [276]. The incorporation of chitosan led to broad hydrogen bonding between BC (O-H) and N-H stretching of chitosan [276]. This resulted in a widening of the O-H region in the composite [276]. Therefore, BC/chitosan composites had the wider region with O-H peaks than pure BC. As the composite's spectrum was dominated by BC peaks, chitosan peaks might not be identified. In addition, the characteristic N-H bend at 1580 cm^{-1} and N-H stretch at 3270 cm^{-1} of chitosan were not clearly visible in the spectra of non-ox BC/WA chitosan.

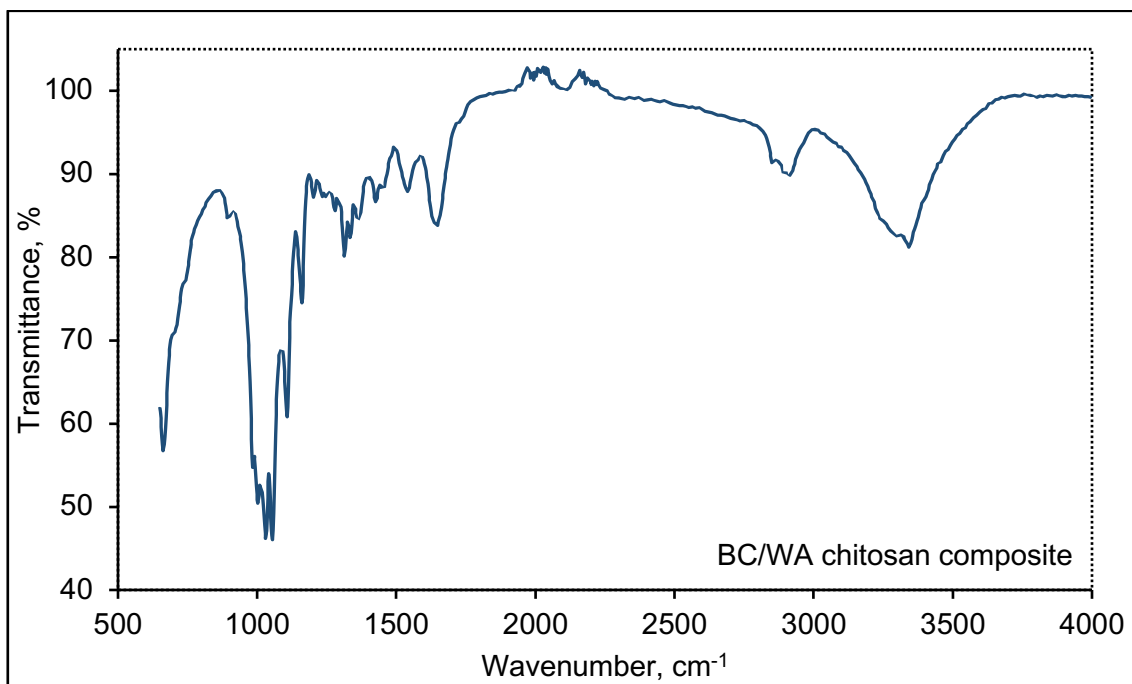


Figure 124. IR spectrum of non-ox BC/WA chitosan composite using FT-IR equipment.

However, non-ox BC/Low MW chitosan and non-ox BC/Medium MW chitosan composite showed the N-H stretch at 3270 cm⁻¹ in IR spectra (Figs. 125-126).

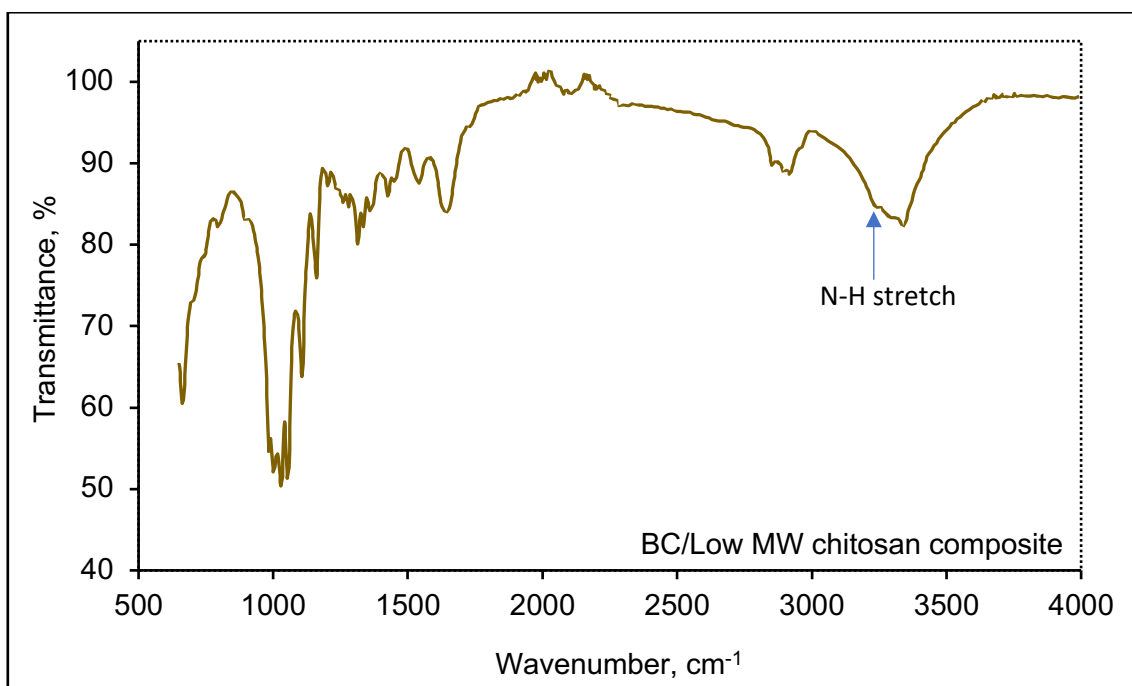


Figure 125. The FT-IR spectrum of non-ox BC/Low MW chitosan composite.

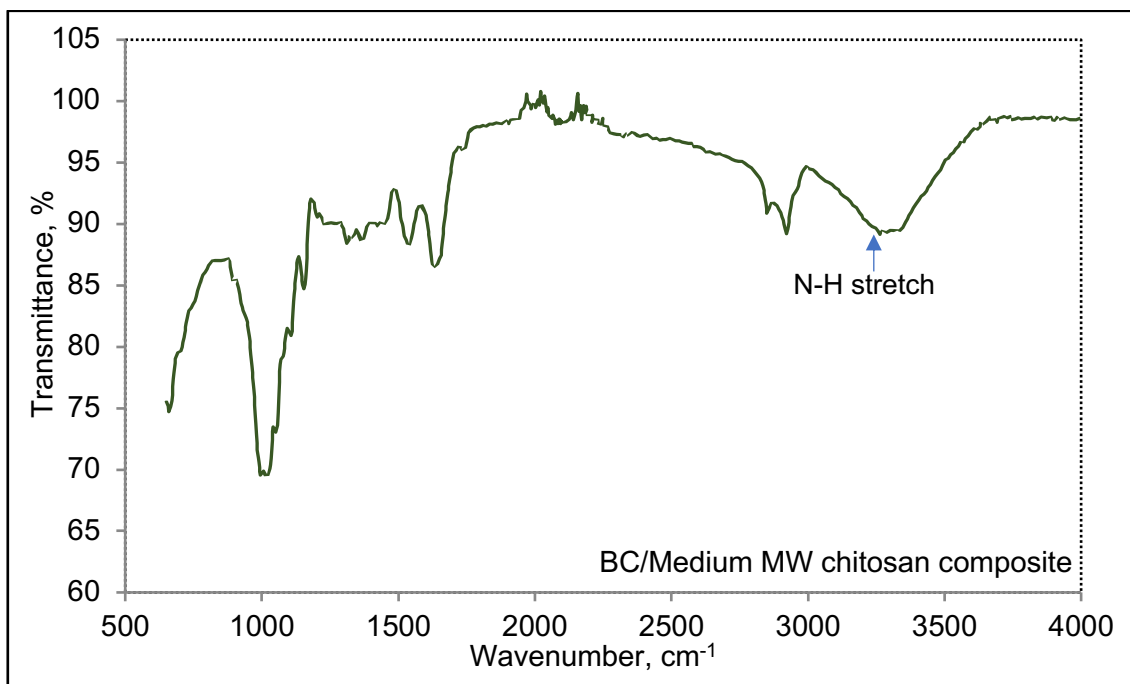


Figure 126. The FT-IR spectrum of non-ox BC/Medium MW chitosan composite.

According to Figs. 124-126, chitosan was either hidden by the predominant peaks of BC or incorporation of chitosan was not achieved. The spectrum of UV-VIS showed the presence of chitosan peak in BC/Low MW chitosan composite, whereas the peaks of chitosan inside other two composites were not detected. The wide region of both O-H and N-H stretching peaks might be due to overlapping these peaks in BC/chitosan composite. It has been stated that the broad peak corresponded to the multiple absorption of hydrogen bonds that could overlap the absorption peaks of the N-H and O-H stretching vibration^[291]. This can lead to moving to the high wavenumber compare to pure BC. The peak indicating N-H stretch was found inside the spectrum of both non-ox BC/Low MW chitosan and non-ox BC/Medium MW chitosan composites.

6.1.5. Ox BC/chitosan composites

Ox BC was immersed into each of 0.5 wt.% solution of WA, low and medium MW chitosan, respectively, for an hour at 25°C. The synthesised ox BC/chitosan composites were compared to both ox BC and chitosan in order to evaluate the attachment of chitosan to BC fibres. The evaluation was carried out using UV-

VIS-NIR and FT-IR spectroscopies. Fig. 127 shows UV-VIS-NIR spectra of ox BC/WA, ox BC/Low and ox BC/Medium MW chitosan composites.

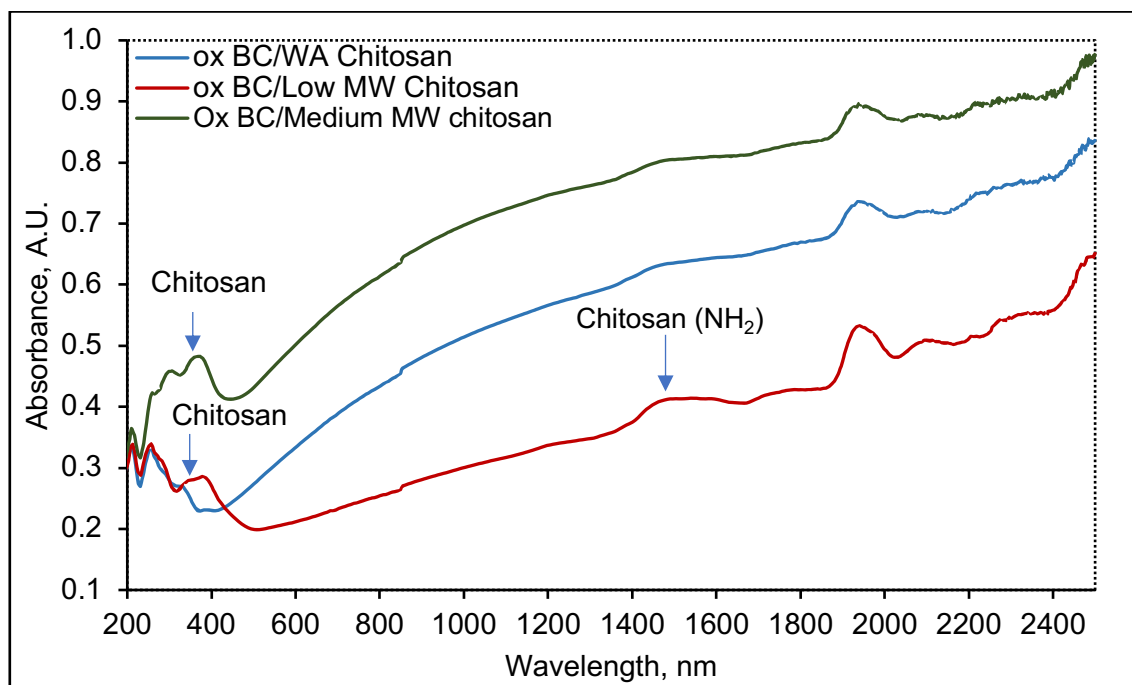


Figure 127. UV-VIS-NIR spectra of ox BC/WA, ox BC/Low and ox BC/Medium MW chitosan composites.

According to UV-VIS-NIR spectra shown in Fig. 127, all three types of the composites had predominant peaks of BC. However, the peaks of chitosan at around 325 can be seen in the all synthesised composites. In addition, the peak of chitosan in NIR spectra was detected in ox BC/Low MW chitosan composite.

The N-H bend of chitosan at 1580 cm^{-1} can be detected in ox BC/Low MW chitosan composite in IR spectra as shown in Fig. 128. Whereas N-H stretch of chitosan at 3270 cm^{-1} can be seen just in ox-BC/Medium chitosan composite (Fig. 128). This might be because the characteristic peak of WA chitosan overlapped with the peaks of BC. As stated previously, the broadening of O-H peak at 3270 cm^{-1} regions could also indicate the presence of chitosan inside the composite.

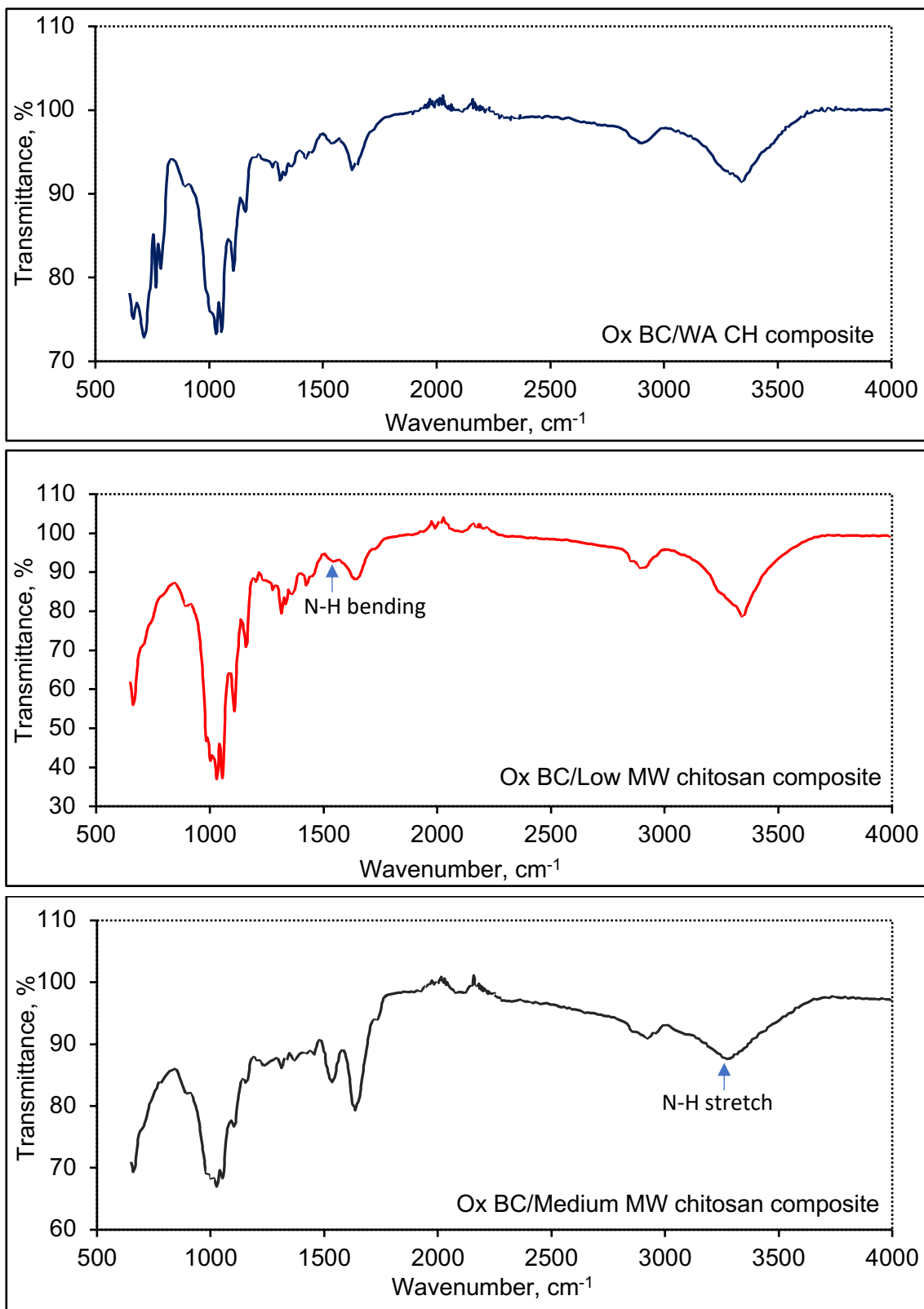


Figure 128. IR spectra of ox BC/WA, ox BC/Low and ox BC/Medium MW chitosan composites.

As a consequence, the most successful incorporation of chitosan could be observed in the oxidised BC/chitosan composites. The presence of chitosan was detected inside the UV spectra of all composites, whereas the characteristic peaks of chitosan can be seen just in ox BC/Low MW chitosan and BC/Medium MW chitosan composites in IR spectra. However, as was stated above, the peaks of WA chitosan might overlap the non-ox BC composites. Therefore, it was challenging to fully evaluate the incorporation of all three types of chitosan inside non-ox BC. However, due to the two detectable peaks of chitosan inside ox BC in UV-VIS and NIR regions, it could be possible to state that oxidation of BC might have improved attachment of chitosan. In addition, the IR spectrum of oxidised and non-oxidised BC/chitosan prepared *via* immersion showed similarities.

6.1.6. Incorporation of chitosan into BC using vacuum self-assembly method

Another method for incorporation *ex situ* of chitosan into the ox and non-ox BC was vacuum self-assembly technique, where pure BC was placed on the Buchner funnel. Each solution containing 0.5 wt.% of WA, low and medium MW chitosan was pumped through the matrix of non-ox and ox BC, respectively. Then, each type of BC/chitosan composite was air-dried at 25°C for 48 hours and analysed by UV-VIS-NIR and FT-IR.

6.1.7. Analysis of synthesised *ex situ* non-ox BC/chitosan composites

Fig. 129 shows the SEM image of BC/WA chitosan composite synthesised using vacuum self-assembly method. As shown in Fig. 129, the fibres of BC were coated with chitosan. This might indicate the successful incorporation of chitosan inside non-ox BC using the pumping-based method.

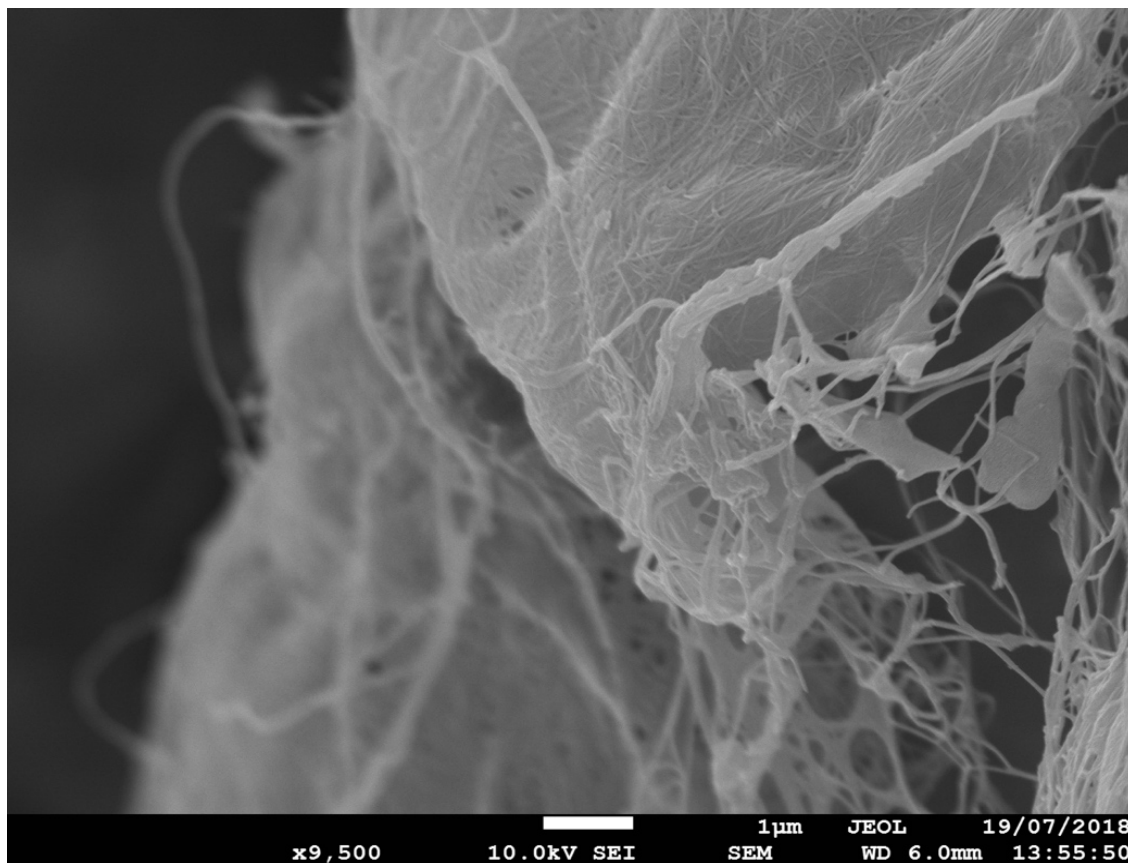


Figure 129. SEM image of BC/WA chitosan synthesised using vacuum self-assembly method.

Fig. 130 shows UV-VIS-NIR spectra of non-ox BC/chitosan composites synthesised using the vacuum pump. Three types of non-ox BC/chitosan had predominantly BC peaks at 265, 860 and 1948 nm. Chitosan peak at 325 nm was detected just in BC/WA chitosan composite.

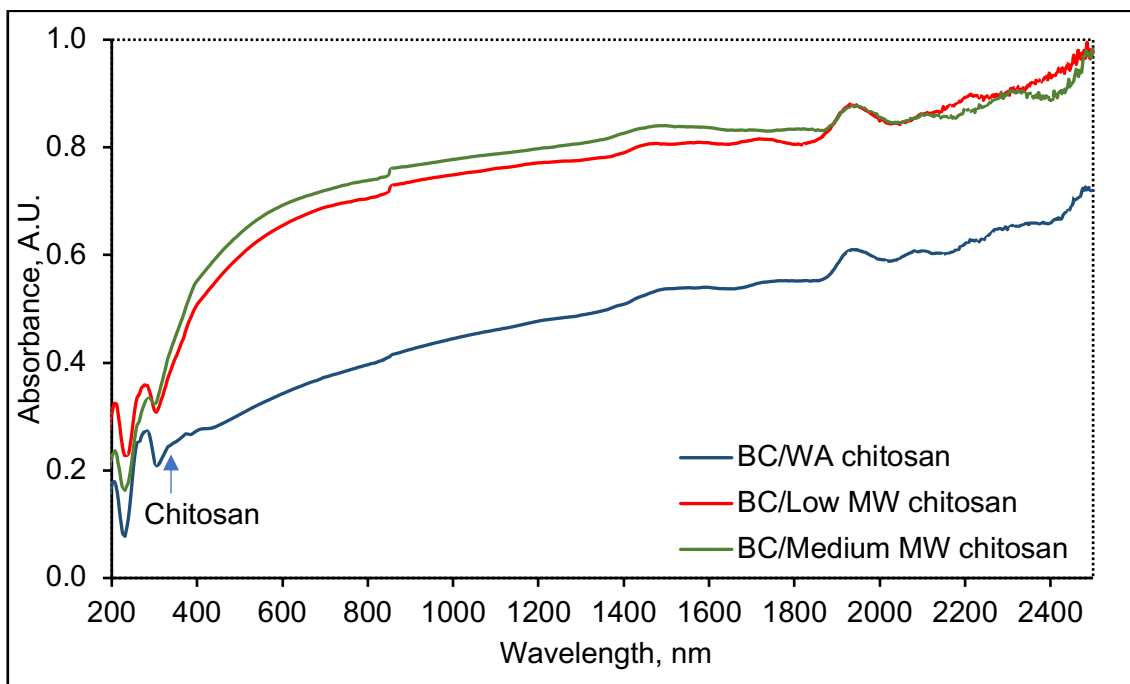


Figure 130. UV-VIS-NIR spectra of non-ox BC/WA, non-ox BC/ Low MW and non-ox BC/Medium MW chitosan composites.

Three types of the composites were analysed by FT-IR (Fig. 131). N-H bend at 1570 cm^{-1} of chitosan were not seen in all composite, whereas N-H stretch could be observed in non-ox BC/WA composite. Regarding O-H stretching, non-ox BC/Medium MW chitosan composite had O-H stretch peak of 3340 cm^{-1} at a transmittance of 91%, whereas the other two composites had such peak at a transmittance of 86%.

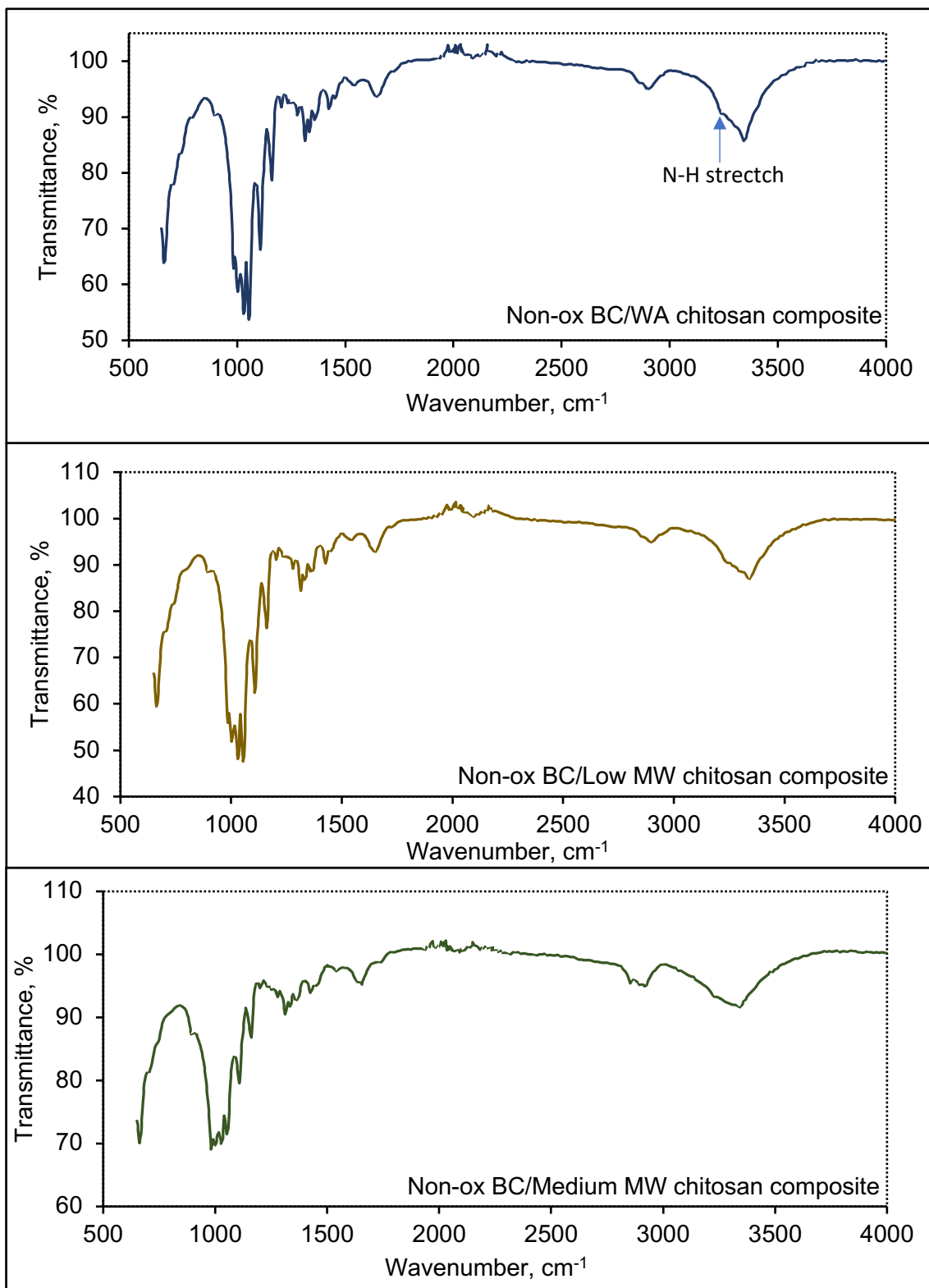


Figure 131. IR spectra of non-ox BC/WA, non-ox BC/ Low MW and non-ox BC/Medium MW chitosan composites.

6.1.8. Analysis of synthesised *ex situ* ox BC/chitosan composites

Fig. 132 shows UV-VIS-NIR spectra of ox BC/chitosan composites prepared using the pump. While UV-VIS analysis of the composites showed all peaks of BC, sharp chitosan peaks at around 325-350 nm can also be observed in all three types of the composites.

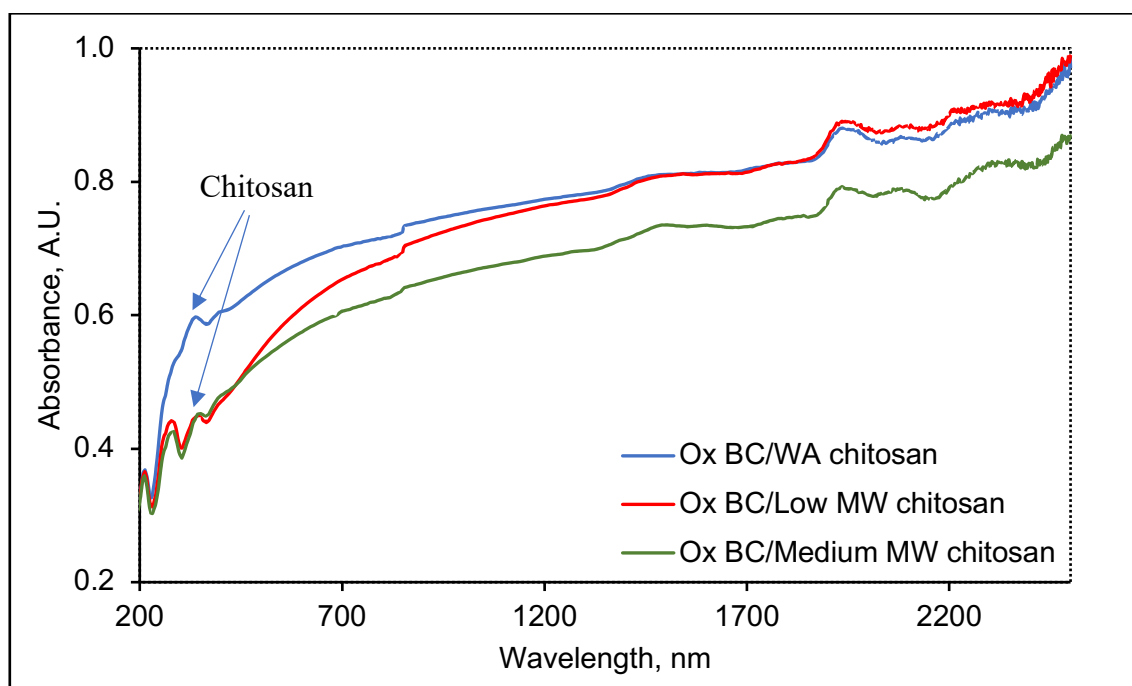


Figure 132. UV-VIS-NIR spectra of ox BC/WA, ox BC/Low and ox BC/Medium MW chitosan composites prepared using the pump.

Fig. 133 shows IR spectra of ox BC/chitosan composites prepared using the pump. According to Fig. 133, the composites synthesised with low MW chitosan had the best integration into BC. The sharp peak of N-H stretch could be identified at 3260 cm^{-1} . This peak was also slightly visible in other tested BC/chitosan composites. Originally, the peak of N-H stretch was at 3270 cm^{-1} in the chitosan powders, but it might shift due to hydrogen bonding.

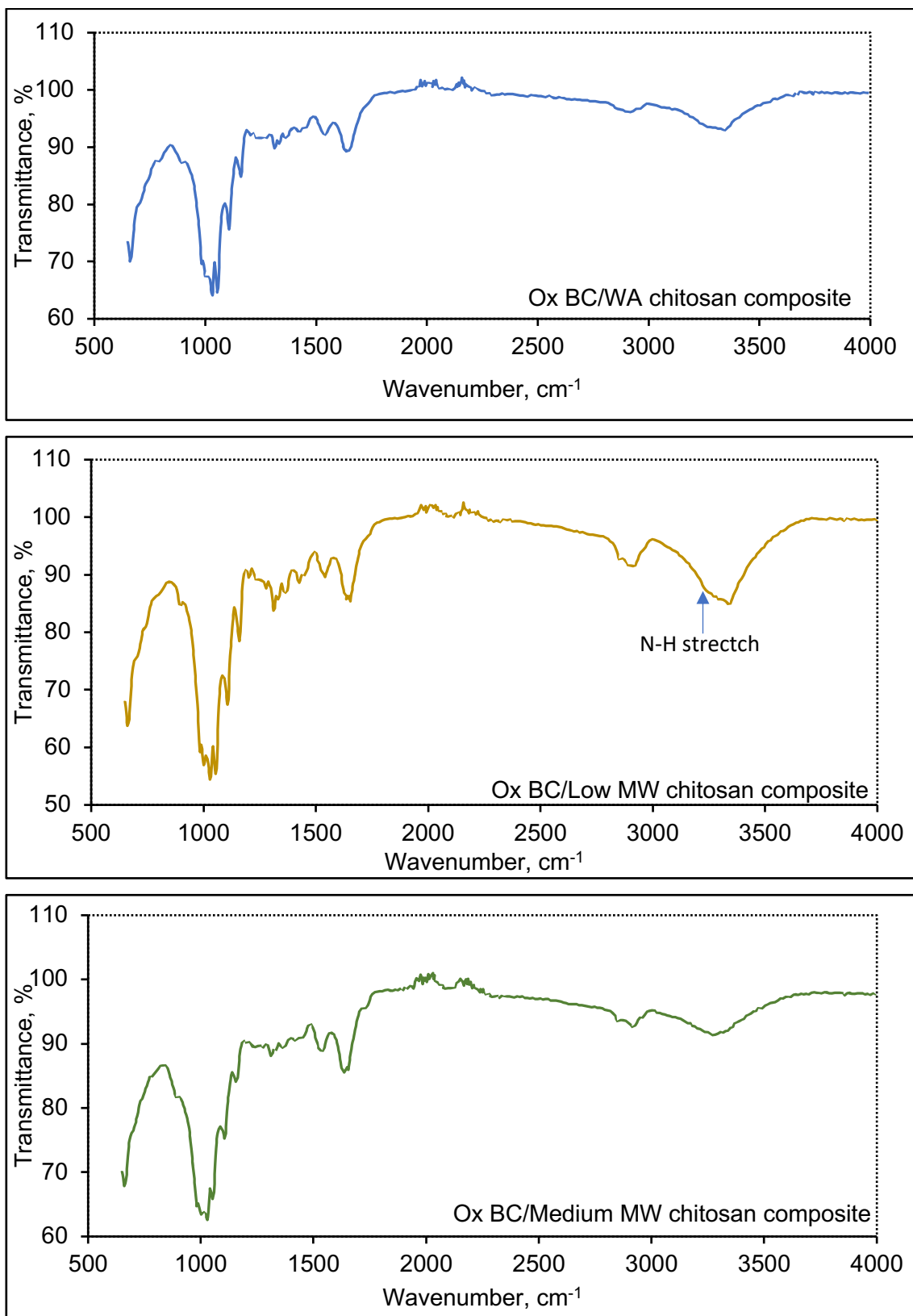


Figure 133. IR spectra of ox BC/WA, ox BC/Low and ox BC/Medium MW chitosan composites prepared using the pump.

Therefore, BC/chitosan composites prepared *via* the vacuum self-assembly method showed that the incorporation of chitosan was more successful using ox BC than non-ox BC. The characteristic peaks of the chitosan were pronounced in the oxidised samples, which is likely due to a reduction in the crystallinity of the BC during oxidation.

6.1.9. Antibacterial activity of synthesised *ex situ* BC/chitosan composites

The antibacterial activity of synthesised *ex situ* BC/chitosan composites was investigated against MRSA, *E. coli* and *P. aeruginosa*, respectively, as described in Section 2.7.3. The control for each antibacterial assay was PBS-resuspended MRSA, *E. coli* and *P. aeruginosa*, respectively, that was placed on the surface of the empty petri dish without agar and covered with the sterile plastic lid.

6.1.9.1. Antibacterial activity of non-ox BC/chitosan composite produced through immersion

The antibacterial activity of non-ox BC/chitosan composites produced through immersion *ex situ* method along with BC treated with 0.1M acetic acid was investigated against MRSA, *E. coli* and *P. aeruginosa* (Figs. 134-136).

According to Fig. 134, the growth of MRSA was reduced to 94% and 85% of control values by using BC/WA chitosan and BC/Low MW chitosan composites, respectively. Non-ox BC/Medium MW chitosan composite decreased the control values to 73%.

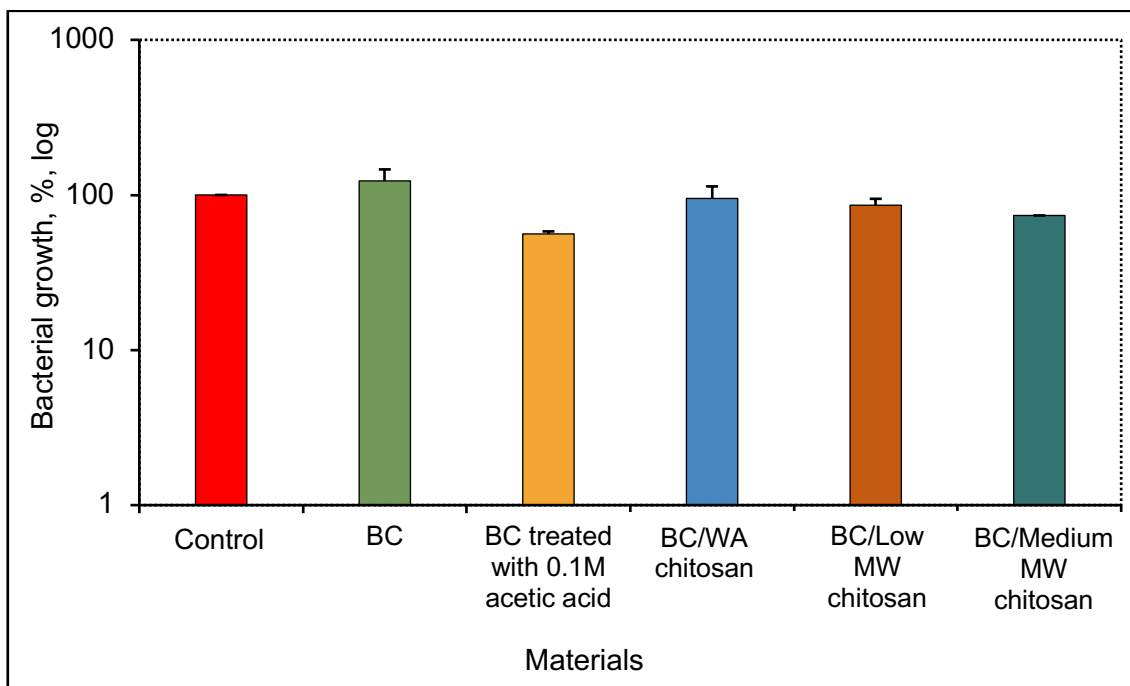


Figure 134. Antibacterial activity of non-ox BC/chitosan composites against MRSA. The control represented PBS-resuspended MRSA that was inoculated on the surface of the empty petri dish without any treatment and covered with a lid. Data shown represent the mean of two independent experiments with error bars of standard deviation.

Fig. 135 shows antibacterial activity of non-ox BC/chitosan composites against *E. coli*. As shown in Fig. 135, non-ox BC/WA chitosan composite decreased the control values to 10%, whereas BC/Medium MW chitosan composite increased the growth of *E. coli* to 304% compare to the control, which was double than pure BC (150%). BC/Low MW chitosan composite did not affect bacterial growth.

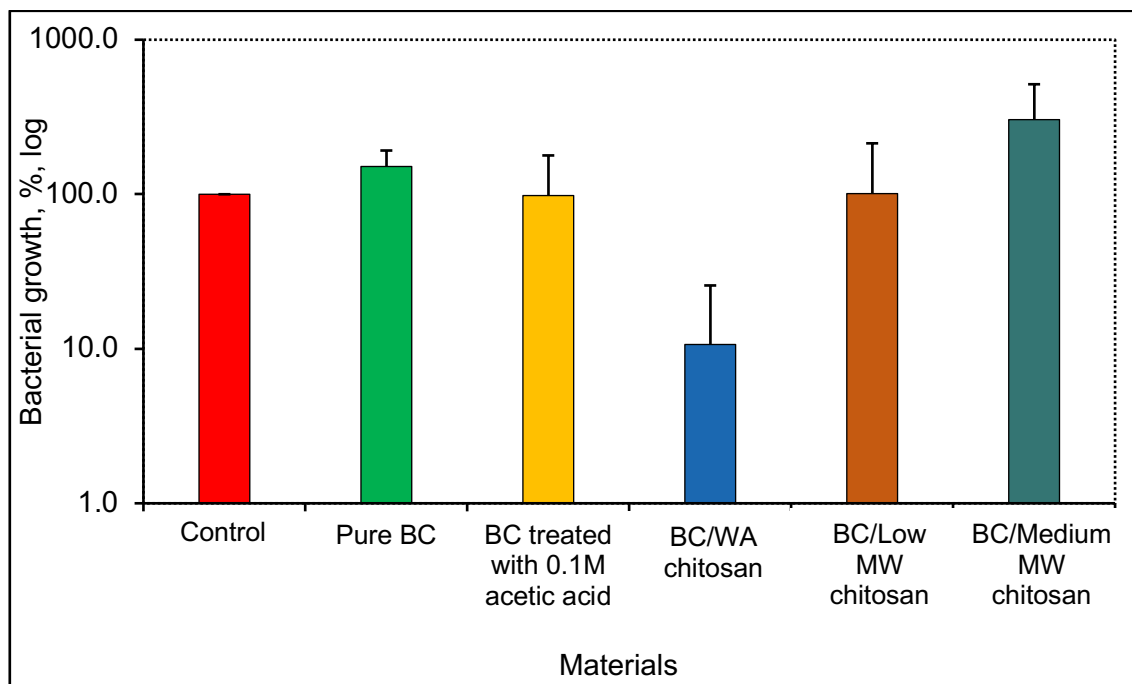


Figure 135. Antibacterial activity of non-ox BC/chitosan composites against *E. coli*. The control represented PBS-resuspended *E. coli* that was inoculated on the surface of the empty petri dish without any treatment and covered with a lid. Data shown represent the mean of two independent experiments with error bars of standard deviation.

However, BC/Low MW chitosan affected the growth of *P. aeruginosa* and decrease it to 67% of the control values, whereas both BC/WA chitosan and BC/Medium MW chitosan promoted the bacterial growth to 150% and 260% compare to the control values, respectively (Fig. 136). Furthermore, both pure BC and BC treated with 0.1M of acetic acid increased the growth of the bacteria to 209% and 192% of the control values, respectively.

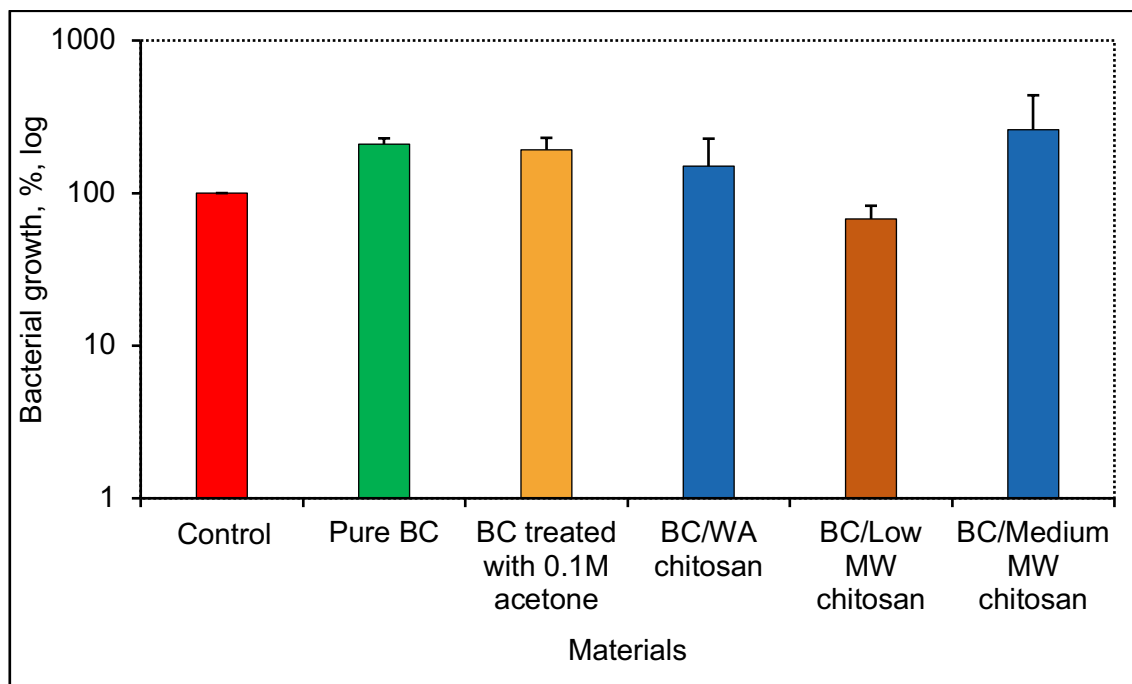


Figure 136. Antibacterial activity of non-ox BC/chitosan composites against *P. aeruginosa*. The control represented PBS-resuspended *P. aeruginosa* that was inoculated on the surface of the empty petri dish without any treatment and covered with a lid. Data represent the mean of two independent experiments with error bars of standard deviation.

6.1.9.2. Antibacterial activity of non-ox BC/chitosan composites prepared through vacuum self-assembly technique

The antibacterial activity of non-ox BC/chitosan composites synthesised using vacuum self-assembly method was investigated (Fig. 137-139). According to Figs. 137-139, all three types of composites showed significantly strong antibacterial activity. The BC/WA chitosan composites reduced the growth of MRSA, *E. coli* and *P. aeruginosa* to 0.3%, 0.002% and 0.8% of control values, respectively. BC/Low MW chitosan decreased the control values of MRSA, *E. coli* and *P. aeruginosa* to 0.8%, 0.006% and 1.8%, respectively. BC/Medium MW chitosan composite reduced the growth of MRSA, *E. coli* and *P. aeruginosa* to 0.7%, 0.5% and 1.8% of control values, respectively. As shown in Figs. 137-139, BC/WA chitosan composite was the most effective treatment against all three

types of bacteria. In addition, pure BC did not affect MRSA and increased the growth of *E. coli* and *P. aeruginosa* to 151% and 209% of the control values, respectively.

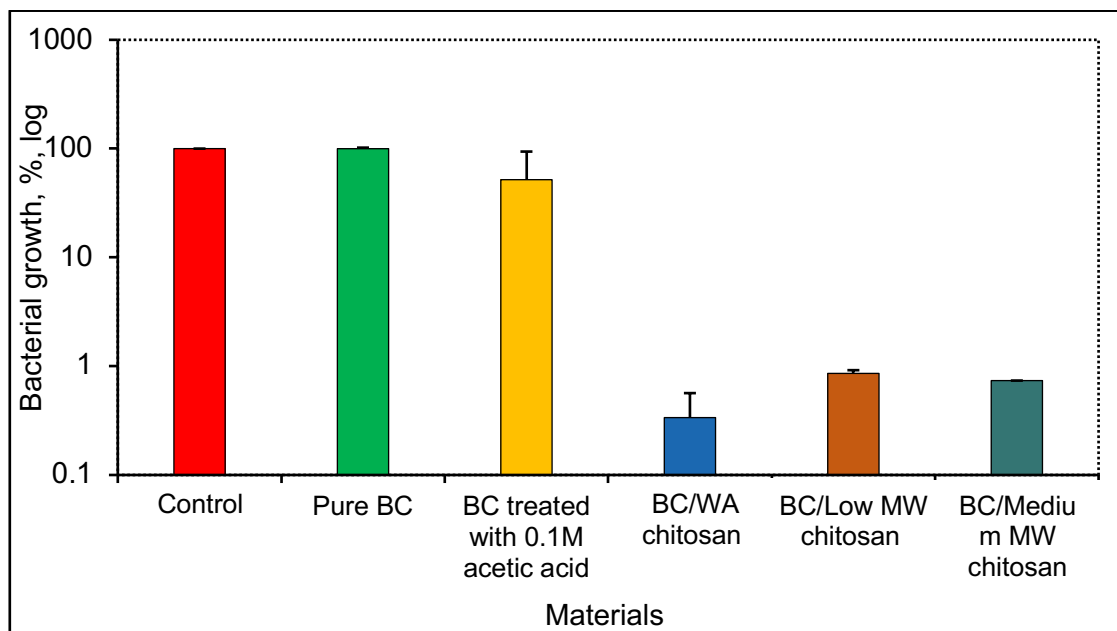


Figure 137. Antibacterial activity of non-ox BC/CH composites prepared through vacuum self-assembly technique against MRSA. The control represented PBS-resuspended MRSA that was inoculated on the surface of the empty petri dish without any treatment and covered with a lid. Data shown represent the mean of three independent experiments with error bars of standard deviation. The treatments were compared to the control. BC/WA, BC/Low MW and BC/Medium MW chitosan composites are significantly different from the control (P -value <0.001).

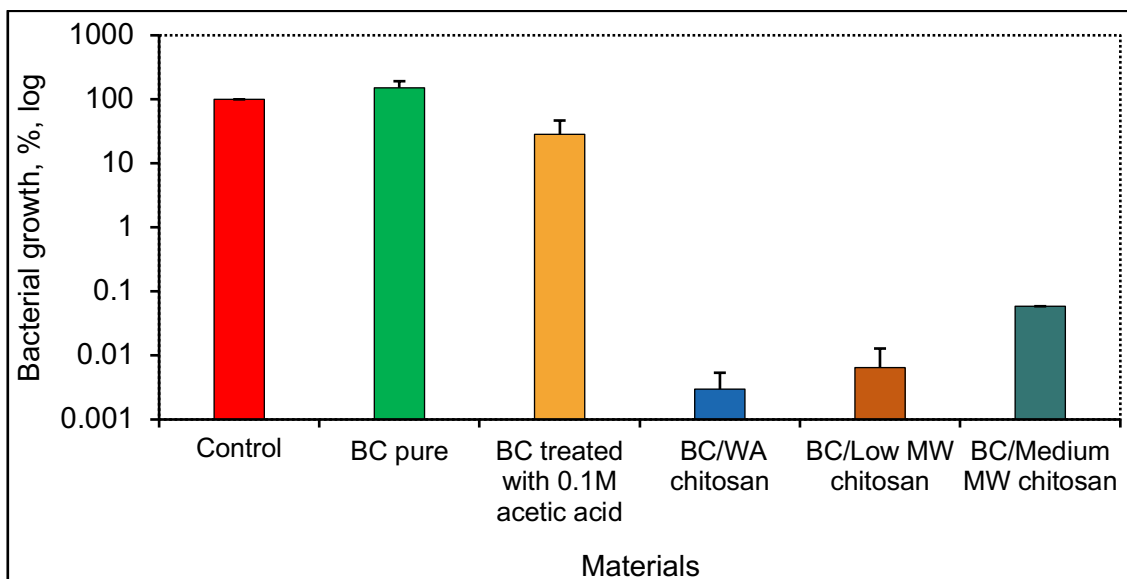


Figure 138. Antibacterial activity of non-ox BC/chitosan composites prepared through vacuum self-assembly technique against *E. coli*. The control represented PBS-resuspended *E. coli* that was inoculated on the surface of the empty petri dish without any treatment and covered with a lid. Data shown represent the mean of three independent experiments with error bars of standard deviation. The treatments were compared to the control. BC/WA, BC/Low MW and BC/Medium MW chitosan composites are significantly different from the control (P -value <0.01).

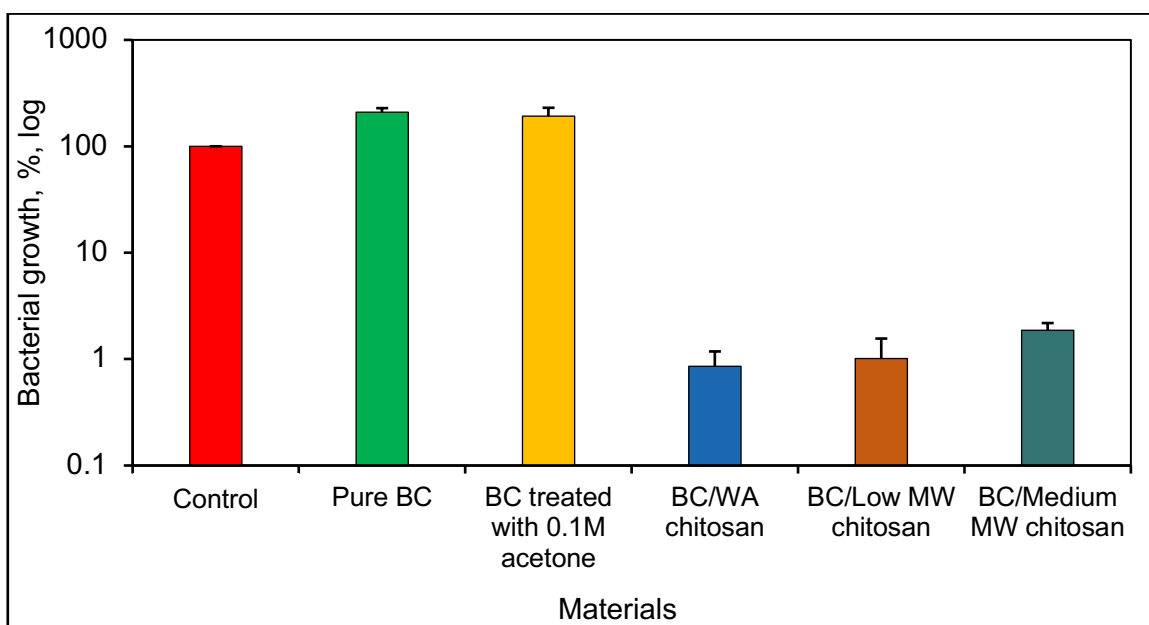


Figure 139. Antibacterial activity of non-ox BC/CH composites prepared through vacuum self-assembly technique against *P. aeruginosa*. The control represented PBS-

resuspended *P. aeruginosa* that was inoculated on the surface of the empty petri dish without any treatment and covered with a lid. Data shown represent the mean of three independent experiments with error bars of standard deviation. The treatments were compared to the control. BC/WA, BC/Low MW and BC/Medium MW chitosan composites are significantly different from the control (P -value <0.01).

6.1.9.3. Antibacterial activity of ox BC/chitosan composites synthesised through vacuum self-assembly technique

The antibacterial properties of pumped-synthesised oxidised BC/chitosan composites were analysed against MRSA, *E. coli* and *P. aeruginosa* (Figs. 140-142). According to Fig. 140, all three composites showed strong antibacterial activity against MRSA. The bacterial growth reduced to 0.0009% of control values using ox BC/WA chitosan, to 0.005% using ox BC/Low MW chitosan and to 0.6% using BC/Medium MW chitosan.

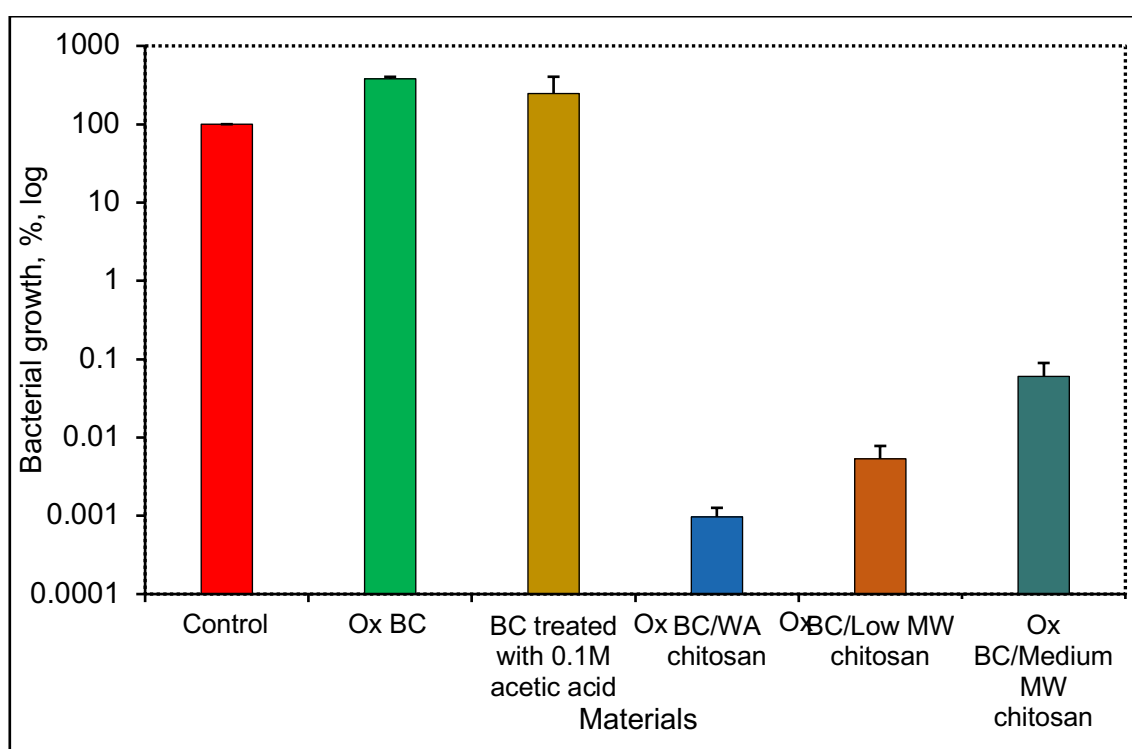


Figure 140. Antibacterial activity of ox BC/chitosan composites prepared through vacuum self-assembly technique against MRSA. The control represented PBS-

resuspended MRSA that was inoculated on the surface of the empty petri dish without any treatment and covered with a lid. Data shown represent the mean of three independent experiments with error bars of standard deviation. Ox BC is different from the control with P -value <0.01 . Ox BC/WA, ox BC/Low MW and ox BC/Medium MW chitosan composites are significantly different from the control (P -value <0.001).

The ox BC/chitosan composites also showed antibacterial activity against *E. coli*. The growth of the bacteria significantly decreased to 2% and 1.8% of control values using ox BC/WA chitosan and ox BC/Medium MW chitosan composites, respectively (Fig. 141). Ox BC/Low MW chitosan composites reduced the growth of *E. coli* to 3.5% of control values. Both pure BC and BC treated with 0.1M acetic acid increased control values to 163% and 115%, respectively.

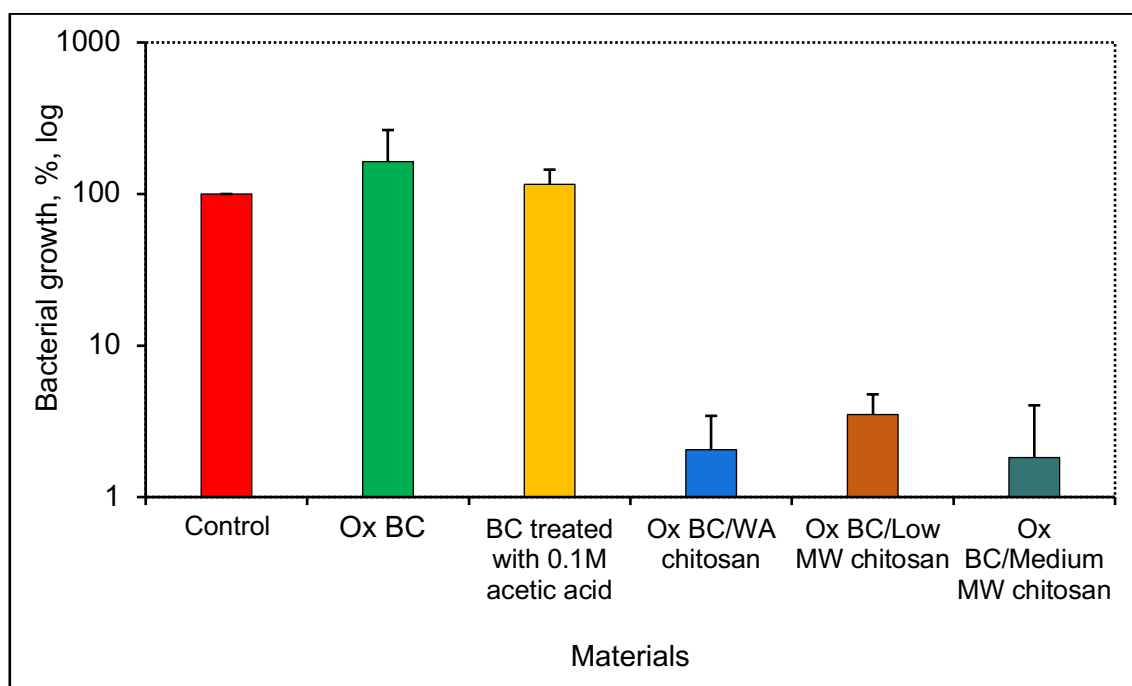


Figure 141. Antibacterial activity of ox BC/chitosan composites prepared through vacuum self-assembly technique against *E. coli*. The control represented PBS-resuspended *E. coli* that was inoculated on the surface of the empty petri dish without any treatment and covered with a lid. Data shown represent the mean of three independent experiments with error bars of standard deviation. The treatments were compared to the control. Ox BC/WA, ox BC/Low MW and ox BC/Medium MW chitosan composites are significantly different from the control (P -value <0.01).

As seen in Fig. 142, the weakest antibacterial activity was observed with ox BC/Medium MW chitosan, which decreased the growth of *P. aeruginosa* to 2.7%, whereas BC/Low MW chitosan and BC/WA chitosan reduced bacterial growth to 0.005% and 0.13% of control values, respectively. However, all treatments shown statistically significant differences.

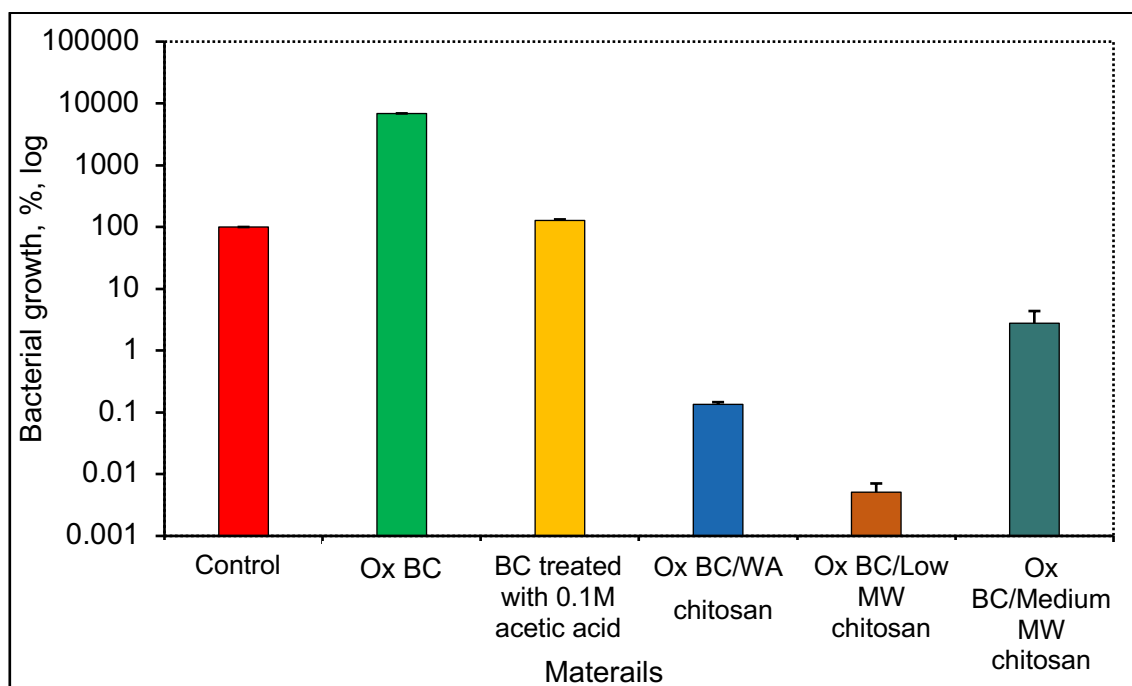


Figure 142. Antibacterial activity of ox BC/CH composites prepared through vacuum self-assembly technique against *P. aeruginosa*. The control represented PBS-resuspended *P. aeruginosa* that was inoculated on the surface of the empty petri dish without any treatment and covered with a lid. Data shown represent the mean of three independent experiments with error bars of standard deviation. All treatments are significantly different from the control. *P*-value for ox BC and ox BC/Low MW chitosan is <0.01 , whereas *P*-value for other treatments is <0.05 .

6.2. Discussion

BC/chitosan composites prepared *via* the vacuum self-assembly method showed that the incorporation of chitosan was more successful using ox BC than non-ox

BC. The characteristic peaks of chitosan were pronounced in the oxidised samples, which is likely due to a reduction in the crystallinity of the BC during oxidation.

6.2.1. Oxidation of BC

Oxidation of BC using sodium periodate (NaIO_4) resulted in the introduction of aldehyde groups to the structure (Fig. 143). This reaction is characterised by cleaving of C2 and C3 bonds between hydroxyl groups of a glucose unit. This results in the formation of two aldehyde groups ($-\text{HC}=\text{O}$) per unit^[292].

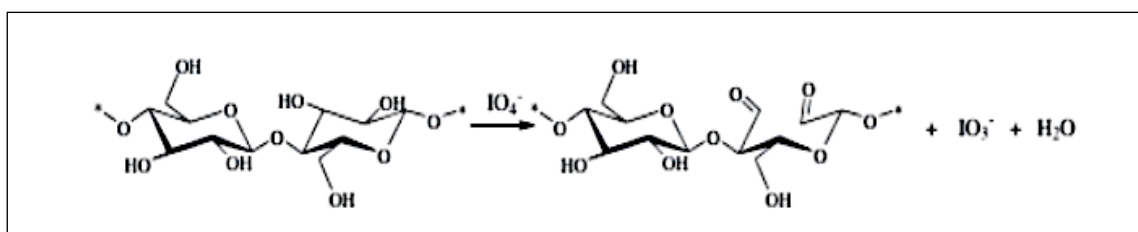


Figure 143. Periodate oxidation of cellulose^[294].

At the end of the oxidation reaction, the hydroxyl groups were replaced with the aldehyde groups. It has been reported that the process of oxidation occurs in the bulk material^[292]. Therefore, the aldehyde groups could be detectable in the FT-IR spectrum. According to the FT-IR result, it was possible to achieve oxidation of BC by using sodium periodate.

The aldehyde groups ($-\text{CHO}$) of the oxidised BC were grafted with amine groups of chitosan by a Schiff's base reaction. In the presence of chitosan, the aldehyde groups could bind to the amino group ($-\text{NH}_2$) of chitosan and form an imine bond ($-\text{C}=\text{NR}$), which is subsequently rearranged to a stable amine ($-\text{C}-\text{NHR}$)^[292]. As was discussed in Section 5.2.1, chitosan could interact with non-ox BC through the intramolecular hydrogen bonds that may be formed between the chemical groups in chitosan ($-\text{OH}$ and NH_2) and BC ($-\text{OH}$). It has been reported that the intramolecular hydrogen bond can break down in order to form BC-chitosan hydrogen bonding^[138, 140]. In addition, chitosan could also coat BC fibres by physical attachment^[291].

It has been reported that oxidised BC and oxidised BC/chitosan composites have a more amorphous structure than pure BC^[295]. This might be due to the oxidant, which could destroy the hydrogen bonding and subsequently the crystal structure of ox BC. In addition, it has been stated that the surface charge of BC changed from negative -8.3 ueq/g to more negative during oxidation -11.4 ueq/g^[291]. However, ox BC has shown positive charge of +34.4 ueq/g in the presence of chitosan^[291].

Oxidation of BC could be beneficial for the chemical interaction with chitosan. However, such a modification of BC may not improve the attachment of clay, because the interaction between clay and BC occurs when silicate particles bind to the OH groups of BC thorough hydrogen and/or weak organic-inorganic bindings^[112, 246].

6.2.2. Antibacterial activity of BC/chitosan composites

The incorporation of chitosan into BC using the immersion method seemed to be uneven. According to the results obtained from UV-VIS and FT-IR, the BC/WA chitosan composite did not show any peaks of WA chitosan inside BC; however, the antibacterial assay exhibits improved antimicrobial properties of the composite and, therefore, incorporation of chitosan. A possible reason behind this might be the relatively short time of the actual immersion, resulting in a low concentration of chitosan penetrating the matrix of BC. It has been reported elsewhere that immersion for 12 hours allowed proper incorporation of 0.6 wt.% of chitosan solution, which resulted in inhibition of 99% of the growth of both *E. coli* and *S. aureus*^[180]. According to UV-VIS and FT-IR results, BC/Medium MW chitosan composite showed more evidence of the presence of chitosan inside the matrix. However, as shown in Figs. 135-136, BC/Medium MW chitosan composite increased bacterial growth, which suggested that chitosan was not fully incorporated into the BC matrix. Alternatively, this might also be because of the lower antibacterial activity of medium MW chitosan^[170]. The antibacterial data obtained were very different from pure chitosan, which might be due to the non-

effective penetration of chitosan inside the matrix, where a very small extent of chitosan was in the BC structure in the materials produced through immersion.

Furthermore, BC treated with 0.1M acetic affected the growth of both MRSA and *E. coli*. The growth of MRSA and *E. coli* was reduced to 51% and 21% of control values, respectively, using BC treated with 0.1M acetic acid. The results might suggest that either BC treated with 0.1M acid was not completely washed after the pumping method or due to porosity of BC, acid could remain inside the matrix and release during the treatment. However, the growth of the bacteria was much lower with the composites than with BC treated with acetic acid. This means that acetic acid was not responsible for the reduction in bacterial growth. In addition, *P. aeruginosa* did not show any sensitivity to BC treated with 0.1M acetic acid as the control values of bacteria increased to 192% (Fig. 139).

The composites synthesised through the immersion showed the least antibacterial activity compared to the composites produced through the vacuum self-assembly technique. Ox BC/chitosan composites synthesised using the vacuum self-assembly technique showed incorporation of chitosan in UV-VIS-NIR and IR spectra as well as strong antibacterial activity. Within all types of synthesised composites, BC/WA chitosan showed the strongest antibacterial activity against MRSA, *E. coli* and *P. aeruginosa*. This might be due to differences in both MW and DDA.

DDA might affect the antimicrobial property of chitosan due to the number of amine groups, which are directly involved in the antibacterial mechanisms that are described in Section 1.4.3.1. WA chitosan had the highest DDA of 90%, whereas WA and low MW chitosan had DDA of 75-85%, respectively. It has been reported elsewhere that an increase in DDA leads to a stronger antimicrobial activity^[132, 157]. In another study, chitosan with 82% DDA reduced the viability to 0.0625% of control values of both *E. coli* and *S. aureus* after 24 hours^[157]. It has been also stated that increasing DDA of chitosan from 75% to 95% leads to

increased antimicrobial activity against *S. aureus* and *E. coli* through nucleotide leakage^[158].

The molecular weight of chitosan is another possible factor that may affect antibacterial activity. It has been reported elsewhere that low MW chitosan could enhance antibacterial properties against Gram-negative bacteria^[164]. Low MW chitosan might penetrate bacterial cell walls and enter bacterial cells^[161]. It has also been reported that chitosan with high MW might showed reduced antibacterial activity against *E. coli* due to the strong binding of intramolecular hydrogen bonds that prevents amine groups from being available to attach bacterial cells^[151]. Furthermore, it has been found that a decrease of MW of chitosan increases the antibacterial activity. As MW decreased chitosan can pass through the channels into the cell^[166]. Low MW chitosan might also be able to affect DNA and inhibit RNA replication^[46]. Inside a bacterial cell, low MW chitosan can bind to DNA electrostatically and reduce a mobility of nucleic acids^[132, 162]. Whereas, high MW of chitosan may form a dense polymer film on the surface of cells and prevent nutrients and oxygen from passing through. This might inhibit the growth of aerobic bacteria^[46]. The present findings confirmed those reports. WA chitosan with the highest 90% DDA and low MW was the most effective, whereas medium MW chitosan showed a weaker antibacterial activity.

The antibacterial activity of the BC/chitosan composites synthesised through the vacuum self-assembly method was much stronger than that of pure chitosan. A possible reason for this might be an experimental error, bacterial adaptation or synergistic effect of chitosan and BC together. A combination of chitosan and BC might lead to increased antibacterial activity^[296]. It has been reported that both antibacterial activity and solubility of chitosan could be increased when chitosan coupling with other materials by a Schiff base reaction^[296]. Schiff base derivatives, where carbonyl groups or aldehyde efficiently coupled with NH₂ groups of chitosan and, subsequently, form the corresponding chitosan Schiff base consisting of the characteristic imine group (-RC=N-), possess

stronger antibacterial activity than pure chitosan due to enhancement of hydrophilicity of chitosan, altering chitosan molecular structure and increasing a number of positively charged cations^[297]. Furthermore, the solubility of chitosan might be improved due to the introduction of groups that could reduce interaction of intramolecular hydrogen bonds^[296]. For example, it has been observed elsewhere that BC/PVA/chitosan composites, which were prepared by magnetic stirring using 0.3 wt.% of chitosan nanoparticles with DDA at 85-90%, showed an increase in both swelling behaviour and solubility in water^[293]. Furthermore, BC/PVA/Chitosan composite has shown higher antibacterial activity against *S. aureus* and *E. coli* than pure chitosan^[293, 298]. Moreover, it has been reported that the combination of ox BC and chitosan (1 wt.%, 200 kDa MW, 90% DDA) could result in the improved antibacterial activity that inhibited growth by 99.9% in *S. aureus* and *E. coli*, respectively^[293]. Such a synergistic effect was observed elsewhere, where chitosan has shown improved antibacterial activity against *S. aureus* in a composite with streptomycin^[296].

6.2.3. Cytotoxicity of BC/chitosan composites

Both spreading and adherence of mammalian cells on a surface of BC might provide an insight into its biocompatibility. It has been reported that fibroblasts hardly adhere on a surface of ox BC after 1, 2 and 3 days, whereas the addition of 1 wt.% of chitosan led to both normal morphology and strong proliferation of the cells on a surface of ox BC/chitosan composite with the number of cells being 2 fold more than just on ox BC after 3 days of incubation^[292]. According to MTT results obtained elsewhere, there were 97.7% of metabolically active fibroblasts adhered to the ox BC/chitosan composite after 24 hours^[292]. Ox BC might have a low pH due to free carboxyl groups, which can result in inhibition of the mammalian cells^[292]. However, this effect can be neutralised by the amine groups of chitosan in ox BC/chitosan composite.

Furthermore, fresh blood has been placed on a surface of both non-ox and ox BC/chitosan composites elsewhere in the blood clotting assay. It has been

observed that ox BC/chitosan composite induced whole blood clotting 2 fold faster with a low number of cells adhered compare to the non-ox BC/chitosan composite^[293]. Such an increase in the rate of blood clotting might be due to the amine groups that can interact with blood, for instance, with the cell membrane of erythrocytes, through electrostatic binding. However, as has been stated elsewhere, the morphology of erythrocytes and platelets adhered to ox BC/chitosan composite remained normal^[293]. Moreover, chitosan can increase expression of integrin $\beta 3$, but inhibit the adhesion of fibroblasts by reorganisation of the actin and integrin $\beta 1$ network^[299].

Furthermore, it has been concluded that BC could not support the adherence of cancer cells, whereas chitosan can rapidly promote the progression of cancer cells showing better biocompatibility than BC^[299]. Effect of non-ox BC/chitosan composite on the adhesion of A2780 (ovarian cancer) cell lines has been analysed elsewhere by culturing the cells on the composite for 1, 3, 5, and 7 days^[299]. It has been observed by phase-contrast microscopic analysis that the cells were very strongly attached to the fibres of BC/chitosan composite, which were produced by immersion of non-ox BC into 2 wt.% chitosan solution^[299]. The formation of A2780 cell aggregates occurred inside the matrix of pure BC from the 1st day^[299]. It has been reported that the size of the aggregates of A2780 cells on a surface of pure BC and BC/chitosan composite was 281 ± 3.5 and $133 \pm 2 \mu\text{m}$, respectively^[299]. It was concluded that the BC/chitosan composite supported the adherence of the cancel cells more than pure BC indicating a high tumorigenic activity of the composite towards the A2780 cells *in vitro*^[299]. Thereby, the addition of chitosan to BC could lead to enhancing the biocompatibility of pure BC in terms of proliferation and adhesion of cells^[299].

There are might be two possible reasons for the stronger adhesion of cells as well as a lower number of cell aggregates with BC/chitosan composite. A BC/chitosan composite might show a strong cell-fibre interaction through electrostatic binding between chitosan and membranes of cancer cells^[299]. In the case of pure BC without chitosan, cells might interact with each other more

strongly than with fibres of BC. In addition, chitosan could produce *N*-acetyl- β -*D*-glucosamine upon a degradation causing a synergistic effect with BC by improving the wound healing ability followed by the reduction in the scar formation^[299].

Therefore, both ox and non-ox BC/chitosan composites could increase the proliferation and adhesion of different cells such as fibroblasts, A2780 and blood cells.

Chapter 7. Synthesis of BC/chitosan hybrid gel through chemical attachment

The novel hybrid of BC gel and chitosan hydrogel was produced using genipin as a crosslinker. Genipin was used due to its low toxicity towards mammalian cells^[300]. Firstly, 0.5 wt.% of WA chitosan was dissolved using 10 vol.% of distilled vinegar at a final pH3. Then, gepin was introduced to the chitosan solution as detailed in Section 2.6.2.3.

7.1. Results

7.1.1. Synthesis of BC/chitosan hybrid gel through chemical attachment of chitosan

The chemical binding between chitosan and genipin cross-linked chitosan to form the hydrogel is as shown in Fig. 144.

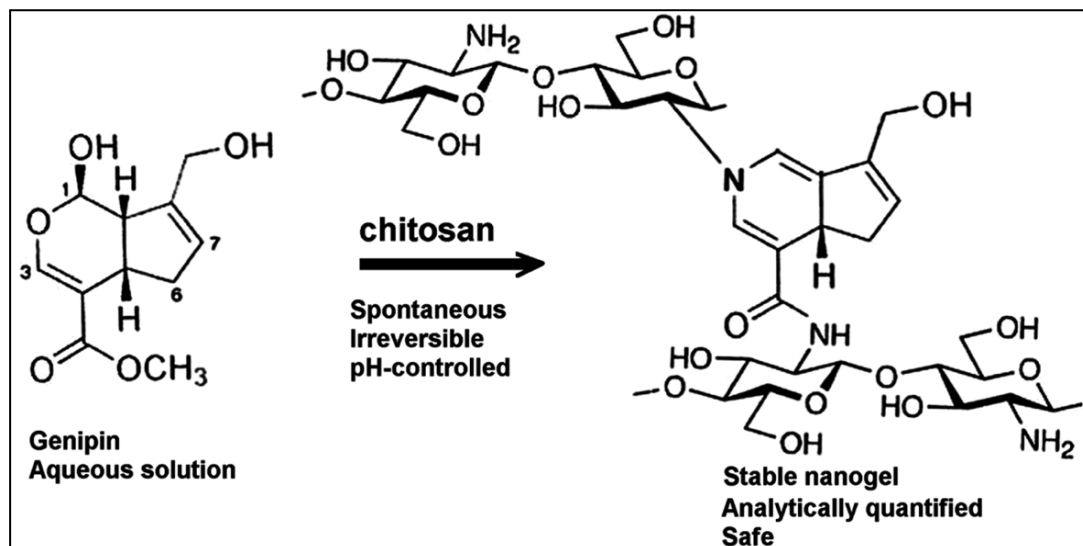


Figure 144. Schematic image of genipin crosslinks with chitosan^[301].

As seen in Fig. 144, two chains of chitosan, which are shown on right side of the picture, react covalently with genipin to form the hydrogel^[301]. The hydrogel was then either settled or incorporated into BC matrix using the vacuum self-assembly technique. Subsequently, BC/chitosan (BC/CH) hybrid was then analysed using

UV-UIS-NIR spectroscopy. Antibacterial activity of the hybrid was investigated against MRSA, *E. coli* and *P. aeruginosa*, respectively.

7.1.2. Analysis of BC/CH hybrid

Fig. 145 shows the appearance of chitosan hydrogel (a) and BC/CH hybrid gel (b) after 24 hours. As seen in Fig. 145a synthesised chitosan hydrogel was dark blue colour due to the presence of genipin. Once the hydrogel was incorporated into BC, the gel formation appeared inside the BC structure. BC/CH hybrid gel was slightly green colour (Fig. 145b).

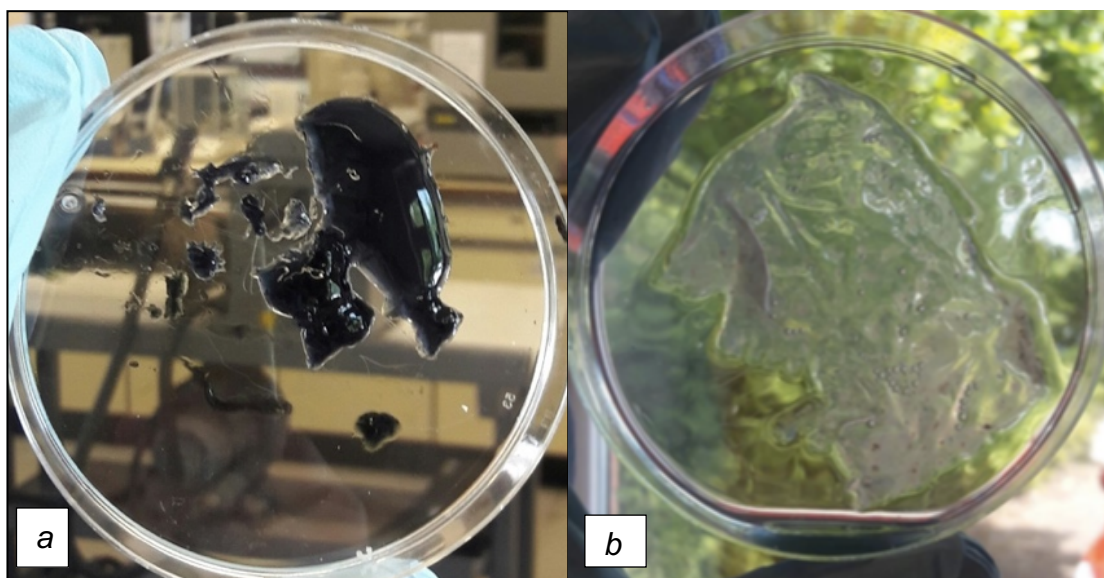


Figure 145. The appearance of chitosan hydrogel (a) BC/CH hybrid gel (b) after 24 hours.

Fig. 146 shows SEM image of BC/CH hybrid gel. As seen in Fig. 146, chitosan hydrogel spread through the matrix and completely covered fibres of BC. Therefore, the strong interaction between the chitosan hydrogel and BC occurred.

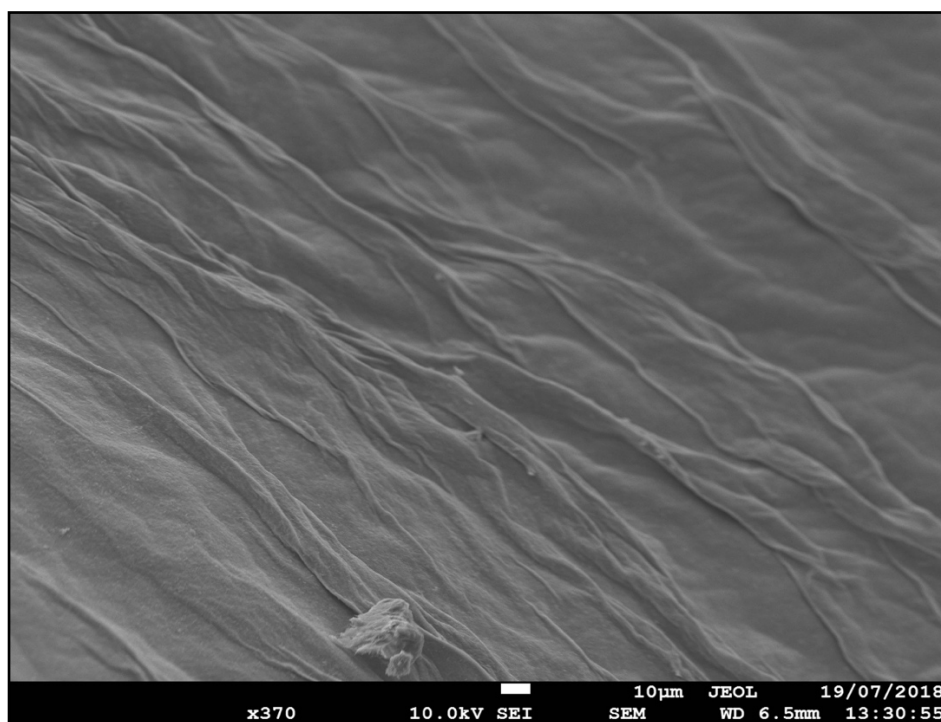


Figure 146. SEM image of BC/CH hybrid gel.

7.1.3. UV-VIS-NIR spectroscopy of BC/CH hybrid gel

BC/CH hybrid gel was analysed using UV-VIS-NIR spectroscopy. In order to investigate the presence of genipin, BC/Genipin composite was observed using UV-VIS spectroscopy (Fig. 147). The characteristic peak of genipin, which is about 683 nm^[301] was not detected inside the composite. Furthermore, Fig. 148 shows UV-VIS spectrum of BC/CH/Genipin hybrid. The double peak of cellulose was detected around 213 nm and 264 nm. The peak of both chitosan at 325 nm and genipin were also not seen inside the hybrid. This might be due to presence of chitosan and genipin inside BC, which was challenging to detect.

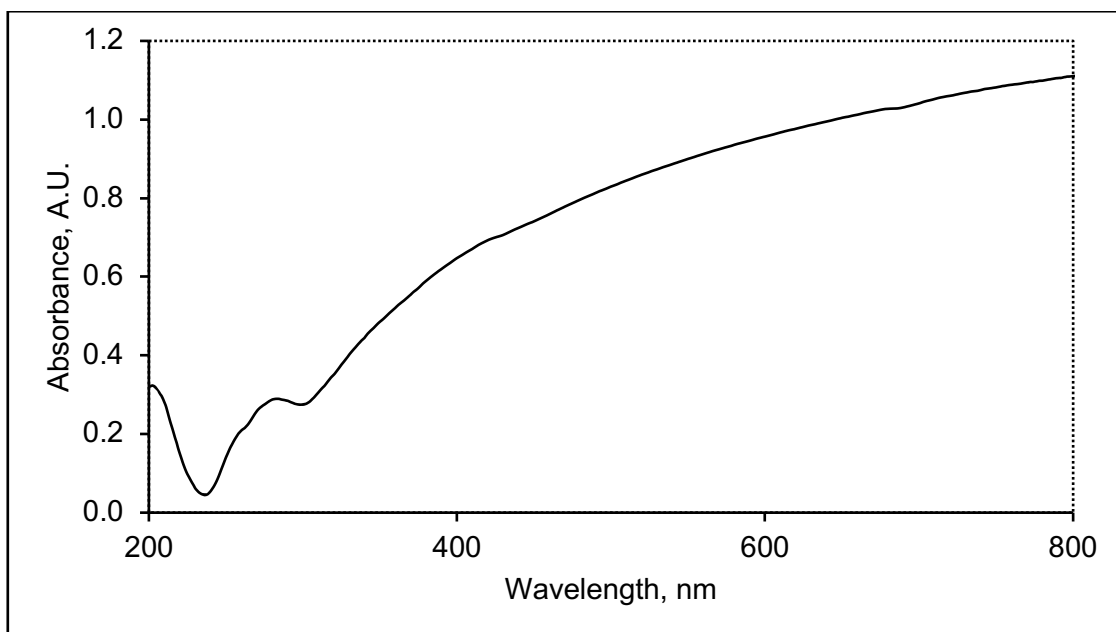


Figure 147. UV-VIS spectrum of BC/Genipin composite.

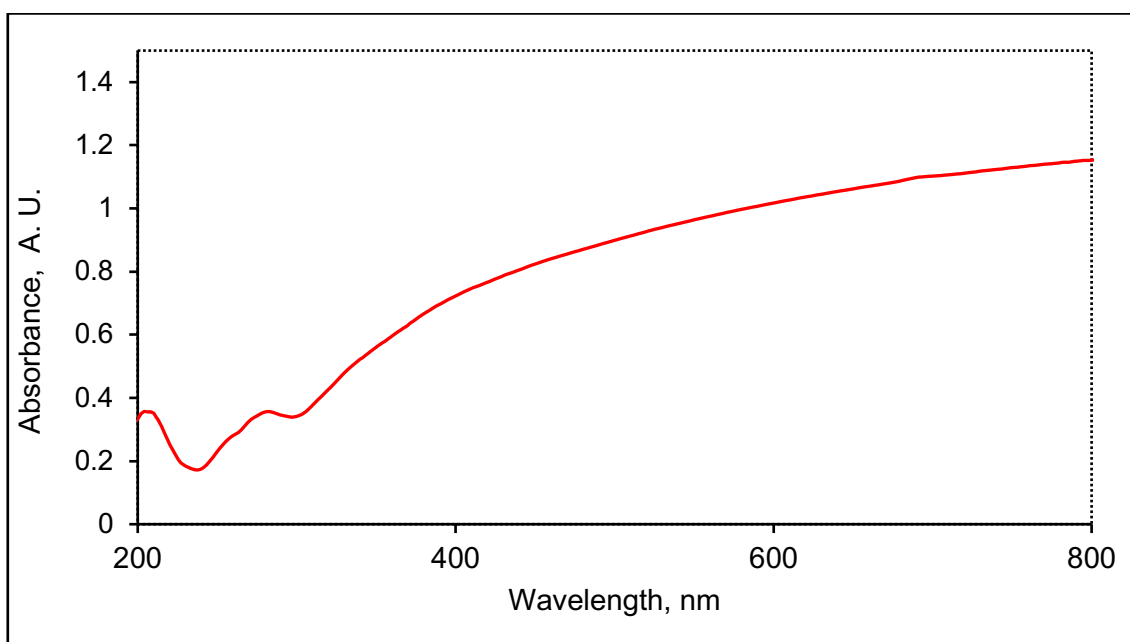


Figure 148. UV-VIS spectrum of BC/CH/Genipin hybrid.

Nonetheless, NIR spectrum of the BC/CH hybrid gel had predominantly BC structure with two characteristic peaks of cellulose at 1940 nm, the peak of chitosan at around 1430-1488 nm might be detectable inside the BC/CH hybrid gel (Fig. 149).

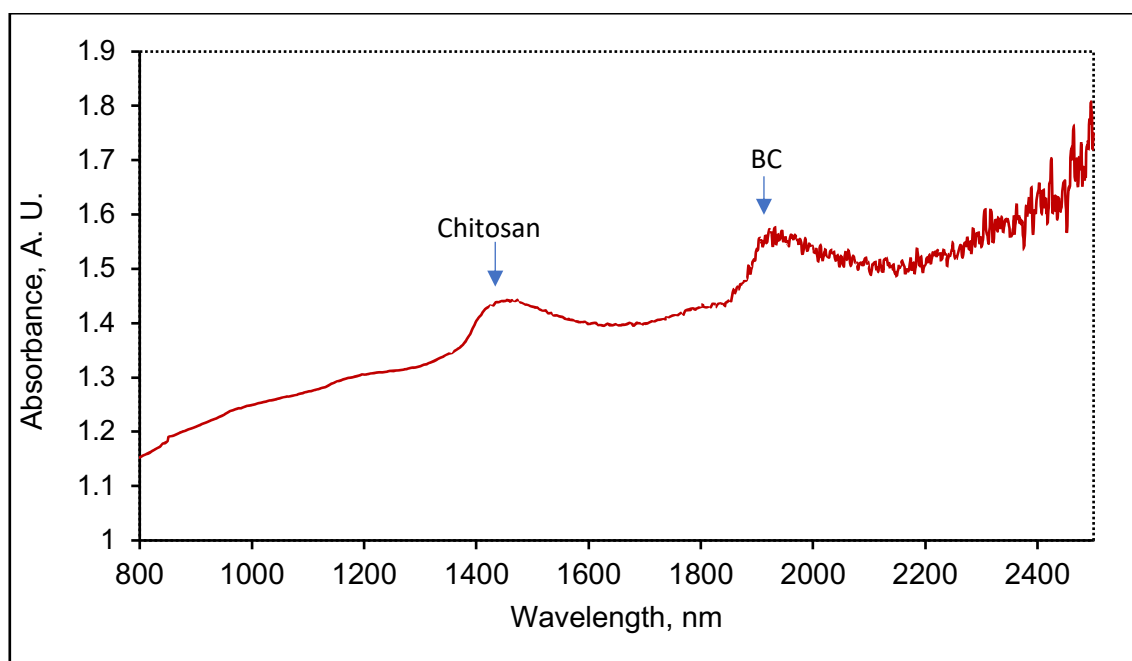


Figure 149. NIR spectrum of BC/CH/Genipin hybrid.

7.1.4. Introduction of exfoliated Cloisite Na⁺ to BC/CH hybrid

Once chitosan hydrogel was successfully incorporated into BC, exfoliated Cloisite Na⁺ clay was introduced to the hybrid. Chitosan at concentration 0.5 wt.% was dissolved using vinegar at pH3. Then, chitosan solution was mixed with 0.6 wt.% exfoliated suspension of Cloisite Na⁺ suspension in the ratio of 1:1, which leaves a final clay concentration of 3 mg/ml. Subsequently, the suspension of chitosan and clay was then pumped through pure BC using the vacuum self-assembly technique. The detailed method of developing BC/CH/Cloisite Na⁺ composite is described in Section 2.6.2.4. The analysis of BC/CH/Cloisite Na⁺ composite was carried out using UV-VIS-NIR spectroscopy.

Fig. 150 shows UV-VIS spectrum of BC/CH/Genipin/Cloisite Na⁺ composite. As shown in Fig. 144, the BC/CH/Cloisite Na⁺ composite contained the peaks of both clay and the cellulose in a range of 209-211 nm. The separate peak of the cellulose at 279 nm was present. The peaks of both genipin and chitosan were not detected.

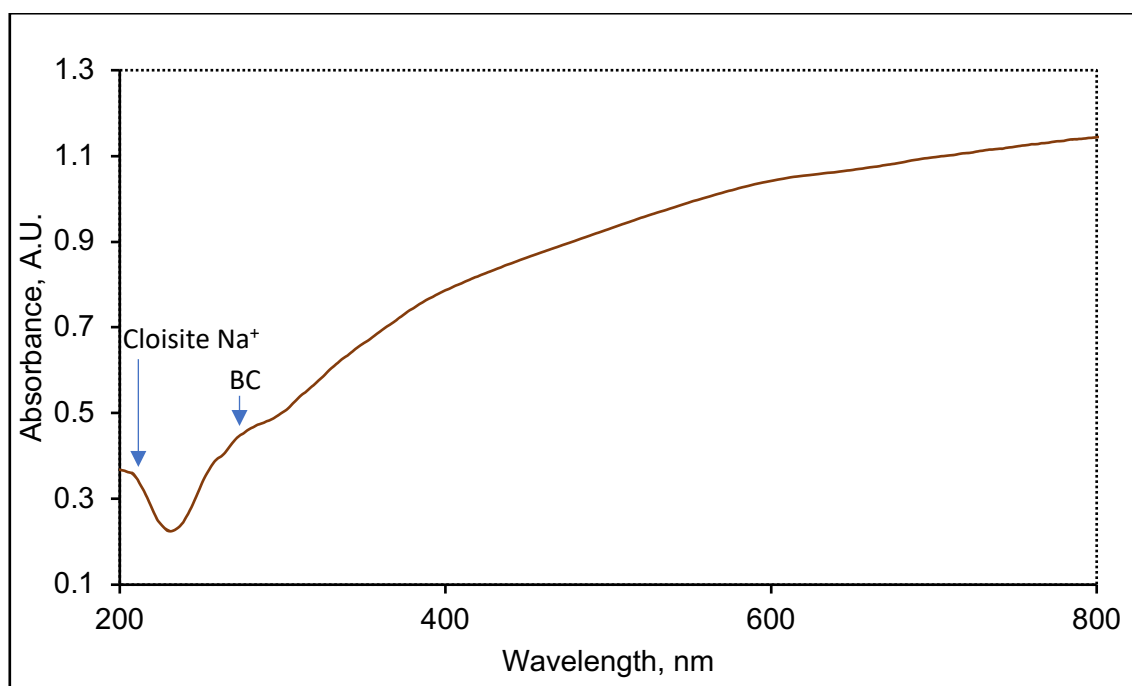


Figure 150. UV-Vis spectrum of BC/CH/Genipin/Cloisite Na⁺ composite.

Fig. 151 shows NIR spectrum of BC/CH/Genipin/Cloisite Na⁺ composite. As seen in Fig. 151, the peak of 1912-1950 nm corresponded to BC. The broad peak around 1400-1500 nm might be due to the presence of both chitosan and clay. Therefore, the presence of clay and chitosan might be detected inside the final structure of BC/CH/Cloisite Na⁺ composite in NIR spectra.

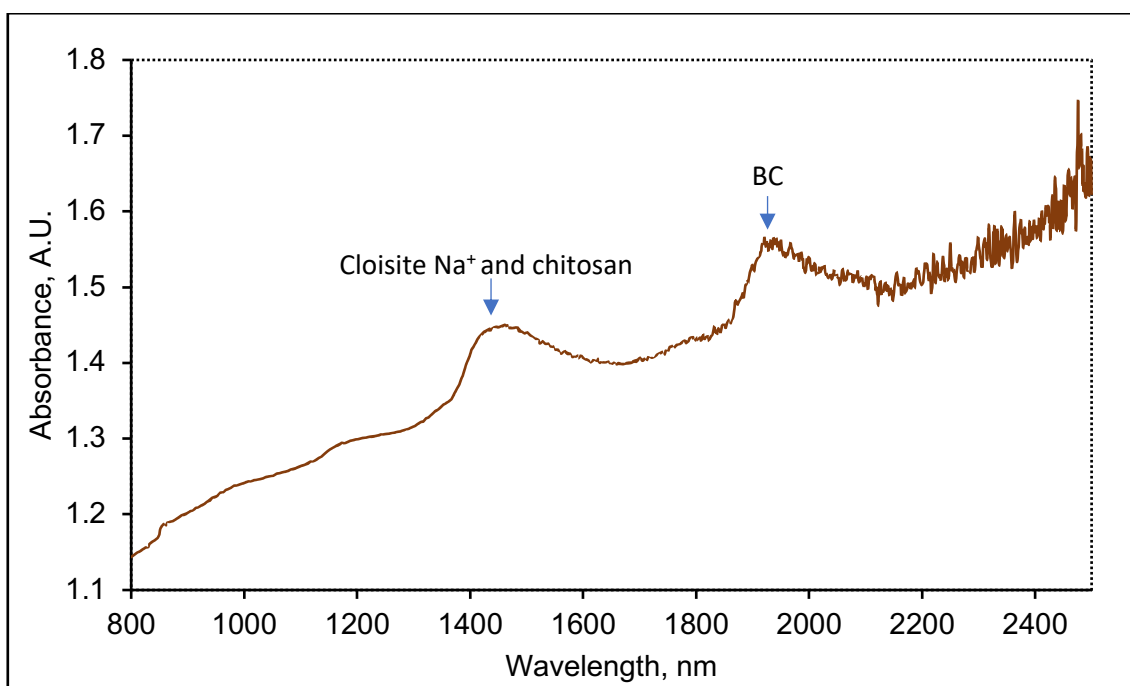


Figure 151. NIR spectrum of BC/CH/Genipin/Cloisite Na⁺ composite.

7.1.5. Antibacterial activity of BC/CH hybrid and BC/CH/Cloisite Na⁺ composite

Antibacterial properties of synthesised BC/CH hybrid and BC/CH/Cloisite Na⁺ composites were investigated against MRSA, *E. coli* and *P. aeruginosa*, respectively, with the results shown in Figs. 152-154. The control represented PBS-resuspended bacteria, which was inoculated on the surface of an empty petri dish without agar and covered with a sterile plastic lid as described in Section 2.7.3. In order to investigate the possible antibacterial activity of vinegar and genipin, each of the solutions was pumped through pure BC.

As shown in Fig. 152, the highest number of MRSA was observed with pure BC, where the growth of the bacteria reached 194% of control values. Both BC/Vinegar and BC/Genipin increased the bacterial growth to 103% and 116% of control values, respectively. It means that neither vinegar nor genipin was toxic

to MRSA. BC/CH hybrid reduced the growth of MRSA to 9% of control values, whereas BC/CH/Cloisite Na⁺ composite showed a reduction to 0.001%.

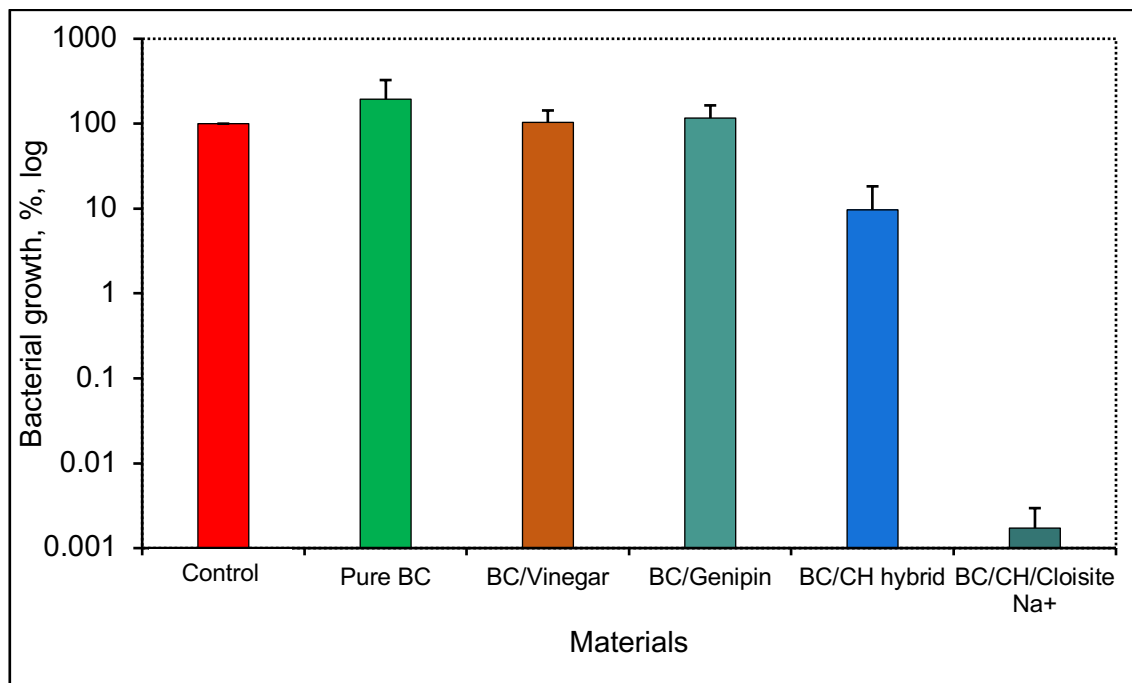


Figure 152. Antibacterial activity of synthesised BC/CH hybrid and BC/CH/Cloisite Na⁺ composite against MRSA. The control represented PBS-resuspended MRSA that was inoculated on the surface of the empty petri dish without agar and covered with a lid. Data shown present the mean of three independent experiments with error bars of standard deviation. BC/CH hybrid and BC/CH/Cloisite Na⁺ are different from the control (P -value <0.001).

As shown in Fig. 153, pure BC, BC/Vinegar and BC/Genipin increased the growth of *E. coli* to 131%, 102% and 136% of control values, respectively. This means that vinegar and genipin were not responsible for the reduction of growth obtained from the hybrid and the composite. BC/CH/Cloisite Na⁺ composite was more effective than BC/CH hybrid and reduced the growth of *E. coli* to 0.5% of control values. BC/CH hybrid decrease the bacterial growth to 50% of control values, which indicated that hybrid was more effective against Gram-positive MRSA than Gram-negative *E. coli*.

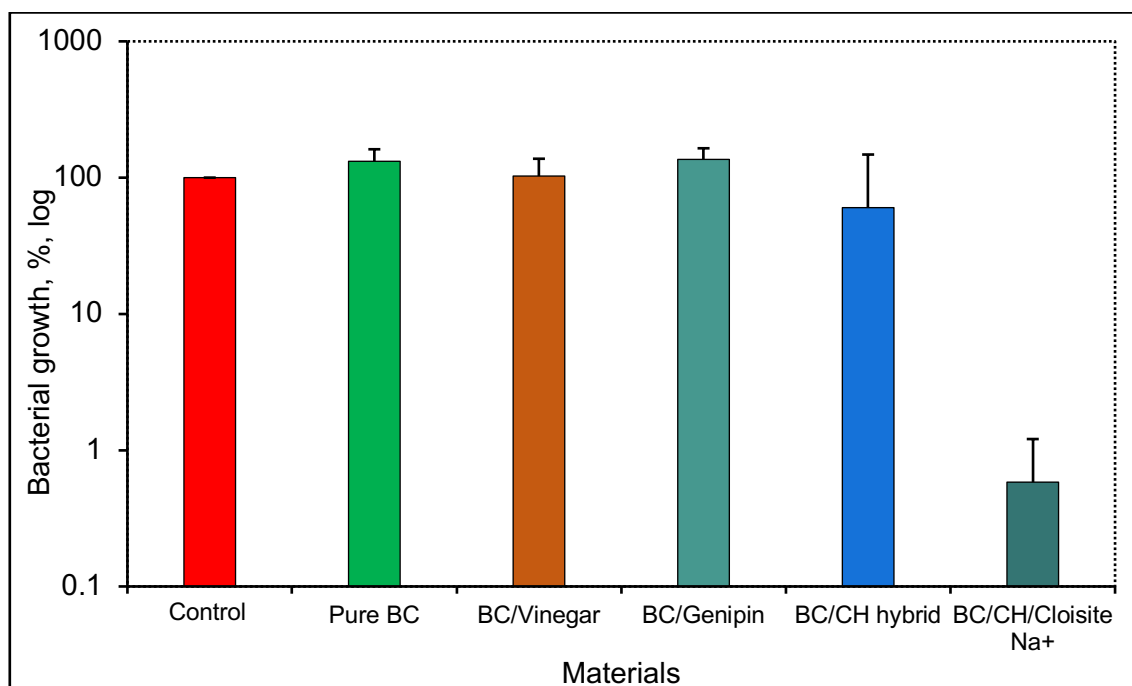


Figure 153. Antibacterial activity of synthesised BC/CH hybrid and BC/CH/ Cloisite Na⁺ composite against *E. coli*. The control represented PBS-resuspended *E. coli* that was inoculated on the surface of the empty petri dish without agar and covered with a lid. Data shown present the mean of three independent experiments with error bars of standard deviation. BC/CH/Cloisite Na⁺ is different compared to the control (P -value<0.001).

Regarding *P. aeruginosa*, BC/CH/Cloisite Na⁺ composite slightly reduced the growth of the bacteria to 93% of control values, whereas BC/CH hybrid promoted the growth of *P. aeruginosa* compared to control values (Fig. 154). The highest level of bacterial growth was observed using BC/Vinegar (299%). Pure BC and BC/Genipin promoted the bacterial growth and increased it to 132% and 108% of control values, respectively.

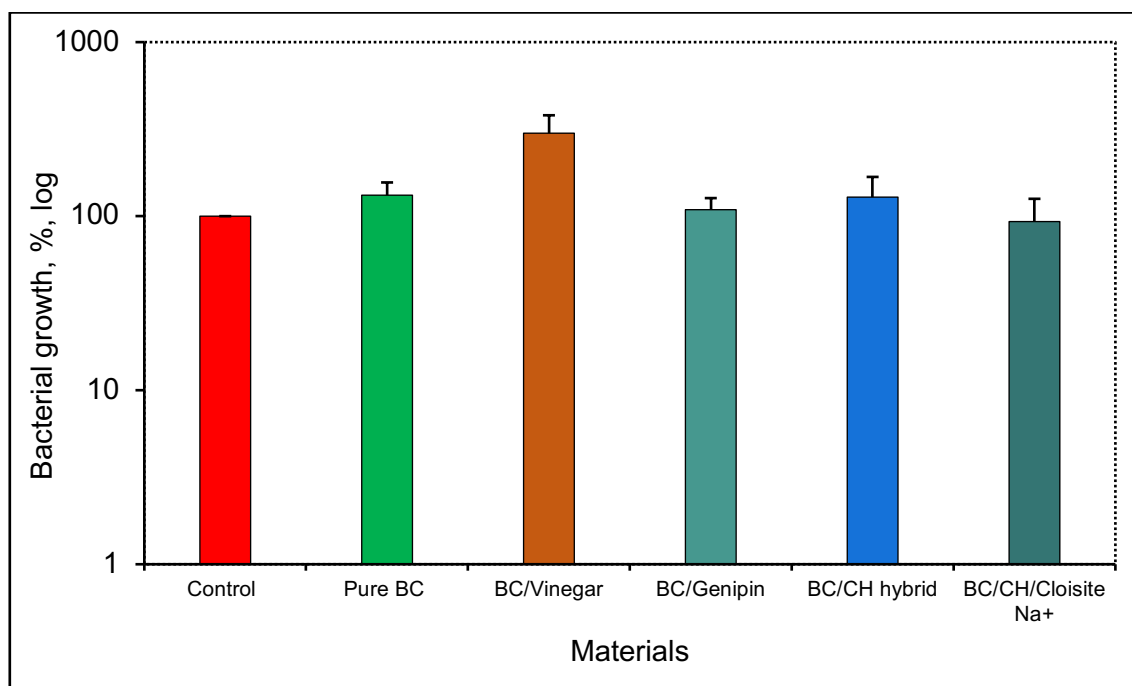


Figure 154. Antibacterial activity of synthesised BC/CH hybrid and BC/CH/Cloisite Na⁺ composite against *P. aeruginosa*. The control represented PBS-resuspended *P. aeruginosa* that was inoculated on the surface of the empty petri dish without agar and covered with a lid. Data shown represent the mean of three independent experiments with error bars of standard deviation. BC/Vinegar is different to the control (P -value<0.05).

7.2. Discussion

7.2.1. Cross-linking of chitosan by genipin

Chitosan can be cross-linked using ionic cross-linkers such as sulphates and phosphates. The cross-linking of chitosan could be achieved by the formation of chemical bridges between reactive amine groups of a polymer chain^[302]. However, a synthesised hydrogel might possess limited stability due to the nature of its chemical bonds, which are based on relatively weak interactions such as dipole–dipole, electrostatic and hydrophobic interactions^[302]. Alternatively, covalent cross-linkers such as formaldehyde and glutaraldehyde could produce hydrogels with stable chemical and physical characteristics^[302]. For instance,

glutaraldehyde is a chemical cross-linking agent that covalently reacts with primary amine groups. The final hydrogel possesses resistance to crush, solubility and the efficacy of metallic cation absorption^[303]. However, glutaraldehyde could exhibit cytotoxicity to mammalian cells^[303].

It has been reported that genipin, which is a natural extract from *Gardenia lasminoides ellis* fruit showed reduced toxicity towards mammals compared to glutaraldehyde and formaldehyde^[302, 303]. Genipin could react with chitosan through a Schiff base reaction leading to the formation of a polymeric network (Fig. 144). A molecule of genipin cross-links two chains of chitosan and, subsequently, creates both a tertiary amine and a mono-substituted amide^[304]. Genipin attacks the primary amine groups on the olefinic carbon atom at C3^[304]. Then, the dihydropyran ring opens followed by a formation of the secondary amine group^[304]. Subsequently, amine groups of chitosan get attacked by the carboxyl group of genipin followed by the formation of amide^[304]. This last reaction could be a relatively slow.

The oxygen radical-induced polymerisation of genipin can occur between genipin molecules that are already linked to amine groups of chitosan. During the polymerisation, the hydrogel has both low cross-linking degree and a low number of covalent bonds^[305]. This means that the hydrogel has a long length of chitosan chains between the links and, therefore, less force is required to deform the hydrogel. As the number of the cross-links increases, the network is tightened, which could lead to a stiffer hydrogel^[305]. Furthermore, a fragile membrane occurs if the degree of cross-linking is low, whereas a high degree of cross-linking leads to an excessively long period of degradation and reduced hydrolysis^[41, 305, 308]. It has been reported that cross-linking degree of hydrogels increases when increasing the concentration of genipin^[305]. For example, it has been stated that the degree of cross-linking using 0.05, 0.10, 0.15 and 0.20 wt.% of genipin was 30%, 32%, 42% and 40, respectively^[311]. The degree of cross-linking could also depend on pH values. For example, it has been reported elsewhere that the

degree of crosslinking of chitosan/genipin was 39.9%, 96%, 45% and 1.4% at pH5, pH 7.4, pH9 and pH13, respectively^[303].

Chitosan is soluble in acidic aqueous solutions that are lower than pH6^[306]. Therefore, an acidic environment can negatively affect chitosan-based hydrogels. In an acidic environment, the links between chitosan and genipin are short, whereas, at alkaline pH, links are long^[306]. At the neutral pH, the cross-linking degree is the highest, whereas the swelling behaviour is the lowest^[306]. The swelling behaviour of a hydrogel occurs at pH values lower than pH3 and higher than pH11 followed by a hydrolysis of amide linkages^[306]. This may lead to a regeneration of amine groups and carboxyl acid in the hydrogel network^[306]. It has been reported elsewhere that formation of the hydrogel can be influenced by DDA of chitosan, as effective formation was observed with a low DDA^[307].

Furthermore, it has been found that CH/Genipin hydrogels show the highest swelling behaviour at pH1 and pH2. This is due to the protonation of amine groups in the chains of chitosan that depend on the pH of the environment^[304]. The number of protonated amine groups might increase by decreasing the pH values of an external solution. At pH1, all amine groups are protonated, which results in a fully charged network^[302]. Protonation of amine groups could also lead to both extension and repulsion of a chain. This may increase the amount of water that enters the polymeric network. An increase in pH of the external solution leads to a decrease in the number of protonated amine groups^[309, 310]. This means that ionic contribution to the swelling capacity decreases. A hydrogel shows negative swelling values at pH6-11^[302].

7.2.2. Antibacterial activity of BC/chitosan hybrid gels

BC/CH and BC/CH/Cloisite Na⁺ were more effective against Gram-positive MRSA than Gram-negative *E. coli* and *P. aeruginosa*. This might be due to the presence of an outer membrane in Gram-negative bacteria, which makes it difficult to inhibit. BC/CH/Cloisite Na⁺ showed stronger antibacterial activity than

BC/CH hybrid. A possible reason why could be that the cross-linking reaction that made the amine groups hidden and ineffective. It has been reported that genipin can decrease the number of residual amine groups^[300]. However, the stronger antibacterial activity of the hybrid was obtained after introducing Cloisite Na⁺ clay. Some amine groups might attach to the negatively charged surface of the clay and not participate in the cross-linking reaction. This could have resulted in the expansion of free movement of the intercalated amine groups. This might lead to enhanced antibacterial properties.

7.2.3. Mammalian toxicity of genipin

Genipin does not possess any cytotoxicity against mammalian cells^[304, 308, 311]. It has been reported that no difference was observed in the proliferation of either hMSCs (human mesenchymal stem cells) or MG63 (human immortalized osteosarcoma) *in vitro* using genipin^[308]. Moreover, L929 fibroblasts have shown good viability on the surfaces of crosslinked CH/Genipin hydrogels (88.4%–90.9%) and chitosan films (92.8%) after 48 hours^[304]. It has been observed elsewhere that the viability of TSA cells was not significantly affected by the presence of 0.20 wt.% of genipin^[311]. In addition, it has also been observed that a degree of cross-linking of 36% of the genipin-gelatin hydrogel can ensure nerve regeneration by developing perineural and epineural organisations, whereas 24% and 51% cross-linking might cause irritation and compression of nerves by the remaining tube walls^[304]. BC/CH/Cloisite Na⁺ composite, which showed the high antibacterial activity against Gram-positive MRSA and Gram-negative *E. coli* was not toxic to mammalian cells and might be a potential material for wound healing applications.

Chapter 8. Kombucha cellulose as an alternative to the conventional BC

The use of Kombucha cellulose (KC) as an alternative to the conventional BC was investigated. KC was synthesised by the isolated microorganisms (IM) obtained from symbiotic culture of bacteria and yeast (SCOBY) on both small and large scales using either glucose or WA chitosan as the main carbon source. Exfoliated Cloisite Na⁺ and SWN clay were *in situ* incorporated into KC, respectively, during the formation. The synthesised KC/Clay, KC/Chitosan and KC/Chitosan/Clay composites were analysed by UV-VIS-NIR spectroscopy. The antibacterial activity of synthesised composites was investigated against MRSA, *E. coli* and *P. aeruginosa*, respectively.

8.1. Results**8.1.1. Optimisation of growing conditions of KC on a small scale**

The optimal conditions for cultivation of KC were investigated on a small scale. The synthesis of KC started with isolation of microorganisms from SCOBY as described in Section 2.8. The SCOBY contained a symbiotic culture of acetic acid bacteria including species of genera of *Gluconacetobacter* and *Acetobacter*, lactic bacteria and yeasts in unknown proportions. The effect of different concentration of IM on the formation of KC was analysed. As the main broth for the cultivation of Kombucha was found to be sugared tea^[312], black tea containing 2 wt.% of glucose was used as the tea broth for inoculation of IM.

The tea broth was adjusted to pH5 and 3.8 RIU (optical reflective unit) of optical reflective index prior to the inoculation. The volume of 100 µl of PBS diluted IM was added to the tea broth, where IM was ranging from 0.1 to 2 OD₆₀₀, and incubated subsequently for 48 hours at 25°C. The mass of wet KC produced by IM at concentration ranging from 0.1 to 2 OD₆₀₀ was measured with the results shown in Fig. 155.

According to Fig. 155, the mass of wet KC was greater for 2 OD₆₀₀ and corresponded to 0.24 grams, whereas the mass of KC decreased to 0.18 and 0.12 grams using 1 and 0.1 OD₆₀₀, respectively.

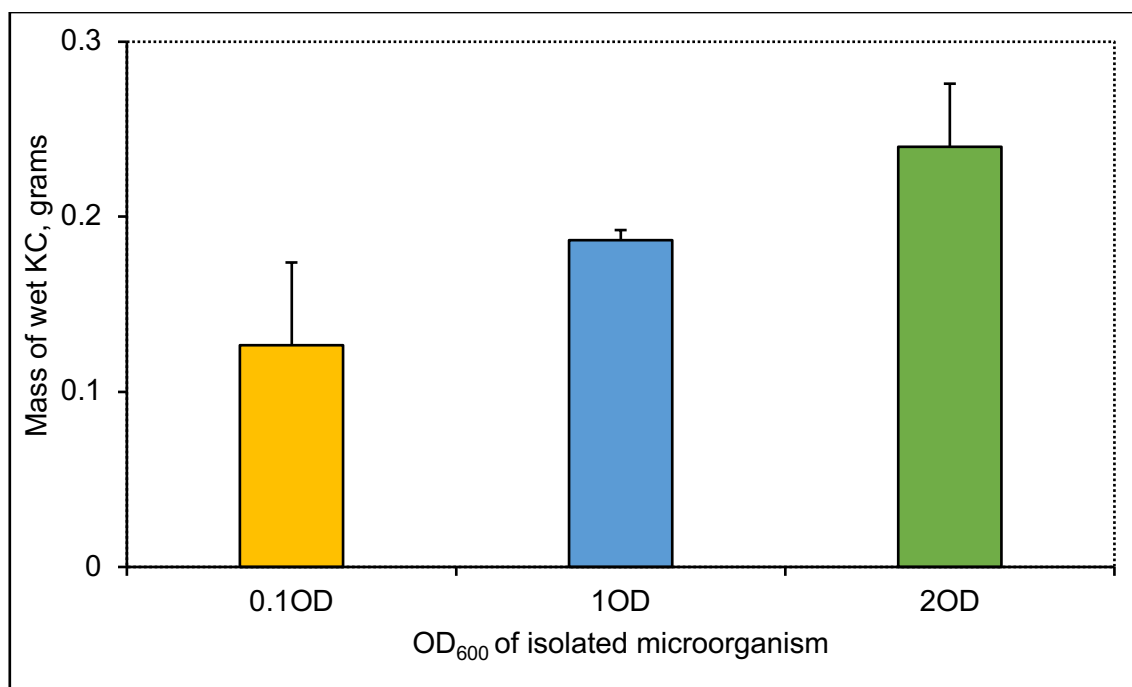


Figure 155. The effect of IM density ranging on the mass of wet KC after 48 hours. KC was produced on a small scale using 2 wt.% of glucose solution and inoculum ranging from 0.1 to 2 OD₆₀₀ at 25°C for 48 hours. Data shown represent the mean of three independent experiments with error bars of standard deviation. OD of 0.1 was compared to either 1 OD or 2 OD. Mass obtained at 2 OD is significantly different in comparison with 1 OD (P -value<0.05).

Therefore, the concentration of PBS-resuspended IM was chosen to be 2 OD₆₀₀. The effect of temperature on KC growth was investigated as detailed in Section 2.8.3. Fig. 156 shows the mass of wet KC formed at 25°C, 30°C and 37°C using 2 OD₆₀₀ concentration of IM after 48 hours. As shown in Fig. 156, the most effective temperature for KC growth was 25°C with the mass reaching 0.23 grams. The mass of wet KC decreased to 0.8 grams at 30°C, whereas no cellulose was detected at 37°C. The 25°C temperature was chosen for further incubation.

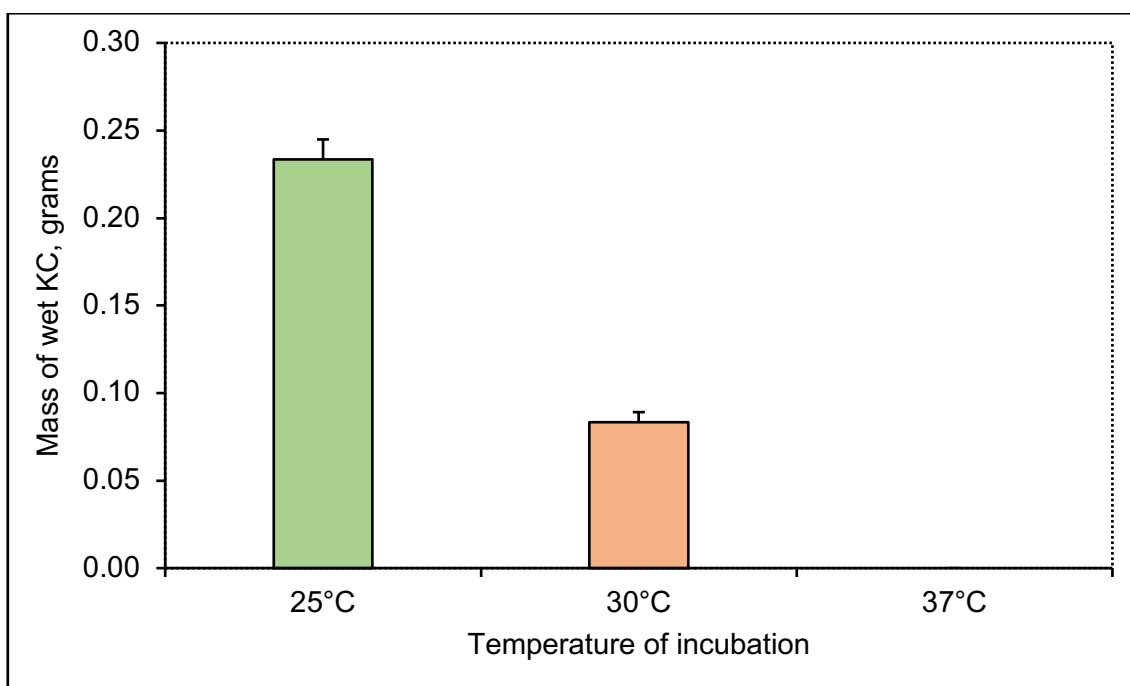


Figure 156. The mass of wet KC produced at 25°C, 30°C and 37°C temperature. KC was produced on a small scale using 2 OD₆₀₀ concentration of IM and incubated for 48 hours. Data shown represent the mean of three independent experiments with error bars of standard deviation. The data obtained at 25°C are significantly different from 30°C (P -value<0.001).

The effect of pH on the formation of KC was investigated with the results shown in Fig. 157. As seen in Fig. 157, the most effective pH for KC growth was pH4, which corresponded to the mass of 0.7 grams. KC produced at pH3 and pH2 was 0.62 and 0.6 grams, respectively. The mass of wet KC decreased to 0.23 and 0.24 grams at pH6 and pH5, respectively. There was no cellulose observed at pH1. Therefore, the chosen pH for inoculation of KC was pH4.

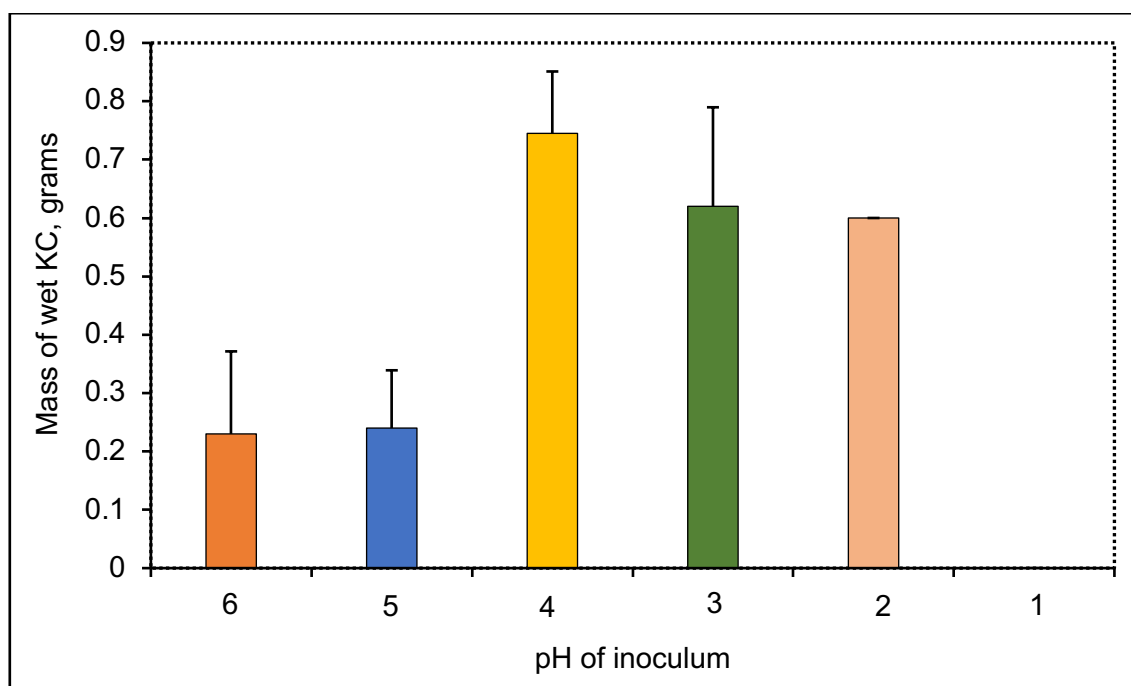


Figure 157. The effect of pH on KC growth. KC was produced using 2 OD₆₀₀ of IM source at pH ranging from pH6 to pH1 at 25°C for 48 hours. Data shown represent the mean of three independent experiments with error bars of standard deviation. Mass produced at pH4 was compared to mass synthesised at other pH values. The data obtained at pH5 and pH6 are significantly different from pH4 (P -value < 0.001).

The effect of tea concentration on the formation of KC was investigated. The stock of the tea broth was diluted using sterilised distilled water. The control represented the inoculum containing 100% of the non-diluted tea broth. The volume of the tea was reduced from 100% to 0%, where the tea broth was completely replaced with distilled water. The pH of tea was adjusted to pH4 using sterile 0.1M HCl. Fig. 158 shows the mass of wet KC synthesised using different concentrations of the tea broth at pH4 with 2 OD₆₀₀ of IM source at 25°C after 48 hours. According to Fig. 158, the mass of wet KC was the heaviest with 75% of the tea broth and reached 0.24 grams. The mass of wet KC produced with 100% of the tea broth was 0.21 grams. The mass of wet KC was continuously decreasing with reducing the concentration of tea. KC was formed without tea, but the cellulose was not robust and hardly weighable. The mass of synthesised KC without tea was approximately 0.02 grams. This means that the formation of

KC might depend on the tea environment. The concentration of the tea broth was chosen to be 75% for further experiments.

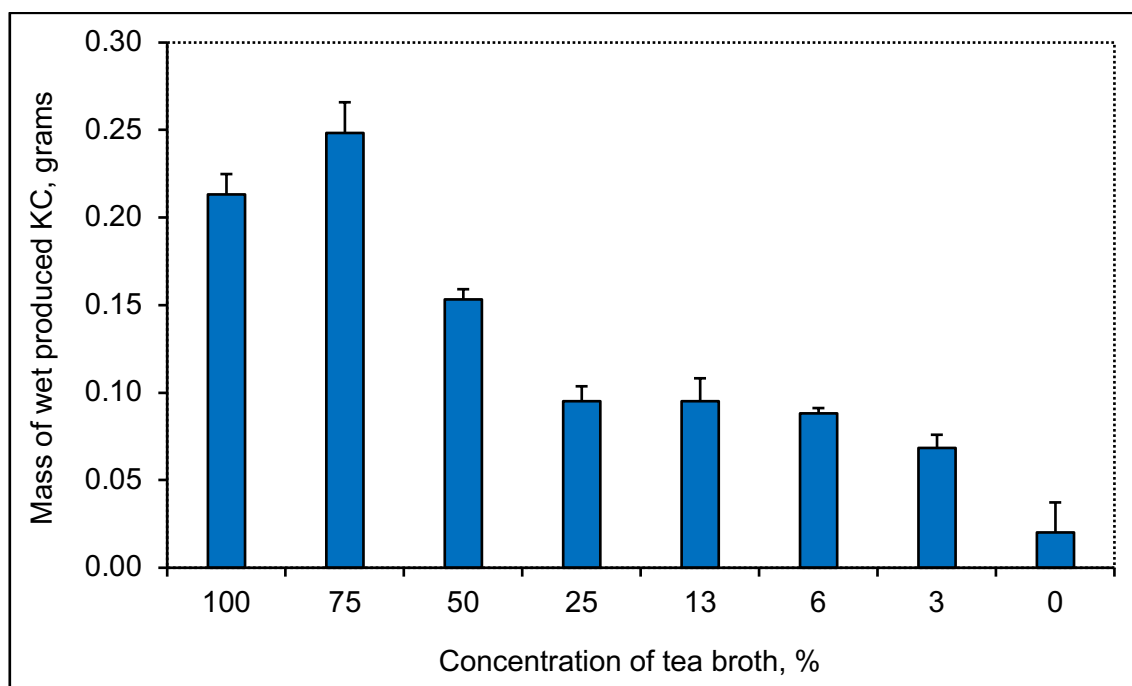


Figure 158. The effect of the concentration of tea broth the mass of wet KC. KC was produced at pH4 using 2 OD₆₀₀ of IM source at 25°C for 48 hours. Data shown represent the mean of three independent experiments with error bars of standard deviation. The control (100% broth) was compared to other broth concentrations. The data obtained using 50%, 25%, 6%, 3% and 0% concentrations are significantly different from 100% (P -value <0.05 for 50% and <0.01 for 25-0%).

The parameters for the synthesis of KC were optimised on a small scale. The chosen concentration of IM was 2 OD₆₀₀. The incubation of PBS-resuspended IM was carried out using 75% of the tea broth adjusted to pH4 at 25°C temperature for 48 hours for further experiments.

8.1.2. Synthesis of KC on a large scale involving glucose

After optimisation of KC growing conditions on a small scale, KC was synthesised on a large scale as described in Section 2.9.2. Fig. 159 shows the synthesised

KC using the optimised parameters such as 75% of tea broth adjusted to pH4 and containing 2 wt.% of glucose as the main carbon source with 2 OD₆₀₀ of IM incubated at 25°C for 48 hours. As seen in Fig. 159, it was possible to produce KC on a large scale. KC was robust enough for further experiments after 48 hours.

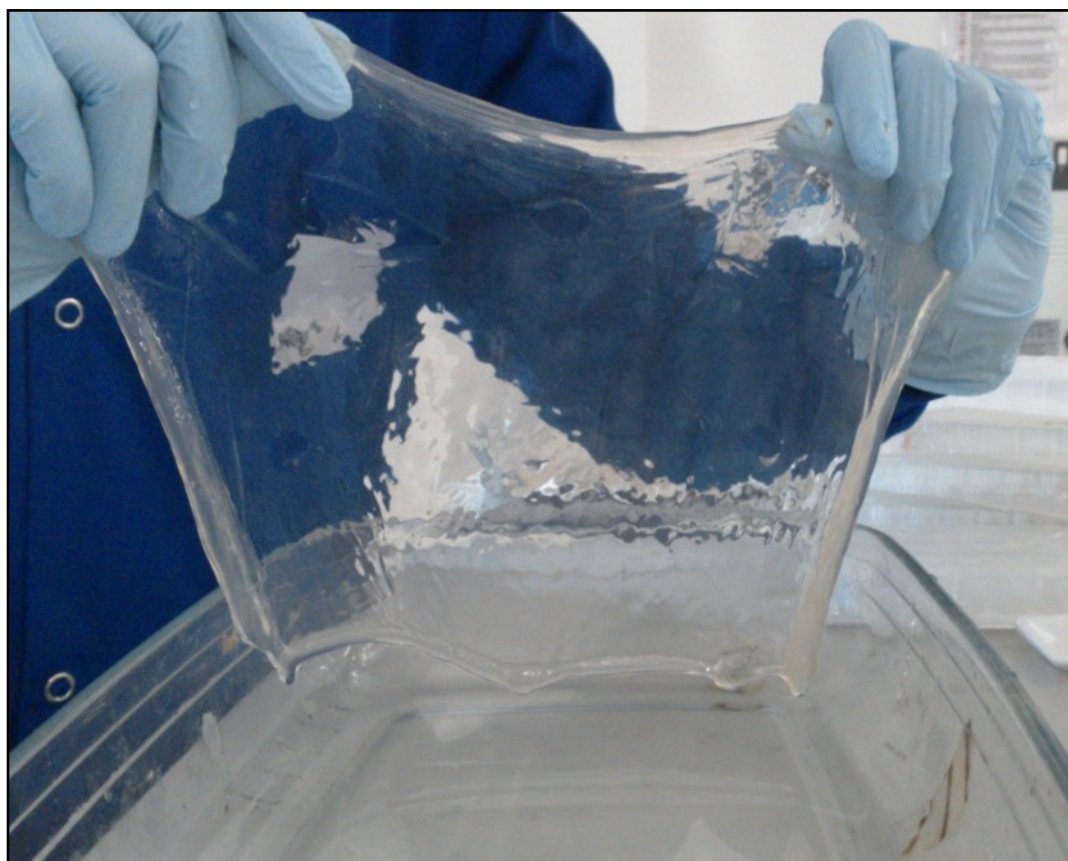


Figure 159. Image of KC produced. KC was inoculated using 75% tea broth at pH4 containing 2 wt.% of glucose as the main carbon source with 2 OD₆₀₀ of IM concentration and incubated at 25°C for 48 hours.

Fig. 160a shows the SEM image of KC produced on a large scale, which was synthesised using all optimised parameters. As seen in Fig. 160a, KC had a porous matrix similar to the conventional BC (Fig. 160b), but the orientation of fibres of KC was more random compare to the pure BC.

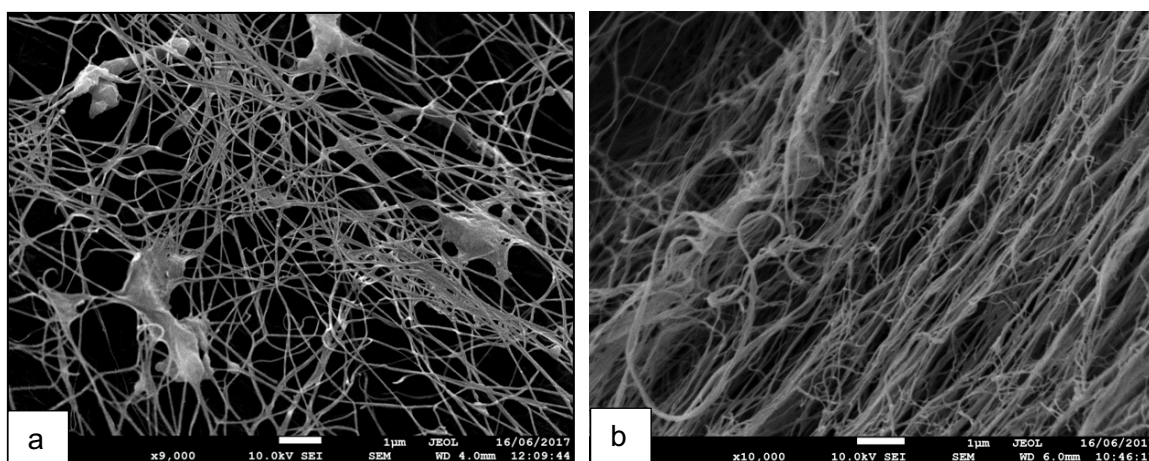


Figure 160. SEM image of KC (a) and pure BC (b) produced on a large scale, respectively. The bars represent a distance in 1µm.

In order to investigate the dependence of the formation of KC on the tea environment on a large scale, 2 OD₆₀₀ of IM were inoculated in distilled water, which was adjusted pH4, using 2 wt.% glucose as the main carbon source and 2 OD₆₀₀ of IM concentration at 25°C for 48 hours (Fig. 161). As shown in Fig. 161, the mass of wet KC synthesised with distilled water was much lower than the mass of KC produced using 75% of the tea broth and corresponded to 19.87 grams. Whereas the mass of wet KC synthesised with 75% of black tea reached 56 grams. This agrees with the results obtained from the small scale experiment. It means that the formation of KC was dependent on the tea environment.

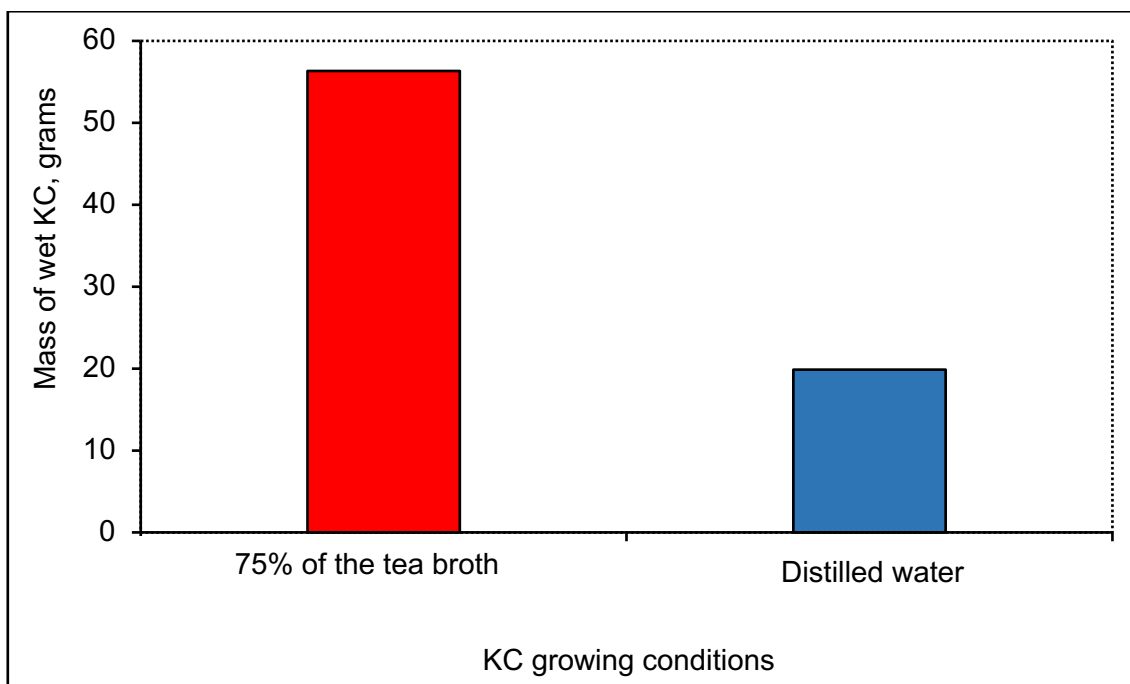


Figure 161. The mass of wet KC produced using either tea or distilled water. KC was produced using 75% of the tea broth and sterile distilled water, respectively, containing 2 wt.% of glucose as the main carbon source and 2 OD₆₀₀ of IM concentration at 25°C for 48 hours. Data shown represent the mean of a single experiment.

8.1.3. *In situ* incorporation of clay into KC on a small scale

The possibility of *in situ* incorporation of clay into KC was firstly investigated on a small scale. Non-exfoliated and exfoliated by the Tefal blender Cloisite Na⁺ and SWN suspensions were added into the tea broth at the concentration of 3 mg/ml, respectively, prior to the incubation with IM as described in Section 2.9.1.

Fig. 162 shows the mass of wet KC produced with non-exfoliated and exfoliated Cloisite Na⁺ and SWN clay, respectively. The control represented pure KC produced without clay. According to Fig. 162, non-exfoliated SWN suspension has reduced the growth of KC, the wet mass of which was 0.7 grams. Whereas, the mass of wet KC produced with exfoliated SWN increased to 1.82 grams. The non-exfoliated and exfoliated Cloisite Na⁺ increased the mass of KC to 1.48 and 2.53 grams, respectively.

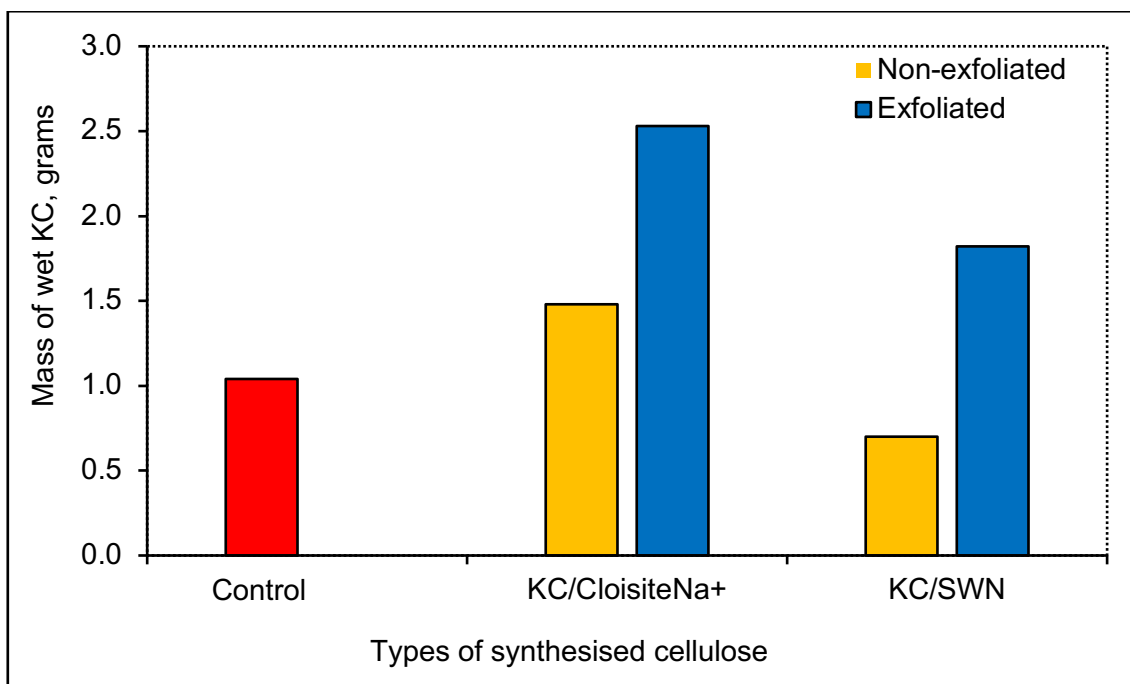


Figure 162. The effect of non-exfoliated and exfoliated Cloisite Na⁺ and SWN clay suspensions on a mass of KC. KC was produced using clay suspensions at the concentration of 3 mg/ml, respectively, and 2 OD₆₀₀ PBS-resuspended IM with 75% the tea broth at pH4 and incubating at 25°C for 48 hours on a small scale. The control was pure KC produced without clay. Data shown represent the mean of a single experiment.

8.1.4. *In situ* incorporation of clay into KC on a large scale

The synthesis of KC/Clay composites was obtained on a large scale. Fig. 163 shows images of KC/Exfoliated Cloisite Na⁺ (a) and KC/Exfoliated SWN (b) composites.

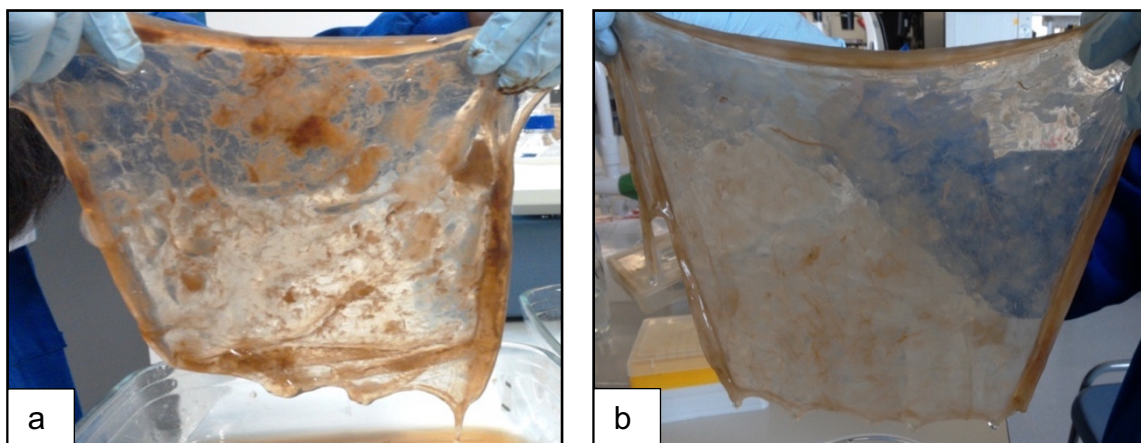


Figure 163. Images of KC/Exfoliated Cloisite Na⁺ (a) and KC/Exfoliated SWN (b) composites. The composites were produced using 2 OD₆₀₀ PBS-resuspended IM incubated with 75% of the tea broth containing 3 mg/ml of each exfoliated clay suspension adjusted subsequently to pH4 for 48 hours at 25°C on a large scale.

The effect of exfoliation of the clay on the mass of KC was investigated on a large scale with the results shown in Fig. 164. As seen in Fig. 164, the mass of both KC/Exfoliated Cloisite Na⁺ and KC/Exfoliated SWN increased from 56 grams of pure KC to 65% and 82%, respectively. This might indicate successful incorporation of the clay inside KC. The mass of wet KC/Non-exfoliated Cloisite Na⁺ was 43 grams. However, KC/Non-exfoliated SWN composite reached 80 grams after 48 hours.

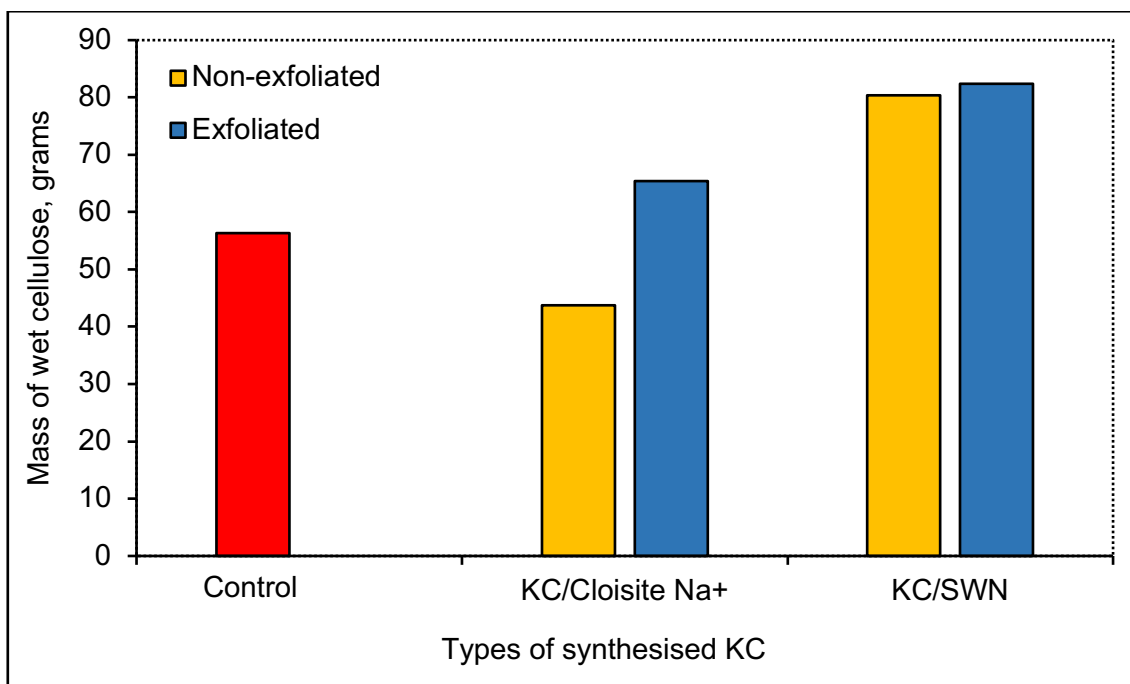


Figure 164. The effect of non-exfoliated and exfoliated Cloisite Na⁺ and SWN clay suspensions on a mass of wet KC. KC was produced using clays at the concentration of 3 mg/ml, respectively, and 2 OD₆₀₀ PBS-resuspended IM and 75% the tea broth at pH4 and incubating at 25°C for 48 hours on a large scale. The control was pure KC produced without clay. Data shown represent the mean of a single experiment.

8.1.4.1. UV-VIS-NIR analysis of synthesised KC/Clay composites

KC/Cloisite Na⁺ and KC/SWN composites, which were produced with exfoliated clay, were analysed using UV-VIS-NIR spectroscopy with the results shown in Figs. 165-166. According to Fig. 165, KC/SWN composites had predominantly KC pattern. The presence of the clay at 211 nm wavelength was not detected in the composites. However, KC/SWN composite showed the peak for SWN at around 1167 nm in NIR region. In addition, UV-VIS spectrum of pure KC was similar to pure BC that was shown in Fig. 56. According to Figs. 57 and 165, pure KC had an additional peak at 1472 nm, which was not detected inside pure BC.

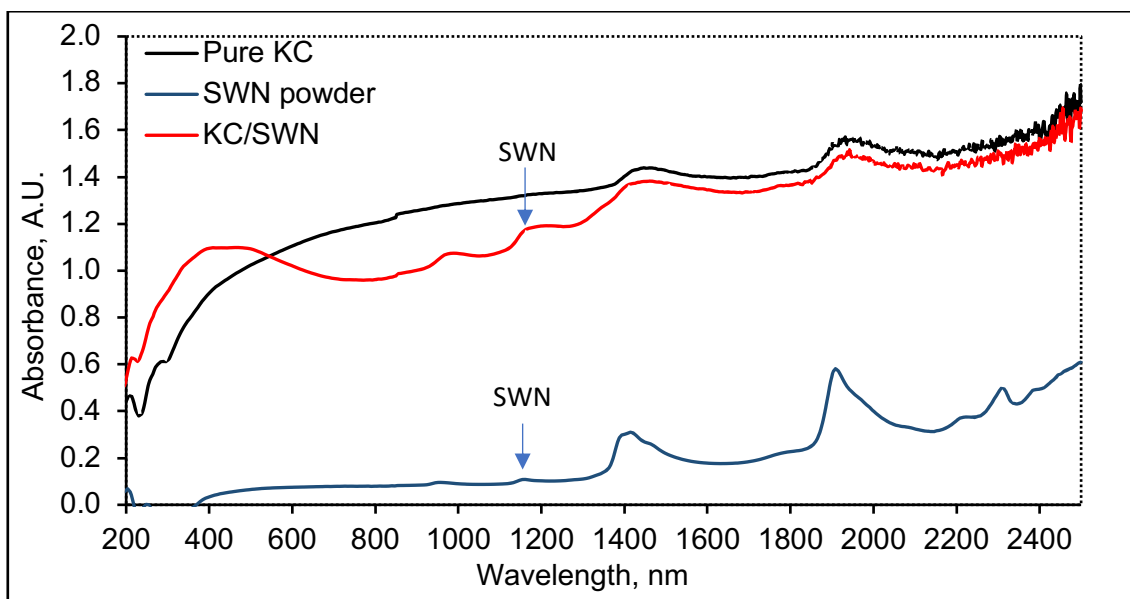


Figure 165. UV-VIS-NIR spectra of pure KC, SWN powder and KC/SWN composite.

According to Fig. 166, KC/Cloisite Na⁺ composites had predominantly KC pattern with a broad peak around 1400 nm, which might indicate both KC and the clay. The clay might be present inside KC, but due to reflective operation of the equipment, such characteristic peaks of the clay were not detected.

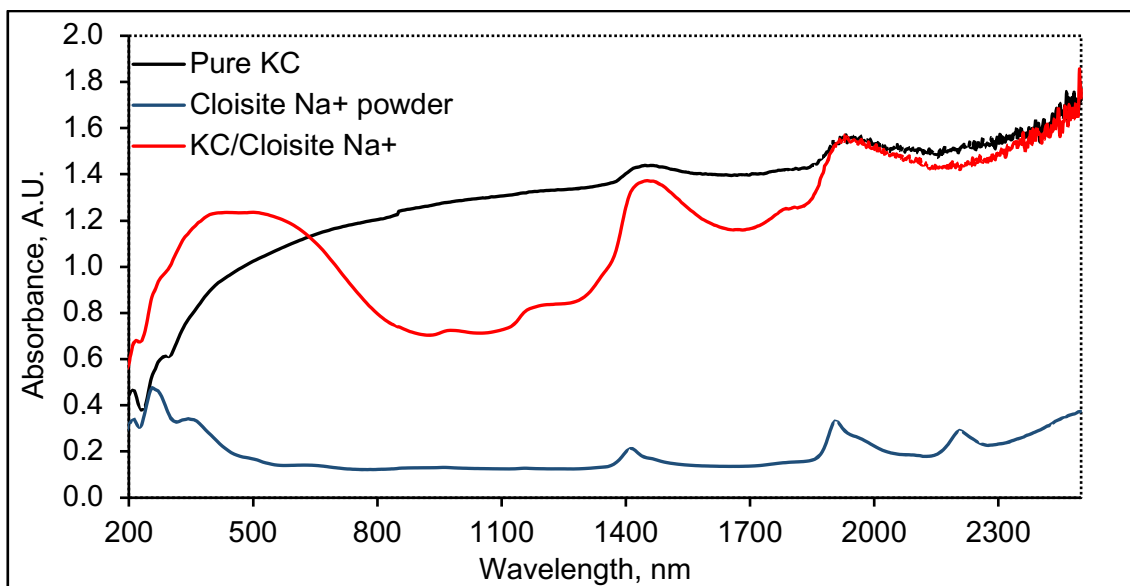


Figure 166. UV-VIS-NIR spectra of pure KC, Cloisite Na⁺ powder and KC/Cloisite Na⁺ composite.

8.1.4.2. Antibacterial activity of synthesised KC/Clay composites

Antibacterial properties of KC/Cloisite Na⁺ and KC/SWN composites prepared using the exfoliated by the Tefal blender clay suspensions were tested against MRSA, *E. coli* and *P. aeruginosa*, respectively, as described in Section 2.9.3. The control represented PBS-resuspended bacteria without any treatment that was placed on the surface of the empty petri dish without agar and covered with a sterile lid. Fig. 167 shows antibacterial activity of the composites against MRSA. As seen in Fig. 167, pure KC increased the growth of MRSA to 227% of control values, whereas KC/Cloisite Na⁺ and KC/SWN composites reduced the control values to 2% and 3%, respectively. This means that pure KC can promote the growth of the bacteria in a similar fashion to pure BC. The results indicated that clay was successfully incorporated inside the matrix of KC.

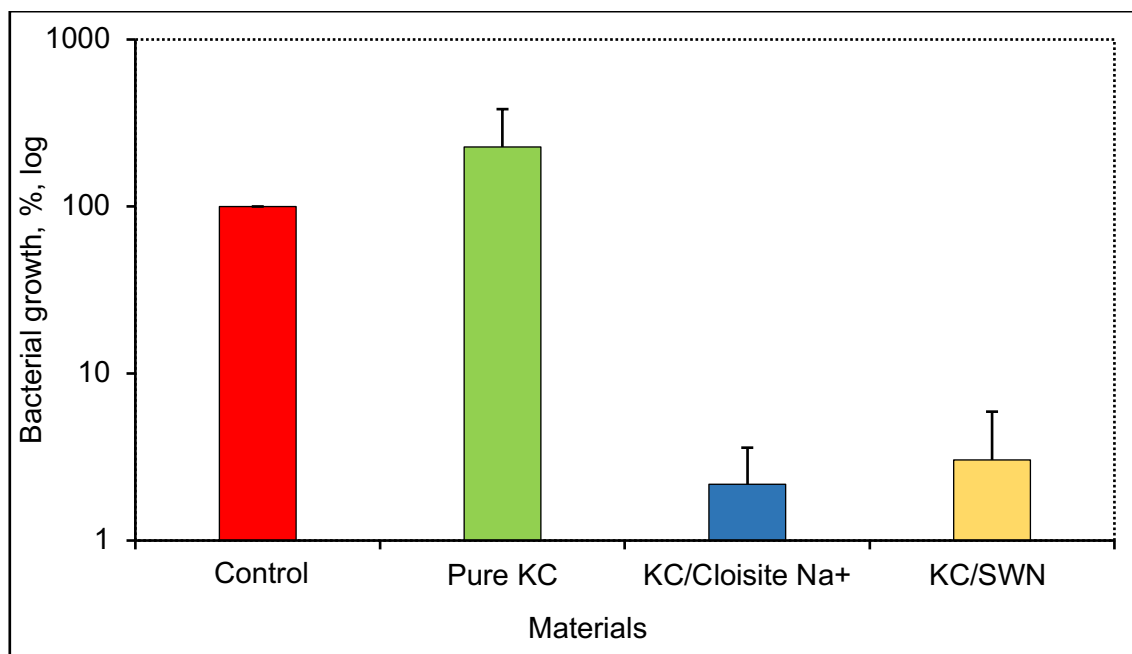


Figure 167. Antibacterial activity of pure KC, KC/Cloisite Na⁺ and KC/SWN composites against MRSA. The control represented PBS-resuspended MRSA that was inoculated on the surface of the empty petri dish without agar and covered with a lid. Bacteria were incubated with treatments for 24 hours at 37°C. Data shown represent the mean of three independent experiments with error bars of standard deviation. The treatments were

compared to the control. Pure KC and KC/Cloisite Na⁺ and KC/SWN are significantly different from the control with *P*-values <0.05, <0.01 and <0.01, respectively.

Antibacterial activity of synthesised KC/Clay composites against *E. coli* is shown in Fig. 168. KC/SWN was more effective than KC/Cloisite Na⁺ and reduced the growth of bacteria to 48% of control values. KC/Cloisite Na⁺ decreased the growth of *E. coli* to 55% of control values. Pure KC slightly increased the bacterial growth to 106% of control values.

The antibacterial activity of KC/Cloisite Na⁺ and KC/SWN composites were weaker compare to the *in situ* synthesised BC/Cloisite Na⁺ and BC/SWN composites, which reduced the growth of *E. coli* to 14.6% and 16.8% of control values, respectively, as shown in Fig. 65. This might be due to not complete penetration of clay particles inside KC during the formation.

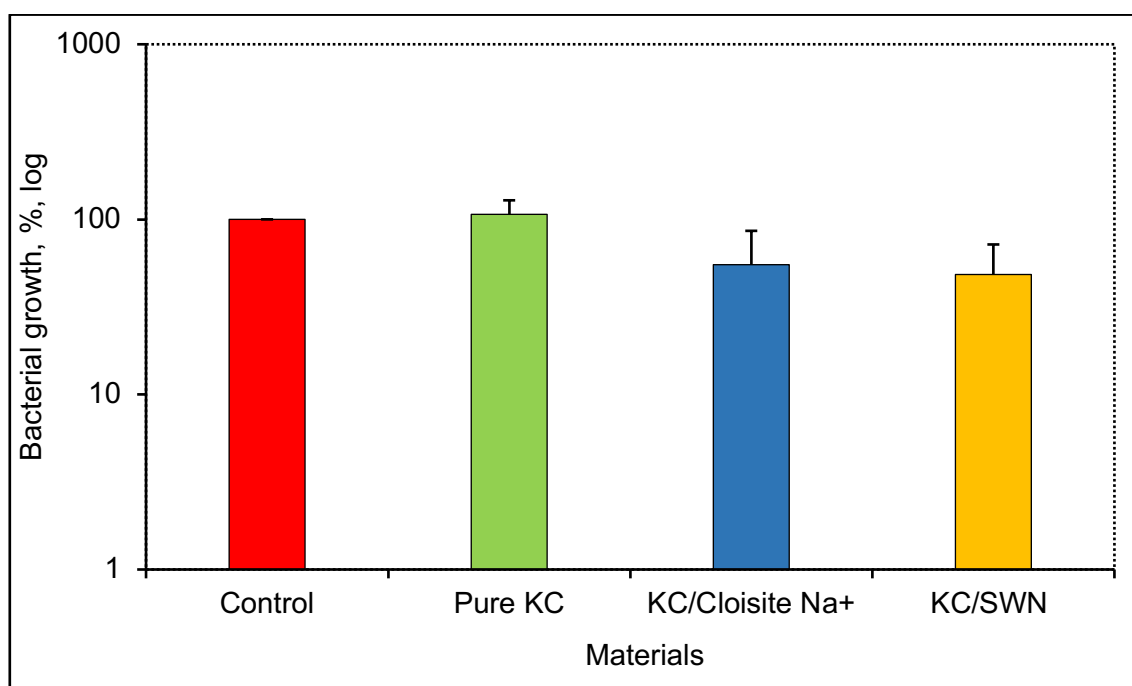


Figure 168. Antibacterial activity of pure KC, KC/Cloisite Na⁺ and KC/SWN composites against *E. coli*. The control represented PBS-resuspended *E. coli* that was inoculated on the surface of the empty petri dish without any treatment and covered with a lid. The data shown represent the mean of three independent experiments with error bars of standard

deviation. The treatments were compared to the control. KC/SWN is significantly different from the control (P -value <0.05).

Furthermore, synthesised KC/Clay composites did not show any antibacterial activity against *P. aeruginosa*. As seen in Fig. 169, all three types of tested KC materials promoted bacterial growth. Pure KC increased the growth of *P. aeruginosa* to 175% of control values. KC/Cloisite Na⁺ and KC/SWN composites raised the growth of *P. aeruginosa* to 172% and 113% of control values, respectively.

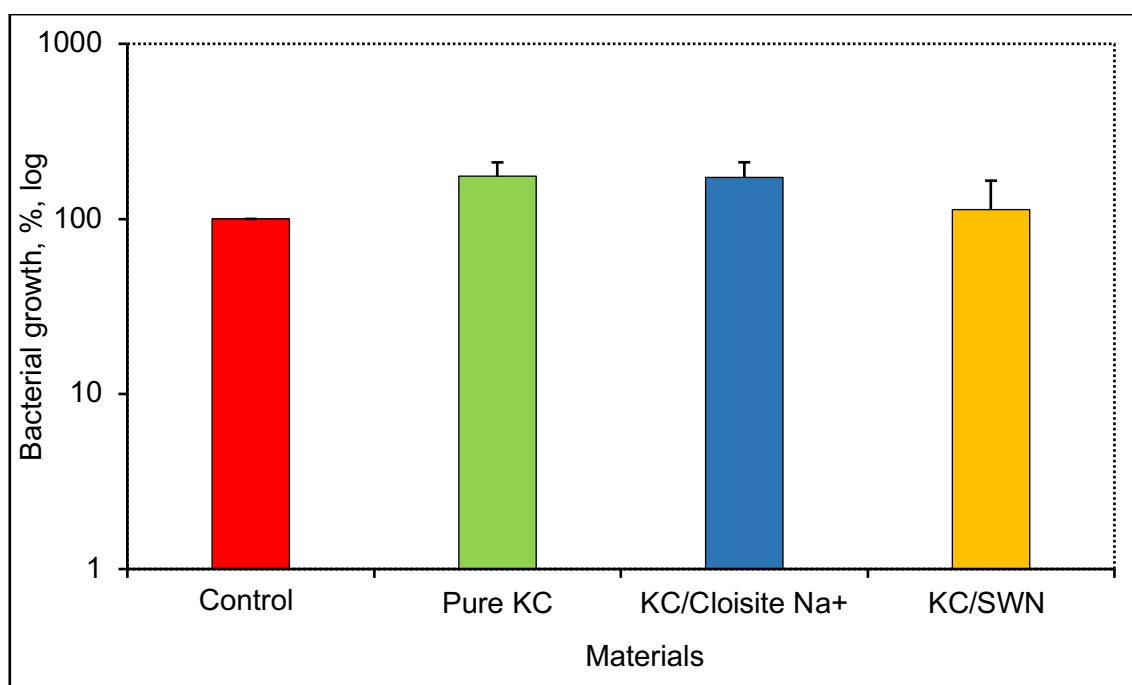


Figure 169. Antibacterial activity of pure KC, KC/Cloisite Na⁺ and KC/SWN composites against *P. aeruginosa*. The control represented PBS-resuspended *P. aeruginosa* that was inoculated on the surface of the empty petri dish without any treatment and covered with a lid. Bacteria were incubated with treatments for 24 hours at 37°C. Data shown represent the mean of three independent experiments with error bars of standard deviation. The treatments were compared to the control. Pure KC and KC/Cloisite Na⁺ are significantly different from the control (P -value <0.05).

KC/Cloisite Na⁺ and KC/SWN composites showed stronger antibacterial activity against Gram-positive MRSA than Gram-negative *E. coli* and *P. aeruginosa*. This might be due to the presence of outer cell wall in Gram-negative bacteria, which made it difficult to inhibit.

8.1.5. *In situ* synthesis of KC/Chitosan using chitosan as the main carbon source on a large scale

Another method of *in situ* synthesis of KC was based on the complete replacement of the main carbon source. Glucose was replaced with 0.5 wt.% of WA chitosan solution, which was prepared using 10 vol.% of distilled vinegar at pH3. IM at concentration of 2 OD₆₀₀ were incubated in the either modified tea broth or distilled water for 48 hours at 25°C. Then, KC/Chitosan was characterised using UV-VIS-NIR spectroscopy. The antibacterial activity of the material was investigated against MRSA, *E. coli* and *P. aeruginosa*, respectively. Fig. 170 shows the image of the produced KC/Chitosan.

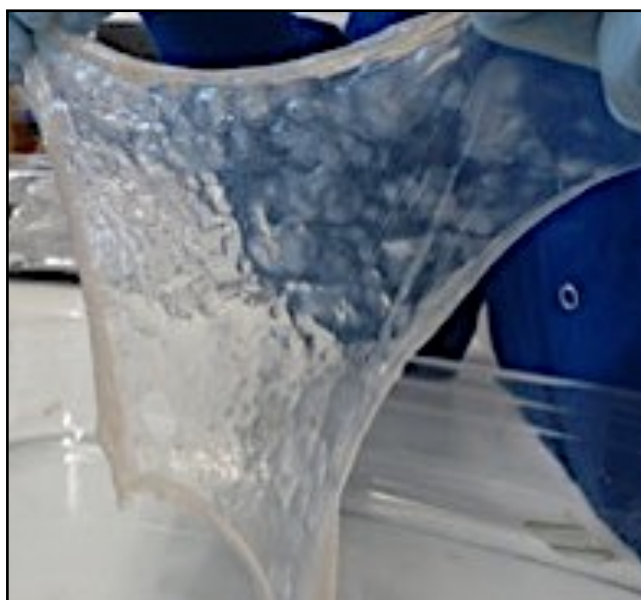


Figure 170. Image of the produced KC/Chitosan using tea. The composite was produced using 75% of the tea broth at pH4 containing 0.5 wt.% of WA chitosan as the main carbon source and 2 OD₆₀₀ of IM concentration at 25°C for 48 hours on a large scale.

KC/Chitosan was then synthesised using sterile distilled water containing 0.5 wt.% of WA chitosan solution as the main carbon source with 2 OD₆₀₀ of IM concentration for 48 hours at 25°C (Fig. 171). As shown in Figs. 170-171, KC/Chitosan formed in distilled water was more robust compared to KC/Chitosan synthesised using the tea broth.

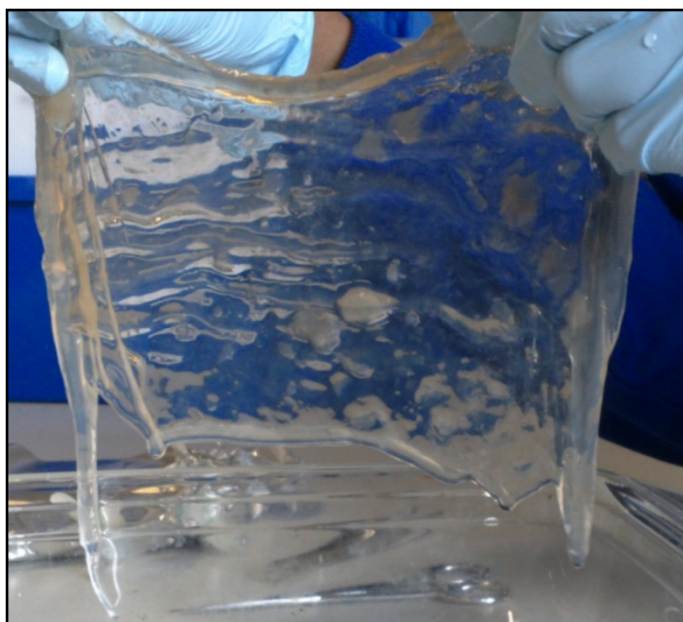


Figure 171. Image of the produced KC/Chitosan using sterile distilled water. KC/Chitosan was produced at pH4 containing 0.5 wt.% of WA chitosan as the main carbon source and 2 OD₆₀₀ of IM concentration at 25°C for 48 hours on a large scale.

The mass of wet KC/Chitosan produced with 75% of tea and sterile distilled water, respectively, is shown in Fig. 172. According to Fig. 172, KC/Chitosan synthesised with distilled water was heavier with the mass reached 42 grams, whereas the mass of wet KC/Chitosan produced with 75% of tea was 10.38 grams.

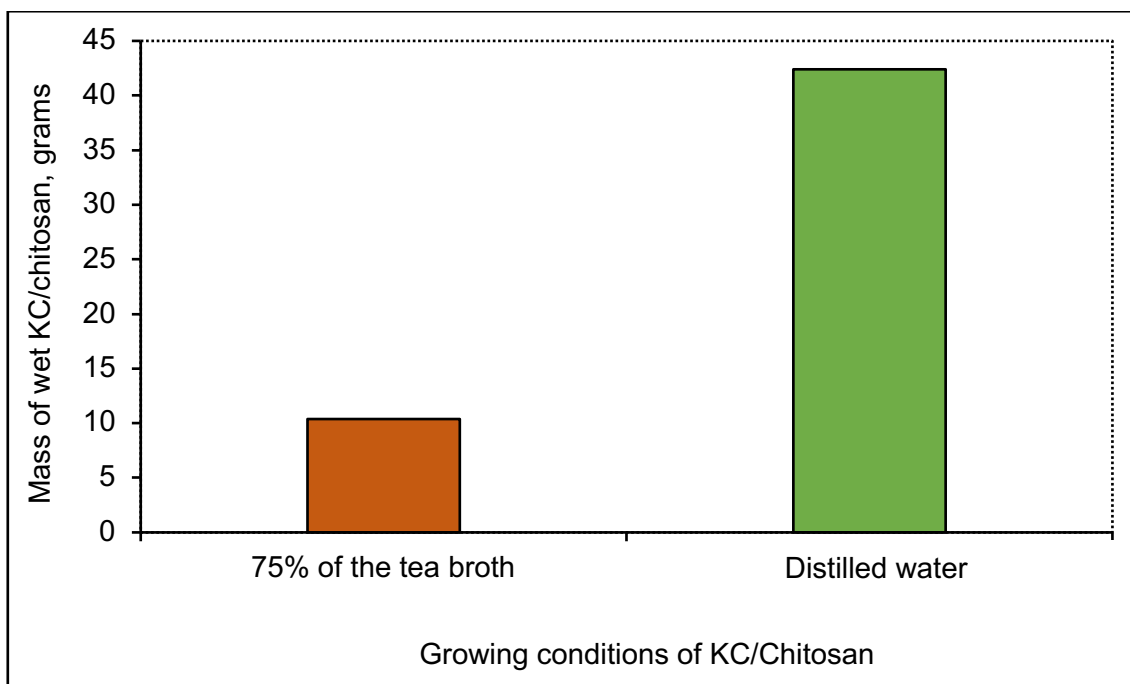


Figure 172. The mass of wet KC/Chitosan produced with either tea broth or distilled water. KC/Chitosan was produced with 75% of the tea broth and sterile distilled water, respectively, at pH4 using 0.5 wt.% WA chitosan as the main carbon source and 2 OD₆₀₀ of IM concentration at 25°C for 48 hours. Data shown represent the mean of a single experiment.

8.1.5.1. UV-VIS-NIR analysis of *in situ* synthesised KC/Chitosan

KC/Chitosan was analysed using UV-VIS-NIR spectroscopy in order to investigate the presence of chitosan. Fig. 173 shows UV-VIS-NIR spectra of pure KC, WA chitosan powder and KC/Chitosan. According to Fig. 173, KC/Chitosan showed a broad peak around 320-400 nm, which might correspond to characteristic peak of chitosan at 325 nm. The peak of chitosan around 1500 nm might overlap with the peak of KC, thus it was difficult to detect the presence of chitosan inside KC/Chitosan.

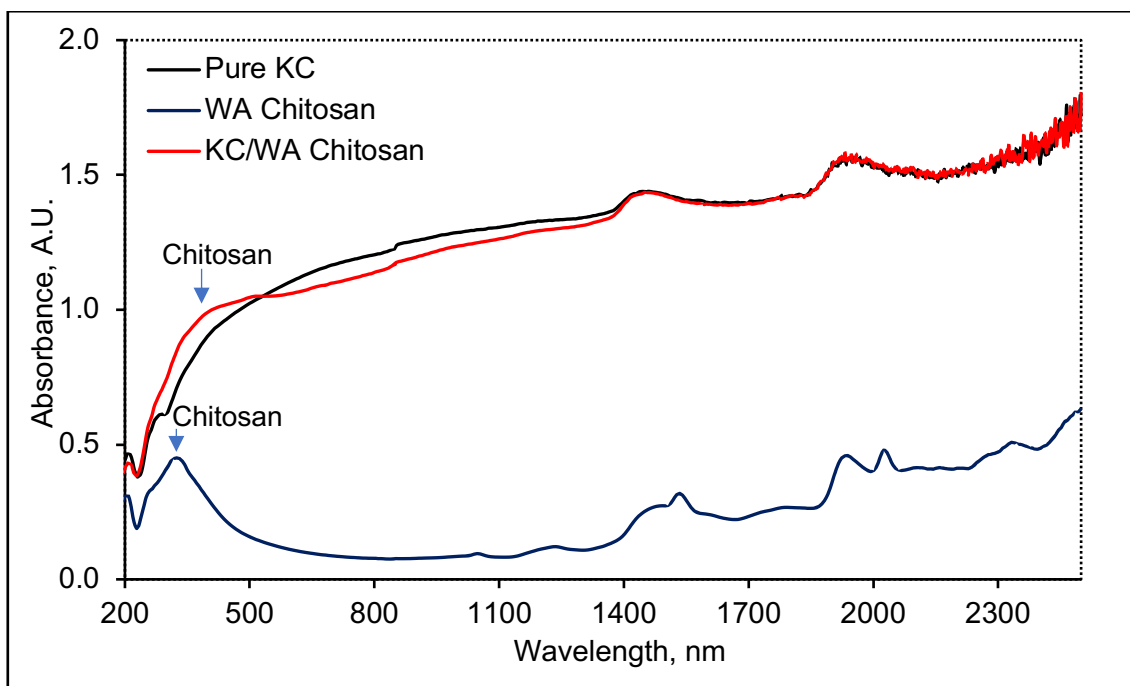


Figure 173. UV-VIS-NIR spectra of pure KC, WA chitosan powder and KC/WA chitosan composite.

8.1.6. Synthesis of KC/Chitosan/Clay composites

The synthesis of KC/Chitosan/Clay composites started on a small scale by adding 3 mg/ml of non-exfoliated and exfoliated Cloisite Na⁺ and SWN suspensions, respectively, into Kombucha inoculum along with 0.5 wt.% of WA chitosan as the main carbon source. Fig. 174 shows the effect of exfoliated and non-exfoliated clay on the mass of wet KC, respectively. As seen in Fig. 174, the mass of wet KC/Chitosan/Clay composites was increased with exfoliated clay suspensions. Wet KC/Chitosan/Exfoliated Cloisite Na⁺ composite had a mass of 2.38 grams, whereas the mass of KC/Chitosan was 1.2 grams. The mass of KC/Chitosan/Non-exfoliated Cloisite Na⁺ composite was 1.6 grams. As shown in Fig. 174, the mass of KC/Chitosan/Exfoliated SWN and KC/Chitosan/Non-exfoliated SWN composites was 1.77 and 0.79 grams, respectively.

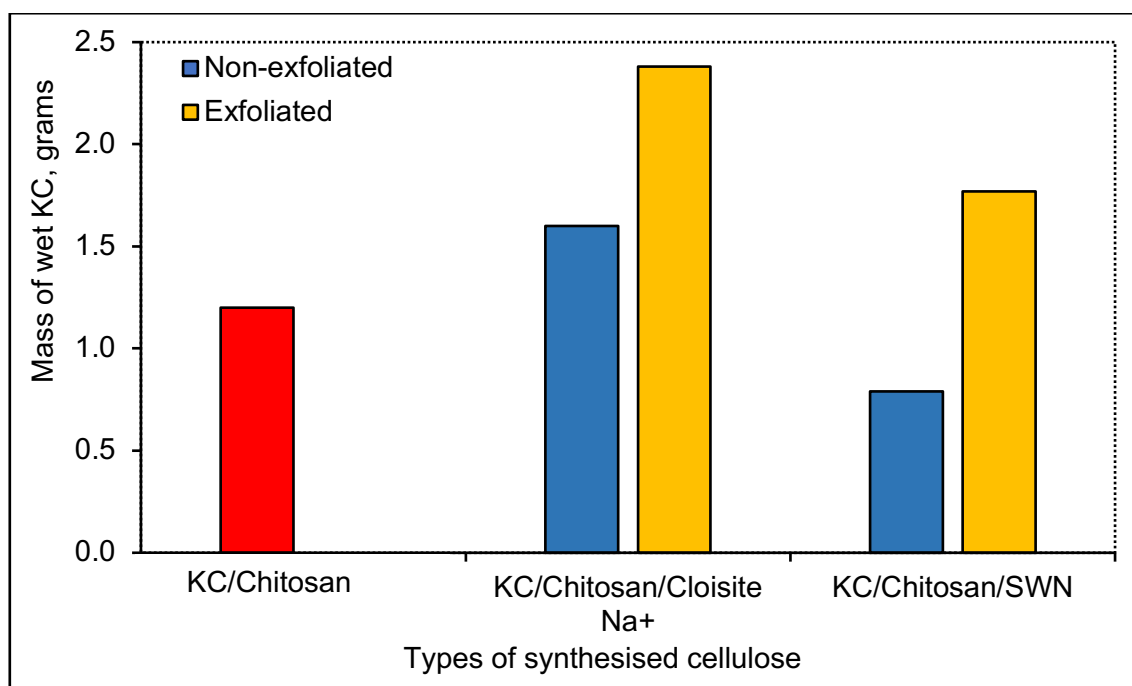


Figure 174. The mass of wet KC/Chitosan, KC/Chitosan/Cloisite Na⁺ and KC/Chitosan/SWN composites on a small scale. The composites were produced with non-exfoliated and exfoliated Cloisite Na⁺ and SWN clay suspensions at the concentration of 3 mg/ml, respectively, using 2 OD₆₀₀ PBS-resuspended IM, 75% the tea broth containing 0.5 wt.% of WA chitosan at pH4 and incubated at 25°C for 48 hours on a small scale. Data shown represent the mean of a single experiment.

The mass of KC/Chitosan/Clay composites using exfoliated and non-exfoliated clay suspensions, respectively, was obtained on a large scale (Fig. 175). As shown in Fig. 175, the mass of the wet KC/Chitosan/Clay composites was heavier than KC/Chitosan. The mass of wet KC/Chitosan/Non-exfoliated Cloisite Na⁺ and KC/Chitosan/Non-exfoliated SWN composites was 15.43 and 26.54 grams, respectively. The mass of KC/Chitosan/Clay composites produced with exfoliated clay suspensions was significantly higher and reached 25.46 grams with Cloisite Na⁺ and 36.57 grams with SWN, respectively. This might indicate that the incorporation of the clay was successfully achieved. As shown in Figs. 174-175, the exfoliation of the clay affected the formation of KC. Non-exfoliated state of the clay reduced the formation of the pellicle.

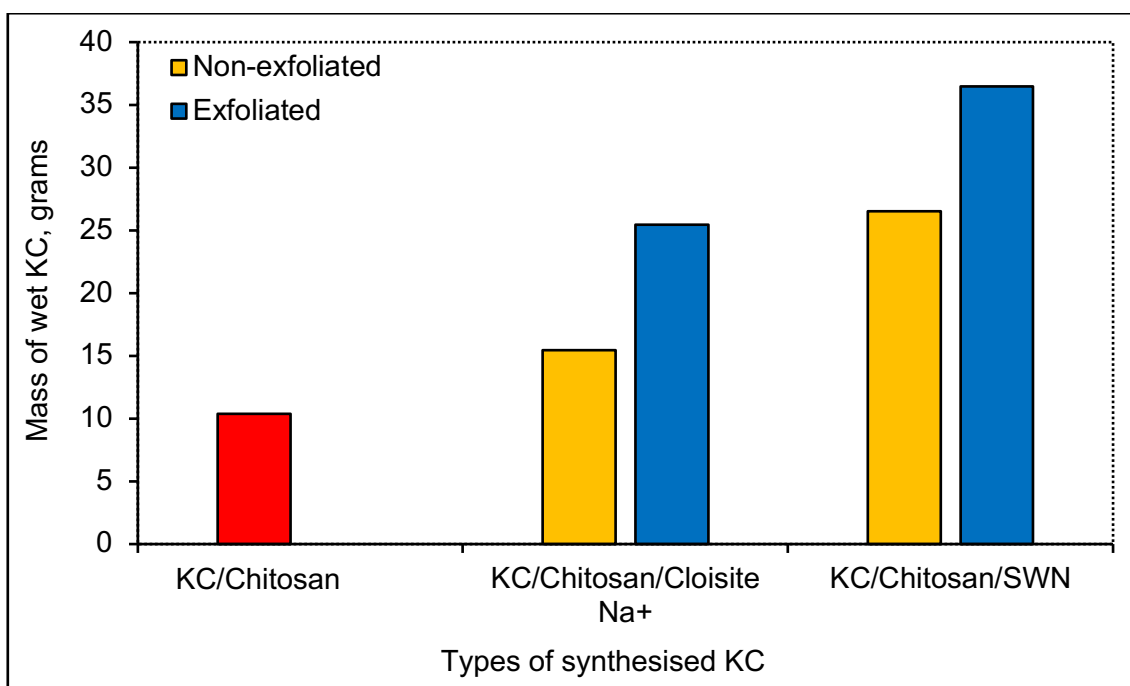


Figure 175. The mass of wet KC/Chitosan, KC/Chitosan/Cloisite Na⁺ and KC/Chitosan/SWN composites produced on a large scale. The composites with non-exfoliated and exfoliated Cloisite Na⁺ and SWN clay suspensions at the concentration of 3 mg/ml, respectively, using 2 OD₆₀₀ PBS-resuspended IM, 75% the tea broth containing 0.5 wt.% of WA chitosan at pH4 and incubated at 25°C for 48 hours on a large scale. Data shown present the mean of a single experiment.

8.1.7. Antibacterial activity of synthesised KC/Chitosan and KC/Chitosan/Clay composites

The antibacterial activity of KC/Chitosan, KC/Chitosan/Cloisite Na⁺ and KC/Chitosan/SWN composites prepared with exfoliated clay suspensions were investigated against MRSA, *E. coli* and *P. aeruginosa*, respectively, with the results shown in Figs. 176-179. As seen in Fig. 176, pure KC increased the growth of MRSA to 302% of control values, whereas KC/Chitosan decreased the growth of the bacteria to 53%. The growth of MRSA was reduced to 12.7% and 3.7% of control values by using KC/Chitosan/Cloisite Na⁺ and KC/Chitosan/SWN composites, respectively.

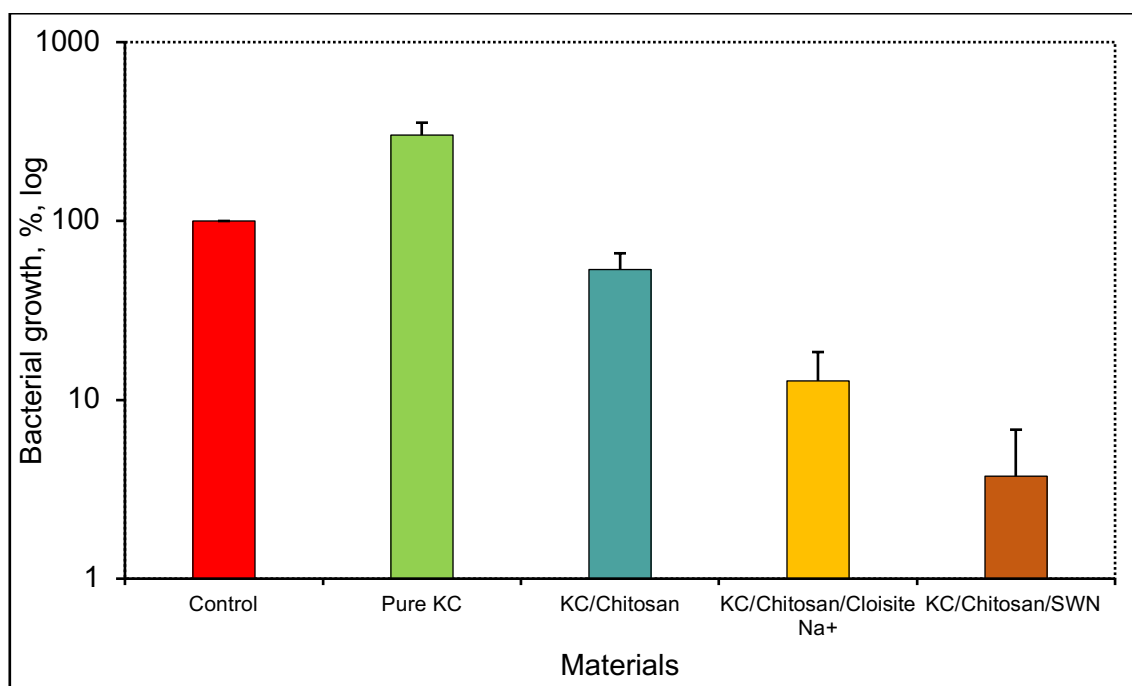


Figure 176. Antibacterial activity of synthesised pure KC, KC/Chitosan, KC/Cloisite Na⁺ and KC/SWN composites against MRSA. The control represented PBS-resuspended MRSA that was inoculated on the surface of the empty petri dish without any treatment and covered with a lid. Bacteria were incubated with treatments for 24 hours at 37°C. Data shown represent the mean of three independent experiments with error bars of standard deviation. The treatments were compared to the control. KC/Chitosan/Cloisite Na⁺ and KC/Chitosan/SWN are significantly different from the control (P -value<0.05).

Similarly, pure KC increased the growth of *E. coli* to 183% of control values (Fig. 177). KC/Chitosan reduced the growth of bacteria to 73% of control values. This indicated the presence of chitosan inside KC/Chitosan composite. Furthermore, KC/Chitosan/Cloisite Na⁺ and KC/Chitosan/SWN composites decreased the growth of *E. coli* to 54% and 46% of control values, respectively. This means that introducing exfoliated clay to already antibacterial material resulted in increased inhibition of bacterial growth.

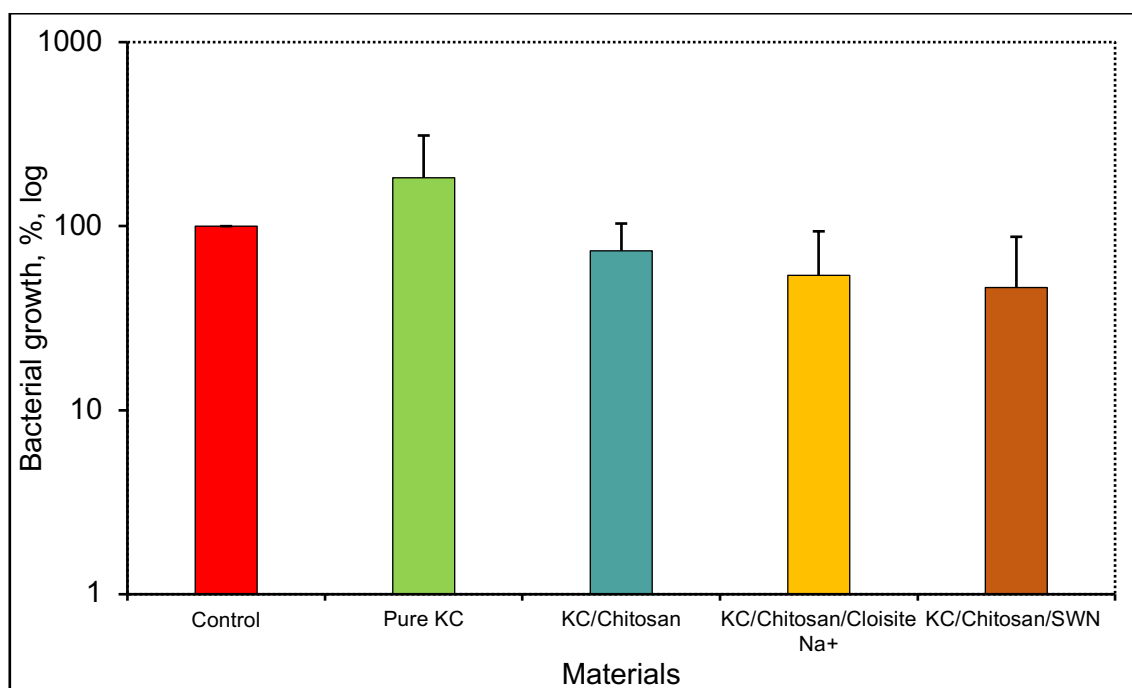


Figure 177. Antibacterial activity of synthesised pure KC, KC/Chitosan, KC/Cloisite Na⁺ and KC/SWN composites against *E. coli*. The control represented PBS-resuspended *E. coli* that was inoculated on the surface of the empty petri dish without agar and covered with a lid. Bacteria were incubated with treatments for 24 hours at 37°C. Data shown represent the mean of three independent experiments with error bars of standard deviation. The treatment outcomes are not significantly different in comparison with the control.

As shown in Fig. 178, only KC/Chitosan/Cloisite Na⁺ showed antibacterial activity against *P. aeruginosa*, the growth of which was reduced to 78% from control values. Pure KC, KC/Chitosan and KC/Chitosan/SWN increased the growth of *P. aeruginosa* to 175%, 125% and 160% of the control values, respectively.

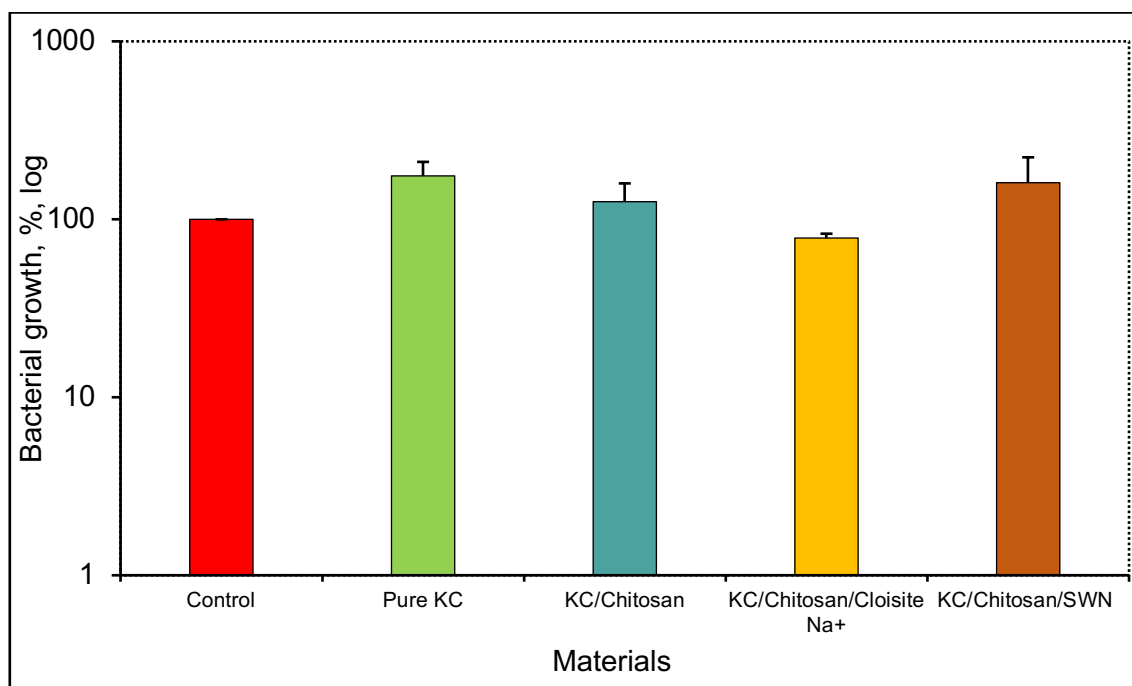


Figure 178. Antibacterial activity of synthesised pure KC, KC/Chitosan, KC/Cloisite Na⁺ and KC/SWN composites against *P. aeruginosa*. The control represented PBS-resuspended *P. aeruginosa* that was inoculated on the surface of the empty petri dish without agar and covered with a lid. Bacteria were incubated with treatments for 24 hours at 37°C. Data shown represent the mean of three independent experiments with error bars of standard deviation. Pure KC and KC/Chitosan/Cloisite Na⁺ are significantly different from the control (P -value<0.05).

8.2. Discussion

It was possible to synthesise KC using IM from the SCOBY. The parameters for the growth of KC were optimised on both small and large scales. The greater mass of wet KC at a higher optical density of IM might be due to a large number of bacteria, which were responsible for the formation of cellulose. It was possible to obtain KC just in 48 hours using 2 OD₆₀₀, whereas, according to the literature, the formation of the pellicle requires approximately 7 to 21 days by using SCOBY^[313]. This might be due to the novelty of the method used in the current research, where IM had direct contact with the tea broth. Therefore, the current

method of isolation of microorganisms might be beneficial for the synthesis of KC in a relatively short period of time.

It has been reported that 25°C was the ideal temperature for the synthesis of Kombucha^[312]. Similar to the formation of the conventional BC, the temperature above 37°C could lead to inhibition of the growth of acetic acid bacteria through the lack of bacterial replication due to the damaging of cell proteins^[217]. Furthermore, KC did not grow at pH1. The mass of KC produced was lower at pH2 and 3 than at pH4. This might be due to the decrease in pH during cultivation. Acetic acid bacteria secrete gluconic acid and 5-keto-gluconic acids, which result in the decrease of pH^[230]. An excessive amount of acidity could inhibit the growth of bacteria. Thus, the inoculation of bacteria at pH1 could lead to the death of bacteria. In addition, a possible reason behind the lower mass of KC obtained from the stock of the tea broth might be that the stock was too concentrated, which slightly inhibited the growth of the bacteria.

The effect of the exfoliation state of the clay was similar to the results obtained with the original BC in Section 3.1.10. As was discussed in Section 3.2.3, a possible reason behind the better growth of the cellulose in the exfoliated SWN clay environment could be a gel formation of non-exfoliated SWN. The viscosity increase during gel formation might restrict the oxygen supply for the bacteria, which were responsible for the formation of KC. Non-exfoliated particle aggregations could also block the access to oxygen supply and, therefore, lead to the reduction in the growth of the bacteria. Moreover, as synthesis of KC was performed at low pH, the number of aggregations of the clay might increase in the acidic environment.

The growth of KC/Chitosan was affected by the tea broth, whereas the mass of KC/Chitosan was heavier in distilled water. Black tea has tannic acid, which could be used as a cross-linker of chitosan. It has been reported that stirring 1 wt.% chitosan with 2, 5, 10 and 20 vol.% of tannic acid led to the formation of hydrogel

due to a reaction between the amine groups of chitosan and OH groups of tannic acid^[314]. This might make chitosan less amenable for bacteria to consume, and, therefore, the formation of KC/Chitosan decreased.

Regarding the antibacterial activity of synthesised KC-based materials, due to exposure of Na⁺ ions during the exfoliation process, the exfoliated clay might be able to inhibit the growth of the bacteria by binding to the negatively charged components of the cell wall (Section 3.2.4.). The antibacterial activity of KC/Cloisite Na⁺ and KC/SWN composites were similar to the synthesised *in situ* BC/Cloisite Na⁺ and BC/SWN composites, respectively.

Therefore, it was possible to synthesise KC from IM of SCOBY on both small and large scales. Similar to the conventional BC, pure KC does not possess any antibacterial activity; However, antibacterial activity can be introduced by *in situ* modification using exfoliated Cloisite Na⁺ and SWN as well as chitosan. KC can be synthesised with chitosan as the main carbon source. KC/Chitosan and KC/Chitosan/Clay composites showed stronger antibacterial activity against MRSA than *E. coli*. The incorporation of exfoliated clay into KC/Chitosan material resulted in improved antibacterial properties. These findings strongly suggest the potential for using KC with incorporated clay and chitosan as a natural and low-cost antibacterial wound healing system.

Chapter 9. Final discussion

9.1. Summary of mechanisms of antibacterial action

The main mechanism for the antibacterial action of the materials synthesised in the current study was based on the electrostatic interactions between positively charged clay or chitosan and the negatively charged bacterial cell wall. Cell walls of Gram-positive and Gram-negative bacteria are negatively charged due to the presence of teichoic acids and LPS, respectively (Section 1.2.3.1)^[132, 151]. Whereas, organoclay and chitosan have positively charged QAC surfactants and amine groups, respectively^[151, 250, 256]. Furthermore, natural clay showed the antibacterial activity in its exfoliated state. As was discussed in Section 3.2.4., this might be due to the release of Na⁺ cations, which were hidden between layers of Cloisite Na⁺ clay^[233]. Thereby, such an electrostatic interaction could lead to permeability and disruption of a cell wall, leakage of vital cell content and the possible penetration of positively charged components of either clay or chitosan through the bacterial cell wall followed by binding to the negatively charged DNA^[254].

However, the mechanism of antibacterial action of clay and chitosan might depend on a number of factors such as a chemical composition of organoclay surfactants, concentration of positively charged compounds, MW and DDA of chitosan, pH of the environment, etc. For instance, C16 hydrophobic tail of QAC was found to be more effective against Gram-negative bacteria than shorter-chain compounds due to the stronger interaction of C16 with the fatty acid portion of Lipid A^[252]. It has been reported that monoalkyl QAC may bind to bacterial surfaces through an ionic interaction of the cationic head groups and hydrophobic connection *via* hydrophobic tails that could be inserted into lipid bilayers^[252]. This can cause re-arrangement of a bacterial cell wall and subsequent leakage of intracellular constituents^[251]. Furthermore, low concentrations of QAC could lead

to damage of the bacterial cell wall, whereas high concentrations of QAC might cause coagulation of the cytoplasm possibly through denaturation of proteins^[98].

Regarding the antibacterial action of chitosan, amine groups could interact with LPS and teichoic acids causing increased permeability of the bacterial cell wall^[132]. For instance, an interaction of chitosan and the outer membrane of Gram-negative bacteria may result in vesicle formation that causes disruption of the outer membrane and the loss of its barrier properties^[53, 152]. Chitosan could bind to metal ions such as Ni²⁺, Fe²⁺, or Cu²⁺ that are present in the cell wall and play an essential role in viability^[132]. The ability of chitosan to penetrate bacterial cell walls might depend on DDA and MW. Increased DDA has been reported to give increased antimicrobial activity due to the presence of free amine groups^[132]. Chitosan with high DDA showed quicker ability to bind and form a stable complex with DNA^[156]. An interaction of chitosan and DNA could lead to DNA dehydration^[156]. Furthermore, the MW of chitosan may also affect its antibacterial activity. As MW decreases chitosan could pass through the channels into a bacterial cell^[161, 166]. Low molecular weight chitosan might also affect DNA and inhibit RNA replication^[46, 132, 162]. Whereas, high MW of chitosan may form a dense polymer film on the cell surface and prevent entry of nutrients and oxygen^[46]. This might inhibit the growth of aerobic bacteria^[46]. In addition, it has been found that Gram-positive bacteria could be more sensitive to antibacterial agents than Gram-negative bacteria (Section 1.2.3.2)^[251].

9.2. *Ex situ* and *in situ* synthesised materials and their significance for antibacterial action

The antibacterial activity of all synthesised materials is presented in Table 4.

Table 4. The antibacterial activity of all tested materials against MRSA, *E. coli* and *P. aeruginosa*. The bold data represents bacterial growth which was less than 1% of control values.

Materials	Growth of bacteria, % of the control values		
	MRSA	<i>E. coli</i>	<i>P. aeruginosa</i>
Pure BC	400	261	300
Pure KC	227	183	126.65
Ox BC	378	163	N/A
BC treated with acetone	190	525	45
BC treated with 0.1M of acetic acid	56	98	192
BC/Cloisite Na ⁺ <i>in situ</i>	1.4	14.6	N/A
KC/Cloisite Na ⁺ <i>in situ</i>	2.17	55.09	172.54
BC/Cloisite Na ⁺ <i>ex situ</i>	40	15.7	130
BC/Cloisite SWN <i>in situ</i>	4.8	16.8	113
KC/SWN <i>in situ</i>	3.03	48.42	N/A
BC/Cloisite SWN <i>ex situ</i>	6.53	13.7	58.27
BC/Cloisite 10A <i>ex situ</i>	0.14	0.2	1.1
BC/Cloisite 15A <i>ex situ</i>	1.86	0.3	1.6
BC/Cloisite 20A <i>ex situ</i>	45	267	1.4
BC/Cloisite 30B <i>ex situ</i>	0.012	0.1	0.4
BC/Cloisite 93A <i>ex situ</i>	69	101	123
BC/chitosan <i>in situ</i>	<0.1	40	337
BC-CH <i>in situ</i>	0.003	1.6	N/A
KC/Chitosan <i>in situ</i>	53.51	73.47	N/A
KC/Chitosan/Cloisite Na ⁺ <i>in situ</i>	12.75	54.06	78.49
KC/Chitosan/SWN <i>in situ</i>	3.74	48.4	160.61
BC/WA chitosan <i>ex situ</i> (immersion)	94	10	150
BC/Low MW chitosan <i>ex situ</i> (immersion)	85	101	67
BC/WA chitosan <i>ex situ</i> (immersion)	73	304	260
BC/WA chitosan <i>ex situ</i> (pumped)	0.3	0.002	0.85
BC/Low MW chitosan <i>ex situ</i> (pumped)	0.8	0.006	1
BC/Medium MW chitosan <i>ex situ</i> (pumped)	0.7	0.58	1.8
Ox BC/WA chitosan <i>ex situ</i> (pumped)	0.0009	2.05	0.13
Ox BC/Low MW chitosan <i>ex situ</i> (pumped)	0.005	3.05	0.005
Ox BC/Medium MW chitosan <i>ex situ</i> (pumped)	0.6	1.8	2.77
BC/CH hybrid	9.5	60.22	128.66
BC/CH/Cloisite Na ⁺ composite	0.0017	0.58	93.11

As shown in Table 4, the strongest antibacterial activity against MRSA was exhibited by BC/Cloisite 10A, BC/Cloisite 30B, all non-ox and ox BC/chitosan composites synthesised *ex situ* using the vacuum self-assembly method,

BC/CH/Cloisite Na⁺ composites as well as BC-CH. *E. coli* was inhibited the most by using BC/Cloisite 10A, BC/Cloisite 15A, BC/Cloisite 30B, non-ox BC/chitosan composites produced *ex situ* by using the vacuum self-assembly method and BC/CH/Cloisite Na⁺ composites. In addition, BC/Cloisite 30B, non-ox and ox BC/WA chitosan and ox BC/Low MW chitosan composites, which were modified *ex situ* using the vacuum self-assembly method, inhibited the growth of *P. aeruginosa* the most.

Nonetheless, BC-based composites synthesised *ex situ* showed higher antibacterial activity than materials produced *in situ*. The antibacterial activity of BC/clay composites synthesised *ex situ* could depend on either Na⁺ cations or QAC. The antibacterial activity of organoclay, mainly Cloisite 10A and Cloisite 30B, was stronger than Cloisite Na⁺ and SWN clay without surfactants. This might be due to both a positive charge and hydrophobic nature of QAC in organoclay^[272]. The organoclays were also more effective against *P. aeruginosa* compared to Cloisite Na⁺ and SWN clay. However, the antibacterial activity of organoclay was associated with the QAC and leaching behaviour, whereas the antibacterial activity of the natural clay was possibly due to the release of Na⁺ cations in the exfoliated state. BC/SWN, however, showed antibacterial activity against the three tested organisms and especially strong inhibition of growth was observed with MRSA. This might be due to the low aspect ratio, which allowed better dispersion within the BC matrix and, therefore, interaction with the bacterial cell wall with subsequent penetration of SWN inside the bacteria. Moreover, the stronger antibacterial activity of SWN against MRSA might be because there is a single cell wall in Gram-positive bacteria, whereas Gram-negative bacteria have an additional outer membrane^[273]. Even though BC/clay composites produced *ex situ* showed stronger antibacterial activity than BC/clay composites synthesised *in situ*, the attachment of the additives might not be permanent. The exception could be BC/CH/ Cloisite Na⁺ composite that was synthesised by the chemical attachment of chitosan to BC. In other cases, the leaching activity of the additive

materials such as organoclay might raise health and safety concerns due to cytotoxicity to fibroblasts.

Antibacterial activity was introduced to BC by incorporation of chitosan both *in situ* and *ex situ*. BC-CH showed stronger antibacterial activity against MRSA than *E. coli*. Chitosan may not cross the outer membrane of Gram-negative bacteria, but could be able to bind to the negatively charged LPS in *E. coli* [168]. *P. aeruginosa* showed high resistance to the BC/chitosan composite. This might be due to the stringer outer membrane of those bacteria, which have different porins from *E. coli*.

BC composites synthesised *ex situ via* immersion showed lower antibacterial activity compared to the composites produced through vacuum self-assembly. Of all types of synthesized composites, BC/WA chitosan possessed the strongest antibacterial activity against MRSA, *E. coli* and *P. aeruginosa*. This might be due to differences in both MW and DDA. WA chitosan had the highest DDA of 90%, whereas WA and low MW chitosan had DDA of 75-85%, respectively. It has been reported elsewhere that increasing DDA of chitosan from 75% to 95% leads to increased antimicrobial activity against *S. aureus* and *E. coli* through nucleotide leakage^[158]. The strong antibacterial activity of BC/chitosan composites synthesised through the vacuum self-assembly method suggests that this technique could be considered more successful than immersion. A major drawback of BC/chitosan synthesised *ex situ* is the ability of chitosan to leach in an acidic environment. However, BC-CH synthesised *in situ* could not be dissolved in acid and, therefore, might overcome the issues associated with the leaching behaviour of chitosan.

BC/CH and BC/CH/Cloisite Na⁺ were more effective against Gram-positive MRSA than Gram-negative *E. coli* and *P. aeruginosa*. BC/CH/Cloisite Na⁺ showed stronger antibacterial activity than BC/CH hybrid. A possible reason behind this could be the cross-linking reaction that made the amine group hidden

and ineffective. It has been reported that genipin can decrease the number of residual amine groups^[300]. However, a stronger antibacterial activity of the hybrid was obtained after introducing Cloisite Na⁺ clay. Some amine groups might attach to the negatively charged surface of the clay and not participate in the cross-linking reaction. This could have resulted in the expansion of free movement of the intercalated amine groups and lead to enhanced antibacterial properties.

9.3. Antibacterial correlation of materials synthesised to other antibacterial agents

As was described in Section 1.2.3.2., different antibacterial materials might affect a bacterial growth through electrostatic interactions and/or inhibition of nucleic acids' activity. Nanoparticles such as silver (Ag), gold (Au), zinc oxide (ZnO), silica (SiO₂), titanium dioxide (TiO₂), alumina (Al₂O₃), and iron oxides (Fe₃O₄, Fe₂O₃) have been used elsewhere as antibacterial agents^[22, 42, 47, 67, 69, 315, 317]. For instance, copper is a broad-spectrum biocide and can inhibit the growth of bacteria such as *Salmonella typhimurium* (*S. typhimurium*), *Listeria monocytogenes* (*L. monocytogenes*), *Salmonella enterica* (*S. enterica*) and *Campylobacter jejuni* (*C. jejuni*) fungi^[42]. Furthermore, silver nanoparticles showed antibacterial activity against pathogens such as *S. aureus*, *Bacillus subtilis* (*B. subtilis*), *Klebsiella pneumoniae* (*K. pneumoniae*), *E. coli* and *P. aeruginosa*^[19, 22, 41, 69, 315, 317]. The mode of antibacterial action of this variety of agents is similar to the mechanisms of both organoclay and chitosan used in the current study. The mechanism of antibacterial action of the materials used is summarised in Section 9.1. Regarding other antibacterial agents, the mechanism of silver ions is also based on the binding of silver to the bacterial cell wall, damaging proteins or altering bacterial function as well as interacting with thiol groups on enzymes and proteins; thus, affecting bacterial cells from inside^[61]. Moreover, silver ions may inhibit the growth of both *S. aureus* and *E. coli* by binding to functional groups of enzymes, causing the release of K⁺ ions from bacteria^[62]. In addition, silver ions can penetrate the cell wall of Gram-positive

bacteria and bind to DNA, which then loses its replication ability, and to cellular proteins leading to protein denaturation^[55]. Furthermore, TiO₂ nanoparticles might adhere to the surface of bacterial cells and produce ROS followed by damaging the structure, composition of the cell wall and leakage of cellular contents^[47]. TiO₂ nanoparticles could also penetrate the cell wall of bacteria and affect DNA degeneration, fragmentation and compression^[47].

The antibacterial activity of nanoparticles might depend on their size, surface morphology, zeta potential and pH of the environment^[47]. Metal oxide nanoparticles can show high stability over a range of pH. For instance, one of the main advantages of ZnO is antibacterial activity at pH7^[68]. The shape of ZnO nanoparticles can also influence their antibacterial mechanism. For example, rods and wire shape nanoparticles might penetrate bacterial cell walls more easily than spherical ZnO nanoparticles, whereas flower-shaped nanoparticles showed stronger antibacterial activity against both *E. coli* and *S. aureus* than spherical nanoparticles^[68]. The size of particles could also play a crucial role in antibacterial activity. It has been reported elsewhere that smaller size ZnO nanoparticles (less than 10 nm) showed stronger antibacterial activity than larger particles against *S. aureus*, *E. coli*, and *B. subtilis*^[69]. Furthermore, small size silver nanoparticles (<10 nm) might pass through the pores in a cell membrane^[63]. In addition, exfoliation of clay to nanoparticles could improve their antibacterial activity against both Gram-positive and Gram-negative bacteria.

Antibacterial agents might be combined with other materials in order to enhance their antibacterial activity. For example, the antibacterial activity of NaMMT has been enhanced by replacing exchangeable Na⁺ cations with silver ions between the layers of MMT clay^[318]. It has been observed that the growth of anaerobic mesophilic bacteria has been decreased from the control by 6.7 log CFU/g to 6.3 log CFU/g using both 10 and 15 mg of AgMMT, whereas 20 mg of AgMMT reduced bacterial growth to 4.5 log CFU/g of control values^[318]. Furthermore, it has been reported that the antibacterial activity of TiO₂/chitosan nanocomposite

was enhanced by introducing chitosan, which is non-toxic to mammals^[316]. Therefore, this nanocomposite might also be an optimal material for bone regeneration and reconstruction due to its biocompatible nature^[316].

In order to introduce antibacterial properties to pure BC, different nanoparticles could be incorporated into its matrix. For example, antimicrobial properties have been introduced into BC by incorporating silver nanoparticles through immersion^[63]. The material produced showed antibacterial activity against both *E. coli* and *S. aureus*^[63]. Furthermore, BC/silver composites, which have been synthesised through immersion elsewhere, inhibited *E. coli* and *S. aureus* by 100% and 99.99%, respectively^[64]. Moreover, BC/sodium alginate with silver sulfadiazine composites showed high antimicrobial properties against both *E. coli* and *S. aureus* bacteria as well as *Candida albicans* (*C. albicans*) yeast^[65]. The bacterial cell wall showed a significant increase in permeability, incapability of regulating transport through the wall followed by cell death^[47, 66]. It has been reported elsewhere that BC/Ag composites, which have been synthesised through immersion of pure BC into 10^{-2} M suspension of AgNO₃ overnight, reduced the control values of *E. coli* from 0.75×10^8 CFU/ml to approximately 0.01×10^8 CFU/ml^[276]. Moreover, BC/Ag composites have been placed either in the medium containing bacteria or on the top of the LB plate for 24 hours. The zones of inhibition of *S. aureus* by Ag/BC composites have been reported to be 6.5 mm due to the release of Ag⁺ ions from the BC^[276]. Furthermore, it has been stated elsewhere that BC/Ag composite showed antibacterial activity greater than 99.99% against both *E. coli* and *S. aureus*^[29, 319]. It has been observed that BC synthesised with copper and copper alloy (Cu_xO_y) nanoparticles by immersion possessed antimicrobial activity against *E. coli*, *S. aureus*, *S. enterica* and *C. albicans*^[42]. Moreover, it has been shown elsewhere that cellulose films coated with 0.046M Cu/NH₃ solution reduced the growth of both *S. aureus* and *E. coli* by 50%, respectively, within an hour of incubation^[278]. Therefore, an antibacterial activity of BC/nanoparticle composites could depend on a leaching behaviour in a similar manner as BC/organoclay synthesised in the current study. In addition,

the immersion technique used in the current study showed that the incorporation of chitosan was uneven, whereas the BC/chitosan composites synthesised through the vacuum self-assembly technique showed stronger antibacterial activity than pure chitosan against MRSA, *E. coli* and *P. aeruginosa*.

The main advantages of inorganic oxides are their stability, robustness, and long shelf life compared to organic antimicrobial agents^[19, 69, 315]. However, most of inorganic oxides could be toxic to mammalian cells. For instance, it has been found that TiO₂ can penetrate the membrane of mammalian cells and could present in the plasma membrane of epithelial cells after 10 days of exposure^[316]. It has been reported that ZnO could be toxic to mammals and may affect both Fe and glucose transports in Caco-2 and HT29-MTX cells^[316]. In addition, organoclay with a strong ability to leach could also exhibit mammalian cytotoxicity^[102, 104], whereas the natural clay and chitosan did not show cytotoxic behaviour to 3t3 cells in the current study.

Furthermore, there are a number of antibiotics that are used against a variety of bacteria. For instance, ceftaroline could inhibit the growth of both Gram-positive bacteria such as *Streptococcus pneumoniae*, *S. aureus* and *Streptococcus pyogenes* as well as Gram-negative species such as *Moraxella catarrhalis* and *Haemophilus influenzae*^[320]. The mechanism of β -lactam derivatives is based on the interaction of antibiotics and the peptidoglycan enzymes^[58]. Both glycopeptide and β -lactam antibiotics can interfere with bacterial cell wall synthesis by either mimicking the peptide stem of peptidoglycan subunits followed by blocking the action of periplasmic transpeptidase enzymes, which are essential for forming and modifying the cell wall or by binding to the peptide stem of precursor molecules and, subsequently, preventing their incorporation into the cell wall^[321]. In Gram-positive bacteria, β -lactam antibiotics may disrupt the peptidoglycan layer followed by the release of teichoic acids^[50-52, 59]. Furthermore, antibiotics such as aminoglycosides, tetracyclines and macrolides could pass through porins in Gram-negative bacteria^[321]. Inside a bacterial cell, antibiotics

such as glycopeptides, oxazolidinones, aminoglycosides, pleuromutilins, tetracyclines and macrolides may also bind to RNA^[320].

However, the main issue is the development of resistance of bacteria to different antibiotics. Organisms that have shown resistance to antibiotics through biofilm production are *S. aureus*, *P. aeruginosa*, *Escherichia coli*, *Pseudomonas pseudomallei*, and *Streptococcus sanguis*^[320]. Such a formation of biofilm may protect bacteria from different antibiotic effects. However, nanoparticles have been found to inhibit a biofilm formation. It has been reported that nanoparticles might be able to prevent the formation of biofilm of *Acinetobacter baumannii*, *P. aeruginosa* and MRSA^[320].

9.4. Mechanical properties of the materials synthesised

BC exhibits high porosity, water holding and release capacities as well as elasticity^[3, 15]. Mechanical properties of BC could be further reinforced *via* the incorporation of different materials, in order to improve thermostability, barrier and mechanical properties of BC such as strength and toughness, NaMMT particles have been introduced to a matrix elsewhere^[112, 113, 118]. Such an incorporation of NaMMT clay into BC could restrict the mobility of the polymer chains and, therefore, increase the toughness and mechanical strength of the final BC/NaMMT composite^[112]. One study has reported that BC/NaMMT composites, which were synthesised by immersion of pure BC into 1 wt.% and 2 wt.% of exfoliated NaMMT suspensions, respectively, showed an increase in the tensile strength from 151.3 MPa for pure BC to 191.2 and 209.6 MPa, respectively^[112]. Whereas, the strain of BC/NaMMT composites decreased from 6.66% of pure BC to 4.51 and 4.45 using 1 wt.% and 2 wt.% of NaMMT suspensions, respectively^[112]. Moreover, the incorporation of clay particles may reduce BC porosity, which then leads to a denser and more compact matrix of BC/NaMMT composites^[29, 112, 113]. This might be due to penetration of nanoparticles into pores of the BC matrix and to BC fibres. Furthermore, it has

been stated that water holding capacities of BC increased from the original 692% to 1923, 2653 and 3460% using 0.5 wt.%, 1 wt.% and 2 wt.% of NaMMT clay, respectively^[325]. Such an increase of water holding capacity might be due to the organophilic nature of NaMMT^[325].

Moreover, the fibres of BC could become thicker when they are coated with high MW chitosan^[138]. This might lead to a decrease in the elastic modulus^[138]. For instance, elasticity of pure BC decreased from 6 GPa to 5.2 GPa in the presence of 0.75 wt.% (MW of 80kDA) chitosan^[180, 323]. The addition of a high concentration of chitosan to pure BC could lead to a decrease in the tensile strength of the final composite^[280]. It has been reported that an increase in concentration of low MW chitosan from 12 wt.% to 45 wt.% led to a decrease in the tensile strength from 160MPa (pure BC) to 130 MPa and 54MPa of final BC/chitosan composites, respectively^[322]. In another study, the tensile strength of a BC/chitosan composite reduced to 82 MPa^[180]. This might be due to stronger intermolecular interactions between OH groups of BC and OH and NH₂ groups of chitosan. However, the concentration of 0.5 wt.% of chitosan used in the current study might not be enough to decrease the tensile strength significantly. In addition, the tensile strength of ox BC was reported to be 30% lower than pure BC^[292]. This might be due to a reduction of interfibrillar interaction caused by the insertion of two additional aldehyde groups.

9.4.1. O₂ diffusion through BC/clay and BC/chitosan composites

Incorporation of different materials into a matrix of BC might cause an increase in barrier properties of the final composite. Such barrier properties of BC can be enhanced by the incorporation of clay particles that have a sufficient aspect ratio to be able to alter the diffusion path of gas molecules that penetrate the matrix^[323]. The main challenge is to obtain an exfoliation and effective dispersion of clay particles^[323]. The presence of exfoliated nanoparticles may slow down the diffusion of gas molecules and increase tortuosity^[323]. An increase in tortuosity

could lead to an extended travelling pathway of diffused gas through the BC matrix^[323]. In addition, the incorporation of clay particles into the matrix of BC may result in a decrease in the available free volume for gas diffusion^[324]. BC/NaMMT composites have been prepared elsewhere by adding 0.5 wt.%, 1 wt.% and 2 wt.% of dispersed NaMMT suspensions, which were exfoliated using ultrasound at an amplitude of 20% for 60 minutes, into HS medium and incubated for 13 days at 30°C^[325]. It was reported that the porosity of BC loaded with 0.5 wt.%, 1 wt.% and 2 wt.% of NaMMT decreased from 12% to 11.8, 9.8 and 6.3%, respectively^[325]. This means that MMT clay particles can be captured inside the matrix of BC and, subsequently, result in a compact structure of BC^[325]. In addition, it has been observed elsewhere that the oxygen permeability of polypropylene decreased from around 56% to 27% by adding 15 wt.% of Cloisite 20A organoclay^[326]. Therefore, the incorporation of MMT clay might lead to a reduction in oxygen permeability. However, the concentrations of both Cloisite Na⁺ and SWN suspensions used in the current study to synthesise BC/clay composites were not higher than 0.6 wt.%. This concentration might not dramatically affect the porosity of BC/clay composites.

Furthermore, it has been observed that the porosity of BC/chitosan composite, which has been prepared *ex situ*, was $80 \pm 1\%$ and $74 \pm 2\%$ using 1.5 wt.% and 2 wt.% of chitosan, respectively^[327]. The diameter of pores in BC/chitosan composite prepared using 1.5 and 2 wt.% of chitosan was found to be $2.5 \pm 1 \mu\text{m}$ and $1.4 \pm 1 \mu\text{m}$, respectively^[327]. Therefore, the incorporation of chitosan into the BC matrix resulted in the formation of a more compact structure of BC with a lower porosity, which could lead to a lower O₂ permeability. The results presented in Fig. 129 showed that the fibres of the BC/WA chitosan composite synthesised *ex situ* through the vacuum self-assembly technique were coated in chitosan, which subsequently might result in a decrease in pore size. However, as seen in Fig. 110, BC-CH had a porous structure similar to pure BC. This means that porosity of BC-CH may not be greatly affected.

Regarding ox BC, the oxidation could lead to a high aggregation of nanofibrils. The diameter of pure non-ox BC fibres is about 8-100 nm, whereas the oxidation of BC led to a compact BC matrix with the width of fibres being 140-300 nm^[1, 291, 292]. It has been stated elsewhere that the porosity of ox BC was reduced by 36%^[292]. Furthermore, the oxidation caused in the shortening of BC fibrils^[292].

To summarise, mechanical properties of pure BC could be increased by incorporation of exfoliated clay that might be beneficial in applications such as food packaging and bone regeneration. On the other hand, the incorporation of chitosan into ox BC might lead to both a decrease in mechanical strength and reduced porosity. A reduction in a porosity might influence the diffusion of oxygen through the gel structures. However, a decrease in porosity might result in an increase in water release capacity. Furthermore, porosity might not be significantly decreased in BC-CH due to similarity in structures of both pure BC and BC-CH. This means that water holding capacity might be similar for both pure BC and BC-CH. In addition, BC/clay composites synthesised *in situ* using a concentration of 0.3 wt.% of exfoliated clay might exhibit increased mechanical strength without affecting the diffusion of oxygen. Therefore, BC/clay composites and BC-CH synthesised *in situ* could be beneficial materials for wound healing applications in terms of mechanical strength and porosity, respectively.

Chapter 10. Conclusion

Significant findings were obtained during this research. Firstly, natural Cloisite Na⁺ and synthetic SWN with antibacterial activity at the exfoliated state, respectively, were identified. The further incorporation of these exfoliated clay into BC led to the final BC/clay composite exhibiting antimicrobial properties against both MRSA and *E. coli*.

Secondly, the novel BC-based material, which was named bacterial chitosan (BC-CH), was developed from chitosan using bacteria as template to produce a new material that has effective antimicrobial properties against MRSA and *E. coli* but cannot be dissolved in acid. This attribute can solve the problem associated with using chitosan in antibacterial applications due to solubility in acidic environment. It could be ideal for not only wound healing but also future textile applications.

The third major finding was the enhancement of the antibacterial activity of BC/chitosan hybrid gels by using the exfoliated Cloisite Na⁺ clay. These findings are novel and based on 100% natural materials that are both non-toxic for mammalian cells and effective against MRSA and *E. coli*. The non-biocidal leaching behaviour of these new materials will widen the application of BC in medical, food and drink sectors.

Furthermore, antibacterial activity was provided to KC using natural biocides. This demonstrates that the new materials can be produced in domestic environments, which may offer potential for future commercialisation and the creation of new industries.

There were other results obtained involving the clay with traditional surfactants as biocides as well as micro-formed clay. Although some of synthesised materials were effective in inhibiting the growth of bacteria, they may have potential

concerns on health and safety due to the structure of the surfactant and biocidal leaching. Therefore, these developments were less important in comparison to those three major findings. In addition, the work provided a solid fundamental understanding of the difference between micro and nanotechnology in this application.

Chapter 11. Future work

The characterisation of the synthesised *in situ* BC/clay composites should be continued. In order to completely investigate the penetration of clay inside the matrix, SEM, FT-IR and X-ray analysis of the composite may be obtained^[325]. The content of incorporated clay inside the matrix of BC could be measured using thermogravimetric analysis (TGA). TGA heats a sample and measures the changes in weight of as a function of temperature and time^[328]. The crystallographic structure of the composite needs to be obtained by differential scanning calorimetry (DSC), which measures the heat flow during thermal changes as a function of temperature and time^[328].

The characterisation of BC-CH should be continued. Firstly, the nature of fibres produced by the bacteria using chitosan as the main carbon source needs to be investigated. The consumption of chitosan followed by the production of the fibres by the bacteria might lead to a presence of chitosan in the chemical structure of the final material. Atomic force and confocal microscopies could offer a better understanding of the structure of the material. The characterisation of BC-CH might also be taken further in an analysis of pore size and size distribution inside the cellulose using the equipment such as Quontochrome.

The mechanism behind the antibacterial activity of exfoliated clay could be analysed, because non-exfoliated clay did not show any antibacterial activity. Such an investigation could include the observation of bacteria under clay treatment using SEM^[325]. If the inhibition is caused by dehydration, the cell membrane would appear shrunken. In addition, the binding of the clay to the bacterial cell wall or even penetration of particles inside the cell can be investigated using either atomic or confocal force microscopies. In addition, if antibacterial activity of exfoliated clay and chitosan is the result of binding to bacterial cell wall, the lysis, which is the breaking down of a cell wall, might be possible to detect by DNA release^[329].

In order to identify changes in cellular proteins and obtain insight into cellular signals, a proteomic approach could be carried out. The proteomic analysis would consist of sample and protein preparation followed by a protein identification^[333]. The most common proteomic analysis involves either identification of specific proteins by, for instance, mass spectrometry following separation by two-dimensional polyacrylamide gel electrophoresis (2D-PAGE)^[330, 334]. Proteins could be purified by ion exchange, affinity or size exclusion chromatography. The analysis of selected proteins may also be obtained by enzyme-linked immunosorbent assay (ELISA) or western blotting^[331]. ELISA is a plate-based assay that is designed for detecting and quantifying proteins, proteins, antibodies, hormones, etc^[335]. However, these techniques might also be used just to analyse selected proteins in cell extracts. Whereas, protein microarrays or chips allow the analysis of protein expression^[331]. In order to determine an amino acid sequence of a particular protein, Edman degradation method could also be used^[334].

Cell-impedance sensing techniques such as real-time cell analysis (RTCA) could also be investigated. RCTA is a technique *in vitro* that is based on monitoring changes in impedance, which is generated by the adherence of cells to microelectrodes to the bottom of microelectronic wells^[332]. This technique might help to monitor cellular changes in real-time without any dyes or labels. Changes in impedance could represent differences in cell proliferation, adhesion or morphology that are caused by exposure to toxic materials over time^[330]. RCTA might be more effective than MTT reduction assay in order to determine a chemical toxicity of organoclay.

In order to investigate the interaction of either clay or chitosan with DNA, comet and micronucleus assays could be performed. The comet assay is known as single cell gel electrophoresis (SCGE) or microgel electrophoresis (MGE)^[333]. This assay could be used to evaluate the genotoxicity of clay in both mammalian and bacterial cells^[333]. Furthermore, the comet assay could be helpful to detect and visualised the breaks in DNA strands^[333]. In addition, the micronucleus assay

may be used to detect both breakage and loss of chromosomes that might occur due to chemical treatment in somatic cells^[333].

The proliferation of the 3t3 cells inside the hydrogels synthesised might also be investigated using CCK-8 and confocal microscopy. The level of expression of genes could be determined by the real-time reverse transcriptase-polymerase chain reaction (RT-PCR)^[334]. The total RNA from the cells, which are embedded in the gels, could be extracted by, for instance, trizol reagent. Then, cDNA could be obtained from RNA by reverse transcription^[334]. The expression of the proteins may also be analysed by immunostaining and visualised by fluorescence microscopy^[334]. In addition, serial analysis of gene expression (SAGE) and DNA microarray technology might also be obtained.

In order to measure oxidative stress and damage of cells caused by clay particles, protein, lipid and DNA oxidation might be analysed. For instance, the oxidation of lysine, proline, arginine and threonine might lead to a formation of carbonyl groups on a protein side of chains^[335]. Therefore, the detection and visualisation of protein carbonyl might be carried out by ELISA or by Western blot analysis^[331].

Regarding cytotoxicity assays, the lactate dehydrogenase assay, which is another type of colorimetric assay can be performed. Lactate dehydrogenase is an enzyme that is present in the cytoplasm and could be released as a result of damage to the plasma membrane^[336]. Furthermore, ATP measurements through luciferase activity could be investigated by CellTiter-Glo Luminescent Cell Viability Assay (Promega) in order to investigate the metabolic activity of cells.

Next, the cytotoxicity of KC and KC-based materials should also be investigated. The investigation of potential healing and antibacterial activity of Kombucha beverage needs to be taken further. The healing properties of the developed materials should be analysed using a scratch assay. The attachment of cells inside the matrix, which may indicate the healing nature of the composite. can be

studied using SEM. In addition, the mechanical properties of the synthesised composites might be investigated using dynamic mechanical testing. Evaluation and comparison of tensile strength and Young's modulus of the composites to the original BC need to be studied.

In order to further investigate the potential of the synthesised materials in medical applications, an animal model can be introduced. Structural damage of the skin of an animal with the subsequent measurements of reepithelisation and granulation of wounded area might provide a better understanding on healing properties of a material^[337]. Swabs from the wounds for any contaminations can prove antibacterial nature of synthesised materials.

References

- [1] A. Bodin, H. Bäckdahl, N. Petersen and P. Gatenholm, "2.22 Bacterial Cellulose as Biomaterial," *Comprehensive Biomaterials II*, vol. 2, pp. 505-511, 2007.
- [2] T. R. Stumpf, X. Yang, J. Zhang and X. Cao, "*In situ* and *ex situ* modifications of bacterial cellulose for applications in tissue engineering," *Materials Science and Engineering: C*, pp. 372-383, 2018.
- [3] J. K. Park, J. Y. Jung and T. Khan, "26-Bacterial cellulose," in *Handbook of Hydrocolloids (Second edition)*, Cambridge, Woodhead Publishing Limited, 2009, pp. 724-739.
- [4] G. F. Picheth, C. L. Pirich, M. R. Sierakowski, M. A. Woehl, C. N. Sakakibara, C. F. Souza, A. A. Martin, R. Silva and R. A. Freitas, "Bacterial cellulose in biomedical applications: A review," *International Journal of Biological Macromolecules*, vol. 104, pp. 97-106, 2017.
- [5] M. Jedrzejczak-Krzepkowska, K. Kubiak, K. Ludwicka and S. Bielecki, "Chapter 2 - Bacterial NanoCellulose Synthesis, Recent Findings," in *Bacterial NanoCellulose (First edition)*, Elsevier, 2016, pp. 19-40.
- [6] P. Ross, R. Mayer and M. Benziman, "Cellulose biosynthesis and function in bacteria," *Microbiological Reviews*, vol. 55, pp. 35-58, 1991.
- [7] K.-Y. Lee, G. M. A. Buldum and A. Bismarck, "More than Meets the Eye in Bacterial Cellulose: Biosynthesis, Bioprocessing, and Applications in Advanced Fiber Composites," *Macromolecule Bioscience*, vol. 14, pp. 10-32, 2013.
- [8] J. L. W. Morgan, J. Strumillo and J. Zimmer, "Crystallographic snapshot of cellulose synthesis and membrane translocation," *Nature*, vol. 493, pp. 181-189, 2013.

- [9] P. Jacek, F. Dourado and M. Gama, "Molecular aspects of bacterial nanocellulose biosynthesis," *Microbial Biotechnology*, vol. 12, pp. 633-649, 2019.
- [10] J. L. W. Morgan, J. Strumillo and J. Zimmer, "Crystallographic snapshot of cellulose synthesis and membrane translocation," *Nature*, vol. 493, pp. 181-186, 2012.
- [11] J. T. McNamara, J. L. W. Morgan and J. Zimmer, "A Molecular Description of Cellulose Biosynthesis," *Annual Review of Biochemistry*, vol. 84, p. 895–921, 2015.
- [12] S. Gordon and Y.-L. Hsieh, "1 - Chemical structure and properties of cotton," in *Cotton*, Woodhead Publishing, 2007, pp. 3-35.
- [13] F. Esa, S. M. Tasirin and N. A. Rahman, "Overview of Bacterial Cellulose Production and Application," *Agriculture and Agricultural Science Procedia*, vol. 2, pp. 113-119, 2014.
- [14] M. Poletto, V. Pistor and A. J. Zattera, "Structural Characteristics and Thermal Properties of Native Cellulose," in *Cellulose-Fundamental Aspects*, 2013, pp. 46-64.
- [15] W. Czaja, A. Krystynowicz, S. Bielecki and R. M. Brown, "Microbial cellulose—the natural power to heal wounds," *Biomaterials*, vol. 27, pp. 145-151, 2006.
- [16] F. G. Torres, S. Commeaux and O. P. Troncoso, "Biocompatibility of bacterial cellulose based biomaterials," *J Funct Biomater*, vol. 4, p. 864–878, 2012.
- [17] M. Martinez-Sanz, F. Pettolino, B. Flanagan, J. M. Gidley and E. P. Gilbert, "Structure of cellulose microfibrils in mature cotton fibres," *Carbohydrate Polymers*, vol. 175, pp. 450-463, 2017.
- [18] R. Q. Cabrera, F. Meersman, P. F. McMillan and V. Dmitriev, "Nanomechanical and Structural Properties of Native Cellulose Under Compressive Stress," *Biomacromolecules*, vol. 12, pp. 2178-83, 2011.

- [19] M. Szymańska-Chargot, J. Cybulska and A. Zdunek, "Sensing the Structural Differences in Cellulose from Apple and Bacterial Cell Wall Materials by Raman and FT-IR Spectroscopy," *Sensors (Basel)*, vol. 11, p. 5543–5560, 2011.
- [20] M. L. Cacicedo, M. C. Castro, I. Servetas, L. Bosnea, K. Boura, P. Tsafrakidou, A. Dima, A. Terpou, A. Koutinas and G. R. Castro, "Review Progress in bacterial cellulose matrices for biotechnological applications," *Bioresource Technology*, vol. 213, pp. 175-180, 2016.
- [21] Z. Shi, Y. Zhang, G. O. Phillips and G. Yang, "Utilization of bacterial cellulose in food," *Food Hydrocolloids*, vol. 35, pp. 539-545, 2014.
- [22] G. F. Picheth, C. L. Pirich, M. R. Sierakowski, M. A. Woehl, C. N. Sakakibara, C. F. Souza, A. A. Martin, R. Silva and R. A. de Freitas, "Bacterial cellulose in biomedical applications: A review," *International Journal of Biological Macromolecules*, vol. 104, pp. 97-106, 2017.
- [23] P.-Y. Chen and J.-T. Lai, "Mechanical Analysis of Biocomposite Materials from Bacterial Cellulose and Hydroxyapatite," *Journal of Medical and Bioengineering*, vol. 2, pp. 228-230, 2013.
- [24] J. Padrao, S. Goncalves, P. J. Silva, V. Sencadas, S. Laceros-Mandez, A. C. Pinheiro, A. A. Vicente, L. R. Rodrigues and F. Dourado, "Bacterial cellulose-lactoferrin as an antimicrobial edible packaging," *Food Hydrocolloids*, vol. 58, pp. 126-140, 2016.
- [25] H. R. Nordli, G. Chinga-Carrasco, A. M. Rokstad and B. Pukstad, "Producing ultrapure wood cellulose nanofibrils and evaluating the cytotoxicity using human skin cells," *Carbohydrate Polymers*, vol. 150, pp. 65-70, 2016.
- [26] L. Nimeskern, H. M. Ávila, J. Sundberg, P. Gatenholm, R. Müller and S. K. Stok, "Mechanical evaluation of bacterial nanocellulose as an implant material for ear cartilage replacement," *Journal of the Mechanical Behavior of Biomedical Materials*, vol. 22, pp. 12-21, 2013.

- [27] M. Scherner, S. Reutter, D. Klemm, A. Sterner-Kock, M. Guschlbauer, T. Richter, G. Langebartels, N. Madershahian, T. Wahlers and J. Wippermann, "In vivo application of tissue-engineered blood vessels of bacterial cellulose as small arterial substitutes: proof of concept?," *Journal of Surgical Research*, vol. 189, pp. 340-347, 2014.
- [28] G. Helenius, H. Backdahl, A. Bodin, U. Nannmark, P. Gateholm and B. Risberg, "In vivo biocompatibility of bacterial cellulose," *Journal of Biomedical Materials Research*, vol. 76, pp. 431-435, 2006.
- [29] H. Ullah, F. Wahid, H. A. Santos and T. Khan, "Advances in biomedical and pharmaceutical applications of functional bacterial cellulose-based nanocomposites," *Carbohydrate Polymers*, vol. 150, pp. 330-350, 2016.
- [30] K. F. Cutting, "Wound exudate: Composition and functions," *British journal of community nursing*, vol. 8, pp. 4-9, 2003.
- [31] H.-C. Huang, L.-C. Chen, S.-B. Lin and H.-H. Chen, "Nano-biomaterials application: In situ modification of bacterial cellulose structure by adding HPMC during fermentation," *Carbohydrate Polymers*, vol. 83, pp. 979-987, 2011.
- [32] H. Orelma, L. O. Morales, L.-S. Johansson, I. C. Hoeger, I. Filpponen, C. Castro, O. J. Rojas and J. Lainea, "Affibody conjugation onto bacterial cellulose tubes and bioseparation of human serum albumin," *RSC Advances*, vol. 4, pp. 3-9, 2014.
- [33] S. Torgbo and P. Sukyai, "Review Bacterial cellulose-based scaffold materials for bone tissue engineering," *Applied materialstoday*, vol. 11, pp. 34-49, 2018.
- [34] H. Ma, C. Feng, J. Chang and C. Wu, "3D-printed bioceramic scaffolds: From bone tissue engineering to tumor therapy," *Acta Biomaterialia*, vol. 79, pp. 37-59, 2018.
- [35] M. Zaborowska, A. Bodin, H. Bäckdahl, J. Popp, A. Goldstein and P. Gatenholm, "Microporous bacterial cellulose as a potential scaffold for bone regeneration," *Acta Biomaterialia*, vol. 6, p. 2540–2547, 2010.

- [36] K. A. Zimmermann, J. M. LeBlanc, K. T. Sheets, R. W. Fox and P. Gatenholm, "Biomimetic design of a bacterial cellulose/hydroxyapatite nanocomposite for bone healing applications," *Materials Science and Engineering: C*, vol. 31, pp. 43-49, 2011.
- [37] C. J. Grande, F. G. Torres, C. M. Gomez and M. C. Bañó, "Nanocomposites of bacterial cellulose/hydroxyapatite for biomedical applications," *Acta Biomaterialia*, vol. 5, pp. 1605-1615, 2009.
- [38] A. M. Barreiro, D. O. S. Recouvreux, D. L. Hotza, M. Porto and C. R. Rambo, "Sand dollar skeleton as templates for bacterial cellulose coating and apatite precipitation," *Journal of Materials Science*, vol. 45, pp. 5252–5256, 2010.
- [39] D. Ciechańska, "Multifunctional Bacterial Cellulose/ Chitosan Composite Materials for Medical Applications," *Institute of Chemical Fibres*, vol. 2, pp. 69-71, 2004.
- [40] G. Yang, J. Xie, F. Hong, Z. Cao and X. Yang, "Antimicrobial activity of silver nanoparticle impregnated bacterial cellulose membrane: Effect of fermentation carbon sources of bacterial cellulose," *Carbohydrate Polymers*, vol. 87, pp. 839-845, 2012.
- [41] V. Dincă, A. Mocanu, G. Isopencu, C. Busuioc, S. Brajnicova, A. V. M. Icriverzi, A. Roseanu, M. Dinescu, M. Stroescu, A. Stoica-Guzun and M. Sucheana, "Biocompatible pure ZnO nanoparticles-3D bacterial cellulose biointerfaces with antibacterial properties," *Arabian Journal of Chemistry*, vol. 13, pp. 3521-3533, 2018.
- [42] I. M. S. Araújo, R. R. Silva, G. Pacheco, W. R. Lustri, A. Tercjak, J. Gutierrez, J. R. S. Júnior, F. H. C. Azevedo, G. S. Figüêredo, M. L. Vega, S. J. L. Ribeiro and H. S. Barud, "Hydrothermal synthesis of bacterial cellulose–copper oxide nanocomposites and evaluation of their antimicrobial activity," *Carbohydrate Polymers*, vol. 179, pp. 341-349, 2018.

- [43] T. J. Silhavy and D. W. Kahne, "The Bacterial Cell Envelope," *Cold Spring Harbor Perspectives in Biology*, vol. 2, pp. 1-4, 2010.
- [44] S. Josset, N. Keller, M.-C. Lett and M. J. Ledoux, "Numeration methods for targeting photoactive materials in the UV-A," *Chemical Society Reviews*, vol. 37, p. 746, 2008.
- [45] S. Brown, J. P. Santa Maria and S. Walker, "Wall Teichoic Acids of Gram-Positive Bacteria," *Annual Review of Microbiology*, vol. 67, pp. 313-316, 2013.
- [46] M. A. Matica, F. L. Aachmann, A. Tøndervik, H. Sletta and V. Ostafe, "Chitosan as a Wound Dressing Starting Material: Antimicrobial Properties and Mode of Action," *International Journal of Molecular Sciences*, vol. 20, pp. 2-31, 2019.
- [47] L. Wang, C. Hu and L. Shao, "The antimicrobial activity of nanoparticles: present situation and prospects for the future," *International Journal of Nanomedicine*, vol. 12, p. 1227–1249, 2017.
- [48] N. Malanovic and K. Lohner, "Gram-positive bacterial cell envelopes: The impact on the activity of antimicrobial peptides," *Biochimica et Biophysica Acta (BBA) - Biomembranes*, vol. 1858, pp. 936-946, 2016.
- [49] J. Kiwi and V. Nadtochenko, "Evidence for the Mechanism of Photocatalytic Degradation of the Bacterial Wall Membrane at the TiO₂ Interface by ATR-FTIR and Laser Kinetic Spectroscopy," *Langmuir*, vol. 21, pp. 4631-4641, 2005.
- [50] G. M. de Tejada, S. Sanchez-Gomez, I. Kowalski, Y. Kaonis, J. Andra, T. Schurhoz, M. Hornef, A. Dupont, P. Garidel, T. Gutschmann, S. A. David and K. Brandenburg, "Bacterial cell wall compounds as promising targets of antimicrobial agents I. Antimicrobial peptides and lipopolyamines," *Current Drug Targets*, vol. 13, pp. 1121-1130, 2012.
- [51] M. Hartmann, M. Berditsch, J. Hawecker, M. F. Ardakani, D. Gerthsen and A. S. Ulrich, "Damage of the Bacterial Cell Envelope by Antimicrobial Peptides Gramicidin S and PGLa as Revealed by Transmission and

- Scanning Electron Microscopy," *Antimicrobial Agents and Chemotherapy*, vol. 54, pp. 3132-3142, 2010.
- [52] H. J. Warshakoon, M. R. Burns and S. A. David, "Structure-Activity Relationships of Antimicrobial and Lipoteichoic Acid-Sequestering Properties in Polyamine Sulfonamides," *Antimicrobial Agents and Chemotherapy*, vol. 53, pp. 57-62, 2009.
- [53] X.-f. Li, X.-q. Feng, S. Yang, G.-q. Fu, T.-p. Wang and Z.-x. Su, "Chitosan kills Escherichia coli through damage to be of cell membrane mechanism," *Carbohydrate Polymers*, vol. 79, pp. 493-499, 2010.
- [54] N. A. Amro, L. P. Kotra, K. Wadu-Mesthrige, A. Bulychev, S. Mobashery and G.-Y. Liu, "High-resolution atomic force microscopy studies of the Escherichia coli outer membrane: structural basis for permeability," *Langmuir*, vol. 16, pp. 2789-2796, 2000.
- [55] I. Sondi and B. Salopek-Sondi, "Silver nanoparticles as antimicrobial agent: a case study on E. coli as a model for Gram-negative bacteria," *Journal of Colloid and Interface Science*, vol. 275, pp. 177-182, 2004.
- [56] E. Sorrentino, P. Tremonte, M. Succi, M. Iorizzo, G. Pannella, S. J. Lombardi, M. Sturchio and R. Coppola, "Detection of Antilisterial Activity of 3-Phenyllactic Acid Using Listeria innocua as a Model," *Frontiers in Microbiology*, vol. 9, pp. 1-9, 2018.
- [57] S. Halder, K. K. S. R. Yadav, S. Mukherjee, P. Saha, S. Haldar, S. Karmakar and T. Sen, "Alteration of Zeta potential and membrane permeability in bacteria: a study with cationic agents," *SpringerPlus*, vol. 4, pp. 1-14, 2015.
- [58] H. Yllah and S. Ali, "Classification of Anti-Bacterial Agents and Their Functions," in *Antibacterial Agents*, Intech, 2017, pp. 1-15.
- [59] D. G. Allison and P. A. Lambert, "Chapter 32 - Modes of Action of Antibacterial Agents," in *Molecular Medical Microbiology (Second Edition)*, Academic Press, 2015, pp. 583-598.

-
- [60] A. L. Meyer, "Prospects and challenges of developing new agents for tough Gram-negatives," *Current Opinion in Pharmacology*, vol. 2, pp. 490-494, 2005.
- [61] S. L. Percival, Bowler, G. P. and D. Russell, "Bacterial resistance to silver in wound care," *Journal of Hospital Infection*, vol. 60, pp. 3-7, 2005.
- [62] W. K. Jung, H. C. Koo, J. W. Kim, S. Shin, S. H. Kim and Y. H. Park, "Antibacterial Activity and Mechanism of Action of the Silver Ion in *Staphylococcus aureus* and *Escherichia coli*," *Applied Environmental Microbiology*, vol. 74, pp. 2171-2178, 2008.
- [63] T. Maneerung, S. Tokura and R. Rujiravanit, "Impregnation of silver nanoparticles into bacterial cellulose for antimicrobial wound dressing," *Carbohydrate Polymers*, vol. 72, pp. 43-51, 2008.
- [64] M. J. Tabaii and G. Emtiazi, "Transparent nontoxic antibacterial wound dressing based on silver nano particle/bacterial cellulose nano composite synthesized in the presence of tripolyphosphate," *Journal of Drug Delivery Science and Technology*, vol. 44, pp. 244-253, 2018.
- [65] W. Shao, H. Liu, X. Liu, S. Wang, J. Wu, R. Zhang, H. Min and M. Huang, "Development of silver sulfadiazine loaded bacterial cellulose/sodium alginate composite films with enhanced antibacterial property," *Carbohydrate Polymers*, vol. 132, pp. 351-358, 2015.
- [66] G. Zhao and S. E. Jr Stevens, "Multiple parameters for the comprehensive evaluation of the susceptibility of *Escherichia coli* to the silver ion," *Biometals*, vol. 11, pp. 27-32, 1998.
- [67] A. Azam, A. S. Ahmed, M. Oves, M. S. Khan, S. Habib and A. Memic, "Antimicrobial activity of metal oxide nanoparticles against Gram-positive and Gram-negative bacteria: a comparative study," *International Journal of Nanomedicine*, vol. 7, pp. 6003-6009, 2012.
- [68] A. Sirelkhatim, S. Mahmud, A. Seeni, N. H. M. Kaus, L. C. Ann, S. K. M. Bakhori, H. Hasan and D. Mohamad, "Review on Zinc Oxide

- Nanoparticles: Antibacterial Activity and Toxicity Mechanism," *Nano-micro Letters*, vol. 7, pp. 219-242, 2015.
- [69] Y. Xie, Y. He, P. L. Irwin, T. Jin and X. Shi, "Antibacterial Activity and Mechanism of Action of Zinc Oxide Nanoparticles against *Campylobacter jejuni*," *Applied Environmental Microbiology*, vol. 77, pp. 2325-2331, 2011.
- [70] Y. Lvov, W. Wang, L. Zhang and R. Fakhruddin, "Halloysite Clay Nanotubes for Loading and Sustained Release of Functional Compounds," *Advanced Materials*, vol. 28, 2015.
- [71] M. Akter, M. T. Sikder, M. M. Rahman, A. Ullah, K. F. B. Hossain, S. Banik, T. Hosokawa, T. Saito and M. Kurasaki, "A systematic review on silver nanoparticles-induced cytotoxicity: Physicochemical properties and perspectives," *Journal of Advanced Research*, vol. 9, pp. 1-16, 2018.
- [72] A. Simon-Deckers, B. Gouget, M. Mayne-L'Hermite, N. Herlin-Boime, C. Reynaud and M. Carrière, "In vitro investigation of oxide nanoparticle and carbon nanotube toxicity and intracellular accumulation in A549 human pneumocytes," *Toxicology*, vol. 253, pp. 137-146, 2008.
- [73] X. Chen and H. J. Schluesener, "Nanosilver: A nanoparticle in medical application," *Toxicology Letters*, vol. 176, pp. 1-12, 2008.
- [74] Y. Ze, L. Zheng, X. Zhao, S. Gui, X. Sang, J. Su, N. Guan, L. Zhu, L. Sheng, R. Hu, J. Cheng, Z. Cheng, Q. Sun, L. Wang and F. Hong, "Molecular mechanism of titanium dioxide nanoparticles-induced oxidative injury in the brain of mice," *Chemosphere*, vol. 92, pp. 1183-1189, 2013.
- [75] C. Carlson, S. M. Hussain, A. M. Schrand, L. K. Braydich-Stolle, K. L. Hess, R. L. Jones and J. J. Schlager, "Unique Cellular Interaction of Silver Nanoparticles: Size-Dependent Generation of Reactive Oxygen Species," *Journal of Physical Chemistry*, vol. 112, p. 13608–13619, 2008.
- [76] W. Liu, Y. Wu, C. Wang, H. C. Li, T. Wang, C. Y. Liao, L. Cui, Q. F. Zhou, B. Yan and G. B. Jiang, "Impact of silver nanoparticles on human cells: Effect of particle size," *Nanotoxicity*, vol. 4, pp. 319-330, 2010.

- [77] X. Wang, Z. Ji, C. H. Chang, H. Zhang, M. Wang, Y. Liao, S. Lin, H. Meng, R. Li, B. Sun, L. V. Winkle, K. E. Pinkerton, J. I. Zink, T. Xia and A. E. Nel, "Use of Coated Silver Nanoparticles to Understand the Relationship of Particle Dissolution and Bioavailability to Cell and Lung Toxicological Potential," *Small*, vol. 10, pp. 385-398, 2013.
- [78] S. I. Kaba and E. M. Egorova, "In vitro studies of the toxic effects of silver nanoparticles on HeLa and U937 cells," *Nanotechnology Science Applied*, vol. 8, pp. 19-29, 2015.
- [79] K. Jlassi, I. Krupa and M. M. Chehimi, "Chapter 1 - Overview: Clay Preparation, Properties, Modification," in *Clay-Polymer Nanocomposites*, Elsevier, 2017, pp. 3-27.
- [80] S. Vogt, "Differences in the production-related properties of the three primary clay minerals kaolinite-illite-montmorillonite (Part 2)," *Brick and Tile Industry International*, no. 6, pp. 15-26, 2014.
- [81] H. H. Murray, "Traditional and new applications for kaolin, smectite, and palygorskite: a general overview," *Applied Clay Science*, pp. 207-221, 2000.
- [82] M. S. Nazir, M. H. M. Kassim, L. Mohapatra, M. A. Gilani, M. R. Raza and K. Majeed, "Characteristic Properties of Nanoclays and Characterization of Nanoparticulates and Nanocomposites," *Nanoclay Reinforced Polymer Composites*, vol. 12, pp. 35-48, 2016.
- [83] P. Leroy, C. T. Bernard, N. Devau and M. Azaroual, "The electrophoretic mobility of montmorillonite. Zeta potential and surface conductivity effects," *Journal of Colloid and Interface Science*, vol. 451, pp. 21-39, 2015.
- [84] K. Emmerich, "Full Characterization of Smectites," in *Handbook of Clay Science*, Elsevier, 2013, pp. 390-391.
- [85] G. Mittal, V. Dhand, K. Y. Rhee and S.-J. Park, "Investigation of seawater effects on the mechanical properties of untreated and treated MMT-based glass fiber/vinylester composites," *Ocean Engineering*, vol. 108, pp. 393-401, 2015.

-
- [86] S. S. Ray, "1-An Overview of Pure and Organically Modified Clays," in *Clay-Containing Polymer Nanocomposites*, Elsevier, 2013, pp. 1-24.
- [87] M. Kotal and A. K. Bhowmick, "Polymer nanocomposites from modified clays: Recent advances and challenges," *Progress in Polymer Science*, vol. 51, pp. 127-187, 2015.
- [88] J.-W. Rhim and S.-I. H. C.-S. Hong, "Tensile, water vapor barrier and antimicrobial properties of PLA/nanoclay composite films," *LWT- Food Science and Technology*, vol. 42, pp. 612-617, 2007.
- [89] W. S. DePolo and D. G. Baird, "Particulate Reinforced PC/PBT Composites. II. Effect of Nano-clay Particles on Dimensional Stability and Structure–Property Relationships," *Polymer Composites*, vol. 30, p. 201, 2009.
- [90] T. J. Pinnavaia and G. W. Beall, *Polymer-Clay Nanocomposites*, John Wiley & Sons Ltd, 2000.
- [91] B. Sun, F.-A. Khan, G. Süss-Fink and B. Therrien, "Chapter 12 - Metal Catalysts Intercalated in Smectite Clays," in *Encapsulated Catalysts*, Tehran, Academic Press, 2017, pp. 387-441.
- [92] V. S. Souza, O. Bianchi, M. F. S. Lima and R. S. Mauler, "Morphological, thermomechanical and thermal behavior of epoxy/MMT nanocomposites," *Journal of Non-Crystalline Solids*, vol. 400, pp. 58-66, 2014.
- [93] N. Meng, N.-L. Z. S.-Q. Zhou and J. Shen, "Synthesis and antimicrobial activity of polymer/montmorillonite-chlorhexidine acetate nanocomposites," *Applied Clay Science*, vol. 42, p. 667, 2009.
- [94] G. Liu, Y. Song, J. Wang, H. Zhuang, L. Ma, C. Li, Y. Liu and J. Zhang, "Effects of nanoclay type on the physical and antimicrobial properties of PVOH-based nanocomposite films," *LWT - Food Science and Technology*, vol. 57, pp. 562-568, 2014.
- [95] A. Roy, M. Joshi, B. S. Butola and S. Malhotra, "Antimicrobial and toxicological behavior of montmorillonite immobilized metal nanoparticles," *Materials Science and Engineering: C*, vol. 93, pp. 704-715, 2018.
-

- [96] A. Brandelli, N. A. Lopes and J. F. Boelter, "2 - Food applications of nanostructured antimicrobials," in *Food Preservation*, Rio Grande do Sul, Academic Press, 2017, pp. 35-74.
- [97] S. Hong and J. W. Rhim, "Antimicrobial activity of organically modified nano-clays," *Journal of Nanoscience and Nanotechnology*, vol. 8, pp. 5818-5824, 2008.
- [98] Russell, Hugo and Aytill's, Principles and practice of Disinfection, Preservation & Sterilization, Blackwell Science Ltd, 2004.
- [99] L. Timofeeva and N. Kleshcheva, "Antimicrobial polymers: mechanism of action, factors of activity, and applications," *Applied Microbiology and Biotechnology*, vol. 89, pp. 475-480, 2011.
- [100] E. Elias, C. C. Sarath, K. Z. Ajesh, V. V. Kumar, M. A. Sunil, B. Suryasarathi, G. S. J. e Fernando and T. Sabu, "Percolated network formation in biocidal 3D porous PCL/clay nanocomposite scaffolds: effect of organic modifier on interfacial and water sorption properties," *RSC Advances*, vol. 6, pp. 85107–85116, 2016.
- [101] J. Houtman, S. Maisanaba, M. Puerto, D. Gutiérrez-Praena, M. Jordá, S. Aucejo and A. Jos, "Toxicity assessment of organomodified clays used in food contact materials on human target cell lines," *Applied Clay Science*, vol. 90, pp. 150-158, 2014.
- [102] A. K. Sharma, B. Schmidt, H. Frandsen, N. R. Jacobsen, E. H. Larsen and M.-L. Binderup, "Genotoxicity of unmodified and organo-modified montmorillonite," *Mutation Research/Genetic Toxicology and Environmental Mutagenesis*, vol. 700, pp. 18-25, 2010.
- [103] S. Mainsanaba, A. I. Prieto, S. Pichardo, M. Jorda-Beneyto, S. Aucejo and A. Jos, "Cytotoxicity and mutagenicity assessment of organomodified clays potentially used in food packaging," *Toxicology in Vitro*, vol. 29, pp. 1222-1230, 2015.
- [104] S. Mainsanaba, M. Puerto, S. Pichardo, M. Jorda, F. J. Moreno, S. Aucejo and A. Jos, "In vitro toxicological assessment of clays for their use in food

- packaging applications," *Food and Chemical Toxicology*, vol. 57, pp. 266-275, 2013.
- [105] S. Lordan, J. E. Kennedy and C. L. Higginbotham, "Cytotoxic effects induced by unmodified and organically modified nanoclays in the human hepatic HepG2 cell line," *Journal of Applied Toxicology*, vol. 31, pp. 27-35, 2011.
- [106] S. Lordan and C. L. Higginbotham, "Effect of serum concentration on the cytotoxicity of clay particles," *Cell Biology International*, vol. 36, pp. 57-61, 2013.
- [107] N. J. Mitchell, J. Kumi, M. Aleser, S. E. Elmore, K. A. Rychlik, K. E. Zychowski, A. A. Romoser, T. D. Phillips and N.-A. Ankrah, "Short-Term Safety and Efficacy of Calcium Montmorillonite Clay (UPSN) in Children," *The American Journal of Tropical Medicine and Hygiene*, vol. 91, pp. 777-785, 2014.
- [108] Y.-H. Lee, T.-F. Kuo, B.-Y. Chen, Y.-K. Feng, Y.-R. Wen, W.-C. Lin and F. H. Lin, "Toxicity assessment of montmorillonite as a drug carrier for pharmaceutical applications: yeast and rats model," *Biomedical engineering applications, basis & communications*, vol. 17, pp. 72-78, 2005.
- [109] M. C. Wiles, H. J. Huebner, E. Afriyie-Gyawu, R. J. Taylor, G. R. Bratton and T. D. Phillips, "Toxicological evaluation and metal bioavailability in pregnant rats following exposure to clay minerals in the diet," *Journal of Toxicology and Environmental Health, Part A*, vol. 67, pp. 863-874, 2010.
- [110] M. D. Subramaniam and I. H. Kim, "Clays as dietary supplements for swine: A review," *Journal of Animal Science and Biotechnology*, vol. 6, pp. 1-9, 2015.
- [111] W. Hu, S. Chen, J. Yang, Z. Li and H. Wang, "Functionalized bacterial cellulose derivatives and nanocomposites," *Carbohydrate Polymers*, vol. 101, pp. 1042-1050, 2014.

- [112] M. Ul-Islam, T. Khan and J. K. Park, "Nanoreinforced bacterial cellulose–montmorillonite composites for biomedical applications," *Carbohydrate Polymers*, vol. 89, pp. 1189-1197, 2012.
- [113] E. E. Kiziltas, A. Kiziltas, M. Blumentritt and D. J. Gardner, "Biosynthesis of bacterial cellulose in the presence of different nanoparticles to create novel hybrid materials," *Carbohydrate Polymers*, vol. 129, pp. 148-155, 2015.
- [114] K.-C. Cheng, J. M. Catchmark and A. Demirci, "Enhanced production of bacterial cellulose by using a biofilm reactor and its material property analysis," *Journal of Biological Engineering*, vol. 3, p. 12, 2009.
- [115] C. Gao, Y. Wan, C. Yang and K. Dai, "Preparation and characterization of bacterial cellulose sponge with hierarchical pore structure as tissue engineering scaffold," *Journal of Porous Materials*, vol. 18, pp. 139-145, 2011.
- [116] S. T. Olalekan, S. A. Muyibi, Q. H. Shah, M. F. Alkhatib, F. Yusof and I. Y. Qudsieh, "Improving the Polypropylene-Clay Composite Using Carbon Nanotubes as Secondary Filler," *Energy Research Journal*, vol. 1, pp. 68-70, 2010.
- [117] S. H. Emami-Razavi, N. Esmaili, S. K. Forouzannia, S. Amanpour, S. Rabbani, A. M. Alizadeh and A. Mohagheghi, "Effect of bentonite on skin wound healing: experimental study in the rat model," *Acta Medica Iranica*, vol. 44, pp. 235-239, 2006.
- [118] M. Ul-Islam, T. Khan, W. A. Khattak and J. K. Park, "Bacterial cellulose-MMTs nanoreinforced composite films: novel wound dressing material with antibacterial properties," *Cellulose*, vol. 20, pp. 589-596, 2013.
- [119] W. Sajjad, T. Khan, M. Ul-Islam, R. Khan, Z. Hussain, A. Khalid and F. Wahid, "Development of modified montmorillonite-bacterial cellulose nanocomposites as a novel substitute for burn skin and tissue regeneration," *Carbohydrated Polymers*, vol. 206, pp. 548-556, 2019.

-
- [120] E. Horvath, C. Murray, G. Vaughan, K. Chung, D. Hospenthal, C. Wade, J. Holcomb, S. Wolf, A. Mason and L. Cancio, "Fungal Wound Infection (Not Colonization) Is Independently Associated With Mortality in Burn Patients," *Annals of Surgery*, vol. 245, pp. 978-985, 2007.
- [121] J. Cabezas-Pizarro, M. Redondo-Solano, C. Umaña-Gamboa and M. L. Arias-Echandi, "Antimicrobial activity of different sodium and potassium salts of carboxylic acid against some common foodborne pathogens and spoilage-associated bacteria," *Revista Argentina de Microbiología Revista Argentina de Microbiología*, vol. 50, pp. 56-61, 2018.
- [122] G. Wu, J. Ding, H. Li, R. Zhao, Z. Shen, X. Fan and T. Xi, "Effects of cations and pH on antimicrobial activity of thanatin and s-thanatin against *Escherichia coli* ATCC25922 and *B. subtilis* ATCC 21332," *Current Microbiology*, vol. 57, pp. 552-557, 2008.
- [123] J. Jantsch, V. Schatz, D. Friedrich, A. Schroder, C. Kopp, I. Siegert, A. Maronna, D. Wendelborn, P. Linz, K. J. Binger, M. Gebhardt, M. Heinig, P. Neubert and F. Fisher, "Cutaneous Na⁺ Storage Strengthens the Antimicrobial Barrier Function of the Skin and Boosts Macrophage-Driven Host Defense," *Cell Metabolism*, vol. 21, pp. 493-501, 2015.
- [124] A. Khalid, R. Khan, M. Ul-Islam, T. Khan and F. Wahid, "Bacterial cellulose-zinc oxide nanocomposites as a novel dressing system for burn wounds," *Carbohydrated Polymers*, vol. 164, pp. 214-221, 2017.
- [125] N. Agnihotri, V. Gupta and M. R. Joshi, "Aerobic bacterial isolates from burn wound infections and their antibiograms—a five-year study," *Burns*, vol. 30, pp. 241-243, 2004.
- [126] G. Borkow, N. Okon-Levy and J. Gabbay, "Copper oxide impregnated wound dressing: Biocidal and safety studies," *Wounds: A Compendium of Clinical Research and Practice*, vol. 22, pp. 301-310, 2010.
- [127] E. Assadian, M. H. Zarei, A. G. Gialni, M. Farshin, H. Degampanah and J. Pourahmad, "Toxicity of Copper Oxide (CuO) Nanoparticles on Human

- Blood Lymphocytes," *Biological Trace Element Research*, vol. 184, pp. 350-357, 2018.
- [128] H. Zhang, C. Chen, C. Zhu and S. Dongping, "Production of bacterial cellulose by acetobacter xylinum: effects of carbon/nitrogen-ratio on cell growth and metabolite production," *Cellulose Chemistry and Technology*, vol. 50, pp. 997-1000, 2014.
- [129] N. N. V. Long, C. Joly and P. Dantigny, "Active packaging with antifungal activities," *International Journal of Food Microbiology*, vol. 220, pp. 73-90, 2016.
- [130] P. R. de Oliveira, M. Takaki, C. T. C. Gorayeb, V. L. Del Bianchi, J. C. Thomeo, M. J. Tiera and V. A. de Oliveira Tiera, "Synthesis, characterization and antifungal activity of quaternary derivatives of chitosan on *Aspergillus flavus*," *Microbiological Research*, vol. 168, pp. 50-55, 2013.
- [131] R. C. Goy, D. de Britto and O. B. G. Assis, "A Review of the Antimicrobial Activity of Chitosan," *Ciência e Tecnologia*, vol. 19, pp. 241-247, 2009.
- [132] D. J. Sullivan, S. Azlin-Hasim, M. Cruz-Romero, E. Cummins, J. P. Kerry and M. A. Morris, "11 - Natural Antimicrobial Materials for Use in Food Packaging," in *Handbook of Antimicrobial Coatings*, Honolulu, Elsevier, 2018, pp. 181-233.
- [133] M. Rinaudo, "Chitin and chitosan: Properties and applications," *Progress in Polymer Science*, vol. 31, pp. 603-632, 2006.
- [134] M. N. V. R. Kumar, "A review of chitin and chitosan applications," *Reactive and Functional Polymers*, vol. 46, pp. 1-27, 2000.
- [135] R. Raftery, F. J. O'Brien and S.-A. Cryan, "Chitosan for Gene Delivery and Orthopedic Tissue Engineering Applications," *Molecules*, vol. 18, pp. 5611-5647, 2013.
- [136] E. Vunain, A. K. Mishra and B. B. Mamba, "1 - Fundamentals of chitosan for biomedical applications," in *Chitosan Based Biomaterials Volume 1*, Woodhead Publishing, 2017, pp. 3-30.

- [137] J. Nilsen-Nygaard, S. Strand, K. M. Varum and K. I. Draget, "Chitosan: Gels and Interfacial Properties," *Polymers*, vol. 7, pp. 552-579, 2015.
- [138] M. Phisalaphong and N. Jatupaiboon, "Biosynthesis and characterization of bacteria cellulose–chitosan film," *Carbohydrate Polymers*, vol. 74, pp. 482-488, 2008.
- [139] H. K. Holme, H. Foros, H. Pettersen, M. Dornish and O. Smidsrod, "Thermal depolymerization of chitosan chloride," *Carbohydrate Polymers*, vol. 46, pp. 287-294, 2001.
- [140] S. Naskar, S. Sharma and K. Kuotsu, "Chitosan-based nanoparticles: An overview of biomedical applications and its preparation," *Journal of Drug Delivery Science and Technology*, vol. 49, pp. 66-81, 2019.
- [141] I. Younes, S. Sellimi, M. Rinaudo, K. Jellouli and M. Nasri, "Influence of acetylation degree and molecular weight of homogeneous chitosans on antibacterial and antifungal activities," *International Journal of Food Microbiology*, vol. 185, pp. 57-63, 2014.
- [142] Y. Yuan, B. M. Chesnutt, W. O. Haggard and J. D. Bumgardner, "Deacetylation of Chitosan: Material Characterization and in vitro Evaluation via Albumin Adsorption and Pre-Osteoblastic Cell Cultures," *Materials*, vol. 4, pp. 1399-1416, 2011.
- [143] T. Jiang, R. James, S. G. Kumbar and C. T. Laurencin, "Chapter 5 - Chitosan as a Biomaterial: Structure, Properties, and Applications in Tissue Engineering and Drug Delivery," in *Natural and Synthetic Biomedical Polymers*, Elsevier Science, 2014, pp. 91-113.
- [144] I.-Y. Kim, S.-J. Seo, H.-S. Moon, M.-K. Yoo, I.-Y. Park, B.-C. Kim and C.-S. Cho, "Chitosan and its derivatives for tissue engineering applications," *Biotechnology Advances*, vol. 26, pp. 1-21, 2008.
- [145] H. Hattori and M. Ishihara, "Changes in blood aggregation with differences in molecular weight and degree of deacetylation of chitosan," *Biomedical Materials*, vol. 10, pp. 1-5, 2015.

- [146] M. L. Tsai and R. H. Chen, "6 - Modifying the molecular weight of chitosan," in *Chitosan Based Biomaterials Volume 1*, Woodhead Publishing, 2017, pp. 135-158.
- [147] C. K. S. Pillai, W. Paul and C. P. Sharma, "Chitin and chitosan polymers: Chemistry, solubility and fiber formation," *Progress in Polymer Science*, vol. 34, pp. 646-649, 2009.
- [148] M. Rinaudo, G. Pavlov and J. Desbrieres, "Influence of acetic acid concentration on the solubilization of chitosan," *Polymer*, vol. 40, p. 7029–7032, 1999.
- [149] J. C. Roy, F. Salaün, S. Giraud and A. Ferri, "Solubility of Chitin: Solvents, Solution Behaviors and Their Related Mechanisms," in *Solubility of Polysaccharides*, IntechOpen, 2017, pp. 110-124.
- [150] N. Kubota and Y. Eguchi, "Facile preparation of water-soluble N-acetylated chitosan and molecular weight dependence of its water-solubility," *Polymer Journal*, vol. 29, pp. 123-127, 1997.
- [151] W. Tachaboonyakiat, "9 - Antimicrobial applications of chitosan," in *Chitosan Based Biomaterials Volume 2. Tissue Engineering and Therapeutics*, Woodhead Publishing, 2017, pp. 245-274.
- [152] J. Tantala, K. Thumanu and C. Rachtanapun, "An assessment of antibacterial mode of action of chitosan on *Listeria innocua* cells using real-time HATR-FTIR spectroscopy," *International Journal of Biological Macromolecules*, vol. 135, pp. 386-393, 2019.
- [153] P. K. Dutta, S. Tripathi, G. K. Mehrota and J. Dutta, "Perspectives for chitosan based antimicrobial films in food applications," *Food Chemistry*, vol. 114, pp. 1173-1182, 2009.
- [154] H. Y. Alay and E. Celik, "Investigations of antibacterial activity of chitosan in the polymeric composite coatings," *Progress in Organic Coatings*, vol. 102, pp. 194-200, 2017.

- [155] S. Panja, P. Aich, B. Jana and T. Basu, "How does plasmid DNA penetrate cell membranes in artificial transformation process of *Escherichia coli*?," *Molecular Membrane Biology*, vol. 4, pp. 411-420, 2008.
- [156] Y. Yang, M. Guo, R. Qian, C. Liu, X. Zong, Y.-Q. Li and W. Li, "Binding efficacy and kinetics of chitosan with DNA duplex: The effects of deacetylation degree and nucleotide sequences," *Carbohydrate Polymers*, vol. 169, pp. 451-457, 2017.
- [157] J. Li, Y. Wu and L. Zhao, "Antibacterial activity and mechanism of chitosan with ultra high molecular weight," *Carbohydrate Polymers*, vol. 148, pp. 200-205, 2016.
- [158] Y.-C. Chung and C.-Y. Chen, "Antibacterial characteristics and activity of acid-soluble chitosan," *Bioresource Technology*, vol. 99, pp. 2806-2814, 2008.
- [159] T. Takahashi, M. Imai, I. Suzuki and J. Sawai, "Growth inhibitory effect on bacteria of chitosan membranes regulated with deacetylation degree," *Biochemical Engineering Journal*, vol. 40, pp. 485-491, 2008.
- [160] K. A. M. O'Callaghan and J. P. Kerry, "Preparation of low- and medium-molecular weight chitosan nanoparticles and their antimicrobial evaluation against a panel of microorganisms, including cheese-derived cultures," *Food Control*, vol. 69, pp. 256-261, 2016.
- [161] F. R. Tamara, C. Lin, F.-L. Mi and Y.-C. Ho, "Antibacterial Effects of Chitosan/Cationic Peptide Nanoparticles," *Nanomaterials*, vol. 8, pp. 1-15, 2017.
- [162] T. T. Zhu, C. H. Zhou, F. B. Kabwe, Q. Q. Wu, C. S. Li and J. R. Zhang, "Exfoliation of montmorillonite and related properties of clay/polymer nanocomposites," *Applied Clay Science*, vol. 169, pp. 48-66, 2019.
- [163] R. C. Goy, S. T. B. Morais and O. B. G. Assis, "Evaluation of the antimicrobial activity of chitosan and its quaternized derivative on *E. coli* and *S. aureus* growth," *Revista Brasileira de Farmacognosia*, vol. 26, pp. 122-127, 2016.

- [164] L.-Y. Zheng and J.-F. Zhu, "Study on antimicrobial activity of chitosan with different molecular weights," *Carbohydrate Polymers*, vol. 54, pp. 527-530, 2003.
- [165] F. C. João, F. K. Tavora, S. C. Fonseca, O. S. Ramos, M. E. Pintado and F. X. Malcata, " In Vitro Screening for Antimicrobial Activity of Chitosans and Chitooligosaccharides, Aiming at Potential Uses in Functional Textiles," *Journal of Microbiology and Biotechnology*, vol. 20, pp. 311-318, 2010.
- [166] M. S. M. Eldin, E. A. Soliman, A. I. Hashem and T. Tamer, "Antibacterial Activity of Chitosan Chemically Modified with New Technique," *Trends in Biomaterials & Artificial Organs*, vol. 22, pp. 127-137, 2008.
- [167] Y.-J. Jeon, P.-J. Park and S.-K. Kim, "Antimicrobial effect of chitooligosaccharides produced by bioreactor," *Carbohydrate Polymers*, vol. 44, pp. 71-76, 2001.
- [168] I. M. Helander, E.-L. Nurmiäho-Lassila, R. Ahvenainen, J. Rhoades and S. Roller, "Chitosan disrupts the barrier properties of the outer membrane of Gram-negative bacteria," *International Journal of Food Microbiology*, vol. 71, pp. 235-244, 2001.
- [169] Z. Abedian, N. Jenabian, A. A. Moghadamnia, E. Zabihi, H. Tashakorian, M. Rajabnia, F. Sadighian and A. Bijani, "Antibacterial activity of high-molecular-weight and low-molecular-weight chitosan upon oral pathogens," *Journal of Conservative Dentistry*, vol. 22, pp. 169-174, 2019.
- [170] M. C. Cruz-Romero, T. Murphy, M. Morris, E. Cummins and J. P. Kerry, "Antimicrobial activity of chitosan, organic acids and nano-sized solubilisates for potential use in smart antimicrobially-active packaging for potential food applications," *Food Control*, vol. 34, pp. 393-397, 2013.
- [171] N. Liu, X.-G. Chen, H.-J. Park, C.-G. Liu, C.-S. Liu, X.-H. Meng and L.-J. Yu, "Effect of MW and concentration of chitosan on antibacterial activity of *Escherichia coli*," *Carbohydrate Polymers*, vol. 64, pp. 60-65, 2006.

- [172] M. S. Benhabiles, R. Salah, H. Lounici, N. Drouiche, M. F. A. Goosen and N. Mameri, "Antibacterial activity of chitin, chitosan and its oligomers prepared from shrimp shell waste," *Food Hydrocolloids*, vol. 29, pp. 48-56, 2012.
- [173] S.-H. Chang, H.-T. Lin, G.-J. Wu and G. J. Tsai, "pH Effects on solubility, zeta potential, and correlation between antibacterial activity and molecular weight of chitosan," *Carbohydrate Polymers*, vol. 134, pp. 74-81, 2015.
- [174] Z. Guo, R. Xing, S. Liu, Z. Zhong, X. Ji, L. Wang and P. Li, "The influence of molecular weight of quaternized chitosan on antifungal activity," *Carbohydrate Polymers*, vol. 71, pp. 694-697, 2008.
- [175] G. I. Marquez, J. Akuaku, I. Cruz, J. Cheemtham, A. Golshani and L. Smith M, "Disruption of protein synthesis as antifungal mode of action by chitosan," *International Journal of Food Microbiology*, vol. 3, pp. 108-112, 2013.
- [176] A. N. Hernández-Lauzardo, S. Bautista-Baños, M. G. Velázquez-del Valle, M. G. Méndez-Montevalvo, M. M. Sánchez-Rivera and L. A. Bello-Pérez, "Antifungal effects of chitosan with different molecular weights on in vitro development of *Rhizopus stolonifer* (Ehrenb.:Fr.) Vuill," *Carbohydrated Polymers*, vol. 73, pp. 541-547, 2008.
- [177] N. Shah, M. Ul-Islam, W. A. Khattar and J. K. Park, "Overview of bacterial cellulose composites: A multipurpose advanced material," *Carbohydrate Polymers*, vol. 98, pp. 1585-1598, 2013.
- [178] F. Wahid, X.-H. Hu, L.-Q. Chu, S.-R. Jia, Y.-Y. Xie and C. Zhong, "Development of bacterial cellulose/chitosan based semi-interpenetrating hydrogels with improved mechanical and antibacterial properties," *International Journal of Biological Macromolecules*, vol. 122, pp. 380-387, 2019.
- [179] Y.-B. Wu, S.-H. Yu, F.-L. Mi, S.-W. Wu, S.-S. Shyu, C.-K. Peng and A.-C. Chao, "Preparation and characterization on mechanical and antibacterial

- properties of chitsoan/cellulose blends," *Carbohydrate Polymers*, vol. 57, pp. 435-440, 2004.
- [180] W.-C. Lin, C.-C. Lien, H.-J. Yeh, C.-M. Yu and S.-h. Hsu, "Bacterial cellulose and bacterial cellulose–chitosan membranes for wound dressing applications," *Carbohydrate Polymers*, vol. 94, pp. 603-611, 2013.
- [181] J. Kingkaew, N. Jatupaiboon, N. Sanchavanakit, P. Pavasant and M. Phisalaphong, "Biocompatibility and growth of human keratinocytes and fibroblasts on biosynthesized cellulose-chitosan film," *Journal of Biomaterials Science, Polymer Edition*, vol. 21, pp. 1009-1021, 2010.
- [182] F. Ostadhossein, N. Mahmoudi, G. Morales-Cid, E. Tamjid, F. J. Navas-Martos, B. Soriano-Cuadrado and J. M. S. A. López Paniza, "Development of Chitosan/Bacterial Cellulose Composite Films Containing Nanodiamonds as a Potential Flexible Platform for Wound Dressing," *Materials (Basel)*, vol. 8, pp. 6401-6418, 2015.
- [183] J. Kim, Z. Cai, H. S. Lee, G. S. Choi, D. H. Lee and C. Jo, "Preparation and characterization of a Bacterial cellulose/Chitosan composite for potential biomedical application," *Journal of Polymer Research*, vol. 18, pp. 739-744, 2011.
- [184] H. Ueno, H. Yamada, I. Tanaka, N. Kaba, M. Matsuura, M. Okumura, T. Kadosawa and T. Fujinaga, "Accelerating effects of chitosan for healing at early phase of experimental open wound in dogs," *Biomaterials*, vol. 20, pp. 1407-1414, 1999.
- [185] H. Ueno, T. Mori and T. Fujinaga, "Topical formulations and wound healing applications of chitosan," *Advanced Drug Delivery Reviews*, vol. 52, pp. 105-115, 2001.
- [186] J. M. Kapp and W. Sumner, "Kombucha: a systematic review of the empirical evidence of human health benefit," *Annals of Epidemiology*, vol. 30, pp. 66-70, 2019.

- [187] C. Greenwalt, K. H. Steinkraus and R. A. Ledford, "Kombucha, the fermented tea: microbiology, composition, and claimed health effects," *Journal of Food Protection*, vol. 63, pp. 976-981, 2000.
- [188] F. De Filippis, A. D. Troise, P. Vitaglione and D. Ercolini, "Different temperatures select distinctive acetic acid bacteria species and promotes organic acids production during Kombucha tea fermentation," *Food Microbiology*, vol. 73, pp. 11-16, 2018.
- [189] R. Jayabalan, R. V. Malbasa, E. S. Loncar, J. S. Vitas and M. Sathishkumar, "A Review on Kombucha Tea—Microbiology, Composition, Fermentation, Beneficial Effects, Toxicity, and Tea Fungus," *Comprehensive Reviews in Food Science and Food Safety*, vol. 13, pp. 538-550, 2014.
- [190] A. Mohammadshirazi and E. B. Kalhor, "Energy and cost analyses of kombucha beverage production," *Renewable and Sustainable Energy Reviews*, vol. 55, pp. 668-673, 2016.
- [191] S. Bhattacharya, R. Gachhui and C. P. Sil, "Effect of Kombucha, a fermented black tea in attenuating oxidative stress mediated tissue damage in alloxan induced diabetic rats," *Food and Chemical Toxicology*, vol. 60, pp. 328-340, 2013.
- [192] R. Jaybalan, R. V. Malbasa and M. Sathishkumar, "Kombucha," in *Reference Module in Food Science*, Elsevier, 2016.
- [193] S. Chakravorty, S. Bhattacharya, A. Chatzinotas, W. Chakraborty, D. Bhattacharya and R. Gachhui, "Kombucha tea fermentation: Microbial and biochemical dynamics," *International Journal of Food Microbiology*, vol. 220, pp. 63-72, 2016.
- [194] S. Bhattacharya, R. Gachhui and P. C. Sil, "Hepatoprotective properties of kombucha tea against TBHP-induced oxidative stress via suppression of mitochondria dependent apoptosis," *Pathophysiology*, vol. 18, pp. 221-234, 2011.

- [195] D. Chaudhary and H. Liu, "Ultrasonic treatment and synthesis of sugar alcohol modified Na⁺-montmorillonite clay," *Ultrasonics Sonochemistry*, vol. 20, pp. 63-68, 2013.
- [196] B. Bittmann, F. Hauptert and A. K. Schlarb, "Ultrasonic dispersion of inorganic nanoparticles in epoxy resin," *Ultrasonics Sonochemistry*, vol. 16, pp. 622-628, 2009.
- [197] X. Zhang, H. Yi, H. Bai, Y. Zhao and F. S. S. Min, "Correlation of montmorillonite exfoliation with interlayer cations in the preparation of two-dimensional nanosheets," *Royal Society of Chemistry*, vol. 7, pp. 41471-41478, 2017.
- [198] H. Bakkih, A. Bakhur and E. Ammar, "Antimicrobial effect of Kombucha analogues," *LWT - Food Science and Technology*, vol. 47, pp. 71-77, 2012.
- [199] R. J. J. Santos, R. A. Batista, S. A. Rodrigues, L. X. Filho and A. S. Lima, "Antimicrobial Activity of Broth Fermented with Kombucha Colonies," *Journal of Microbial & Biochemical Technology*, vol. 1, pp. 72-77, 2009.
- [200] C. J. Greenwalt, R. A. Ledford and K. H. Steinkraus, "Determination and Characterization of the Antimicrobial Activity of the Fermented Tea Kombucha," *Department of Applied Microbiology and Gene Technology*, vol. 31, pp. 291-296, 1998.
- [201] A. Ashrafi, M. Jokar and A. M. Nafchi, "Preparation and characterization of biocomposite film based on chitosan and kombucha tea as active food packaging," *International Journal of Biological Macromolecules*, vol. 108, 2018.
- [202] K. H. Steinkraus, K. B. Shapiro, J. H. Hotchkiss and R. P. Mortlock, "Investigations into the Antibiotic Activity of Tea Fungus/Kombucha Beverage," *Acta Biochnology*, vol. 16, pp. 199-205, 1996.
- [203] N. Halib, I. Ahmad, M. Grassi and G. Grassi, "The remarkable three-dimensional network structure of bacterial cellulose for tissue engineering

- applications," *International Journal of Pharmaceutics*, vol. 566, pp. 631-640, 2019.
- [204] Y. Andriani, K. S. Jack, E. P. Gilbert, G. A. Edwards, T. L. Schiller, E. Strounin, A. F. Osman and D. J. Martin, "Organization of mixed dimethyldioctadecylammonium and choline modifiers on the surface of synthetic hectorite," *Journal of Colloid and Interface Science*, vol. 409, pp. 72-75, 2013.
- [205] L. Yu and P. Cebe, "Crystal polymorphism in electrospun composite nanofibers of poly(vinylidene fluoride) with nanoclay," *Polymer*, vol. 50, pp. 2133-2141, 2009.
- [206] B. Sun, M. Zhang, N. Zhou, X. Chu, P. Yuan, C. Chi, F. Wu and J. Shen, "Study on montmorillonite–chlorhexidine acetate–terbinafine hydrochloride intercalation composites as drug release systems," *RSC Advances*, vol. 8, pp. 21369–21377, 2018.
- [207] V. Kuete, O. Karaosmanoglu and H. Sivas, "Chapter 10 - Anticancer Activities of African Medicinal Spices and Vegetables," in *Medicinal Spices and Vegetables from Africa*, Academic Press, 2017, pp. 271-297.
- [208] T. L. Riss, R. A. Movarec, A. L. Nilis, S. Duellman, H. A. Benink, T. J. Worzella and L. Minor, "Cell Viability Assays," in *Assay Guidance Manual*, Eli Lilly & Company and the National Center for Advancing Translational Sciences, 2013, pp. 2-5.
- [209] T. Mosmann, "Rapid colorimetric assay for cellular growth and survival: application to proliferation and cytotoxicity assays," *The Journal of Immunological Methods*, vol. 65, pp. 55-63, 1983.
- [210] S. E. McBirney, K. Trinh, A. Wong-Beringer and A. M. Armani, "Wavelength-normalized spectroscopic analysis of *Staphylococcus aureus* and *Pseudomonas aeruginosa* growth rates," *Biomedical Optics Express*, vol. 7, pp. 4034-4042, 2016.

- [211] A. Basu, S. V. Vadanam and S. Lim, "A Novel Platform for Evaluating the Environmental Impacts on Bacterial Cellulose Production," *Scientific Reports*, vol. 8, pp. 1-5, 2018.
- [212] B. Ruzicka, E. Zaccarelli, L. Zulian, R. Angelini, M. Sztucki, A. Moussaïd, T. Narayanan and F. Sciortino, "Observation of empty liquids and equilibrium gels in a colloidal clay," *Nature Materials*, vol. 50, pp. 56-60, 2011.
- [213] A. Rodger and K. Sanders, "UV-Visible Absorption Spectroscopy, Biomacromolecular Applications," *Encyclopedia of Spectroscopy and Spectrometry (Third Edition)*, vol. 3, pp. 495-502, 2017.
- [214] S. Mallakpour and M. Dinari, "Synthesis and Properties of Biodegradable Poly(vinyl alcohol)/ Organo-nanoclay Bionanocomposites," *Journal of Polymer Environment*, vol. 20, pp. 732-737, 2012.
- [215] N. K. Verma, E. Moore, W. Blau, Y. Yolkov and P. R. Babu, "Cytotoxicity evaluation of nanoclays in human epithelial cell line A549 using high content screening and real-time impedance analysis," *Journal of Nanoparticle Research*, vol. 14, p. 1137, 2012.
- [216] A. Seluanov, C. Hine, J. Azpurua, M. Feigenson, M. Bozzella, Z. Mao, K. C. Catania and V. Gorbunova, "Hypersensitivity to contact inhibition provides a clue to cancer resistance of naked mole-rat," *Proceedings of the National Academy of Sciences of the United States of America*, vol. 106, p. 19352–19357, 2009.
- [217] K. A. Zahan, "Effect of Incubation Temperature on Growth of *Acetobacter xylinum* 0416 and Bacterial Cellulose Production," *Applied Mechanics and Materials*, pp. 3-6, 2015.
- [218] D. Raghunathan, "Production of Microbial Cellulose from the New Bacterial Strain Isolated From Temple Wash Waters," *Internatioanl Journal of Current Microbiology and Applied Sciences*, vol. 2, pp. 275-283, 2013.
- [219] E. P. Çoban and H. Biyik, "Evaluation of different pH and temperatures for bacterial cellulose production in HS (Hestrin-Scharmm) medium and beet

- molasses medium," *African Journal of Microbiology Research*, vol. 5, pp. 1037-1040, 2011.
- [220] D. R. Ruka, G. P. Simon and K. M. Dean, "Altering the growth conditions of *Gluconacetobacter xylinus* to maximize the yield of bacterial cellulose," *Carbohydrate Polymers*, vol. 89, pp. 613-622, 2012.
- [221] P. Lestari, N. Elfrida, A. Suryani and Y. Suryadi, "Study on the Production of Bacterial Cellulose from *Acetobacter Xylinum* Using Agro - Waste," *Jordan Journal of Biological Sciences*, vol. 7, pp. 75-80, 2014.
- [222] A. F. Jozala, R. A. N. Pértile, C. A. dos Santos, V. d. C. Santos-Ebinuma, M. M. Seckler, F. M. Gama and A. Pessoa, "Bacterial cellulose production by *Gluconacetobacter xylinus* by employing alternative culture media," *Applied Microbiology Biotechnology*, vol. 99, pp. 1181-1190, 2015.
- [223] G. Lagaly and I. Dekany, "Chapter 8 - Colloid Clay Science," in *Developments in Clay Science*, Elsevier, 2013, pp. 243-345.
- [224] N. Lu and M. Khorshidi, "Mechanisms for Soil-Water Retention and Hysteresis at High Suction Range," *Journal of Geotechnical and Geoenvironmental Engineering*, vol. 141, pp. 1-15, 2015.
- [225] H. Li, Y. Zhao, S. Song, Y. Hu and Y. Nahmad, "Delamination of Na-Montmorillonite Particles in Aqueous Solutions and Isopropanol under Shear Forces," *Journal of Dispersion Science and Technology*, vol. 38, pp. 1117-1123, 2016.
- [226] D. R. Katti, K. B. Thapa and K. S. Katti, "The role of fluid polarity in the swelling of sodium-montmorillonite clay: A molecular dynamics and Fourier transform infrared spectroscopy study," *Journal of Rock Mechanics and Geotechnical Engineering*, vol. 10, pp. 1133-1144, 2018.
- [227] L. Wu, S. Cao and G. Lv, "Influence of Energy State of Montmorillonite Interlayer Cations on Organic Intercalation," *Advances in Materials Science and Engineering*, vol. 2018, p. 8, 2018.

- [228] V. A. Agubra, P. S. Owuor and M. V. Hosur, "Influence of Nanoclay Dispersion Methods on the Mechanical Behavior of E-Glass/Epoxy Nanocomposites," *Nanomaterials*, vol. 3, pp. 555-560, 2013.
- [229] A. L. Poli, T. Batista, C. C. Schmitt, F. Gessner and M. G. Neumann, "Effect of sonication on the particle size of montmorillonite clays," *Journal of Colloid and Interface Science*, vol. 325, pp. 386-390, 2008.
- [230] H. M. Azeredo, H. Barud, C. S. Farinas, V. M. Vasconcellos and A. M. Claro, "Bacterial Cellulose as a Raw Material for Food and Food Packaging Applications," *Frontiers in Sustainable Food Systems*, vol. 3, pp. 1-7, 2019.
- [231] A. Marchuk, P. Rengasamy and A. McNeill, "Influence of organic matter, clay mineralogy, and pH on the effects of CROSS on soil structure is related to the zeta potential of the dispersed clay," *Soil Research*, vol. 51, pp. 34-40, 2013.
- [232] E. Cortes-Trivino and I. Martinez, "Wheat gluten/montmorillonite biocomposites: Effect of pH on the mechanical properties and clay dispersion," *Express Polymer Letters*, vol. 12, pp. 616-627, 2018.
- [233] L. B. Williams, D. W. Metge, D. D. Eberl, R. W. Harvey, A. G. Turner, P. Prapaipong and A. T. Poret-Peterson, "What Makes a Natural Clay Antibacterial?," *Environmental Science and Technology*, vol. 45, pp. 3768-3773, 2011.
- [234] J.-C. Wei, Y.-T. Yen, H.-L. Su and J.-J. Lin, "Inhibition of Bacterial Growth by the Exfoliated Clays and Observation of Physical Capturing Mechanism," *The Journal of Physical Chemistry*, vol. 115, pp. 18770-18775, 2011.
- [235] J.-C. Wei, Y.-T. Wang and J.-J. Lin, "First evidence of singlet oxygen species mechanism in silicate clay for antimicrobial behavior," *Applied Clay Science*, vol. 99, pp. 18-23, 2014.
- [236] J. Shephard, A. J. McQuillan and P. J. Bremer, "Mechanisms of Cation Exchange by *Pseudomonas aeruginosa* PAO1 and PAO1 wbpL, a Strain

- with a Truncated Lipopolysaccharide," *Applied and Environmental Microbiology*, vol. 74, p. 6980–6986, 2008.
- [237] B. J. Wilkinson, K. J. Dorian and L. D. Sabath, "Cell Wall Composition and Associated Properties of Methicillin-Resistant *Staphylococcus aureus* Strains," *Journal of Bacteriology*, vol. 136, pp. 976-980, 1978.
- [238] L.-A. B. Rawlinson, J. P. O'Gara, D. S. Jones and D. J. Brayden, "Resistance of *Staphylococcus aureus* to the cationic antimicrobial agent poly(2-(dimethylamino ethyl)methacrylate) (pDMAEMA) is influenced by cell-surface charge and hydrophobicity," *Journal in Medical Microbiology*, vol. 60, pp. 968-976, 2011.
- [239] W. Saiiad, T. K. R. Khan, Z. Hussain, A. Khalid and F. Wahid, "Development of modified montmorillonite-bacterial cellulose nanocomposites as a novel substitute for burn skin and tissue regeneration," *Carbohydrate Polymers*, vol. 206, pp. 548-556, 2019.
- [240] S.-h. Hsu, H.-J. Tseng, H.-S. Hung, M.-C. Wang, C.-H. Hung, P.-R. Li and J.-J. Lin, "Antimicrobial Activities and Cellular Responses to Natural Silicate Clays and Derivatives Modified by Cationic Alkylamine Salts," *Applied Materials and Interfaces*, vol. 1, pp. 2556-2564, 2009.
- [241] P.-R. Li, J.-C. Wei, Y.-F. Chiu, H.-L. Su, F.-C. Peng and J.-J. Lin, "Evaluation on Cytotoxicity and Genotoxicity of the Exfoliated Silicate Nanoclay," *Applied Materials and Interfaces*, vol. 2, pp. 1608-1613, 2010.
- [242] A. Gujjari, B. V. Rodriguez, J. Pescador, C. Maeder, G. W. Beali and K. L. Lewis, "Factors affecting the association of single- and double-stranded RNAs with montmorillonite nanoclays," *International Journal of Biological Macromolecules*, vol. 109, pp. 551-559, 2017.
- [243] A. Taki, B. John, S. Arakawa and M. Okamoto, "Structure and rheology of nanocomposite hydrogels composed of DNA and clay," *European Polymer Journal*, vol. 49, pp. 923-931, 2013.
- [244] S.-J. Choi, "Cytotoxicity and Biokinetic Evaluation of Clay Minerals," *Clays and Clay Minerals*, vol. 67, pp. 91-98, 2019.

- [245] M. Baek, J.-A. Lee and S.-J. Choi, "Toxicological effects of a cationic clay, montmorillonite in vitro and vivo," *Molecular & Cellular Toxicology*, vol. 8, pp. 95-101, 2012.
- [246] S.-M. Li, N. Jia, J.-F. Zhu, M.-G. Ma and R.-C. Sun, "Synthesis of cellulose–calcium silicate nanocomposites in ethanol/water mixed solvents and their characterization," *Carbohydrate Polymers*, vol. 80, pp. 270-275, 2010.
- [247] J. Shah, M. K. Mishra, A. D. Shukla, T. Imae and D. O. Shah, "Controlling wettability and hydrophobicity of organoclays modified with quaternary ammonium surfactants," *Journal of Colloid and Interface Science*, vol. 407, pp. 493-499, 2013.
- [248] A. Ammala, C. Bell and K. Dean, "Poly(ethylene terephthalate) clay nanocomposites: Improved dispersion based on an aqueous ionomer," *Composites Science and Technology*, vol. 68, pp. 1328-1337, 2008.
- [249] K. C. Baker, M. Manitiu, R. Bellair, C. Gratopp, H. N. Herkowitz and R. Kannan, "Supercritical carbon dioxide processed resorbable polymer nanocomposite bone graft substitutes," *Acta Biomater*, vol. 7, pp. 3382-3389, 2011.
- [250] M. C. Jennings, K. P. C. Minbiole and W. M. Wuest, "Quaternary Ammonium Compounds: An Antimicrobial Mainstay and Platform for Innovation to Address Bacterial Resistance," *Infectious Diseases*, vol. 1, pp. 288-298, 2015.
- [251] N. V. Shtyrlin, S. V. Sapozhnikov, A. S. Galiullina, A. R. Kayumov, O. V. Bondar, E. Mirchink, E. B. Isakova, A. A. Firsov, K. V. Balakin and Y. G. Shtyrlin, "Synthesis and Antibacterial Activity of Quaternary Ammonium 4-Deoxyriboxine Derivatives," *BioMed Research International*, vol. 1, pp. 1-8, 2016.
- [252] C. J. Iannou, G. W. Hanlon and S. P. Denyer, "Action of Disinfectant Quaternary Ammonium Compounds against *Staphylococcus aureus*," *Antimicrobial Agents and Chemotherapy*, vol. 51, pp. 296-306, 2007.

-
- [253] M. Tischer, G. Pradel, K. Ohlsen and U. Holzgrabe, "Quaternary Ammonium Salts and Their Antimicrobial Potential: Targets or Nonspecific Interactions?," *ChemMedChem*, vol. 7, pp. 22-31, 2012.
- [254] R. Nayak and R. Padhye, "12 - Antimicrobial finishes for textiles," in *Functional Finishes for Textiles*, Woodhead Publishing, 2015, pp. 361-385.
- [255] M. M. Sugii, F. A. d. S. Ferreira, K. C. Müller, P. U. R. Filho, F. Henrique and B. Aguiar, "Chapter 5 - Quaternary ammonium compound derivatives for biomedical applications," in *Materials for Biomedical Engineering*, Elsevier, 2019, pp. 153-175.
- [256] C. Zhang, F. Cui, G.-m. Zeng, M. Jiang, Z.-z. Yang, Z.-g. Yu, M.-y. Zhu and L.-q. Shen, "Quaternary ammonium compounds (QACs): A review on occurrence, fate and toxicity in the environment," *Science of The Total Environment*, vol. 518, pp. 352-362, 2015.
- [257] R. Nigmatullin, F. Gao and V. Konovalova, "Polymer-layered silicate nanocomposites in the design of antimicrobial materials," *Journal of Materials Science*, vol. 43, pp. 5728-5733, 2008.
- [258] C. Johnston, "Infrared Studies of Clay Mineral-Water Interactions," *Developments in Clay Science*, vol. 8, pp. 288-309, 2017.
- [259] M. Chorom and P. Pengasamy, "Dispersion and zeta potential of pure clays as related to net particle charge under varying pH, electrolyte concentration and cation type," *European Journal of Soil Science*, vol. 46, pp. 657-665, 1995.
- [260] B. Bate and S. E. Burns, "Effect of total organic carbon content and structure on the electrokinetic behavior of organoclay suspensions," *Journal of Colloid and Interface Science*, vol. 343, p. 58-64, 2010.
- [261] S. Z. I. Marras and C. Panayiotou, "Nanostructure vs. microstructure: Morphological and thermomechanical characterization of poly(L-lactic acid)/layered silicate hybrids," *European Polymer Journal*, vol. 43, pp. 2191-2206, 2007.
-

-
- [262] R. Khatem, R. Celis and C. M. Hermosin, "Cationic and anionic clay nanoformulations of imazamox for minimizing environmental risk," *Applied Clay Science*, vol. 168, pp. 106-115, 2019.
- [263] J. H. Huh, M. M. Rahman and H.-D. Kim, "Properties of Waterborne Polyurethane/Clay Nanocomposite Adhesives," *Journal of Adhesion Science and Technology*, vol. 23, p. 739–751, 2012.
- [264] A. Borges, C. Ferreira, J. M. Saavedra and M. Simoes, "Antibacterial Activity and Mode of Action of Ferulic and Gallic Acids Against Pathogenic Bacteria," *Microbial Drug Resistance*, vol. 19, pp. 256-265, 2013.
- [265] E. Birkenhauer and S. Neethirajan, "Characterization of electrical surface properties of mono- and co-cultures of *Pseudomonas aeruginosa* and methicillin-resistant *Staphylococcus aureus* using Kelvin probe force microscopy," *RSC Advances*, vol. 4, pp. 41431-42435, 2014.
- [266] S. Halder, K. K. Yadav, R. Sarkar, S. Mukherjee, P. Saha, S. Haldar, S. Karmakar and T. Sen, "Alteration of Zeta potential and membrane permeability in bacteria: a study with cationic agents," *Springerplus*, vol. 4, pp. 1-14, 2015.
- [267] A. Hanizan, R. W. Sharudin, Z. Ahmad, I. Subuki and A. A. Rahman, "Wettability Behavior of XLPE Nanocomposite with Surface Modified Nanofiller," *International Journal of Recent Technology and Engineering*, vol. 8, pp. 9652-9656, 2019.
- [268] A. Pegoretti, A. Dorigato, M. Brugnara and A. Penati, "Contact angle measurements as a tool to investigate the filler–matrix interactions in polyurethane–clay nanocomposites from blocked prepolymer," *European Polymer Journal*, vol. 44, pp. 1662-1672, 2008.
- [269] H. He, J. Zhu, P. Yuan, Q. Zhou, Y. Ma and R. Frost, "Pore Structure of Surfactant Modified Montmorillonites," *The Proceedings of the Ninth International Congress for Applied Mineralogy*, vol. 1, pp. 1-7, 2008.
- [270] P. Johnson, A. Trybala and V. Starov, "Kinetics of Spreading over Porous Substrates," *Colloids and Interfaces*, vol. 3, pp. 1-13, 2019.

- [271] B. Rafiei and A. F. Ghomi, "Preparation and characterization of the Cloisite Na⁺ modified with cationic surfactants," *Journal of Crystallography and Mineralogy*, vol. 21, pp. 25-27, 2013.
- [272] S. S. Babu, S. Mathew, N. Kalarikkal, S. Thomas and E. K. Radhakrishnan, "Antimicrobial, antibiofilm, and microbial barrier properties of poly (ϵ -caprolactone)/cloisite 30B thin films," *3 Boitech*, vol. 6, pp. 1-9, 2016.
- [273] Q. Feng, J. Wu, G. Chen, F. Cui, T. Kim and J. Kim, "A mechanistic study of the antibacterial effect of silver ions on Escherichia coli and Staphylococcus aureus," *Journal of Biomedical Materials Research*, vol. 52, pp. 662-668, 2000.
- [274] S. B. Aziz, O. G. Abdullah, D. R. Saber, M. A. Rasheed and H. M. Ahmed, "Investigation of Metallic Silver Nanoparticles through UV-Vis and Optical Micrograph Techniques," *International Journal of Electrochemical Science*, vol. 12, pp. 363-365, 2017.
- [275] J. Kumirska, M. Czerwicka, Z. Kaczyński, A. Bychowska, K. Brzozowski, J. Thöming and P. Stepnowski, "Application of Spectroscopic Methods for Structural Analysis of Chitin and Chitosan," *Marine Drugs*, vol. 8, pp. 1567-1636, 2010.
- [276] S. Pal, R. Nisi, M. Stoppa and A. Licciulli, "Silver-Functionalized Bacterial Cellulose as Antibacterial Membrane for Wound-Healing Applications," *American Chemical Society*, vol. 2, pp. 3632-3639, 2017.
- [277] J.-W. Oh, S. C. Chun and M. Chandrasekaran, "Preparation and In Vitro Characterization of Chitosan Nanoparticles and Their Broad-Spectrum Antifungal Action Compared to Antibacterial Activities against Phytopathogens of Tomato," *Agronomy*, vol. 9, pp. 1-12, 2019.
- [278] B. Jia, Y. Mei, L. Cheng, J. Zhou and L. Zhang, "Preparation of copper nanoparticles coated cellulose films with antibacterial properties through one-step reduction," *Applied materials & interfaces*, vol. 4, pp. 2897-2902, 2014.

- [279] D. Zvezdova and C. Uzov, "Determination of the degree of deacetylation of chitin and chitosan by X-ray powder diffraction," *Management and Education*, vol. 8, pp. 85-88, 2012.
- [280] L. Urbina, O. Guaresti, J. Requies, N. Gabilondo, A. Eceiza, M. A. Corcuera and A. Retegi, "Design of reusable novel membranes based on bacterial cellulose and chitosan for the filtration of copper in wastewaters," *Carbohydrate Polymers*, vol. 193, pp. 362-372, 2018.
- [281] M. R. Barer, "Bacterial Growth, Culturability and Viability," in *Molecular Medical Microbiology (Second Edition)*, Academic Press, 2015, pp. 181-199.
- [282] J. R. Allen and B. Waclaw, "Bacterial growth: a statistical physicist's guide," *Reports on Progress in Physics*, vol. 82, pp. 1-12, 2019.
- [283] R. M. Maier, "Bacterial Growth," in *Soil, Water and Environmental Science*, Elsevier Inc., 2008, pp. 37-54.
- [284] R. J. Gomes, M. d. F. Borges, M. d. F. Rosa, R. J. H. Castro-Gomez and W. A. Spinosa, "Acetic Acid Bacteria in the Food Industry: Systematics, Characteristics and Applications," *Food Technology and Biotechnology*, vol. 56, pp. 139-151, 2018.
- [285] M. Bonnet, J. C. Lagier, D. Raoult and S. Khelaifia, "Bacterial culture through selective and non-selective conditions: the evolution of culture media in clinical microbiology," *New Microbes New Infections*, vol. 34, pp. 1-5, 2020.
- [286] E. Tsouko, C. Koutmentza, D. Ladakis, N. Kopsahelis, I. Mandala, S. Papanikolaou, F. Paloukis, V. Alves and A. Kountinas, "Bacterial Cellulose Production from Industrial Waste and by-Product Streams," *International Journal of Molecular Sciences*, vol. 16, pp. 14832-14839, 2015.
- [287] Z. Gromet-Elhanan and S. Hestrin, "Synthesis of cellulose by *Acetobacter xylinus*," *Journal of Bacteriology*, vol. 85, pp. 284-290, 1963.
- [288] H. Kommann, P. Duboc, I. Marison and U. von Stockar, "Influence of Nutritional Factors on the Nature, Yield, and Composition of

- Exopolysaccharides Produced by *Gluconacetobacter xylinus* I-2281," *Applied Environmental Microbiology*, vol. 69, pp. 6091–6098, 2003.
- [289] F. Yassine, N. Bassil, R. Flouty, A. Chokr, A. A. Samrani, G. Boiteux and M. E. Tahchi, "Culture medium pH influence on *Gluconacetobacter* physiology: Cellulose production rate and yield enhancement in presence of multiple carbon sources," *Carbohydrate Polymers*, vol. 146, pp. 282-291, 2016.
- [290] F. Ostadhossein, N. Mahmoudi, G. Morales-Cid, E. Tamjid, F. J. Navas-Martos, B. Soriano-Cuadrado, J. M. L. Paniza and A. Simchi, "Development of Chitosan/Bacterial Cellulose Composite Films Containing Nanodiamonds as a Potential Flexible Platform for Wound Dressing," *Materials*, vol. 8, pp. 6401-6418, 2015.
- [291] X. Liu, Y. Wang, Z. Cheng, J. Sheng and R. Yang, "Nano-sized fibrils dispersed from bacterial cellulose grafted with chitosan," *Carbohydrate Polymers*, vol. 214, pp. 311-316, 2019.
- [292] N. F. Vasconcelos, F. K. Andrade, L. d. A. P. Vieira, R. S. Viera, J. M. Vaz, P. Chevallier, D. Mantovani, M. d. F. Borges and M. d. F. Rosa, "Oxidized bacterial cellulose membrane as support for enzyme immobilization: properties and morphological features," *Cellulose*, vol. 27, pp. 3055–3083, 2020.
- [293] H. Yuan, L. Chen and F. F. Hong, "A Biodegradable Antibacterial Nanocomposite Based on Oxidized Bacterial Nanocellulose for Rapid Hemostasis and Wound Healing," *Applied Materials and Interfaces*, vol. 12, pp. 3382-3392, 2020.
- [294] S. Coseri, G. Biliuta, B. C. Simionescu, K. Stana-Kleinsch, V. Ribitsch and V. Harabagiu, "Oxidized cellulose—Survey of the most recent achievements," *Carbohydrate Polymers*, vol. 93, pp. 207-215, 2013.
- [295] K. A. Kristiansen, A. Potthast and B. E. Christensen, "Periodate oxidation of polysaccharides for modification of chemical and physical properties," *Carbohydrate Research*, vol. 345, pp. 1264-1271, 2010.

- [296] Y. Qin and P. Li, "Antimicrobial Chitosan Conjugates: Current Synthetic Strategies and Potential Applications," *International Journal of Molecular Sciences*, vol. 21, pp. 4-19, 2019.
- [297] M. A. Hassan, A. M. Omer, E. Abbas, W. M. A. Baset and T. M. Tamer, "Preparation, physicochemical characterization and antimicrobial activities of novel two phenolic chitosan Schiff base derivatives," *Scientific reports*, vol. 8, pp. 1-11, 2018.
- [298] S. Ju, F. Zhang, J. Duan and J. Jiang, "Characterization of bacterial cellulose composite films incorporated with bulk chitosan and chitosan nanoparticles: A comparative study," *Carbohydrate Polymers*, vol. 237, pp. 1-10, 2020.
- [299] M. Ul-Islam, F. Subhan, S. Ul Islam, S. Khan, N. Shah, S. Manan, M. W. Ullah and G. Yang, "Development of three-dimensional bacterial cellulose/chitosan scaffolds: Analysis of cell-scaffold interaction for potential application in the diagnosis of ovarian cancer," *International Journal of Biological Macromolecules*, vol. 137, pp. 1050-1059, 2019.
- [300] J. S. Yoo, Y. Kim, S. H. Kim and S. H. Choi, "Study on Genipin: A New Alternative Natural Crosslinking Agent for Fixing Heterograft Tissue," *The Korean Journal of Thoracic and Cardiovascular Surgery*, vol. 44, pp. 197–207, 2011.
- [301] R. A. A. Muzzarelli, M. El Mehtedi, C. Bottegoni, A. Aquili and A. Gigante, "Genipin-Crosslinked Chitosan Gels and Scaffolds for Tissue Engineering and Regeneration of Cartilage and Bone," *Marine Drugs*, vol. 13, pp. 7314–7338, 2015.
- [302] S. Dimida, C. Demitri, V. M. De Benedictis, F. Scalera, F. Gervaso and A. Sannino, "Genipin-cross-linked chitosan-based hydrogels: Reaction kinetics and structure-related characteristics," *Journal of Applied Polymer Science*, vol. 132, pp. 1-8, 2015.
- [303] F.-L. Mi, S.-S. Shyu and C.-K. Peng, "Characterization of ring-opening polymerization of genipin and pH-dependent cross-linking reactions

- between chitosan and genipin," *Journal of Polymer Science: Part A: Polymer Chemistry*, vol. 43, pp. 1985-2000, 2005.
- [304] R. A. A. Muzzarelli, "Genipin-crosslinked chitosan hydrogels as biomedical and pharmaceutical aids," *Carbohydrate Polymers*, vol. 77, pp. 1-9, 2009.
- [305] M. Grolík, K. Szczubialka, B. Wowra, D. Dobrowolski, B. Orzechowska-Wylegate, E. Wyegata and M. Nowakowska, "Hydrogel membranes based on genipin-cross-linked chitosan blends for corneal epithelium tissue engineering," *Journal of Materials Science*, vol. 23, pp. 1991-2000, 2012.
- [306] K. Delmar and H. Bianco-Peled, "The dramatic effect of small pH changes on the properties of chitosan hydrogels crosslinked with genipin," *Carbohydrated Polymers*, vol. 127, pp. 28-37, 2015.
- [307] O. A. C. J. Monteiro and C. Airoidi, "Some studies of crosslinking chitosan–glutaraldehyde interaction in a homogeneous system," *International Journal of Biological Macromolecules*, vol. 26, pp. 119-128, 1999.
- [308] S. Dimida, A. Barca, N. Cancelli, V. De Benedictis, M. G. Raucci and C. Demitri, "Effects of Genipin Concentration on Cross-Linked Chitosan Scaffolds for Bone Tissue Engineering: Structural Characterization and Evidence of Biocompatibility Features," *International Journal of Polymer Science*, vol. 1, pp. 1-8, 2017.
- [309] A. A. d. N. Pomari, T. L. d. A. Montanheiro, C. P. de Siqueira, R. S. Silva, D. B. Tada and A. P. Lemes, "Chitosan Hydrogels Crosslinked by Genipin and Reinforced with Cellulose Nanocrystals: Production and Characterization," *Journal of Composites Science*, vol. 3, pp. 1-12, 2019.
- [310] J. E. Arikibe, R. Lata, K. Kuboyama, T. Ougizawa and D. Rohindra, "pH-Responsive Studies of Bacterial Cellulose/Chitosan Hydrogels Crosslinked with Genipin: Swelling and Drug Release Behaviour," *ChemistrySelect*, vol. 4, pp. 9915 – 9926, 2019.
- [311] M. J. Moura, H. Faneca, M. P. Lima, M. H. Gil and M. M. Figueiredo, "In Situ Forming Chitosan Hydrogels Prepared via Ionic/Covalent Co-Cross-Linking," *Biomacromolecules*, vol. 12, pp. 3275-3284, 2011.

- [312] S. A. Villarreal-Soto, J. Bouajila, J.-P. Souchard and P. Taillandier, "Understanding Kombucha Tea Fermentation: A Review," *Journal of Food Science*, vol. 83, pp. 580-586, 2018.
- [313] S. C. Chu and C. Chen, "Effects of origins and fermentation time on the antioxidant activities of Kombucha," *Food Chemistry*, vol. 98, pp. 501-507, 2006.
- [314] A. Sionkowska, B. Kaczmarek and K. Lewandowska, "Characterisation of chitosan after cross-linking by tannic acid," *Progress on Chemistry and Application of Chitin and its Derivatives*, vol. 19, pp. 135-138, 2014.
- [315] K. R. Raghupathi, R. T. Koodali and A. C. Manna, "Size-Dependent Bacterial Growth Inhibition and Mechanism of Antibacterial Activity of Zinc Oxide Nanoparticles," *Lagmuir*, vol. 27, pp. 4020-4028, 2011.
- [316] Y. Huang, L. Mei, X. Chen and Q. Wang, "Recent Developments in Food Packaging Based on Nanomaterials," *Nanomaterials*, vol. 830, pp. 1-12, 2018.
- [317] S. Mohanbaba and S. Gurunathan, "Chapter 6 - Differential biological activities of silver nanoparticles against Gram-negative and Gram-positive bacteria: A novel approach for antimicrobial therapy," in *Nanobiomaterials in Antimicrobial Therapy*, William Andrew Applied Science Publishers, 2016, pp. 193-277.
- [318] C. Costa, A. Conte, G. G. Buonocore and M. A. Del Nobile, "Antimicrobial silver-montmorillonite nanoparticles to prolong the shelf life of fresh fruit salad," *International Journal of Food Microbiology*, vol. 148, pp. 164-167, 2011.
- [319] I. Armentano, C. R. Arciola, E. Fortunati, D. Ferrari, S. Mattioli, C. F. Amoroso, J. Rizzo, J. M. Kenny, M. Imbriani and L. Vissai, "The Interaction of Bacteria with Engineered Nanostructured Polymeric Materials: A Review," *Scientific World Journal*, vol. 1, pp. 1-18, 2014.
- [320] Y. D. Boakye, N. Osafo, C. A. Danquah, F. Adu and C. Agyare, "Antimicrobial Agents: Antibacterial Agents, Anti-biofilm Agents,

- Antibacterial Natural Compounds, and Antibacterial Chemicals," in *Antimicrobials*, IntechOpen, 2019, pp. 1-20.
- [321] R. L. Guest and T. L. Raivio, "Role of the Gram-Negative Envelope Stress Response in the Presence of Antimicrobial Agents," *Trends in Microbiology*, vol. 24, pp. 377-390, 2016.
- [322] Z. Cai, P. Chen, H.-J. Jin and J. Kim, "The effect of chitosan content on the crystallinity, thermal stability, and mechanical properties of bacterial cellulose–chitosan composites," *Journal of Mechanical Engineering Science*, vol. 223, pp. 2225-2230, 2008.
- [323] R. Portela, C. R. Leal, P. L. Almeida and R. G. Sobral, " Bacterial cellulose: a versatile biopolymer for wound dressing applications," *Microbial Biotechnology*, vol. 12, pp. 1-20, 2019.
- [324] Y. Cui, S. Kumar, B. R. Kona and D. van Houcke, "Gas barrier properties of polymer/clay nanocomposites," *RSC Advances*, vol. 5, pp. 63669-63690, 2015.
- [325] I. Algar, C. Garcia-Astrain, A. Gonzalez, L. Martin, N. Gabilondo, A. Retegi and A. Eceiza, "Improved Permeability Properties for Bacterial Cellulose/Montmorillonite Hybrid Bionanocomposite Membranes by In-Situ Assembling," *Journal of Renewable Materials*, vol. 4, pp. 57-65, 2016.
- [326] M. Gomez, H. Palza and R. Quijada, "Influence of Organically-Modified Montmorillonite and Synthesized Layered Silica Nanoparticles on the Properties of Polypropylene and Polyamide-6 Nanocomposites," *Polymers (Basel)*, vol. 8, pp. 1-15, 2016.
- [327] G. Li, A. G. Nandgaonkar, Y. Habibi, W. E. Krause, Q. Wei and L. A. Lucia, "An environmentally benign approach to achieving vectorial alignment and high microporosity in bacterial cellulose/chitosan scaffolds," *RSC Advances*, vol. 7, pp. 13678–13688, 2017.
- [328] T. M. Tengku-Rozania and E. J. Birch, "Thermal analysis of Lipid Decomposition by DSC and TGA," *Encyclopedia of Food Chemistry*, vol. 2, p. 346, 2019.

- [329] O. M. de Bruin and H. C. Birnboim, "A method for assessing efficiency of bacterial cell disruption and DNA release," *BMC Microbiology*, vol. 16, p. 199, 2016.
- [330] B. M. Kadakkuzha, X.-a. Liu, S. Swarnkar and Y. Chen, "Chapter 18 - Genomic and Proteomic Mechanisms and Models in Toxicity and Safety Evaluation of Nutraceuticals," in *Nutraceuticals*, Academic Press, 2016, pp. 227-237.
- [331] B. Aslam, M. Basit, M. A. Nisar, M. Khurshid and M. H. Rassol, "Proteomics: Technologies and Their Applications," *Journal of Chromatographic Science*, vol. 55, pp. 182-196, 2017.
- [332] B. Moe, S. Gabos and X.-F. Li, "Real-time cell-microelectronic sensing of nanoparticle-induced cytotoxic effects," *Analytica Chimica Acta*, vol. 789, pp. 83-90, 2013.
- [333] R. P. Araldi, T. C. de Melo, T. B. Mendes, P. L. de Sa Junior, B. H. N. Nozima, E. T. Ito, R. F. de Carvalho, E. B. de Souza and R. d. C. Stocco, "Using the comet and micronucleus assays for genotoxicity studies: A review," *Biomedicine & Pharmacotherapy*, vol. 27, pp. 74-82, 2015.
- [334] K.-C. Cheng, C.-F. Huang, Y. Wei and S.-h. Hsu, "Novel chitosan–cellulose nanofiber self-healing hydrogels to correlate self-healing properties of hydrogels with neural regeneration effects," *NPG Asia Materials*, vol. 11, pp. 2-17, 2019.
- [335] M. I. Mitov, V. S. Patil, M. C. Alstott, T. Dziuba and A. D. Butterfield, "Chapter Six - In Vitro Cellular Assays for Oxidative Stress and Biomaterial Response," in *Oxidative Stress and Biomaterials*, Academic Press, 2016, pp. 145-150.
- [336] P. Kumar and A. U. P. D. Nagarajan, "Analysis of Cell Viability by the Lactate Dehydrogenase Assay," *Cold Spring Harbor Protocols*, vol. 6, pp. 1-7, 2018.
- [337] H. Troustrup, K. Thomsen, H. Calum, N. Hoiby and C. Moser, "Animal model of chronic wound care: the application of biofilms in clinical

research," *Chronic Wound Care Management and Research*, vol. 3, pp. 123-132, 2016.